



APAT

Agenzia per la protezione dell'ambiente e per i servizi tecnici

Servizio Geologico d'Italia

DIPARTIMENTO DIFESA DEL SUOLO

Organo Cartografico dello Stato (legge n°68 del 2.2.1960)

MEMORIE

DESCRITTIVE DELLA

CARTA GEOLOGICA D'ITALIA

VOLUME LXXXII



STRUCTURAL STYLES & DOLOMITES FIELD TRIP

Carlo Doglioni & Eugenio Carminati





A P A T

Agenzia per la protezione dell'ambiente e per i servizi tecnici
Servizio Geologico d'Italia
DIPARTIMENTO DIFESA DEL SUOLO
Organo Cartografico dello Stato (legge n° 68 del 2.2.1960)

MEMORIE
DESCRITTIVE DELLA
CARTA GEOLOGICA D'ITALIA
VOLUME LXXXII

STRUCTURAL STYLES
&
DOLOMITES FIELD TRIP

Stili strutturali ed escursione nelle Dolomiti

di

CARLO DOGLIONI & EUGENIO CARMINATI
Dipartimento di Scienze della Terra - Università La Sapienza, Roma

2008



This book is conceived more as an atlas rather than a text-book. It provides few introductory concepts in structural styles and the main topics of a field trip in the Dolomites (Southern Alps, northeast Italy). The main issues will be related to brittle deformation examples, and to the tectonics-sedimentation interplay.

Direttore responsabile : Leonello SERVA

REDAZIONE a cura del Servizio Cartografico, coordinamento base dati e tavoli europei

Dirigente: Norman ACCARDI

Capo Settore: Domenico TACCHIA

Coordinatore Editoriale: Marina COSCI, Maria Luisa VATOVEC

Allestimento digitale Cartografico ed Editoriale: Silvana FALCETTI

Introduction

Search and use of fossil energy sources, underground storage of natural gas during summer for the re-use during the cold season or whenever needed. They are only two out of several hot topics which brittle structural geology can provide a basic contribution to. However, many others might be listed. For all of them, knowledge of rock geometry, tectonics and interrelation between stress and strain, are crucial. The ways these information can be accessed are discussed in this volume which, in the first part, describes the state-of-the-art of the knowledge on rock mechanics and traditional tectonic structures. That knowledge is then applied to tectonic and geodynamic contexts in which these structures were formed. A large part of the volume shows examples of buried and outcropping structures, from the meter to the kilometric scales, in the Dolomites and in the Prealpi Bellunesi areas.

These examples are thematically and geographically grouped in order to create also a guide for the understanding of the central-eastern Southern Alps geology.

Therefore, the volume proposes different reading and use levels. It can either be considered a way to go further in depth in the basic knowledge on structural geology acquired during their studies by geologists, engineers or naturalists. Or it can be used as a didactic tool for university courses.

Introduzione

Ricerca e utilizzo di risorse energetiche fossili, stoccaggio di gas naturale nel sottosuolo in estate per un futuro riutilizzo nei mesi più freddi o in caso di crisi di rifornimento. Questi sono solamente due temi scottanti ai quali la geologia strutturale del fragile può contribuire in modo fondamentale. Ma molti altri potrebbero esserne elencati. Per tutti questi argomenti è cruciale la conoscenza della geometria dei corpi rocciosi nel sottosuolo, della tettonica e delle relazioni tra sforzo e deformazione. Le modalità con cui queste informazioni possono essere raggiunte sono trattate in questo volume, che nella prima parte presenta lo stato dell'arte sulla meccanica delle rocce e le strutture tettoniche classiche. Queste conoscenze sono poi inserite nei possibili contesti tettonici e geodinamici in cui si formano. Buona parte del volume illustra esempi di sottosuolo e di affioramenti, dalla scala metrica a quella chilometrica provenienti dalle Dolomiti e dalle Prealpi Bellunesi. Questi esempi sono raggruppati tematicamente e geograficamente in modo da costituire anche una guida alla geologia del Sudalpino centro-orientale. Il volume propone pertanto diversi piani di lettura e di utilizzo. Può essere un approfondimento delle conoscenze elementari di geologia strutturale acquisite durante gli studi per geologi, ingegneri e naturalisti. Oppure può essere utilizzato come uno strumento didattico per corsi universitari.

Il Direttore del
Servizio Geologico d'Italia
Dr. LEONELLO SERVA

Preface

Eni, in collaboration with the Italian Geological Survey, is pleased to present this volume on structural styles. This volume is the result of a long and stimulating scientific collaboration with Professor Carlo Doglioni and Professor Eugenio Carminati from the Dipartimento Scienze della Terra (Earth Sciences Department) – Università La Sapienza, Rome and is based on the extensive notes compiled during various editions of a course that Professor Doglioni has been presenting for Eni geoscientists for more than a decade.

The experience acquired from this course, together with the continuous field research of the authors in the Dolomites over the last 25 years, has provided a natural opportunity to present an updated vision of the Geology of the Dolomites and an excellent example of the true benefits of the integration of the core geoscience disciplines of Field Geology, Structural Interpretation and Predictive Geological Modelling. The models described in this volume will find a practical application in geological interpretation and reservoir modelling of many carbonate complexes and successions worldwide. It will also provide inspiration for geoscientists and engineers with a wide range of scientific experiences and technicalities.

This contribution witnesses the importance that Petroleum Industry in general, and Eni Exploration & Production Division in particular, attribute to high quality geological field work. Indeed, we consider that is still possible – perhaps even mandatory – for geoscientists and engineers to learn key lessons from the direct observation of rocks and outcrop geometries in the field, particularly in an industry characterised by intense and aggressive development of workstation-based interpretation technology.

Eni welcomes this opportunity to collaborate once again with the Italian Geological Survey, which continues to generate major progress in the comprehension of the complex, marvellous, Italian geological environment.

Eni

Abstract

During the last 30 years, structural geology had relevant advances thanks to a wealth of data provided by geological and geophysical investigations. In this volume we propose a sort of handbook for basic tectonic features. We review the fundamental mechanics, and the most common features associated to brittle deformation. The main geometries and kinematics of compressional, transpressive, strike-slip, transtensive and extensional tectonic environments are presented. Moreover the migration of rupture along faults and the elementary evolution of diapirs are discussed. Few instances on how tectonics influences sedimentation, compaction, and the sedimentary architecture controls tectonics are highlighted. The structural features are then inserted in a wider geodynamic scenario in which the basic element is the basal decollement, with its depth, temperature, pressure and strain rate. The regional subsidence or uplift is combined with the growth rate of single tectonic features, which may locally increase or decrease the regional motions. This points to the computation for example of the fold total uplift, e.g., the uplift of an anticline minus the regional subsidence rate of the foredeep, that can even exceed the vertical growth rate of the fold. The combination with variable sedimentation rates may further differentiate the growth structures. The geodynamics of subduction zones and rift zones is discussed in the frame of the westward drift of the lithosphere, generating a worldwide asymmetry, which can be recognized as well as between the subduction zones in the Mediterranean realm. Unlike the Apennines, the Alps do not have a coaxial rifting in the hangingwall of the subduction, i.e., a backarc basin as the Tyrrhenian Sea. In this context, the Southern Alps and the Dolomites in particular, are rather the compressive retro-belt of the Alpine orogen, which is associated to the right-lateral transpressive subduction along the E-W trending segment of the belt. The Dolomites were undergoing rifting episodes during the Permo-Mesozoic. Fast subsidence rates during the Ladinian would support a backarc origin in the hangingwall of a W-directed subduction zone, possibly located in the present Pannonian Basin. The Dolomites are located half on the N-trending Trento Horst to the west, and the other half on the Belluno Graben to the east, both extensional features of Permo-Mesozoic age. The Trento Horst determined an undulation in the Alpine thrusting, being located in a recess since the early phases of shortening, generating left-lateral transpression along the western border (Giudicarie system), and right-lateral transpression on its eastern margin (Paleogene WSW-verging thrusts of the central-eastern Dolomites). The adjacent Lombard Graben (and basin) to the west, and the Belluno Basin to the east have rather been the seat of salients. The description of a five days field trip illustrates well exposed examples of tectonic features generated by the Mesozoic rifting and the later Cenozoic Alpine inversion that generated a classic thrust belt with imbricate fan geometry.

KEY WORDS: *Structural Geology, Tectonics-Sedimentation interplay, Geodynamics, Dolomites.*

Riassunto

Negli ultimi 30 anni, la geologia strutturale ha avuto un profondo avanzamento grazie ad una gran mole di nuovi dati geologici e geofisici. Questo volume è concepito come un piccolo manuale per le strutture tettoniche elementari. Dopo una breve descrizione di elementi di meccanica delle rocce, vengono descritte le strutture più comuni degli ambienti fragili, dagli ambienti compressivi a quelli transpressivi, trascorrenti, transtensivi e estensionali. Inoltre sono discusse le migrazioni della rottura lungo le faglie, e gli elementi di base dell'evoluzione dei diapiri. Vengono illustrati alcuni esempi di come la tettonica controlli la sedimentazione, la compattazione, e di come l'architettura stratigrafica influenzi la tettonica. Gli elementi strutturali sono poi inseriti in un contesto geodinamico più ampio, dove l'elemento di base è il piano di scollamento basale, con la propria temperatura, pressione e tasso di deformazione. La subsidenza o il sollevamento regionali sono combinati con la crescita di singole strutture tettoniche, che possono localmen-

te aumentare o diminuire il trend regionale. Questo porta ad esempio al concetto di sollevamento totale di un'anticlinale, dato dal tasso di sollevamento della piega, meno la subsidenza regionale dell'avanfossa, che può addirittura superare quella del sollevamento della piega. L'ulteriore combinazione col tasso di sedimentazione differenzia ulteriormente vari casi di anticlinali di crescita.

La geodinamica delle zone di subduzione e di rift viene sommariamente analizzata nell'ambito della rotazione verso ovest della litosfera rispetto al mantello sottostante, rotazione che genera un'asimmetria globale che può essere riconosciuta anche comparando le subduzioni del Mediterraneo. Al contrario degli Appennini, le Alpi non hanno un rift coassiale a tetto della subduzione, cioè un bacino di retroarco come il Tirreno. Il Sudalpino e le Dolomiti in particolare sono invece la retrocatena in compressione dell'orogene alpino, generato dalla subduzione transpressiva destra lungo il tratto E-W della catena. Le Dolomiti sono state oggetto di tettonica estensionale durante il Permo-Mesozoico. Una fase di rifting con tassi di subsidenza molto rapida durante il Ladinico indicherebbe un'origine di bacino di retroarco a tetto di una subduzione diretta ad ovest, subduzione che in quest'ipotesi si sarebbe dovuta trovare nell'area attualmente occupata dal Bacino Pannonico. Le Dolomiti si trovano a cavallo tra l'Horst di Trento e il Graben di Belluno, strutture estensionali orientate N-S. L'Horst di Trento ha determinato un'ondulazione assiale nei sovrascorrimenti, generando un recesso fin dalle prime fasi del raccorciamento alpino, con transpressione sinistra sul lato occidentale (sistema Giudicariense), e transpressione destra sul lato orientale (strutture paleogeniche OSO-vergenti delle Dolomiti centro-orientali). I graben adiacenti Lombardo e Bellunese (coincidenti con facies bacinali) sono stati invece sedi di salienti. La descrizione di un'escursione di cinque giorni illustra esemplari affioramenti di strutture tettoniche generate dal rifting Mesozoico e dalla successiva inversione Alpina Cenozoica che ha prodotto un classico esempio di catena di sovrascorrimenti con geometria a ventaglio embricato.

PAROLE CHIAVE: Geologia Strutturale, Rapporto Tettonica-Sedimentazione, Geodinamica, Dolomiti.

1. Elements of rheology



The kinds of structures that develop in rocks during deformation depend on: 1) the orientation and intensity of the forces applied to the rocks; 2) the physical conditions (mainly temperature, pressure, occurrence and pressure of fluids) under which the rocks are deformed; 3) the mechanical properties of rocks, which are strongly dependent on the physical conditions. At relatively low temperature and pressure and for high intensity of the applied forces, rocks generally undergo brittle deformation, i.e., rocks are characterised by loss of cohesion along discrete surfaces (either faults or fractures) and deformation is accommodated by the mechanism of fracturing (e.g., cataclastic flow). At higher temperature and pressure, rocks normally undergo ductile deformation, i.e., a solid state deformation in which no cohesion loss occurs both at the crystalline scale and at larger scales (no evidence of brittle fracturing). The deformation is accommodated by intracrystalline plastic mechanisms (e.g., from low to high temperature: pressure solution, intracrystalline deformation, twinning, recovery, recrystallization, solid-state diffusion creep, superplasticity). Ductile deformation is generally associa-

ted to the generation of folds, stretching and thinning of layers, generation of planar (foliations) and linear (lineations) tectonic fabrics. It is however stressed that not necessarily folding of a sedimentary succession may be accommodated by plastic deformation mechanisms. More frequently, folding in foreland fold-and-thrust belts is accommodated both at meso- and micro-scales by brittle fracturing. In this case the term brittle-ductile deformation is adopted to indicate that geometries of structures may be similar to those occurring in ductile regimes but deformation is accommodated by brittle deformation mechanisms.

The strength of rocks in the brittle regime (brittle yield stress, expressed in terms of differential stress, $\sigma_1 - \sigma_3$) is described by the Sibson's law (SIBSON, 1981). This law, based on the Coulomb-Navier frictional criterion, predicts a linear increase with depth of the yield stress:

$$\sigma_1 - \sigma_3 = \beta \rho g z (1 - \lambda) \quad (1)$$

where β is a parameter depending on the fault type, ρ is the density, g is the gravity acceleration, z is the depth and λ is the pore fluid pres-

sure ratio (i.e., the ratio between fluid pressure and lithostatic load). It is immediately clear that brittle rock strength is quite independent on rock type (with the exception of particular lithologies such as shales and evaporites, characterised by very low strengths) and increases linearly with depth. It is however dependent on the type (extensional, strike slip or compressional) of the structural setting and on fluid pressure.

The ductile behaviour of rocks is described by various power law creep relations, such as, for example:

$$\sigma_1 - \sigma_3 = \left(\frac{\dot{\epsilon}}{A} \right)^{1/n} \exp\left(\frac{Q}{nRT} \right) \quad (2)$$

where $\dot{\epsilon}$ is the effective strain rate, A is the generalised viscosity coefficient, n is the stress power law exponent, Q is the activation energy,

R is the gas constant and T is the absolute temperature (e.g., CARTER & TSENN, 1987). A , n and Q are typically lithology dependent and are determined by laboratory experiments on rock or mineral samples. The ductile strength of rocks diminishes exponentially with depth and is strongly lithology, strain rate and temperature dependent (fig. 1).

The differential yield stress required to produce failure is given by the lesser of the brittle and ductile yield stresses (GOETZE & EVANS, 1979). In the upper crust, at shallow levels, brittle strength is lower than ductile strength and fracturing occurs. At deeper depths ductile strength is lower and plastic deformation occurs. The depth at which brittle and ductile strengths are equal is called brittle-ductile (or alternatively brittle-plastic) transition depth (BDTD) and is the border between the brittle and ductile deformation fields. Such depth is not constant since it varies

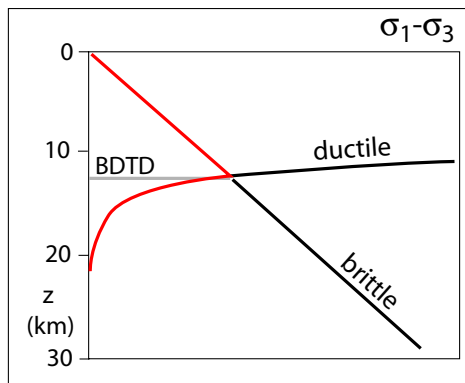


Fig. 1 - Schematic representation of the strength of rocks (yield stress, expressed in terms of differential stress, $\sigma_1 - \sigma_3$) in the brittle and ductile regime. Brittle strength is linearly increasing with depth whereas ductile strength diminishes exponentially with depth. The depth at which the two curves cross each other is named brittle-ductile transition depth (BDTD). Above such depth, rocks will undergo brittle deformation, whereas below they will deform ductilely. The strength of rocks with depth will follow the red line.

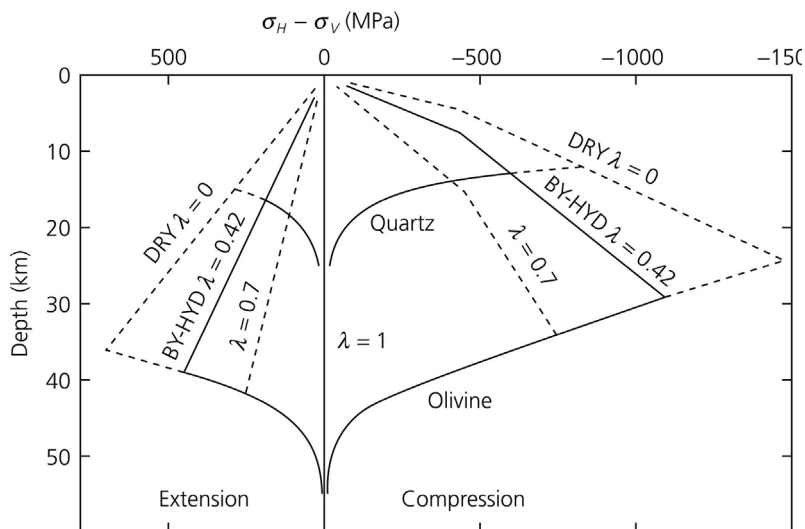


Fig. 2 - The effects of fluid pressure on the depth of brittle to ductile transition are shown. An increase of fluid pressure (increasing λ) induces a lowering of the brittle yield stress and consequently a deepening of the brittle-ductile transition. Brittle strength curves are provided for extensional and compressional settings. Notice also that, for a fixed depth, the ductile strength is larger for olivine than for quartz. Quartz (that is the main mineralogical component of upper crustal crystalline rocks) is therefore characterised by shallower brittle-ductile transitions than olivine (that is the main component of the lithospheric mantle). (After BRACE & KOHLSTEDT, 1980).

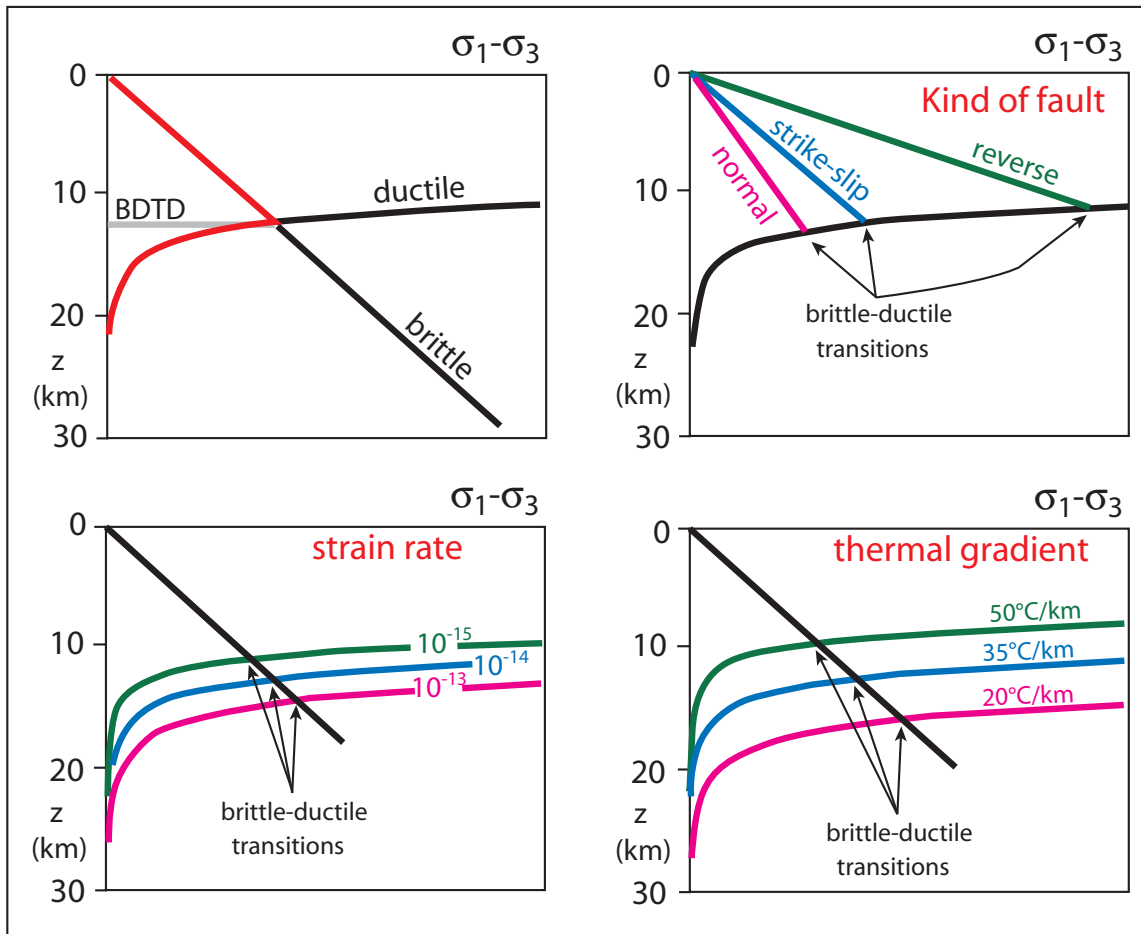


Fig. 3 - The brittle-ductile transition depth (BDTD) is strongly dependent on the kind of structural regime active in a given region, on the strain rate and on the thermal gradient. In this figure, the sensitivity of the BDTD on these parameters is schematically shown. In all the panels the lithology is kept constant. Areas characterised by thrust faulting are characterised by larger brittle strength with respect to areas characterised by strike-slip and normal faulting. As a consequence, keeping constant the other controlling parameters, the brittle-ductile transition depth in contractional areas will be shallower than in strike-slip (intermediate depth) and extensional (deeper depth) areas. Strain rate strongly controls the ductile strength. Typical strain rates in deforming areas vary between 10^{-15} s⁻¹ (slow deformation) and 10^{-13} s⁻¹ (fast deformation). Increasing strain rates induce higher ductile rock strengths. This is mainly due to the fact that, for fast deformations, migration of lattice defects, recrystallization and other plastic deformation mechanisms are not capable to keep the pace with deformation. Keeping constant the other controlling parameters, areas characterised by faster deformations will be characterised by deeper brittle-ductile transition depths. The thermal gradient of an area is controlled by the regional mantle heat flow, by the crustal radiogenic heat production (that is in turn controlled by crustal lithologies) and by local effects (e.g., magmatic intrusions, heat production generated along major regional faults). An area characterised by larger thermal gradient will be characterised, at a fixed depth, by higher temperatures with respect to areas characterised by low thermal gradients. Since ductile strength is inversely proportional to temperature, at the same depth areas characterised by high gradients will also be characterised by low ductile strength. Therefore, keeping constant the other controlling parameters, larger thermal gradients will be associated to shallower brittle-ductile transition depths.

considerably from region to region. This is mainly due to the variation of the factors controlling brittle (structural setting, fluid pressure) and ductile (temperature gradient, lithology, strain rate) strengths (fig. 2, 3). It has to be stressed that the brittle-ductile transition does not occur sharply and at the same depth in a given region. This is mainly due to the fact that the

factors controlling the brittle-ductile transition depth may vary even along short distances (for example the fluid pressure may be controlled by laterally discontinuous aquifers) and the mineralogical content of rocks may also vary significantly. Moreover, the different minerals forming one single lithology (e.g., phyllosilicates, quartz and feldspars in an upper crustal

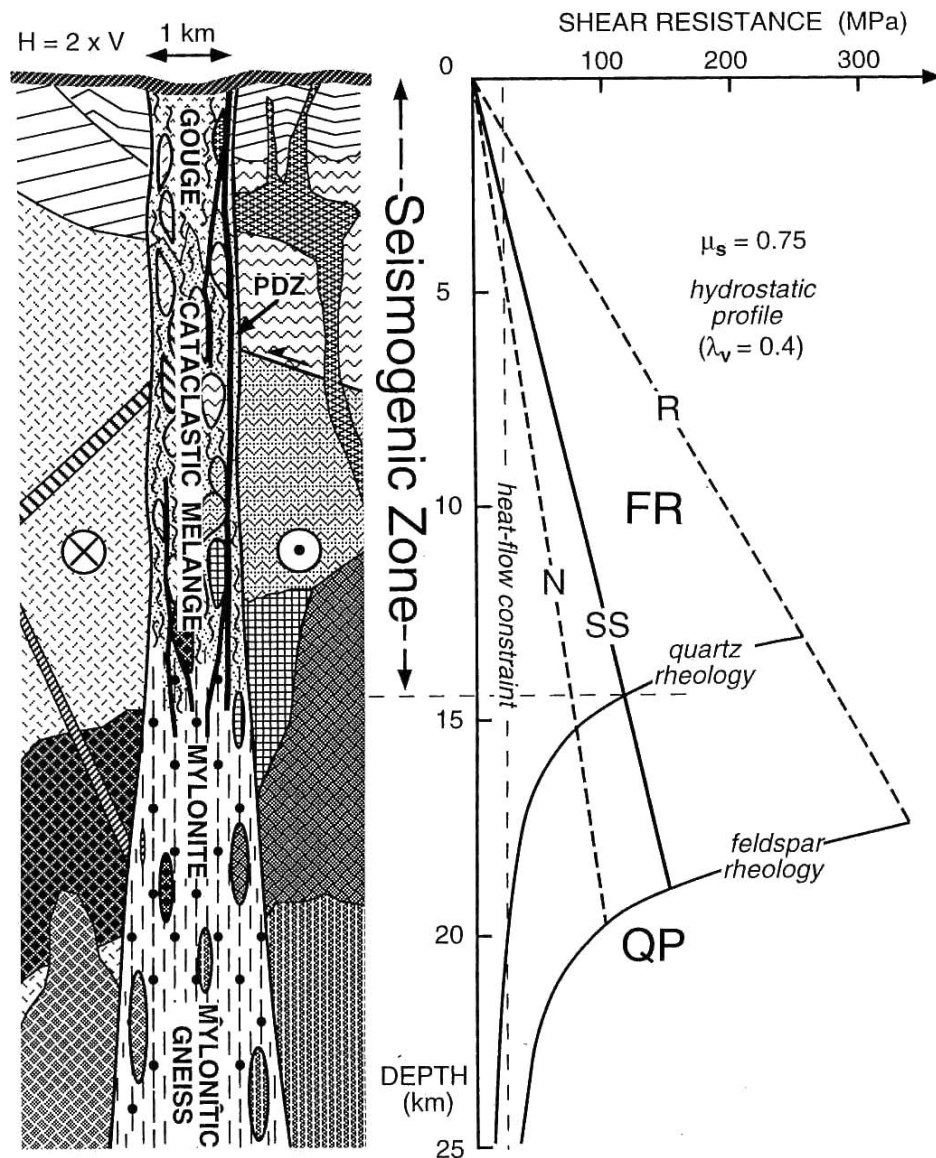


Fig. 4 - Fault rocks associated to brittle (breccias, fault gouge and foliated/non-foliated cataclasites) and ductile (mylonites) structural settings (left panel). Notice that the transition from brittle to ductile behavior is rather distributed. This is mainly due to the fact that the brittle ductile transition for different rock forming minerals occurs at different depths. In the right panel the intersection between the brittle strength curves (for normal faults, N, for strike slip, SS and for reverse faults, R) and the ductile strength curves for quartz and feldspar is shown. Quartz and feldspar are typical mineralogical components of upper crustal rocks, such as gneisses. In this example, at depths of about 15-18 km, quartz may deform plastically whereas feldspar may be still characterised by fracturing (after SIBSON, 2001).

gneiss) may be characterised by different brittle-ductile transition depths.

The active deformation mechanism will control the kinds of rocks generated along fault zones (fig. 4). A major fault zone crossing the upper crust from the surface down to depths of 15-20 km will be characterised by brittle (most probably seismogenic) behavior at shallow depths and ductile (aseismic) behavior below

the brittle ductile transition. Typical fault lithologies associated to brittle regimes are breccias, gouge and cataclasites (that can be either foliated or characterised by absence of internal organization). Ductile portions of faults are associated to mylonites.

The minerals constituting the main lithologies forming the lithosphere are characterised by radically different ductile strength (fig. 5). As a

consequence, the lithological layering of the lithosphere (sedimentary covers, upper crustal crystalline basement, lower crust, lithospheric mantle) will determine a rheological layering within the lithosphere. The rheological layering of the lithosphere varies according to the type of lithosphere (continental vs. oceanic), to the thickness of the various layers and to the parameters controlling brittle and ductile strength (fig. 6). Typical lithospheric rheological profiles are characterised by the alternance of brittle and ductile levels and have a christmas-tree (or saw-tooth) shape. The occurrence of ductile low strength levels between stronger brittle layers is a major factor controlling the deep geometry of extensional (e.g., rift zones) and compressional areas (e.g., mountain belts). Weak ductile layers, that may be located both in the sedimentary covers and in the crustal crystalline rocks, will, in fact, behave as lithospheric scale detachment levels.

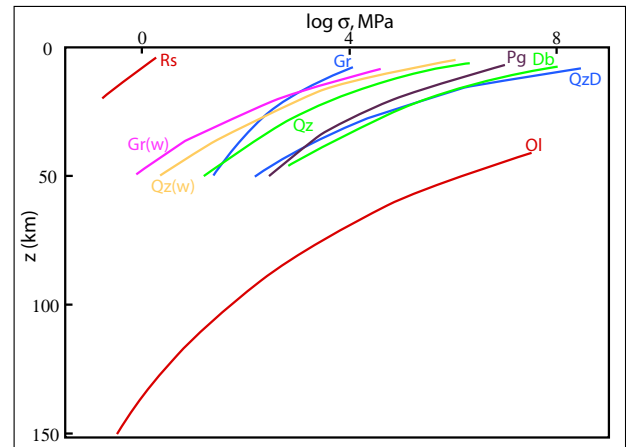


Fig. 5 - Ductile strength of different rocks and rock forming minerals calculated for a cold continental geothermal gradient. Rs, rock salt; Gr(w), wet (i.e., hydrated) granite; Gr, granite; Qz, quartz; Qz(w), wet quartz; Pg, plagioclase; Db, diabase; QzD, quartz-diorite; Ol, olivine. Calcite and limestones have strength intermediate between salt and quartz. Quartz, plagioclase and olivine are the main constituents of upper crust, lower crust and lithospheric mantle. Notice that the ductile strength of the lithosphere increases with depth. The minerals of the crust have lower strength than the minerals of the mantle (after RANALLI & MURPHY, 1987).

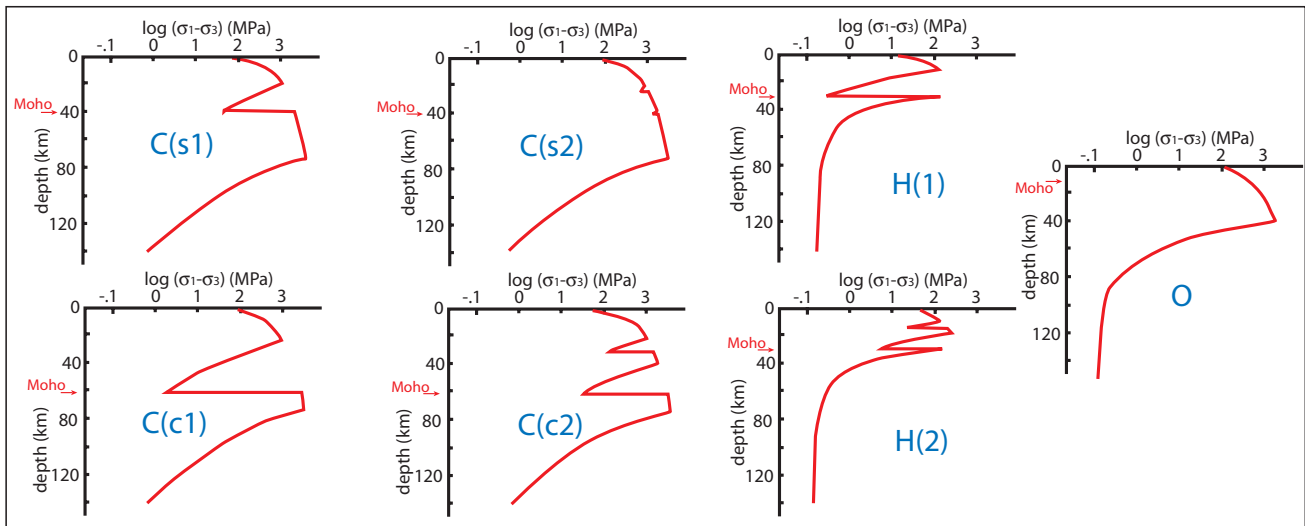
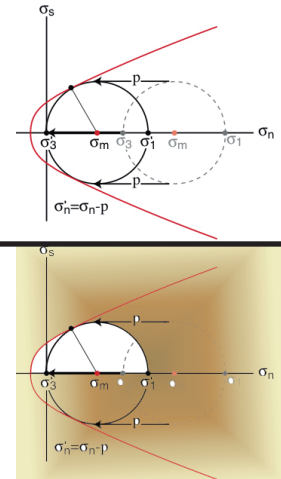


Fig. 6 - Lithospheric scale rheological profiles are characterised by the alternance of brittle and ductile structural levels. Ductile layers may act as major detachment levels along deforming plate margins (e.g., rift zones and collisional belts). The profiles were calculated for different geodynamic setting: C(s1), precambrian shields with 150 km thick lithosphere and unlayered (i.e., quartz-granitic) 40 km thick crust; C(s2), precambrian shields with 150 km thick lithosphere and layered (i.e., quartz-granitic over intermediate basic) 40 km thick crust; C(c1) continental convergence zones with 150 km thick lithosphere and unlayered 60 km thick crust; C(c2) continental convergence zones with 150 km thick lithosphere and layered 60 km thick crust; H(1), continental extensional zones with 50 km thick lithosphere and unlayered 30 km thick crust; H(2), continental extensional zones with 50 km thick lithosphere and layered 30 km thick crust; O, mature oceanic lithosphere, 75 km thick and with a 10 km thick basic crust. The lithospheric rheological profile is even more complicated if one considers sedimentary cover as well. As discussed in the previous figures, evaporites and limestones are characterised by ductile strengths lower than crystalline rocks. Additional brittle-ductile transitions may therefore occur within the sediment succession (after RANALLI & MURPHY, 1987).

2. Fault mechanics: some basic aspects



The behavior of rocks in the shallow crust (fig. 7) has been extensively investigated with rock mechanics laboratory experiments. The results of experiments on the failure of intact rocks are graphically expressed using Mohr diagrams that relate principal stresses acting on a rock volume to shear stresses acting on planes differently oriented within the body. In Mohr diagrams (figs. 8, 9, 10), the composite failure envelope for intact isotropic rock is constructed by merging the Griffith and

Coulomb criteria (JAEGER & COOK, 1979; SIBSON, 1998). Three failure modes of intact rock have been recognized (ENGELDER, 1999; SIBSON, 1998): tensional fracturing, transitional-tensional fracturing (also called in literature extensional-shear fracturing, e.g., SIBSON, 1998) and compressional failure (also called in literature compressional shear failure, e.g., SIBSON, 1998). The first two failure modes occur when the effective minimum stress is tensional and are generally considered to occur only for fluid pressures greater than lithostatic in thrust regimes or at shallow depths in normal fault regions (SIBSON, 1998). Tensional fracturing mainly controls the development of extensional fractures in rocks, whereas the compressional failure applies to development of faults and is governed by the Coulomb fracture criterion: $\tau = C + \sigma\mu$ where τ is the shear stress, C is the cohesive shear stress, σ is the normal stress and μ is the angle of rock internal friction. The slope of the Coulomb envelope is controlled by the coefficient of internal friction of rocks involved in the deformation. Laboratory strength tests on a wide range of rock types have shown that



Fig. 7 - Plumose structure on a fracture in lavas at Colcuc (Dolomites). Note on the left the center of nucleation of the fracture.

the internal friction coefficient ranges between 0.5 and 1.0 (e.g., JAEGER & COOK, 1979). It has been shown that in isotropic bodies (quite a rare situation in the Earth's crust), thrust faults are most likely to form from

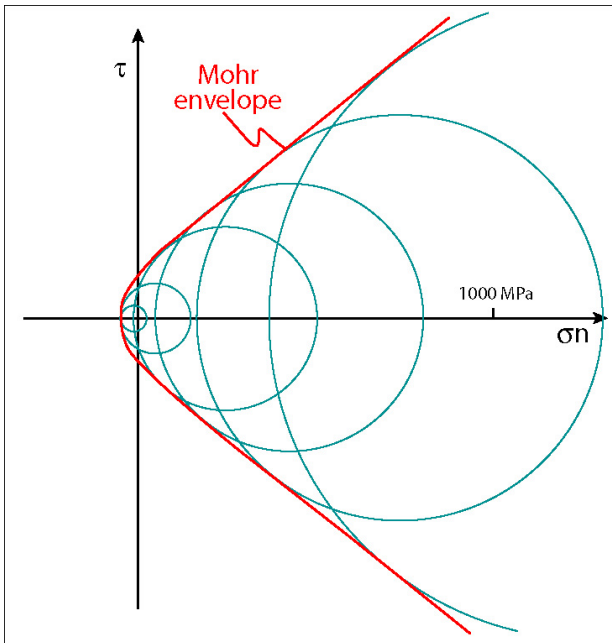


Fig. 8 - Mohr diagram showing the state of effective stress at failure for various experiments (varying the confining and the axial load) with intact Fredrick Diabase. Each circle represents the state of stress at failure at a different mean stress ($(\sigma_1 + \sigma_2 + \sigma_3)/3$). The locus of stress states that bounds the field of stable and unstable stresses is called the Mohr envelope (after SUPPE, 1985).

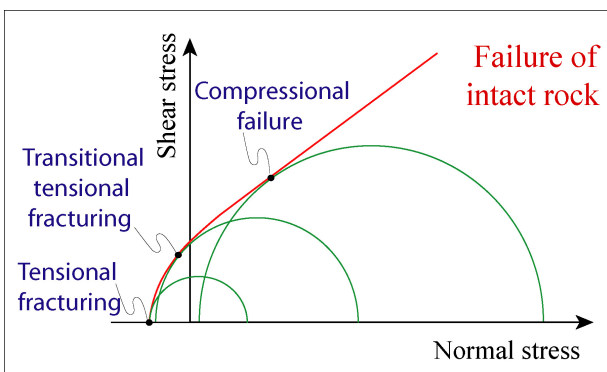


Fig. 9 - Generic Mohr diagram showing a composite Griffith-Coulomb failure envelope for intact rocks. The three shown critical stress circles represent different failure modes: tensional fracturing, transitional-tensional fracturing (also called in literature extensional-shear fracturing) and compressional failure (also called in literature compressional shear failure).

intact rocks at an angle of about 30° to σ_1 (fig. 11). ANDERSON (1905) used the Coulomb-Mohr theory to explain conjugate faults and the different mean dip of the various types of faults. The Anderson's theory applies close to the Earth's surface, where one of the principal stresses needs to be vertical and the two remaining horizontal (due to the fact that, being a solid-air interface, the Earth's surface cannot sustain shear stresses). The main compressional stress σ_1 is vertical in extensional regimes and consequently normal faults normally develop with high (dip around 60°) angle, whereas it is horizontal in contractional areas and thrust faults consequently develop with low angle (around 30°). In strike slip settings σ_2 is vertical and strike-slip faults are mainly subvertical. Important classes of faults that appear to contradict the Anderson's theory are low angle normal faults and high angle reverse faults.

Fluid (e.g., water and hydrocarbons) pressure affects significantly the mechanics of faulting (fig. 12). High fluid pressures (caused by rapid burial of impermeable strata, thermal water pressuring and dehydration reactions occurring during burial and metamorphism) reduce drastically the stress needed to generate rock fracturing and formation of faults, since it supports part of the normal stress that would otherwise act across rock grain boundaries. The normal stress is then reduced to a lower effective normal stress. Extremely high pore fluid pressure will promote hydrofracturing (a process normally induced in oil wells to increase the permeability of reservoir rocks) and vein development. Normally, faults are associated with hydrothermal extensional vein systems (fig. 13). Veins are mainly horizontal when associated to thrust faults and subvertical for normal faults.

Reactivation of existing faults accounts for most of the deformation within the frictional seismogenic crust (fig. 14). In Mohr diagrams, the frictional failure envelope follows the

linear Amonton's law and, for faults characterised by cohesive strength, is a form of the Coulomb envelope (fig. 15). The slope of the Amonton envelope is controlled by the sliding coefficient of friction of the fault, which has been shown to have typical values as high as 0.85 in the shallow crust (BYERLEE, 1978). The frictional resistance along pre-existing planes is expressed by the Byerlee's law: $\tau = 0.85\sigma$. The Byerlee's law is broadly lithology-insensitive. Fault surfaces that contain a layer of gouge also obey Byerlee's law and display a frictional behavior similar to clean rock surfaces involving either strong and weak lithologies. The only silicatic minerals that display significant lower friction than Byerlee's law are montmorillonite, vermiculite and illite. Other platy minerals (e.g., chlorite, kaolinite and serpentine) display normal frictional properties.

The existence of near optimally oriented faults (at an angle close to 30° from σ_1) normally inhibits the development of new planes by brittle failure. As the orientation of existing faults becomes less favourable, reactivation occurs for increasingly higher effective stresses until the angle of frictional lockup is reached and Coulomb mode rupture is expected to occur (HANDIN, 1969). For example, in compressional settings characterised by pre-existing normal faults unfavourably oriented

with respect to σ_1 pre-existing normal faults are expected to remain unsheared and new fault planes may develop. Domino tilting of faults in extensional and compressional areas may progressively rotate the active fault plane so that they may acquire an unfavourable orientation for re-shearing, may lock-up and be abandoned. Further deformation will require the nucleation of new, favourably oriented faults.

Most of the theory on fault mechanics is based on the assumption of isotropic rock. This assumption is largely inconsistent with the observations both in sedimentary and basement rocks, where stratification, schistosity and other metamorphic and igneous foliations occur. In strongly anisotropic rocks, the orientation of the forming fractures is generally influenced by the foliation. Only in case of planes of anisotropy nearly perpendicular to the σ_1 direction, unisotropy is unimportant in localizing fractures (fig. 16).

The displacement distribution along normal and thrust faults is maximum at the fault center and dies out to the fault margins. The thickness of the fault gouge is direct function of total slip along the surface (fig. 17).

The mechanics of thrust faulting has been the subject of animated discussion since when large thrust sheets were recognized. The mechanical problem is that thrust sheets are

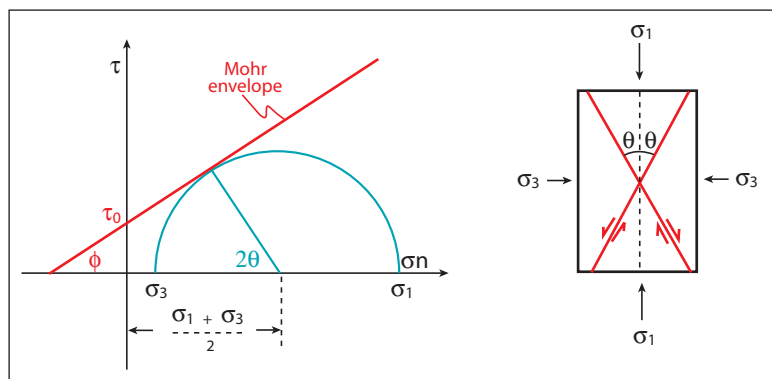


Fig. 10 - Mohr-Coulomb failure criterion for isotropic intact rocks (left panel). The point of tangency of the Mohr circle represents the state of stress on the plane which is at an angle Θ from the σ_1 axis of the right panel.

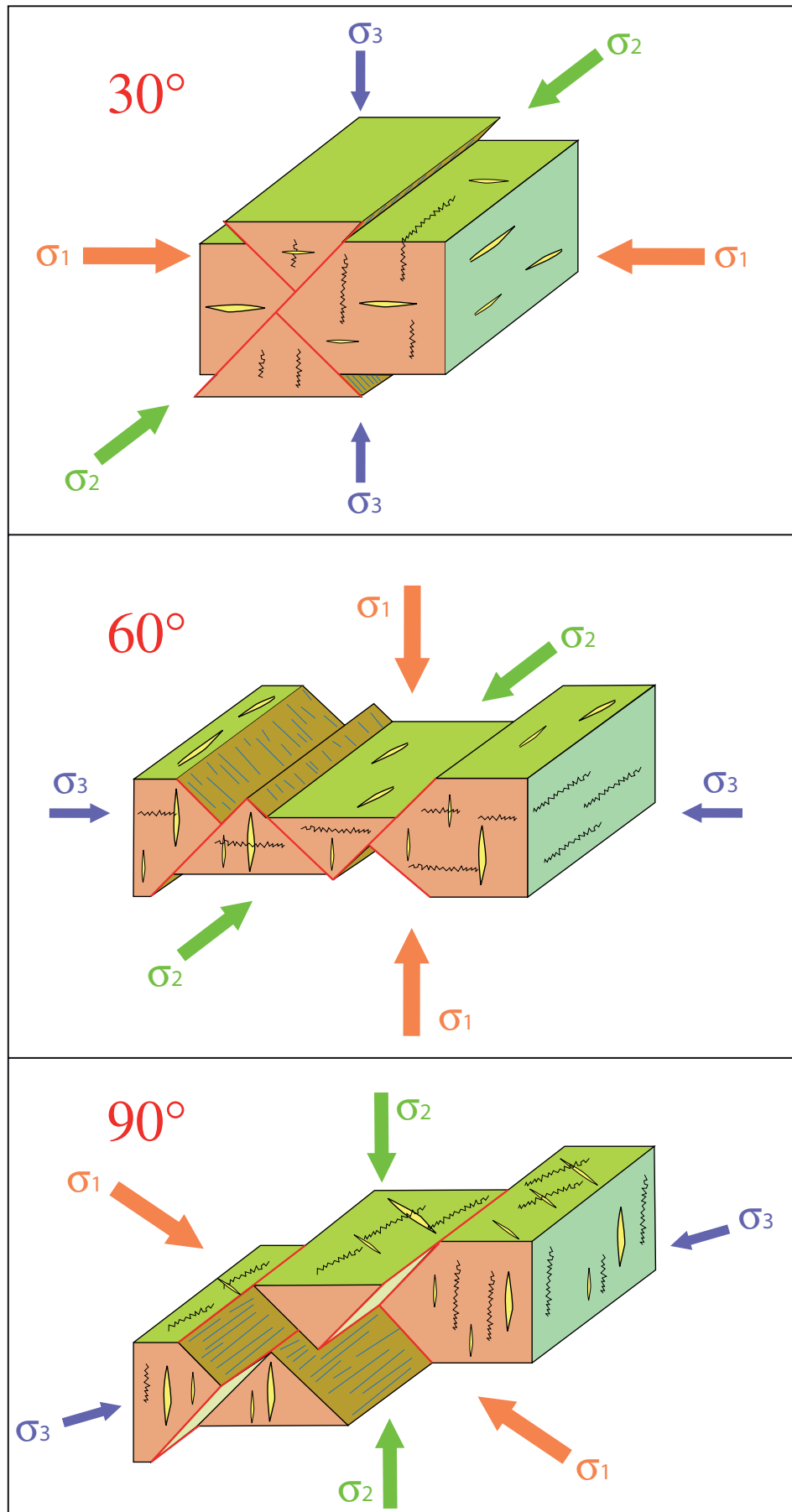


Fig. 11 - Anderson's theory of faulting. The structures associated to fault planes (i.e., stylolites, extensional fractures and veins) are also shown.

very thin relative to their apparent frictional resistance. When thrust faulting is reduced to the elementary physics problem of pushing a rigid block over a rigid base, the force with which the thin sheet has to be pushed determines stresses that are even an order of magnitude larger than the yield stress of common rocks.

Several solutions were proposed to solve this enigma: 1) the basal resistance is not expressed by Coulomb friction but is viscous or plastic (i.e., lower than expected); 2) thrusts are not pushed from behind but slide along dipping planes; 3) fluid pressures may lower the frictional resistance along the basal surface and enhance thrusting; 4) mountain belts are plastic masses that flow outward under their own

weight; 5) mountain belts may be modelled as critical tapers, similar to the deformed wedges of snow or sand developing in front of a bulldozer.

At present the two more accepted explanations invoke the role of fluids and the critical taper behavior of thrust faults. Two lines of evidence suggest that fluid pressures play a significant role: 1) pumping of fluids in reservoirs near active faults produces small earthquakes; 2) fluid pressure measurements in active regions show that major thrusts are confined to overpressured rock volumes.

The critical taper theory suggests that fold-and-thrust belts and accretionary prisms are first characterised by internal deformation and development of a topographic gradient

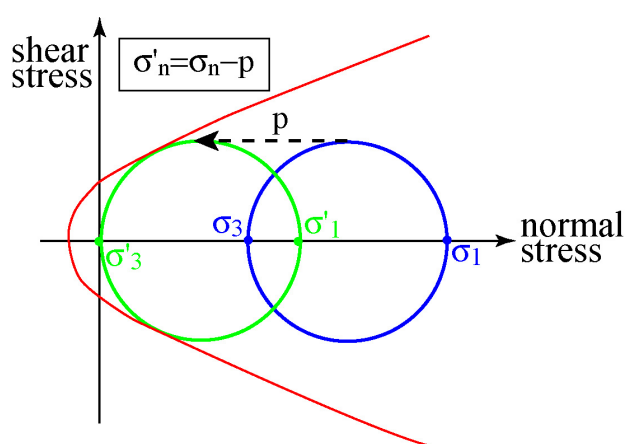


Fig. 12 - Mohr stress diagram showing the effects of pore fluid pressure on the state of stress of a rock volume. An increase of pore fluid pressure p lowers the principal stresses acting on the body and shifts the corresponding Mohr circle to the left. In this example, the dry rock is stable (i.e., it does not fracture since it does not reach the Mohr envelope) whereas the same rock volume, when subject to fluid pressure, may be unstable, i.e., characterised by a Mohr circle tangent to the Mohr envelope. σ_n is the normal stress.

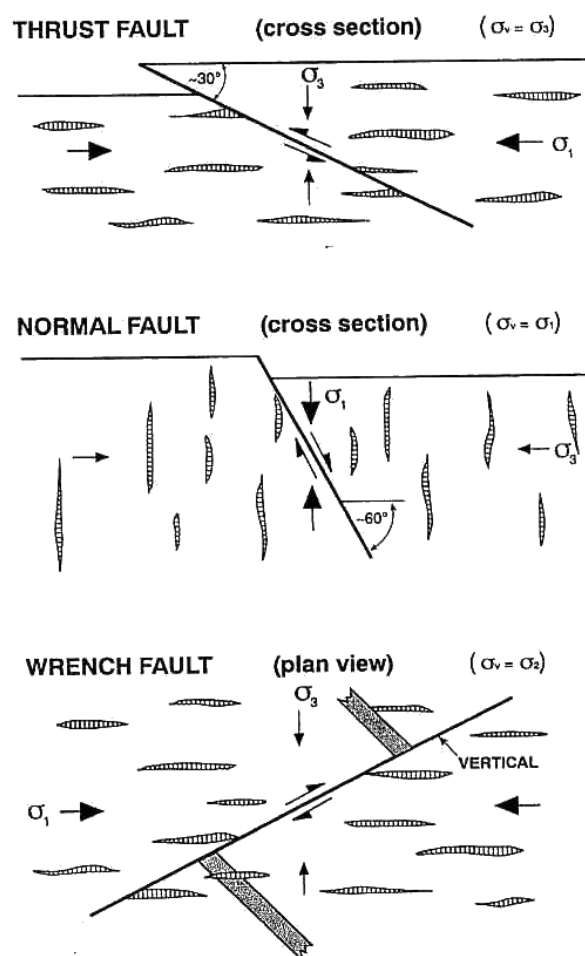


Fig. 13 - Hydrothermal extensional vein systems associated to Anderson style fault systems (after SIBSON, 1990).

without sliding on the basal surface (or decollement) and developing a wedge shape (figs. 18, 19, 20). Only when the wedge attains its critical taper (given by the sum of α , the surface slope dip, and β , the basal decollement dip), the belt starts sliding stably, continuing to growth at constant taper as additional material

enters the belt at the front. If, at a specific point, the critical taper of a wedge is less than the critical value (because of erosion, for example), then the material will deform in more internal sectors (for example with the development of out of sequence thrusts) until the critical value is once again attained. At this

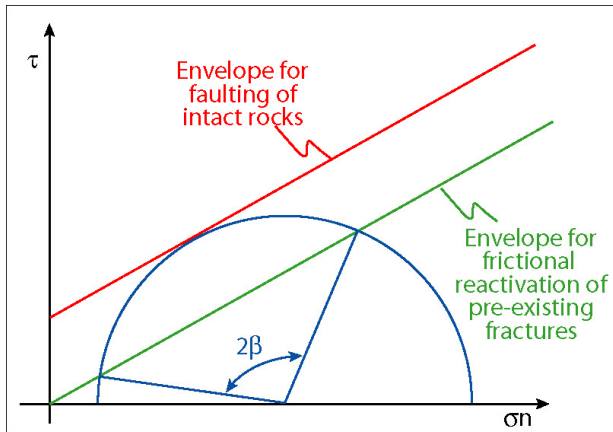


Fig. 14 - Fracturing of intact rocks vs. frictional reactivation of pre-existing faults. The frictional reactivation envelope for pre-existing faults is lower than that for faulting of intact rocks. The stress required for frictional sliding along pre-existing fractures is significantly less than the fracture strength. Two circles for fracture of intact rock (i.e., tangent to the Mohr envelope labeled as "faulting of intact rock") are shown. For the stress distributions associated to the two circles, frictional sliding on pre-existing fractures should anticipate the development of a new fault plane provided that such fractures have orientations comprised in the 2β angles shown in figure

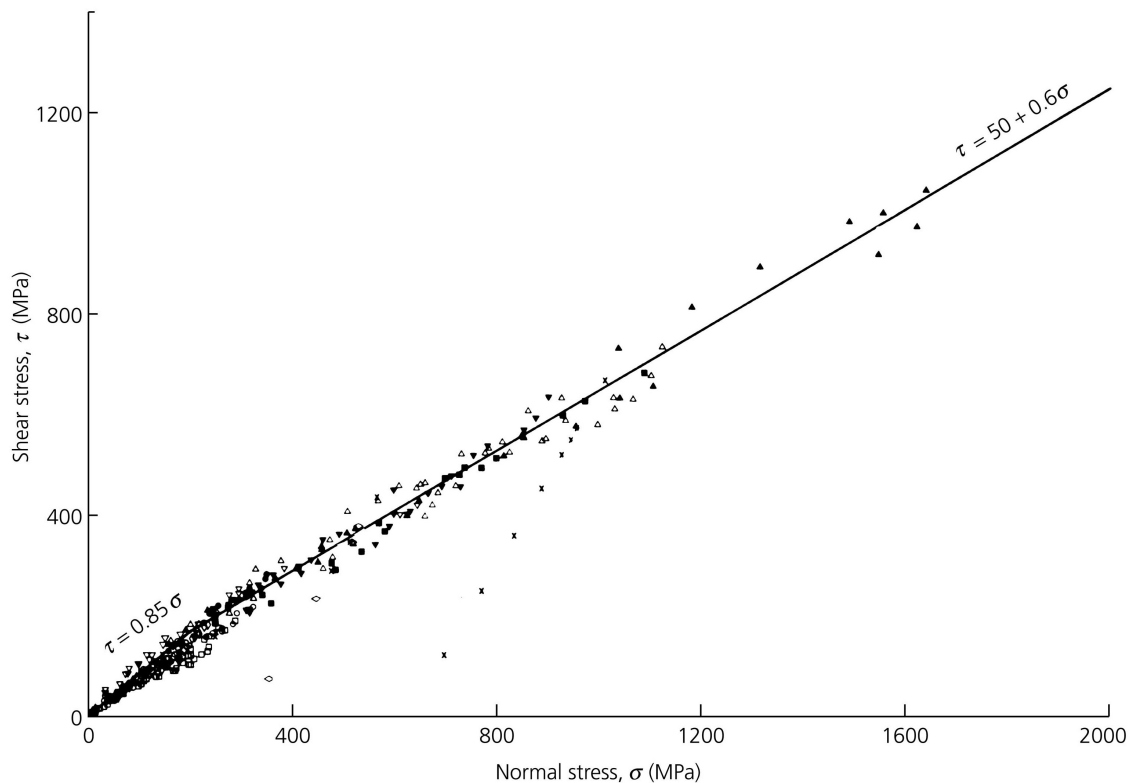


Fig. 15 - Measurements of maximum friction in sandstone, limestone and graywacke. The frictional resistance along pre-existing planes is expressed by the Byerlee's law: $\tau = 0.85\sigma$. Notice that, in the shallow crust (for lithostatic pressure lower than 0.2 GPa) the cohesion is null. The Byerlee's law is broadly lithology-insensitive and is valid for fault surfaces involving either strong and weak lithologies that may contain a layer of gouge as well. The only silicatic minerals that display significant lower friction than Byerlee's law are montmorillonite, vermiculite and illite (after BYERLEE, 1978).

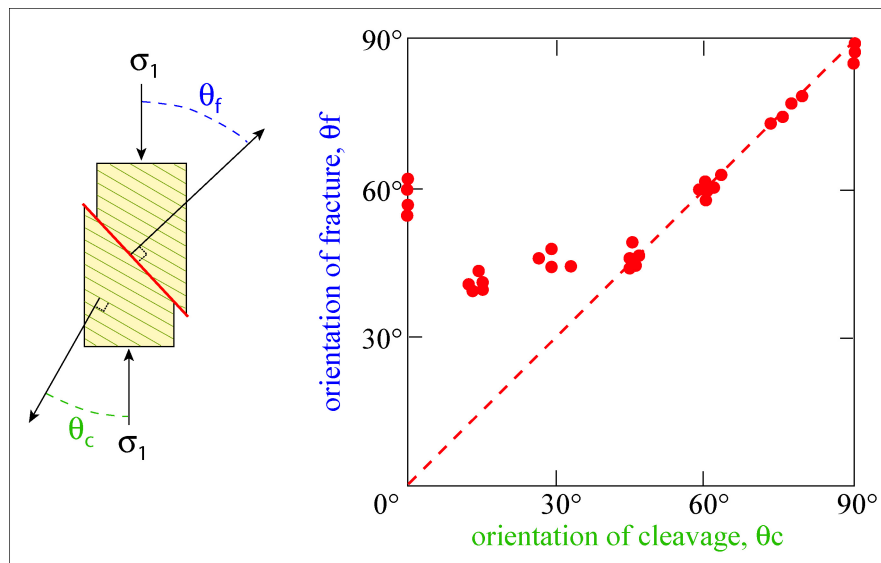


Fig. 16 - Fracturing in anisotropic rocks. The effect of the orientation of the plane of slaty cleavage on a fracture orientation is investigated in compressive fracture experiments on Martinsburg Slate. The orientation of the forming fractures is generally influenced by the foliation. For inclination of the slaty cleavage to the σ_1 of as much as 45°, the fracture always lay parallel to the cleavage. Only in cases for which the plane of anisotropy is nearly perpendicular to the σ_1 direction, anisotropy is unimportant in localizing fractures (after SUPPE, 1985).

point migration of the belt and accretion of material at the thrust front will start again. Typical values of surface slope dips are between 1° and 10°, whereas decollement dips

may be as high as ca. 20°. When the basal decollement runs within low-friction or ductile rocks, then the surface slope becomes about horizontal and plateaus develop.

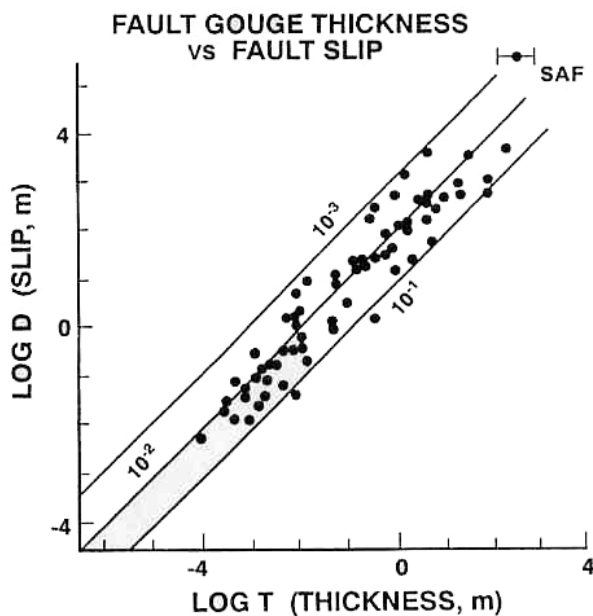


Fig. 17 - Fault gouge thickness (T) vs. total slip (D) for faults mainly developed in crystalline rocks (after SCHOLZ, 1990).

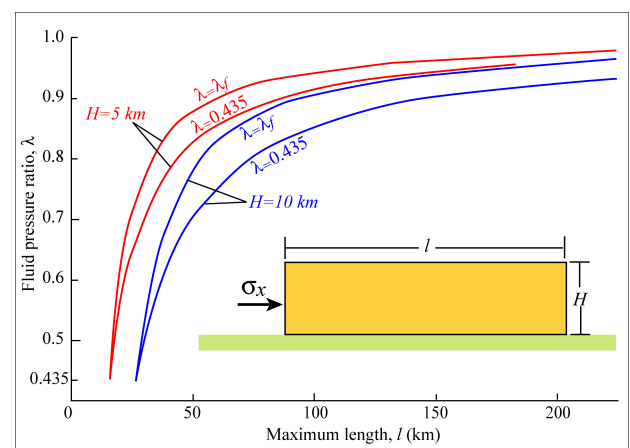


Fig. 18 - Maximum length (l), as a function of fluid pressure ratio ($\lambda = P_f/P_l$, where P_f is the fluid pressure and P_l is the lithostatic pressure) of a rectangular thrust sheet that can be pushed along a horizontal decollement without fracturing. λ is the fluid pressure within the thrust sheet and λ_f is the fluid pressure along the fault (after SUPPE, 1985).

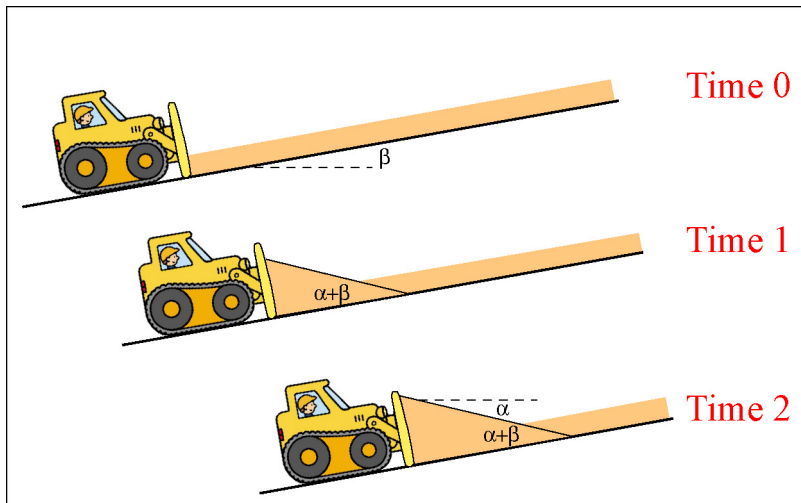


Fig. 19 - Contractional belts are normally modelled as purely brittle critical tapers deforming internally and spreading under the action of body (gravity) and surface (tectonic) forces (upper panel). These models successfully reproduce large scale topographic signatures of several wedge-shaped deformed regions (accretionary wedges) overlying a basal décollement. Surface slope and basal decollement dips predicted for submarine and subaerial accretionary wedges worldwide are shown in the bottom panel (after DAVIS *et alii* 1983).

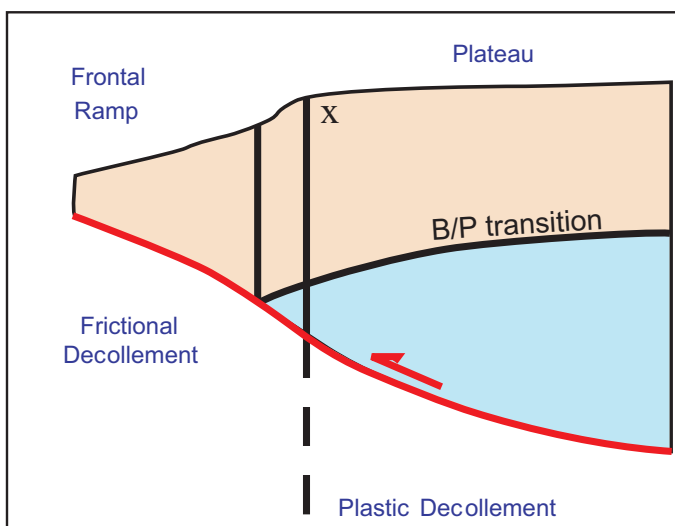
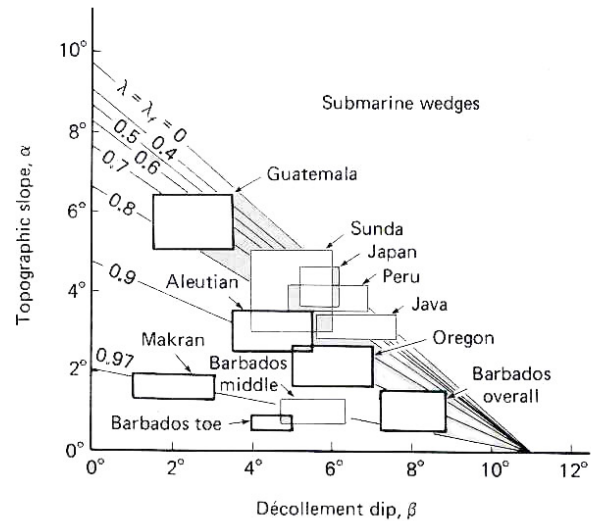
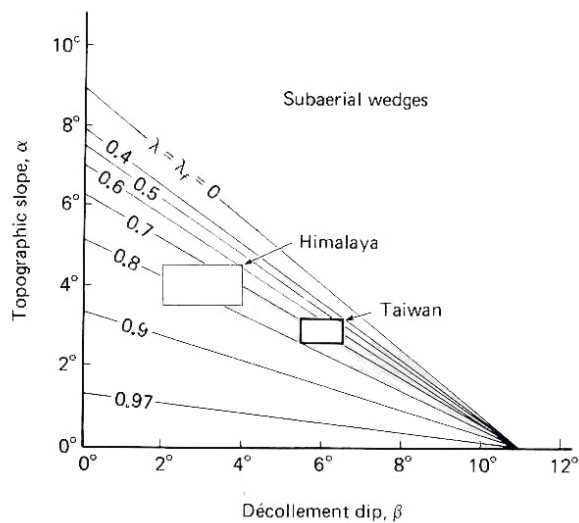
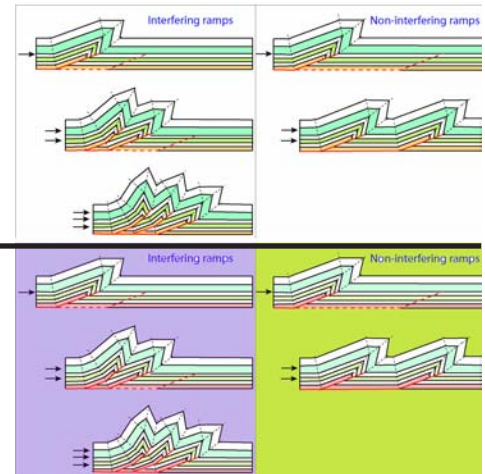


Fig. 20 - The topographic features of mountain belts are controlled by the rheological behavior of the basal décollement. Low-angle surface slopes, typical of frontal sectors of wedges deforming with a purely brittle (frictional) behavior, are interrupted by relatively steeper slopes, where the lowermost part of the wedge (wedge base) crosses the brittle/plastic transition and starts creeping while the basal décollement, deforming at higher strain rates, still behaves frictionally. Further to the rear, where both the wedge base and the décollement are plastic, the surface slope flattens (plateau). After CARMINATI & SILETTO (1997).

3. Thrusts, folds and orogens



Reverse faults or thrusts are found in the following tectonic regimes:

- Contractional orogenic systems or collisional zones (metamorphic terranes in the axial parts of collisional orogens and low-grade to non-metamorphic foreland fold and thrust belts);
- Subduction zones (i.e., accretionary wedges and Andine-type orogens);
- Strike-slip systems (restraining bends, restraining step-overs);
- Inverted basins.

Folds are found in the same tectonic regimes and, in addition, in extensional settings (normal fault-propagation folds, rollover anticlines and synclines).

Thrust systems consist of one (or more) basal detachment (or decollement, or sole thrust) and more steeply dipping (often with ramp-flat geometries) thrusts or imbricate thrusts (combined into imbricate fan or duplex structures) that branch off from the basal thrust. When rocks involved in thrusting are limited to sedimentary cover, the tectonics is termed thin-skinned. When the basement rocks are involved as well, the term thick-skinned tectonics is used.

Thrust faults (figs. 21, 22, 23) normally accom-

plish the following general (but reversible) rules: 1) they cut undeformed and subhorizontal sedimentary successions (unless they affect a folded succession or a pre-existing thrust or the faults occur along an unconformity, fig. 24); 2) thrusts cut upsection; 3) they propagate in the direction of transport (unless out of sequence thrusts develop, fig. 25).

Thrust faults are regularly associated in thrust fault systems that can be of two types: 1) Duplexes (fig. 26), bounded to the top and to the bottom by roof and floor thrusts respectively; depending on the relationship between fault spacing and displacement, hinterland dipping duplexes (when displacement is smaller than ramp spacing), antiformal stacks (when displacement equals ramp spacing) and foreland dipping duplexes (when displacement is larger than ramp spacing) may develop. 2) Imbricate fans (figs. 27, 28, 29, 30, 31, 32), characterised by the absence of a roof thrust.

Thrust faults and thrust fronts of orogenic belts are often laterally segmented. Faults that locally link segmented thrusts are called transfer faults (figs. 34, 35). Displacement may be, however, transferred also by diffuse strain. In this case the term transfer zone is adopted.

The spacing between successive thrust faults in fold-and-thrust belts is controlled by the thickness of the sediments entering the belt at the deformation front (figs. 36, 37).

The geometry of the wedge is controlled by friction along the basal decollement. Highly frictional decollements are associated to narrow belts with a steep topographic slope. Low friction decollement are associated to wide and flat mountain belts (fig. 38). These characters are well documented in the Zagros that display different geometries of the wedge in areas characterised by absence or occurrence of Cambrian salt (figs. 39, 40).

In foreland belts, thrust faults produce folding (figs. 41-45). Folds created by thrust faulting are called forced folds and can be of three types (figs. 46-75): 1) fault-bend faults, generated when the hangingwall of a thrust sheet pas-

ses over a stepped (ramp-and-flat) thrust fault. Above each kink of the thrust fault surface folds are generated to accommodate slip; 2) fault-propagation folds, generated by folding strain at the tip of the ramp of a blind thrust, where displacement dies to zero; 3) detachment folds, generated above the tip line of a thrust that developed along a bedding-parallel detachment surface (i.e., along a flat).

Another structure typical of fault-and-thrust belts are triangle structures (figs. 76-88), also called structural wedges. They develop according to the conjugate faulting theory and consist of two connected fault segments that bound a triangular block. The two faults may be either two ramps or a ramp and a detachment. Slip occurs along both faults allowing propagation of the wedge and determining the folding of the hangingwall.

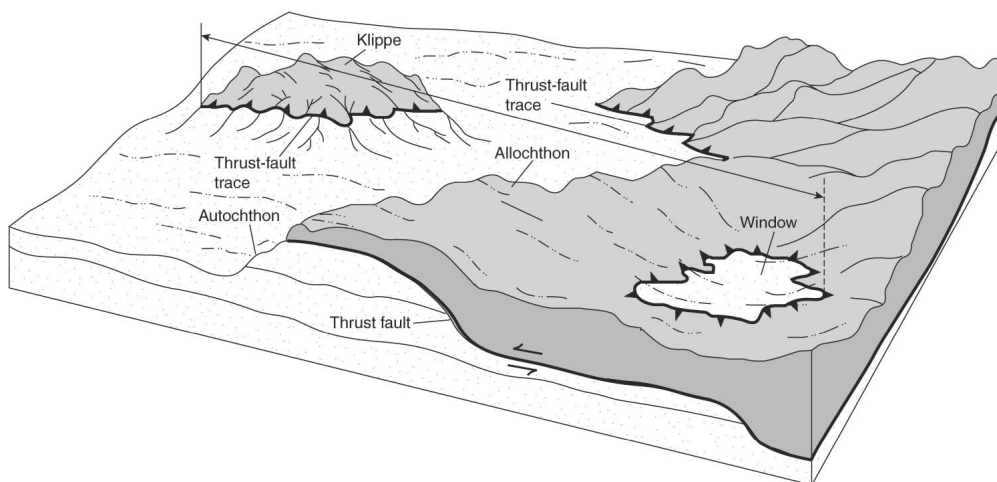
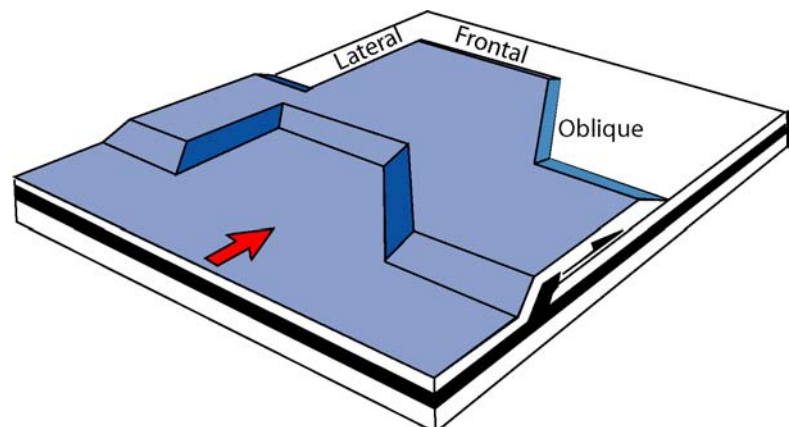


Fig. 21 - Basic nomenclature of thrust fault systems. Upper panel after TWISS & MOORES, 1992.



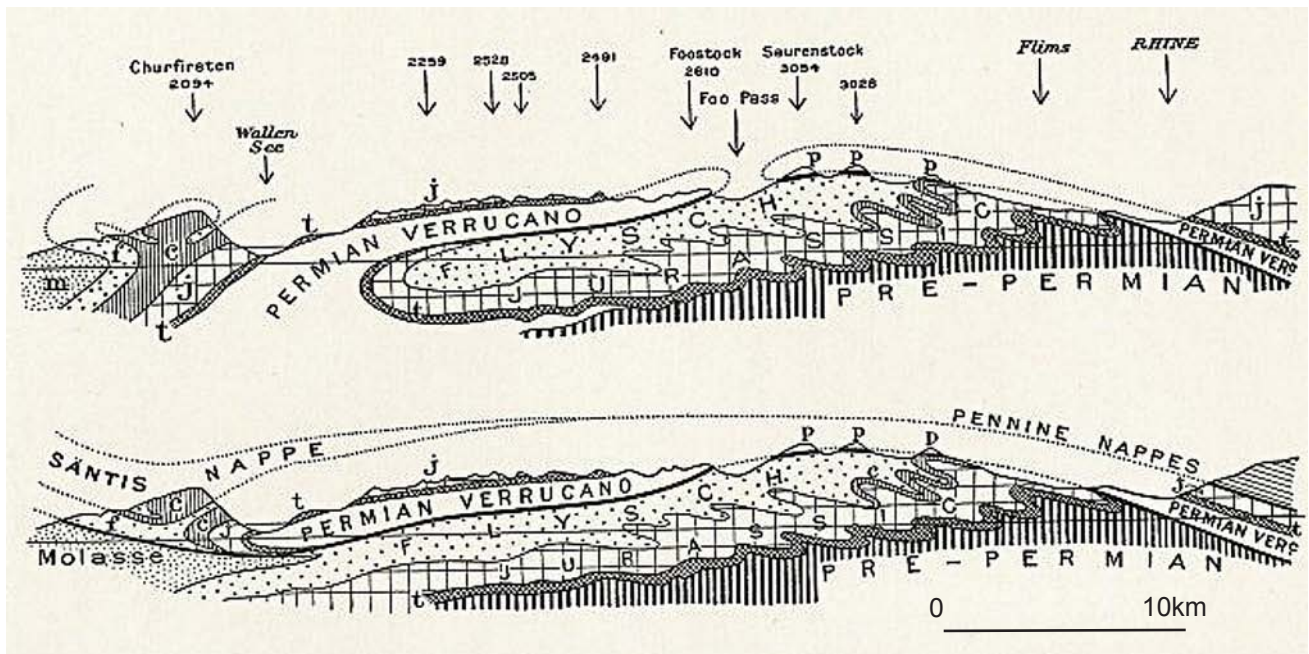


Fig. 22 - Upper panel. Glarus thrust, Swiss Alps. The dark rocks above the thrust (the Permian Verrucano Fm.) have been emplaced on the lighter Mesozoic limestones. Lower panel. Although the age and nature of the lithologies was recognised since the early beginning, the tectonic nature of the contact (by thrust fault) was only later recognised. To explain the regional geology of the Glarus area, Arnold Escher (1807-1872) and his student Albert Heim (1849-1937) proposed a strange "double fold" structure. Heim's clear descriptions in his classic 1878 text on mountain building led, in 1884, to the re-interpretation of the Glarus structure as a single, southward-derived thrust sheet by Marcel Bertrand (1847-1907) - although Bertrand had never visited the area. (after Butler, 2006; earth.leeds.ac.uk/tectonics/thrust_tectonics/index.htm).

Fig. 23 - Possible 2-D geometries of thrust faults. The thrust can either reach the Earth's surface or not (blind faults). Note the staircase (ramp and flat) geometry of the fault plane. Redrawn after MCCLAY (1992).

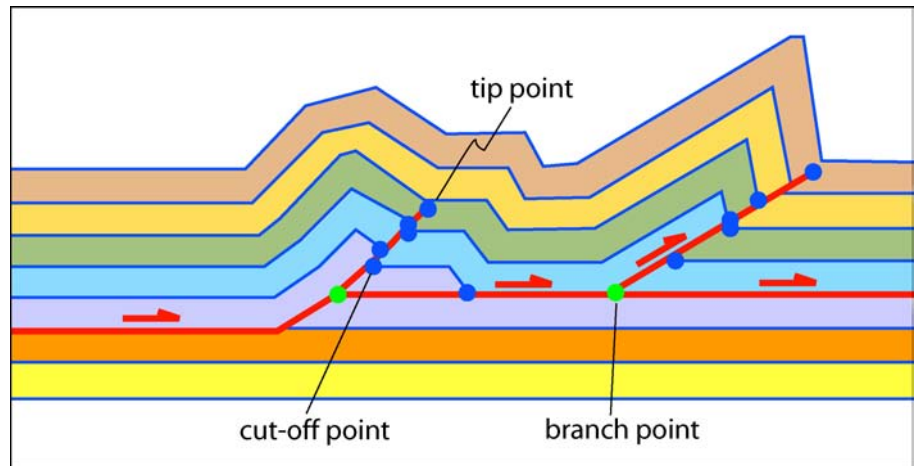


Fig. 24 - Generally older thrusts are carried on younger thrusts (in sequence thrusting). Higher older thrusts become folded as younger thrusts climb ramps. The opposite occurs when out-of-sequence thrusts develop. Redrawn after MCCLAY (1992).

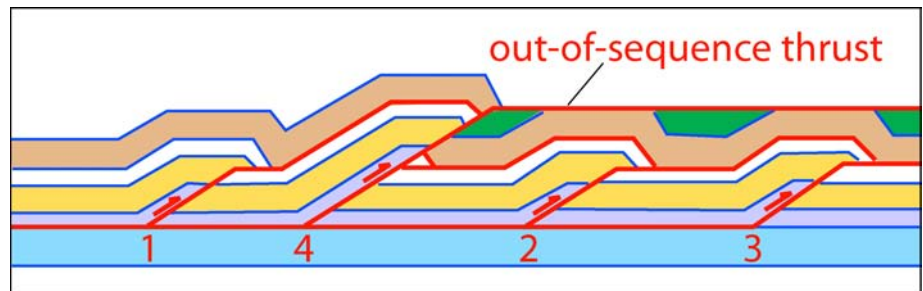
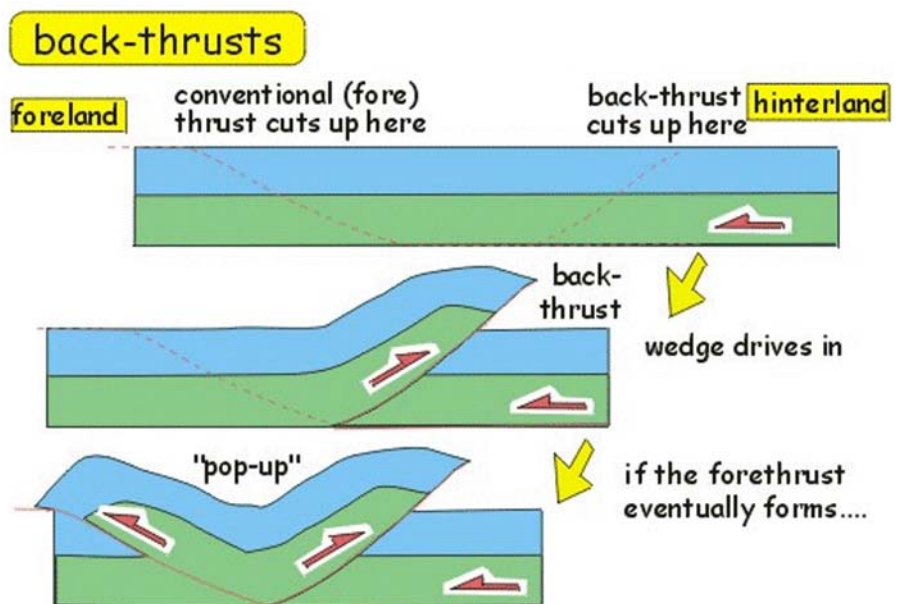


Fig. 25 - In a fold-and-thrust belt the sense of transport along thrust faults is generally towards the foreland (fore-thrusts). In some thrust faults (named backthrusts), however, the sense of transport may be toward the hinterland. The combination of thrusts and backthrusts determine the development of pop-up structures (after <http://earth.leeds.ac.uk/assynt-geology/thrusts/what/backthrust.htm>).



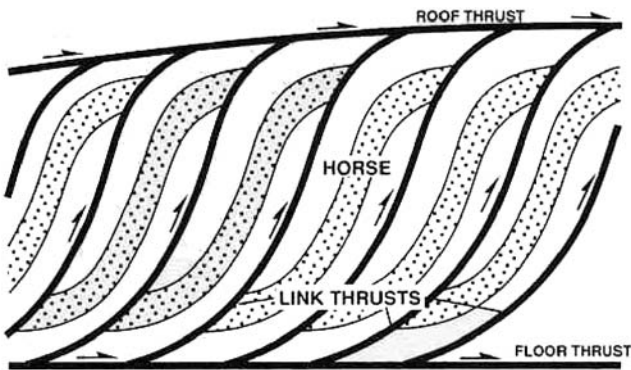
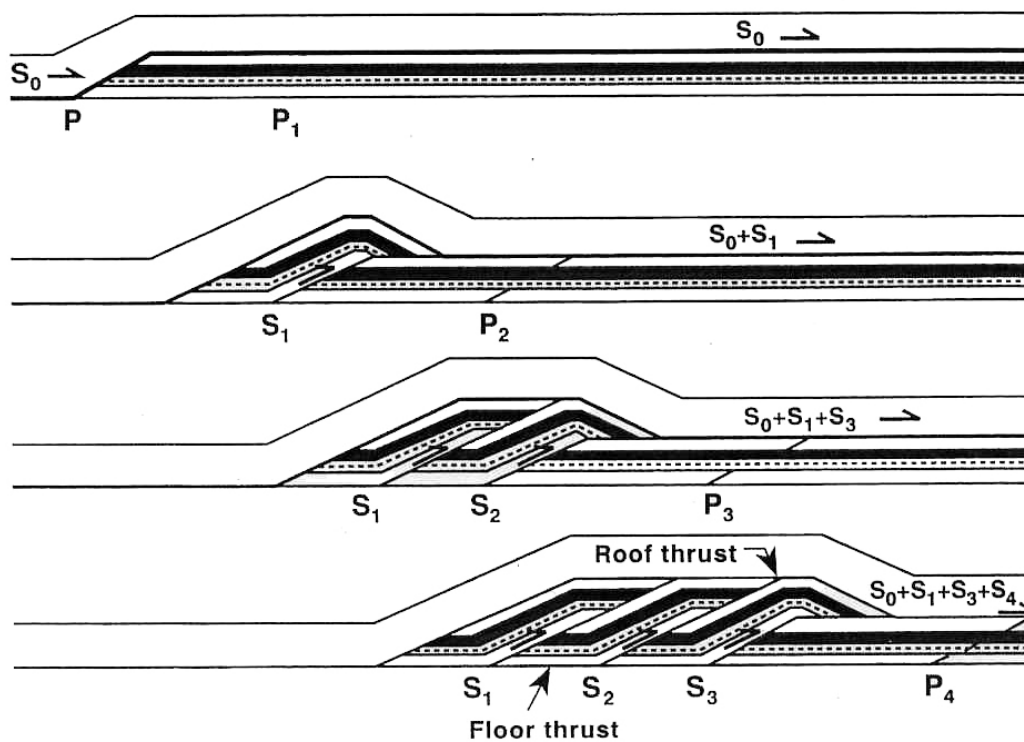
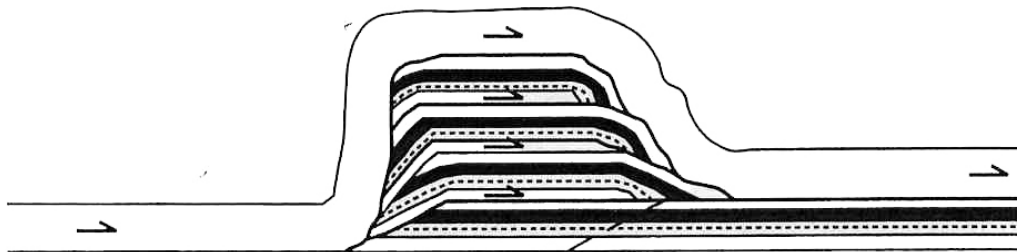


Fig. 26 - Duplexes are one of the two major geometries of thrust-fault systems. They are bounded to the top and to the bottom by roof and floor thrusts respectively. Depending on the relationship between fault spacing and displacement, three different duplex geometries may develop: hinterland dipping duplexes (when displacement is smaller than ramp spacing), antiformal stacks (when displacement equals ramp spacing) and foreland dipping duplexes (when displacement is larger than ramp spacing). After RAMSAY & HUBER (1987).

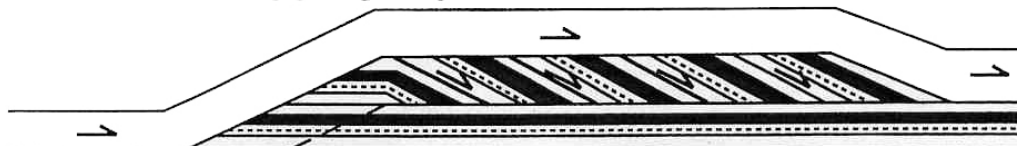
A. Hinterland dipping duplex



B. Antiformal stack



C. Foreland dipping duplex



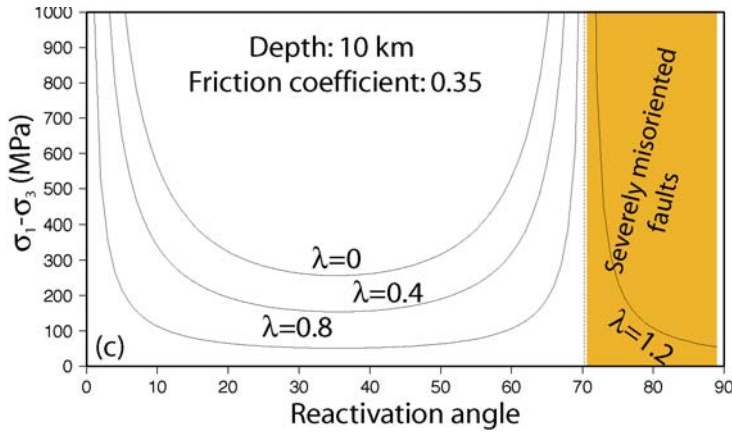


Fig. 29 - Plot of differential stresses needed in order to reactivate thrust faults with different dips at a depth 10 km for variable pore fluid pressure ratios ($\lambda = P_f/P_l$, where P_f is the fluid pressure and P_l is the lithostatic pressure). The coefficient of friction is 0.35. Notice that, even for very high fluid pressure, thrust faulting along planes more inclined than ca. 70° would need far too high differential stresses. Such faults are therefore severely misoriented to be re-sheared in a compressional regime (after CARMINATI & SILETTO, 2005).

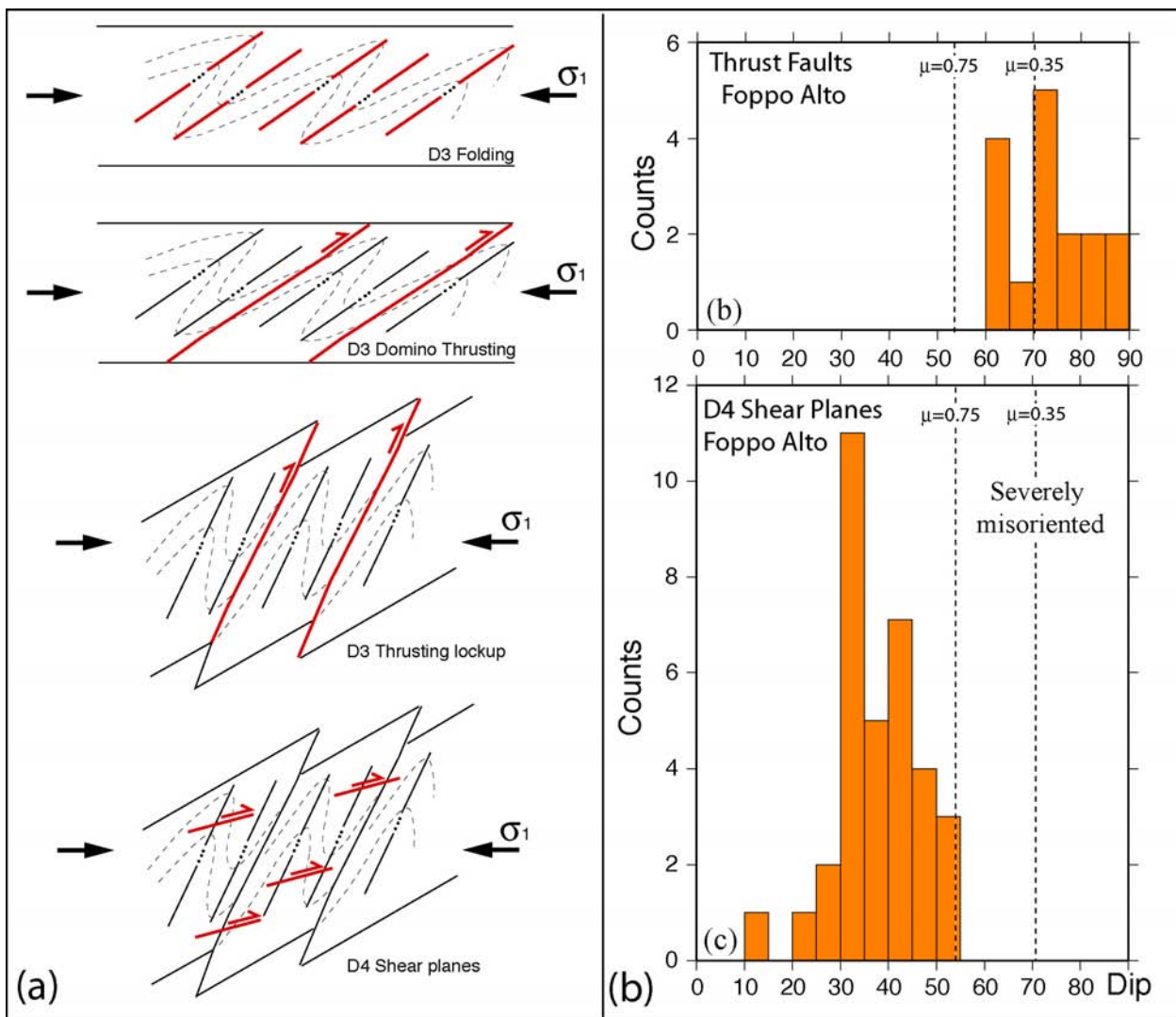


Fig. 30 - a) The thrust faults of the Foppo Alto area are severely misoriented (far too steep; see previous figures) for fault reactivation in a sublithostatic fluid pressure regime. Thrust motion likely started when the faults were less steep and the faults were progressively rotated up to the present day dip by domino tilting. When the faults became inclined beyond the fault lock-up angle, no further thrusting was accommodated along them. At later stages regional shortening was accommodated by newly formed lower angle shear planes (dipping around 30° - 40°), consistently with predictions from fault mechanics. b) Dip distribution for the thrust faults and for the later (D4) shear planes of the Foppo Alto area (after CARMINATI & SILETTO, 2005).

Fig. 31 - Erosion may remove any indication of a roof thrust in a duplex thrust system, making it difficult to distinguish it from an imbricate fan. Redrawn after McCAY (1992).

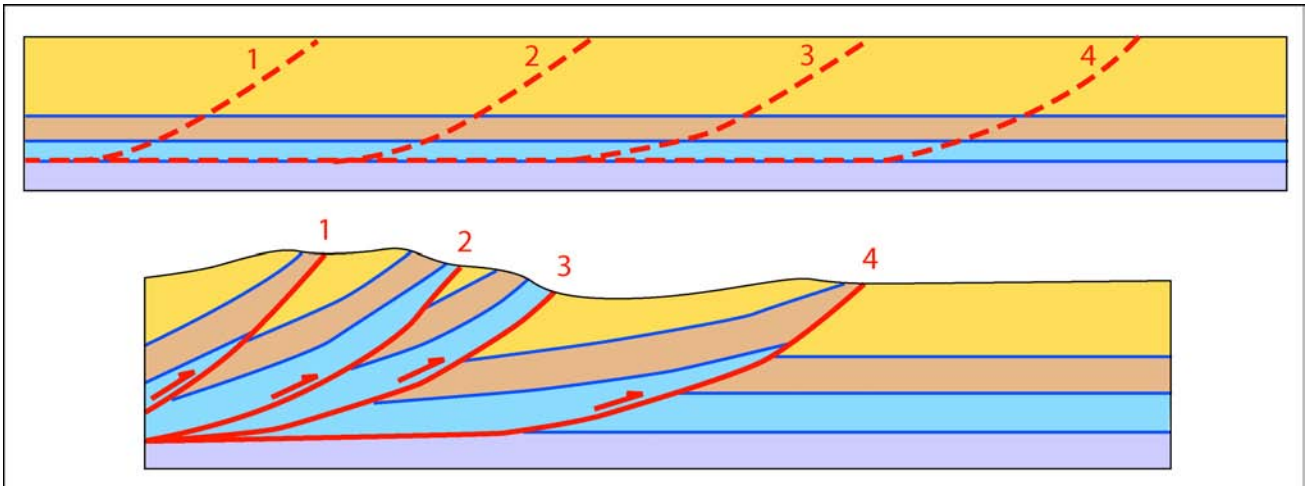
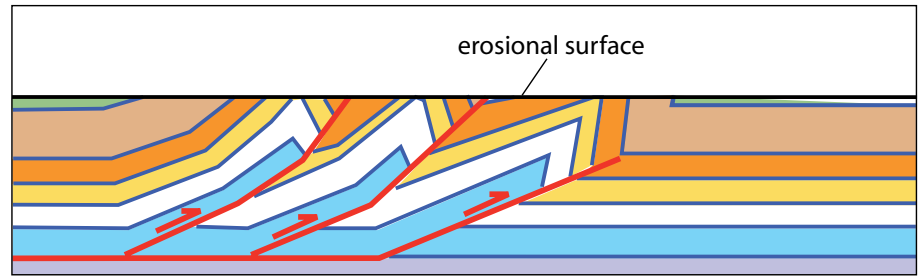


Fig. 32 - The different spacing of thrust fault ramps in the lower panel may be misinterpreted as the result of a variable spacing of fault nucleation points. When the section is retro-deformed, in this case the original spacing was constant, which is not the rule. The variable spacing in the deformed section is related to the variable displacement along the faults.

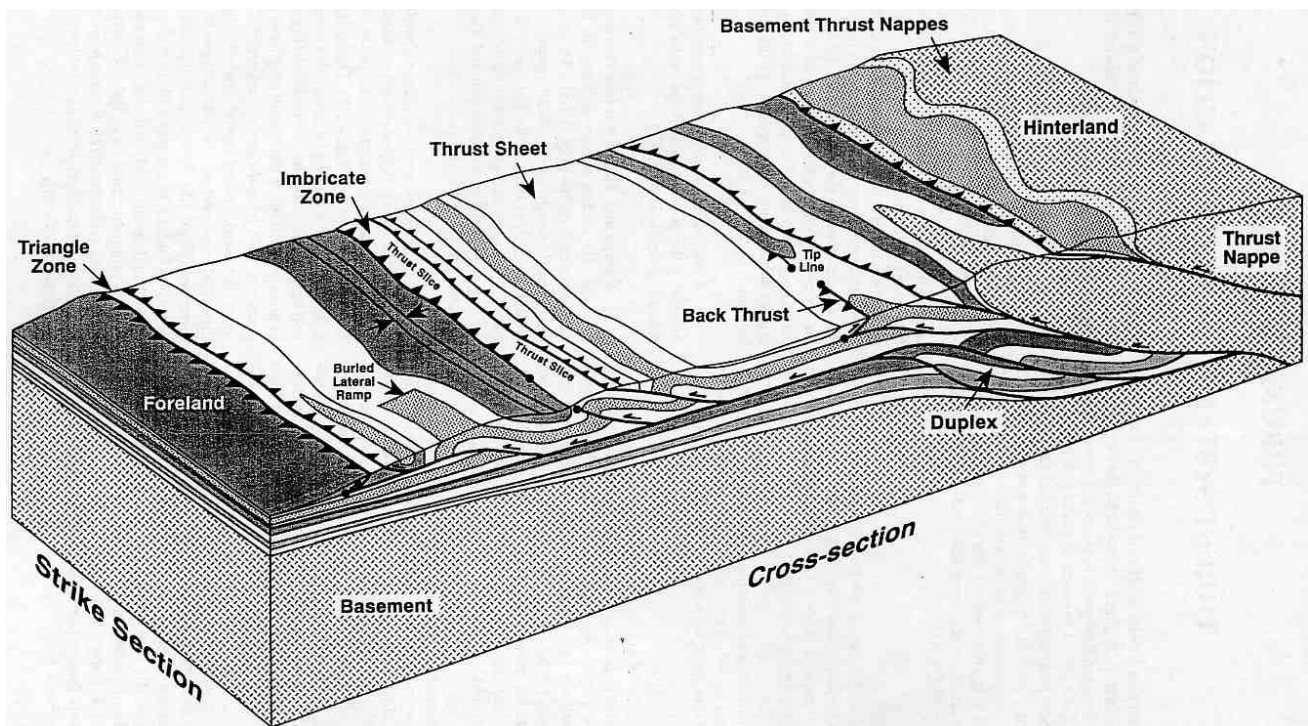


Fig. 33 - Thrust systems may be extremely complicated and all the structures so far described may coexist in fold-and-thrust belts (after DE PAOR, 1988).

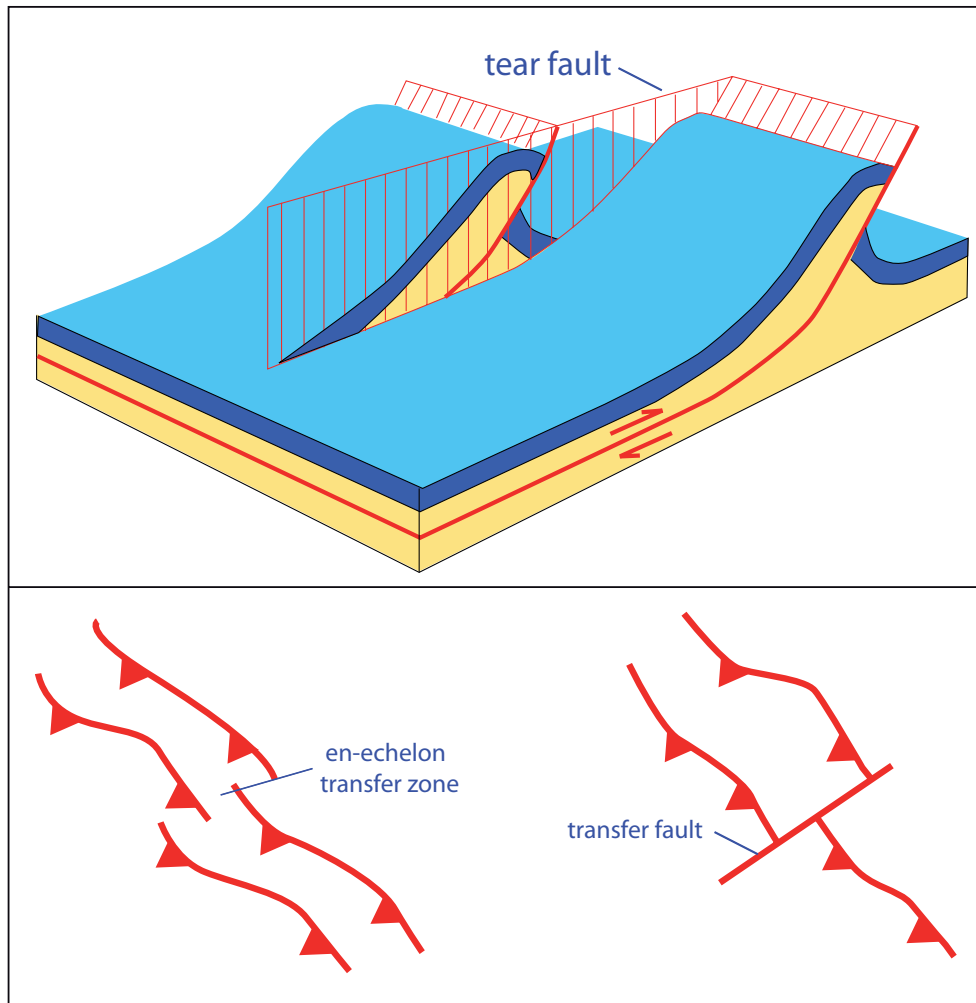


Fig. 34 - Thrust faults are normally laterally segmented. Local faults segmenting thrusts are called tear faults. At regional scale, the thrust faults may be segmented by a single fault (transfer fault) or displacement may be transferred laterally to other faults along transfer zones (modified after TWISS & MOORES, 1992).

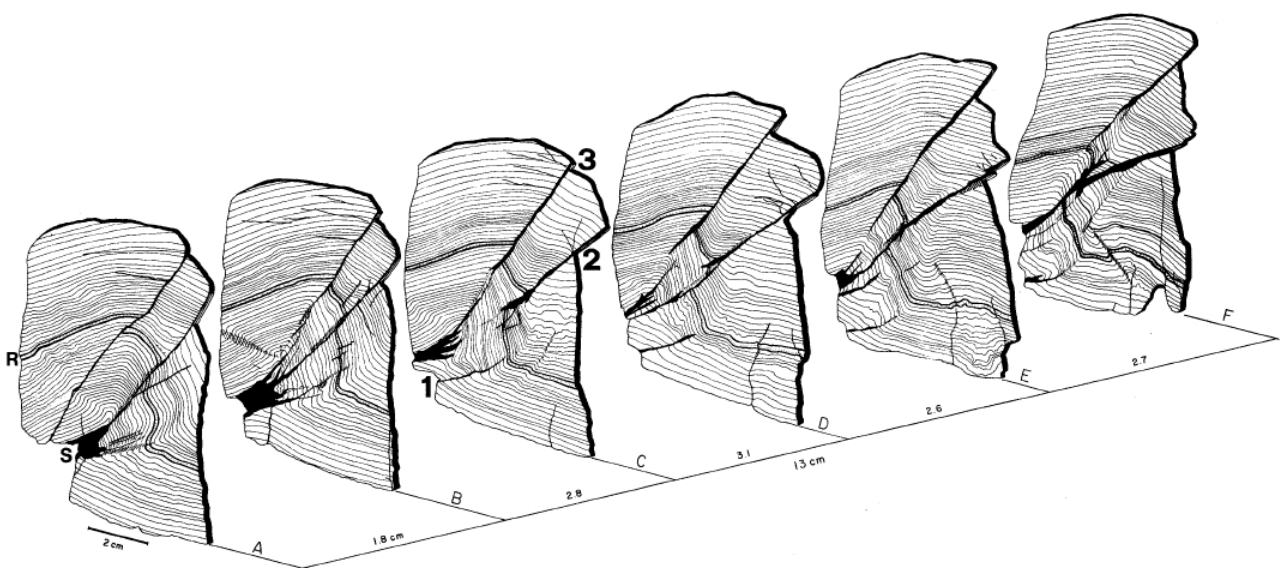


Fig. 35 - Small-scale example of transfer zones. A 30 cm wide kink-band has been cross-cut, showing how each single slice has different geometries, number of thrusts, distance among them, etc. Similar along strike variations typically occur along fold and thrust belts.

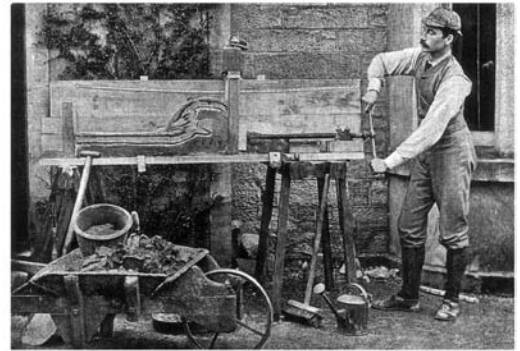
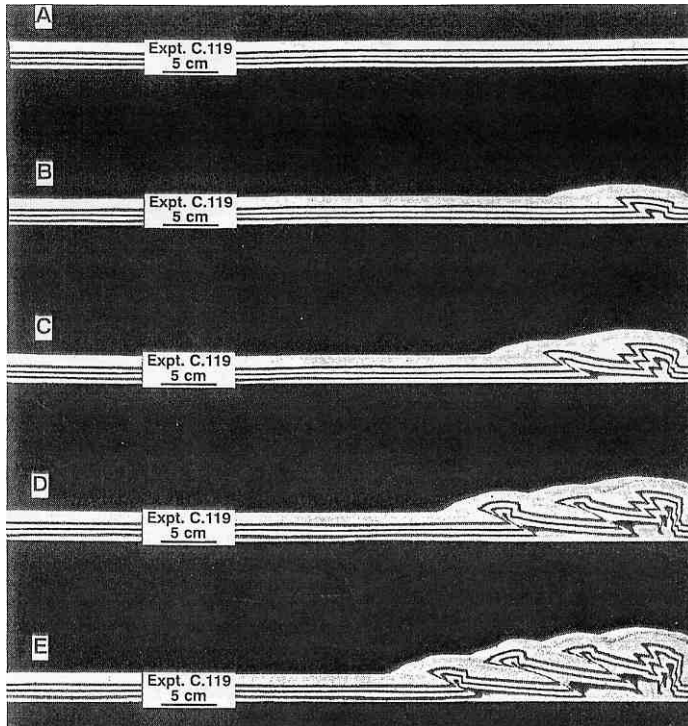


Fig. 36 - The progressive development of fold-and-thrust belts has been studied extensively (since the pioneering work of CADELL 1889, above picture) with analogue models that simulate thrust faults formation pushing laterally a multilayer of sand (plus additional materials). Notice in the left panel the foreland propagation of thrust faulting. When new thrust faults form, older thrusts are abandoned, rotated and transported passively toward the foreland (after HUIQI *et alii*, 1992).

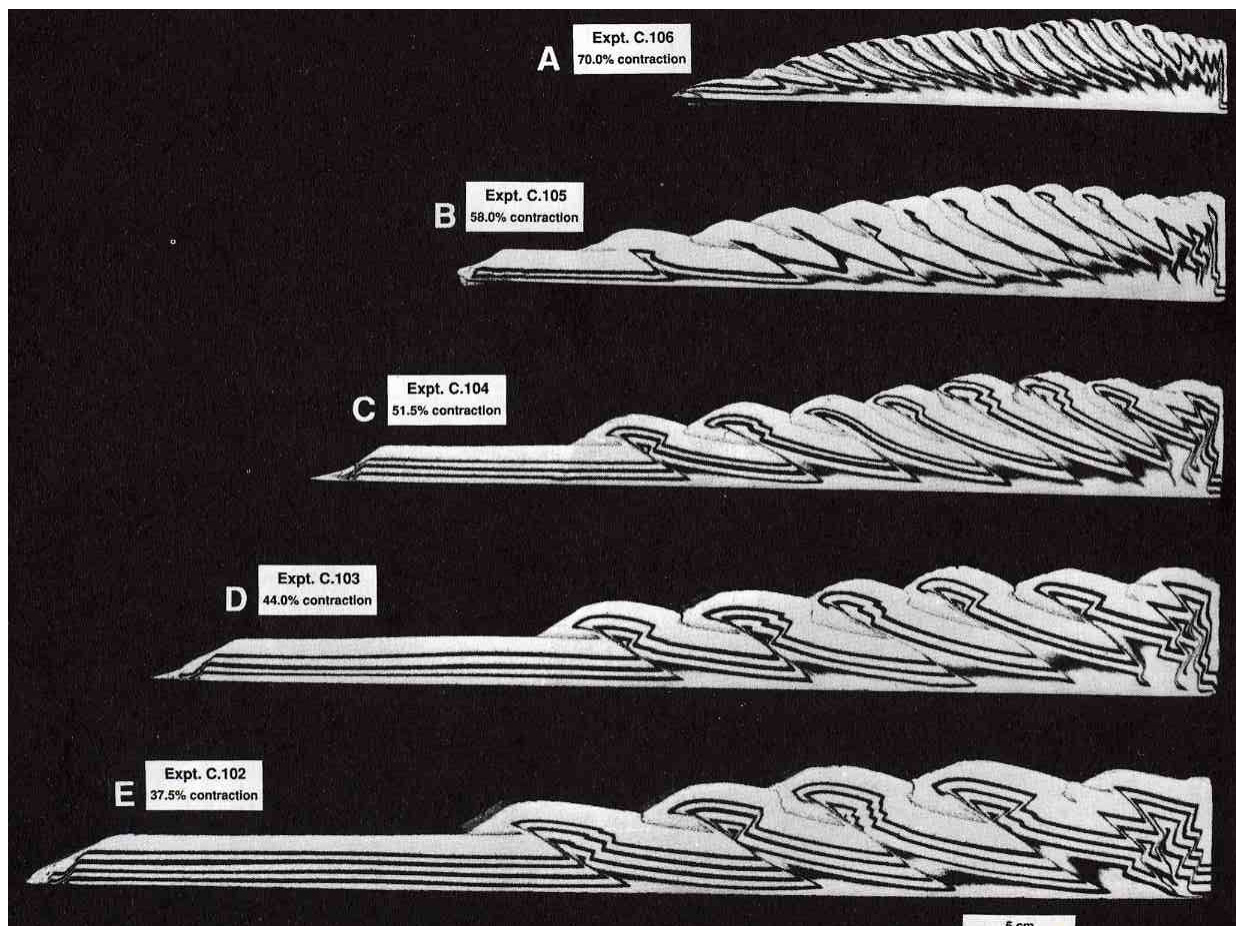


Fig. 37 - The spacing of thrust faults is controlled by the thickness of the foreland sedimentary cover above the basal decollement. The larger the thickness, the larger the spacing (after HUIQI, *et alii* 1992).

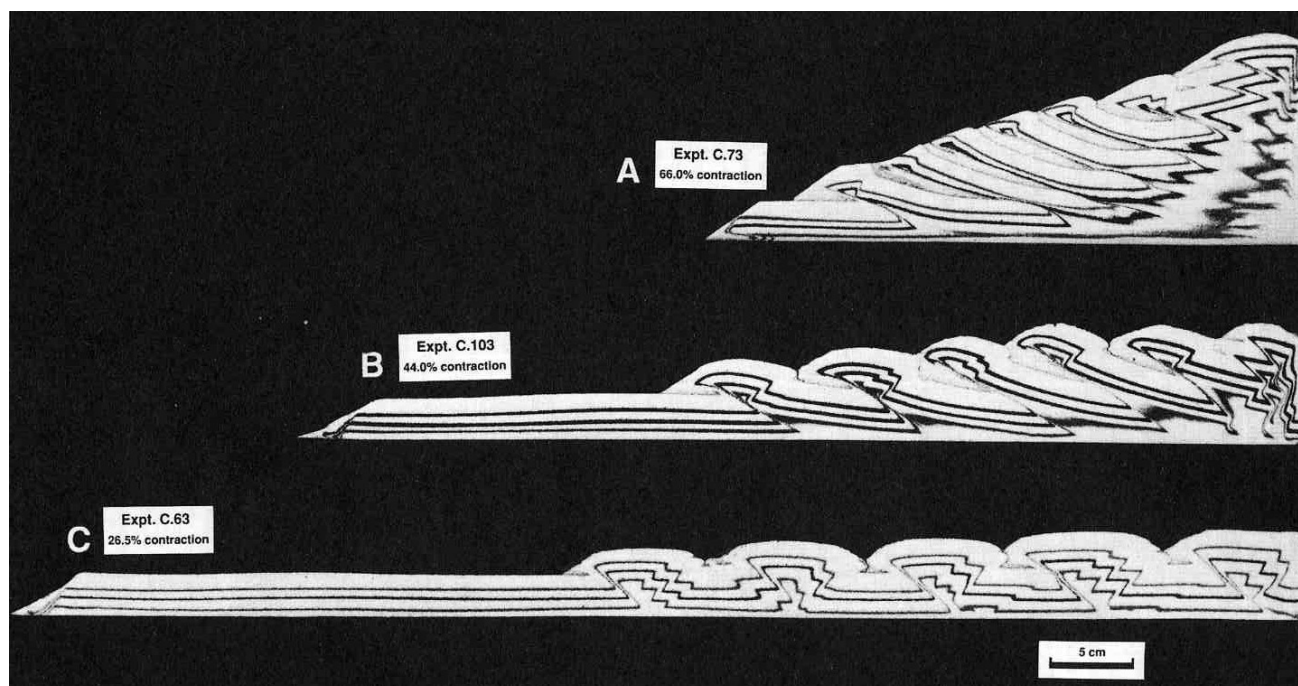


Fig. 38 - The geometry of the wedge is controlled by the friction along the basal decollement. Highly frictional decollements are associated to narrow belts with a very steep topographic slope. Low friction decollements are associated to wide and flat mountain belts. In experiments a-c, the friction coefficient of the decollement is 0.55, 0.47 and 0.37 respectively. Compare these geometries with the following two figures.

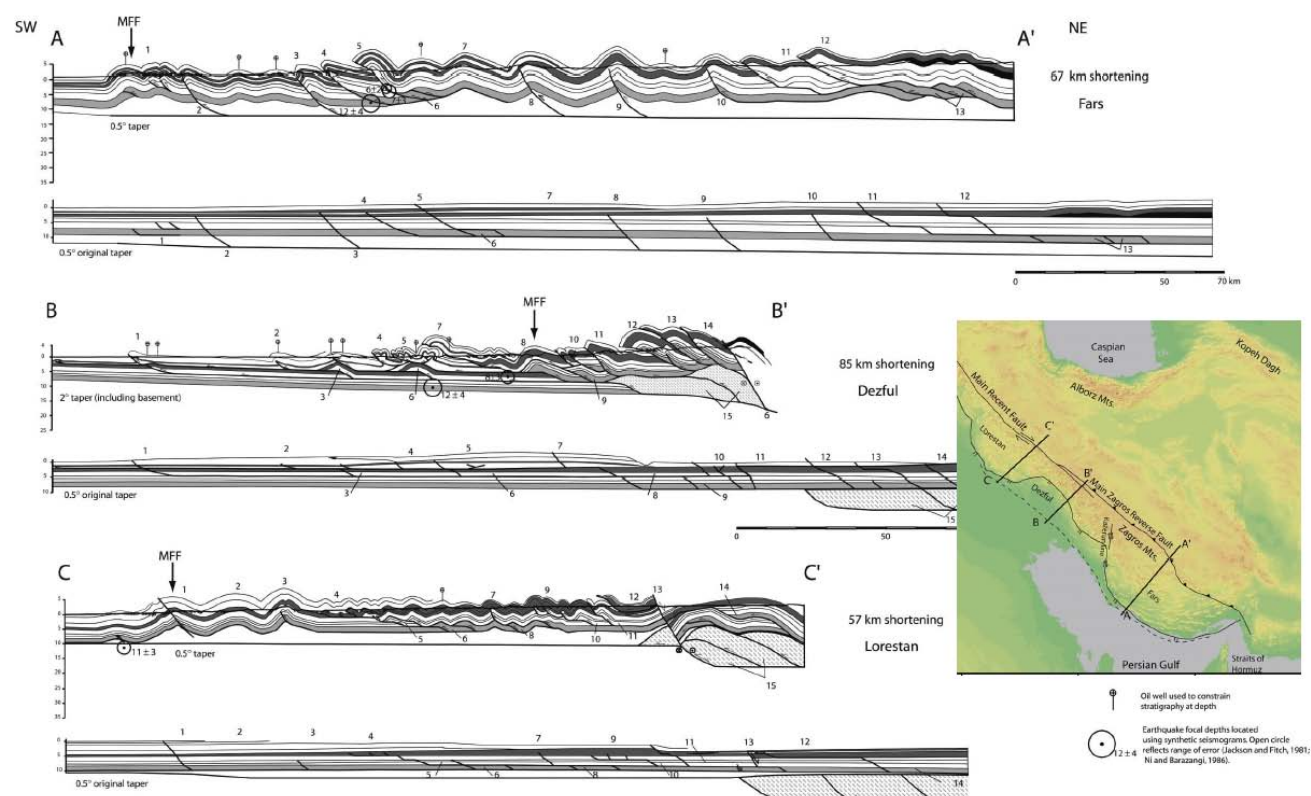


Fig. 39 - Three cross sections through the Zagros show different fold-and-thrust geometries. The basal decollement of sections A and C runs through the Cambrian Hormoz Fm. (salt) and the chain is wide. Along section B no salt occurs along the basal decollement and the surface slope is steeper and the belt is narrower with thrust faults characterised by larger displacement (after McQUARRIE, 2004).

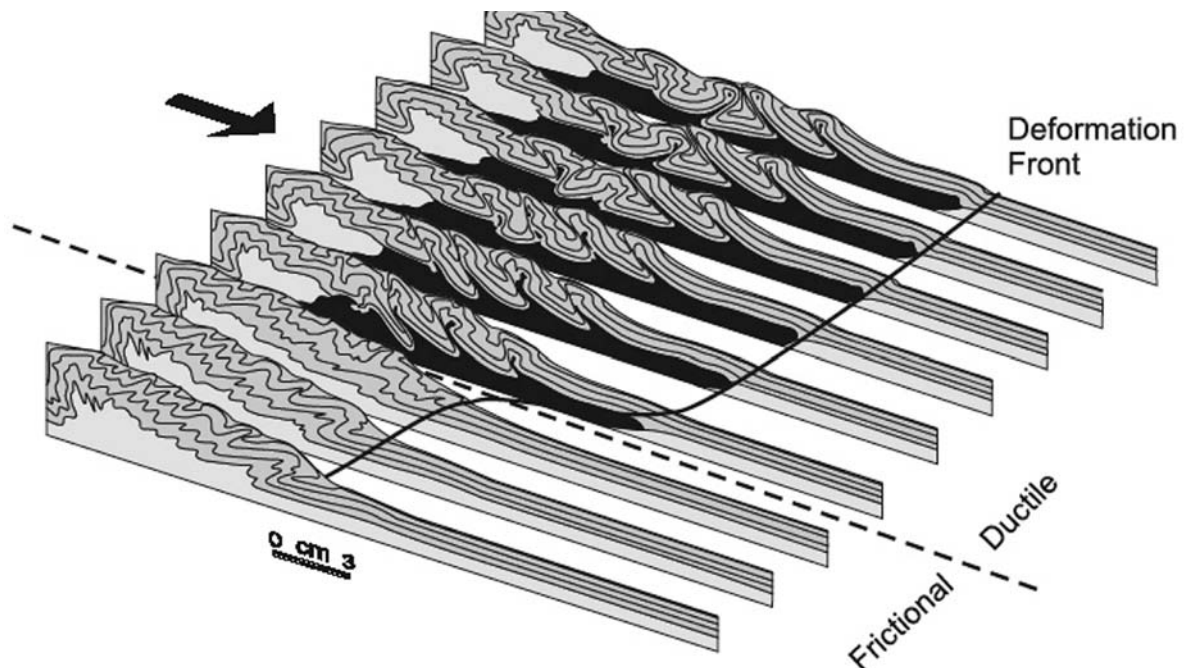
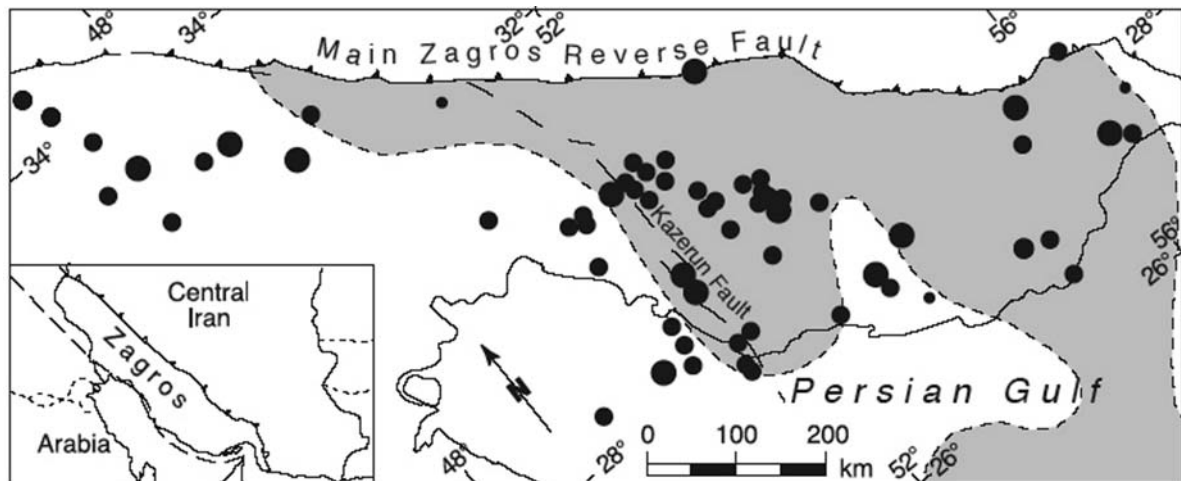


Fig. 40 - Upper figure: In the portion of the Zagros shortened above a low-friction ductile decollement (rock salt, grey area), low- to moderate-magnitude earthquakes ($M_w = 5.3-5.6$), distributed over a wide area, occur along several long-lived thrust faults. Conversely, in areas shortened above high-friction decollements large-magnitude earthquakes ($M_w = 6.6 - 6.8$), distributed over a narrow zone are likely to occur along few short-lived thrust ramps (after KOYI *et alii*, 2000).

Lower figure: Above the ductile domain, both forward- and rearward-vergent thrusts form, whereas above the frictional domain, only forward-vergent thrusts prevail. The thrust belt is characterised by salients above ductile decollements and by recesses above frictional layers (after COTTON & KOYI, 2000).

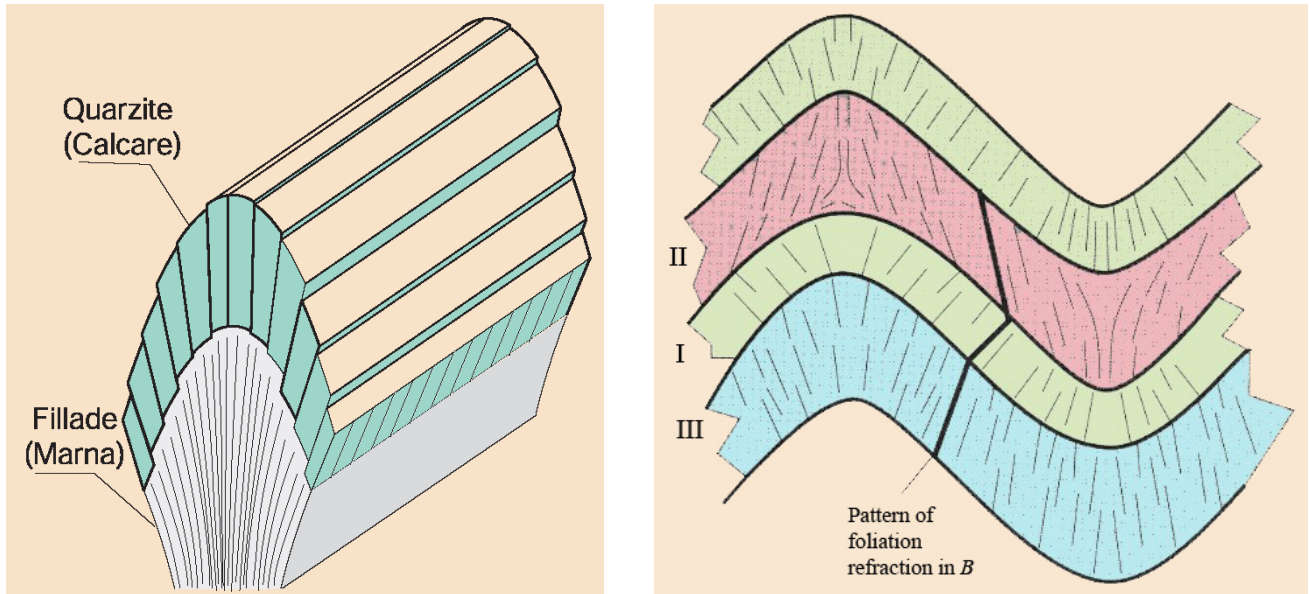


Fig. 41 - Cleavage formation is often associated to folding. When cleavage is subparallel to fold axial planes it is termed axial plane cleavage. However, the axial plane cleavage is often refracted between competent and incompetent layers and the spacing is dependent on lithology (larger in more competent lithologies). Cleavage may represent an important source for rock permeability. Modified after TWISS & MOORES (1992).

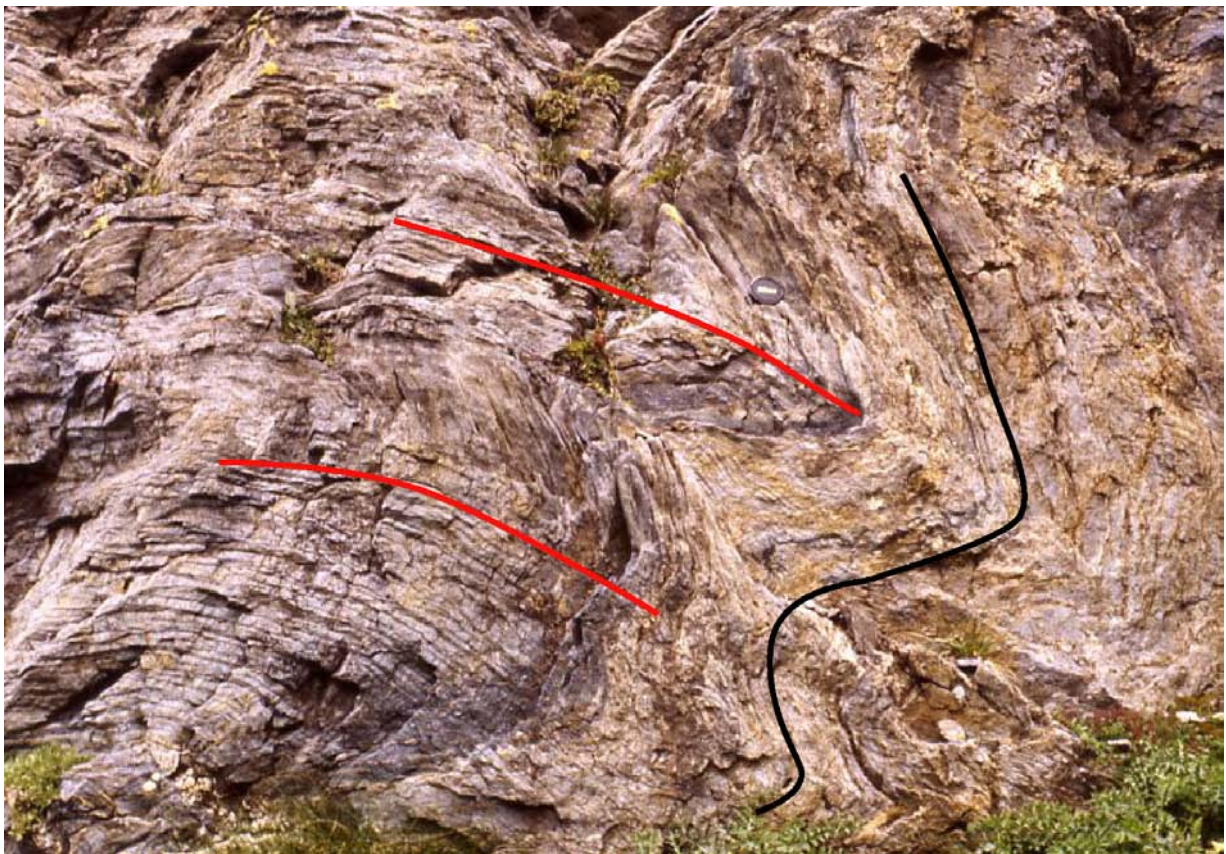


Fig. 42 - Folded volcaniclastic rocks of the Permian Collio Fm. (the original stratigraphic layers are indicated by the black line). Notice the development of a strong axial plane cleavage (red lines) that is unevenly distributed. Some layers (normally those characterised by higher percentages of phyllosilicates, such as micas for example) are characterised by a sharp cleavage, whereas in other layers (more competent) cleavage is absent. In some layers, cleavage may have obliterated continuously the original strata. Val Belviso, Central Southern Alps.



Fig. 43 - Microphotograph of an axial plane cleavage developed in marly limestones from the Alpi Apuane, Central Italy. Notice that one of the main processes controlling cleavage development in this sample was pressure solution.

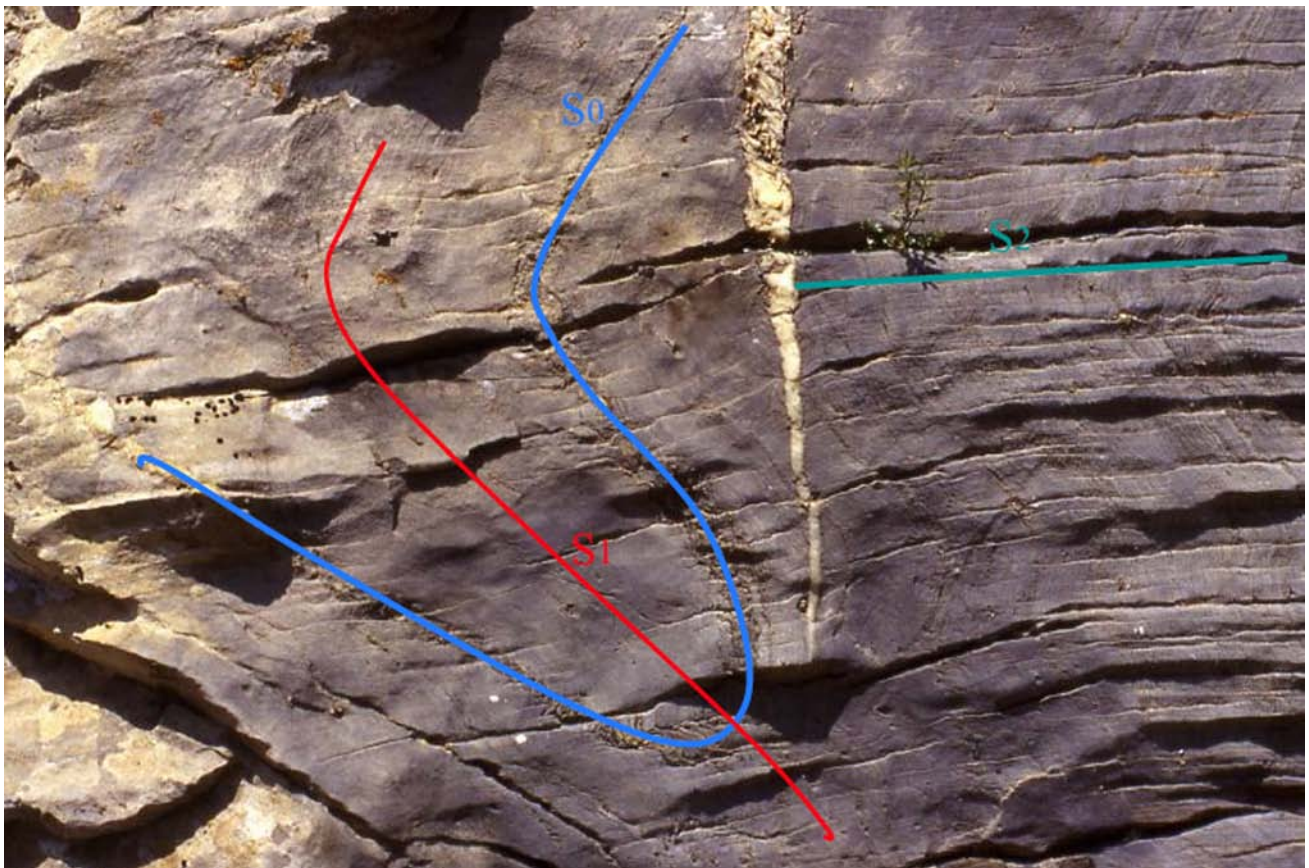


Fig. 44 - In terrains involved in more than one phase of folding, different generations of cleavage may develop. For example in these Cretaceous marly limestones from the Mt. Marguareis area (Ligurian Briançonnais, Western Alps) two generations of folds and corresponding axial plane cleavages (labelled as S1 and S2) can be observed. The original stratigraphic surfaces are labelled S0.

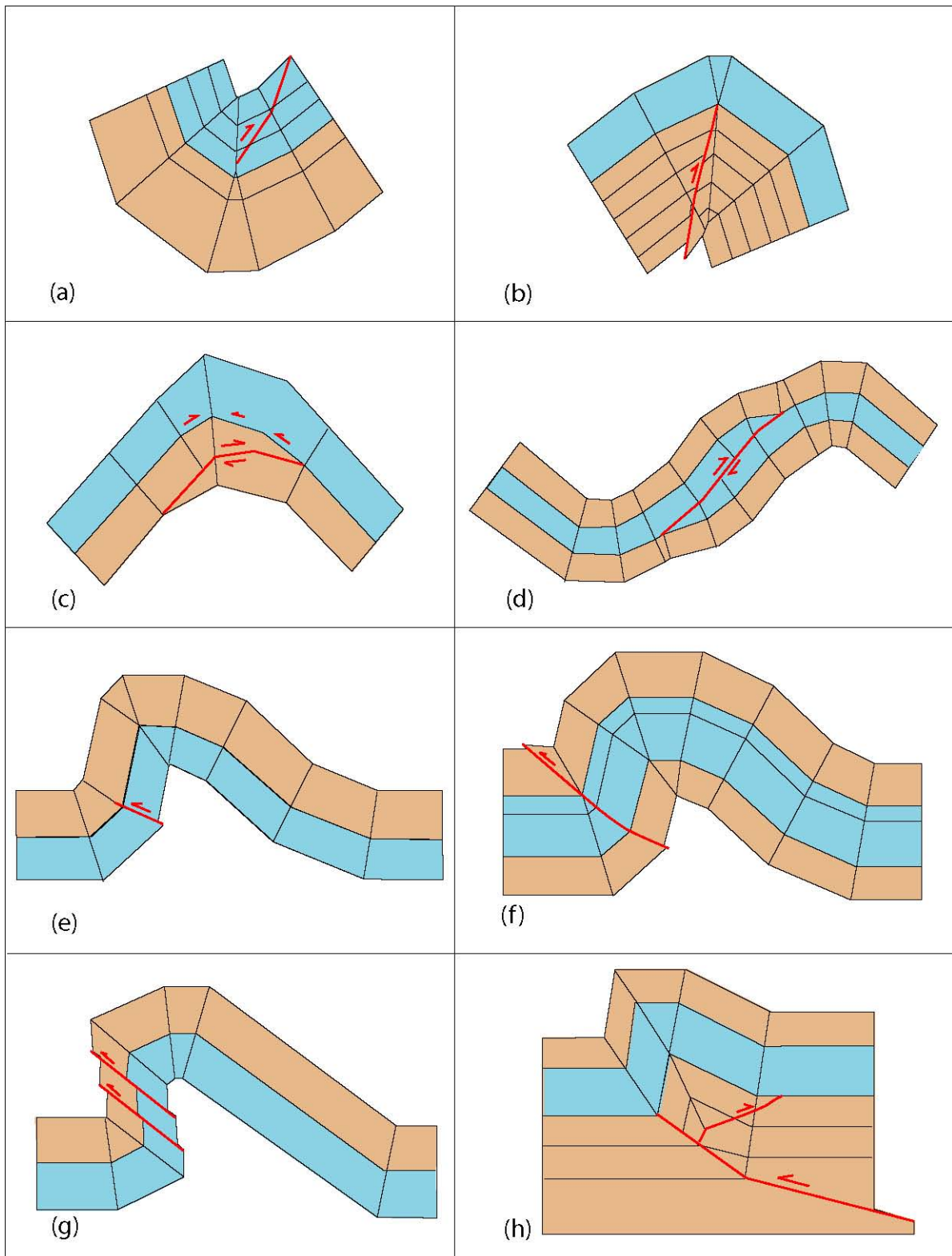


Fig. 45 - Normally folding is induced by thrusting. At shallow levels, however, rocks display brittle behaviour during folding and minor faults associated to folding may form. Common types of fold-accommodation faults: (a) out-of-syncline thrust propagating on the gently dipping limb; (b) into-anticline thrust propagating on the gently dipping limb; (c) hinge wedge thrust; (d) limb wedge thrust; (e) forelimb space accommodation thrust; (f) forelimb-backlimb thrust; (g) forelimb shear thrusts; (h) back thrust (after MITRA, 2002).

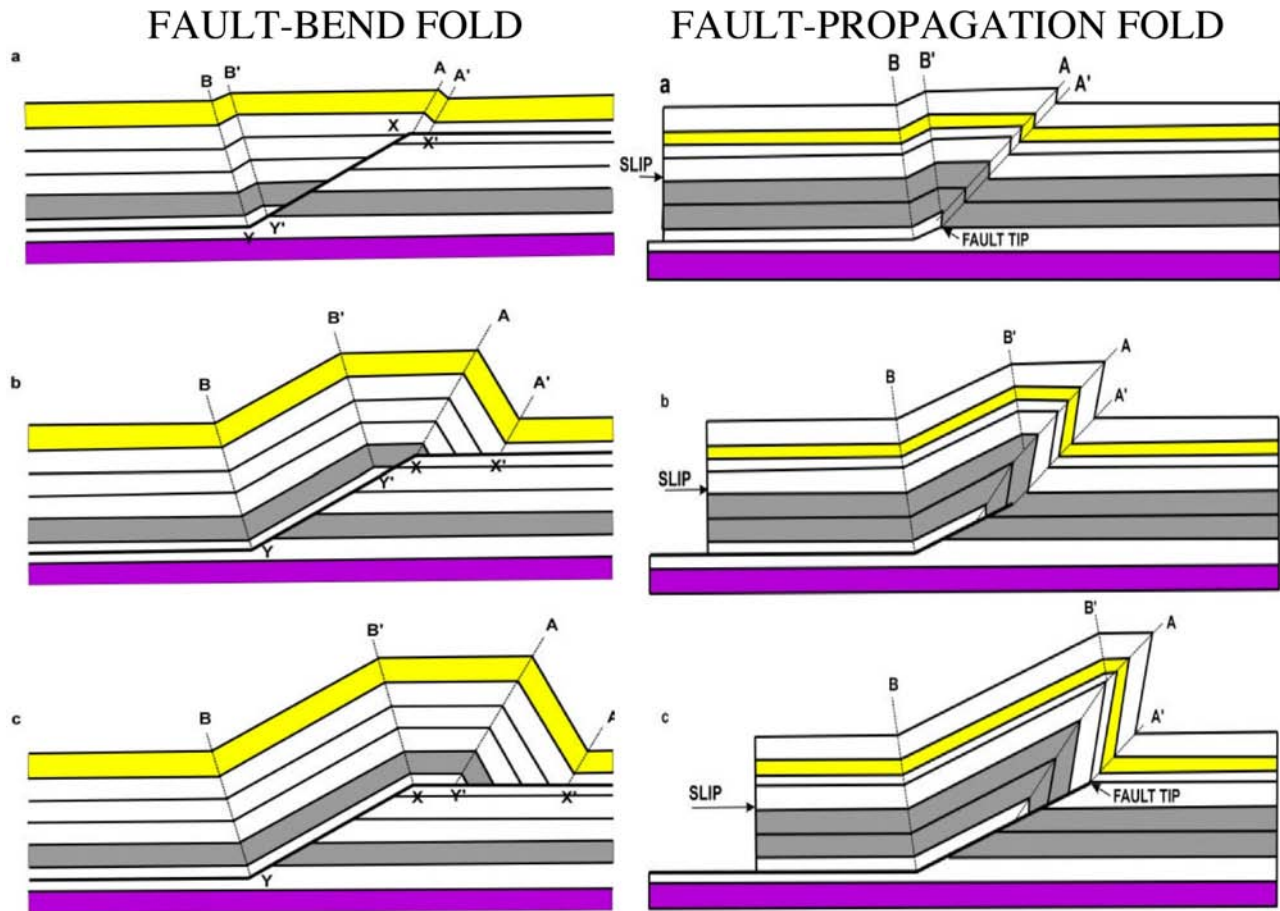


Fig. 46 - Classic relations between thrust shape, propagation and fold development (SUPPE, 1983; 1985). In both cases the back-limb of the fold is parallel to the footwall ramp. Fault-bend folds are generated when the hangingwall of a thrust sheet passes over a stepped (ramp-and-flat) thrust fault. Above each kink of the thrust fault surface folds are generated to accommodate slip.

Fault-propagation folds are generated by the folding strain at the tip of the ramp of a blind thrust, where displacement dies to zero. Above this point, an asymmetric fold with a steep or overturned forelimb (indicating the vergence of the thrust) is formed. With the progressive upward migration of the thrust fault tip, the fold may be dissected and in part transported in the hangingwall of the thrust sheet, with a relict footwall syncline. The forelimb is less inclined in the fault-bend fold, whereas it is often overturned and subject to elongation and flattening in fault-propagation folds.

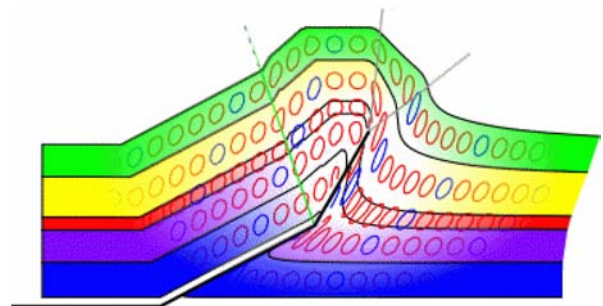
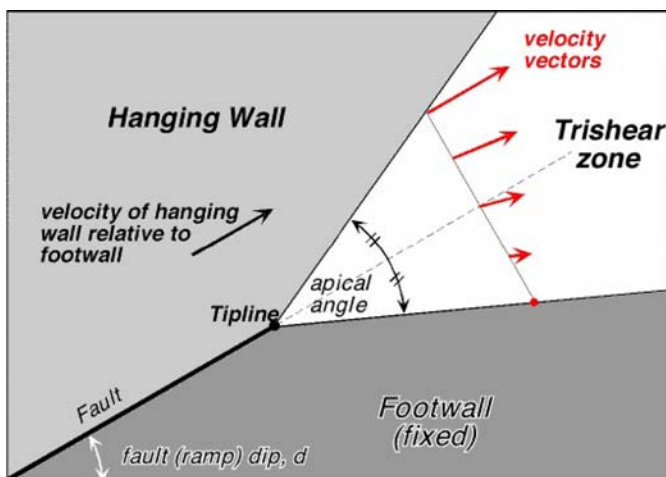
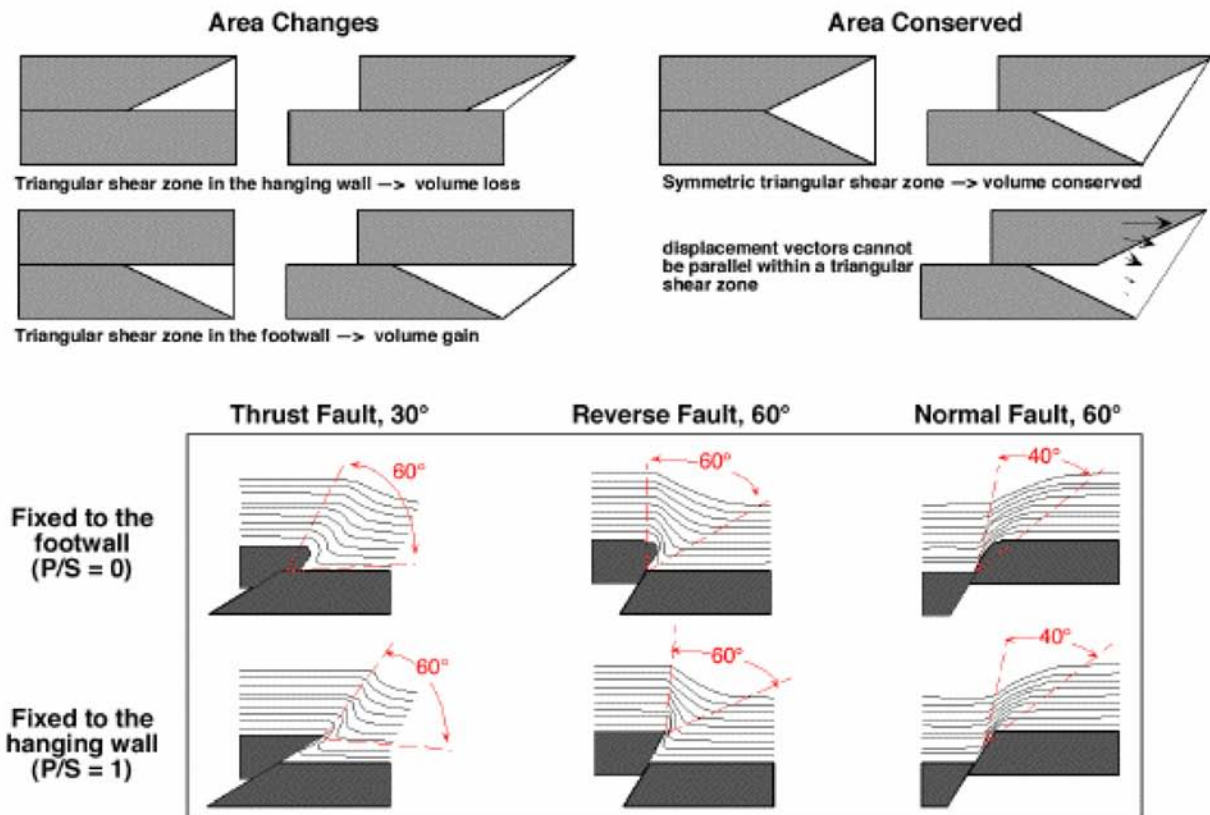


Fig. 47 - The trishear model (ERSLEV, 1991, ALLMENDINGER, 1998) explains most of the deformation occurring at the tip line of faults.

<http://www.geo.cornell.edu/RWA/trishear/default.html>

The Trishear concept of Erslev (1991)



Growth Triangles in Trishear Fault-propagation Folds

Allmendinger (1998)

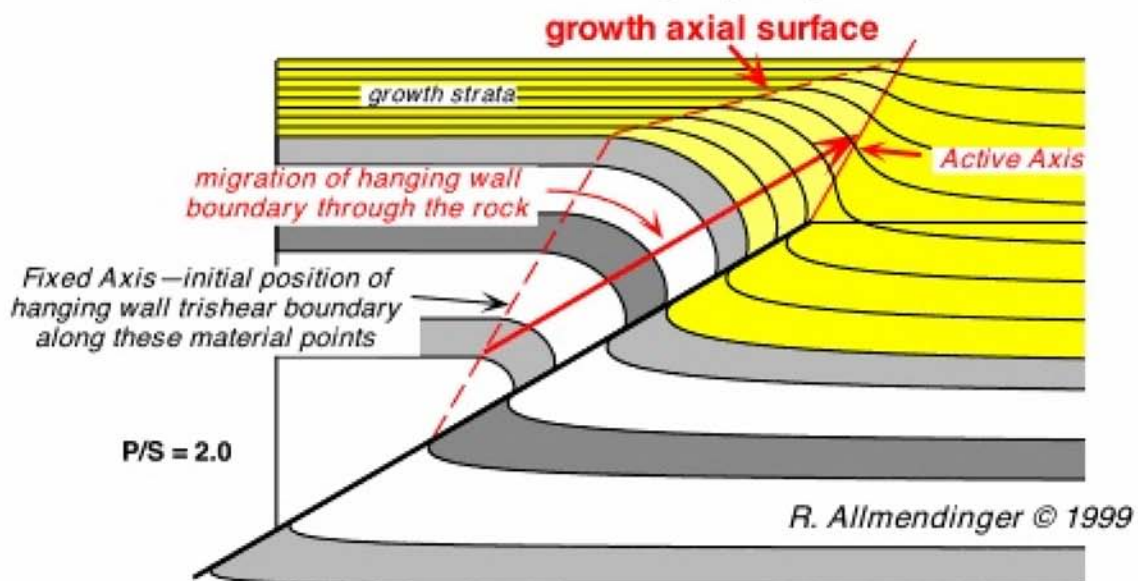


Fig. 48 - The trishear concept as expressed by ERSLEV (1991) and ALLMENDINGER (1998).

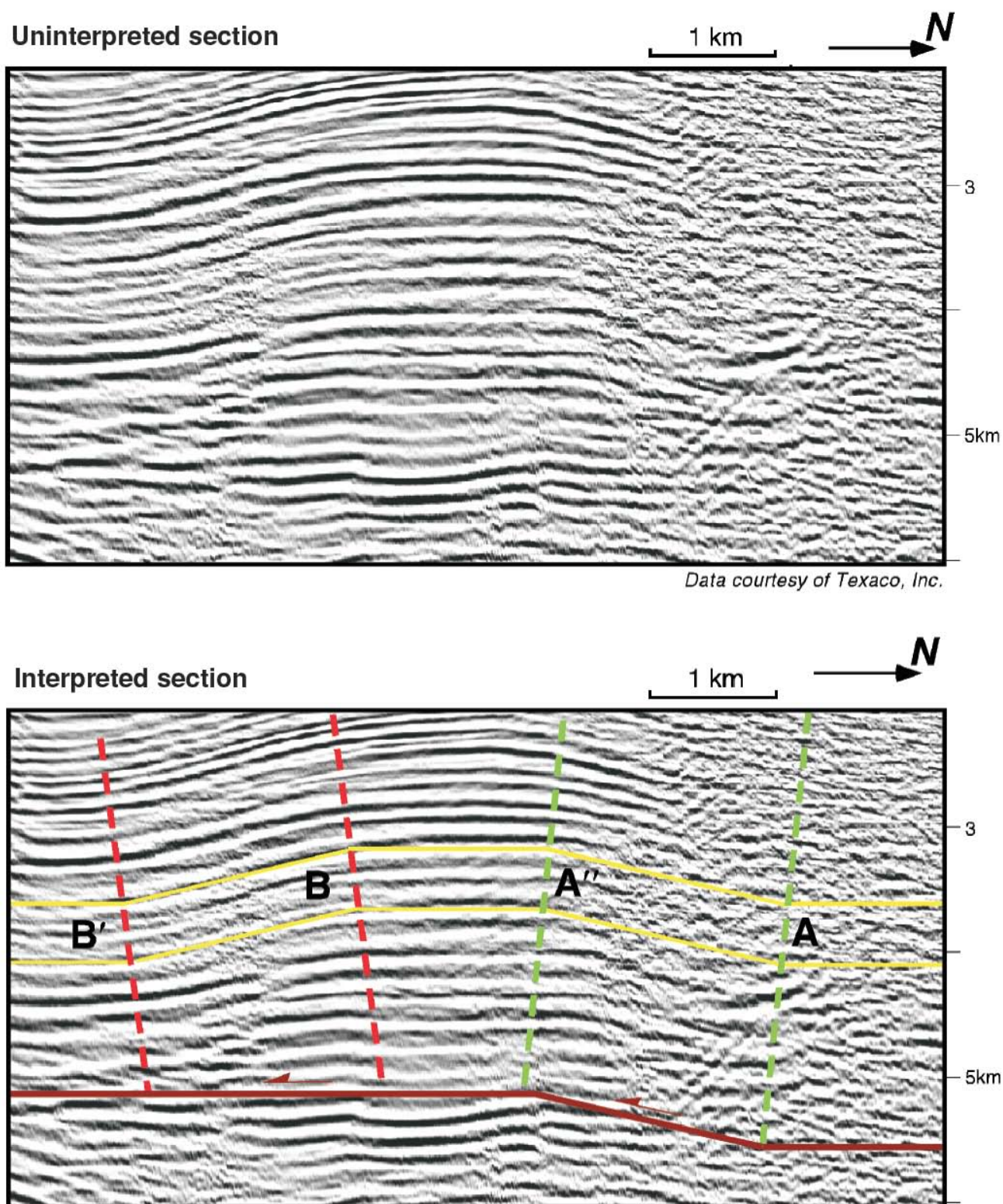


Fig. 49 - Seismic section of a fault bend fold. Pitas Point, Santa Barbara Channel, California, USA. After SHAW *et alii* (2005) AAPG©, reprinted by permission of the AAPG whose permission is required for further use.

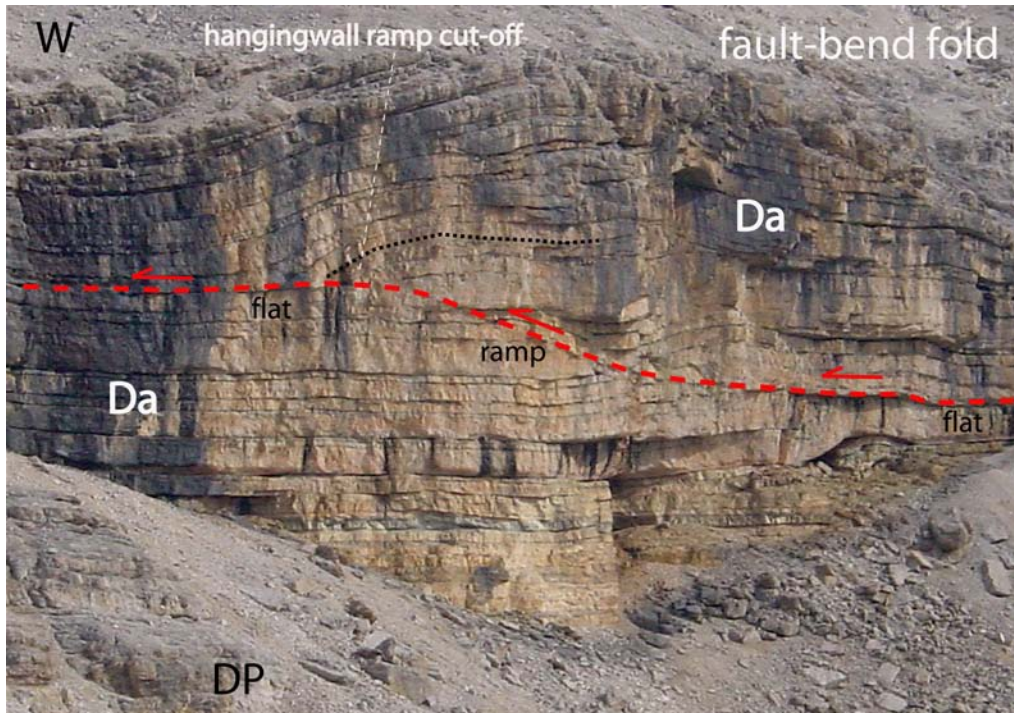


Fig. 50 - Fault-bend fold in the Dachstein Limestone (Da) of the southern cliff of the Piz Boè, Sella Massif, Dolomites. Note the fore-limb inclined toward the vergence. Dolomia Principale (DP). The cliff is about 20 m high.

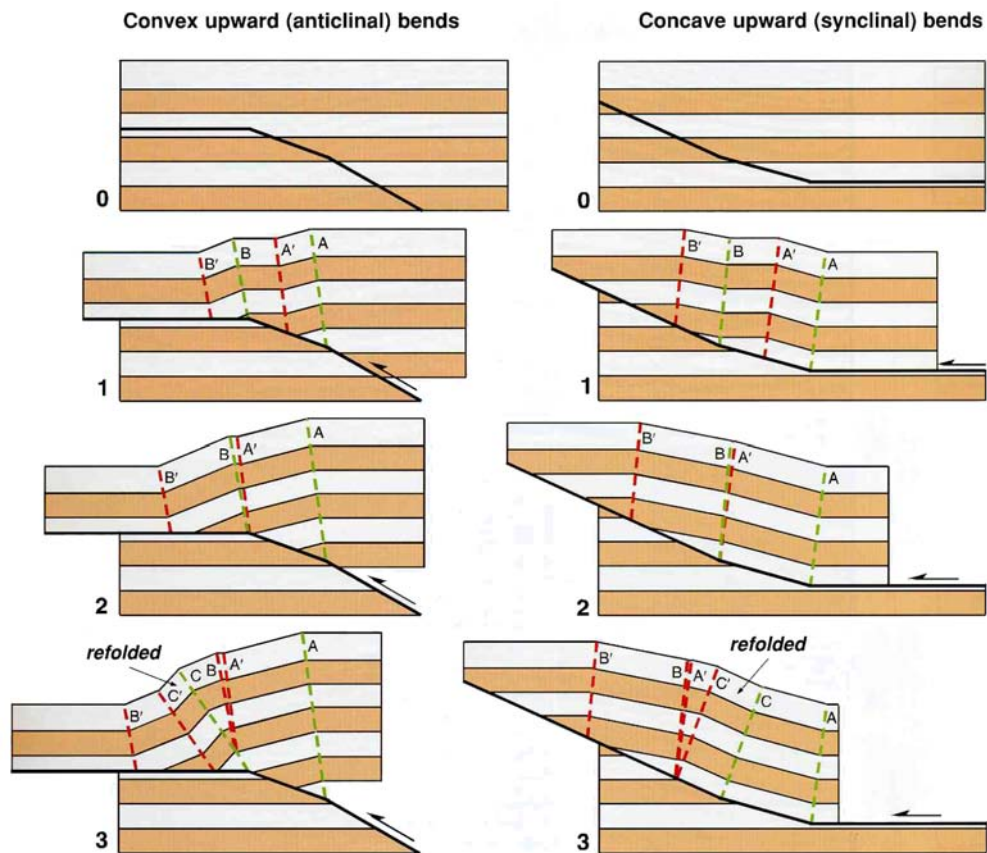


Fig. 51 - Fault trajectories may be characterised by two or more bends with the same concavity or convexity. These features produce multi-bend fault-bend folds. After SHAW *et alii* (2005) AAPG©, reprinted by permission of the AAPG whose permission is required for further use.

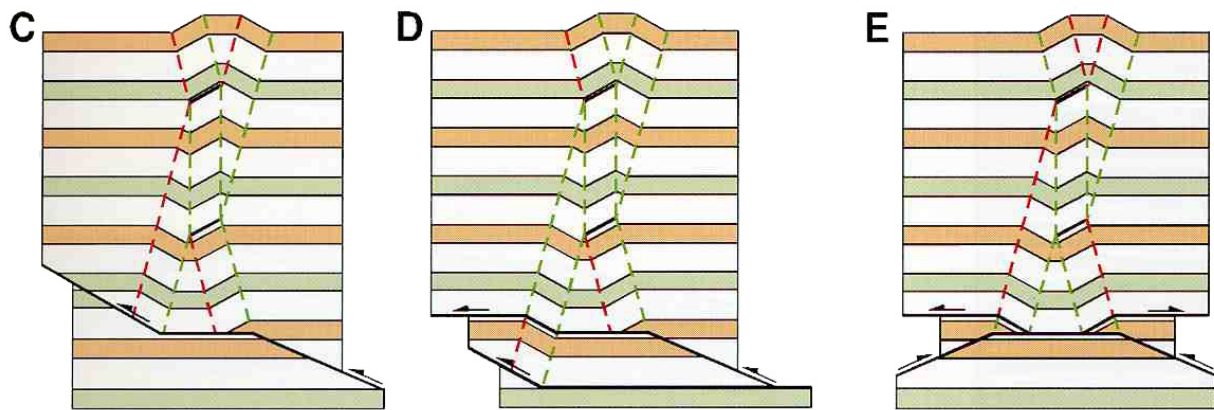


Fig. 52 - Fold interference structures form when two or more fault-bend kink bends intersect. This produces for example anticlines over synclines. After SHAW *et alii* (2005) AAPG©, reprinted by permission of the AAPG whose permission is required for further use.

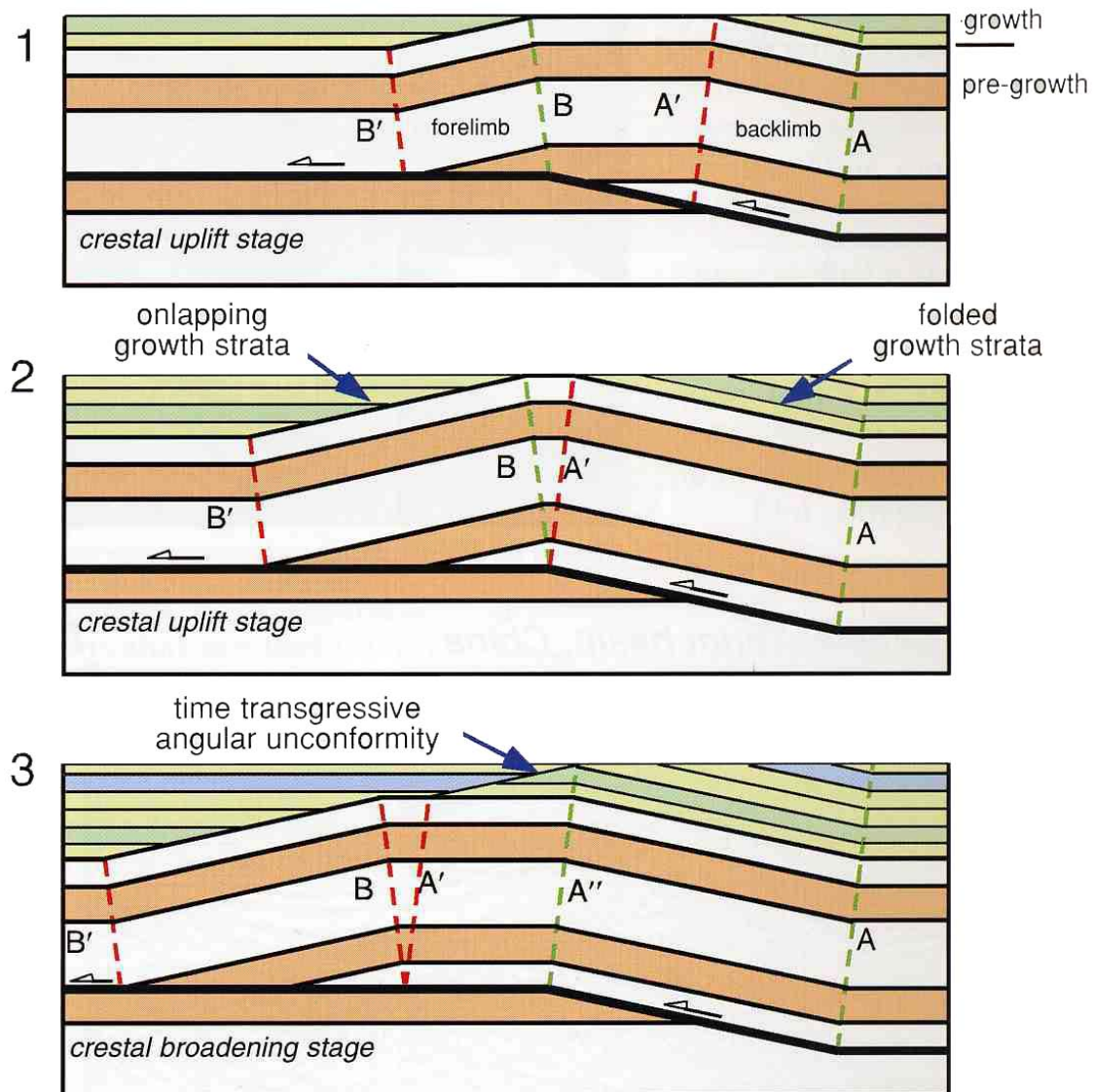


Fig. 53 - Growth-fold associated to fault bending with low sedimentation rates (i.e., sedimentation rates slower or equal to uplift rates). After SHAW *et alii* (2005) AAPG©, reprinted by permission of the AAPG whose permission is required for further use.

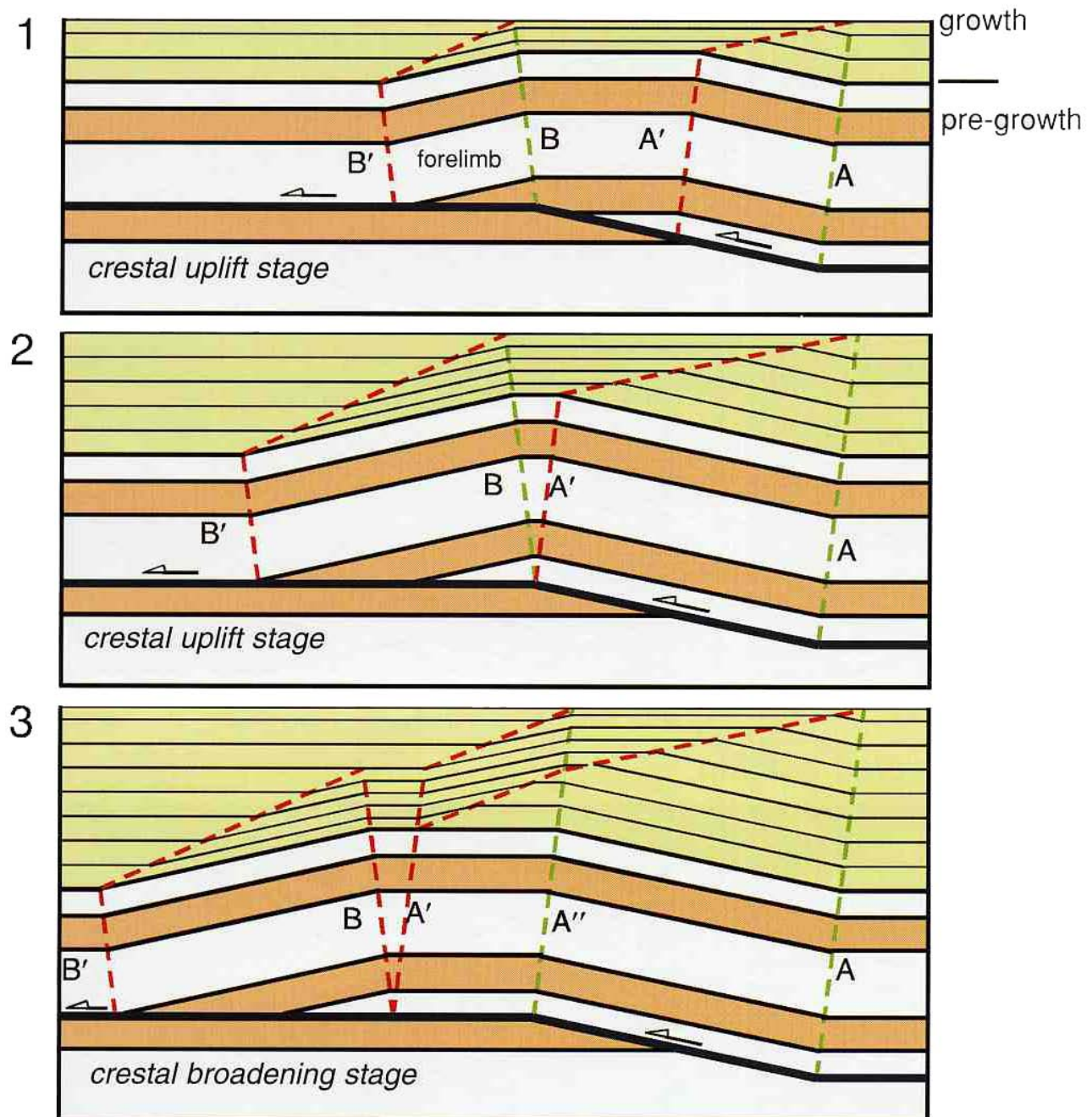
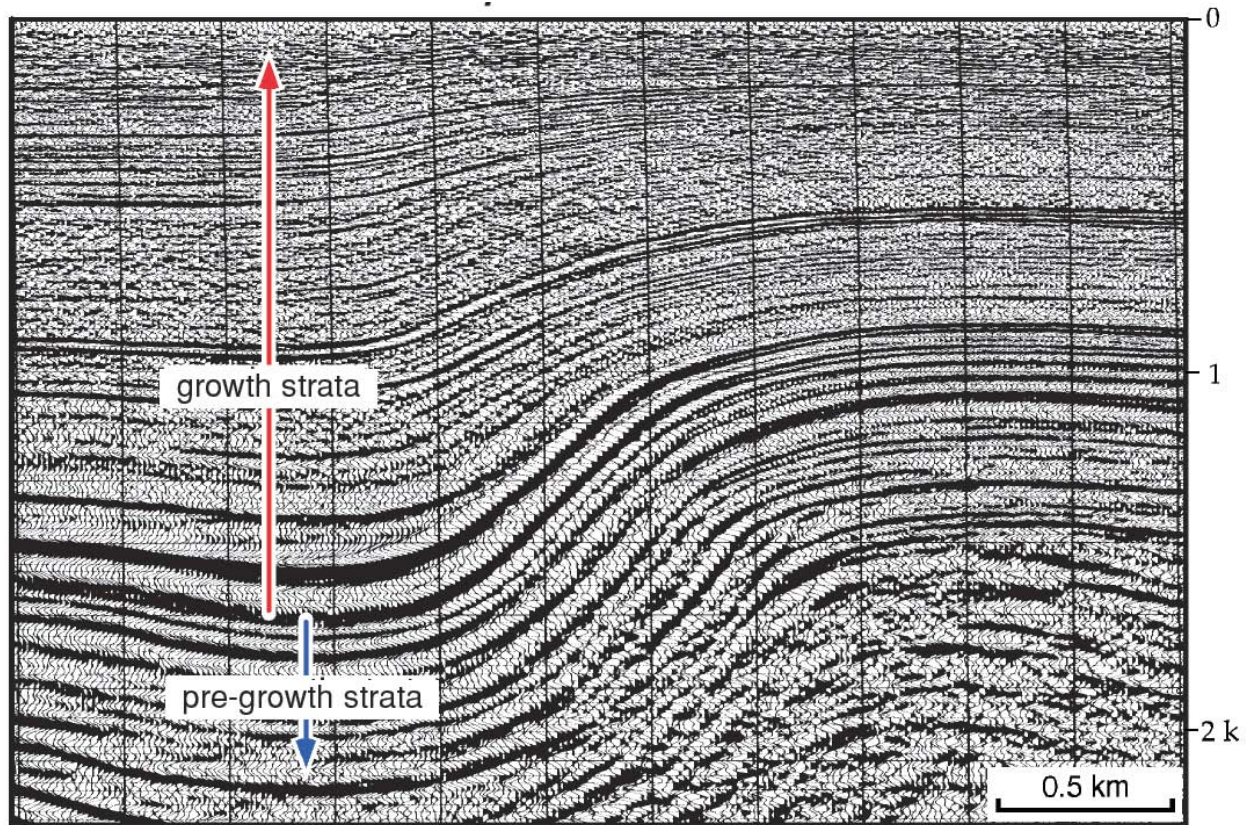
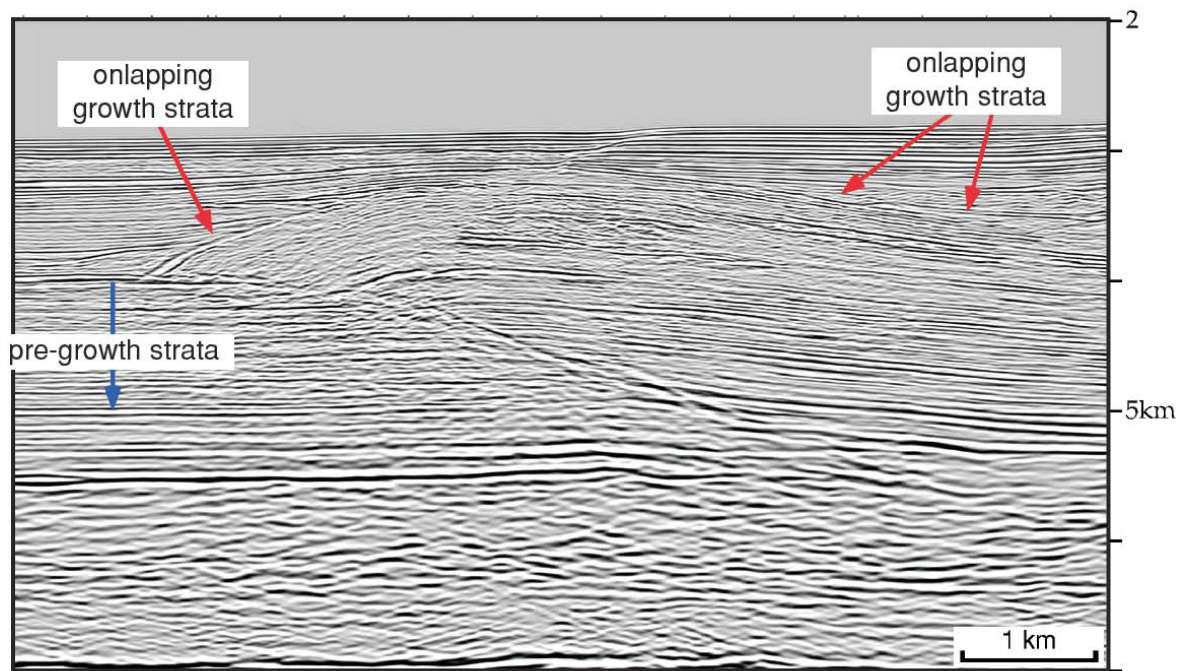


Fig. 54 - Growth fold associated to fault bending with high sedimentation rates (i.e., sedimentation rates faster than uplift rates). After SHAW *et alii* (2005) AAPG©, reprinted by permission of the AAPG whose permission is required for further use.



Data courtesy of Caltex and Texaco, Inc.

Fig. 55 - Growth fold characterised by sedimentation exceeding uplift. Notice that the growth strata, bounded by two seismic reflections, thin towards the structural high. After SHAW *et alii* (2005) AAPG©, reprinted by permission of the AAPG whose permission is required for further use.



Data courtesy of VERITAS DGC Limited

Fig. 56 - Growth fold characterised by uplift exceeding sedimentation. Growth-strata typically thin toward and onlap the structural high. Growth strata do not occur on the crest of the anticline. After SHAW *et alii* (2005) AAPG©, reprinted by permission of the AAPG whose permission is required for further use.

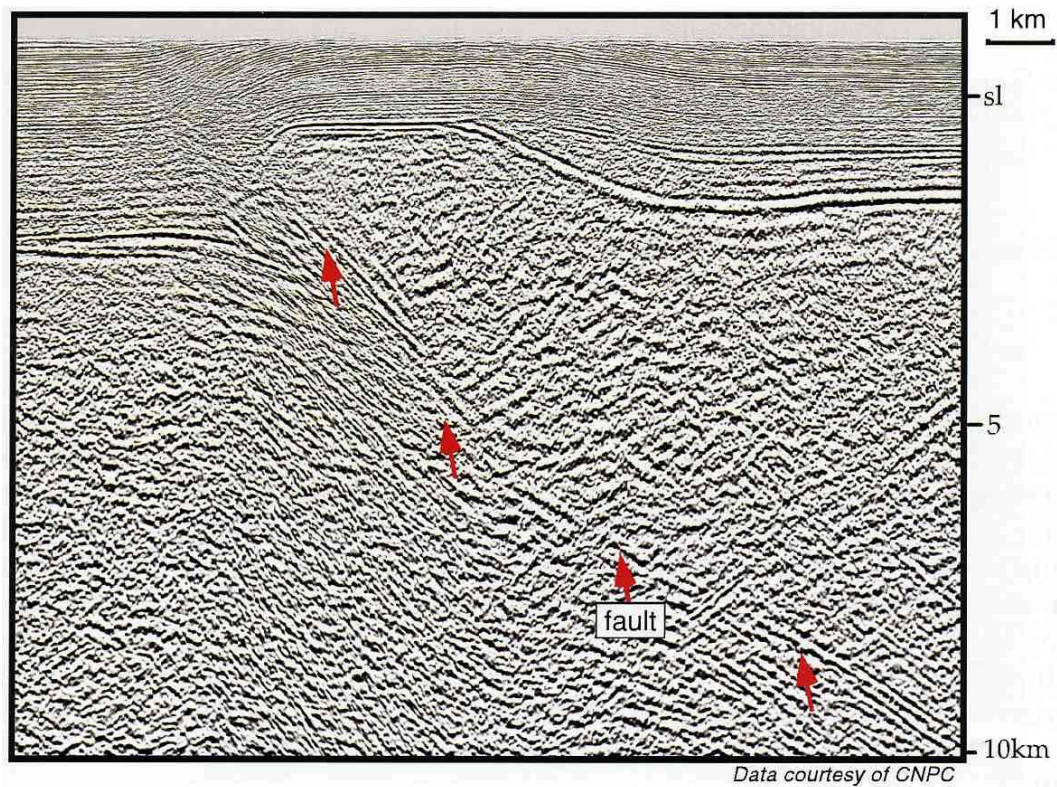


Fig. 57 - Seismic section through a fault-propagation fold in the Tarim Basin, China. After SHAW *et alii* (2005) AAPG©, reprinted by permission of the AAPG whose permission is required for further use.



Fig. 58 - Fault-propagation fold, southeastern cliff of Col Bechei, Dolomites. This type of structure is the most common for brittle regime in the orogens worldwide.

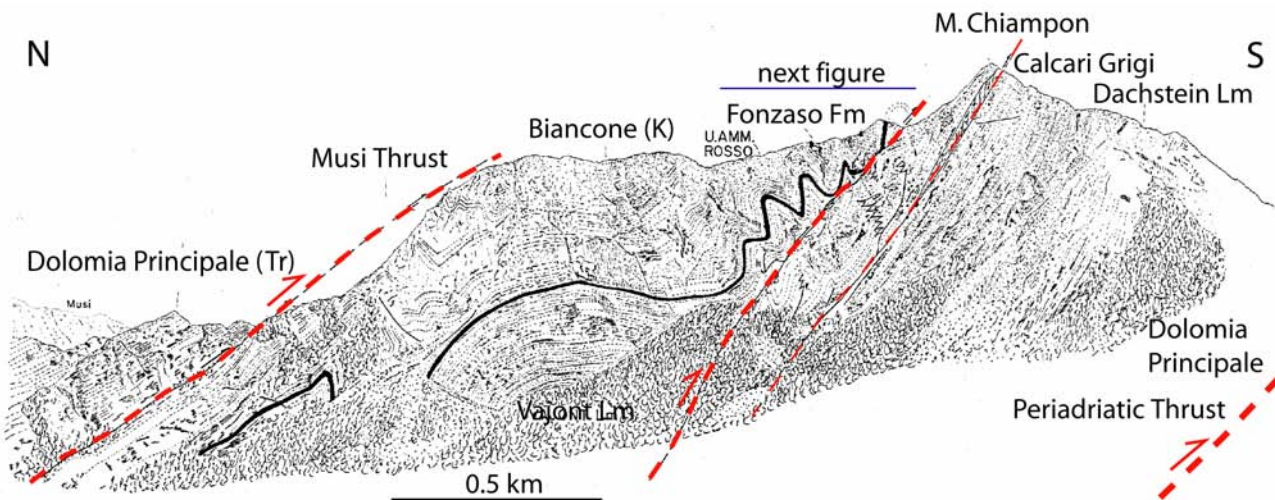


Fig. 59 - Natural section of the Mt. Chiampon, near Venzone, Friuli, eastern Southern Alps. Two major thrusts (Musi Thrust, eastward prolongation of the Valsugana Thrust, and Periadriatic Thrust) contain an intervening folded and internally sheared slice of Mesozoic rocks (platform facies up to Liassic, and deep water up to the Cretaceous).

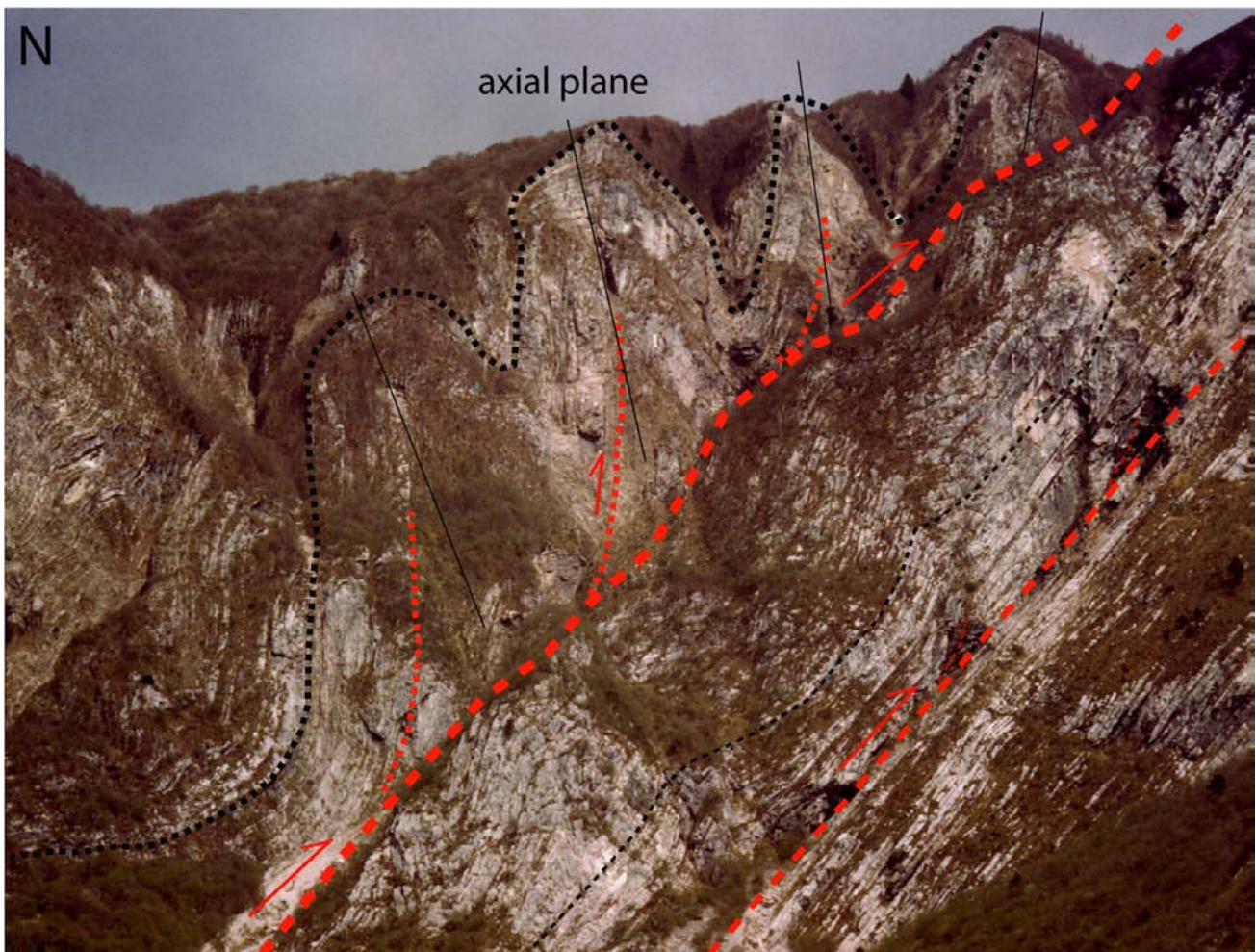


Fig. 60 - Detail of the previous figure. The upper decollement is older and has been tilted and folded by the deeper decollements. Note the gradual counter-clockwise rotation of the axial planes of the detached folds due to piggy back forward propagation of the imbricate fan.

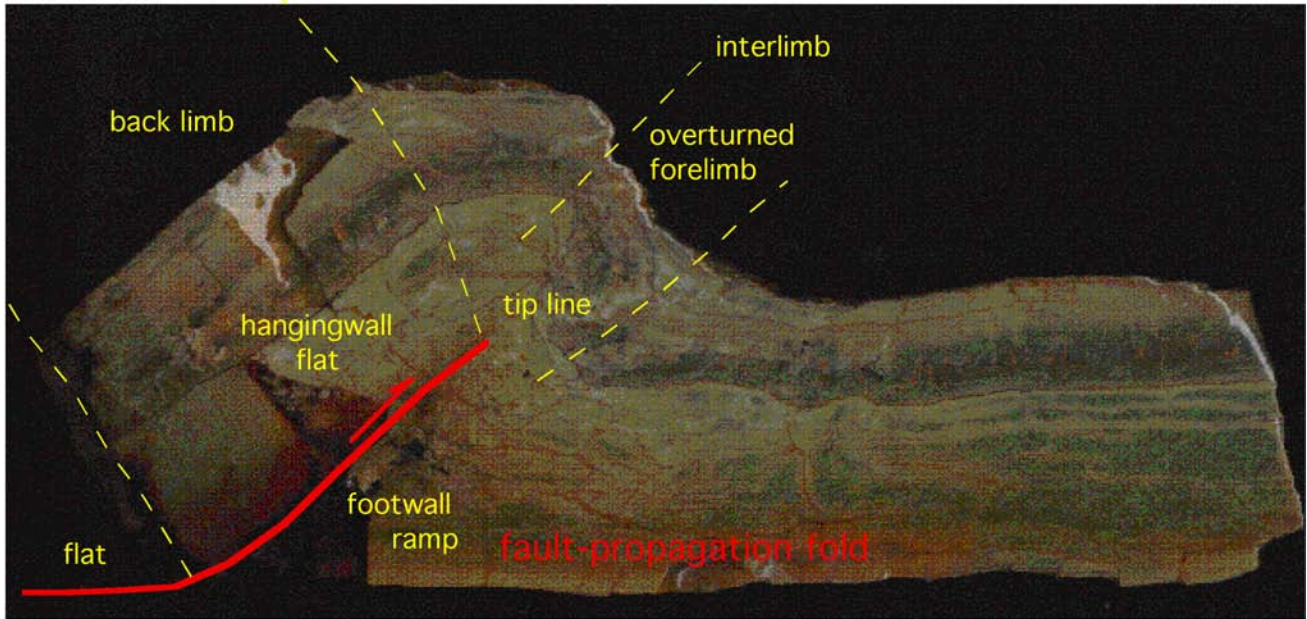


Fig. 61 - Fault-propagation fold in a 25 cm wide specimen of the Lagonegro Jurassic Scisti Silicei, Southern Apennines. Notice the transfer of shortening from the thrust to the fold. Unlike the fault-bend fold mechanism, the forelimb tends to be vertical or overturned. The backlimb has the inclination of the ramp.

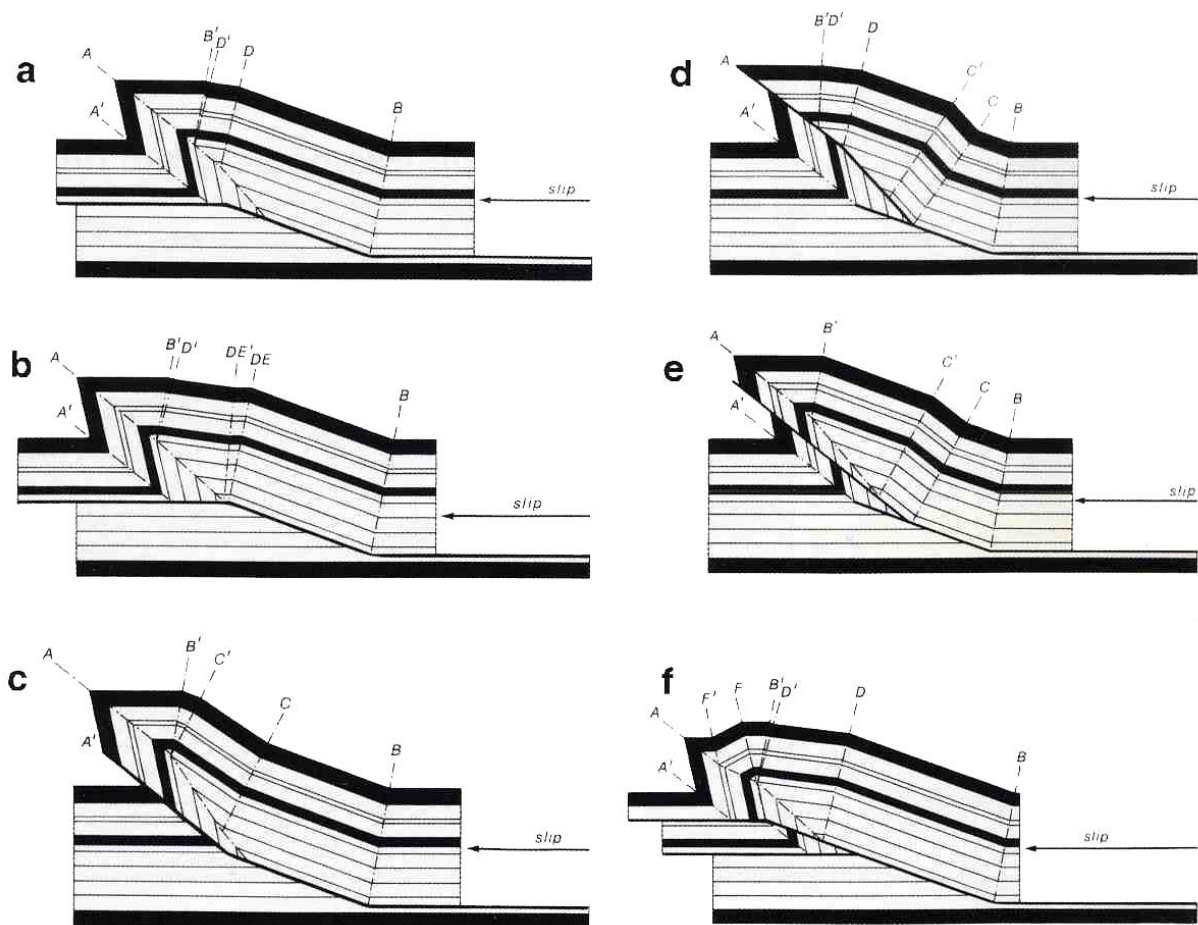


Fig. 62 - Cartoon showing the possible breakthrough structures associated to fault-propagations folds. a) and b) decollement breakthrough; c) synclinal breakthrough; d) anticlinal breakthrough; e) high-angle-forelimb breakthrough; f) low-angle breakthrough. After SHAW *et alii* (2005) AAPG©, reprinted by permission of the AAPG whose permission is required for further use.

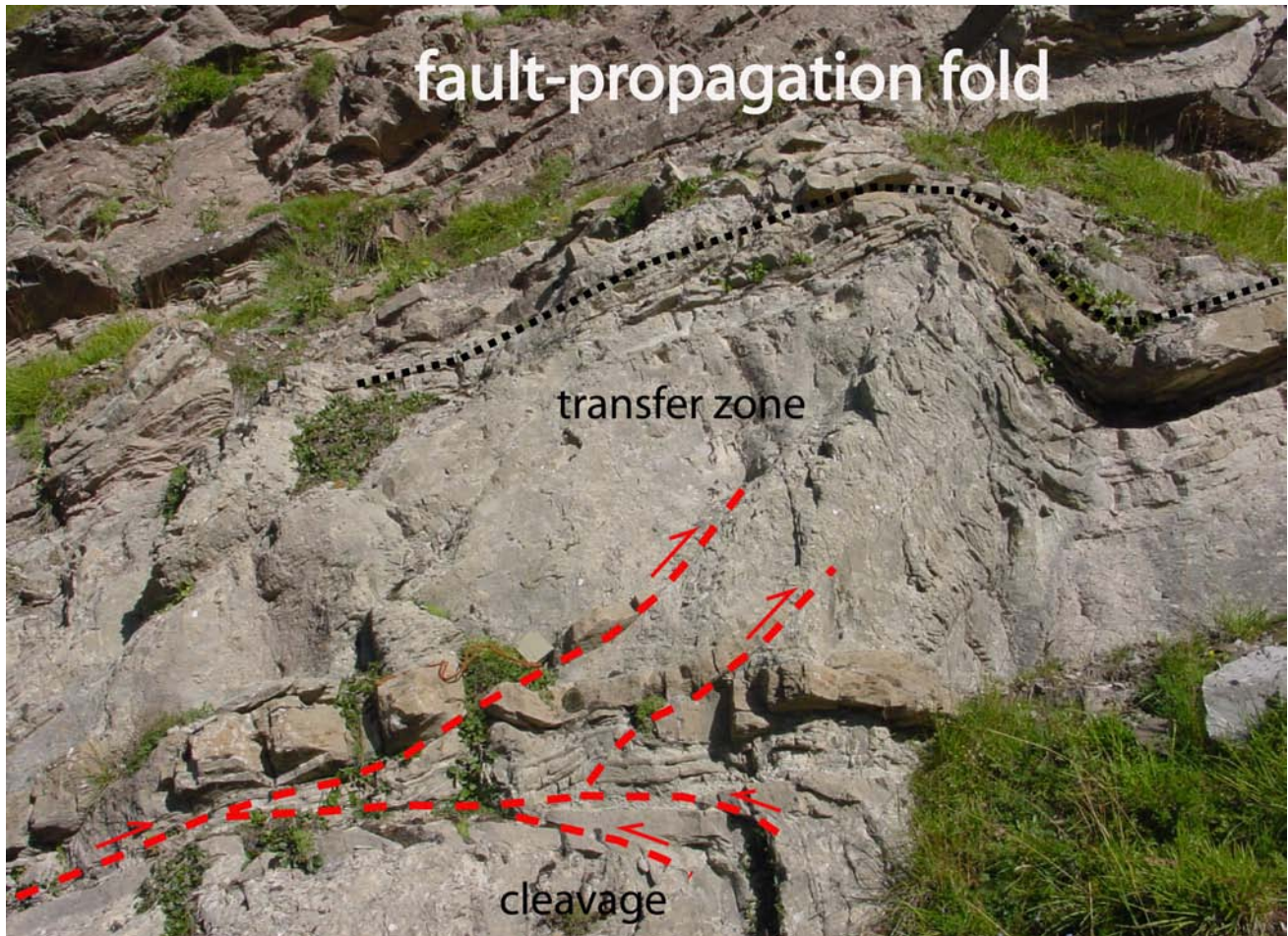


Fig. 63 - Fault-propagation fold in the Siusi Member, within the olistholith of Werfen Fm at Varda (Dolomites). Note the partitioning of the strain associated to the shortening. In the transfer zone thrusting gradually decreases and passes into folding. In the lower part, small backthrusts disappear at depth into vertical slaty cleavage accommodating the shortening.

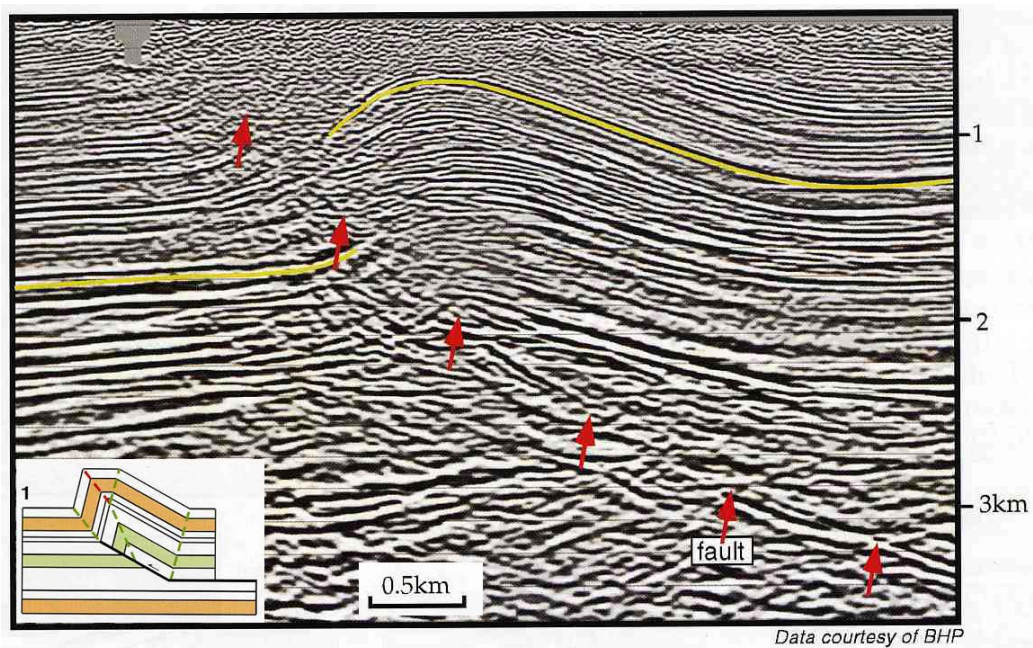


Fig. 64 - Seismic section showing a forelimb breakthrough pattern. After SHAW *et alii* (2005) AAPG©, reprinted by permission of the AAPG whose permission is required for further use.



Fig. 65 - Fault-propagation fold at the hinge of a chevron fold in the Ladinian basinal Livinallongo Fm. 1 km west of Livinallongo del Col di Lana, Dolomites.



Fig. 66 - Tight syncline in Tertiary flysch, Castiglioncello, Tuscany. Note the hinge thickening of shales, whereas the sandstone beds maintain their thickness.

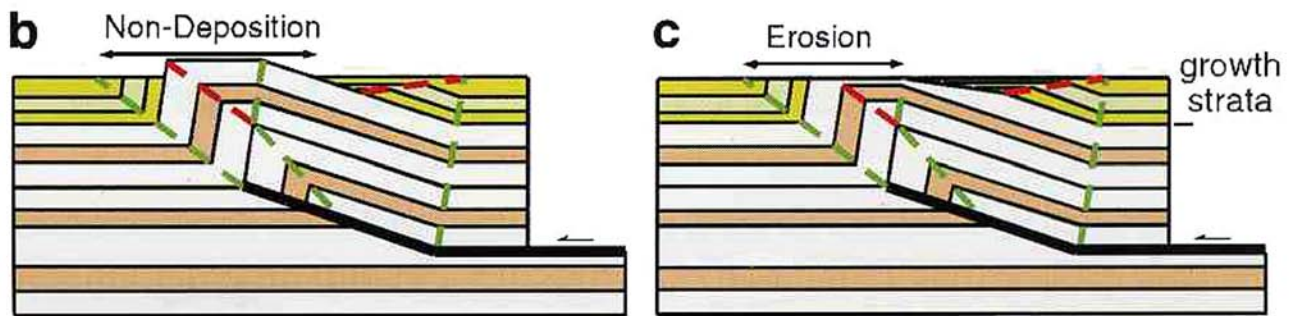


Fig. 67 - Growth fault-propagation folding with sedimentation rates slower than uplift rates. Notice that in submarine conditions the crest of the growing anticline may be characterised by non-deposition, whereas it may be eroded in subaerial conditions. After SHAW *et alii* (2005) AAPG©, reprinted by permission of the AAPG whose permission is required for further use.

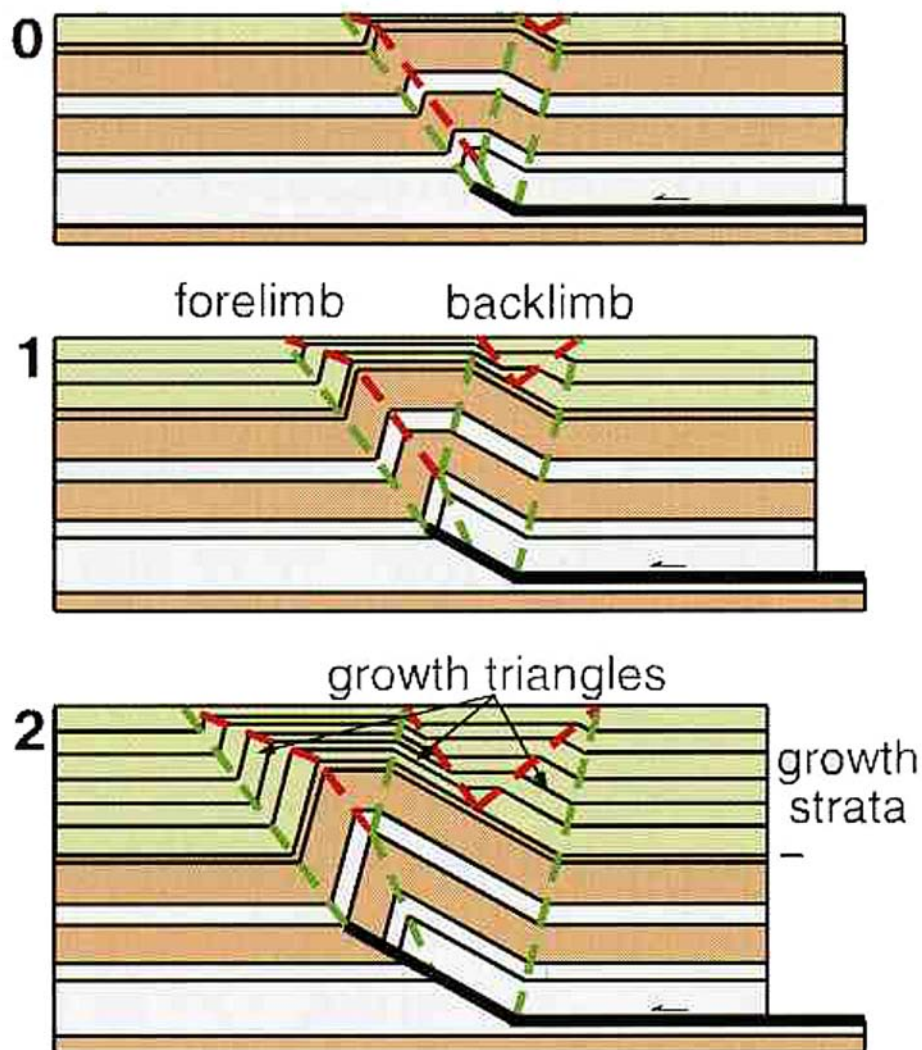


Fig. 68 - Growth fault-propagation folding with sedimentation rates greater than uplift rates. After SHAW *et alii* (2005) AAPG©, reprinted by permission of the AAPG whose permission is required for further use.



Fig. 69 - Growth fault-propagation fold in Pleistocene conglomerates. Alianello, Southern Apennines. Notice the thinning of syn-tectonic sediments toward the crest of the anticline.

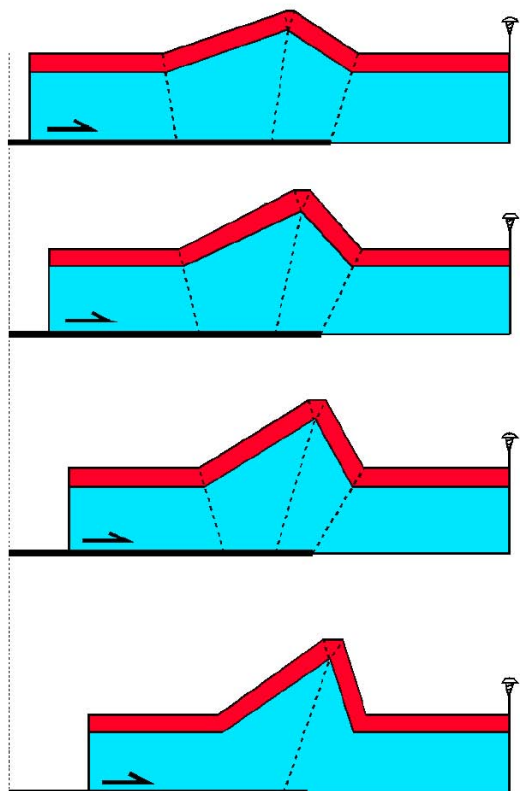


Fig. 70 - Detachment or decollement folds are generated above the tip line of a thrust that developed along a bedding-parallel detachment surface (i.e., along a flat). Where the thrust displacement dies to zero, the deformation is accommodated by folding in the hanging-wall. Modified after SHAW *et alii* (2005). AAPG©, reprinted by permission of the AAPG whose permission is required for further use.

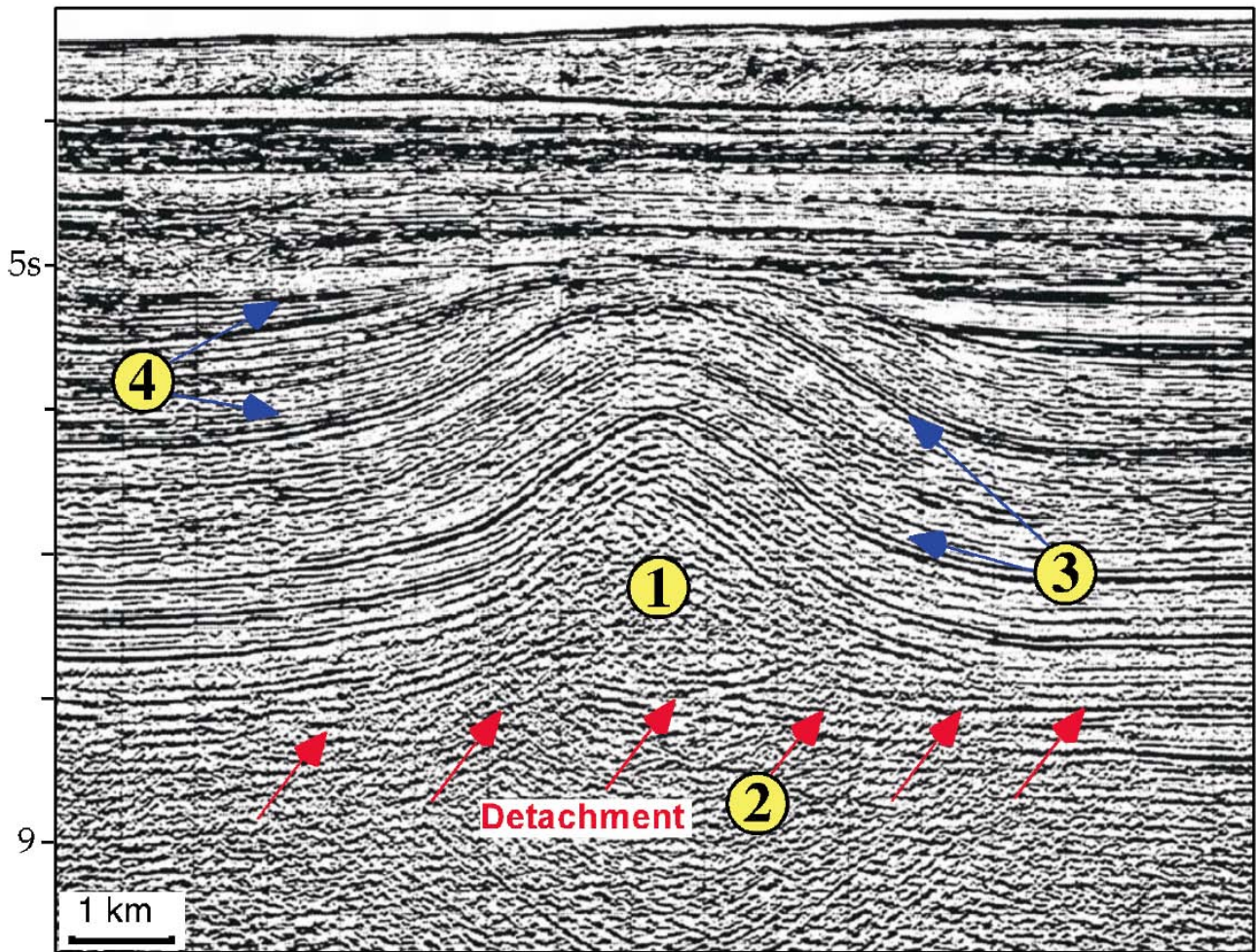


Fig. 71 - Seismic line of a detachment fold in the Gulf of Mexico. After SHAW *et alii* (2005) AAPG©, reprinted by permission of the AAPG whose permission is required for further use.



Fig. 72 - Detachment fold cropping out in the Opal Mt., Canadian Rocky Mountains. Modified after BONS, 2007 (<http://homepages.uni-tuebingen.de/paul.bons/paul/lectures/structure/index.html>).

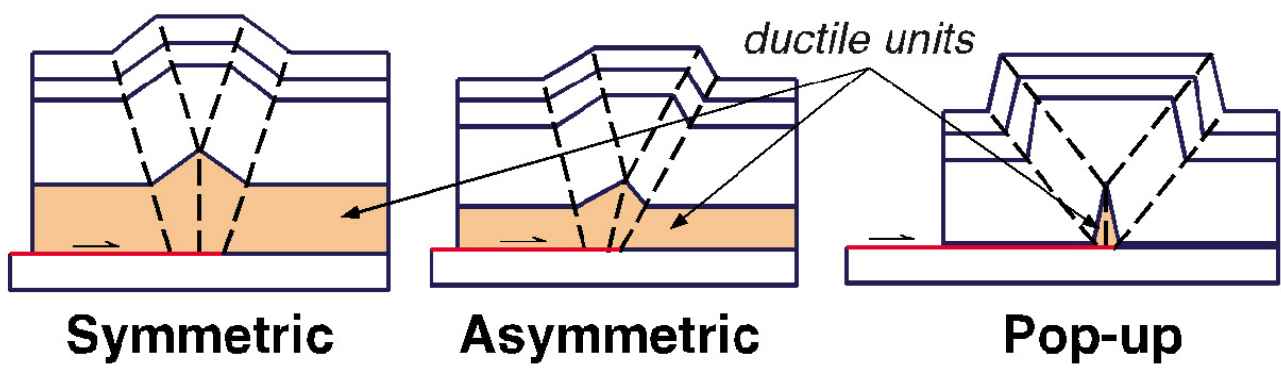


Fig. 73 - Possible geometries of detachment folds. After SHAW *et alii* (2005) AAPG©, reprinted by permission of the AAPG whose permission is required for further use.

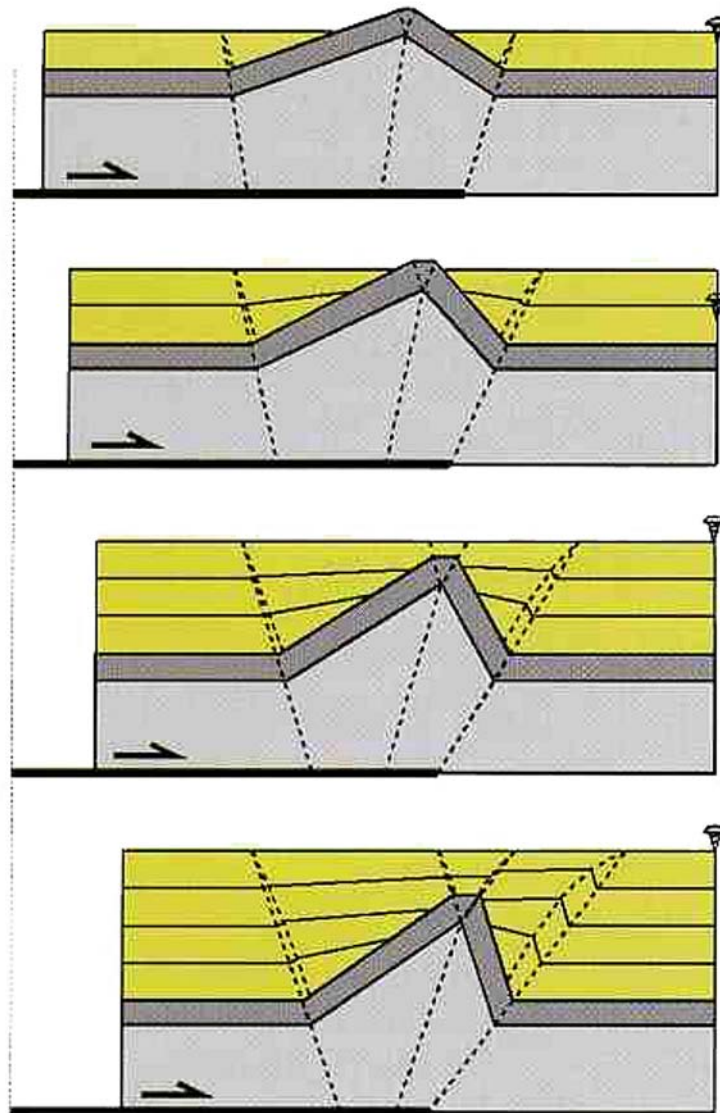


Fig. 74 - Models of growth detachment folds. Different ratios of sedimentation vs. uplift rates (increasing toward the bottom of the figure) are shown. After SHAW *et alii* (2005) AAPG©, reprinted by permission of the AAPG whose permission is required for further use.



Fig. 75 - Chevron folds in the Livinallongo Fm. Note the decoupling surface above where the thickness of the beds increase and the underlying tight folds disappear. The fold axis is NNW-trending. Gasoline station, Pieve di Livinallongo.

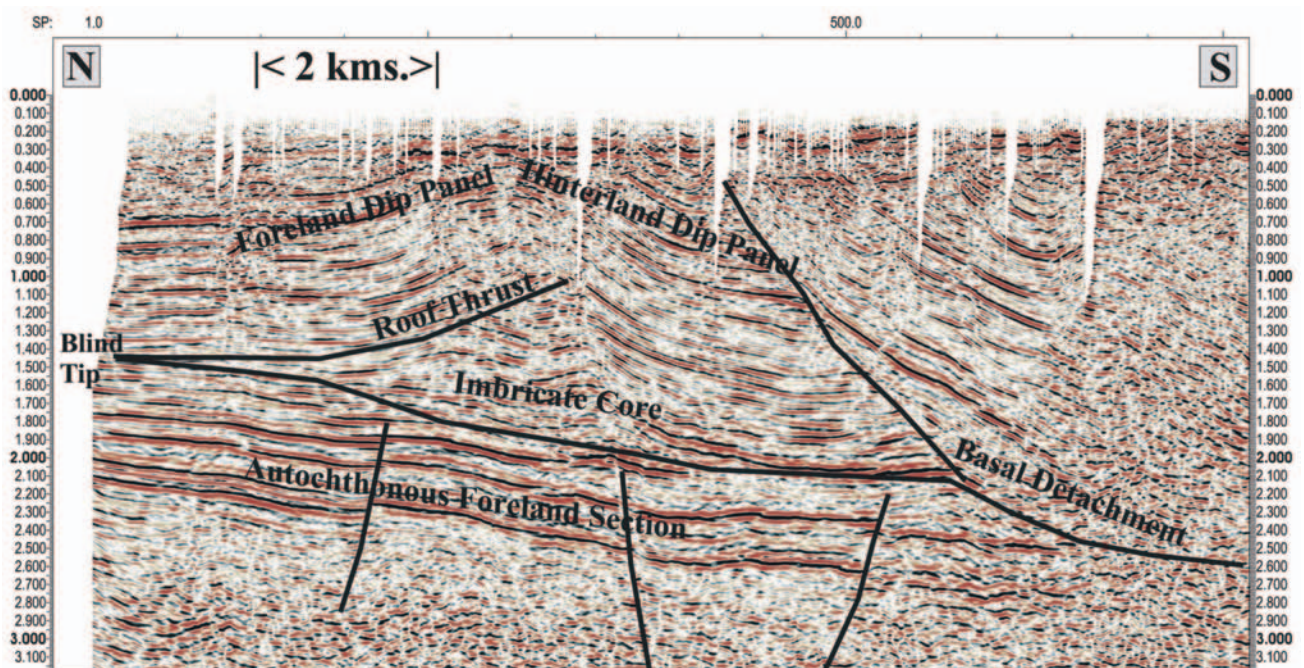


Fig. 76 - Example of triangle zone at the Alpine front in Bavaria (after BERGE & VEAL, 2005)

DECOLLEMENT DEPTH 2.5 km

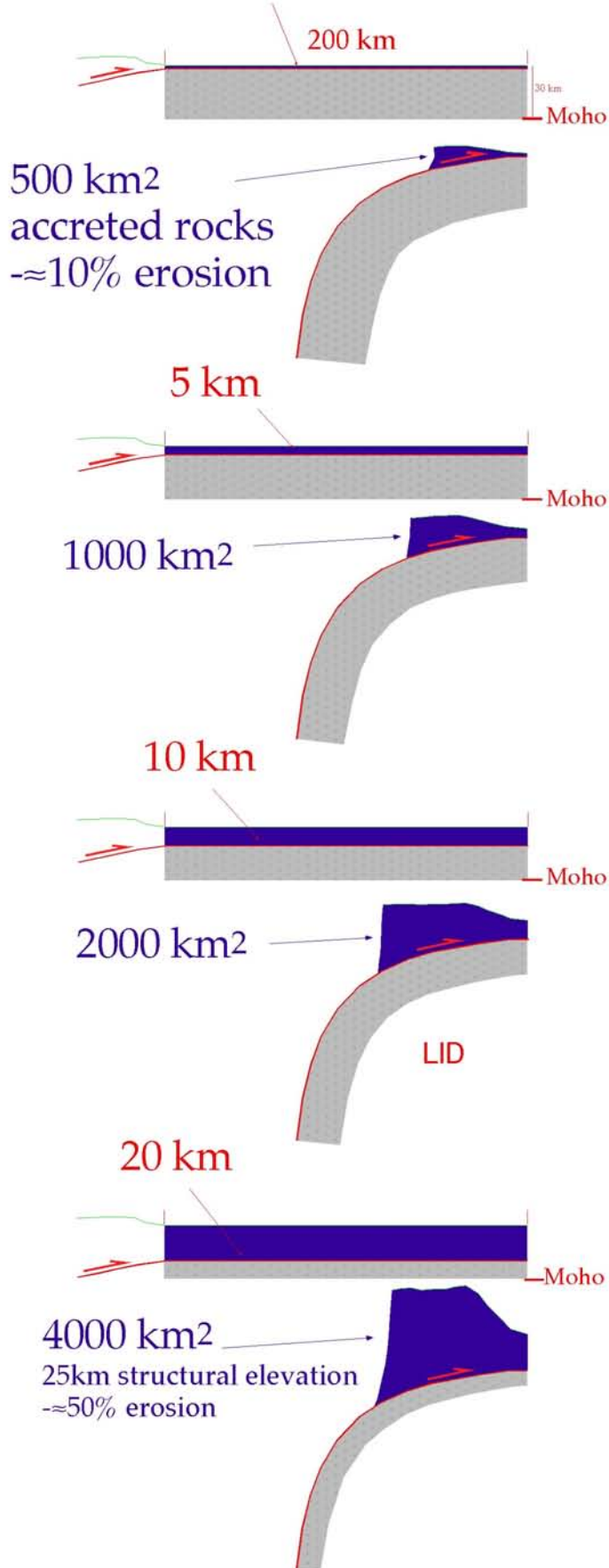


Fig. 77 - The volumes involved by orogens and accretionary prisms are a function of the length of subduction and the depth of the basal decollement. Here are examples of an idealized subduction of 200 km and incremental depths of the decollement. As the decollement becomes deeper, the volume of the orogen will be larger, and its structural and morphologic elevation greater. In nature, the basal decollement is more undulating and shallower for west-directed subduction zones, which in fact present lower volumes in the hangingwall.

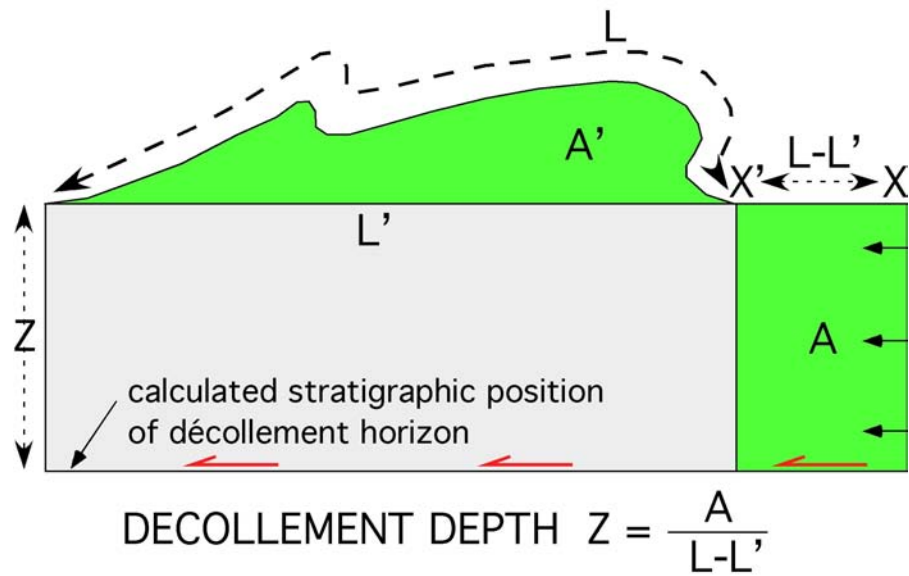


Fig. 78 - The décollement depth (Z) is the fundamental information for tectonic reconstructions. The depth can be estimated once the length of a marker bed (L) and the uplifted area (A) is measured. The uplifted area is equal to the shortened area. The area (A) divided by the difference between the original marker length (L) and the final shortened length (L') gives the calculated depth, after CHAMBERLIN, (1910) and MITRA & NAMSON (1989).



Fig. 79 - Folds in the Zagros. The large scale wavelength and amplitude of the folds indicate a deep décollement (10-14 km), which is located in early Paleozoic salt. Note three diapiric intrusions (darker rocks). USGS-Nasa picture.

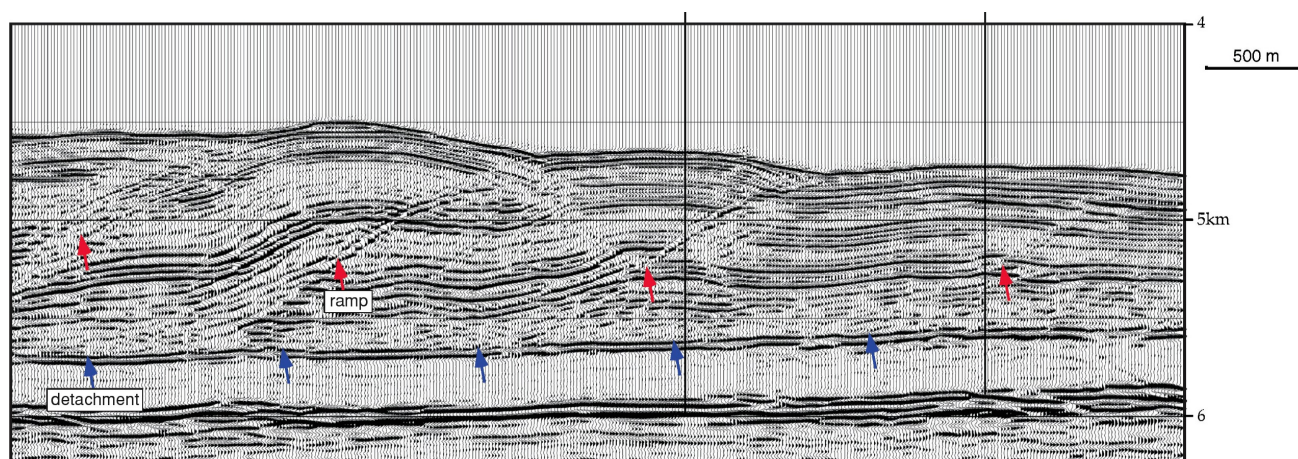


Fig. 80 - Seismic line through the Nankai Trough, Japan, showing the active front of the accretionary wedge associated to the Nankai subduction zone. Notice the ramps generating from a nearly subhorizontal basal decollement. Fault-bend folds accommodate the displacement along the ramp-flat thrust faults. After SHAW *et alii* (2005) AAPG©, reprinted by permission of the AAPG whose permission is required for further use.

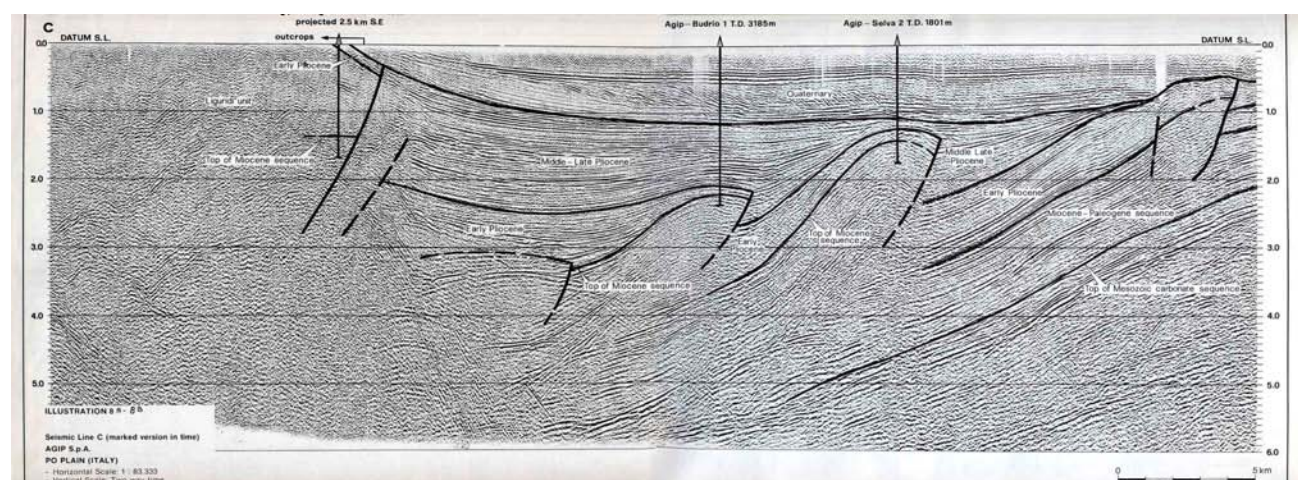
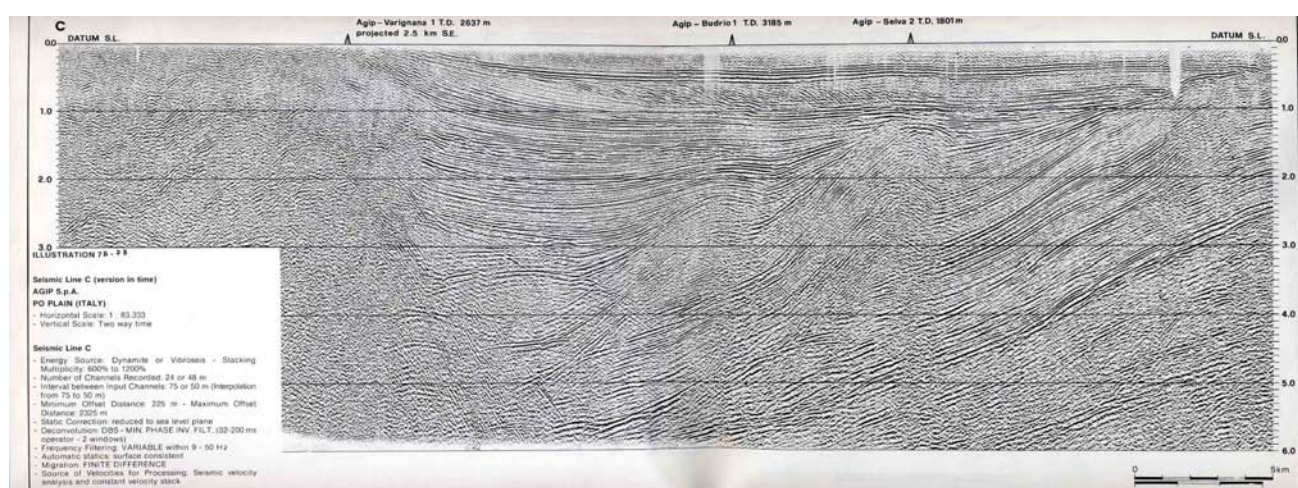


Fig. 81 - Seismic sections through the front of the Northern Apennines beneath the Po Plain. Notice that the two central growth fault-propagation folds are characterised by sedimentation faster than uplift (after PIERI, 1983).

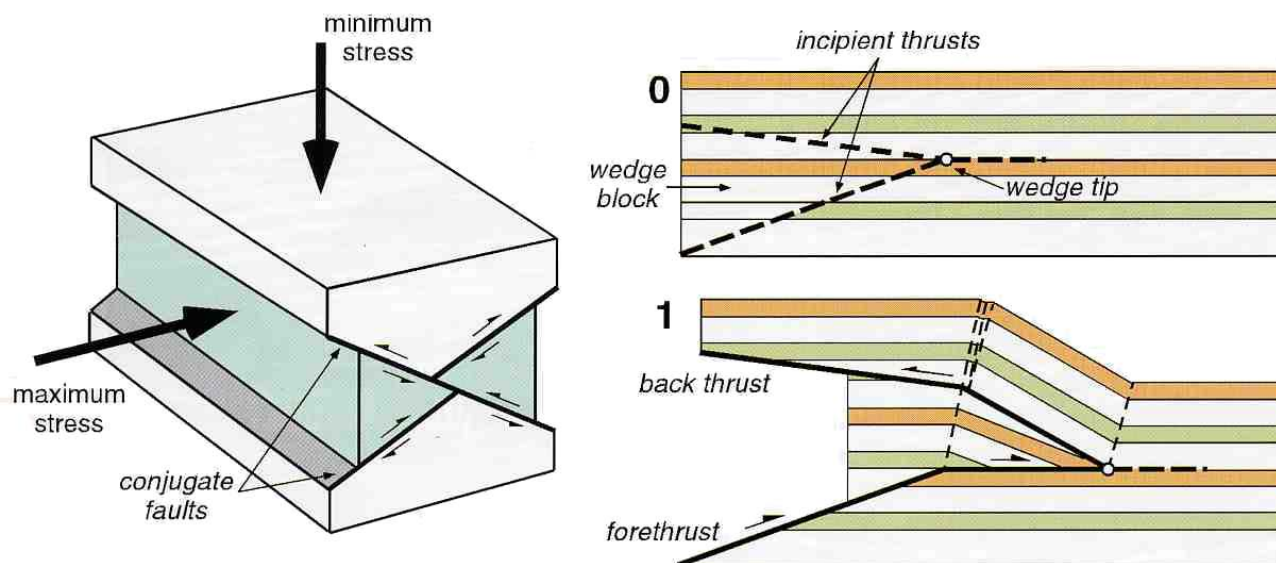


Fig. 82 - Structural wedges contain two connected fault segments that bound a triangular block. The two faults may be either two ramps or a ramp and a detachment. Structural wedges nucleate in agreement with the conjugate fault theory. Once nucleated, slip occurs along both faults allowing propagation of the wedge and determining the folding of the hangingwall. The lower thrust is named roof-thrust whereas the upper thrust is the back- (or roof-) thrust. At large scales wedges are referred to as triangle zones. After SHAW *et alii* (2005) AAPG©, reprinted by permission of the AAPG whose permission is required for further use.

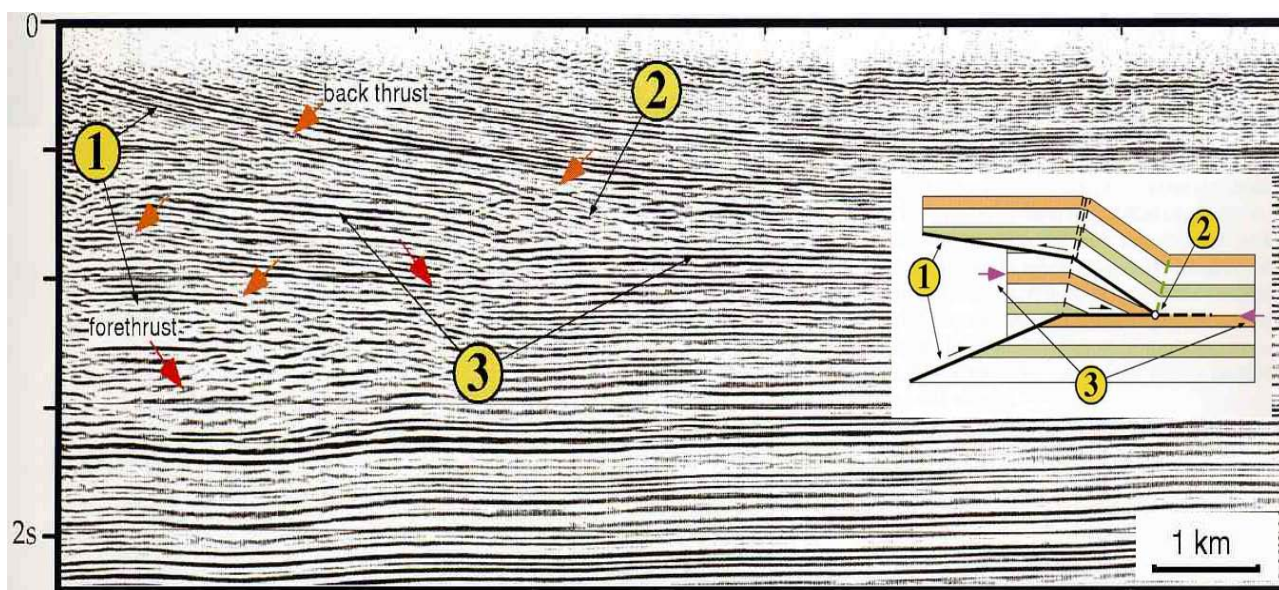


Fig. 83 - Seismic line showing a triangle zone imaged in the Alberta Foothills, Canada. The various structures highlighted by numbers are interpreted in the inset. After SHAW *et alii* (2005) AAPG©, reprinted by permission of the AAPG whose permission is required for further use.



Fig. 84 - Triangle zone in the Liassic Calcarei Grigi, Tofana II, Dolomites. The outcrop is about 20 m wide.

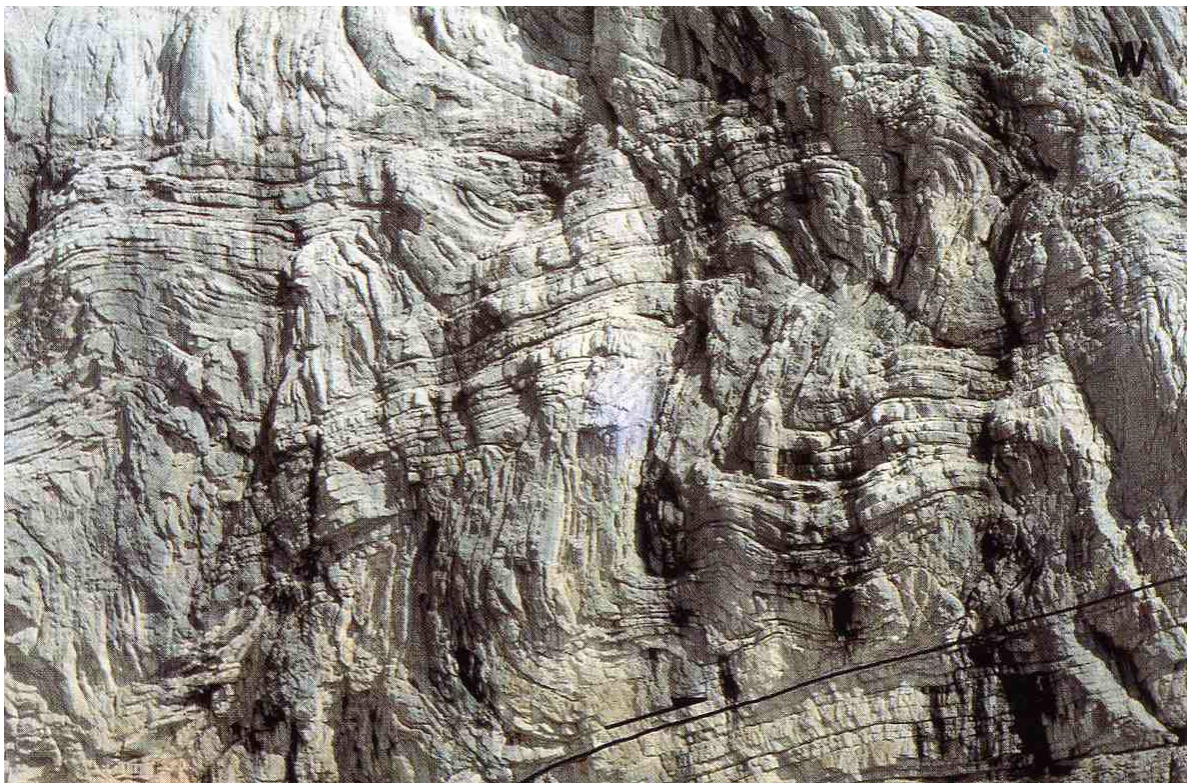


Fig. 85 - WSW-verging chevron folds in Liassic Calcarei Grigi in the hangingwall of the basal thrust of the Civetta klippe, Dolomites.

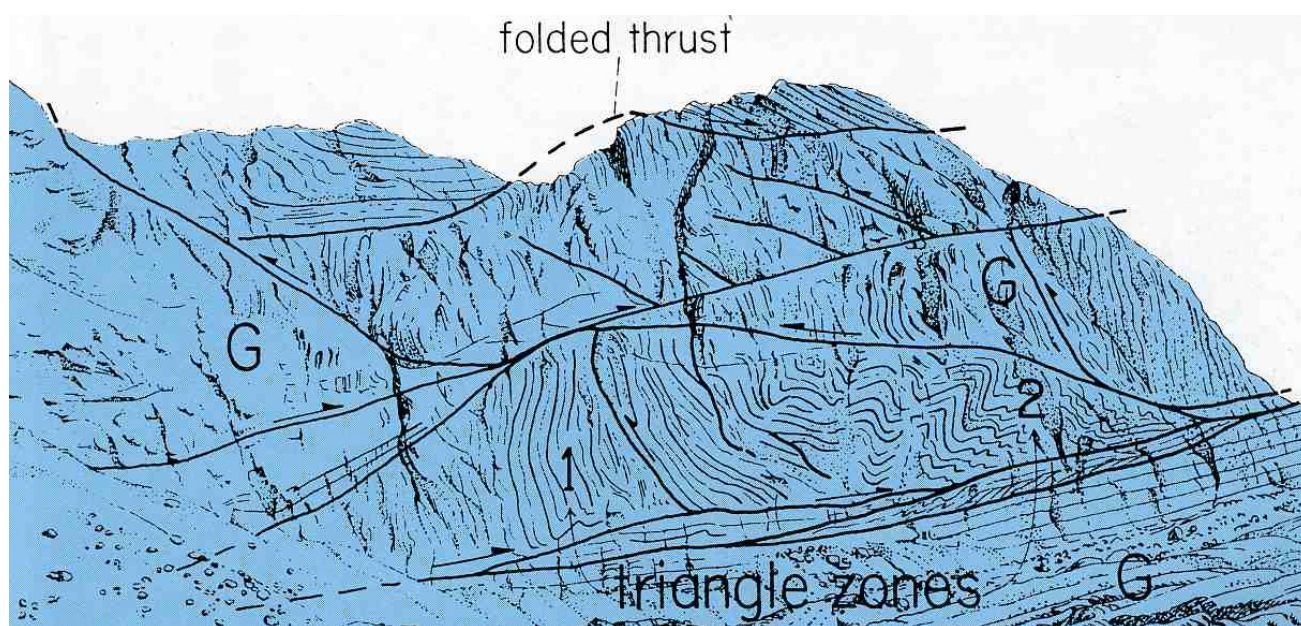


Fig. 86 - Examples of triangle zones in the Civetta Massif (Van dei Sass, central Dolomites). Numbers indicate the kinematic progression of the triangles. Front of the WSW-vergent Paleogene belt. G, Liassic Calcarei Grigi.

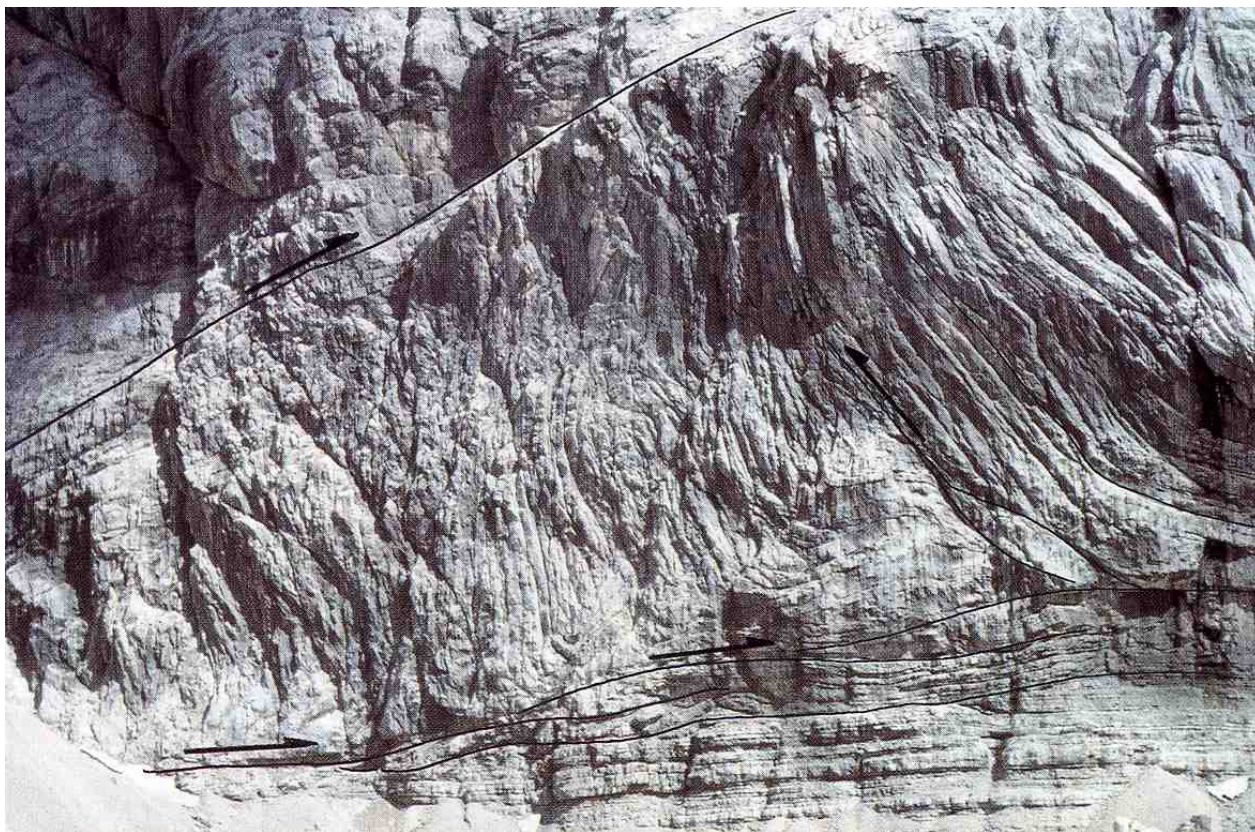
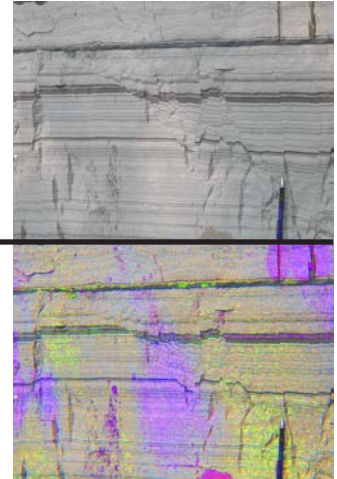


Fig. 87 - Detail of the central part of the previous picture. Triangle structure in Liassic Calcari Grigi, Van Dei Sass, Civetta Massif. The backthrust on the right side is folded and tilted.



Fig. 88 - Triangle structure developed in Carboniferous Rocks. Front Ranges of the Canadian Rockies. After SHAW *et alii* (2005) AAPG©, reprinted by permission of the AAPG whose permission is required for further use.

4. Normal faults and rift zones



Crustal-scale extensional fault systems develop in the following tectonic regimes:

- Intracontinental rift systems (East African Rift)
 - Passive continental margins (North America and Europe passive margins)
 - Mid ocean Ridge systems (Mid Atlantic - Iceland ridge)
 - Back-Arc basin (Lau basin-Tyrrhenian Sea)
 - Extensional collapse Basins (West Norway, Basin and Range)
 - Strike-slip pull apart basins (Dead sea Basin)
- Shallow detached extensional fault systems (i.e., limited to sedimentary cover above a detachment level, normally located in evaporites and shales) are found in the following tectonic regimes:
- Progradational delta systems (Niger Delta)
 - Passive continental margins (West Africa, Brazil and Gulf of Mexico)
 - Submarine Scarps Collapse (East Coast USA).

Normal faults are of three kinds (fig. 89): 1) planar non-rotational (fig. 90), 2) planar with rotation of beds and faults (domino faults) (figs. 91 - 93) and 3) curvilinear with rotation

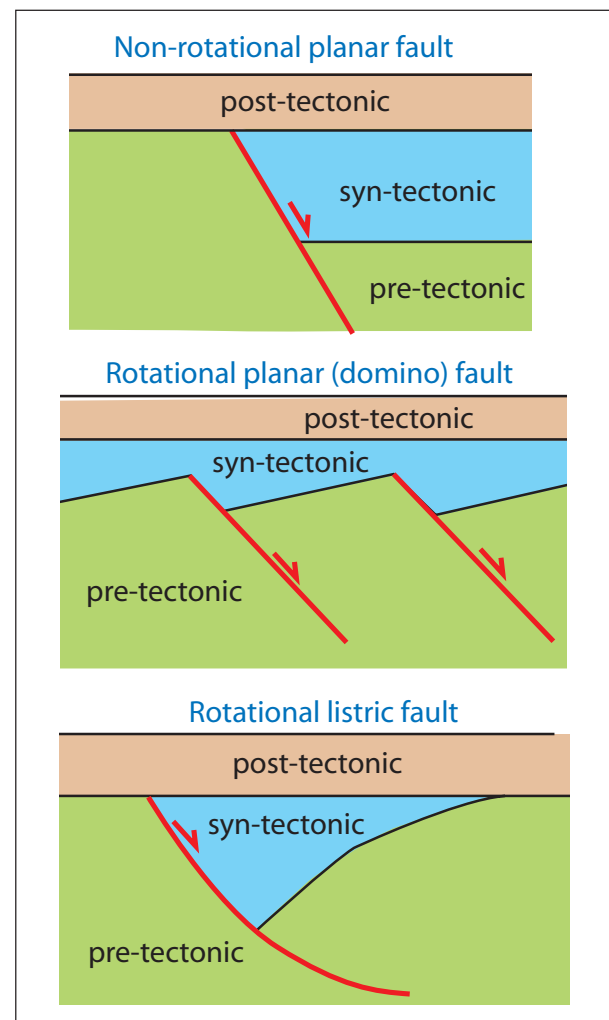


Fig. 89 - 2D geometric classification of normal faults. The classification is based on the effects that faults have on beds and on other faults.

of the beds (listric faults) (figs. 94 - 96).

Types 1 and 2 are found in intercontinental rifts, passive continental margins, mid-oceanic ridges, back-arc basins and pull apart basins. Type 3 occurs in delta systems, passive continental margins, areas characterised by salt detachments and diapirs, areas characterised by collapses of submarine scarps and extensional collapse (mostly post-orogenic) basins.

When investigated in 2D, normal faults are classified as rotational or non-rotational and their fault plane may be planar, listric or kinked. Planar faults can be non-rotational or rotational (fomino faults). In this latter case both beds and fault planes rotate. Both domino and listric faults necessitate of a detachment level. Curved or kinked normal fault planes pose severe space accommodation problems that are eliminated either by folding of the hangingwall with the formation of synforms and antiforms or by tectonic erosion of the fault walls.

Listric faults are associated to rotations of the hangingwall beds. Such rotation generates roll-over anticlines that may be characterised by crestal collapse normal faults delimiting a graben (figs. 97 - 99).

Syn-sedimentary or growth faults (figs. 100 - 106) are characterised by differences in sedi-

ment thicknesses between hangingwall and footwall. Rotational growth faults (either listric or planar) are characterised by the development of a wedge geometry of hangingwall syn-rift sediments that thicken towards the fault plane.

As also discussed for thrust faults, normal faults may be associated to folding (normal fault propagation folds) (figs. 107, 108). Folding occurs during the vertical and lateral propagation of a normal fault involving a rigid basement and a ductile sedimentary cover. Fault tips are associated with the development of a monoclinal fold above the blind, upward and laterally propagating normal fault.

When normal fault systems are discussed in 3D, it is to be emphasized that normal faults are laterally segmented and connected by transfer zones (figs. 109 - 114). In transfer zones displacement is transferred from one fault to the adjacent fault either by strike-slip transfer faults (hard linkage) or by relay ramps (soft linkage). Rift systems (figs. 115, 116) are markedly asymmetric with dominant half-graben structures. In intracontinental rift systems and in passive margins extensional fault systems (i.e., semi-grabens) change frequently polarity along strike. The different semi-grabens are connected by accommodation zones.



Fig. 90 - Planar non-rotational conjugate extensional faults affecting volcanic deposits along the Panamerican Road in El Salvador. Fabrizio Innocenti for scale.

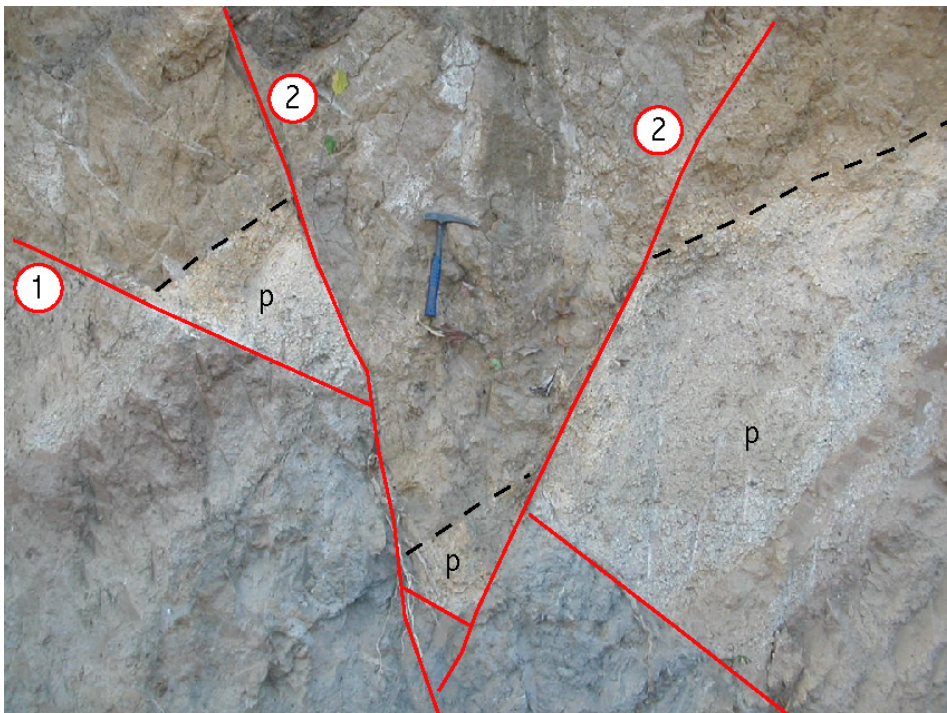
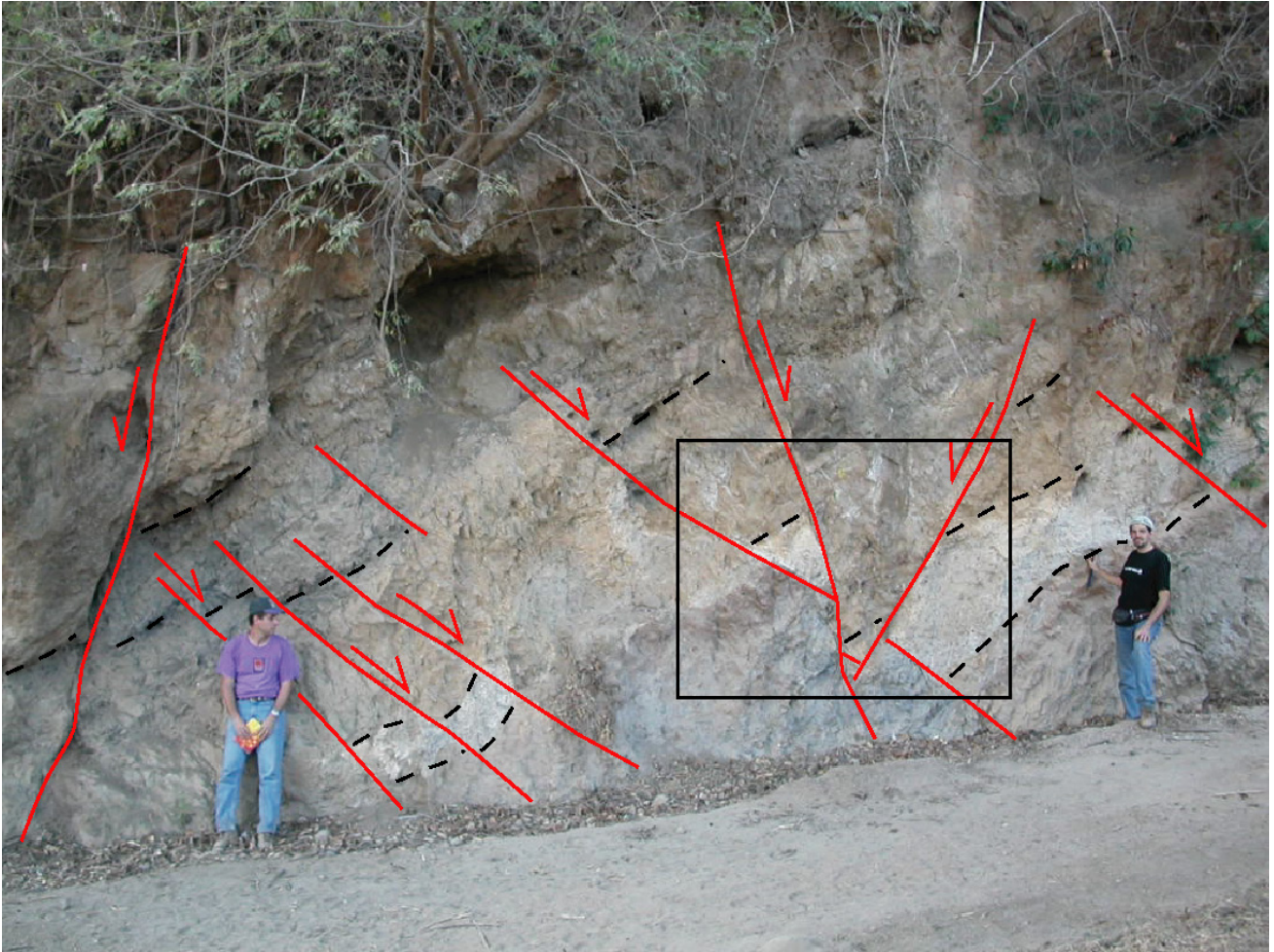


Fig. 91 - Domino normal faults in Pleistocene-Holocene volcanic deposits near the Laguna de Llano, western El Salvador. Notice that a first generation of normal faults (labelled 1 in the close up) were characterised by strong rotations that lowered considerably the fault dip. This produced a severe misorientation of the faults with respect to the direction of active extension. The first fault generation was therefore unsuitable to accommodate further stretching and a new generation of steeply dipping normal faults (labelled 2 in the close up) developed. A sketch of the structural evolution of the area is shown in figure 93. Courtesy of Giacomo Corti and Samuele Agostini.



Fig. 92 - Domino set of planar rotational normal faults, Liassic Medolo Fm, Lake Maggiore, Lombardy. The faults are decoupled along the marly intrabed layers. Courtesy of Daniel Bernoulli.

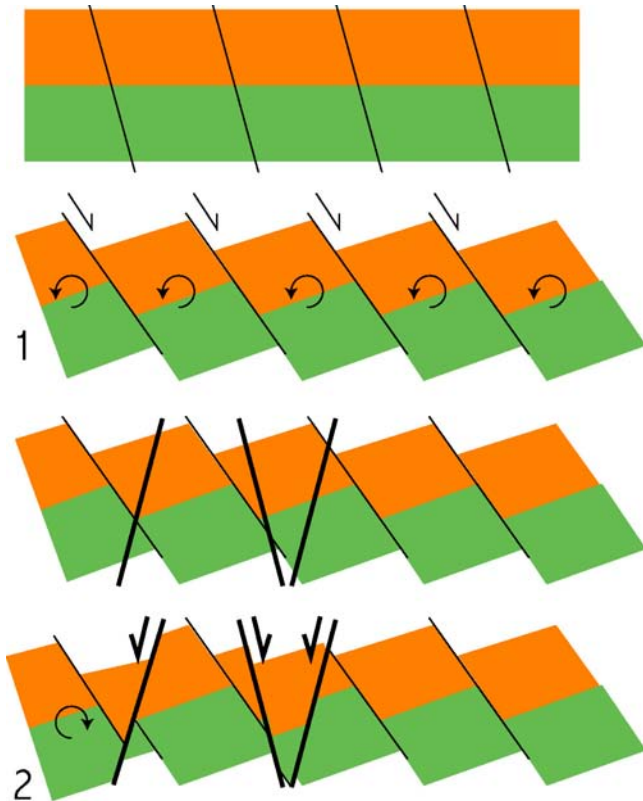


Fig. 93 - Sketch of the structural evolution of the area portrayed in figure 91. Four evolutionary stages are represented. The faults labelled 1 and 2 refer to the two generations of normal faults that developed in the Laguna de Llano (El Salvador) area. The faults of the first generation were rotated and entered the field of extreme misorientation with respect to the active extensional stress field and were therefore abandoned. The faults of second generation nucleated at high angle, compatibly with the predictions of the Anderson's faulting model. Courtesy of Giacomo Corti and Samuele Agostini.

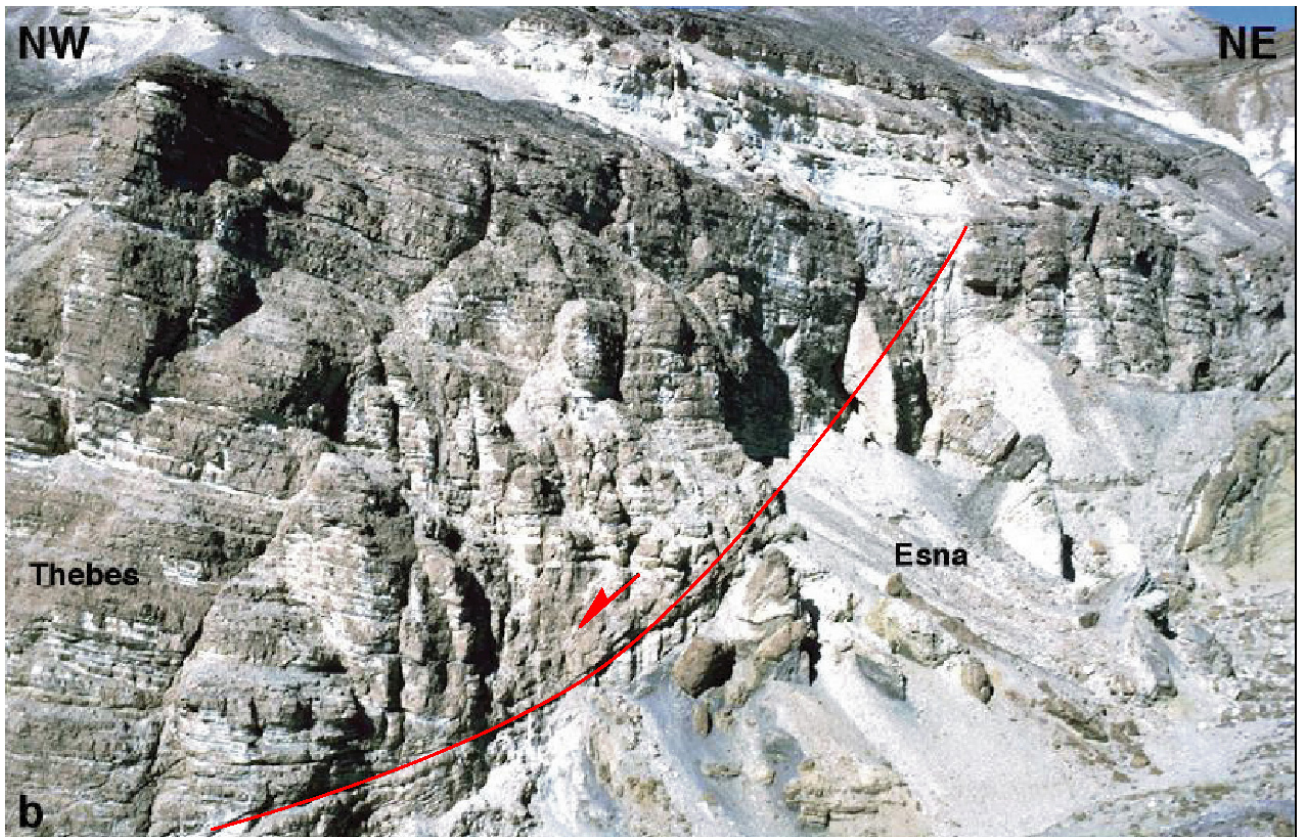


Fig. 94 - Listric fault cropping out in the Sinai Peninsula, Egypt (after KHALIL, 1998).



Fig. 95 - Seismic line showing a rotational, mainly planar domino set of extensional faults. Gulf of Mexico.

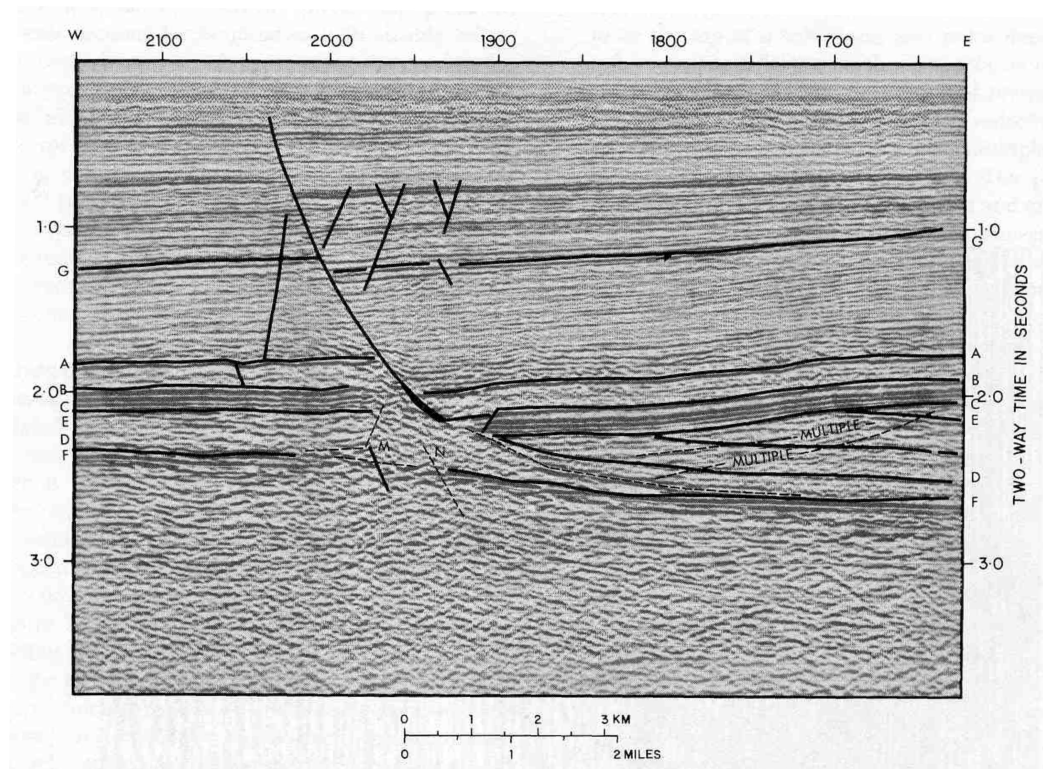
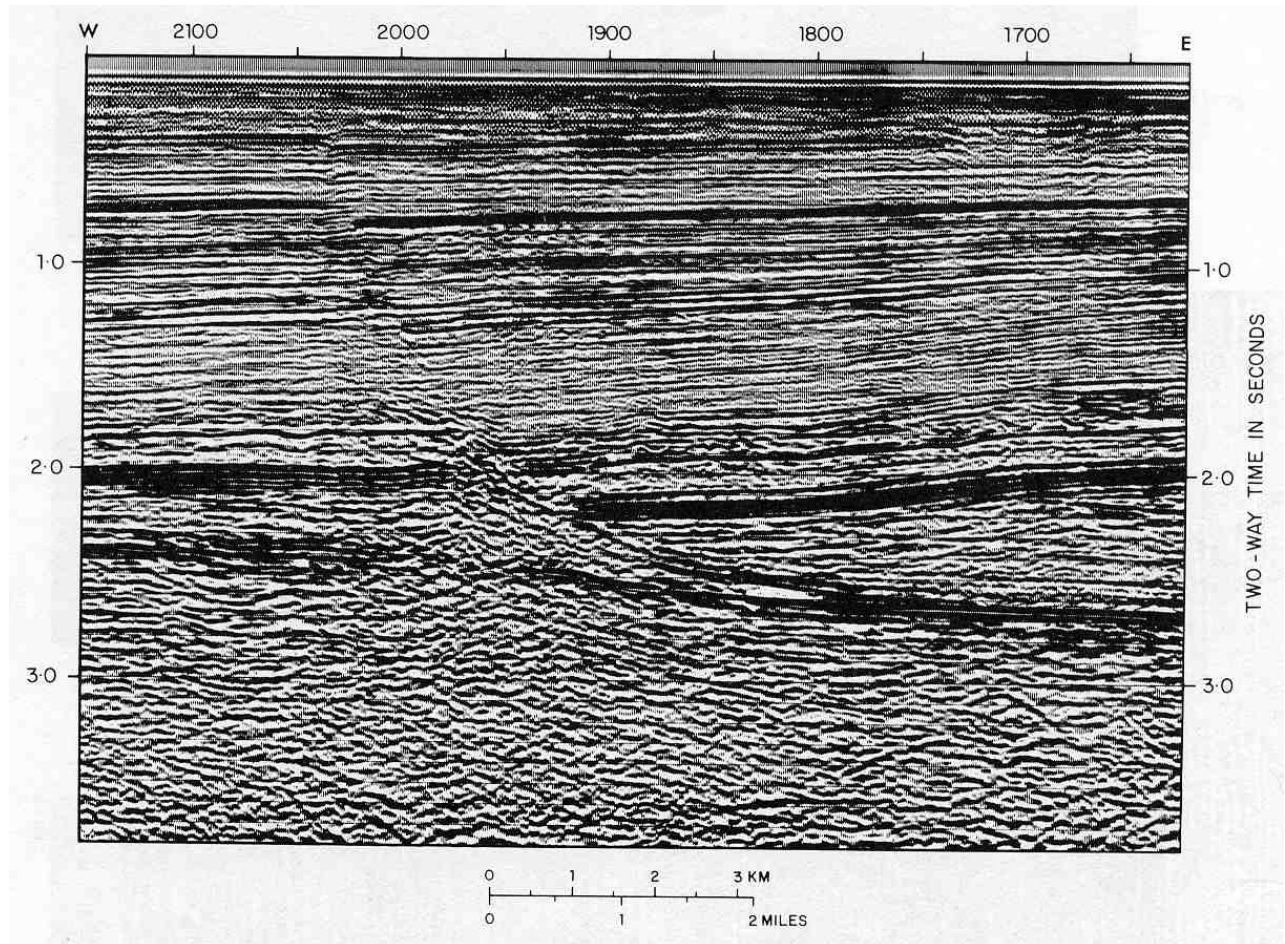


Fig. 96 - Seismic line and interpretation showing a listric normal fault. Notice that the upper half of the figure shows, in the hanging-wall, sedimentary wedges that thicken toward the fault, indicating that they were deposited when the fault was active (after BADLEY, 1985).

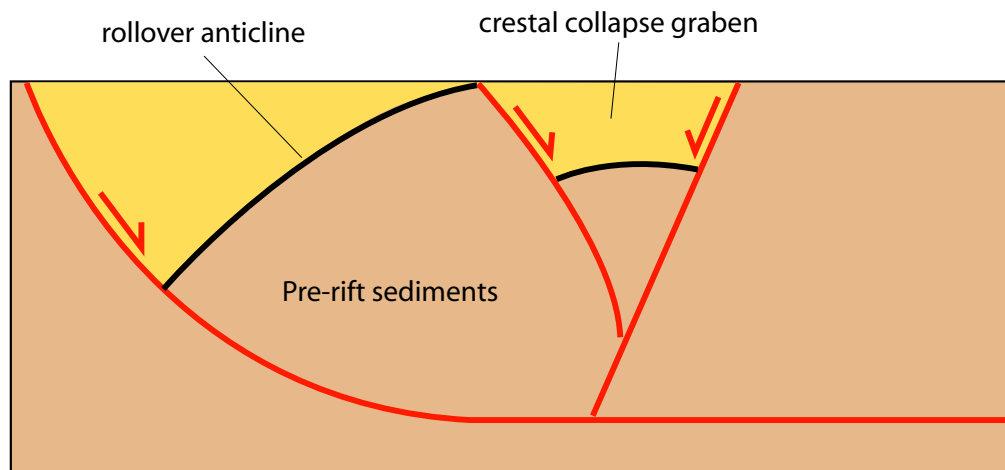


Fig. 97 - Listric faults are characterised, in the hangingwall, by the occurrence of rollover anticlines. Such structures accommodate the slip along the curved fault plane and are possibly characterised at their top by a crestal collapse, with the development of graben like structures.

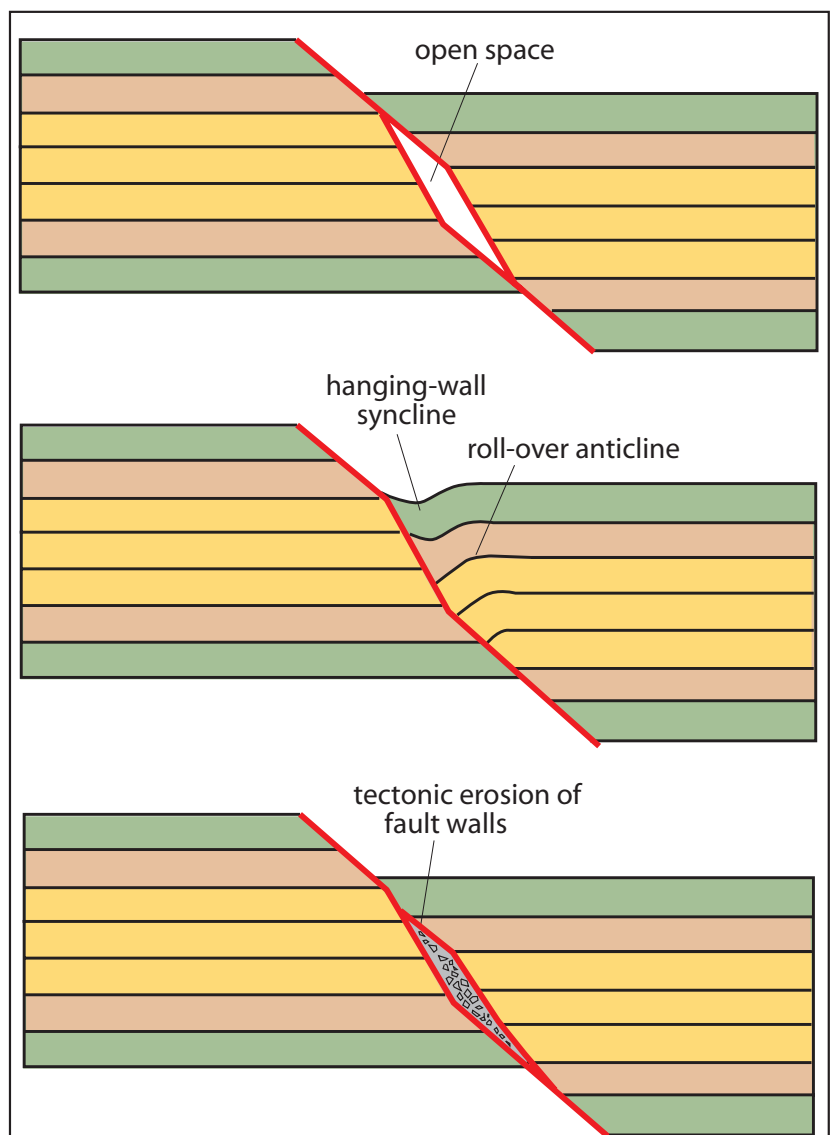


Fig. 98 - Curved or kinked normal fault planes pose severe space accommodation problems (opening of voids) when the fault kinematics are investigated. In nature, the voids may be eliminated either by folding of the hangingwall with the formation of synforms and antiforms or by tectonic erosion of the fault walls (after RAMSAY & HUBER, 1987).

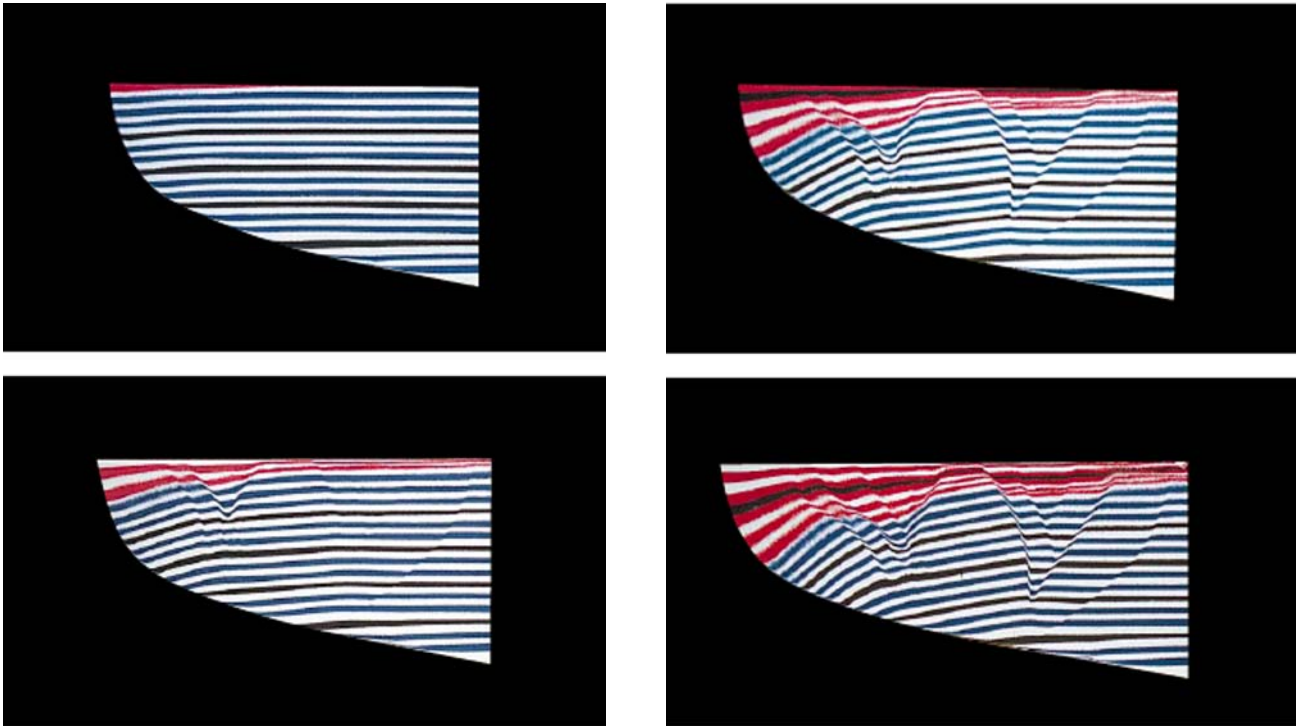


Fig. 99 - Analogue modeling showing the development of a rollover anticline and of the associated crestal collapse graben (after PLATT *et alii*, 1993).

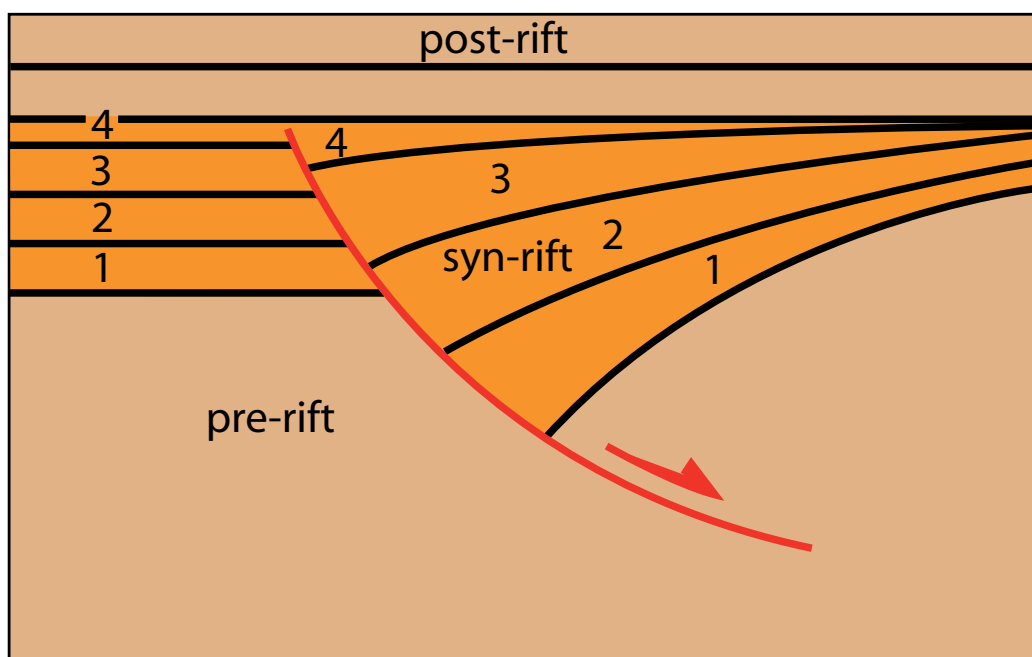


Fig. 100 - Synsedimentary listric fault. The syn-rift strata show in the hangingwall a wedge-like thickening towards the fault.

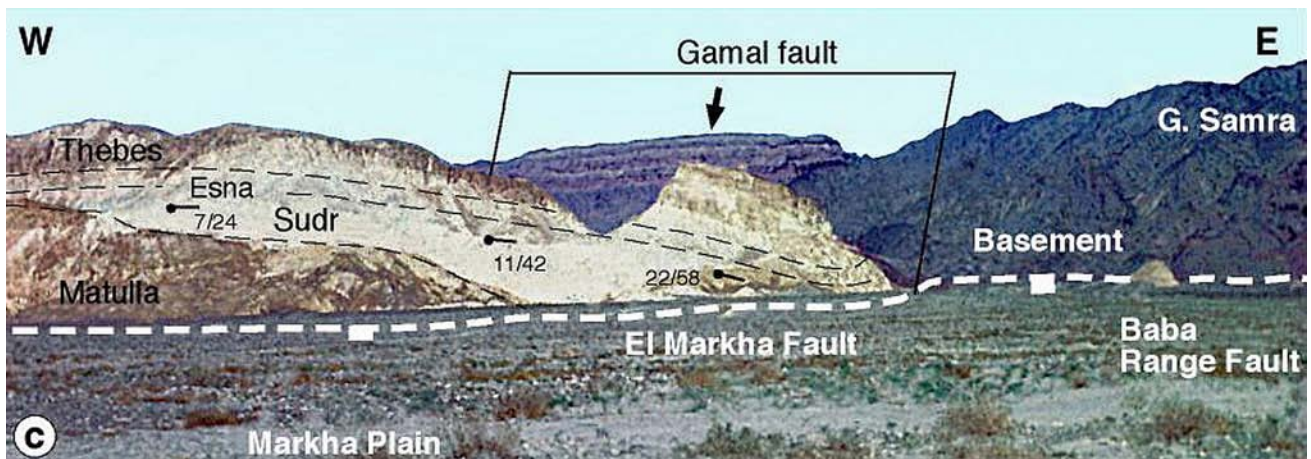
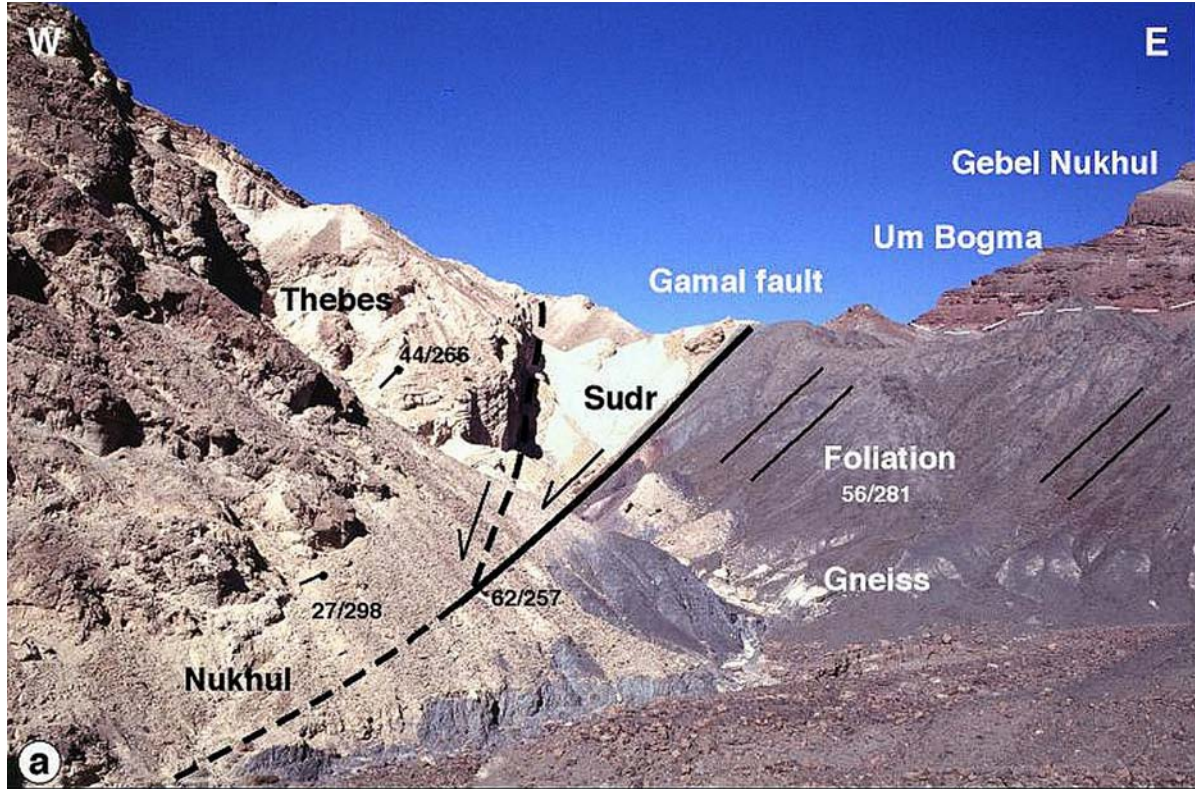


Fig. 101 - An example of rollover anticline cropping out in the Sinai Peninsula. The Gamal fault has a listric geometry (upper panel). In the lower panel it is shown that the Paleozoic sediments overlying the basement are horizontal (just below the black arrow), whereas the hangingwall sediments of the Thebes, Esna and Sudr Fms. progressively bend producing a rollover anticline geometry (after KHALIL, 1998).

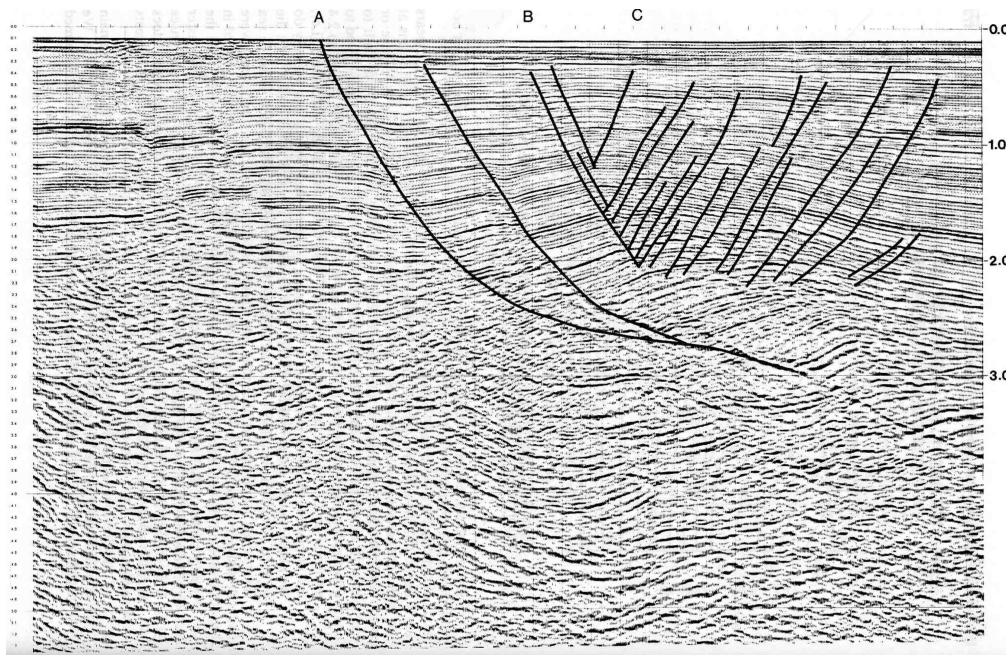


Fig. 102 - Seismic section showing a listric fault associated with a rollover anticline characterised by crestal collapse (after XIAO & SUPPE, 1992).

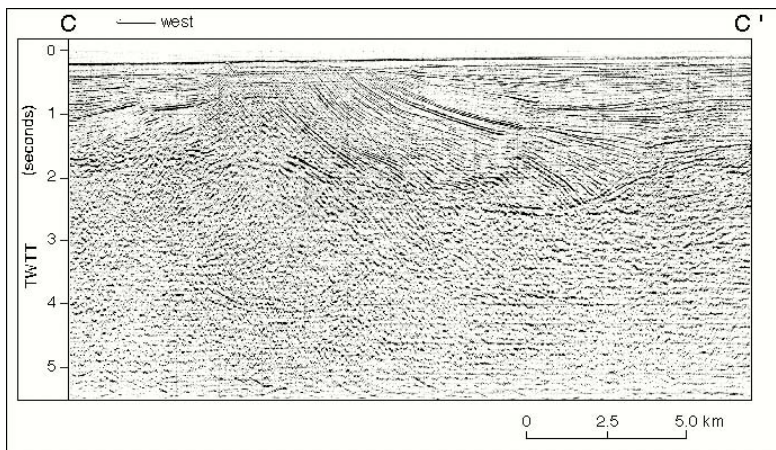


Fig. 103 - Seismic line and interpretation showing syn-sedimentary listric faults from the Cascadia subduction zone (after McNEILL *et alii*, 1997).

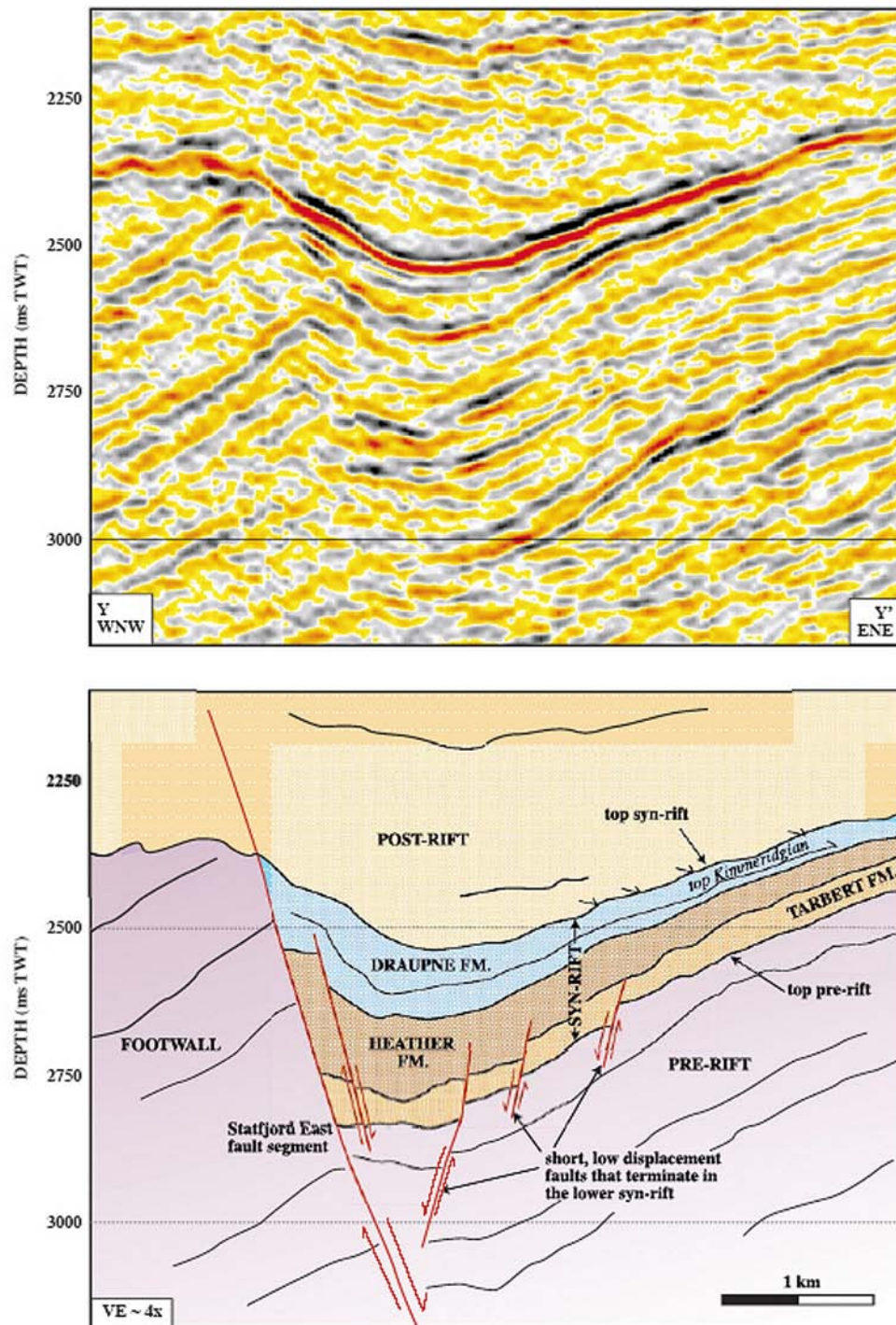


Fig. 104 - Seismic section and interpretation of a growth fault from the North Sea. Notice that the master listric fault is associated to synthetic and antithetic normal faults (after DAVIES *et alii*, 2000).

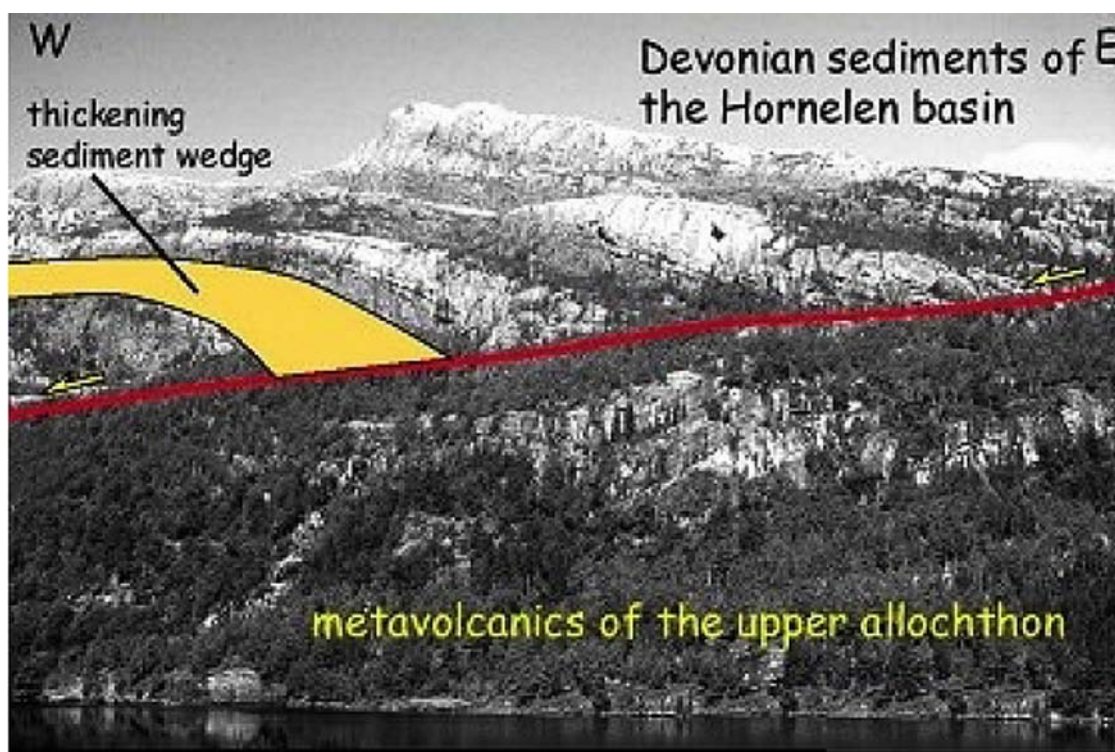


Fig. 105 - Growth normal fault in the Devonian Hornelen Basin, Norway (after DAVIES & REYNOLDS, 1996).

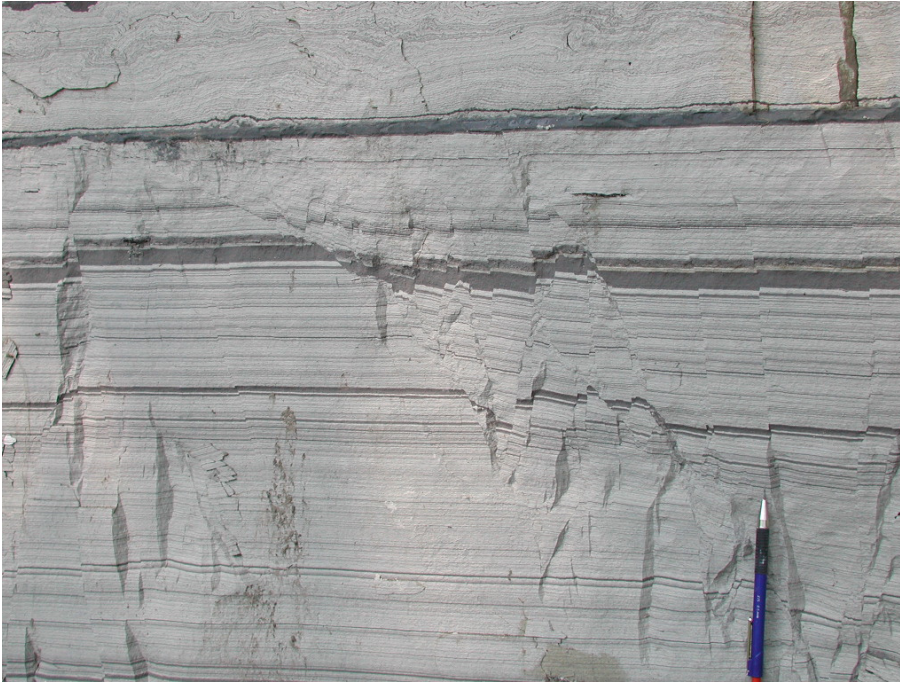


Fig. 106 - Syn-sedimentary normal faults in lacustrine sediments of the Pianico Basin, Lombardy. Courtesy of Fabrizio Berra.

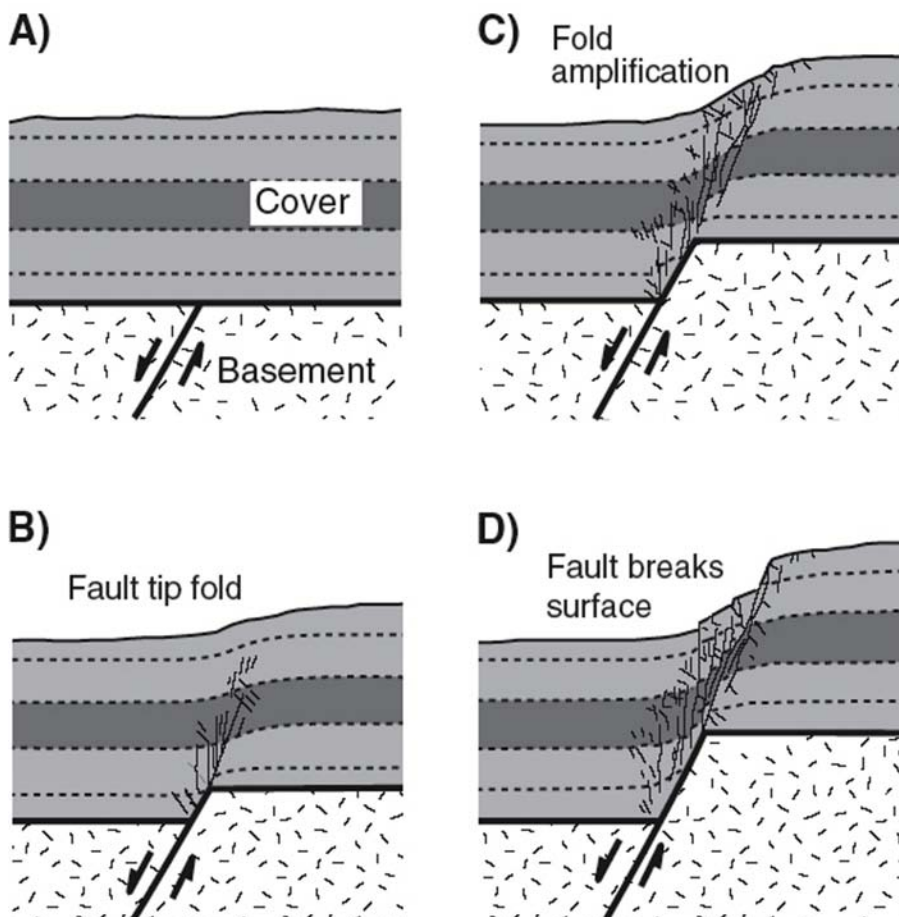


Fig. 107 - Forced folds may develop above blind normal faults. Extensional fault-propagation folds form above steeply dipping normal faults typically, though not exclusively, where there is a distinct mechanical contrast between basement and sedimentary cover or a ductile unit overlies the basement and acts to decouple the basement and the overlying sediments (after GAWTHORPE & LEEDER, 2000).

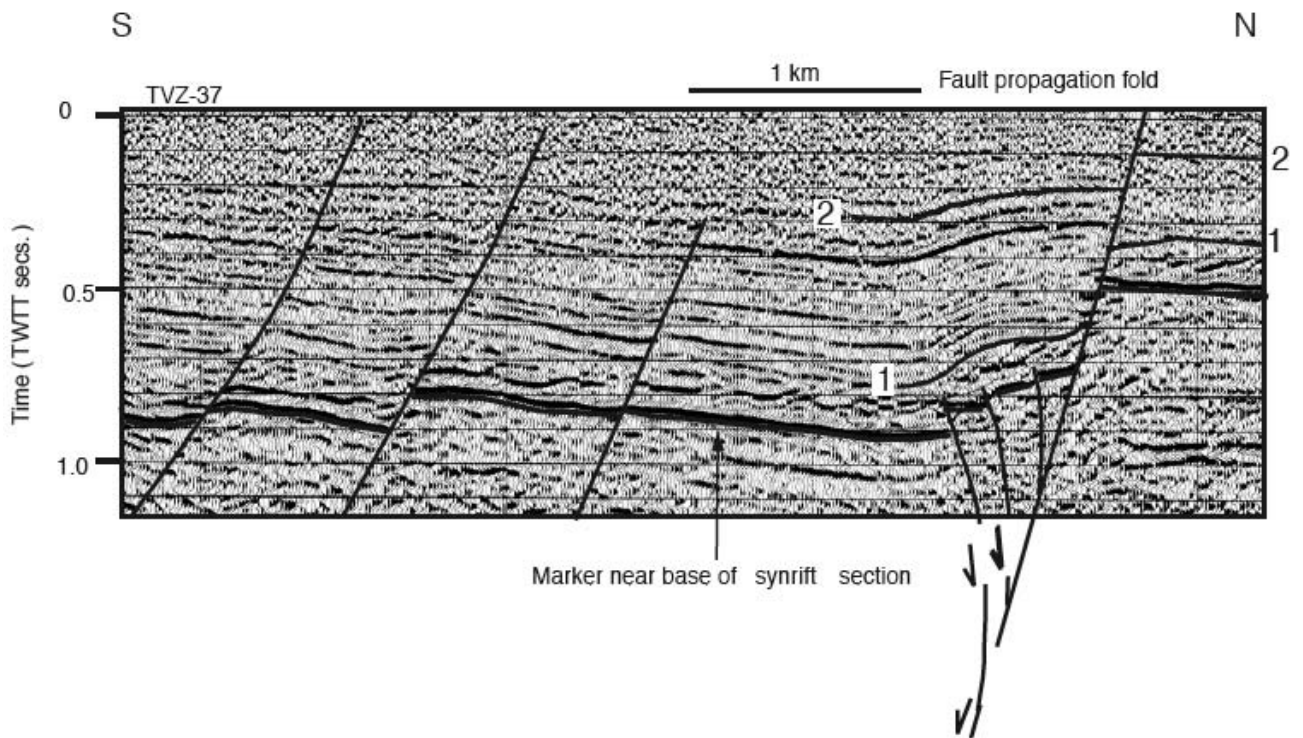


Fig. 108 - Seismic section showing a normal fault-propagation fold developed in the Usungu Flats, Tanzania (after MORLEY, 2002).

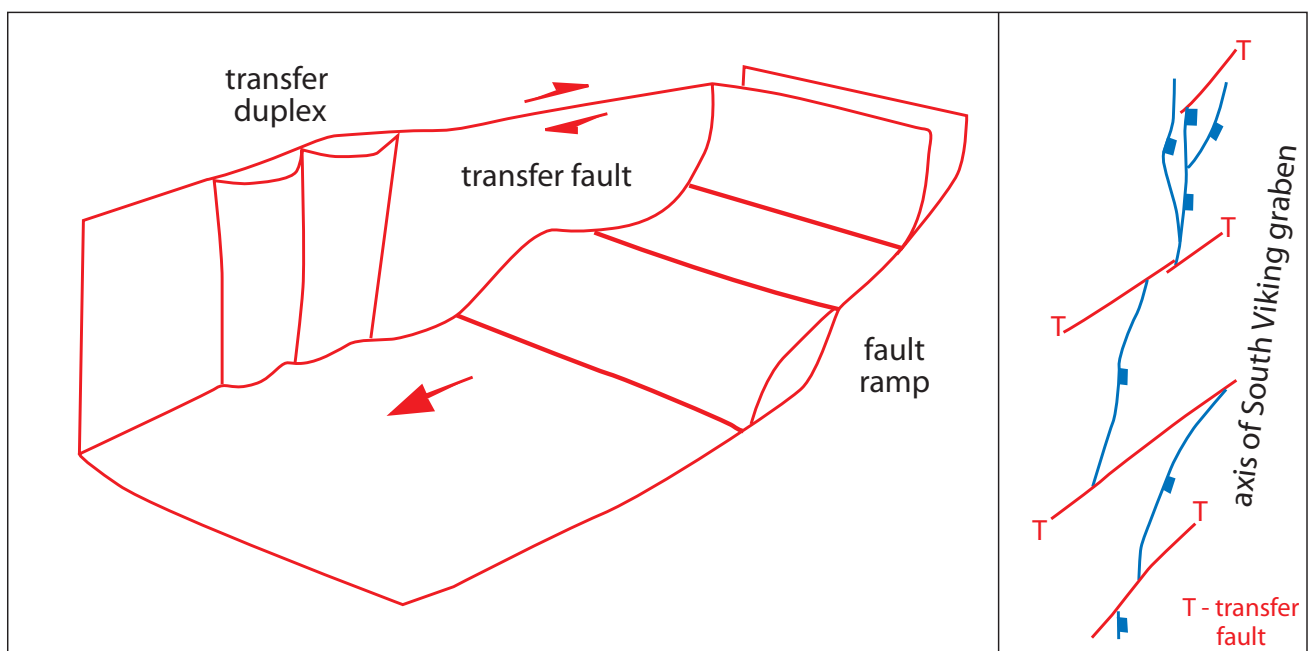


Fig. 109 - The development of mainly strike-slip (transfer) faults may accommodate normal fault segmentation. In this case the displacement between two normal faults is transmitted by hard linkage. The panel to the right shows a tectonic map from the Viking graben showing extensional faults offset by transfer faults (after GIBBS, 1984 and 1990).

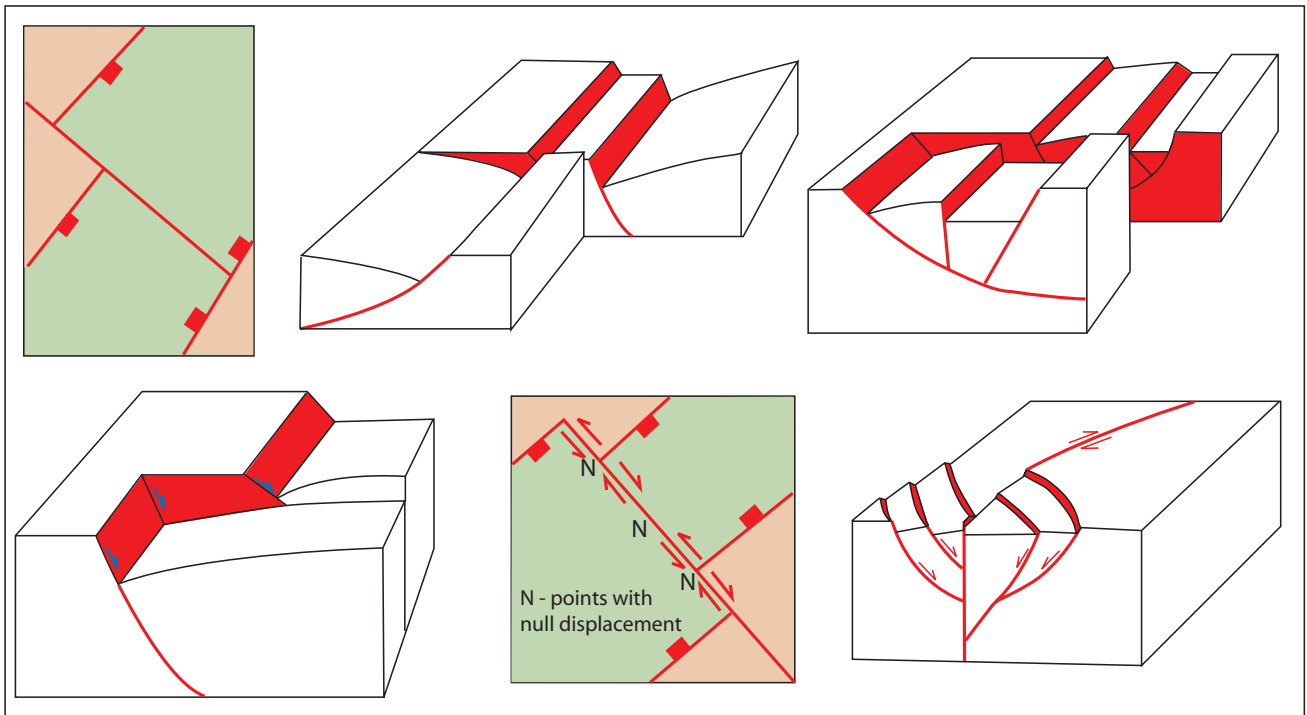


Fig. 110 - Hard linkage structures may link normal faults or semi-grabens with opposing or common dips. After MILANI & DAVISON (1988).

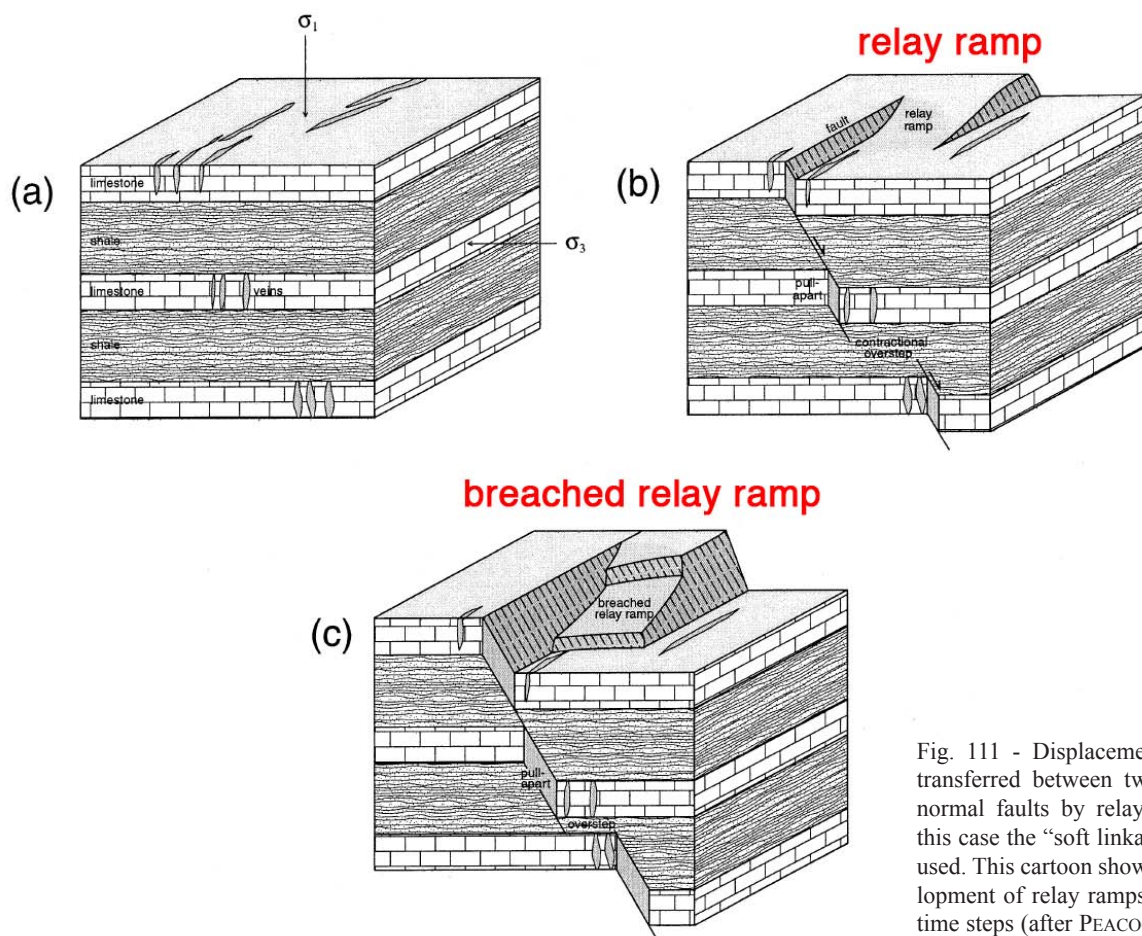


Fig. 111 - Displacement may be transferred between two adjacent normal faults by relay ramps. In this case the “soft linkage” term is used. This cartoon shows the development of relay ramps in various time steps (after PEACOCK, 2002).



Fig. 112 - Relay ramps develop at very different scales. In this case decimeter-scale relay ramps are exposed in limestones, East Quantoxhead, Somerset, UK (after PEACOCK & SANDERSON, 1994).

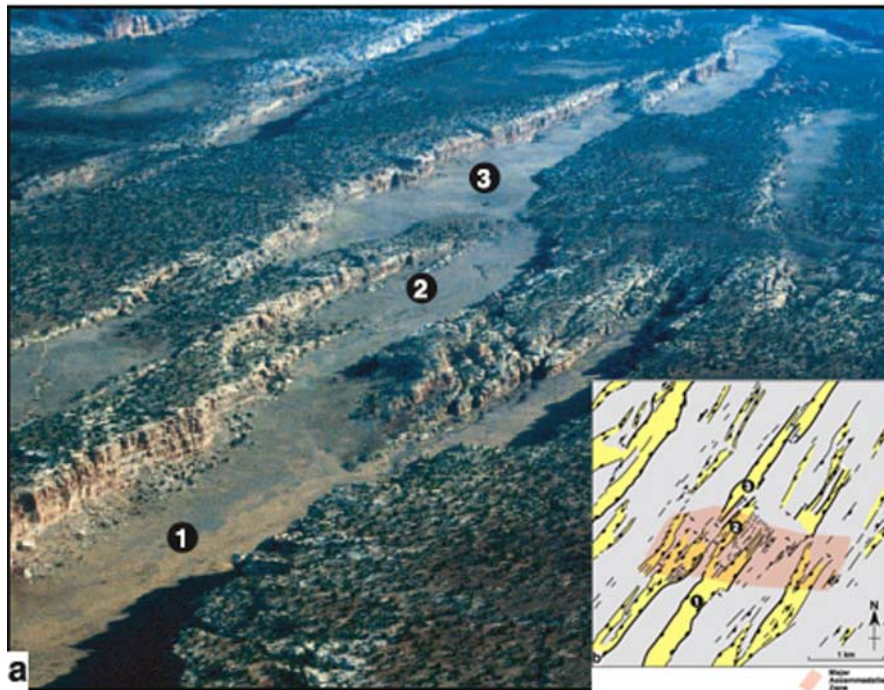


Fig. 113 - Relay ramps develop at very different scales. In this case kilometre-scale relay ramps are imaged by an aerial photograph (the inset is the interpretation) taken in the Canyonlands National Park, Utah, USA. At the terminations of individual grabens, the main faults branch into a series of splays that form relay ramps between overlapping, like-dipping faults (after McCLAY *et alii* 2002).

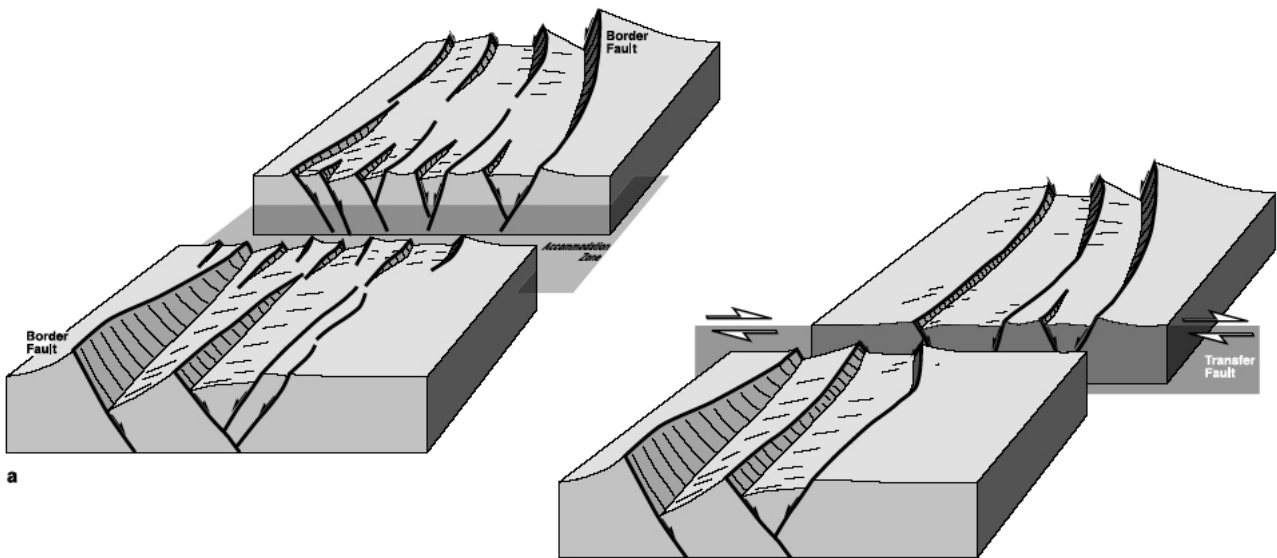


Fig. 114 - Conceptual models of displacement transfer in rift systems. (a) Synoptic model of a low-strain intracontinental rift with along-axis segmentation. Individual half grabens are separated by soft-linked accommodation zones formed by overlapping fault segments. (b) Synoptic model of hardlinked, strike-slip, rift transfer fault system (after McCLAY *et alii*, 2002).

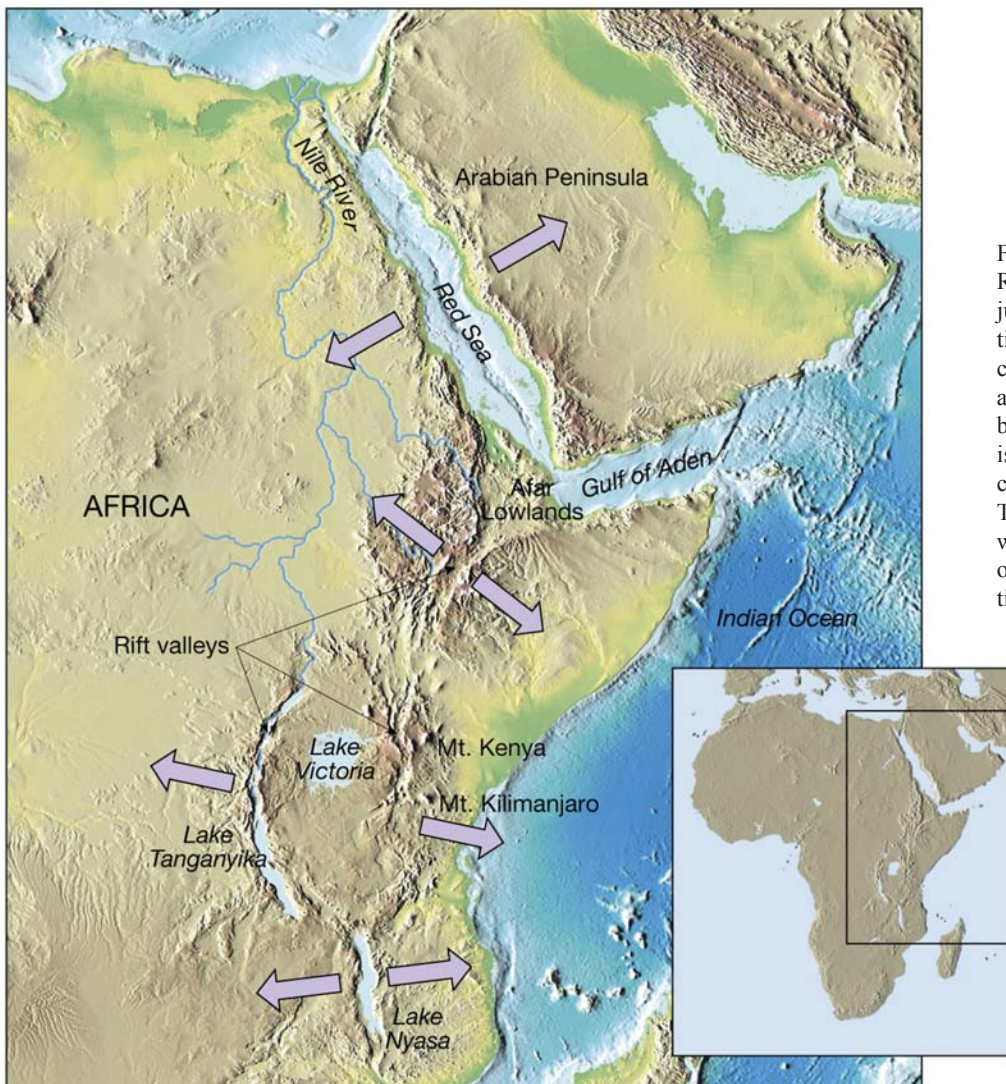


Fig. 115 - The East African Rift system and the Afar triple junction. Notice the organization of the rift system in branches (west and east branches, around the Lake Victoria block) and zones. Each zone is laterally segmented and constituted by semi-grabens. The transfer of extension between adjacent semigrabens occurs through accommodation zones. See next picture.

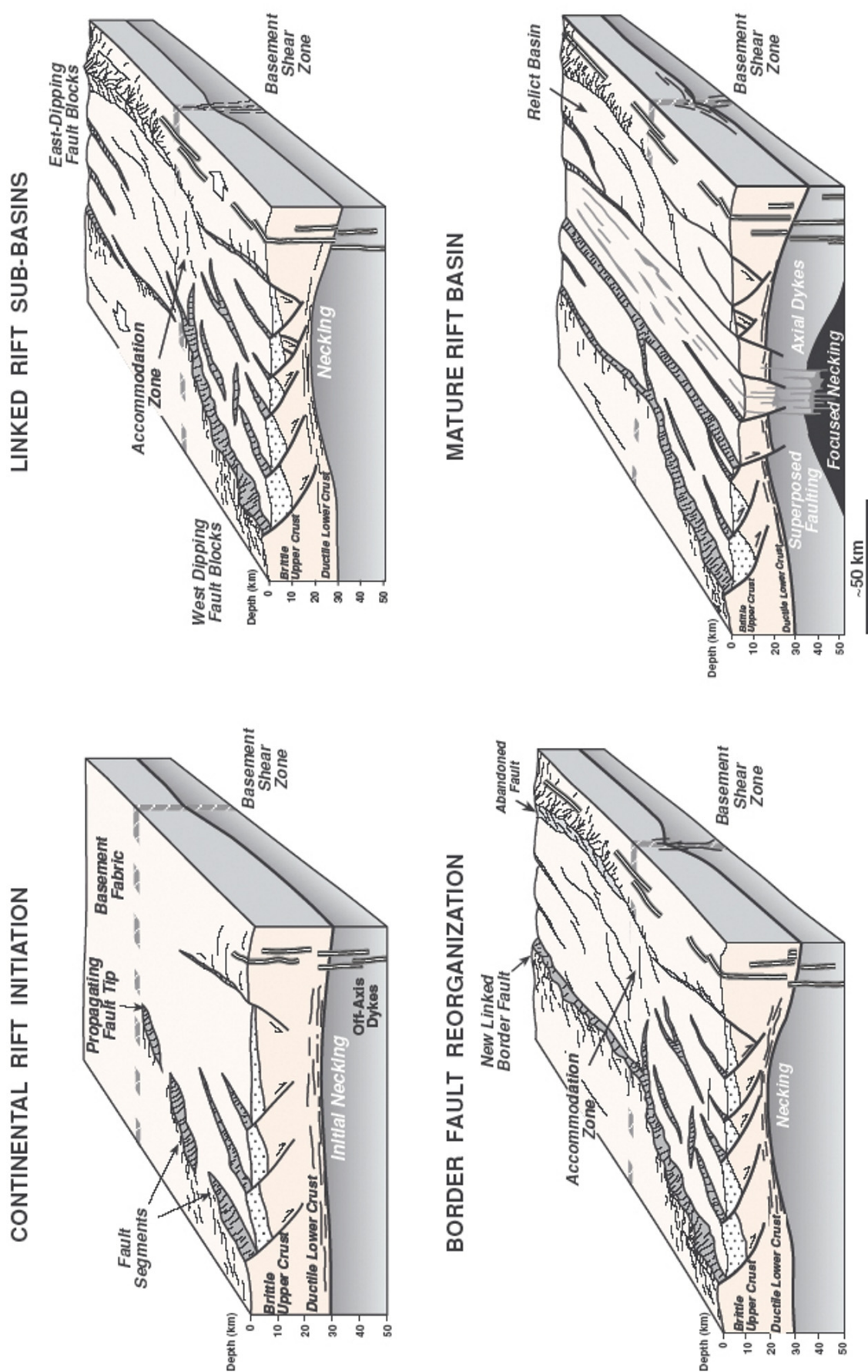
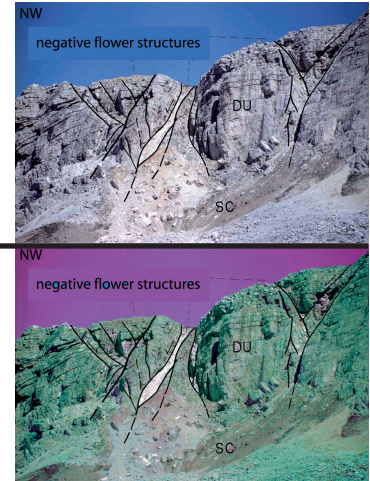


Fig. 116 - Evolutionary model of the Gulf of Suez and the Northern Red Sea system. The various stages of the transition from rifting to drifting are portrayed. Notice the marked asymmetric nature of semi-grabens and the development of accommodation zones in the early stages of rift development (after KHALIL & MCCRAY, 2001).

5. Strike-slip faults



Strike slip fault systems occur in all geodynamic settings, although they are typical of transform plate margins. Strike-slip systems are often segmented and show various fault arrangements (en-echelon, relay, anastomosing or stepping) (fig. 117). Strike slip faults are normally associated to other structures, such as synthetic and antithetic minor strike-slip faults, folds, normal and reverse faults (fig. 118). Oblique strike-slip motions (i.e., displacements characterised by a minor dip slip component) produce transpression (i.e., contractional deformation along the strike-slip fault) or transtension (i.e., dilational deformation along the fault).

In seismic sections strike slip fault zones are characterised by complex flower structures (figs. 119 - 123). Such structures are normally characterised by single or groups of steeply-dipping to vertical faults nucleating from the main strike-slip fault. These faults show either dominantly extensional (negative flower structures) or compressional (positive flower structures) displacements. Flower structures mainly develop at strike-slip fault bends that, depending on fault geometry and sense of shear, can be of two kinds: releasing bends,

associated to extension, and restraining bends, associated to shortening. Fault bends may also be associated to strike-slip extensional or contractional duplexes.

Strike-slip faults are often segmented and fault stepovers occur when single fault segments are arranged in en-echelon geometry. Stepovers of fault segments may drive to the development of contractional areas (restraining stepovers) and extensional areas (releasing stepovers). The most common structures associated to releasing stepovers are pull-apart basins (figs. 124 - 128). At the tips of major strike-slip faults displacements die to zero. Slip is here accommodated by the formation of (both extensional or compressional) faults fans (fig. 129).

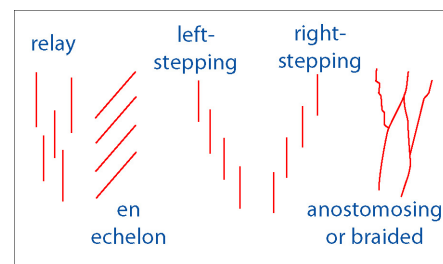


Fig. 117 - Typical geometry of strike-slip fault systems.

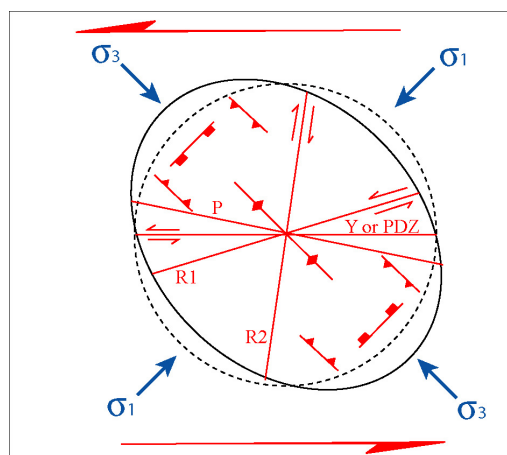


Fig. 118 - Structures associated to strike-slip faults. PDZ (principal displacement zone) or Y-Shear is the principal strike-slip zone. R1 (synthetic Riedel, at 15-20° to the PDZ) and R2 (antithetic Riedel at 70-75° to the PDZ) shears develop in response to Navier-Coulomb shear failure with respect to σ_1 and σ_3 . P synthetic shear develops at low angle (15°) to the PDZ as a consequence of the rotation of the principal stress axes at the tips of R1 shears as faulting develops. Minor thrust and normal faulting also may develop.

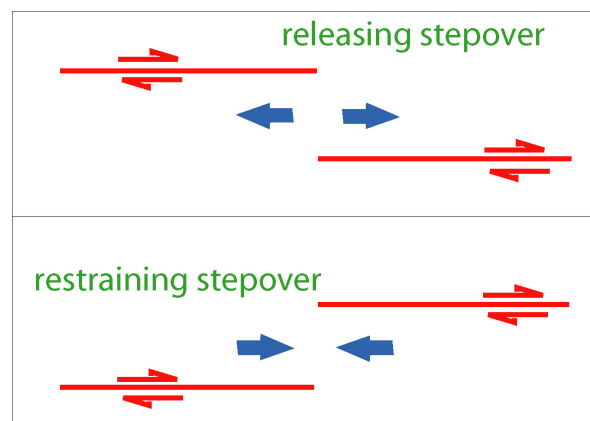


Fig. 120 - Strike slip segmentation and en-echelon stepover geometries may cause local shortening (restraining stepovers) or stretching (releasing stepovers). Stretching areas associated to releasing stepovers are called pull-apart basins, whereas the opposite restraining stepovers generate push-ups.

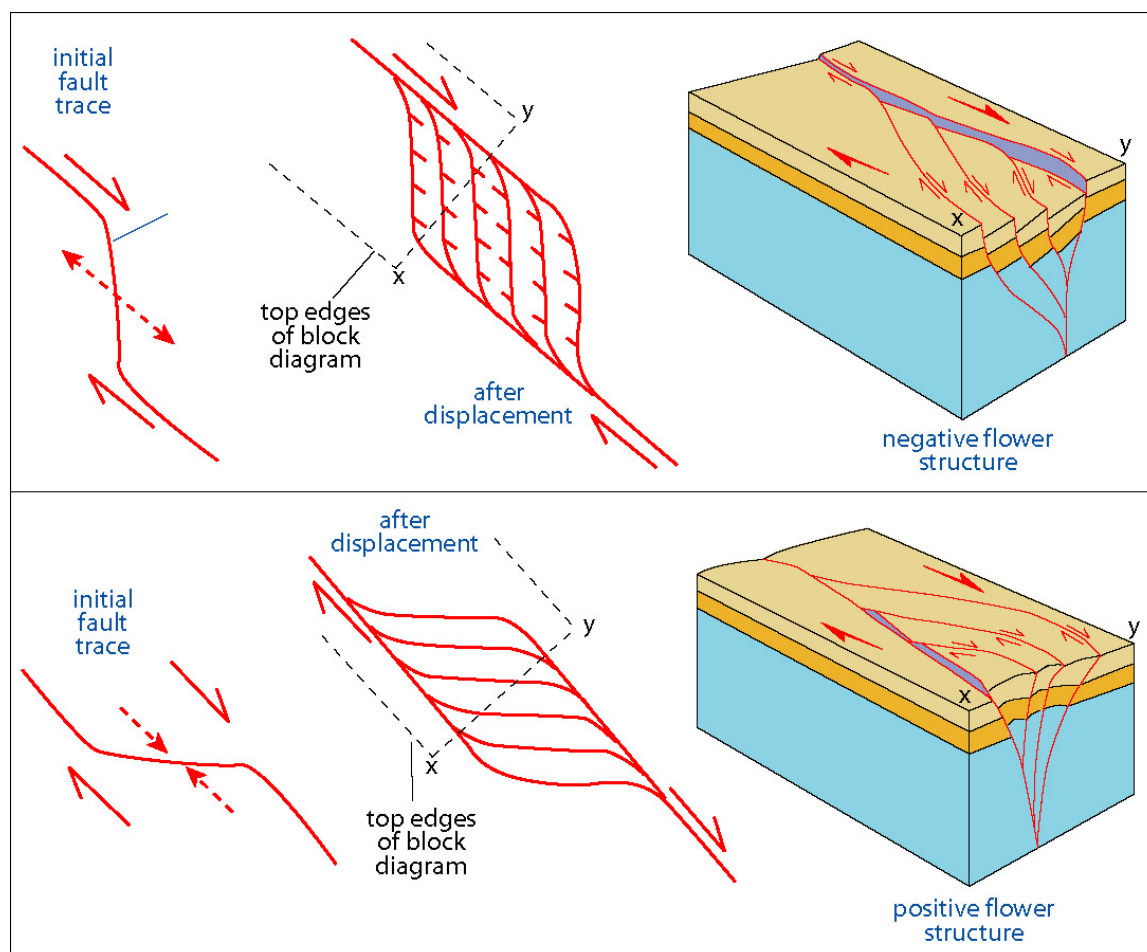


Fig. 119 - Undulated strike-slip faults give rise to local extensional (releasing bends; upper panel) or compressional (restraining bends; lower panel) zones. Releasing bends are associated to negative flower structures, whereas restraining bends to positive flower structures. In map view, these features are also called strike-slip duplexes. Modified after TWISS & MOORES (1992).

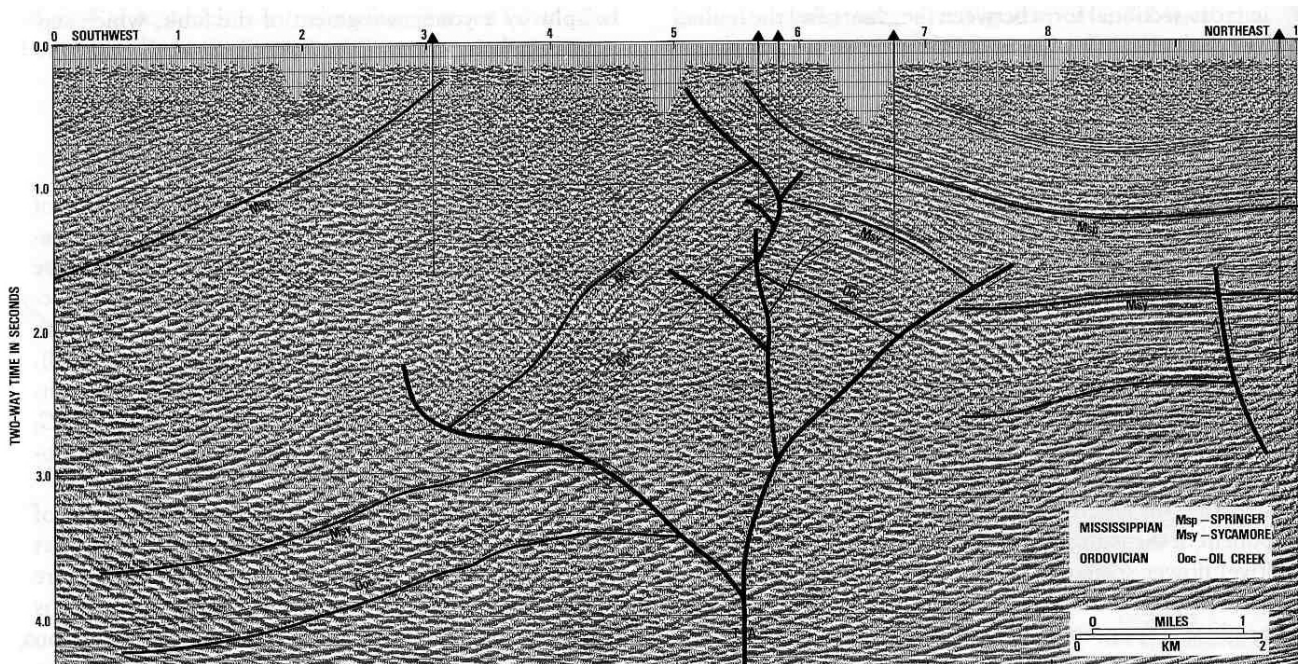
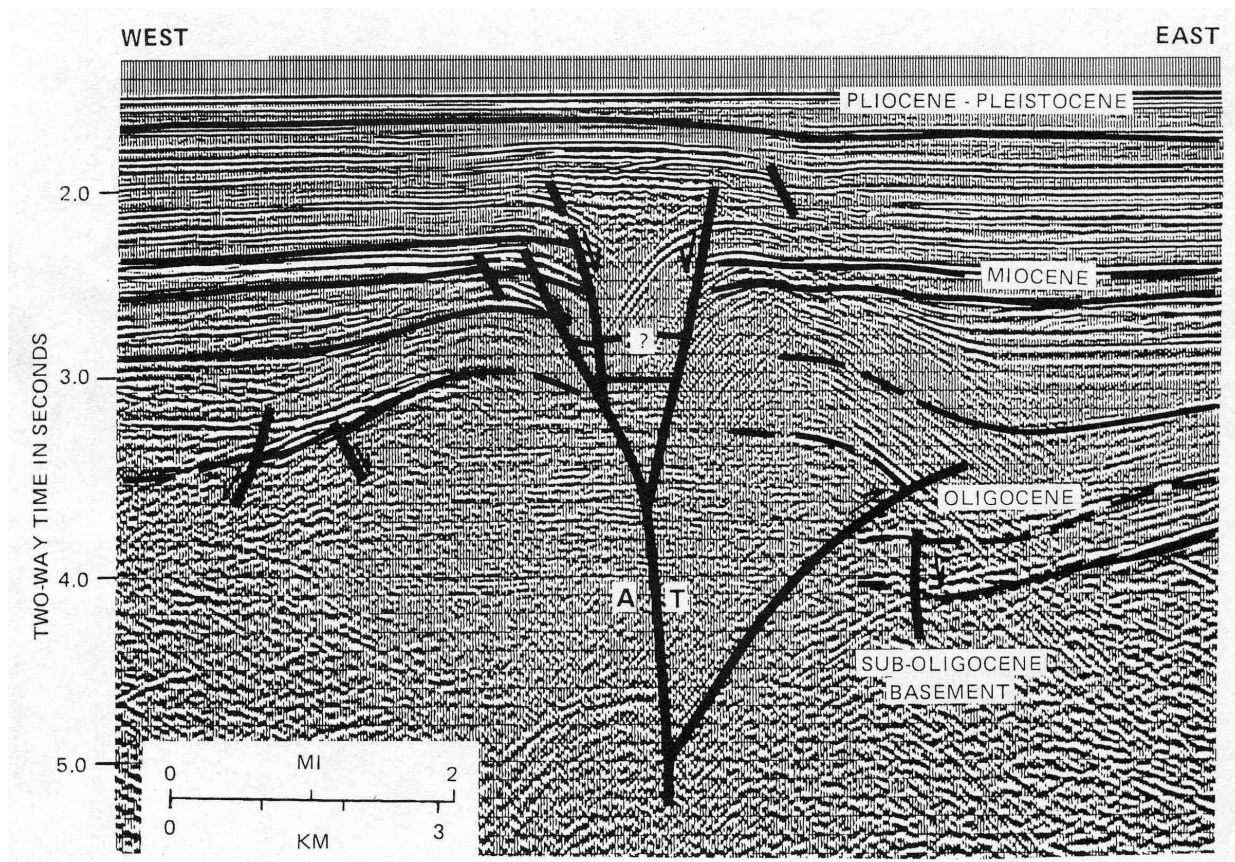


Fig. 121 - Seismic sections showing negative (above) and positive (below) flower structures. After HARDING (1983) and HARDING *et alii* (1983), in TWISS & MOORES (1992).

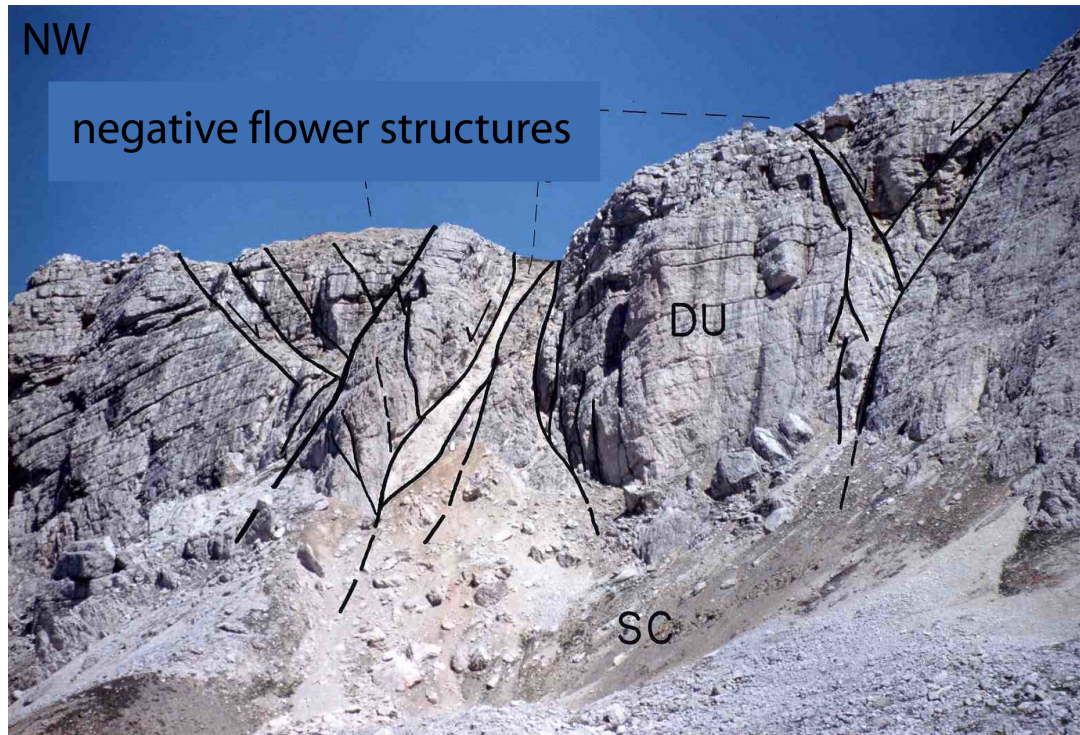


Fig. 122 - Negative flower structure related to sinistral strike-slip alpine tectonics in the Settsass Massif (Dolomites).

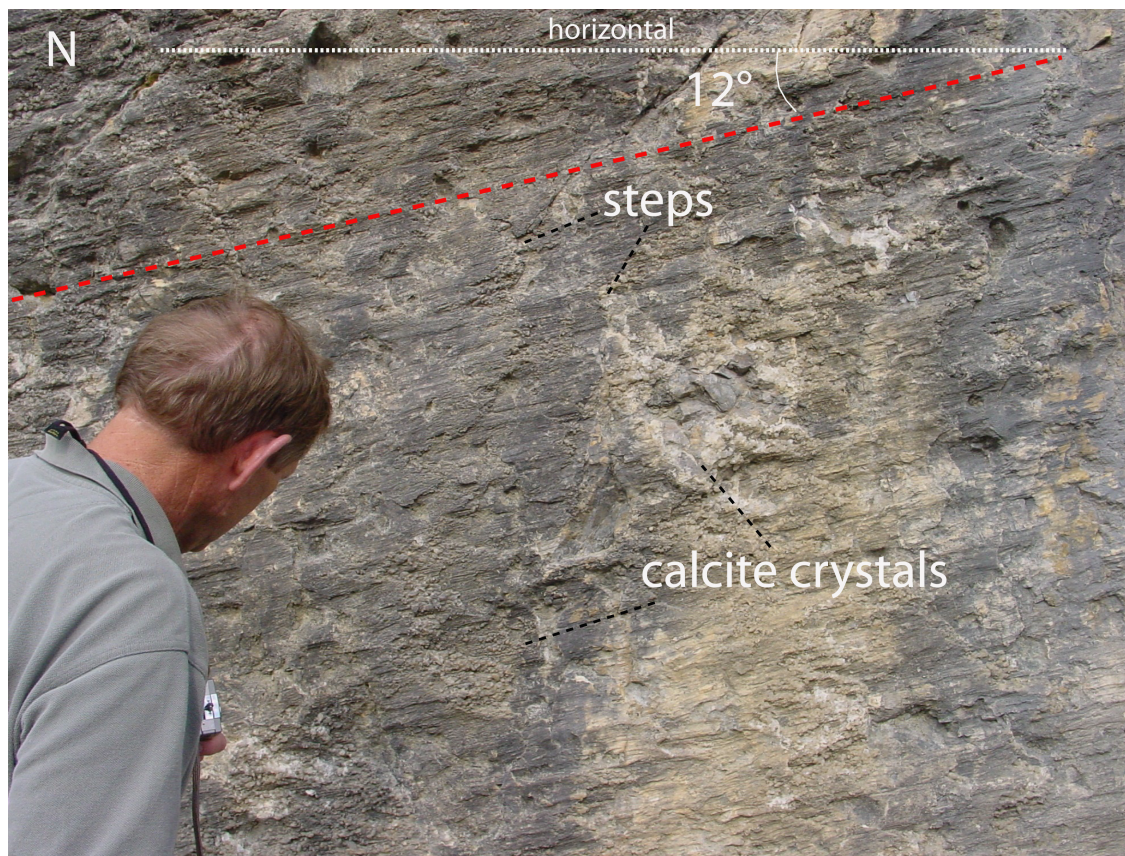


Fig. 123 - Transtensional N-S trending left-lateral fault in the Caotico Eterogeneo. Slickensides are more developed in conglomerates than in more homogeneous rocks. The striations have a pitch of 12° left (northward). The left-lateral sense of motion is indicated by the steps in the fault plane, and by the crystals of calcite grown in their shadow. Road between Caprile and Selva di Cadore (Dolomites). Casey Moore for scale.

Fig. 124 - The Angara Graben is a pull apart basin northeast of Lake Baikal developed on a left stepover in a left-lateral strike slip zone (after TAPPONNIER & MOLNAR, 1977).

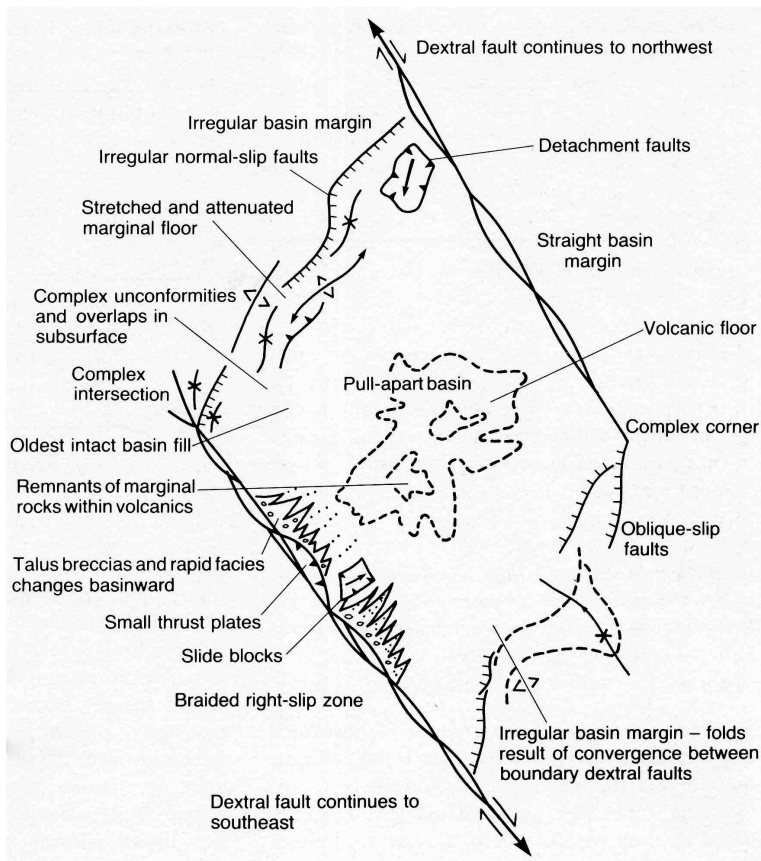
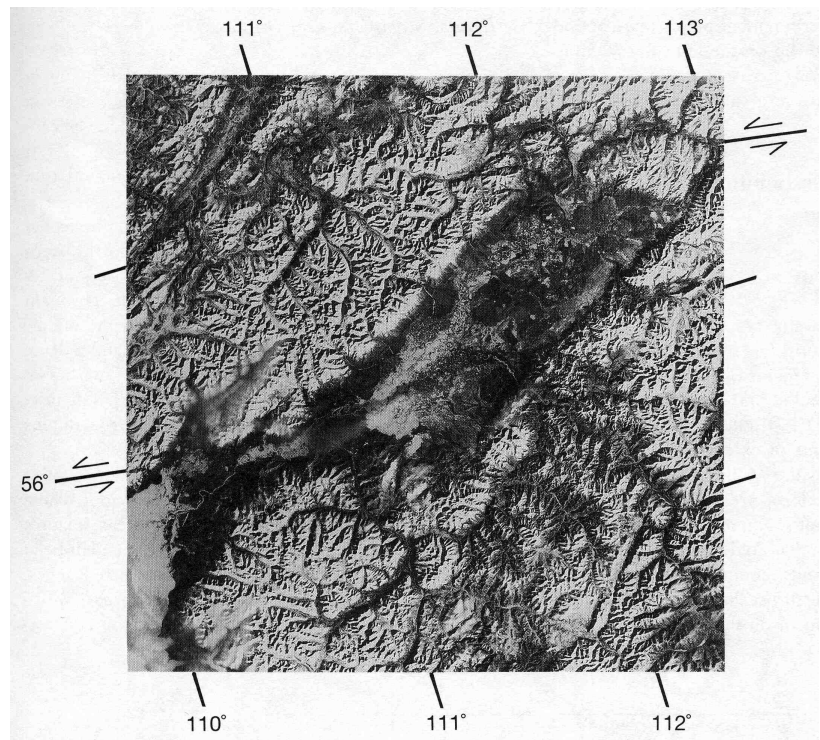


Fig. 125 - Tectonic structures and sedimentary features typical of pull apart basins. Subsidence may be abrupt and very fast. Volcanism may also be associated to extensional tectonics (after CROWELL, 1974).

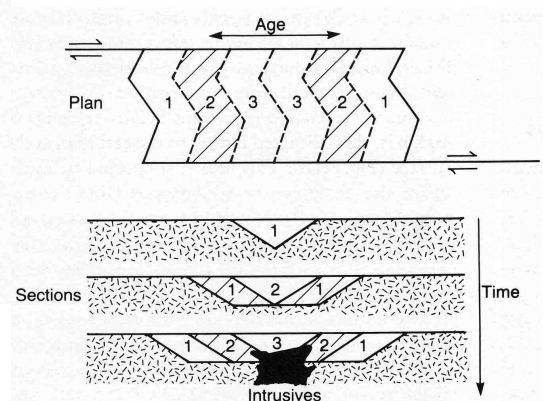


Fig. 126 - Stages of formation of a pull-apart basin (after KEAREY & VINE, 1992).

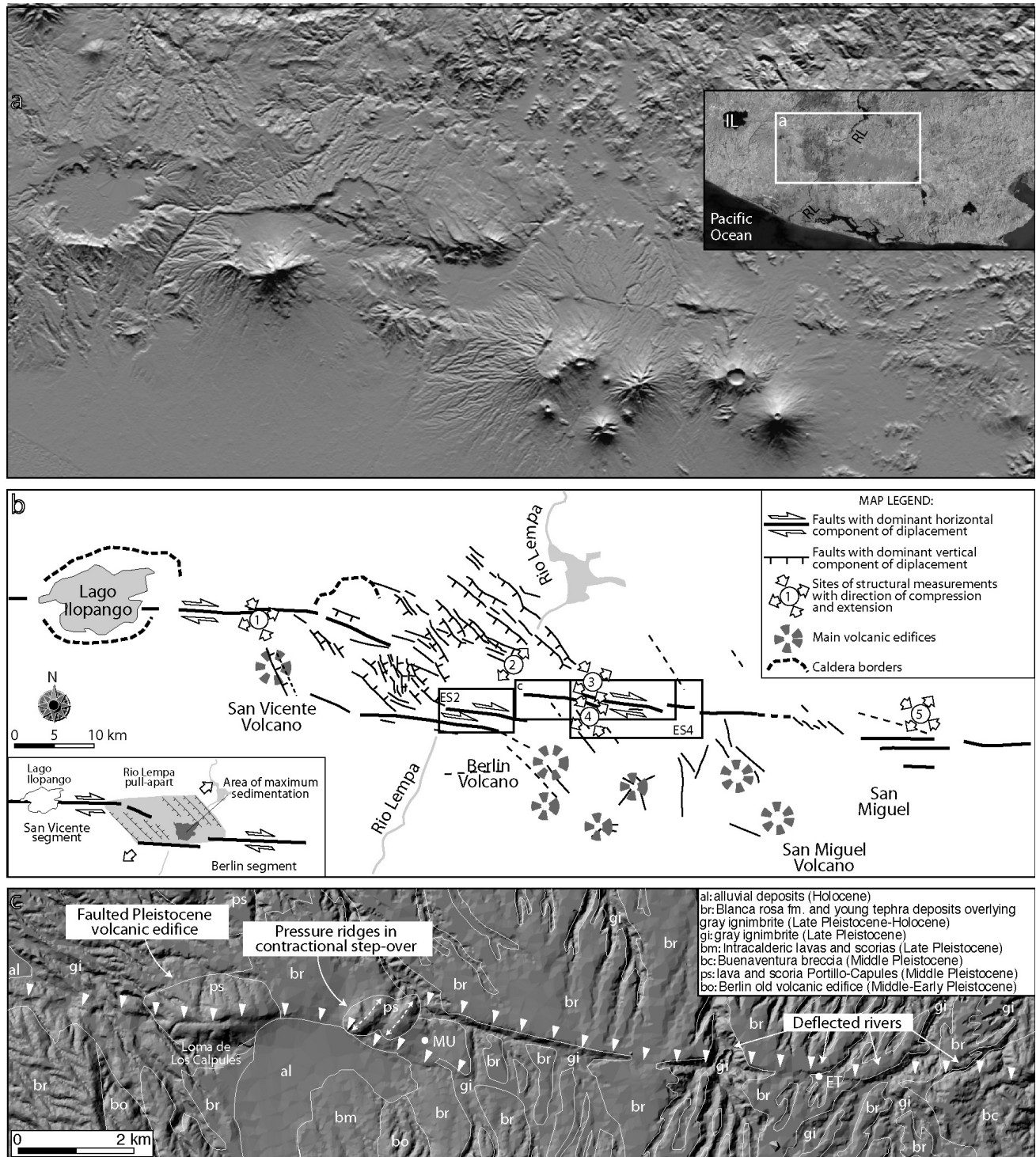


Fig. 127 - Along the El-Salvador fault zone, a major strike-slip fault system, the Rio Lempa pull-apart basin, developed in Quaternary times. (a) Digital elevation model of the region. (b) Line-drawing of the active structures forming the El Salvador Fault Zone (ESFZ) in the area, with also reported palaeostress orientations. Inset shows the interpretation of the regional fault pattern. (c) Geological map superimposed on a DEM of the region. Arrows indicate the fault trace. After CORTI *et alii* (2005).

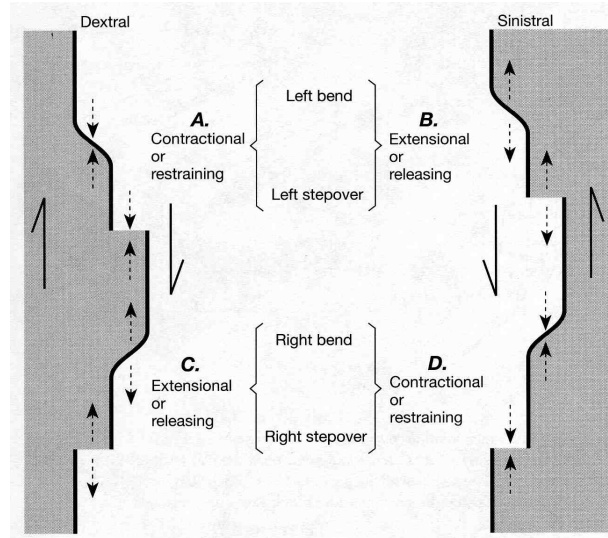


Fig. 128 - Terminology and stress state for bends and stepovers along strike-slip fault systems (after TWISS & MOORES, 1992).

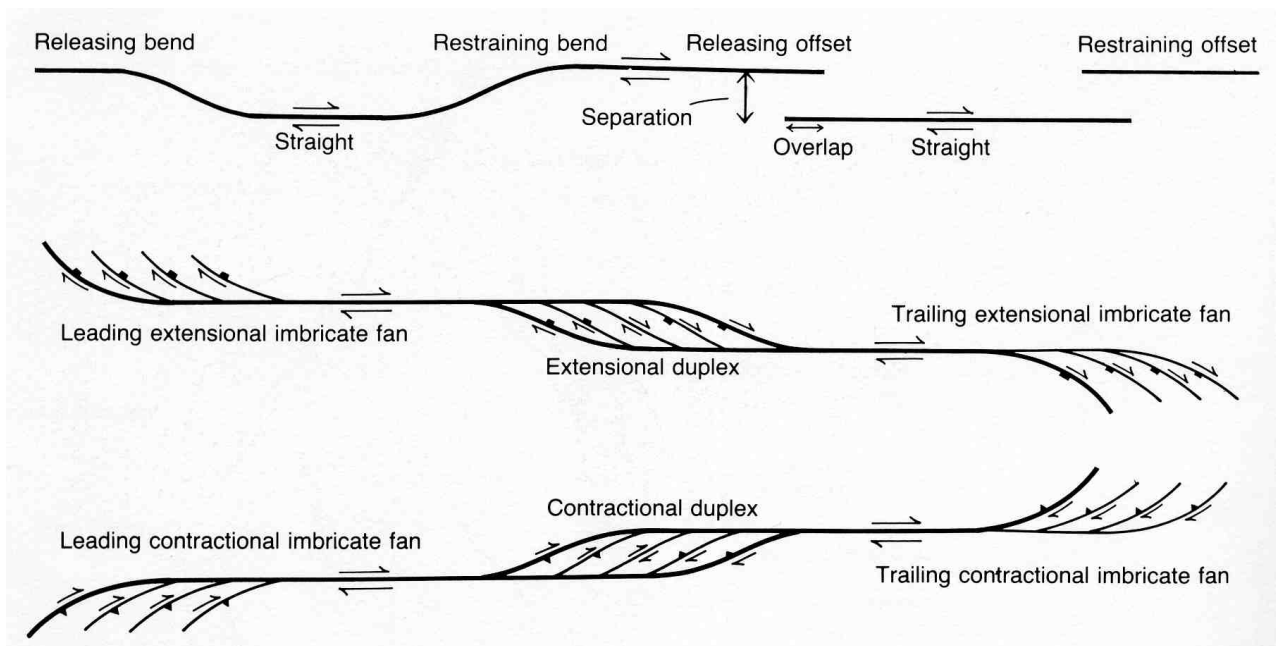
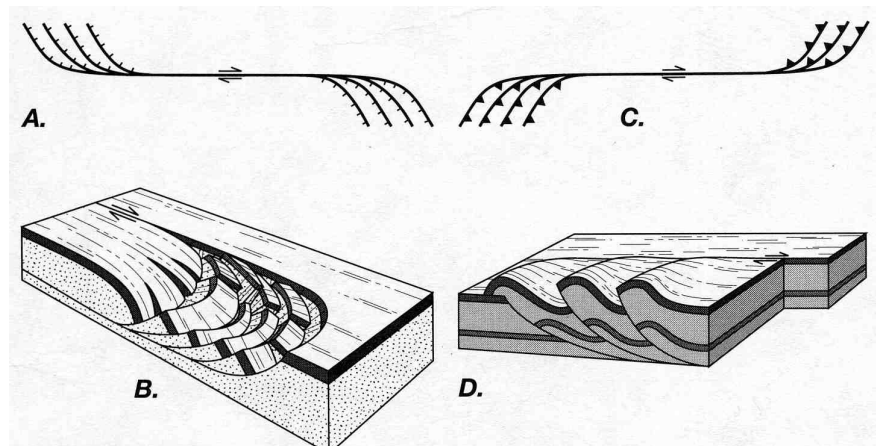
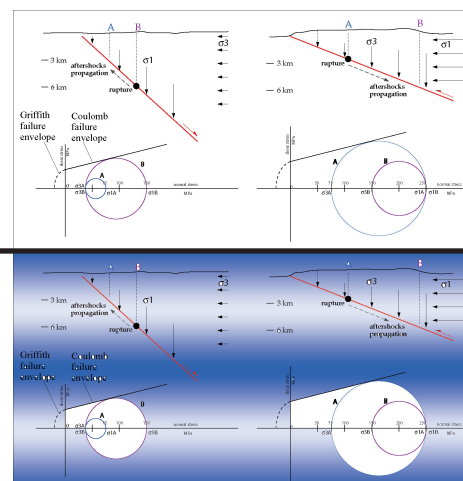


Fig. 129 - Strike-slip fault systems may include fault geometries similar to those of duplexes in contractional terrains. In this case however, the faults are subvertical and characterized mainly by strike-slip motion. Duplexes, either extensional or contractional, form at fault bends. At the termination of major strike slip faults, displacement may be accommodated by extensional (a,b) or contractional (c,d) imbricate fan structures. After WOODCOCK & FISHER (1986) and TWISS & MOORES (1992).



5.1 Opposite migration of seismicity



CARMINATI *et alii* (2004) showed that, along thrust faults, shallow initial rupture and downward migration of seismicity generally occur. On the contrary, along normal faults, rupture generally occurs at deeper levels and aftershocks are shallower. This opposite behavior is exemplified by Figs. 130 and 131 that show the opposite migration of seismicity associated to the Irpinia 1980 normal fault-related earthquake sequence and to the Friuli 1976 earthquake sequences occurred in a compressive environment.

This reverse behavior can be explained by a simple fault mechanical model.

The following discussion, based on Fig. 132, assumes that the pore fluid factor λ (equal to pore fluid pressure divided by the overburden pressure) is approximately constant with depth. It should be, however, noted that major differences from model predictions would occur with λ varying significantly with depth. Overpressured compartments bounded by sealing horizons (e.g., clay rich stratigraphic horizons or impermeable faults) are typical in sedimentary basins.

In crystalline rocks the base of the upper crustal hydrostatic fluid pressure regime is likely to be limited, during interseismic periods, to the first 3-7 km. This is in agreement with recent data from deep wells. Townsend and

Zoback (2000) analysed in situ stress and permeability measurements from deep (down to 9.1 km) boreholes and concluded that both these datasets suggest hydrostatic fluid pressures.

According to the Anderson fault theory, the vertical stress is the least principal stress in compressional regimes, whereas it is the maximum principal stress in extensional tectonic regimes.

Let us consider the state of stress of two points (A and B) positioned at different depths along hypothetical thrust and normal faults (Fig. 132).

Since A is shallower than B, the vertical load increases from point A to point B. It is here further assumed that the horizontal stress remains constant with depth. In compressional regimes the vertical load is σ_3 . Moving upward from location B to A, the differential stress (the diameter of the Mohr circle) increases.

As a consequence, moving upward along a thrust fault, the decrease of σ_3 enlarges the Mohr circle making the fault plane more unstable.

This means that rupture along the fault is likely to occur at shallower depths and that both the fracture and early aftershocks are expected to propagate downward, consistently with the

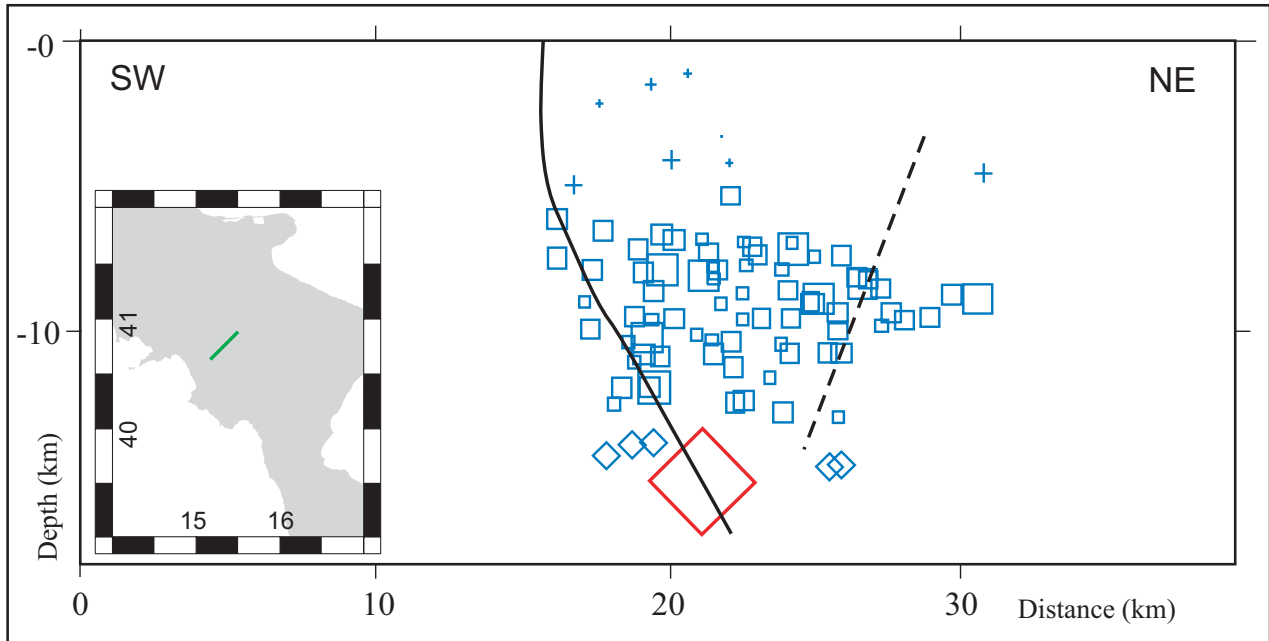


Fig. 130 - Cross-section of the Irpinia 1980 normal fault-related earthquake sequence. The largest red square is the mainshock. The blue squares are aftershocks. The earthquake was generated by two normal faults dipping north-eastward and one conjugate, and was characterised by M_s 6.9. The earthquake showed the largest moment release at a depth of 8-13 km and a possible nucleation at about 10 km. Most of the aftershocks were generated in the hanging wall of the main fault, between this and an antithetic normal fault dipping to the south-west. All the aftershocks occurred at depths (3-10 km) shallower than the mainshock. Modified after CARMINATI *et alii* (2004).

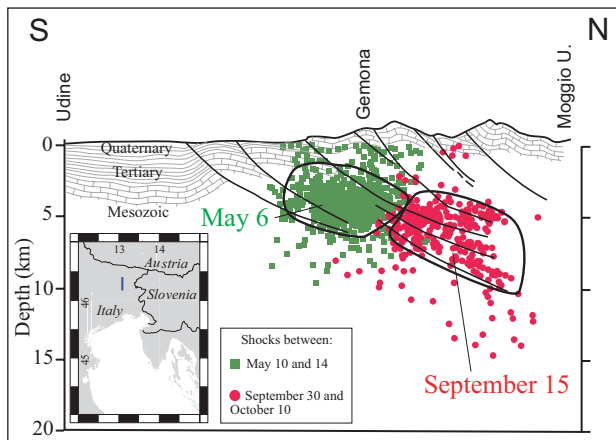


Fig. 131 - Cross-section of the Friuli 1976 earthquake sequences occurred in a compressive environment. The seismicity occurred in two main episodes, May 6 and September 15, with magnitude 6.4 and 6.1 respectively. The focal mechanisms are mainly compressional, with a slight transpressional component. They were associated with N-dipping thrust planes in the eastern part of the Southern Alps, at the intersection with the Dinarides thrust belt in north-east Italy. The maximum energy released by the aftershocks of the May 6 earthquake was very shallow, between 2 and 8 km. The highest energy release density has been evaluated to be located at a depth of about 4 km. The epicentres of the later September quakes and related aftershocks were about 8 km northward. The September hypocentres were deeper (down to 16-17 km) and characterised by a maximum energy release density at about 5-6 km. The timing of groups of events clearly shows a deepening of seismic activity with time. Modified after CARMINATI *et alii* (2004).

observations outlined above. On the other hand, if a small earthquake occurs at greater depths, it is unlikely to propagate upward and to grow into a larger one.

In extensional regimes the opposite occurs. The vertical load is σ_1 . Moving from location B to A the differential stress decreases. The decrease of σ_1 diminishes the Mohr circle making the fault plane more stable at shallower depth. As a consequence rupture is expected to occur, along normal faults, at deeper depths and early aftershocks are expected to propagate upwards, as observed in several natural cases.

Several researchers have proposed mechanical models assuming that non tectonic horizontal stress varies as $\sigma_h = [\nu / (1 - \nu)] \sigma_v$ (Poisson effect, see e.g., TWISS & MOORE, 1992), where ν is the Poisson's ratio (values between 0.25 and 0.33 are common for rocks). According to this relation, assuming $\nu = 0.25$, the non-tectonic component of horizontal stress is $\sigma_v/3$.

This relation is based on the assumption that the uppermost brittle crust behaves elastically

and upper crustal rocks are laterally constrained (and therefore the horizontal strain is imposed equal to zero). Since we deal with the shallow brittle portion of the crust such

assumptions seem to be reasonable. Fig. 133 shows that, even considering a horizontal stress growing with depth, the above discussion holds.

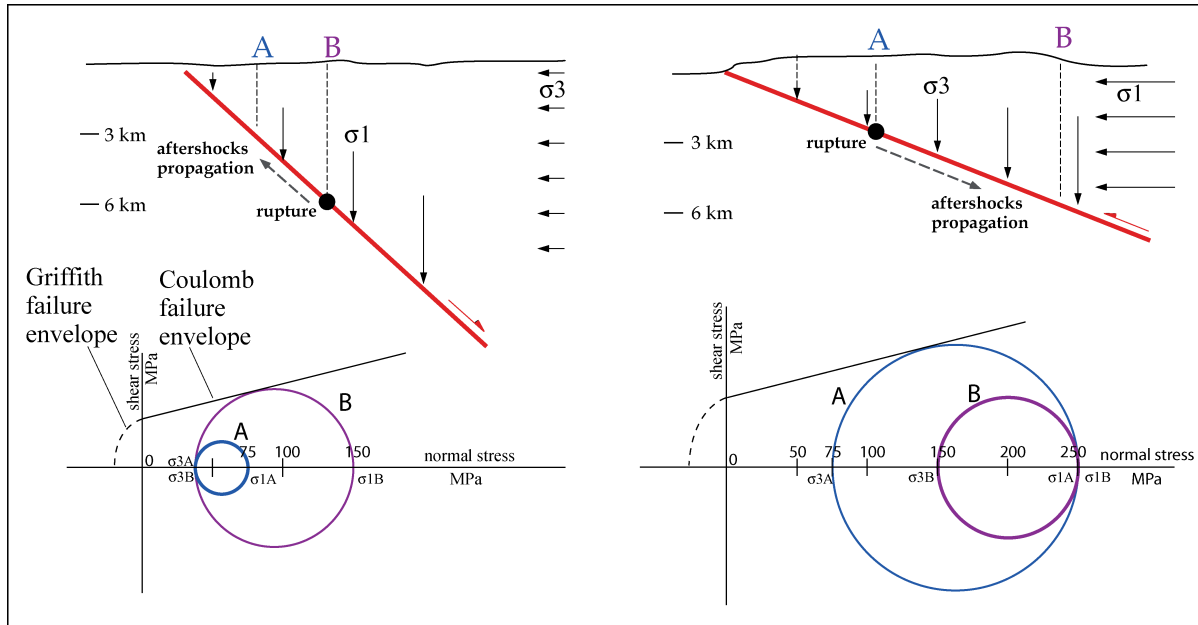


Fig. 132 - Left, sketch and Mohr diagram of the variation of σ_1 (vertical load) and σ_3 (horizontal load) along normal faults. Right, sketch and Mohr diagrams of the variation of σ_3 (vertical load) and σ_1 (horizontal load) along thrust faults. For the sake of simplicity horizontal stress is assumed to remain constant with depth. It is shown in the next figure that such a rough assumption does not hamper the validity of the model. Along thrust faults, shallow initial ruptures and downward migration of seismicity is more likely. On the contrary, along normal faults, rupture should generally occur at deeper levels and aftershocks are expected to be shallower.

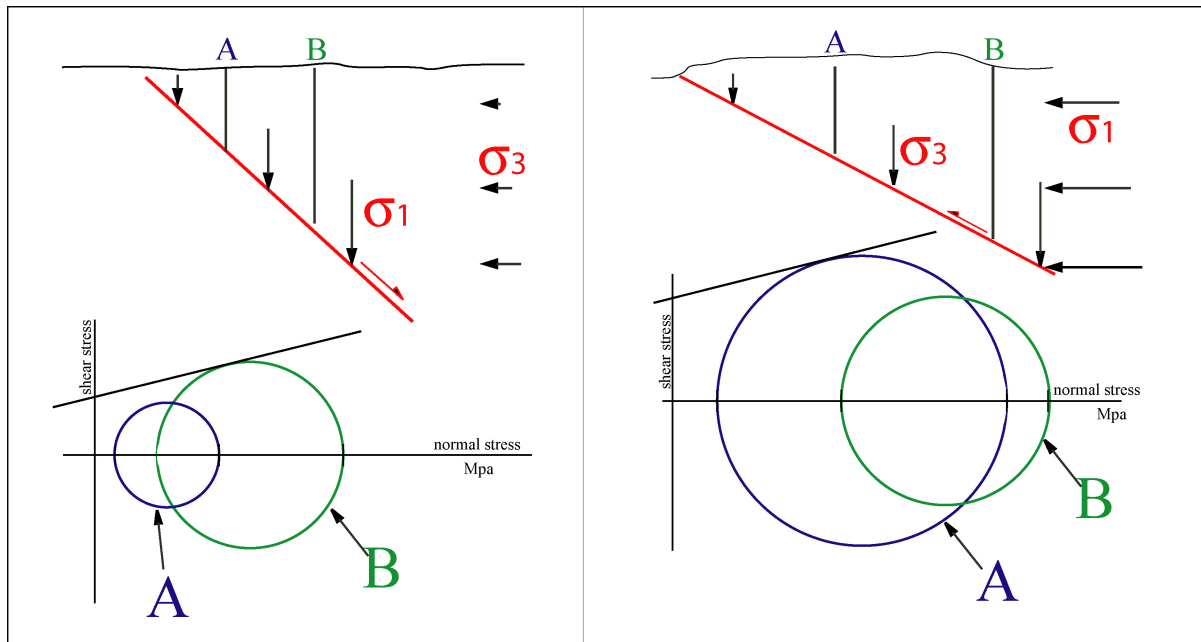
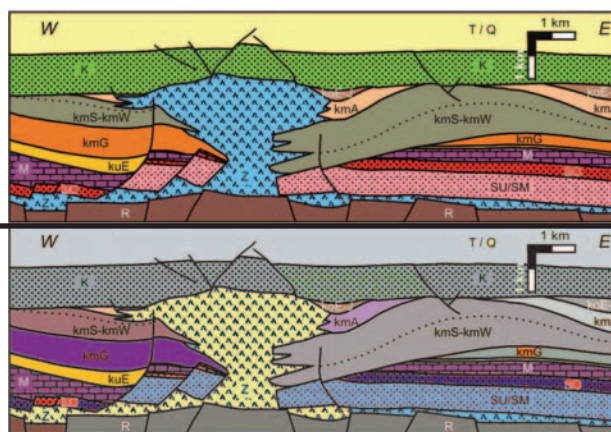


Fig. 133 - Left, sketch and Mohr diagram of the variation of σ_1 (vertical load) and σ_3 (horizontal load) along normal faults. Right, sketch and Mohr diagrams of the variation of σ_3 (vertical load) and σ_1 (horizontal load) along thrust faults. The horizontal stress increases with depth according to the Poisson effect. Along thrust faults, shallow initial ruptures and downward migration of seismicity is more likely. On the contrary, along normal faults, rupture should generally occur at deeper levels and aftershocks are expected to be shallower. Modified after CARMINATI *et alii* (2004).

6. Salt tectonics



Salt and evaporites in general deposited as the intermediate layer of passive continental margins (fluvial red beds, evaporites and carbonates). At depth deeper than ca. 1000 m salt rocks are less dense than common sedimentary rocks. This produces buoyancy forces that, when associated to triggering processes (e.g., faulting) may generate the upwelling of salt (figs. 134 - 137). Salt structures may have point sources (producing salt pillows or diapirs) or line sources (producing salt walls or salt anticlines).

Diapirs form in any tectonic environment (fig. 138) (compression, extension, strike-slip) and are longlasting features, being active as long they are loaded and gravitationally unstable. Salt is the component of the sedimentary cover that is characterised by the shallowmost brittle-ductile transition. Salt layers normally behave as detachment layers even at shallow depth. In passive margins, a basinward tilting of the sedimentary cover resting on salt layers normally induces gravitally driven downslope sliding of the sediment succession. This typically occurs on the two conjugate margins of the Southern Atlantic Ocean (i.e., along the Brazilian Margin and in the Kwanza Basin, in the Angolan offshore) (figs. 139 - 142). Passive

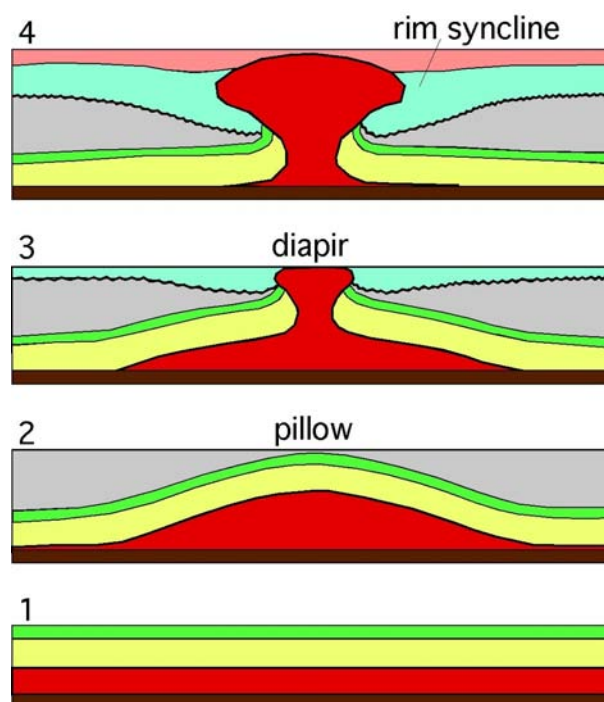


Fig. 134 - Classic model of salt (red layer) evolution when loaded. First it forms a pillow uplifting the overlying cover (2). Then the diapiric piercing starts (3) and the mother salt layer is eventually entirely evacuated (4) to generate a subsidence around the diapir and producing a basin surrounding the diapir (rim syncline). Note the yellow layer which is first uplifted (pillow stage) determining a thinning of the growth (gray) strata. Then it subsides (diapiric stage) forming an overlying thickening of the cover. An unconformity separates the two stages at the base of the azure (after TRUSHEIM, 1960).

margins affected by gravity salt tectonics are characterised by three major domains: 1) raft domain in the internal part (close to the continent), with sedimentary blocks bounded by listric normal faults rooted in a shallow detachment level characterised by the occurrence

of remnant bodies of salt; 2) a diapir domain in the middle part, characterised by wide and numerous diapirs; 3) a salt nappe domain, close to the abyssal plain, characterised by trusts and folds, occurring where the sliding sediments accumulate.

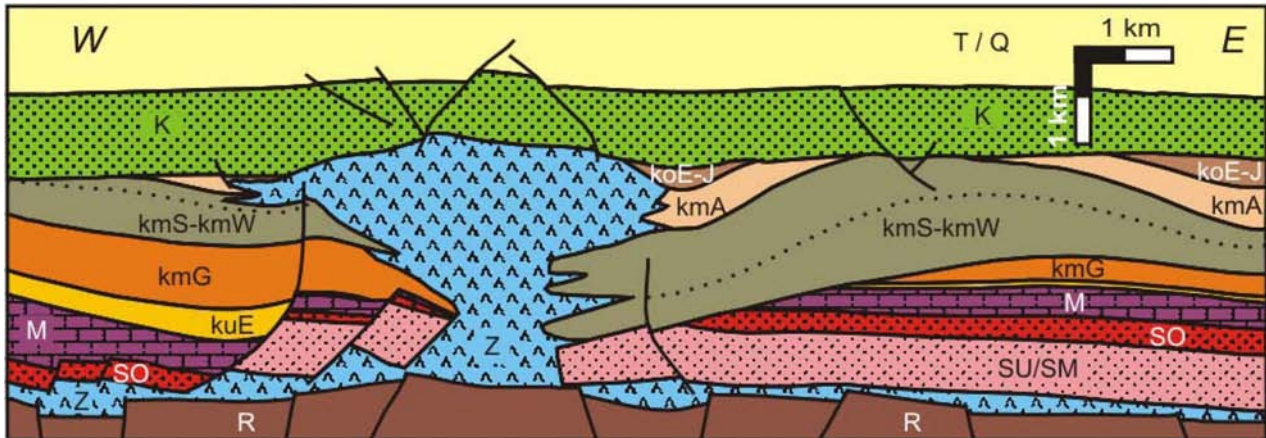


Fig. 135 - Example of diapir from the Permian Zechstein salt in northern Germany after MOHR *et alii* (2006). Note the two major unconformities, one at the base of the Cretaceous (K), and a deeper one at the base of the kmS-kmW, marking the transition between the pillow stage and related uplift producing erosion, followed by the rim syncline which occurred with the evacuation of the salt from the mother layer.

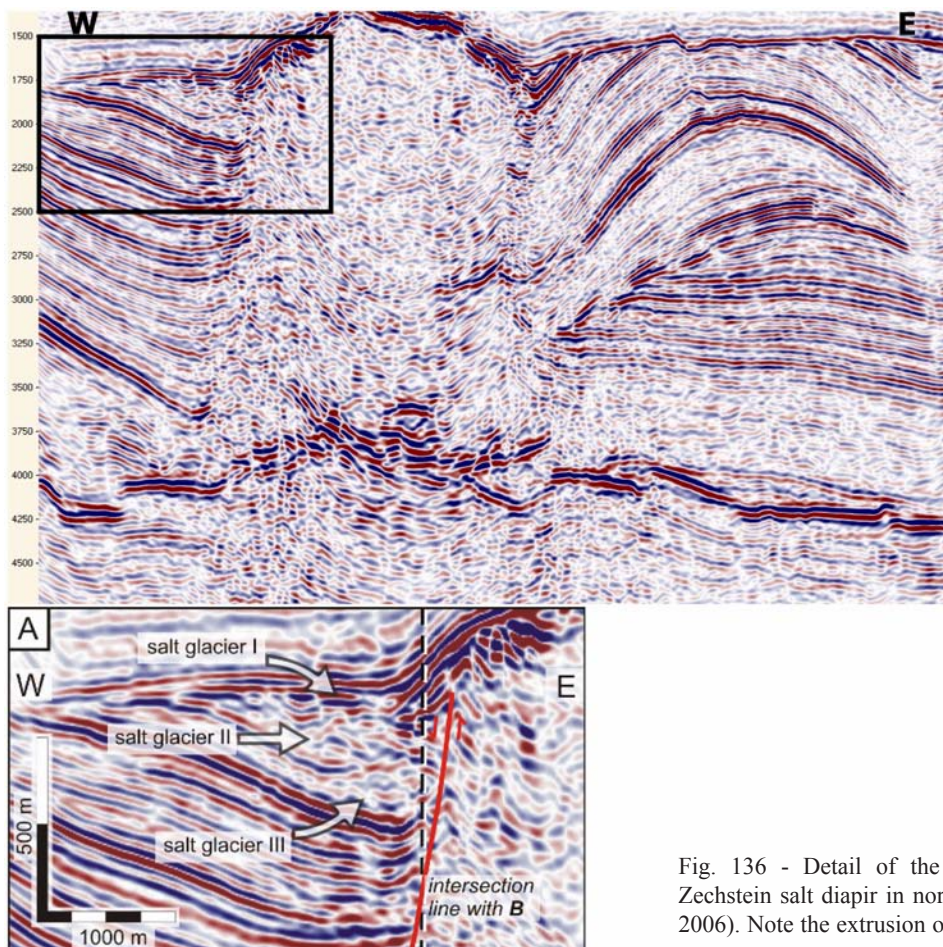


Fig. 136 - Detail of the previous section of the Permian Zechstein salt diapir in northern Germany (after MOHR *et alii*, 2006). Note the extrusion of salt (salt glacier).

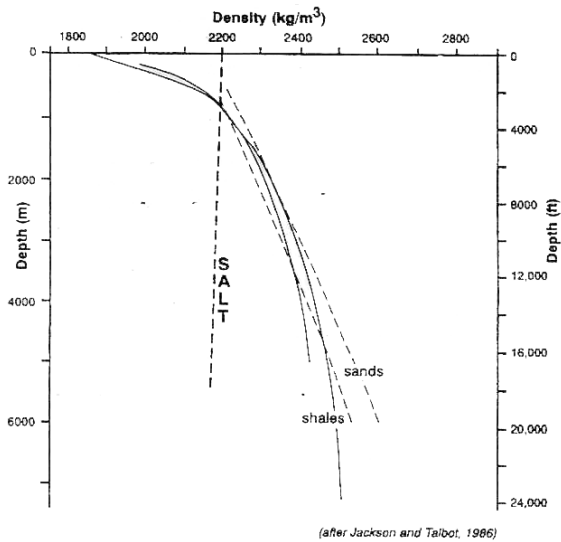
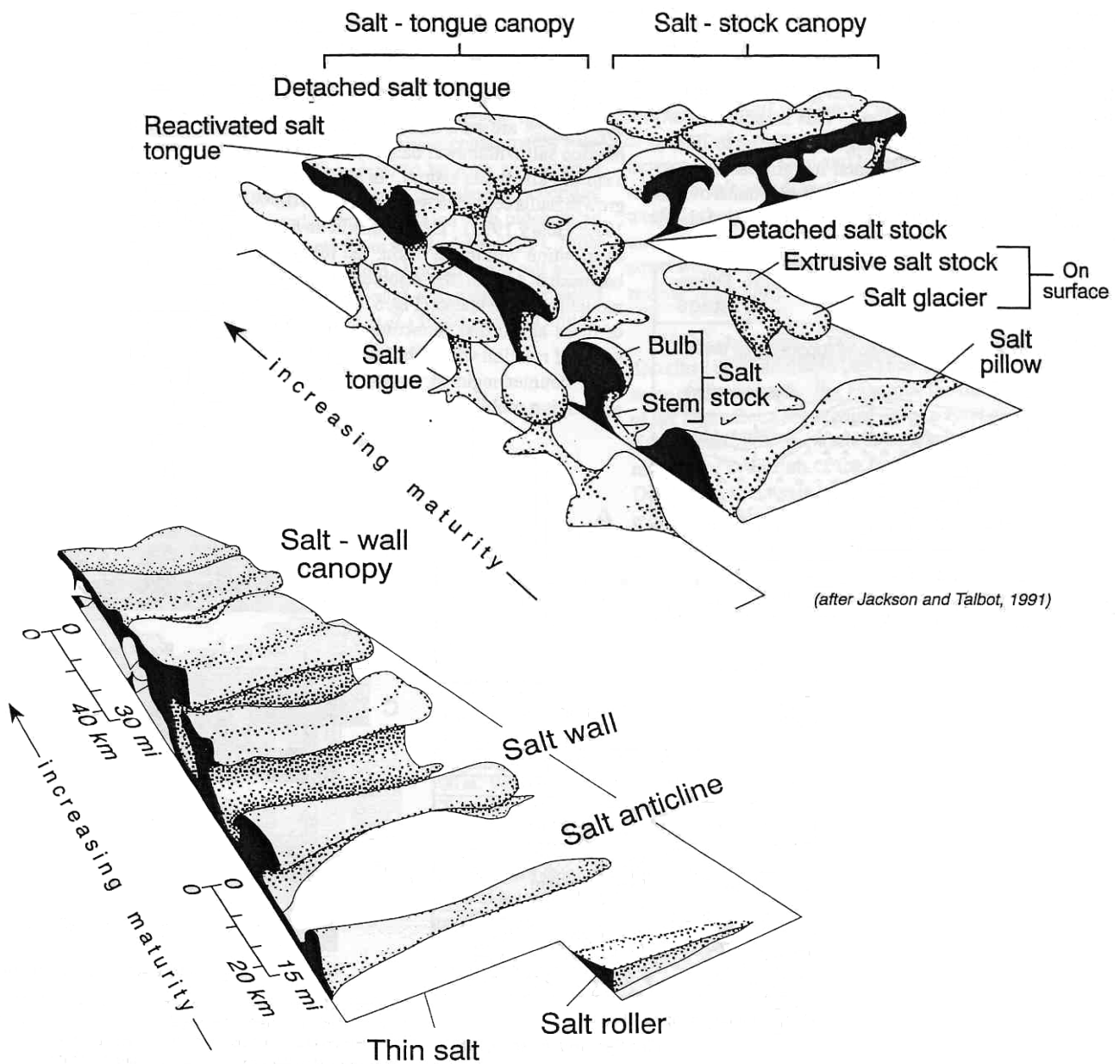


Fig. 137 - At depths greater than 1000 m the density of salt is smaller than that of common sediments (upper panel). This causes the onset of buoyancy forces that may lead to the development of salt diapirs. Salt structures may be punctual (middle panel) or planar (bottom panel). After JACKSON & TALBOT (1991).



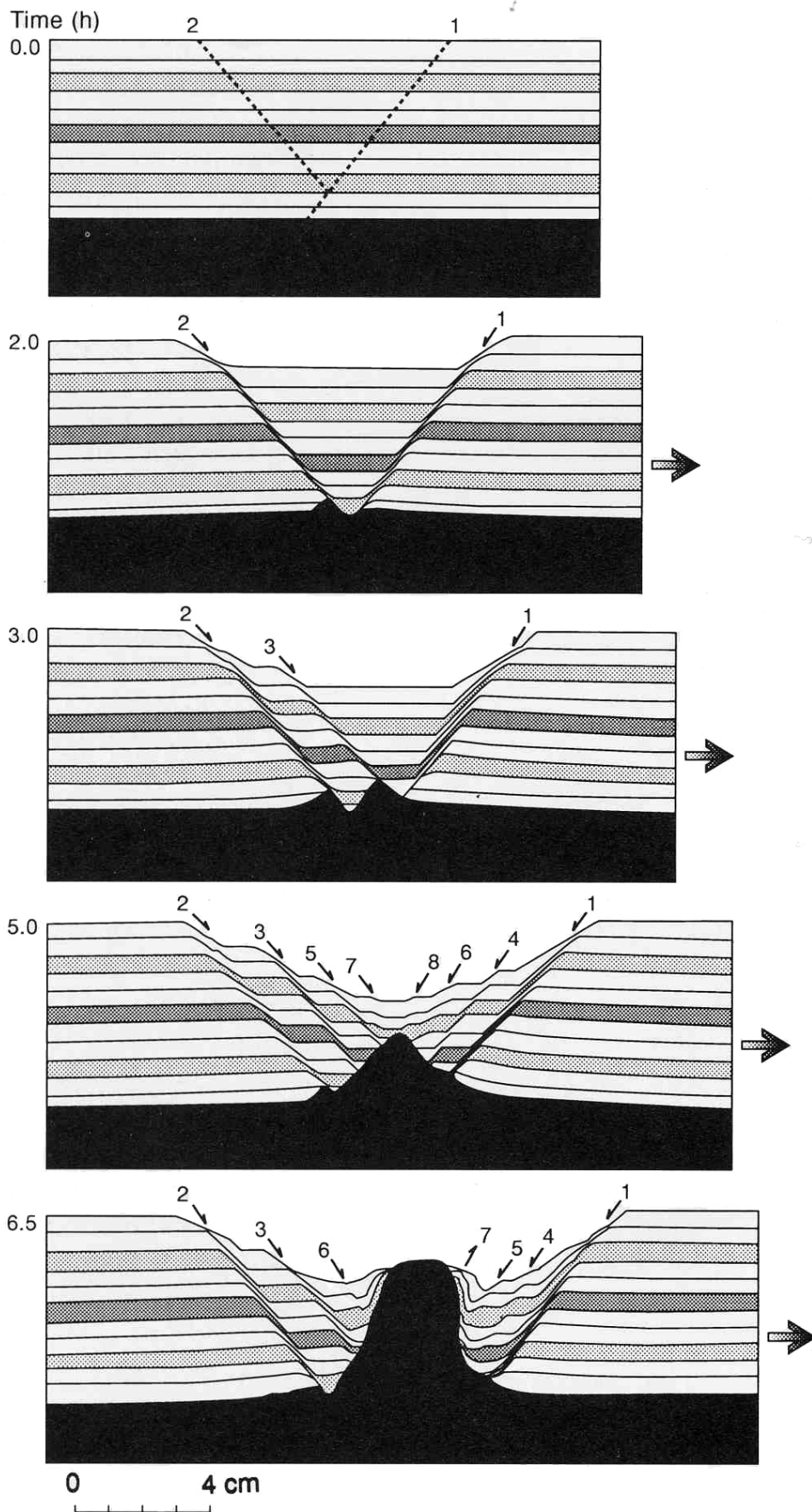


Fig. 138 - Diapirs are normally triggered by local tectonic features, such as normal faults, as in this case. Notice the formation of rim synclines (after JACKSON & VENDEVILLE, 1994).

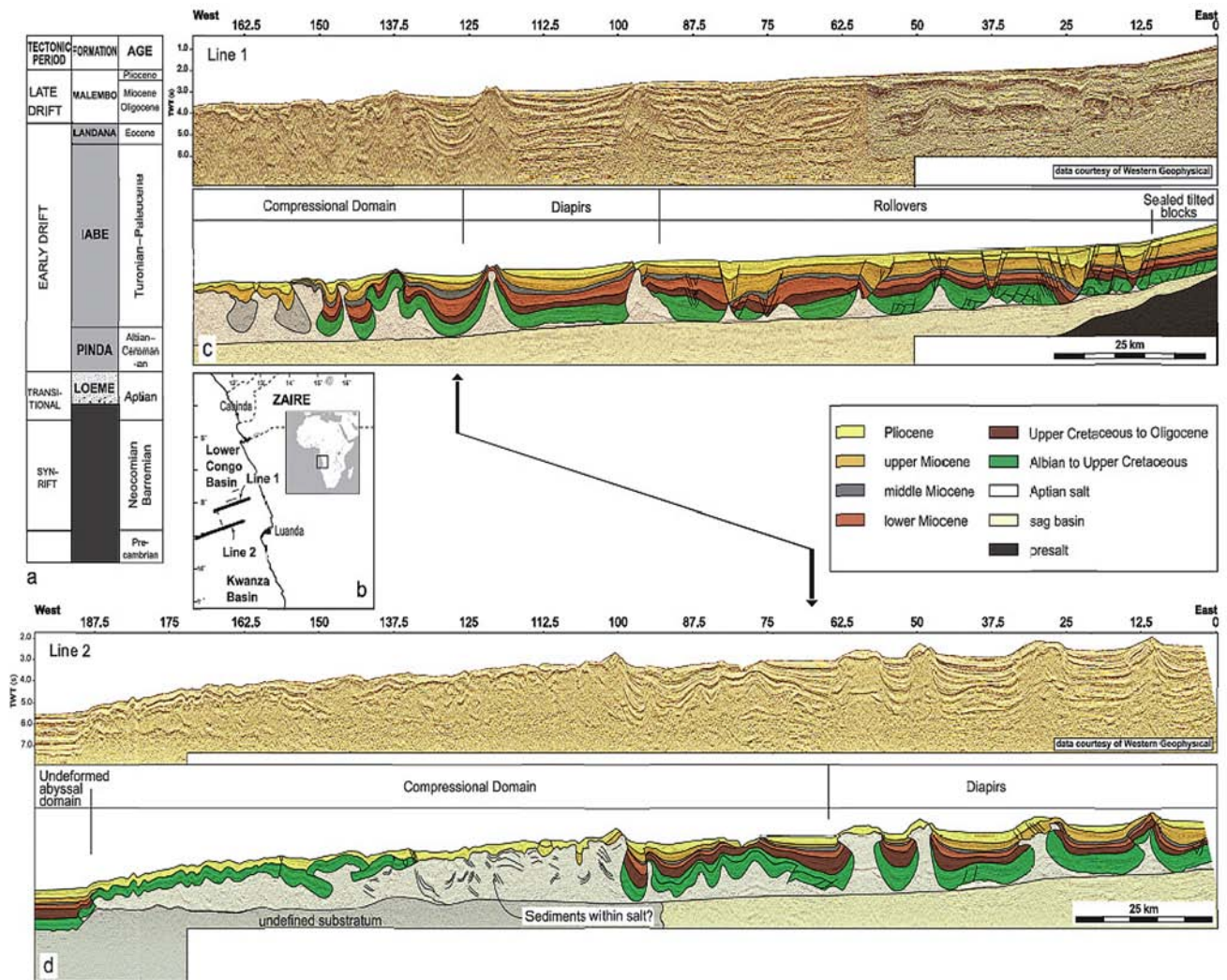


Fig. 139 - Gravity salt tectonics in the Kwanza Basin, offshore Angola. Notice the extensional tectonics in the internal sectors (close to the continent; raft domain) with listric normal faults rooted in a shallow detachment level characterised by the occurrence of remnant bodies of salt. The central part of the section is characterised by wide and numerous diapirs, while the external part is a compressional domain characterised by thrusts and folds. Shortening is due to accumulation of sliding sedimentary cover at the transition between the continental ramp and the abyssal plain (after FORT *et alii*, 2004).

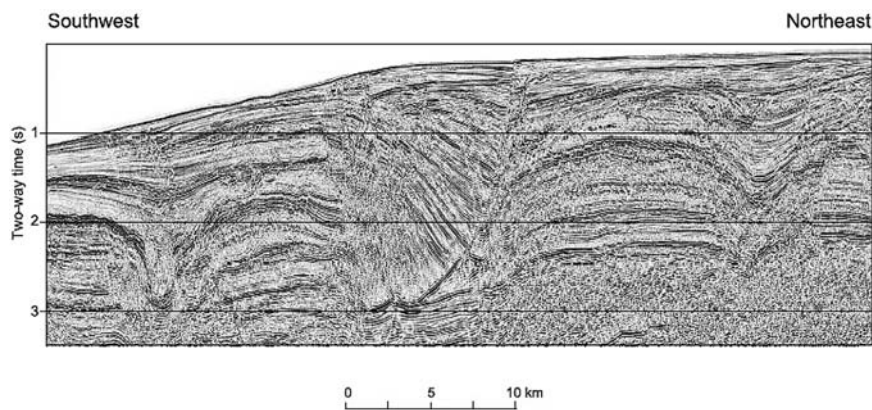


Fig. 140 - Seismic section showing listric faults in the raft domain of the Kwanza Basin, offshore Angola. The raft domain contains large sedimentary depotroughs separated by almost undeformed Cretaceous rafts (after HUDECK & JACKSON, 2004).

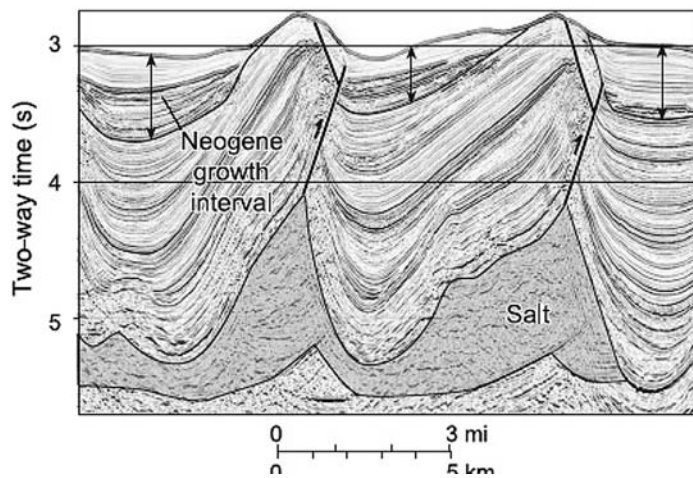
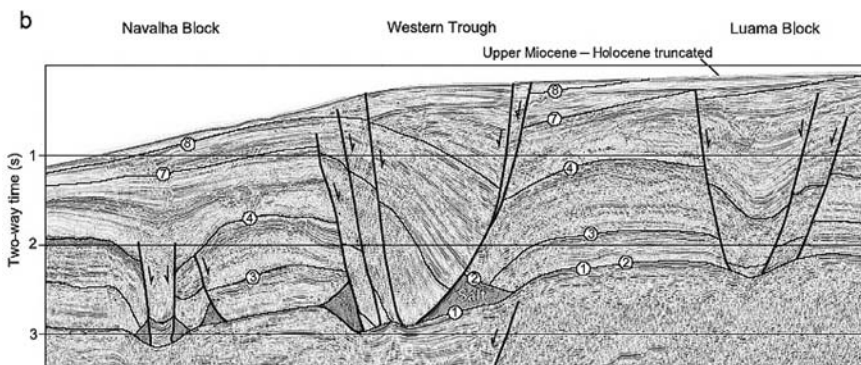
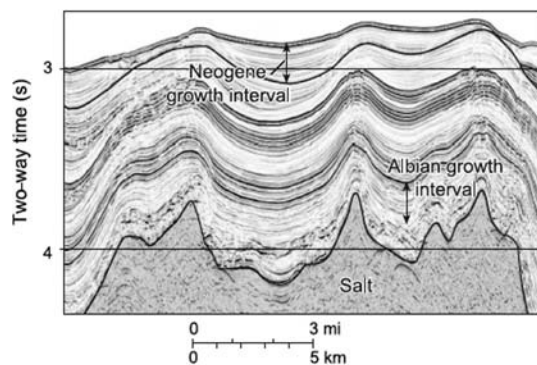


Fig. 141 - Seismic sections from the diapir domain of the Kwanza Basin, offshore Angola. After HUDECK & JACKSON (2004).



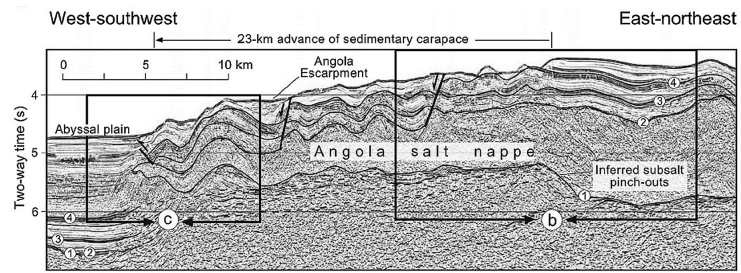


Fig. 142 - Seismic section from the salt nappe domain of the Kwanza basin, offshore Angola. Notice the development of folds and thrust faults. The bottom panel is an enlargement of box *c* of the upper panel (after HUDECK & JACKSON, 2004).

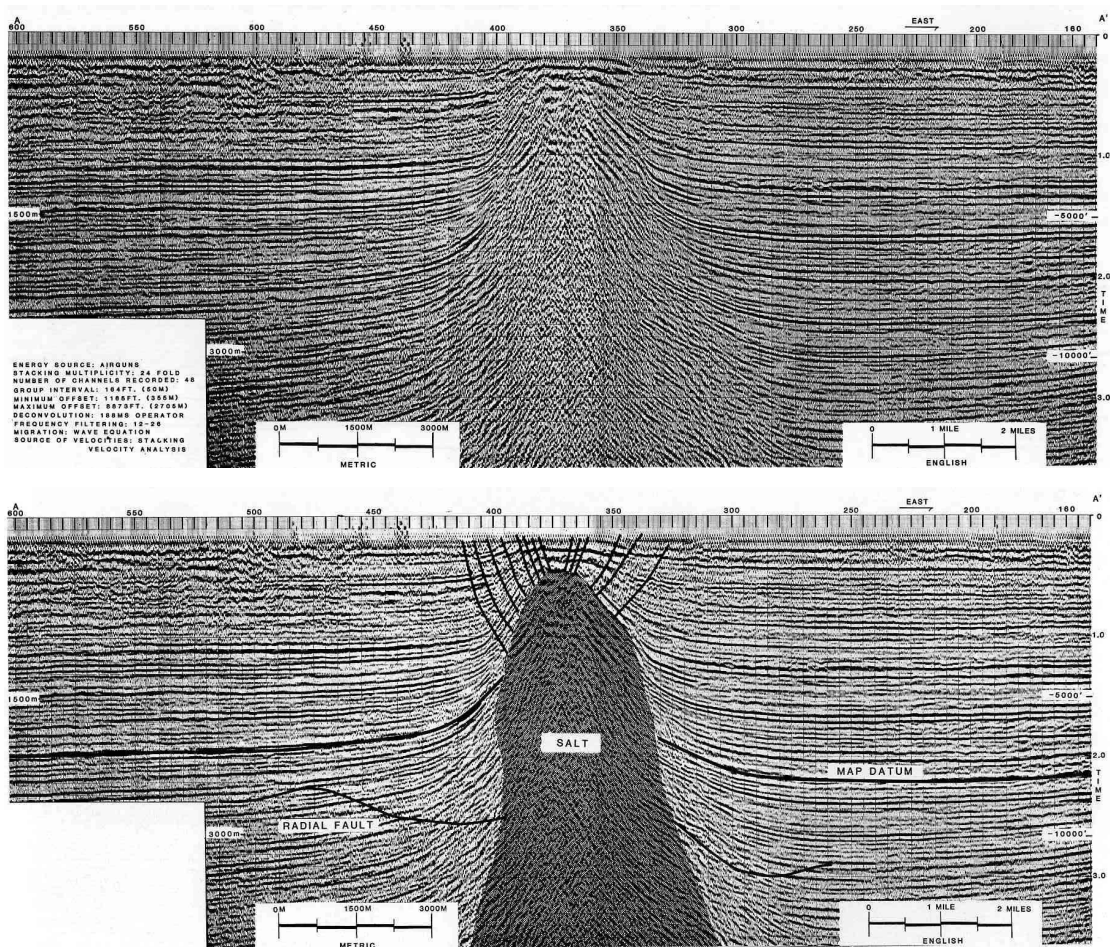
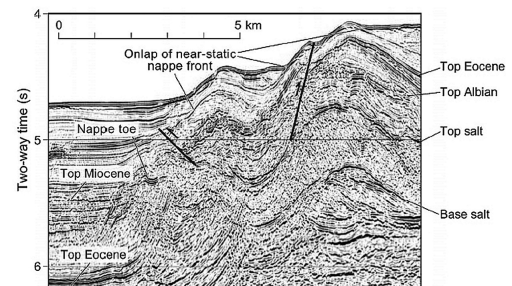
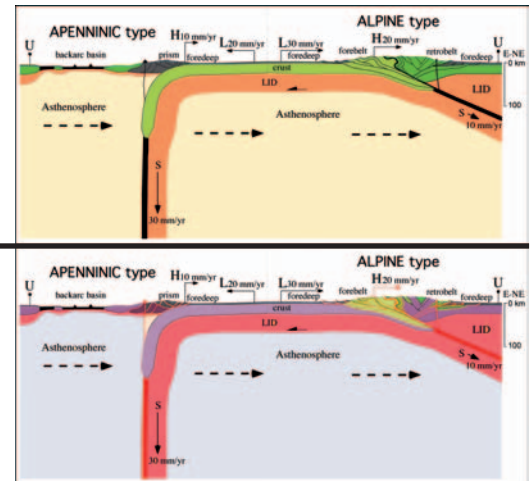


Fig. 143 - Salt diapirs with crestal collapse normal faults from the US Gulf coast (after SUNWALL *et alii*, 1983).

7. Geodynamic framework of subduction zones



The kinematics of subduction zones shows a variety of settings that can provide clues for dynamic understandings. Two reference frames are used here to describe simple 2D kinematics of subduction zones (fig. 144). In the first, the upper plate is assumed fixed, whereas in the second frame upper and lower plates move relative to the mantle.

Relative to a fixed point in the upper plate U, the transient subduction hinge H can converge, diverge, or be stationary. Similarly, the lower plate L can converge, diverge or be stationary. The subduction rate VS is given by the velocity of the hinge VH minus the velocity of the lower plate VL ($VS = VH - VL$). The subduction rate 1) increases when H diverges, and 2) decreases when H converges.

Combining the different movements, at least 14 kinematic settings can be distinguished along the subduction zones. Variable settings can coexist even along a single subduction zone, as for the 5 different cases occurring along the Apennines subduction zone (DOGLIONI *et alii*, 2007). Apart from few exceptions, the subduction hinge converges toward the upper plate more frequently along E- or NE-directed subduction zone, whereas mainly

diverges from the upper plate along W-directed subduction zones accompanying backarc extension.

Before collision, orogen growth occurs mostly at the expenses of the upper plate shortening along E- NE-directed subduction zones, whereas the accretionary prism of W-directed subduction zones increases at the expenses of the shallow layers of the lower plate.

Backarc spreading forms in two settings: along the W-directed subduction zones it is determined by the hinge divergence relative to the upper plate, minus the volume of the accretionary prism, or, in case of scarce or no accretion, minus the volume of the asthenospheric intrusion at the subduction hinge. Since the volume of the accretionary prism is proportional to the depth of the decollement plane, the backarc rifting is inversely proportional to the depth of the decollement. On the other hand, along E- or NE-directed subduction zones, few backarc basins form (e.g., Aegean, Andaman) and can be explained by the velocity gradient within the hangingwall lithosphere, separated into two plates.

When referring to the mantle, the kinematics of subduction zones can be computed either in

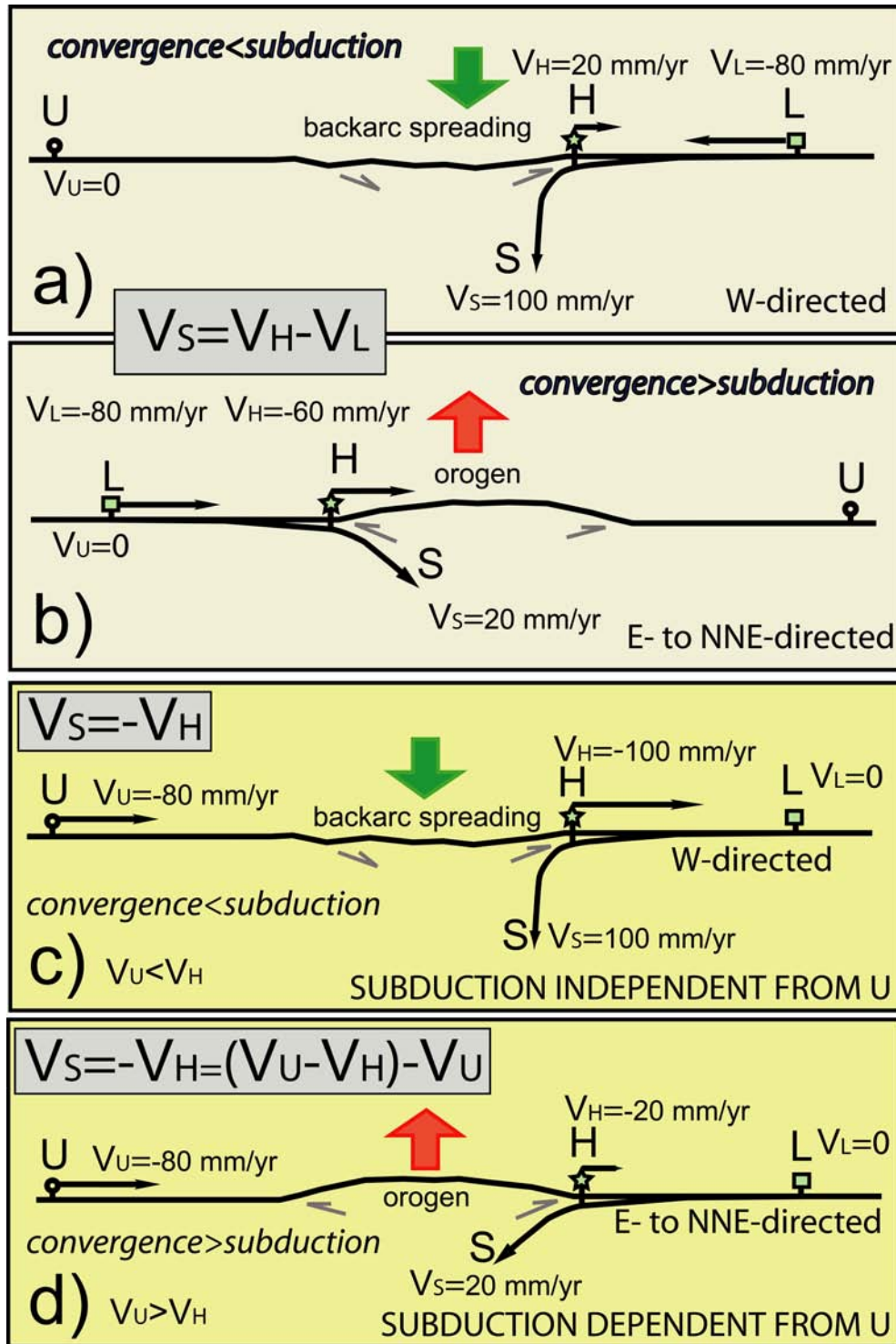


Fig. 144 - Upper panels a) and b): Basic kinematics of subduction zones, assuming a fixed upper plate U, a converging lower plate L, and a transient subduction hinge, H. The subduction rate S is given by $V_S = V_H - V_L$. Values are only as an example. S increases when H diverges relative to the upper plate (a), whereas S decreases if H converges (b). The movements diverging from the upper plate are positive, whereas they are negative when converging. The case a) is accompanied by backarc spreading, a low prism and is typical of W-directed subduction zones, whereas in case b) double verging and elevated orogens form and is more frequent along E- to NNE-directed subduction zones. Note that in both W- and E- NE-directed subduction zones, the hinge migrates eastward relative to the upper plate, suggesting a global tuning in subduction processes. Lower panels c) and d): kinematics of subduction zones assuming fixed the lower plate. Note that the velocity of the hinge equals the velocity of the subduction in both cases. In case c) the subduction is independent from the upper plate velocity, whereas in case d) is a function of it. These opposite kinematic settings indicate different dynamic origin of the subduction, i.e., slab/mantle interaction for c), and upper/lower plates interaction for case d).

the deep or in the shallow hotspot reference frames. The subduction hinge is mostly stationary being the slab anchored to the mantle along W-directed subduction zones, whereas it moves W- or SW-ward along E- or NE-directed subduction zones. Surprisingly, along E- or NE-directed subduction zones, the slab moves "out" of the mantle, i.e., the slab slips relative to the mantle opposite to the subduction direction. Kinematically, this subduction occurs because the upper plate overrides the lower plate, pushing it down into the mantle. As an example, the Hellenic slab moves out relative to the mantle, i.e., SW-ward, opposite to its subduction direction, both in the deep and shallow hotspot reference frames. In the shallow hotspot reference frame, upper and lower plates move "westward" relative to the mantle along all subduction zones.

This kinematic observation casts serious doubts on the slab negative buoyancy as the primary driving mechanism of subduction and plate motions.

W-directed subduction zones rather provide about 2-3 times larger volumes of lithosphere re-entering into the mantle, and the slab is pushed down. This opposite behavior is consistent with the down-dip extension seismicity along E-NE-directed subduction zones, and the frequent down-dip compression along the W-directed subduction zones.

Subduction kinematics show that plate velocity is not dictated by the rate of subduction. Along the W-directed subduction zones, the rate of subduction is rather controlled i) by the hinge migration due to the slab interaction with the "easterly" trending horizontal mantle wind along the global tectonic mainstream, ii) by the far field plate velocities, and, iii) by the value of negative buoyancy of the slab relative to the country mantle.

Alternatively, E-NE-NNE-directed subduction zones have rates of sinking chiefly determined i) by the far field velocity of plates, and ii) by the value of negative buoyancy of the slab relative to the country mantle. Along this

type of subduction, the subduction hinge generally advances E-NE-ward toward the upper plate decreasing the subduction rate, but it moves W-SW-ward relative to the mantle.

All this indicates that subduction zones have different origin as a function of their geographic polarity, and the subduction process is more a passive feature rather than being the driving mechanism of plate motions. A rotational component combined with mantle density and viscosity anisotropies seems more plausible for generating the global tuning in the asymmetry of subduction zones.

Subduction zones and related orogens show significant differences as a function of their polarity. It is referred here as polarity the direction of subduction with respect to the tectonic mainstream, which is not E-W, but undulates around the Earth. Therefore, the asymmetry can be recognized not simply comparing W-directed versus E-directed subduction zones, but subductions along the sinusoidal flow of absolute plate motions that undulates from WNW in the Pacific, E-W in the Atlantic, and NE to NNE from eastern Africa, Indian Ocean and Himalayas. In the hotspot reference frame a "westward" rotation of the lithosphere can be observed. The origin of this net rotation of the lithosphere (BOSTROM, 1971) is still under debate (SCOPPOLA *et alii*, 2006), but it should range between 4.9 cm/yr (GRIPP & GORDON, 2002) and 13.4 cm/yr (CRESPI *et alii*, 2007) at its equator. This implies that the plate motions flow is significantly polarized toward the "west" (Doglioni *et al.*, 1999), and subduction zones follow or oppose the relative "eastward" relative mantle flow. Subduction zones following the flow are: North and South America cordilleras, Dinarides, Hellenides, Caucasus, Zagros, Makran, Himalayas, Indonesia-Sunda arc, Taiwan, New Guinea, New Hebrides, southern New Zealand. Subduction zones opposing the flow are: Barbados, Sandwich, Apennines, Carpathians, Banda, Molucca, Tonga, Kermadec, Marianas, Izu-Bonin,

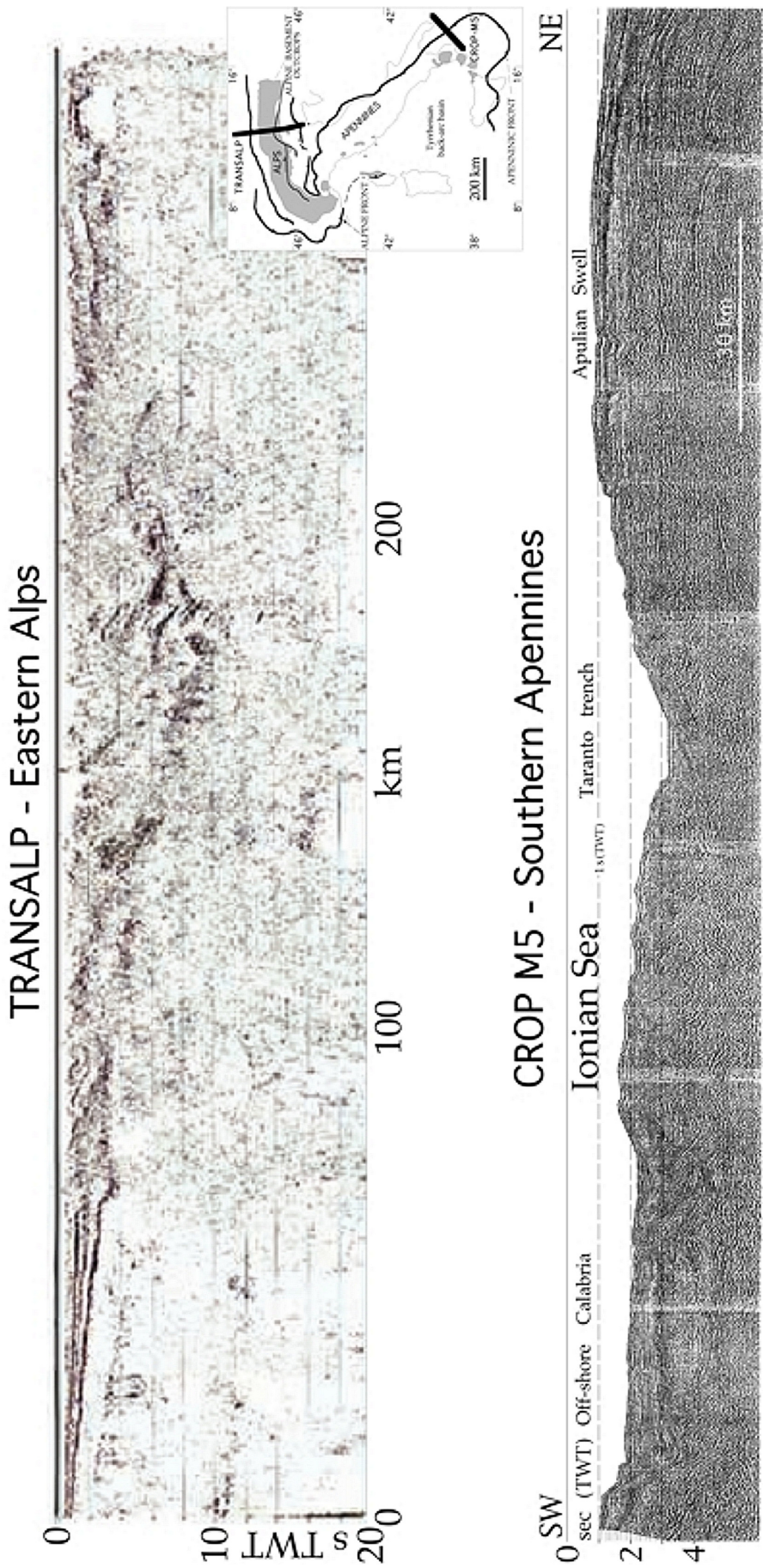


Fig. 145 - Seismic sections of the Alps (Transalp, 2002) and of the Apennines (SCROCCA *et alii*, 2003).

Nankai, Philippine, Kurili, Aleutians. The Japan subduction appears as a transitional subduction zone.

Since many subduction zones have undulations or arcs along strike, their dip and strike can be oblique or parallel to the proposed tectonic mainstream. For example, in the transfer zone between Makran and Himalayas NNE-directed subduction zones, along the Chaman left-lateral transpressive system, the tectonic mainstream is about parallel to the belt. Another emblematic case is the Aleutians arc, here considered as a subduction opposing the flow (W-directed). Along their western termination, they almost parallel the Pacific subduction direction (WNW), where the slab is a right-lateral ramp of the subduction, and it dips to the NNE.

The W-directed slabs are generally very steep (up to 90°) and deep, apart few cases as Japan. They have a co-genetic backarc basin, and the related single verging accretionary prism has low elevation (e.g., Barbados, Sandwich, Nankai), is mostly composed of shallow rocks, and has a frontal deep trench or foredeep (DOGLIONI *et alii*, 1999). The E- or NE-directed subduction zones are less inclined (15-70°), and the seismicity generally dies at about 300 km, apart some deeper clusters close to the upper-lower mantle transition. The related orogens have high morphological and structural elevation (e.g., Andes, Himalayas, Alps), wide outcrops of basement rocks, and two shallower trenches or foredeeps at the fronts of the double verging belt, i.e., the forebelt and the retrobelt. The retrobelt decreases its development when the upper plate is subject to extension (e.g., Central America, Aegean and Andaman Seas).

But, even more striking, surface geology and topography of the orogens contrast dramatically with a number of differences between the opposite subduction zones such as shallow vs. deep rocks, steep vs. shallow dip of the foreland monocline, low vs. higher inclination of the topographic and structural envelop, small

vs. wider area above sea-level, etc., respectively for W- vs. E- or NE-directed subduction zones (e.g., LENCI & DOGLIONI, 2007).

Moreover backarc spreading occurs mostly in W-directed subduction zones. Two counterexamples are proposed as proofs that this statement is not correct, i.e., the Aegean and the Andaman Seas, which are related to NE- to NNE-directed subduction zones. However these two cases have a different kinematics and geodynamic setting with respect to the W-directed subduction zones, where upper plate extension is concomitant to subduction hinge migrating away with respect to the upper plate, being the lithospheric deficit due to subduction, compensated by mantle replacement. Along the Aegean and Andaman rift zones the extension rather accommodates only the differential velocity within the upper lithospheric plate, which is split into two plates overriding the subduction (e.g., DOGLIONI *et alii*, 2002). Along the Andaman-Sunda-Indonesia arc for example, the flow of plates is NE- to NNE-directed. Extension or "backarc" spreading is not diffused along the entire arc, but rather concentrated at the western margin, along the transfer zone between the SW-ward faster advancing of Indonesia upper plate over the lower oceanic plate (about 60 mm/yr) with respect to the slower velocity of Eurasia upper plate in overriding the continental Indian lithosphere along the Himalayas belt (about 40 mm/yr). Where upper plate extension occurs along these settings, the retrobelt of the orogen is poorly developed and narrower. Another example seems the Central America subduction zone (e.g. Guatemala, El Salvador, Nicaragua, Costa Rica), in which the upper plate extension accommodates the faster westward motion of North America relative to South America.

DOGLIONI *et alii* (2006) rather suggested that the subduction system is primarily sensitive to the behavior of the subduction hinge, i.e., moving toward or away from the upper plate, regardless the convergence rate. The resulting

subduction rate is faster than the convergence rate where the hinge migrates away from the upper plate, whereas it is slower than the convergence where the hinge converges or advances toward the upper plate. The two end members appear sensitive to the geographic polarity of the subduction zones, being the asymmetry not among E-W subduction zones, but following or opposing an undulated "westerly" directed lithospheric flow (DOGLIONI, 1993), recently validated by space geodesy and statistical analysis (CRESPI *et alii*, 2007). This tectonic mainstream implies a relative mantle undulated counterflow, "easterly" directed.

The result of the asymmetry among opposite subduction zones (figs. 145 - 147) is that along the W-directed subduction zones only the shallow rocks on the subduction hinge are accreted (sedimentary cover and slices of the topmost basement) because the accretionary

prism basal decollement is located at the top of the subduction, without an actively thrusting upper plate. In the opposite E- or NE-directed subduction hinge, the lithosphere basal decollement is ramping upwards, providing a mechanism for uplifting deep-seated rocks. As a consequence, the shortening is concentrated in the shallow layers of the lower plate along W-directed subduction zones, both during the oceanic and the continental stages of subduction, providing small volumes to the orogen and maintaining a low elevation of the critical taper. The shortening is rather mostly concentrated in the upper continental lithosphere in E- or NE-directed oceanic subduction zones. Andean type trenches are in fact often characterized by tectonic erosion, rather than accretion. It is unclear how deep is transported the material offscraped by the tectonic erosion. It could eventually be re-transferred to the upper

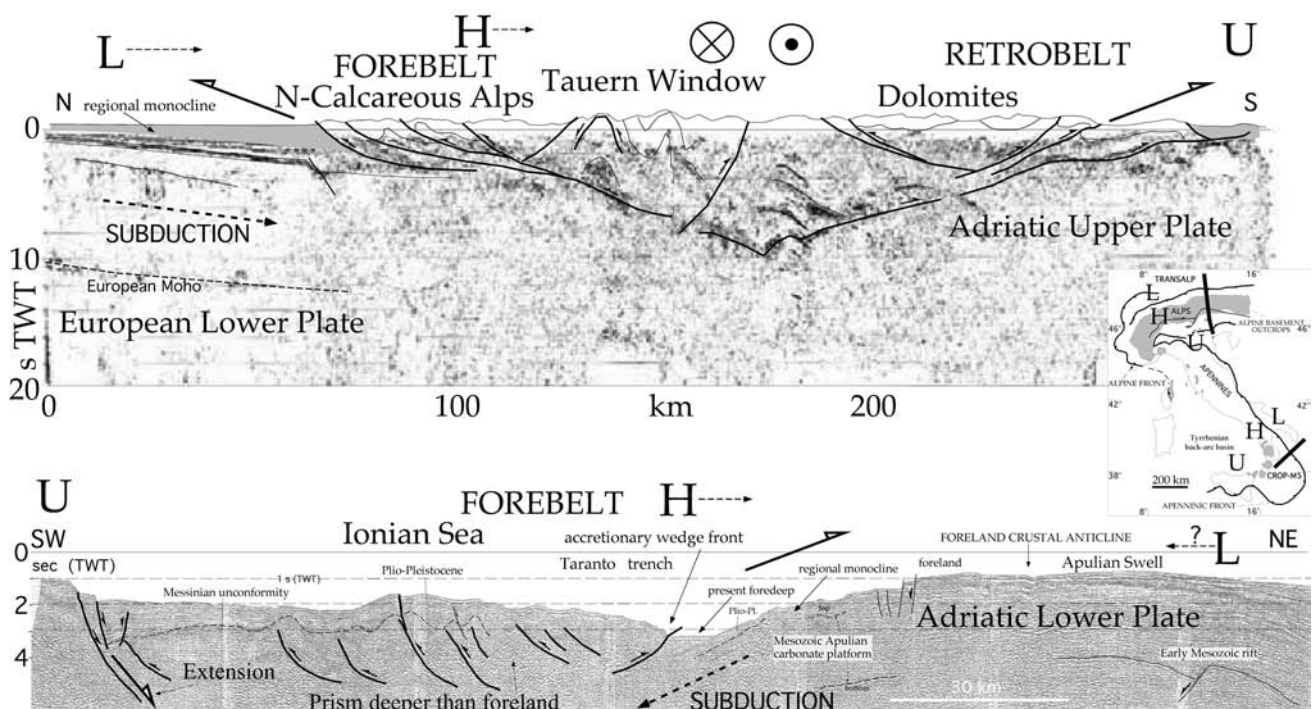


Fig. 146 - Same sections as in the previous figure with some interpretation (modified after TRANSALP, 2002; DOGLIONI *et alii*, 1999c). Note the Alpine double vergence versus the single Apennines vergence, where the prism is even deeper than the foreland and followed by extension to the left. L, lower plate, H, subduction hinge, U, upper plate. In the Alps H migrated toward the upper plate, whereas it moves toward the lower plate in the Apennines. The Adriatic plate is the upper plate U in the Alps, while it is the lower plate U in the Apennines. The E-W segment of the Alps formed under right-lateral transpression (After DOGLIONI *et alii*, 2007).

plate in the lower crust or upper mantle, and later re-exhumed during shortening progression.

However, accretion is documented along the Cascadia, Indonesia and several other segments of this type of subduction zones, thus providing a transfer of shallow rocks from the lower to the upper plate. But it is only at a collisional stage that the lower plate is eventually entirely involved and shortened. During this final stage, the lower plate contributes significantly to the volume increase of the orogen because shear zones and decollement planes enter much deeper in the continental crust of the footwall plate.

The term accretionary prism is often confused with the term forearc, which is the region between the subduction trench and the volcanic arc, having not always a unique tectonic meaning. The arc is also a misleading term used both to define a volcanic belt or a structural undulation of a thrust system. Moreover in the so-called forearc, extension can be widespread, without active accretion.

The shortening in prisms of W-directed subductions can be larger than the convergence rate, whereas it is in general smaller than the convergence in orogens of E- or NE-related subductions. This occurs because along W-directed slabs the shortening is confined in the lower plate and directly equivalent to the amount of subduction, which is larger than the convergence rate. In the E- or NE-directed slabs, the shortening is smaller than the convergence because the convergence is partitioned partly in the subduction rate, and partly in the contraction of the upper plate. While W-subduction-related prisms have a forebelt and a backarc basin, E-NE-subduction-related orogens have a forebelt and a widely developed retrobelt since the very early stages.

The different rock exhumation in the different subduction settings is highlighted by peculiar petrography of transported sediments (GARZANTI *et alii*, 2007). Regional foreland monoclines at the accretionary prism fronts

also show steep dip and fast subsidence rates along W-directed subduction zones, and shallow dip and slow subsidence rates for E- or NE-directed subduction zones. This is a paradox because if the foredeep subsidence is generated only by the mountain load, along the highest mountains as the Andes and Himalayas we should expect the deepest trenches and foredeeps, but we rather observe these features along the opposite subduction zones where there is not a significant lithostatic load, like the Marianas trench, the Apennines and Carpathians foredeep. The relative "eastward" mantle flow could favor the bending of the slab and the foredeep fast subsidence along the hinge of W-directed subduction zones. The mantle counter flow should rather contrast the subsidence along the opposite subduction zones, providing a force sustaining the slab. While W-directed subduction-related prisms have low-grade metamorphism, the E- or NE-subduction-related orogens at the collisional stage may exhibit UHP rocks. Metallogenesis appears also controlled by subduction style. The Mariana type subduction is characterized by Kuroko or similar volcanogenic sulphide deposits. Porphyry copper deposits are instead concentrated in collisional settings and Andean type subduction zones.

The seismicity of the slabs is mostly characterized by down-dip compression along W-directed subduction zones, whereas it is quite often down-dip extensional along E- or NE-directed subduction zones. Japan subduction shows a different case, having two separate layers of slab seismicity, i.e., an upper one characterized by down-dip compression, and a lower one where down-dip extension prevails. However, Japan seems an intermediate case of subduction, where the Neogene W-directed subduction system is presently initiating to flip, having the backarc basin started to shrink. The seismicity is frequently down-dip extensional all along the subduction hinges of both subduction polarities, possibly related to

the bending of the lithosphere.

Within the two opposite end-members, a number of different settings can occur. For example along the E-NE-directed subduction zones there are oceanic slabs under continental lithosphere as in the Andes, which may or may not evolve to continent-continent collision such as the Alps or Himalayas. Along W-directed subduction zones there also are variable compositions of the lower plate (both oceanic and continental lithosphere, e.g., Marianas and Apennines, Banda arc) and variable depth of the basal decollement plane, determining variations in the volume of the related accretionary prism.

The vertical and lateral growth of orogens is strongly asymmetric. In fact prism or orogens related to W-directed subduction zones mostly generate an E-ward migrating wave, never reaching high structural and morphologic elevation, where the volumes and elevation rates of the prism are constrained by the subduction rate and the depth of the basal decollement plane of the accretionary prism. On the other hand, orogens related to E- or NE-directed subduction zones are much more elevated and their growth occurs both vertically and horizontally.

As prototypes of different subduction zones, the Alps and the Apennines are orogens formed above opposite slabs. Along the first belt, since the Cretaceous, the European plate subducted SE-ward underneath the Adriatic plate, whereas along the second belt, since the Late Oligocene, the Adriatic plate subducted W-ward below the European plate, with fast slab rollback and backarc spreading in the western Mediterranean. The Alps, unlike the Apennines, have double vergence, high structural and morphologic elevation, and no backarc basin. The Alps have two shallow foreland monoclines at the base of two foredeep basins, whereas the Apennines have a single deep foredeep, with steeper monocline and faster subsidence rates. Beneath the Alps the crust is about doubled, and the lithosphere

base is deeper than 100 km. Below the Apennines, a new shallow Moho formed in the western backarc side, and the asthenosphere is very shallow (30-40 km, PANZA *et alii*, 2003). The new Moho is kinematically required by the replacement of the original Moho, now subducted, on which the present surface thrust sheets were originally lying, being part of a pre-existing passive margin section. A new mantle section from west has replaced the subducted crustal section, the pre-subduction Moho and the lithospheric mantle of the lower plate, since the slab is eastward retreating (DOGLIONI, 1991).

The Alps have widespread outcrops of basement rocks. In fact along the Alpine belt, thrusts are deeply rooted, cross-cutting the whole crust and upper mantle (DAL PIAZ *et alii*, 2003). Seismic tomography shows large involvement of continental lithosphere in the subduction system (MUELLER & PANZA, 1986). In the Apenninic belt, the prism is rather mostly composed of shallow (mostly sedimentary) crustal rocks of the lower plate because the decoupling surface is traveling atop the downgoing lithosphere (BALLY *et alii*, 1986).

The different structural settings of Alps and Apennines suggest different dynamic and consequently kinematic evolution of the related subduction zones. These asymmetries are diffused worldwide in the orogens, and appear controlled by the polarity of the subduction, i.e., following or opposing the polarized undulated flow of plate motions.

A number of exceptions occur to these two end members. For example, Japan has low elevation and other characteristics of W-directed subduction zones, such as the backarc basin and an accretionary prism mostly composed of shallow rocks. However the slab has low dip of the subduction plane, and there is no active hangingwall extension, in spite of an onshore morphology suggesting widely distributed structural depressions. The GPS data confirm that the Japan Sea backarc is not opening anymore, but it is rather closing. This

indicates that the system possibly arrived at an end, and its inversion started. Unlike other living W-directed subduction zones, the slab hinge in Northern Japan is moving toward the upper plate.

W-directed subduction zones formed mostly along the retrobelt of pre-existing E-NE-directed subduction zones, provided that oceanic lithosphere was present in the foreland to the east. This would explain why, for example, the Barbados and Sandwich arcs formed only where the Northern and Southern America continental lithospheres narrow, and slices of Cordillera type are boudinaged and scattered in the backarc setting. Similarly, the Japanese W-directed subduction, developed during the Neogene, to the east of a retrobelt of an earlier Cretaceous Andean type orogen, generated by an E-directed subduction. This is also supported by the outcrops of Andean type co-genetic porphyry copper deposits in Japan and Chorea.

W-directed subduction zones on Earth appear as short lived. If the Marianas or Japan subduc-

tions were active since the Cretaceous with a steady state E-ward hinge retreat, they should be now positioned in the middle of the Pacific. Backarc spreading in the hangingwall of W-directed subduction zones are mostly Cenozoic, pointing out that the related subduction should have a similar age. Backarc basins probably arrive to a critical opening stage, and then they become closed, until a new subduction starts. The non-standard Japan subduction in fact shows scattered intermediate deep seismicity, unlike it typically occurs along similar slabs.

Another apparent discrepancy to the W-directed versus E-NE-directed slabs asymmetry is the occurrence of backarc basins also in the hangingwall of E- or NE-directed subduction zones. However these types of rifts rarely arrive to oceanic spreading as W-directed subduction do in their hangingwall. Moreover they may be post-subduction (e.g., Basin and Range, DOGLIONI, 1995), or sin-subduction but accommodating differential advancement of the upper plate over the lower plate.

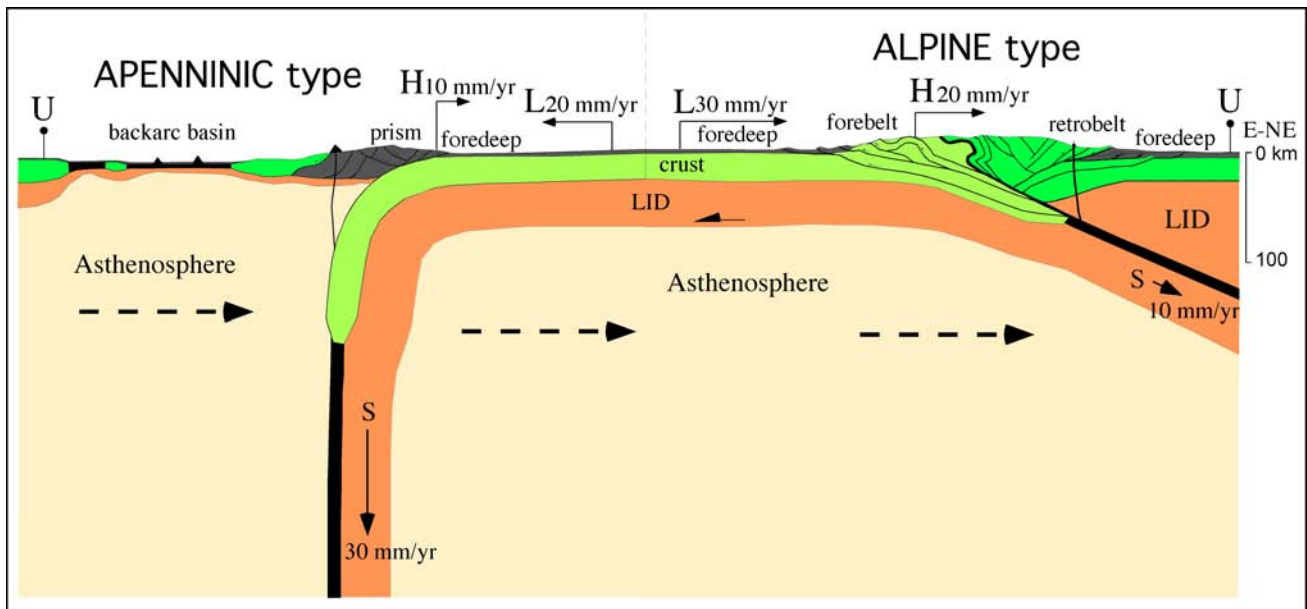


Fig. 147 - Schematic sections showing how in an Alpine setting, the subduction rate is decreased by the migration of the hinge H toward the upper plate U, and the orogen in the final collisional stage is composed both by the upper and lower plate L rocks. In the opposed Apenninic setting, the subduction rate is rather increased by the migration of H away from U, and the accretionary prism is made of shallow rocks of the lower plate. Note also the shallower asthenosphere in the hangingwall, which is typical of W-directed subduction zones (after DOGLIONI *et alii*, 2007).

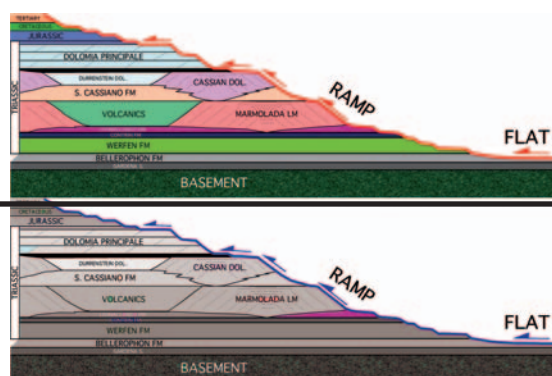
Examples of this type are the aforementioned Aegean and the Andaman rifts. The extension in western Turkey, Aegean sea, Greece and Bulgaria can be interpreted as a result of the differential convergence rates between the NE-ward directed subduction of Africa relative to the hangingwall disrupted Eurasian lithosphere (DOGLIONI *et alii*, 2002). Considering fixed Africa, the faster SW-ward motion of Greece relative to Cyprus-Anatolia determines the Aegean extension. The differences in velocity can be ascribed to differential decoupling with the asthenosphere. Unlike west-Pacific backarc basins, where the asthenosphere replaces a subducted and retreated slab, the Aegean rift represents a different type of extension associated to a subduction zone, where the hangingwall plate overrode the slab at different velocities, implying internal deformation. While W-directed subductions occur with the rollback of the lower plate relative to the upper plate, the Aegean setting needs three plates, i.e., a common lower plate, and two plates overriding at different velocities. Analogously, assuming only few mm/yr of relative motion between the Indian and Australian plates, along the Himalayas collision, the Indo-Australian plates converge relative to Asia at about 36 mm/yr, while the same Indo-Australian plates along their oceanic northern part are overridden by the Sumatra-Burma plate at around 64 mm/yr. Therefore, assuming a relatively coherent lower plate, the hangingwall plates move SSW-ward at different velocity, this gradient being responsible for the extension between Asia and Sumatra-Burma, and generating the Andaman rift. In this type of geodynamic setting the subduction hinge still moves toward the upper plate, as in the normal E- or NE-directed subduction zones.

There are belts that are apparently not following the global trend of plate motions, like orogens that are E-W trending, and related to N-S convergence (e.g., the Pyrenees, Venezuela-Colombia belt). They have Alpine

character and may kinematically be explained as related to subrotation of plates (CUFFARO *et alii*, 2004). The Atlas is not directly related to a subduction zone, but has been interpreted as an intraplate inversion structure, while the E-W-trending Maghrebides (FRIZON DE LAMOTTE *et alii*, 2000) are rather the right-lateral prolongation in northwestern Africa of the arcuate Apennines-Maghrebides subduction system. Along this segment of the belt, the right-lateral transpression coexisted with an about 5 times slower roughly N-S component of Africa-Europe convergence (GUEGUEN *et alii*, 1998). The E-W-trending Himalaya is instead almost perpendicular to the global tectonic mainstream (DOGLIONI, 1990).

Mantle convection could satisfy a steady state speed of the lithosphere, assuming low or no decoupling at the asthenosphere interface. However, mantle convection is kinematically problematic in explaining the migration of plate boundaries and the occurrence of a decoupling surface at the lithosphere base. Although a combination of all forces acting on the lithosphere is likely, the decoupling between lithosphere and mantle suggests that a torque acts on the lithosphere independently of the mantle drag. Slab pull and ridge push are candidates for generating this torque, but, unlike these boundary forces, the advantage of the Earth's rotation and related tidal drag is to be a volume force, acting simultaneously and tangentially on the whole plates. Tidal drag maintains the lithosphere under a permanent high frequency vibration, polarized and sheared toward the "west". Earth's rotation and the break exerted by the lag of the tidal bulge (BOSTROM, 1971) can be efficient only if very low viscosity occur at the lithosphere-asthenosphere transition (JORDAN, 1974), but growing evidences are emerging on the presence of an ultra-low viscosity layer at the very top of the asthenosphere, possibly related also to higher fluids concentration in the mantle. Lateral variations in the low-velocity layer viscosity could control the different velocity of plates.

8. Tectonics and Sedimentation



Relationships among extensional tectonics, stratigraphy and inversion.

The interactions between tectonics and stratigraphy are schematically two-folds: 1) the effects of tectonics on the control of depositional sequences; 2) the control of paleotectonics and depositional sequences on the location of subsequent deformation.

Stratigraphy is mainly controlled by the combination of tectonics and eustatism. Oversimplified models considering only pure tectonic or eustatic control on stratigraphy are misleading. Their relative importance has to be taken into account considering the magnitude and origin of the different orders of eustatic oscillations and their association with the tectonically controlled vertical motions occurring in the various geodynamic and tectonic scenarios in which they operate. For example, along passive margins the interference between tectonics and eustatism is different during rifting and drifting stages. During rifting tectonic subsidence prevails, whereas thermal subsidence is more important during drifting. Therefore, as in contractional environments, also in extensional settings the interference

between tectonics and eustatism varies as a function of how, where (kind of geodynamic environment) and when (one of the various stages of third order cycles that develop during sea-level rises or falls of second cycle) it occurs. An important relationship between tectonics and stratigraphy can be observed in extensional or transpressional growth faults. If subsidence rate is slower than the velocity of the environment to re-equilibrate and maintain the same facies along the fault, then subsidence across the fault plane will control only the sedimentary thickness at the two sides of the fault, since sedimentation will manage to level continuously the structural step. However, when the velocity of the fault is faster than sedimentation rates, the fault will produce a morphological step and will control both facies changes and sedimentary thickness variations between hangingwall and footwall. In this second case, local depositional sequences, not globally correlatable, can develop: debris flows associated to fault escarpment or to rollover anticline flanks cannot be considered as low-stand wedges.

The aggradation of a carbonate platform is controlled by subsidence and carbonate pro-

duction. The platform break of a carbonate platform is therefore direct function of the subsidence rates of an area. In the Dolomites, for example, coeval carbonate platforms show different shapes of the platform break surface. This is due to the fact that such platforms grew in areas characterised by different subsidence rates generated by the Triassic transtensional tectonics. A strong and fast subsidence generates a subvertical platform break surface, whereas a subhorizontal platform break surface is generated during phases of low or null subsidence.

A frequently disregarded parameter is the subsidence component related to compaction of the sedimentary cover. The more the sediment succession is heterogeneous, the more compaction is irregular: this can produce depositional sequences confined to restricted basins controlled by differential compaction.

The three dimensional reconstruction of inversion structures remains an open problem.

Generally, inversion is considered in two dimensions (e.g., a graben inverted to produce a pop-up). However, the direction of compression can vary widely with respect to the preceding extension. In the Southern Alps, for example, alpine compression ($N0^{\circ}-30^{\circ}W$) is oblique to Mesozoic extensional paleostructures (i.e., extensional growth faults oriented $N10^{\circ}E-N10^{\circ}W$) (fig. 148). Extensional paleofaults dipping to the east were easily cut and transported passively along thrust faults, whereas those dipping to the west were easily re-sheared as sinistral transpressional faults. As already mentioned, inversion (or re-shear) of a fault occurs when peculiar conditions are respected (e.g., low angle both for strike and dip between the thrust fault and the pre-existing normal fault; high fluid pressure). The shortening of a platform-basin system can produce different interference geometries for different directions of compression relative to the direction of the platform margin. The concept

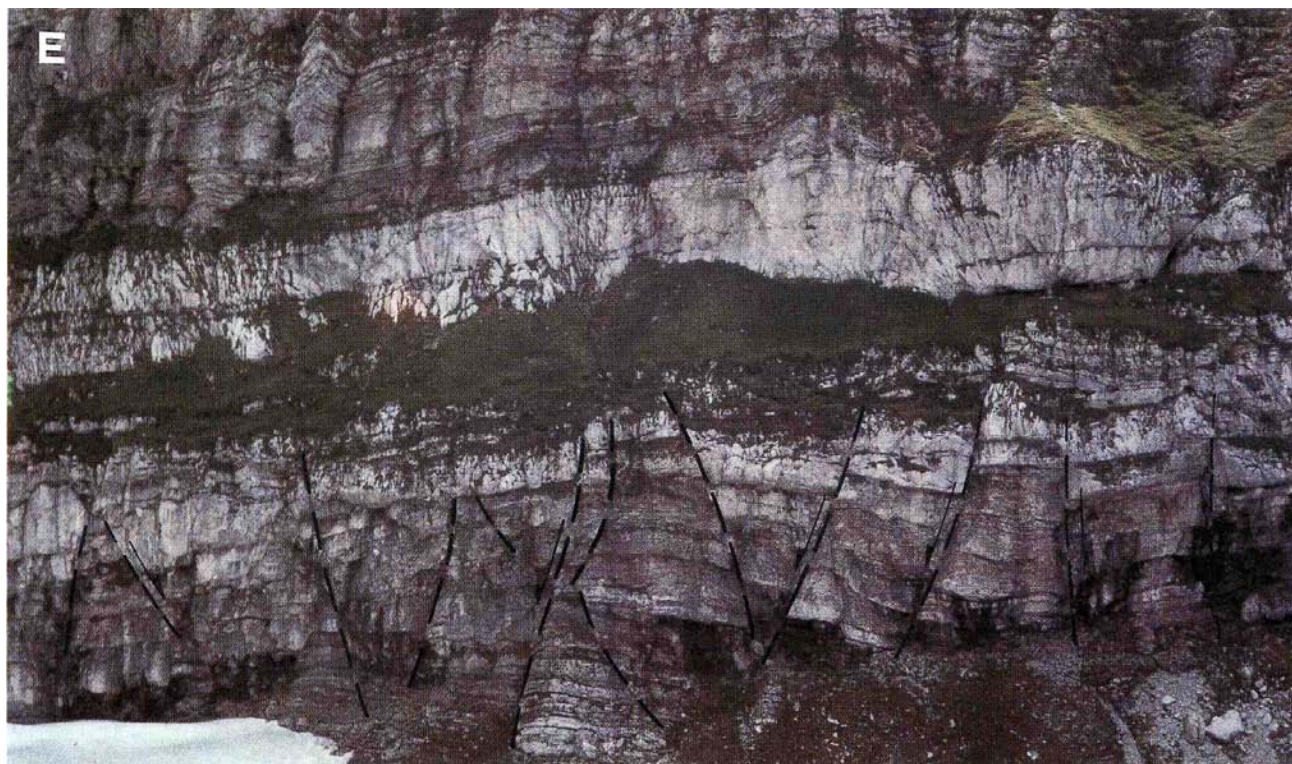


Fig. 148 - System of grabens with N-S direction in Dogger sediments (synchronous to the deposition of the Fonzaso and Calcare del Vajont Fms.) cropping out along the northern flank of Mt. Mangart (area of Tarvisio). It can be considered as a field example of the Mesozoic Southalpine extensional tectonics.

of platform should however be split in two concepts: structural platform (that is generally retrograde since extensional tectonics migrates and induces a margin retrogression) and sedimentary platform (that is generally prograde due to the advancement of a carbonate platform or of a delta).

The front of a fold-and-thrust belt is generally of three types: 1) triangle zone; 2) fault propagation fold; 3) fault bend fold. A syn-sedimentary fault in the upper crust of a certain region represents a strong anisotropy due to the different thickness of lithologies in hanging-wall and footwall. Differences in the embrication structural style can be frequently observed at the two sides of the fault: for example, an imbricate fan on one side and a pop-up on the other side. In nature the three above mentioned front geometries may develop separately or may be combined and coexist. Rheology controls and determines the predominance of one of the three mechanisms on the others. For example, triangle zones are best developed in basin sedimentary successions, rich in shales and therefore more prone to flexural slip. The activation of flexural slip processes is also necessary in fault-propagation folds. Fault-propagation folds and fault-bend folds can coexist in the same structure both in section and along strike. For example, the propagation of a fault at the hinge of a fold may occur with a ramp-and-flat trajectory, so that the two folding mechanisms may be superimposed.

Some examples from the Southern Alps (interactions among Mesozoic extensional tectonics, stratigraphy and Alpine shortening)

The Southern Alps are a regional example for some general considerations on the relationships among extensional tectonics, lithological and facies variations (both horizontal and vertical) and alpine inversion (both Southalpine and Dinaric) (figs. 149 - 163).

The irregular rheology of the Southern Alps sedimentary cover is evident observing the

ramp and flat trajectories of the thrust surfaces. It can be commonly observed that sequence boundaries or maximum flooding surfaces acted as preferential decollement levels. Obviously evaporitic and shaly levels or horizons characterised by strong lithological contrasts constitute major detachment surfaces. The main detachment levels are: Bellerophon Fm (Upper Permian) and Werfen Fm (Scythian) in the Dolomites, together with the pelagic deposits of the Livinallongo Fm (Ladinian) and San Cassiano Fm (Carnian). In the Venetian Prealps, the major decollements are concentrated in the Cretaceous pelagic deposits (Biancone and Scaglia Rossa Fms.) and in the flyschoid deposits of Paleocene-Eocene age. Ramp geometries of thrust faults are frequent at the margins of carbonate platforms and along clinostratifications. The horsts are often located along frontal, oblique or lateral ramps, as a function of their geometry with respect to the direction of maximum compression.

Some paleostructures can be identified by structural undulations in the thrust belt. Such undulations occur frequently above inherited normal syn-sedimentary faults or in correspondence with facies and thickness variations. Several physical parameters affect the final structure of the belt. In particular, a strong influence is exerted by the orientation of shortening with respect to pre-existing extensional faults and by the facies involved. For example, high angle normal faults dipping in a direction opposite to that of the thrust surfaces are seldom reactivated, whereas normal faults dipping to the same direction or at low angle to the thrust surface are more easily inverted as transpressional or reverse faults. Normal faults or facies limits oriented perpendicularly to subsequent thrusts are often loci of structural undulations in the belt or of transfer zones.

From the structural analysis of the Southalpine belt it is evident that each structural undulation is controlled by pre-existing

rheological anisotropies (variations of thickness and facies, inherited faults, etc.). Consequently we may hypothesize the occurrence of paleostructures, even where these are undiscovered, on the basis of the occurrence of structural undulations within the belt. The largest structural undulation of the Southern Alps occurs along the Giudicarie fault lineament, which is most probably one of the largest Mesozoic crustal anisotropies between the Trento Platform to the east and the Lombard Basin to the west. Towards the east, further first order structural undulations occur at the transitions between Trento Platform and Belluno Basin and between Belluno Basin and Friuli Platform, which are the more significant structural features of the area. Various second order undulations occur in correspondence with the minor paleostructures at the margins or within the above mentioned major structural domains, which were unstable features through time. As analogously observed in seismic lines at the margins of present-day plate margins, such domains were progressively cut by extensional and transfer faults that dissected the structural highs and were active at different places in different times. For example, the eastern margin of the Trento Platform retrogressed, from a structural point of view, to the west from the Jurassic to the Cretaceous. This controlled the thickness and sometimes the facies of sediments. The differences on the two sides of the Mesozoic extensional fault system separating the Friuli Platform and the Belluno Basin controlled the geometry of the front of the Venetian Southern Alps front. To the west, within the Belluno Basin, the front is accommodated by a triangle zone (Bassano Line) and the foredeep clastic sediments are folded and tilted to the south, whereas to the east the frontal thrust front crops out along the Maniago Line and the clastic foredeep sediments are overthrust.

The structural undulations at the front of the belt also control the syn-tectonic clastic depo-

sition in the foreland basin. The onlaps on the growing flank of the frontal fold of the belt occur unconformably only along dip if the fold is cylindrical (i.e., without axial undulations). On the contrary, the unconformity will occur both along dip and strike in non-cylindrical folds (i.e., along deep anisotropies inherited by compressional tectonics).

Interactions between tectonics, eustasy, compaction and sedimentation.

In general, thrust fault activation migrates towards the foreland in fold-and-thrust belts. Consequently, also syntectonic clastic deposits migrate towards the foreland. In several works, the evolution of fold-and-thrust belts is described in terms of orogenic phases or pulses. This may suggest misleadingly that shortening is limited to periods separated by quiescence stages. It is here stressed that the shortening in contractional belts is rather constant through time and follows the rate of plate motions that is rather regular, as indicated by the spreading rates at middle-oceanic ridges. Such continuous shortening is accomplished by the growth of folds related to fault-propagation and fault-bending. These folds generate episodic and local uplifts within a belt that constantly migrates towards the foreland. However, such local events may not be interpreted as the evidence of a phase-like evolution of shortening in fold-and-thrust belts (figs. 164, 165).

For example, a single fold with a 1-3 km amplitude can develop in a time span variable between 0.5 and 5 Ma. During the growth of an anticline (either sub-aerial or marine) the clastic sedimentation drapes and onlaps the uplifting zone.

The anticlines are eroded and represent the source area for the foredeep deposits. The growth of an anticline may occur during a part of a third order cycle (e.g., low stand, transgressive, high stand) and consequently sedimentation may be controlled by the interplay

between uplift rates and eustatic fluctuations. Such a combination may be highly variable and random. The uplift rates of an anticline may in general be considered constant through time, but may also be irregular, especially in transpressional settings.

During a low stand, the uplift rates of the anticline and the rates of eustatic fall need to be summed up. This time interval obviously will register the largest relative sea-level fall and the period will be characterised by strong erosion of the anticline. During a transgression stage, the effects of tectonic uplift may be in part or

totally compensated by the eustatic rise. As a result the relative sea-level may remain approximately constant along the flanks of a growth anticline and erosion may be minimal. The subsequent high stand represents an intermediate situation, in which the structural uplift is only in part (or not at all) compensated by the eustatic rise. Consequently also erosion is intermediate between that occurring in low stand and transgressive phases. Therefore, each fold has its own tectonic and eustatic history. The resulting syntectonic stratigraphy is therefore highly dependent on when, where and

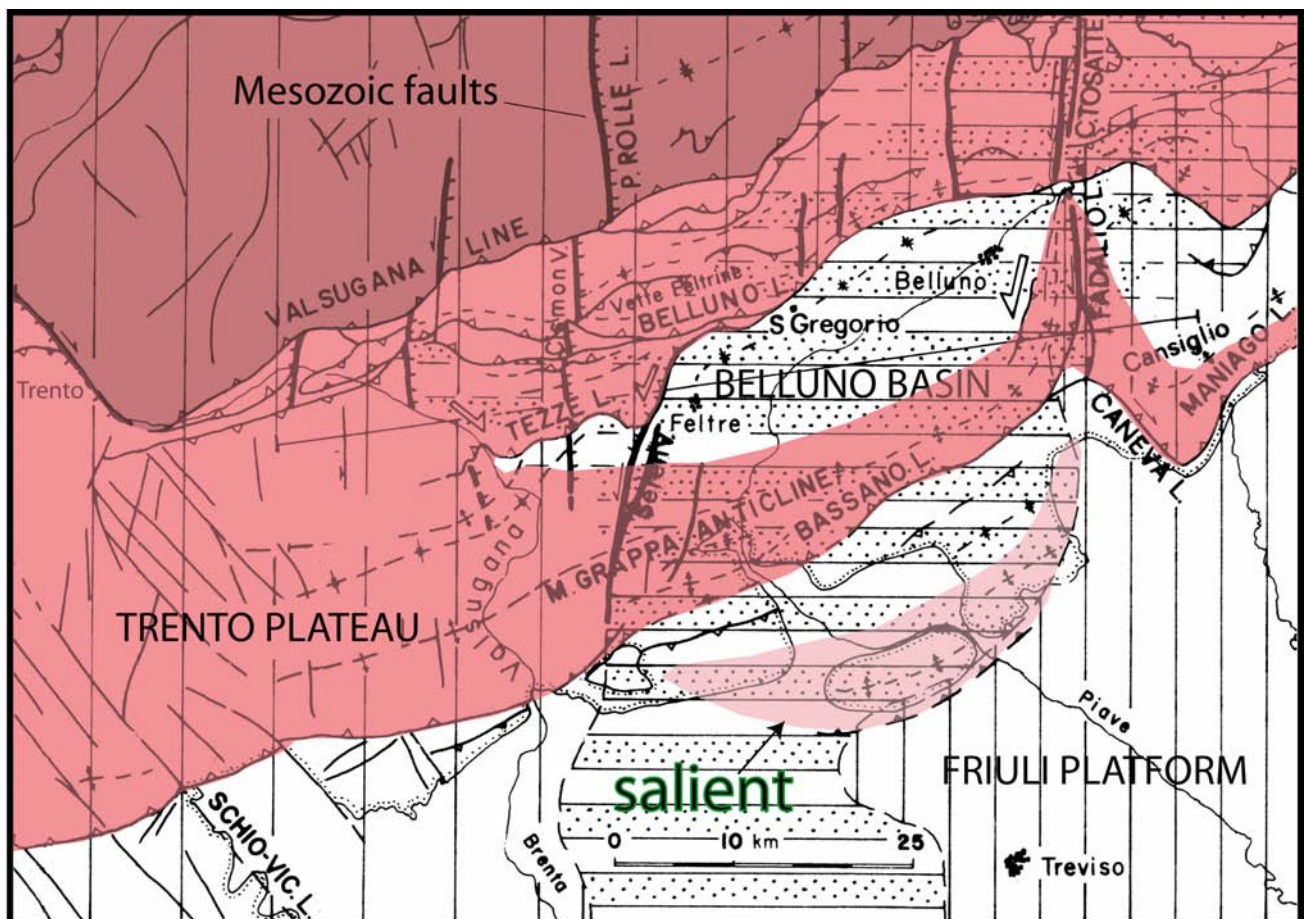


Fig. 149 - The Mesozoic horts and grabens and facies transitions controlled the geometry of the Venetian Alps fold-and-thrust belt, producing undulations of the structures that are characterised by non-cylindrical shape. Transpressional fault systems and transfer faults are localised along inherited Mesozoic extensional faults and along thickness and facies variations of the sedimentary cover. The shaded pink zone represents the morphological and structural relief of the area. The darker colors are toward the more internal thrust sheets. Note that such a relief diminishes rapidly from the Trento Platform towards the east where compressional tectonics affected the sediments of the Belluno Basin. At the eastern margin of the basin, a major sinistral transpressional zone occurs at the intersection with the Friuli carbonate platform. The structural relief is lower but more diffuse within the Belluno Basin which is richer in shaly content, allowing lower friction in the decollement zones, and forming a salient of the thrust belt front (after DOGLIONI, 1992). In the salient, ramp distance is wider and the topography is lower.

how the fold develops. A fold is therefore a local process that represents only a spatial and temporal element of a mountain belt that needs to be studied in all its aspects. Dating a fold, filtering the effects of the eustatic oscillations, means deciphering one single step of the complex evolution of a belt.

A crucial point in the study of mountain belts is the dating of the deformation phases. The stratigraphic chronologies, based on transgressive conglomerates may however be misleading. For example, in the Venetian Southern Alps a strong Messinian deformation phase, characterised by strong conglomeratic sedimentation (Montello and Pontico Conglomerates), has been proposed for a long time. However, the eustatic curve shows a sharp global low stand phase during the Messinian.

It may be thus alternatively proposed that the Venetian Southern Alps developed quite regularly from the Oligocene and that the Messinian sea-level fall, even if restricted to the

Mediterranean, may have induced a strong erosional phase, non necessarily associated to a tectonic pulse.

The geometry of sediments onlapping normal fault escarpments or the flanks of anticlines, is normally considered to be controlled by the relationship between tectonics and sedimentation but it may be additionally controlled by differential sediment compaction. For example, in the Apennines the basinal strata onlapping platform sediments along Mesozoic normal fault paleoescarpments commonly dip considerably (as much as 20°-30°) toward the basin when platform strata are retrodeformed to horizontal so to eliminate the geometrical effects of Tertiary compressional tectonics. These geometries are usually interpreted, in the field and in seismic lines, as the effects of normal drag along synsedimentary faults. Similarly, basinward dip affecting clastic sediments onlapping anticlines flanks in the Po Plain has been interpreted as the effect of synsedimentary growth of the anticline. Although



Fig. 150 - Satellite image of the Venetian Alps. Notice that the dimension of the morphological high of the Asiago Plateau (A), corresponding to the Mesozoic Trento Platform, drastically reduces to the east within the Belluno Basin, broadly correspondent with the Belluno syncline (S) located between Feltre (F) and Belluno (B). To the right the undulation of the Mt. Grappa-Visentin Anticline can be observed. This anticline developed in a transpressional system, at the intersection between the Belluno Basin and the Friuli Platform. V, Vittorio Veneto.

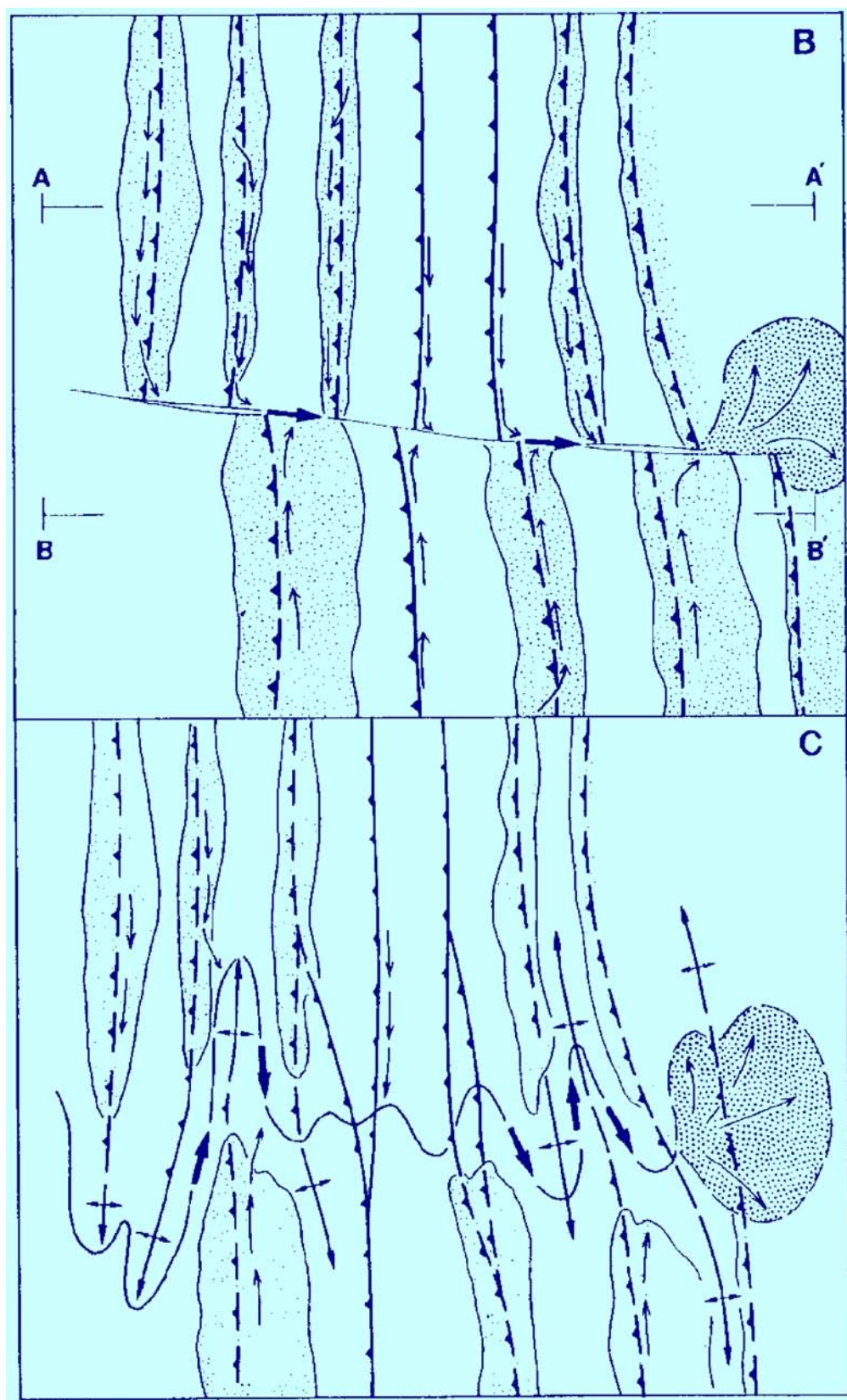


Fig. 151 - Structural undulations along strike, and transfer zones in general, control the hydrographic pattern. Therefore the coarser and larger accumulation of clastic material at the front of the thrust belts occurs more frequently where internally in the belt there are transfer zones (after LAWTON *et alii*, 1994).

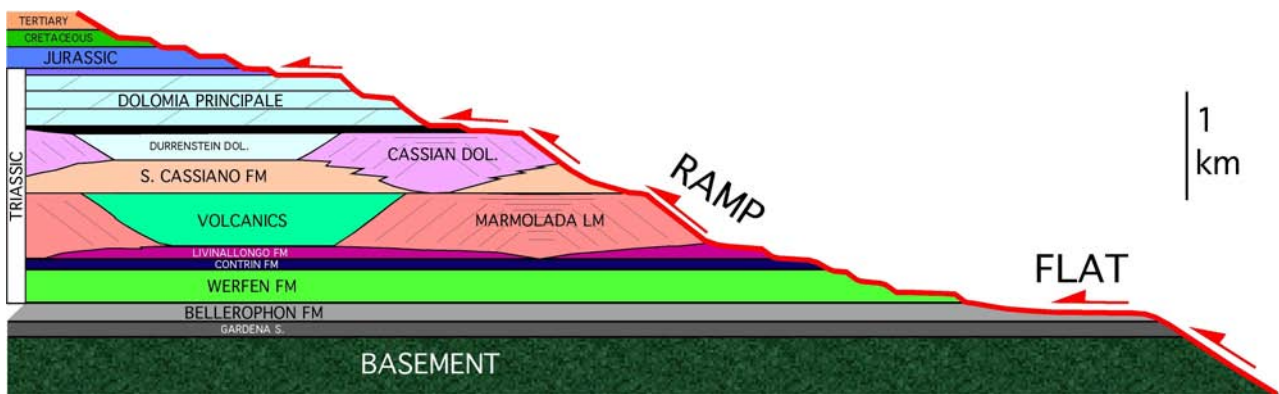


Fig. 152 - Potential control of the stratigraphic succession on the localization of ramps and flats (decollement surfaces) of thrust faults in the Dolomites region. The basement includes the Gardena Sandstone, the older Permian porphyrites and the underlying Hercynian crystalline basement. Notice the occurrence of margins of Ladinian and Carnian carbonate platforms (Marmolada Limestone and Cassian Dolomite respectively) that can be the loci of thrust ramps. The Bellerophon Fm (Upper Permian), consisting mainly of evaporitic sediments such as gypsum, shales and marls, is characterised by flat geometries of thrust faults, similarly to other relatively less competent formations (e.g., Andraz Horizon of the Werfen Fm and Raibl Fm).

the feasibility of such an interpretation is not neglected, the results of numerical simulations of sedimentation demonstrate that the dips observed in the field or in seismic lines can also (or in part) be explained by differential compaction (SKUCE, 1994; CARMINATI & SANTANTONIO, 2005; SCROCCA *et alii*, 2007). The role of differential compaction is supported by numerical modeling (figs. 166, 167).

The evolution of the belt will be therefore registered by punctual information provided by the unconformities. The dip of the basement monocline varies between 0° and 5° in belts associated to subductions that follow the flow of the mantle (i.e., directed to the E-NE), and between 5° and 10° in the belts associated to subductions contrasting the mantle flow (i.e., directed to the W). In this latter case, cha-

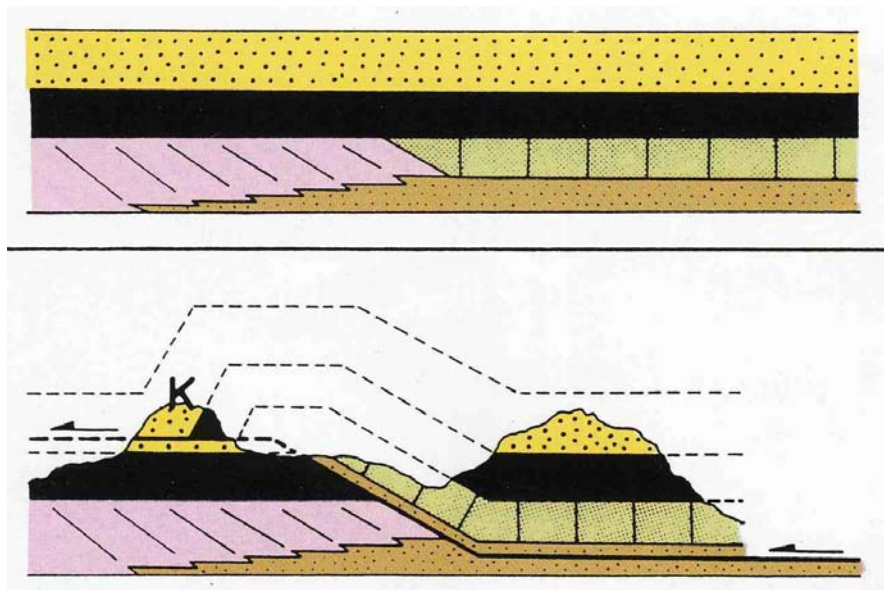


Fig. 153 - Schematic section of a carbonate platform (violet) and of the adjacent basin covered and levelled by later sediments. The margin of the platform becomes the area where compressional stresses are focussed. For this reason, the chance that ramp geometries of the thrust faults may form in this inherited structure is rather high. The klippen (K) of the Dolomites are interpreted as remaining parts of the hanging-wall of thrust faults similar to that shown in this figure.

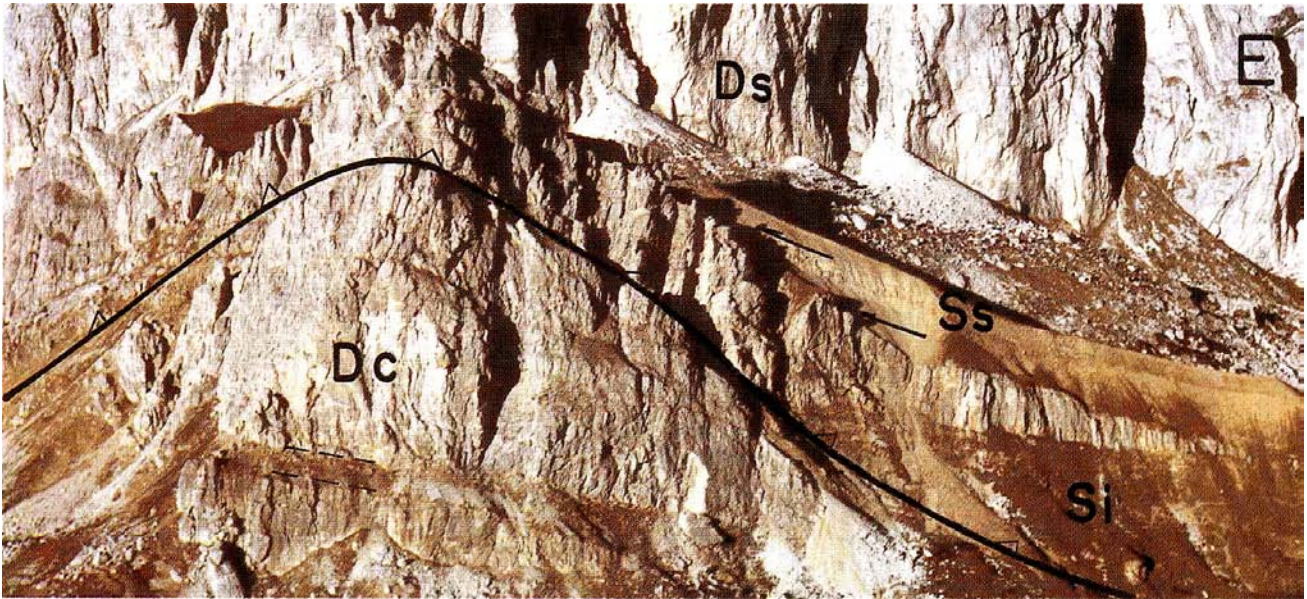


Fig. 154 - The Sasso di Richthofen (central Dolomites) is a prograding edge of the Lower Cassian Dolomite (lower Carnian, D1) that was doubled by a thrust that partially used as a ramp the clinostratification of the megabreccias. Notice within the San Cassiano Fm the thinning of the body of megabreccias towards the right that onlaps the same body. D2, Upper Cassian Dolomite; S1, Lower San Cassiano Fm; S2, Upper San Cassiano Fm.

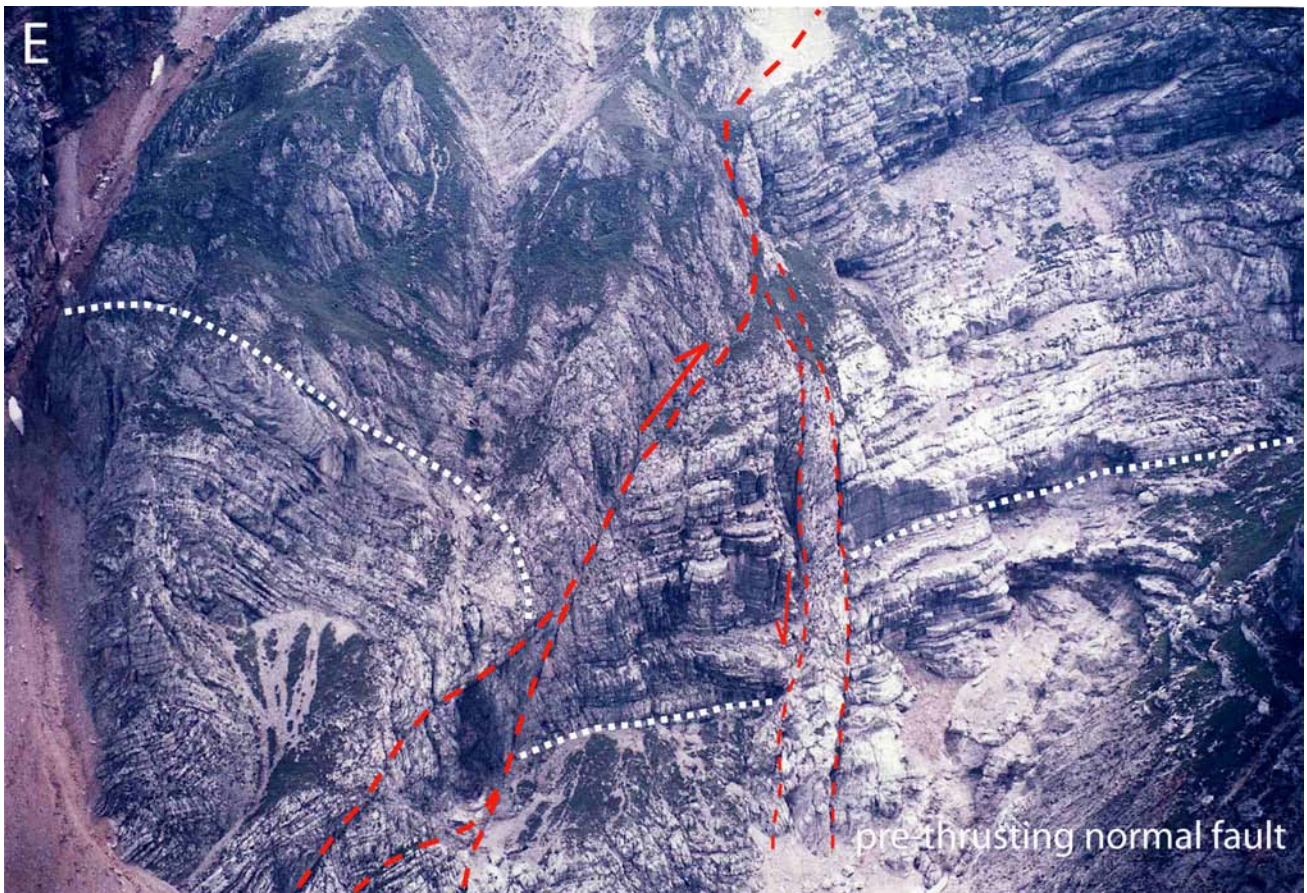


Fig. 155 - Northern wall of the Croda del Vallon Bianco (Ampezzo Dolomites), consisting of Liassic Calcarei Grigi in which a W-verging thrust cuts a pre-existing extensional fault of Upper Jurassic - Lower Cretaceous? age.



Fig. 156 - WSW-verging thrust of the Remeda Rossa in the Ampezzo Plateau. The thrust surface is sub-horizontal, the hanging-wall consisting of folded and partly overturned Calcarei Grigi (G) and the footwall consisting of Cretaceous marls (K; in the meadows), extremely deformed by the shear zone.



Fig. 157 - Detail of the previous figure. In the hanging-wall of the Remeda Rossa thrust the Calcarei Grigi sediments are overturned along the broken flank of a fault-propagation fold. In these sediments, a shear zone can be observed. If the sediments are retro-deformed to the pre-overturning position, the shear zone is interpretable as a syn-sedimentary extensional fault. Notice that the fault is sutured at the bottom of the picture. It may, however, be argued that the flexural slip necessary to accommodate the fold formation may have obliterated such an inherited shear zone. In this case the shear zone could be interpreted as an antithetic Riedel fault of the main thrust plane.

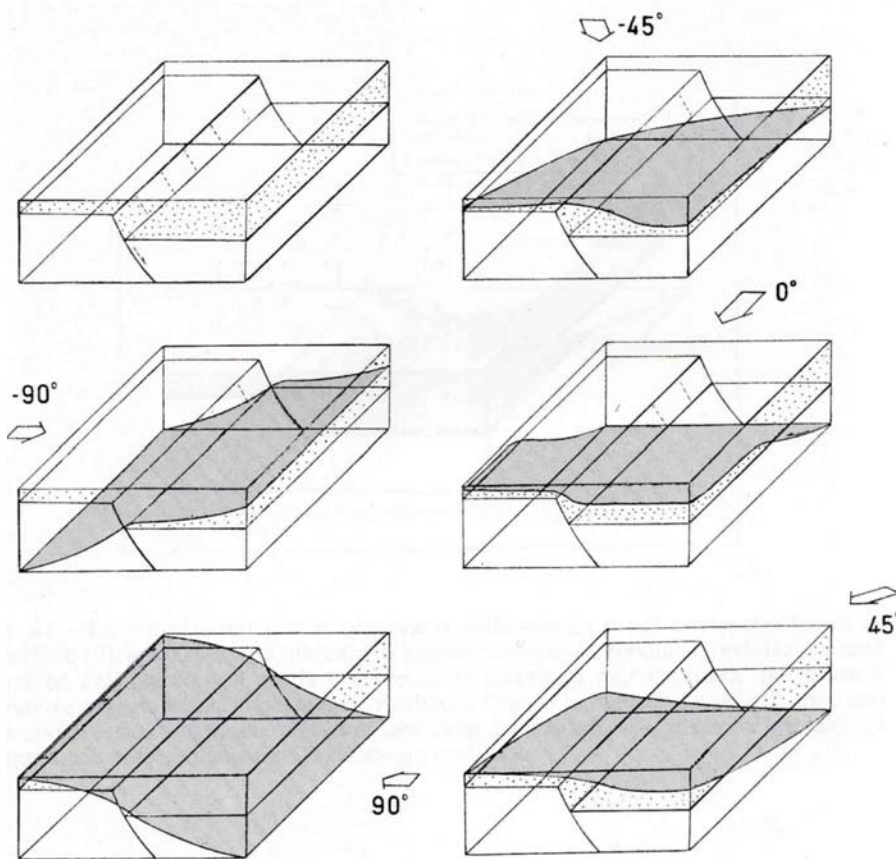


Fig. 158 - During inversion stages, a given normal syn-sedimentary fault can be shortened with very variable angles. The fault-hinge zone represents a strong anisotropy within the shortened body and compressional stresses may easily focus around the extensional lineament. The stress field in the vicinity of the fault is, however, controlled also by the angle between the principal stresses directions and the inherited geometry (both strike and dip) and by the rheology of the rocks constituting both hanging-wall and foot-wall. The entity of inversion is surely influenced by the direction of compression with respect to the attitude of the paleostructure. Lateral ramps frequently develop in the areas of inherited fault hinge. A compression oriented at -90° to the strike of the paleostructure may cut the paleostructure without producing appreciable inversion along the old extensional lineament, with the exception of minor backthrusting. The more significant inversions develop when the extensional paleofaults dip to the same direction of the thrust fault planes and the angle between the shortening direction and the dip direction of the extensional fault is small. For example, in the Southalpine belt, the Mesozoic extensional faults striking about N-S and dipping to the east were cut and involved in the alpine folding without significant deformation. In other words they are much more preserved and recognizable than Mesozoic normal faults with the same strike but dipping to the west that were frequently reactivated as sinistral transpressional faults.

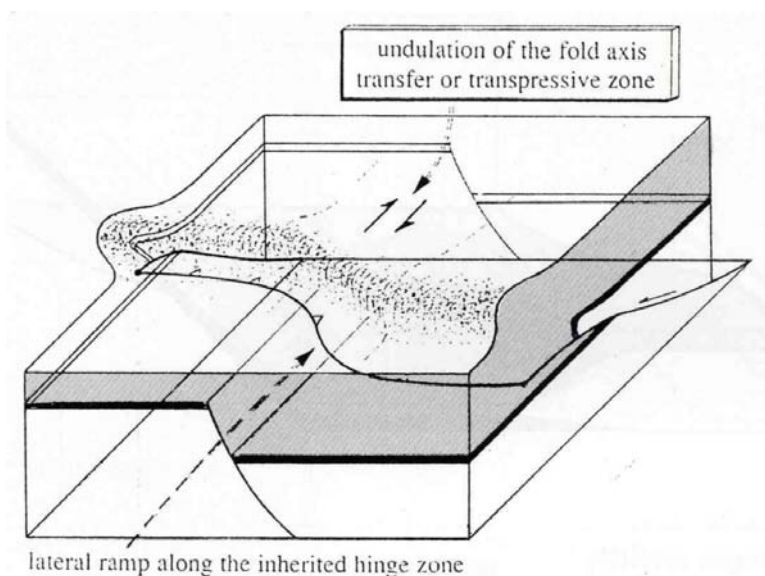


Fig. 159 - Undulations of fold axis and thrust plane reflect the presence of paleostructures (i.e. normal faults or facies changes) at depth. The undulation of the fault-propagation fold will be a function of the angle of compression with respect to the buried feature. The drawing represents the case of 0° , with compression parallel to the pre-existing normal fault strike. Lateral ramp forms along the inherited anisotropy. Between 0° and 30° - 40° , there are the strongest undulations as in the example of the next figure.

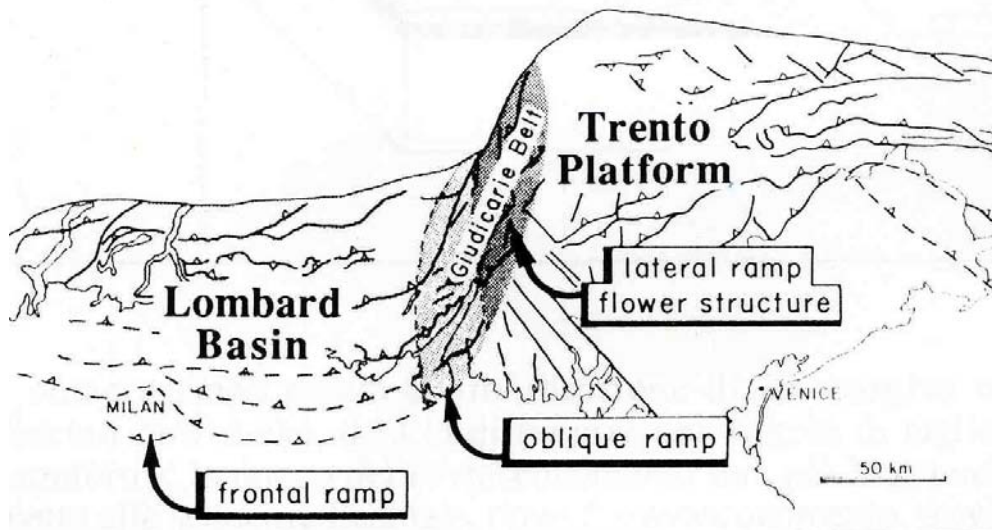


Fig. 160 - The sinistral transpression along the Giudicarie fault system represents the strongest structural undulation of the Alps and developed as a sinistral transpressional reactivation of a system of extensional faults dipping to the west (one of the major fault is the Ballino Line; CASTELLARIN, 1972). This undulation developed at the border between the Lombardian Basin to the west and the Trento Platform to the east (DOGLIONI & BOSELLINI, 1987).

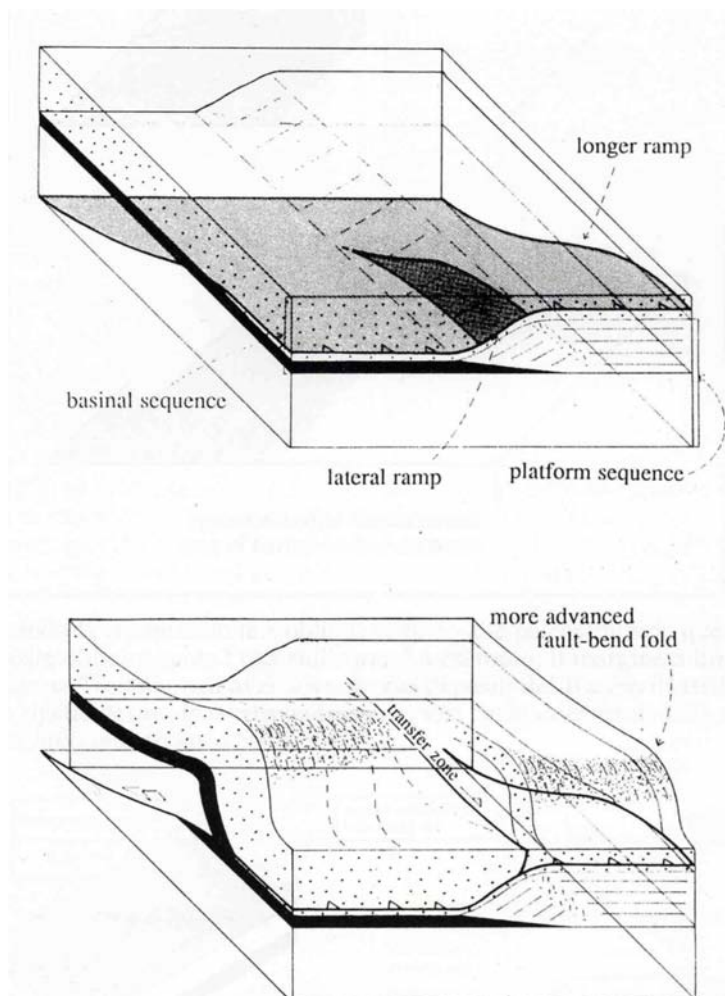


Fig. 161 - Example of shortening parallel to the margin between a carbonate platform and a basin. In this case the difference of ramp dips between basin and platform sediments will produce a longer thrust ramp in the platform sequence with respect to the basin sequence, where the thrust surface, propagating in less competent sediments, will tend to become horizontal. This will produce a more advanced anticline in the platform sequence with respect to that in the basin sequence, with a transfer lateral ramp connecting the two structures. This model could be applied to the western margin of the Friuli Platform, where the Cansiglio anticline developed in the platform sediments in the hanging-wall of the Maniago Line is more advanced than the Mt. Grappa-Visentin Anticline developed in the Belluno Basin. The two anticlines are connected by the Fadalto - Caneva transfer zone. It is, however, to be noticed that the Mt. Grappa-Visentin Anticline is not the front of the belt, which coincides with the more external Montello Anticline, within the salient in the Belluno Basin.

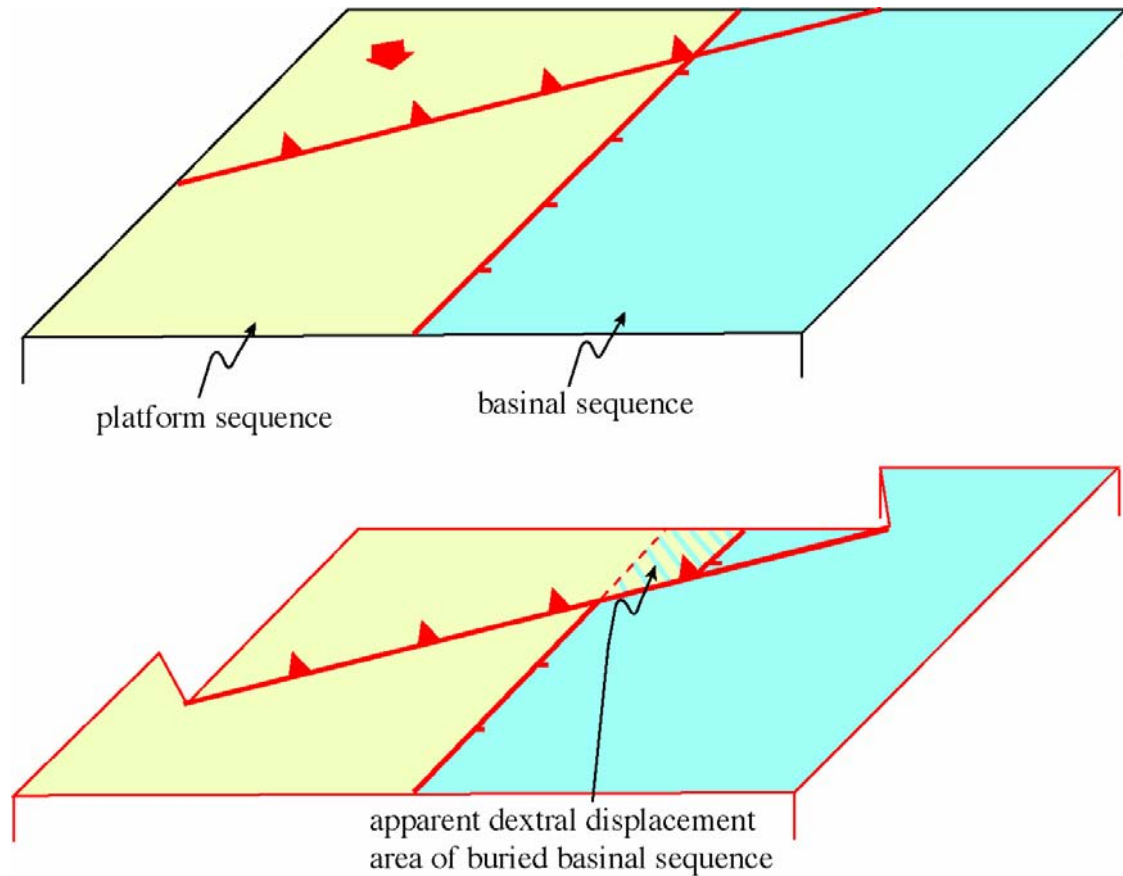


Fig. 162 - A thrust obliquely affecting a platform-basin margin will produce an apparent dextral displacement. For instance the Trento Platform was thrust towards southeast over the Belluno Basin in the Venetian Prealps along the Belluno Thrust, due to the southalpine N20°-30°W compression oblique to the Mesozoic N-S trending margin.

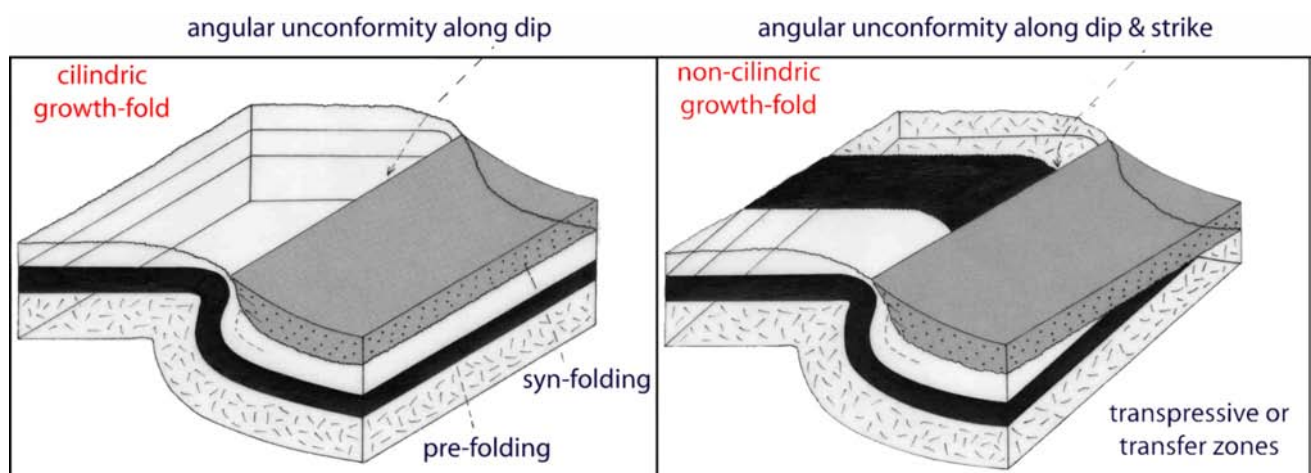


Fig. 163 - The front of the fold-and-thrust belt is characterised by clastic syntectonic deposition. With the progressive growth of the belt, the molassic deposits tend to onlap the flank of the frontal growth anticline. If the frontal anticline is cylindrical, the resulting unconformity will interest only the dip angle. In anticlines characterised by axial undulations, the resulting unconformity will occur both along dip and strike.

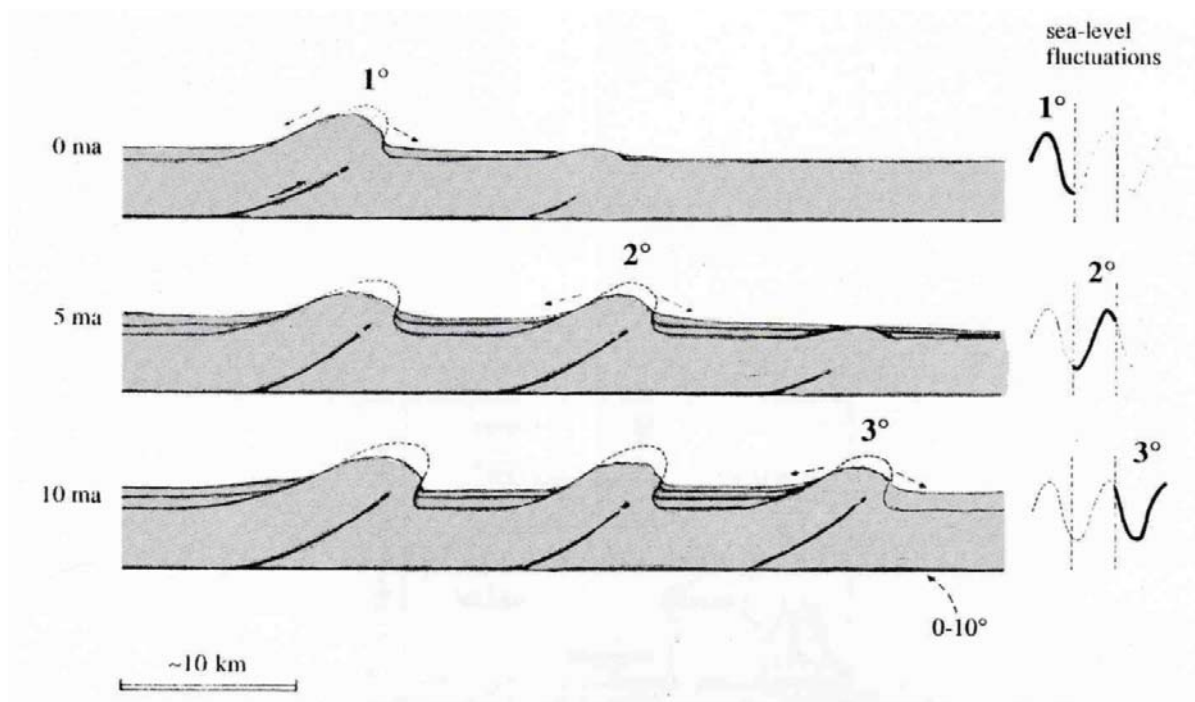


Fig. 164 - Three tectonic cycles may occur during three different segments of a eustatic curve. The depositional sequences may thus be characterised by different interference patterns between tectonics and eustatism. The fault-propagation folds of an accretionary prism produce episodic and localised uplifts of the belt, which migrate regularly towards the foreland together with the foredeep basin and the depositional sequences associated to the growth of any anticline.

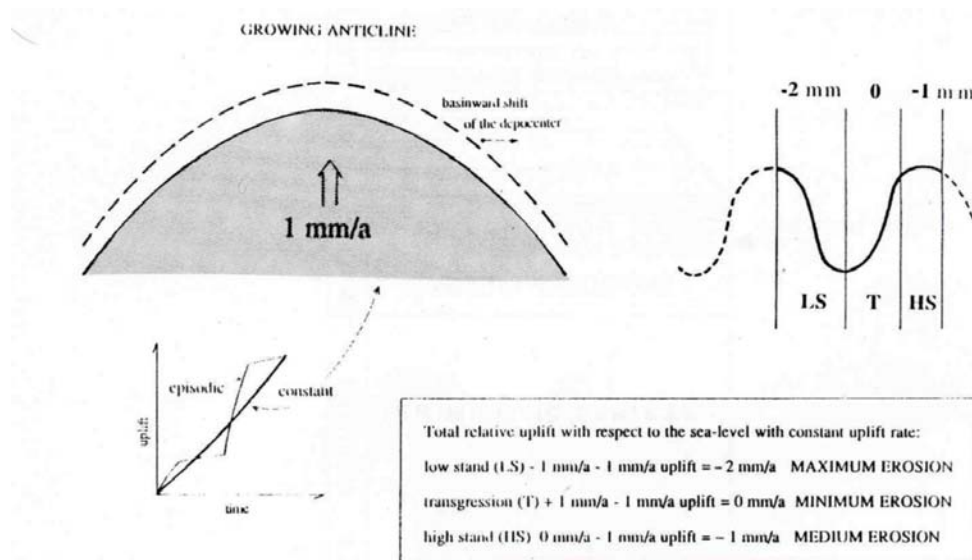


Fig. 165 - The growth of an anticline may be episodic or constant (like the slow steady-state plate motions). In this figure it is shown a scenario characterised by an uplift rate of 1 mm/yr. The uplift is superimposed to a eustatic cycle of third order, represented to the right. During the low stand, with a eustatic sea level fall of 1 mm/yr, the relative sea-level fall at the growing anticline will occur at rates of 2 mm/yr, producing a significant erosion of the anticline. During a transgressional stage with rates of 1 mm/yr, the tectonic uplift will be compensated by the eustatic rise and the relative sea-level will remain constant, inducing minimum rates of erosion of the fold. The assumed uplift and eustatic rates are hypothetical. However, they may help in understanding the problem of the relationship between tectonics and sequence stratigraphy.

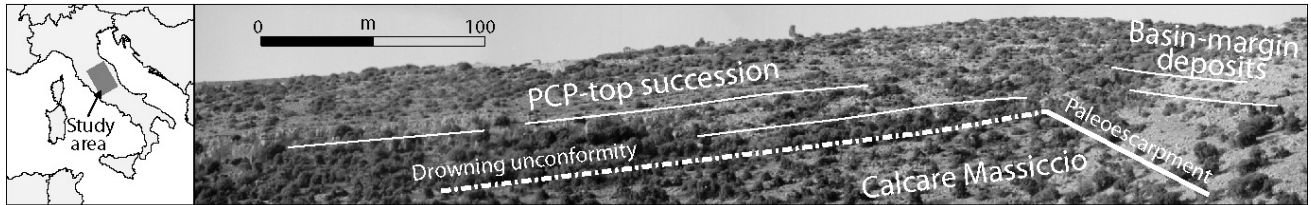


Fig. 166 - Panoramic view of platform-to-basin transition at Castiglione (Sabina region, Central Apennines). Notice that the onlapping basinal sediments are at an angle of approximately 20° with respect to the sediments deposited onto the structural high. Such an angle is interpreted as the result of differential compaction affecting basinal sediments in the hangingwall of the paleoescarpment. PCP- pelagic carbonate platforms, (after CARMINATI & SANTANTONIO, 2005).

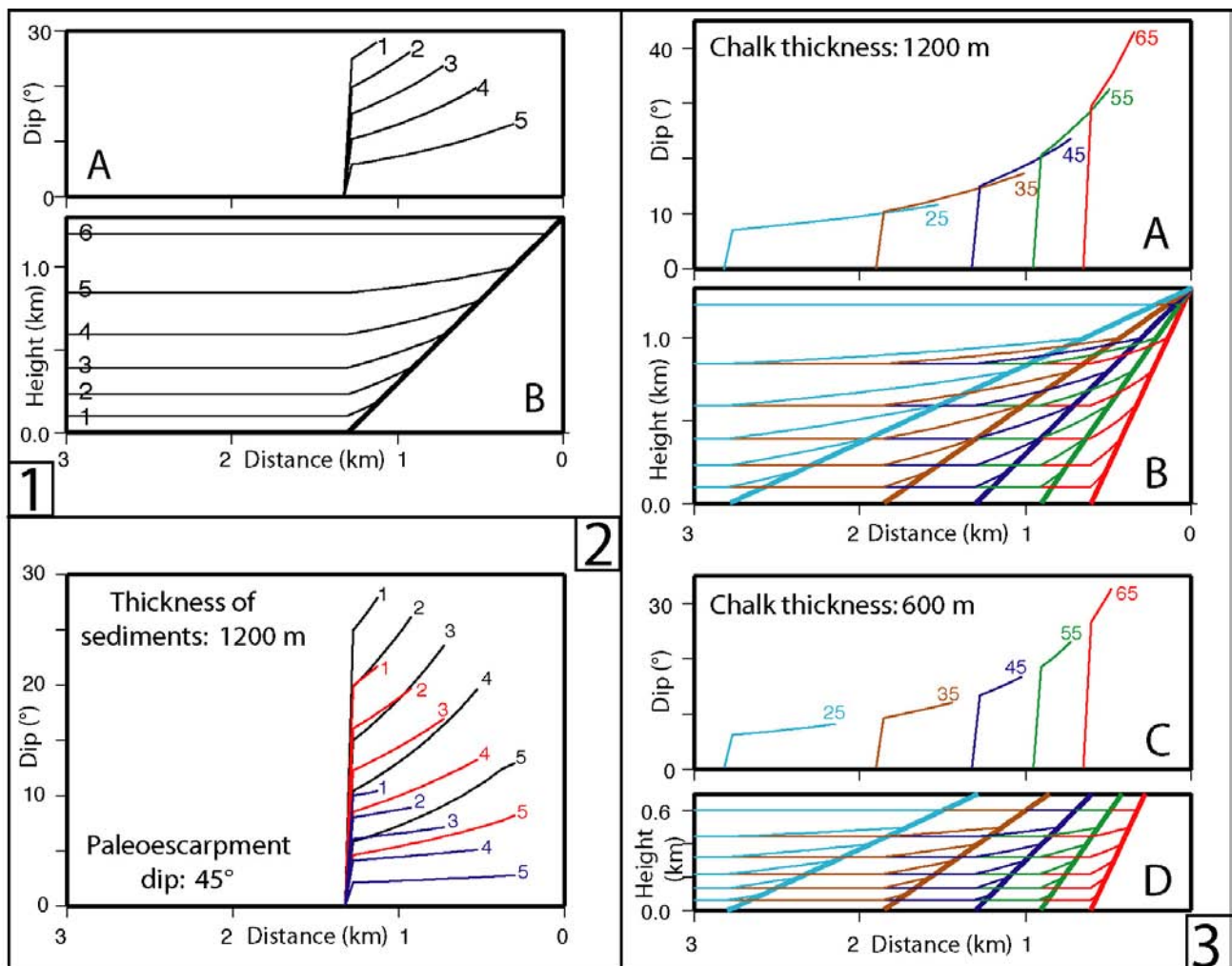


Fig. 167 - This figure shows the results of numerical models of compaction of the basal sediments onlapping a normal fault paleoescarpment. Such results may be, however, extended to sediments onlapping the flanks of anticlines in compressional settings. Notice that the geometry and dip of basal sediments vary consistently with the variation of the sediment nature and of the fault dip. (1) (A) Dip and (B) geometry predicted for a 1200-m-thick succession of chalk onlapping an escarpment dipping 45° . (2) Dip predicted for 1200-m-thick chalk (black), shale (red), and sandstone (blue) successions onlapping an escarpment dipping 45° . (3) (A, C) Dip and (B, D) geometry predicted for chalk section (1200 m and 600 m thick, respectively) onlapping escarpments with dips ranging between 25° and 65° . In A and C, dip is referred to level 3. Colors indicate simulations with different escarpment dips: cyan, 25° ; brown, 35° ; blue, 45° ; green, 55° ; red, 65° (after CARMINATI & SANTANTONIO, 2005).

racterised by more inclined basement monoclines, the internal synclines may be filled by larger volumes of clastic deposits (figs. 168, 169).

Fold uplifts compete during their development with regional subsidence in the frontal parts of thrust belts and accretionary wedges. Two cases exist in frontal thrust belts. In the first, most common case, the uplift rate of the external folds is higher than the subsidence rate of the foredeep. In the second case the fold uplift is less than the regional subsidence. The total fold uplift may be considered as the fold uplift rate minus the regional subsidence rate; this value can be either positive or negative. The positive total fold uplift occurs when folds rise faster than regional subsidence and the envelope of the fold crest rises toward the hinterland of the accretionary wedge. In the opposite case, the negative total fold uplift, the envelope dips toward the hinterland because

folds rise slower than the regional subsidence. In the first positive case the folds are deeply eroded and the onlap of the growing strata moves away from the fold crest if the sedimentation rate is lower than the fold uplift rate in marine or alluvial environments. In the second negative case, where folds rise at lower rates than the regional subsidence, the onlap moves toward the fold crest if the sedimentation rate is higher than the fold uplift rate. This is also the more favorable case for hydrocarbon traps where growth strata can seal the fold. Moreover the fast subsidence rates in the foredeep provide a higher thermal maturation. This second tectonic setting is commonly associated with accretionary wedges forming along west-dipping subduction zones, which are characterized by high subsidence rates in the foredeep or trench, due to the fast "eastward" roll-back of the subduction hinge (e.g. Apennines, Carpathians, Banda arc).

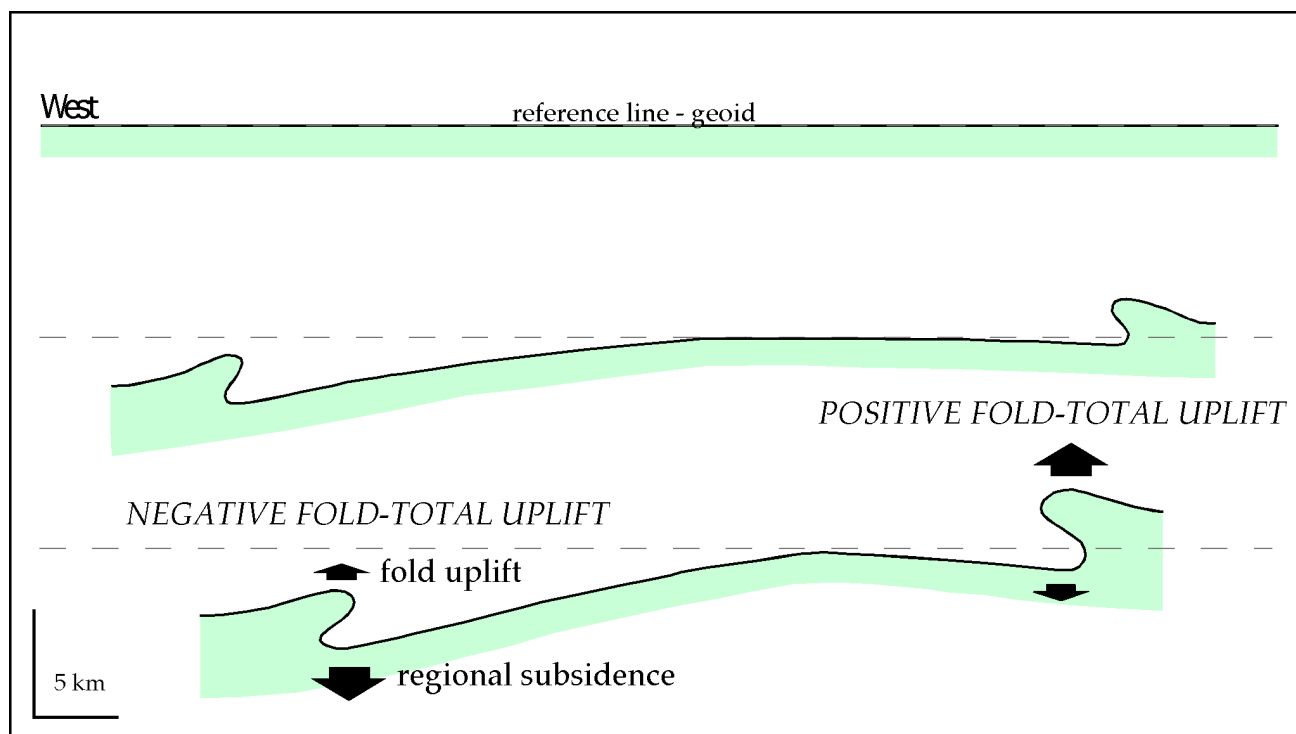


Fig. 168 - The fold-total uplift may be defined as the single fold uplift minus the regional subsidence. This value can be either positive or negative. This last case may occur along the front of W-directed subduction zones where the subsidence rates may be faster than the fold uplift rate.

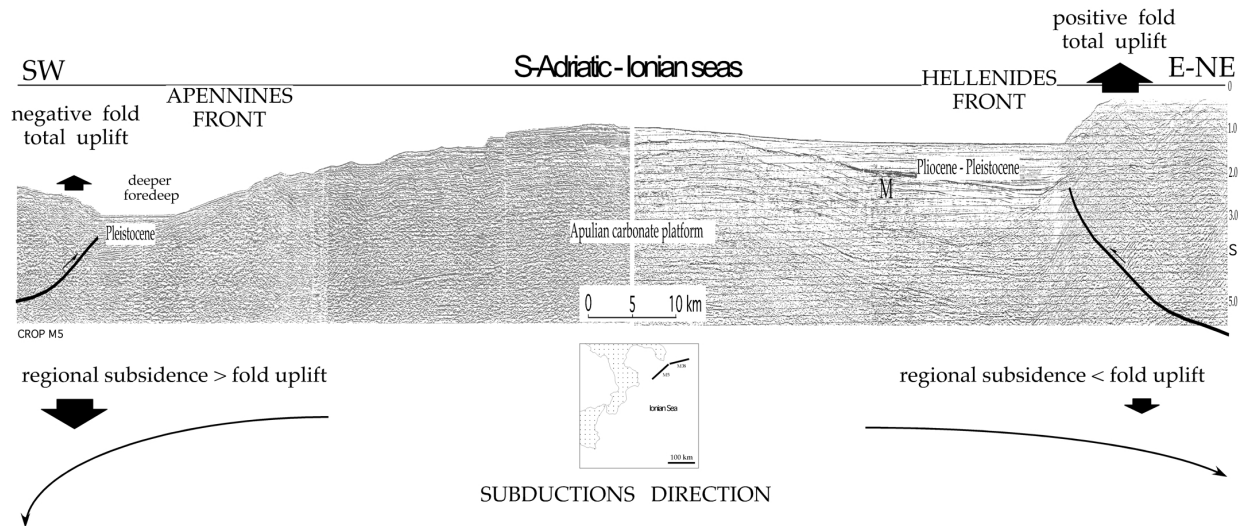


Fig. 169 - Comparison between the Apennines and Dinarides-Hellenides front in the southern Adriatic-Ionian seas. Note the deepest foredeep along the Apennines subduction and the higher structural elevation of the Hellenides front. M, Messinian. The Apenninic front has negative fold-total uplift, whereas in the Hellenides it is positive.

Normal faults occur in a variety of geodynamic environments, both in subsiding and uplifting areas (figs. 170 -174). Normal faults may have slip rates faster or slower than regional subsidence or uplift rates. The total subsidence may be defined as the sum of the hangingwall subsidence generated by the normal fault and the regional subsidence or uplift rate. Positive total subsidence obviously increases the accommodation space (e.g. passive margins

and back-arc basins), in contrast with negative total subsidence (e.g. orogens). Where the hangingwall subsidence rate is faster than the sedimentation rate in case of both positive and negative total subsidence, the facies and thickness of the syntectonic stratigraphic package may vary from the hangingwall to the footwall. A hangingwall subsidence rate slower than sedimentation rate only results in a larger thickness of the strata growing in the hangin-

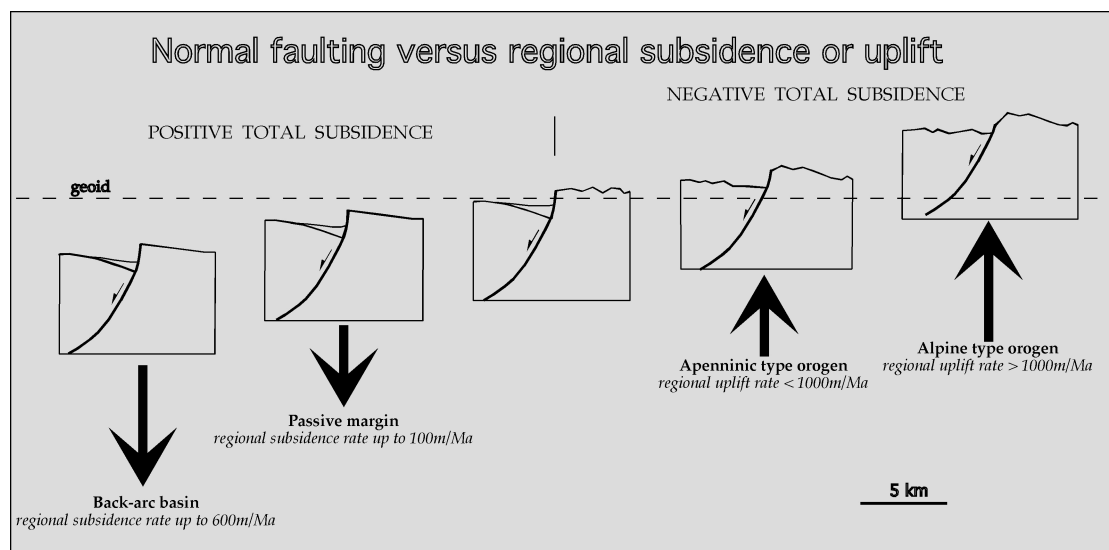


Fig. 170 - Normal faults form in almost all geodynamic settings. The subsidence they generate competes with regional thermal subsidence, lithospheric thinning or uplifting orogens along subduction zones.

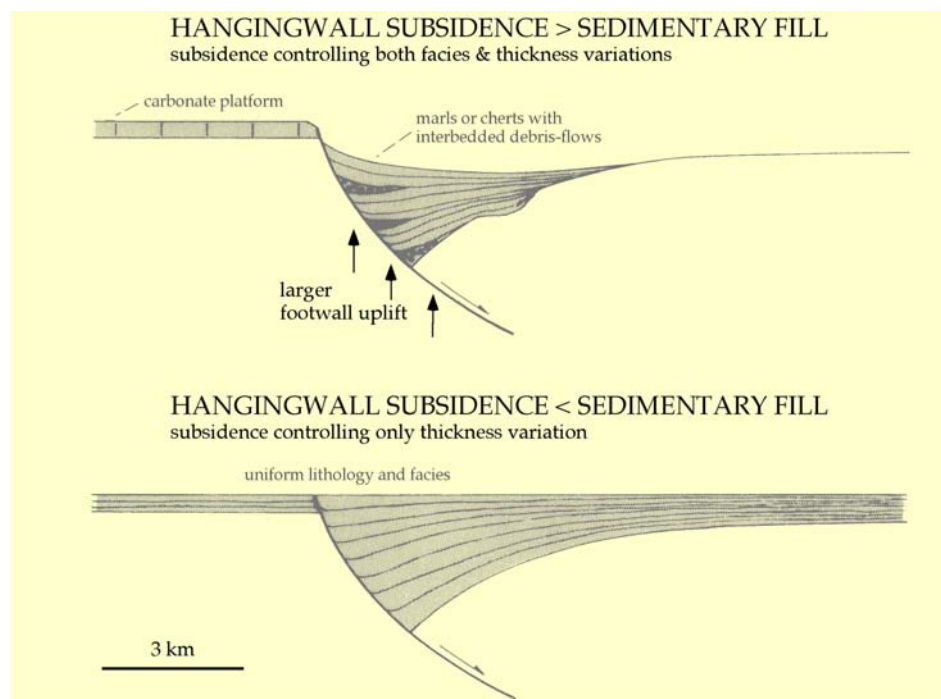


Fig. 171 - Relationship between tectonics and stratigraphy across an extensional syn-sedimentary fault. Subsidence rates and sediment supply are independent factors that have different values in different geodynamic settings. When the subsidence rate along a fault is larger than the sedimentation rate, there is a morphological step at the fault and this may generate lateral facies changes (upper panel). When the subsidence rate is lower than the sedimentation rate, the fault only controls the thickness of the syntectonic sediments and the morphological gradient is absent in any kind of sedimentary environment, e.g., both subaerial and shallow or deep marine facies (lower panel). In the former case, a higher footwall uplift should be expected due to the mass deficit. Interbedded debris flows may be sourced both by the fault scarp and by the limb of the rollover anticline. Debris-flow deposits (megabreccias) of this origin intercalated in a sedimentary successions should not be confused with low-stand wedge deposits generated by global eustatic falls.

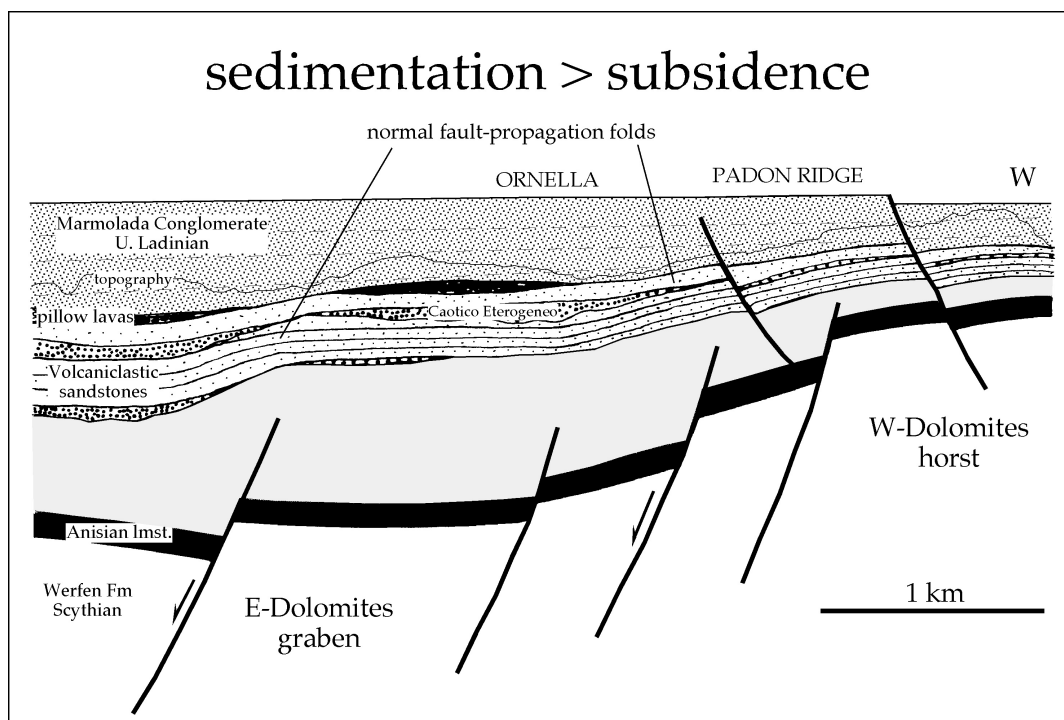


Fig. 172 - Cross-section at the end of the Ladinian along the Padon Massif (Dolomites). Synsedimentary N-S trending normal faults formed with subsidence rates slower than sedimentation rate and no facies changes occur across the faults.

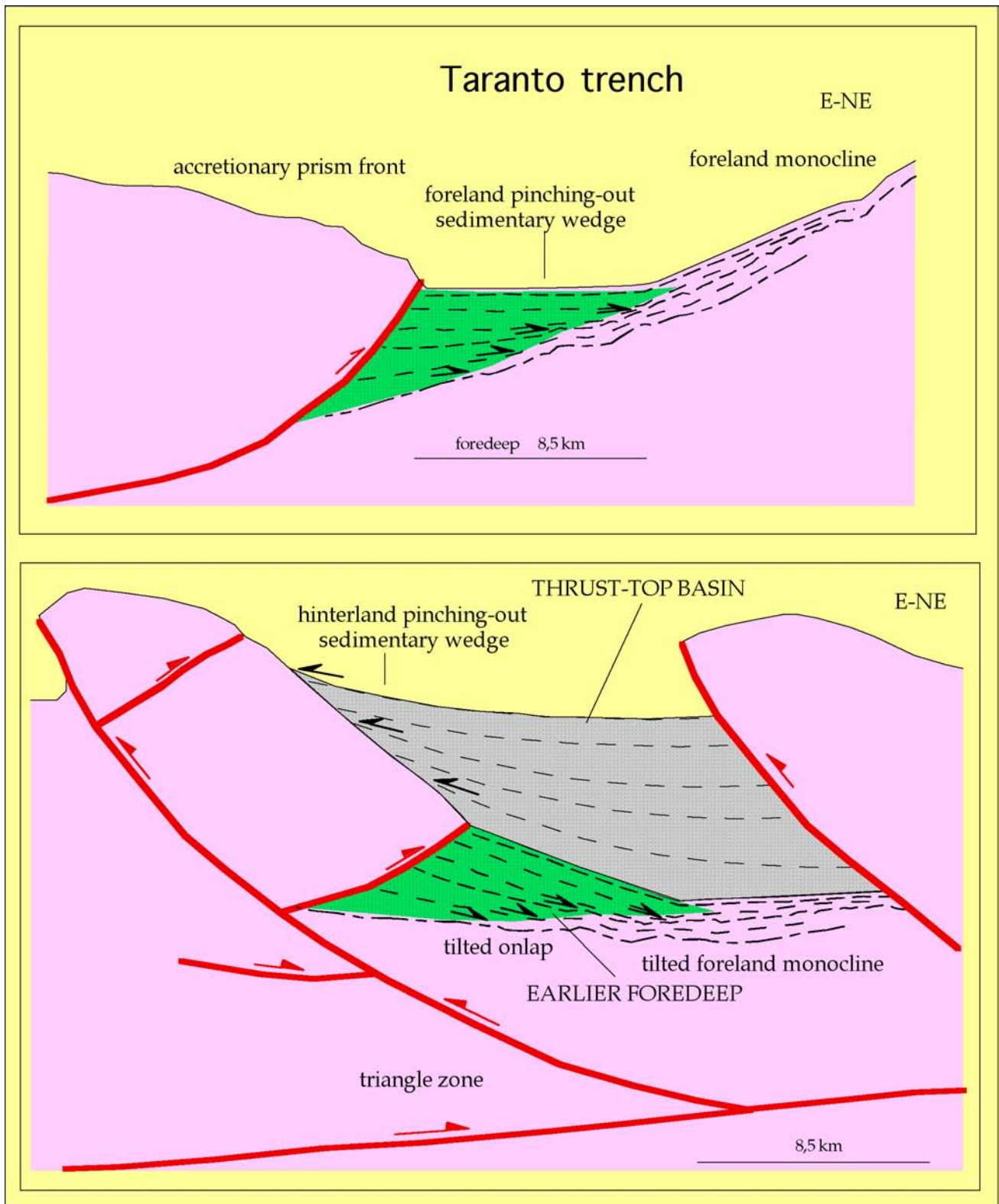


Fig. 173 - Interpretation of the geometric structural and stratigraphic pattern at the front and within the Apennines accretionary prism in the Ionian Sea. The present front (above) could represent the early foredeep stage later tilted by backthrusting (below). The original onlap onto the foreland regional monocline, and pinching-out of the sedimentary packages, once tilted, mimics an apparent downlap in the internal section below. The shape and width of the basin is controlled by ramp distances and vergences.



Fig. 174 - Example of the Apennines history. Pizzo Intermesoli, Gran Sasso Range, central Apennines. Jurassic transtensional tectonics sealed by Cretaceous basinal facies are preserved in a thrust sheet presently cross-cut by active normal faults to the left. Active thrusting is presently displaced eastward in the Adriatic coast.

gwall, with no facies changes and no morphological step at the surface. The isostatic foot-wall uplift is also proportional to the amount and density of the sediments filling the half-graben and therefore it should be more significant when the hangingwall subsidence rate is higher than sedimentation rate.

The foreland monocline dips underneath thrust belts and accretionary wedges, both in oceanic and continental subduction zones (fig. 175). Figure 176 shows the dip of the monocline in the frontal part of two orogens, the Alps and the Apennines. There is an overall difference between the dip of the relative monoclines, and there is also a strong lateral variation along both arcs. In the Alps, the regional dip varies between 0° in the remote foreland, to an average of $2-3^\circ$ at the front of the thrust belt below the foredeep, to about 5° beneath the external thrust-sheets within 40 km from the leading edge of the accretionary wedge. The regional dip of the monocline in the

Apennines has an average of $4-5^\circ$ at the front of the thrust belt below the foredeep, to about 10° beneath the external thrusts-sheets within 40 km from the leading edge of the accretionary wedge. There are areas where the dip exceeds 20° .

The Apennines though topographically lower than the Alps present higher monocline dips and a deeper foredeep. Moreover, there are variations in the dip of the monocline moving along strike of the two belts: the low values coincide with Permian-Mesozoic inherited horsts, whereas the steeper values correspond to basinal areas, and they usually match the salients of the thrust belt front. Within the salients the distance between thrusts ramps increases.

Therefore there are two orders of mean values of the dip of the foreland monocline, the first at the orogen scale (more than 1000 km wavelength), the second at the regional scale (100-200 km wavelength) within the single orogen.

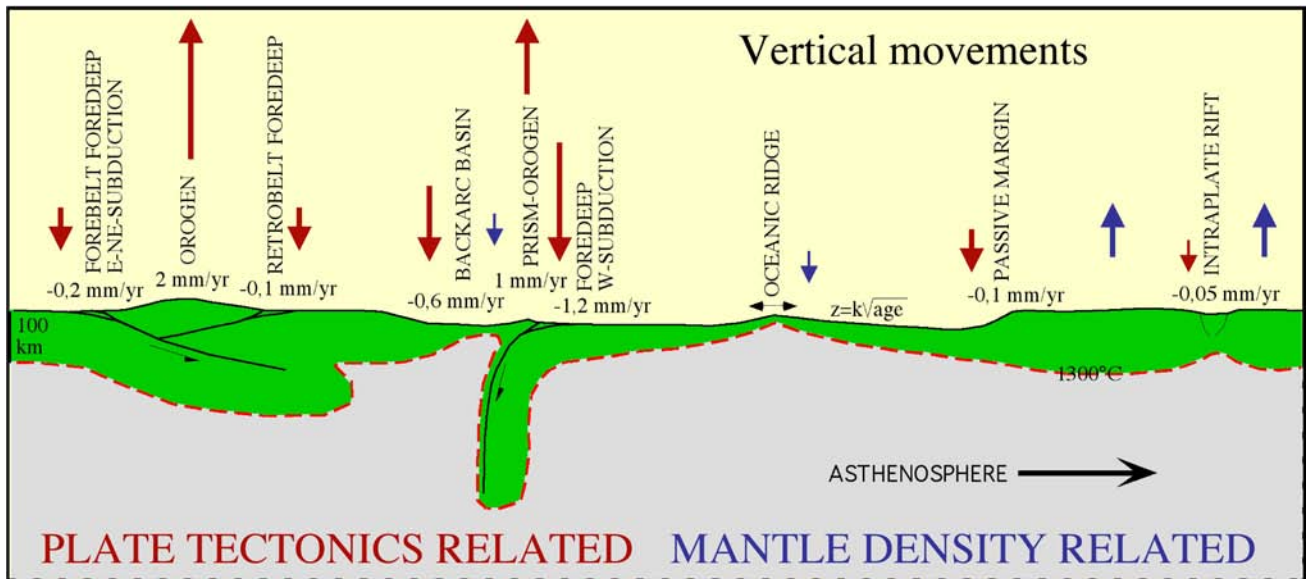


Fig. 175 - Mean vertical movements along the main geodynamic settings, i.e., foredeeps, passive continental margins, and rifts. Foredeeps subside for the flexure of the lithosphere generated by the loading of the upper plate along E- to NE-directed subduction zones, whereas they are possibly generated by the flexure generated by the opposite mantle flow along W-directed subduction zones. Oceanic embayments are subsiding mostly for the cooling and thickening of the lithosphere, where z is the depth of the ocean floor relative to the ridge, and K is a constant (320). Backarc rifts, passive margins and intraplate rifts are generated primarily by thinning of the lithosphere, plus thermal and loading effects. The red dashed line indicates the inferred trend of the isotherm marking the lithosphere base.

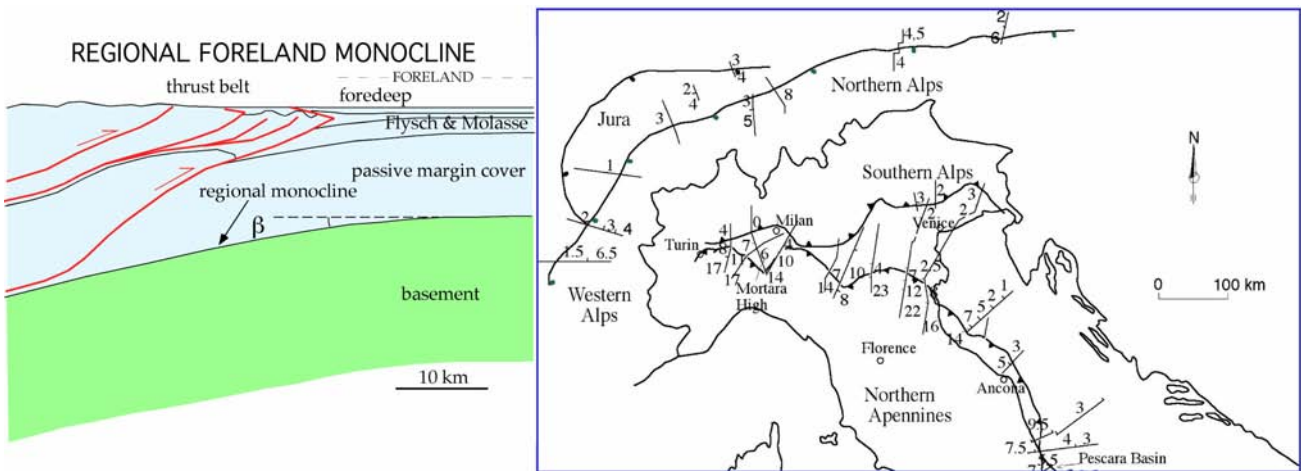


Fig. 176 - The dip of the regional foreland monocline is a significant signature of thrust belts. In spite of the higher elevation, the Alps have in average lower dip of the monocline with respect to the Apennines. This asymmetry might be ascribed to the different polarity of the subduction (after MARIOTTI & DOGLIONI, 2000).

Lateral variations in the lithospheric buoyancy due to the inherited Mesozoic stretching may explain the second order variations in foreland dip, but not the first order mean values which seem to be more sensitive to the geographic polarity of the subduction rather than to the lithospheric composition which is

rather similar in the Alpine and in the central-northern Apennines slabs.

The geological characteristics of foredeeps and accretionary wedges suggest that these features are distinguishable on the basis of the direction of the associated subduction (figs. 177 - 179). East- northeast-dipping subduction-related

accretionary wedges show high relief and broad outcrops of metamorphic rocks. They are associated with shallow foredeeps with low subsidence rates. In contrast west-dipping subduction-related accretionary wedges show low relief and involve mainly sedimentary cover. The related foredeeps are deep and have high subsidence rates (figs. 180, 181). This differentiation is useful both for oceanic and continental subductions, e.g., eastern vs. western Pacific subductions, or east-dipping Alpine vs. west-dipping Apenninic subductions (figs. 182, 183, 185). In a cross-section of the Alps the ratio of the area of the orogen to the area of the foredeeps is at least 2:1, whereas this ratio is 0.22:1 for the Apennines. These ratios explain why foredeeps related to east- or northeast-dipping subduction are quickly filled

and bypassed by clastic supply, whereas foredeeps related to west-dipping subduction maintain longer deep water environment. These differences support the presence of an "eastward" asthenospheric counterflow relative to the "westward" drift of the lithosphere detected in the hot-spot reference frame, even in the Mediterranean where no hot spots are present (fig. 184). In this interpretation, the Apennines foredeep was caused by the "eastward" push of the mantle acting on the subducted slab, whereas the foredeeps in the Alps were caused by the load of the thrust sheets and the downward component of movement of the upper Adriatic plate; these forces contrast with the upward component of the "eastward" mantle flow.

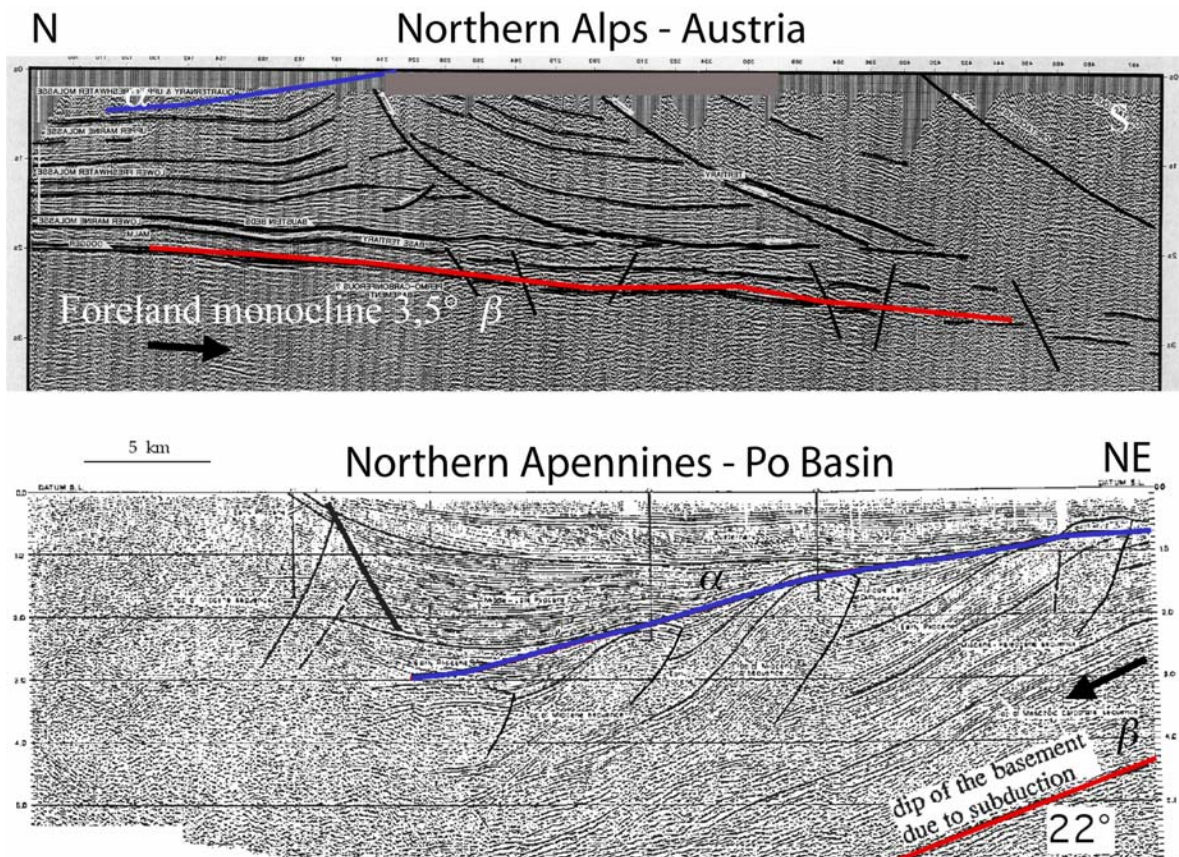
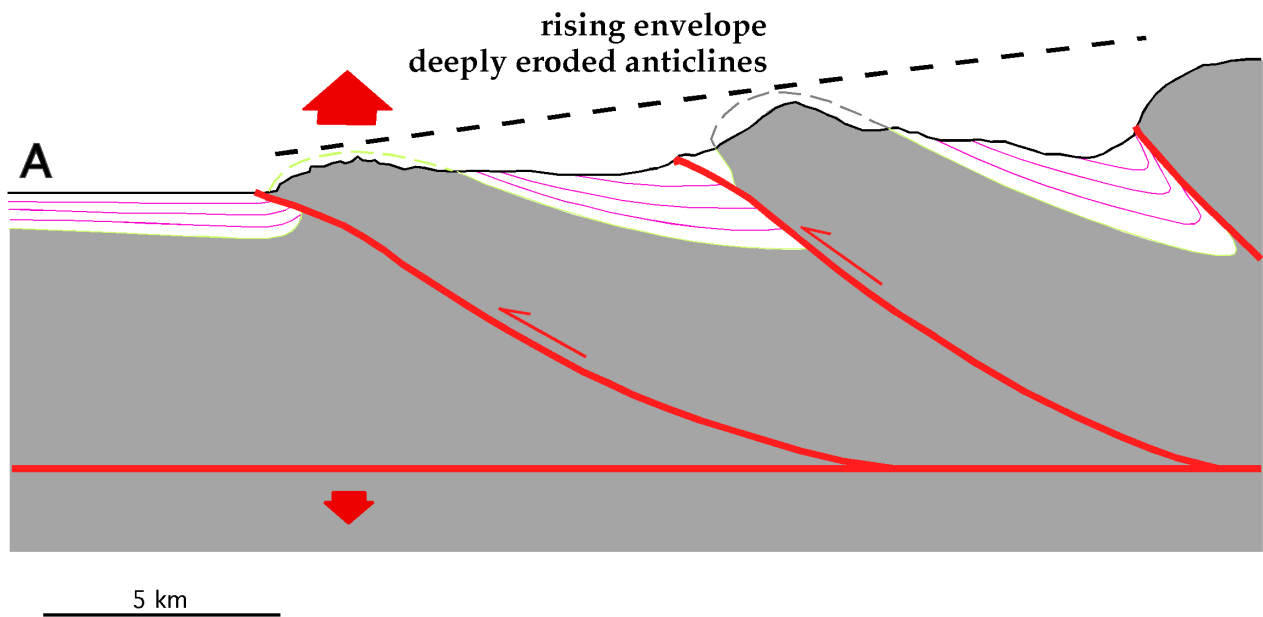


Fig. 177 - Two examples of the regional foreland monocline dip in red (β) from the Alps, above, and the Apennines, below. The envelope of the fold crests in blue (α) rises toward the interior of the belt in the Alps, whereas it may dip toward the interior of the prism in the Apennines. This last geometry occurs if the regional subsidence is faster than the fold uplift. Seismic sections after BACHMANN & KOCH (1983) and PIERI (1983).

FOLD UPLIFT > REGIONAL SUBSIDENCE



FOLD UPLIFT < REGIONAL SUBSIDENCE

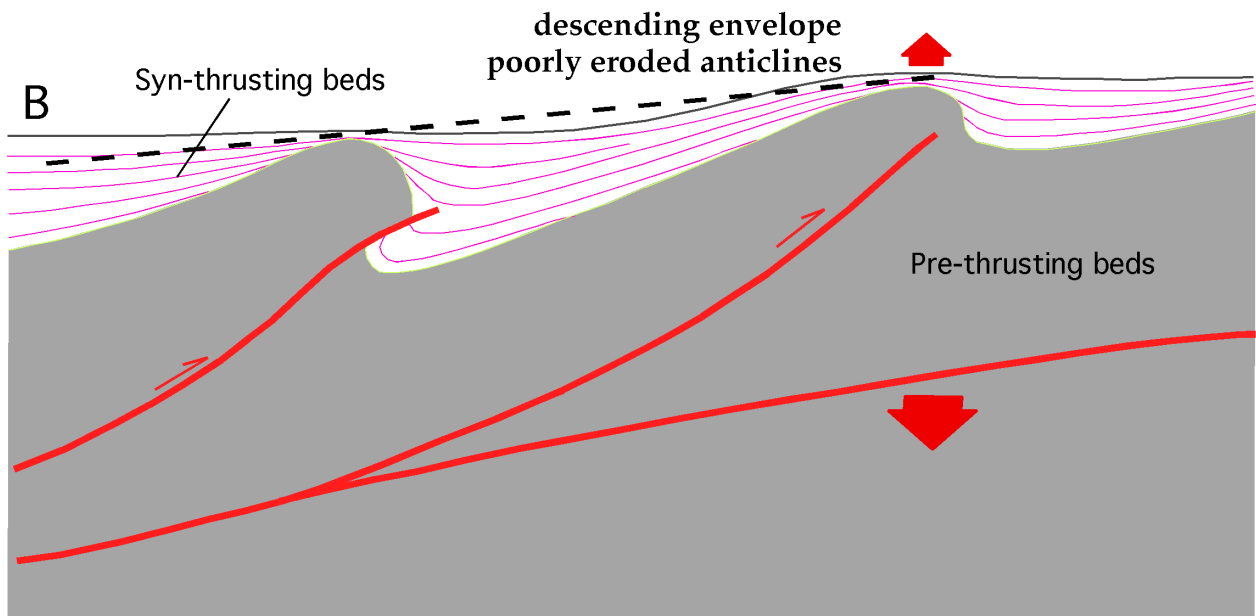


Fig. 178 - Fold uplift rates may be higher or lower than the regional subsidence of the foredeeps. In the classic case A, the envelope of the fold crests is rising toward the hinterland, and the anticlines are deeply eroded. In the case B the fold uplift rate is lower than the regional subsidence rate, as a result of which, the envelope to the fold crests descends toward the hinterland and the anticlines are not significantly eroded (after DOGLIONI & PROSSER, 1997).

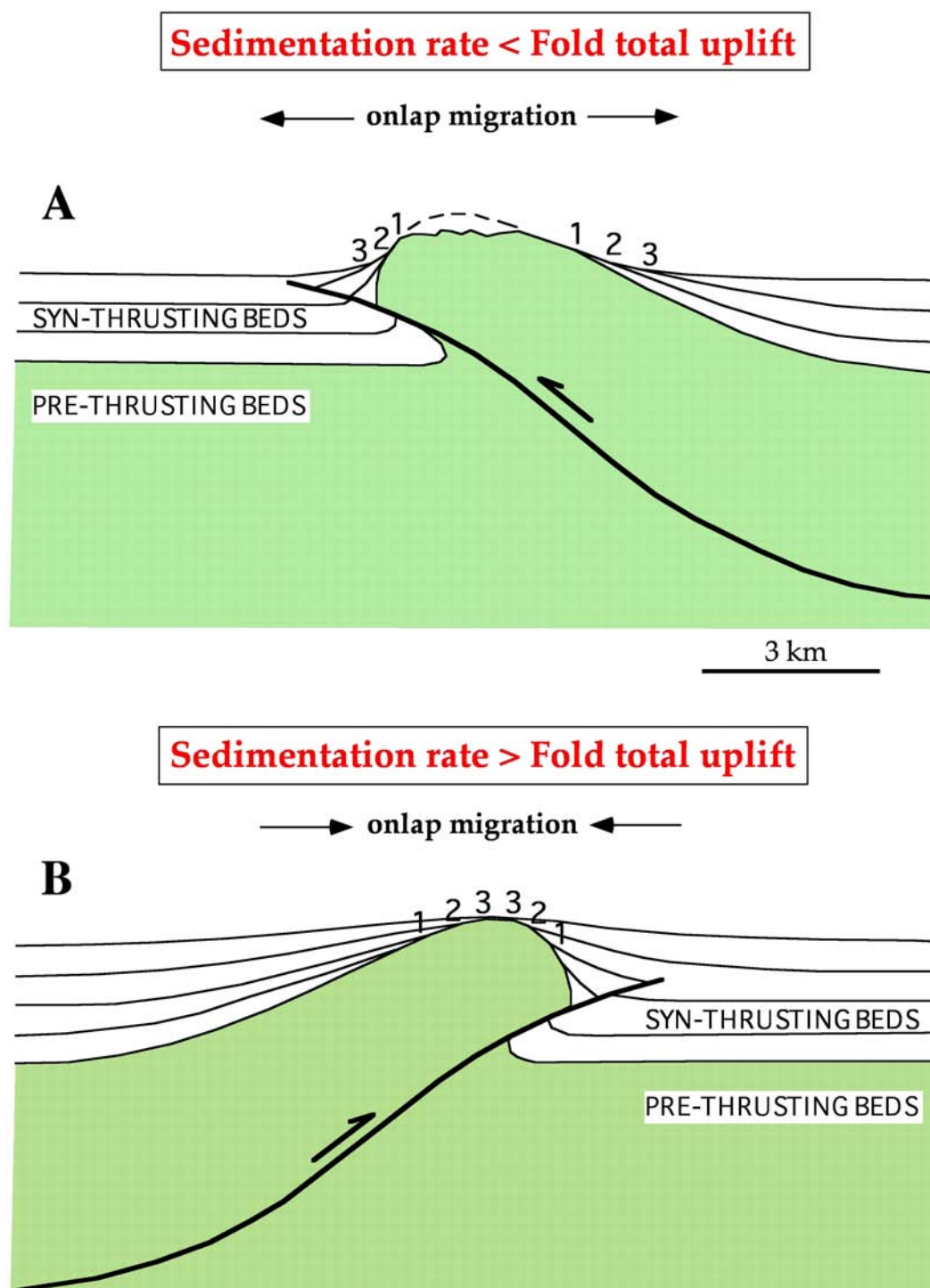


Fig. 179 - Where the fold uplift rate is greater than regional subsidence rate, the onlaps of the syntectonic beds move away from the fold crest, and the sedimentation rate is lower than the fold total uplift (A). On the other hand, onlaps may migrate toward the fold crest where the fold uplift rate is less than the regional subsidence rate, and the sedimentation rate is higher than the fold total uplift (B). The two end members may alternate on the limbs of a fold when for instance in B the fold uplift is lower than the regional subsidence, but the sea-level drops at higher rates exposing the fold.

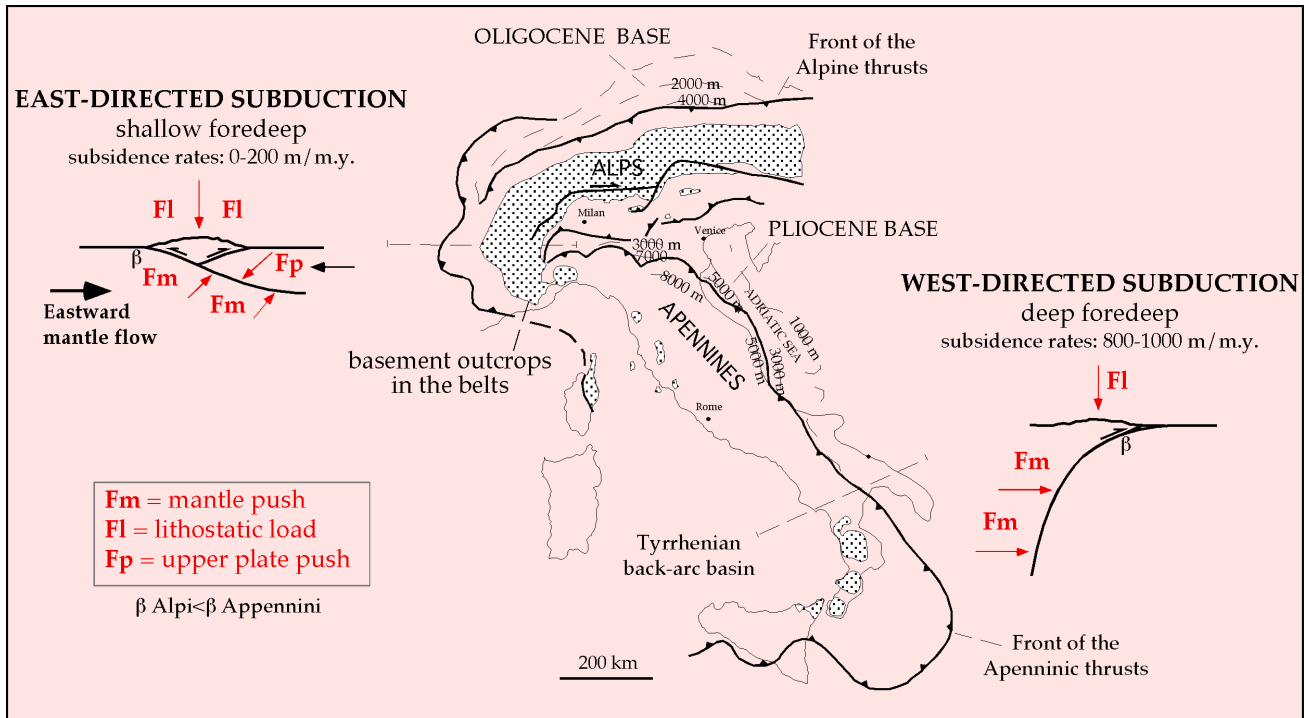


Fig. 180 - Alps and Apennines are thrust belts with very different characters. The Alps have a shallow foredeep, broad outcrops of metamorphic rocks, and high structural and morphologic relief. The Apennines have deep foredeep, few outcrops of basement rocks (partly inherited from earlier Alpine phase), low structural and morphologic elevation, and the Tyrrhenian back-arc basin. These differences mimic asymmetries of Pacific east-directed Chilean and west-directed Marianas subductions. For E-NE-directed subduction foredeep and trench, the origin may be interpreted as controlled by the lithostatic load and the downward component of upper plate push, minus the upward component of the "eastward" mantle flow (upper left panel). For the W-directed subduction where subsidence rate is much higher, the foredeep origin may rather be interpreted as due to the horizontal mantle push and the lithostatic load, panel in the lower right (after DOGLIONI, 1994).

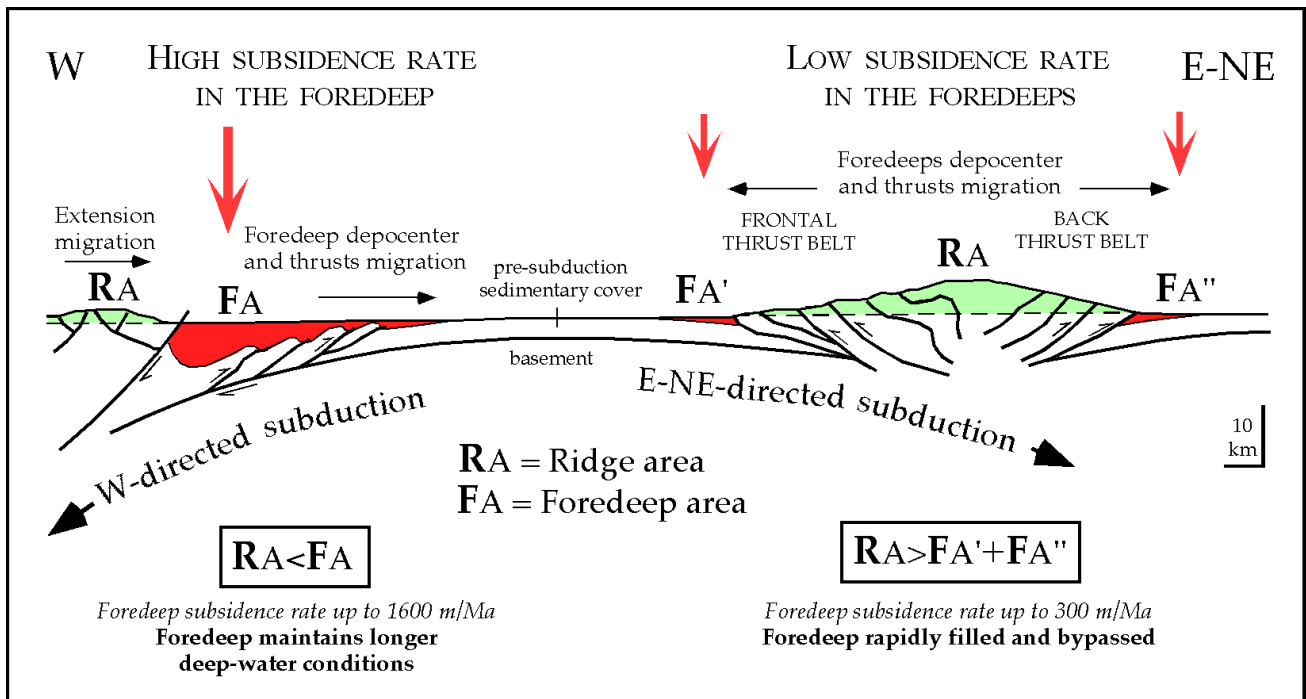


Fig. 181 - Strong asymmetry of the geologic parameters is observed between foredeeps related to west-directed subduction (left), and foredeeps related to east-northeast-directed subduction (right). In the west-directed case, the area of foredeep (filled or unfilled) is wider than the area of mountainous ridge, whereas foredeeps areas are smaller in opposite directed subductions (after DOGLIONI, 1994).

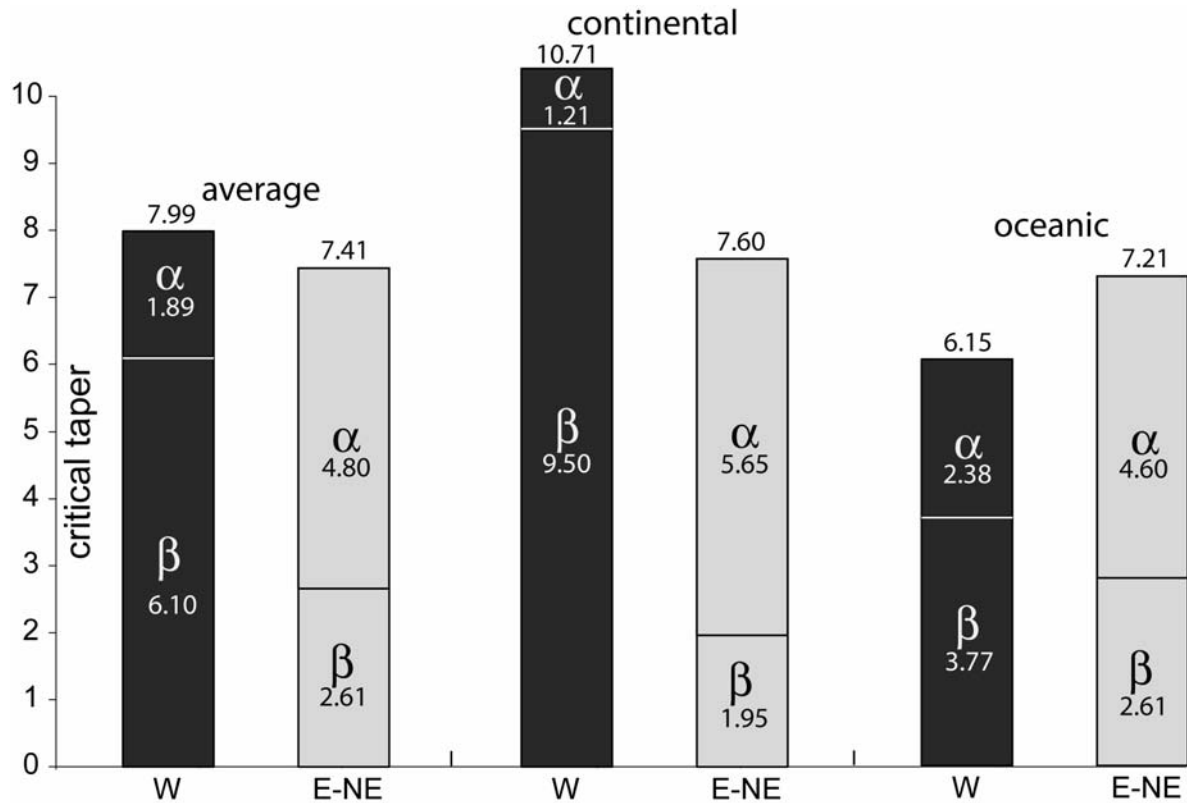


Fig. 182 - Average values of the topographic envelope (α), dip of the foreland monocline (β), and critical taper ($=\alpha+\beta$) for the two classes of subduction zones, i.e., W-directed and E- or NE-directed. Note that the "western" classes show lower values of α and steeper values of β (after LENCI & DOGLIONI, 2007).

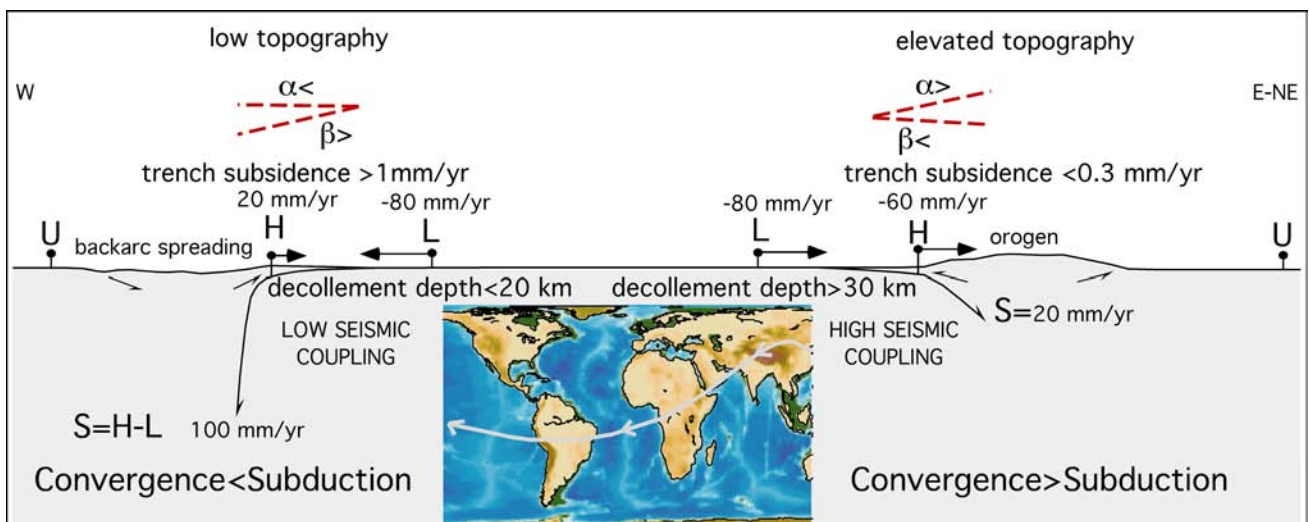


Fig. 183 - Assuming fixed the upper plate U, along west-directed subduction zones the subduction hinge H frequently diverges relative to U, whereas it converges along the opposite subduction zones. L, lower plate. Note that the subduction S is larger than the convergence along W-directed slabs, whereas S is smaller in the opposite case. The two end-members of hinge behavior are respectively accompanied in average by low and high topography, steep and shallow foreland monocline, fast and slower subsidence rates in the trench or foreland basin, single vs. double verging orogens, etc., highlighting a worldwide subduction asymmetry along the flow lines of plate motions indicated in the inset (after DOGLIONI *et alii*, 2007).

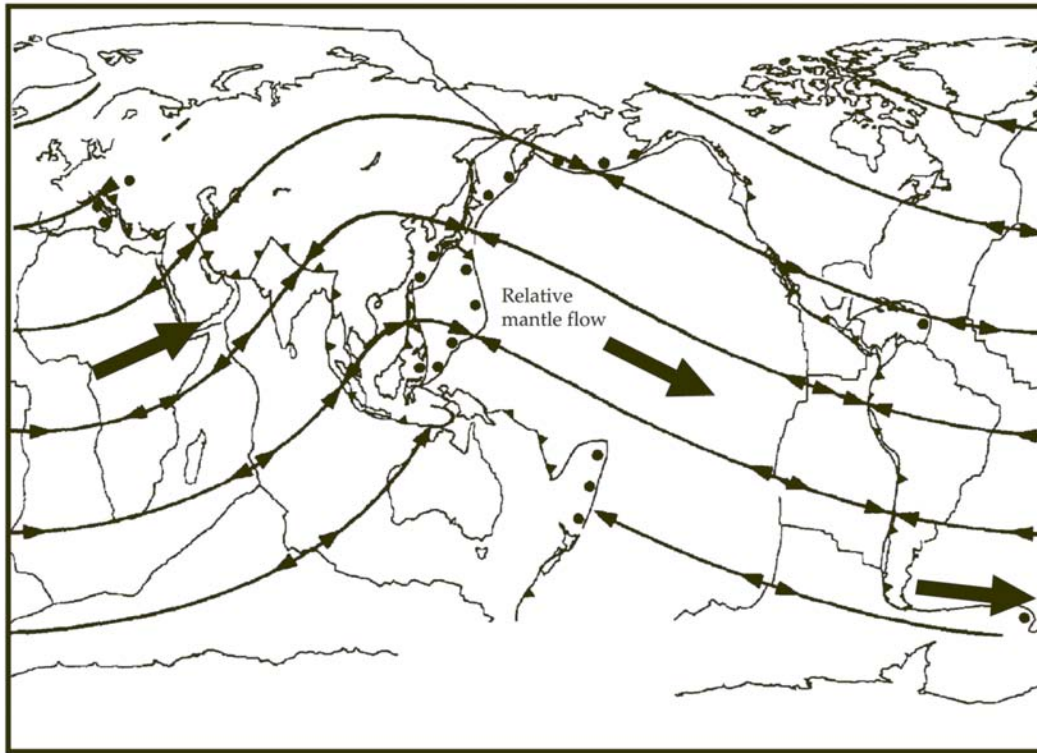


Fig. 184 - Tectonic undulated mainstream along which plates move with a few cm/yr "westward" delay relative to the underlying mantle.

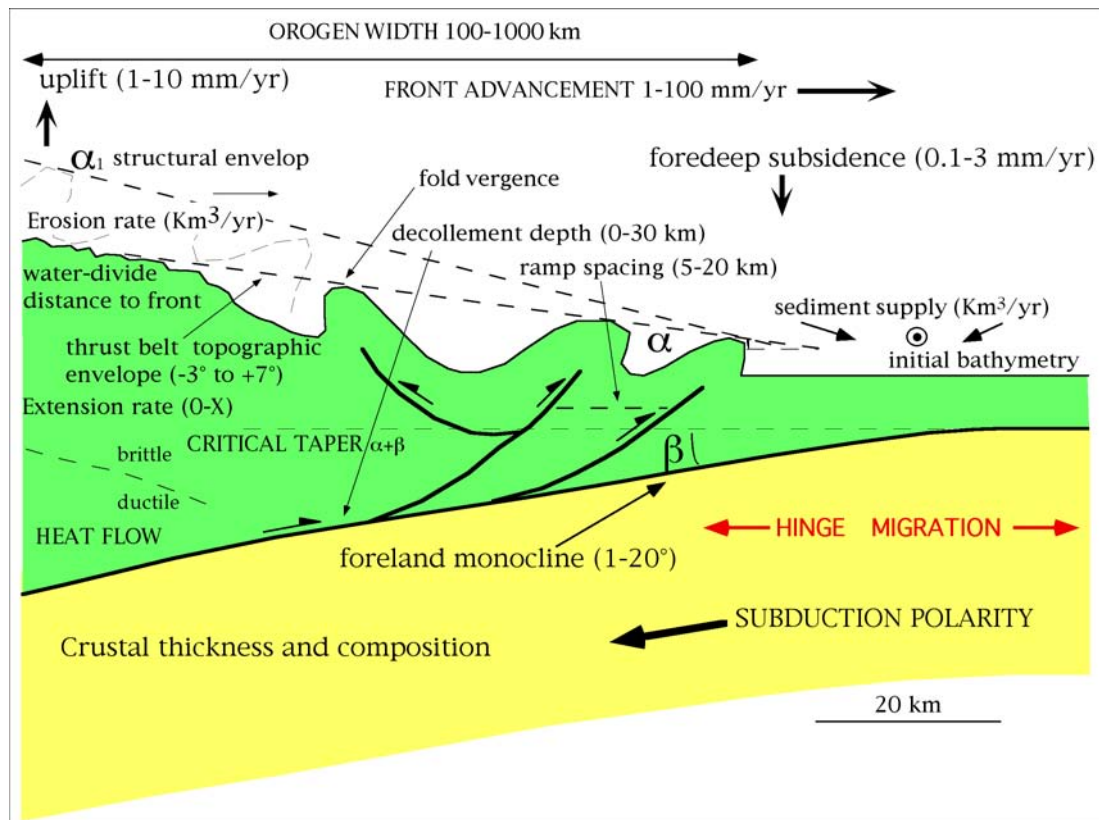
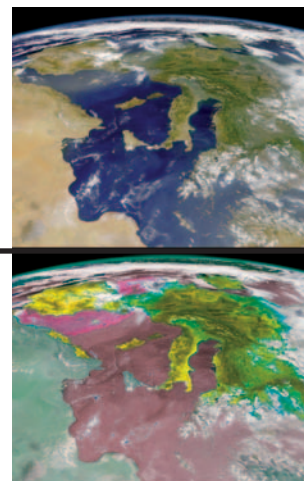


Fig. 185 - The orogens are structured by the combination of a number of parameters. The most important are listed in the figure (after LENCI & DOGLIONI, 2007).

9. Mediterranean geodynamics



It is commonly accepted that the Mediterranean geology has been shaped by the interplay between two plates, i.e., Africa and Europe (fig. 186), and possibly smaller intervening microplates. The Mediterranean was mainly affected by rifting after the Variscan orogeny: during the Mesozoic, oceanic Tethys areas and passive continental margins developed, where widespread carbonate platforms grew up. During the late Mesozoic, the Mediterranean area was rather dominated by subduction zones (from east to west, Cimmerian, Dinarides, Alps-Betics), which inverted the extensional regime, consuming the previously formed Tethyan oceanic lithosphere and the adjacent continental margins. The composition (i.e., oceanic or continental), density and thickness of the lithosphere inherited from the Mesozoic rift controlled the location, distribution and evolution of the later subduction zones. The shorter wavelength of the Mediterranean orogens with respect to other belts (e.g., Cordillera, Himalayas) is due to the smaller wavelength of the lithospheric anisotropies inherited from the Tethyan rift.

The Mediterranean basin was and still is the collector of sediments coming from the erosion of the surrounding continents and orogens: the best examples are the Nile and Rhone deltas. In the past, other deltas deposited at the bottom of the Mediterranean, and their rivers were later disconnected or abandoned: an example is the Upper Oligocene-Lower Miocene Numidian Sandstone, which was supplied from Africa, deposited in the central Mediterranean basin, and partly uplifted by the Apennines accretionary prism. It is notorious also that during the Messinian eustatic low-stand, the Mediterranean dried several times, generating the salinity crisis in which thick sequences of evaporites deposited in the basin. This episode generated a pulsating loading oscillation in the Mediterranean, because the repetitive removal of the water should have generated significant isostatic rebound in most of the basin, particularly where it was deeper as in Ionian, in the Provençal and in the central Tyrrhenian seas.

The Neogene to present direction of Africa-Europe relative motion is still under debate. Most of the reconstructions show directions of

relative motion spanning between northwest to northeast. Recent space geodesy data confirm this main frame, where Africa has about 5 mm/yr of N-S component of convergence relative to Europe, but they also show that the absolute plate motions directions of both Europe and Africa are northeast oriented and not north or northwest directed as usually assumed (see the NASA data base on present global plate motions, <http://sideshow.jpl.nasa.gov:80/mbh/series.html>). The main Cenozoic subductions of the Mediterranean are the Alps-Betics, the Apennines-Maghrebides, and the Dinarides-Hellenides-Taurides (figs. 187 - 193). Closely related to the Mediterranean geodynamics are

the Carpathians subduction and the Pyrenees. The Mediterranean orogens show two distinct signatures similar to those occurring in the opposite sides of the Pacific Ocean. High morphologic and structural elevation, double vergence, thick crust, involvement of deep crustal rocks, and shallow foredeeps characterize E- or NE-directed subduction zones (Alps-Betics, Dinarides-Hellenides-Taurides). On the other hand, low morphologic and structural elevation, single vergence, thin crust, involvement of shallow rocks, deep foredeep and a widely developed backarc basin characterize W-directed subduction zones (Apennines, Carpathians). This asymmetry can be ascribed to the "W"-ward drift of the lithosphere relati-

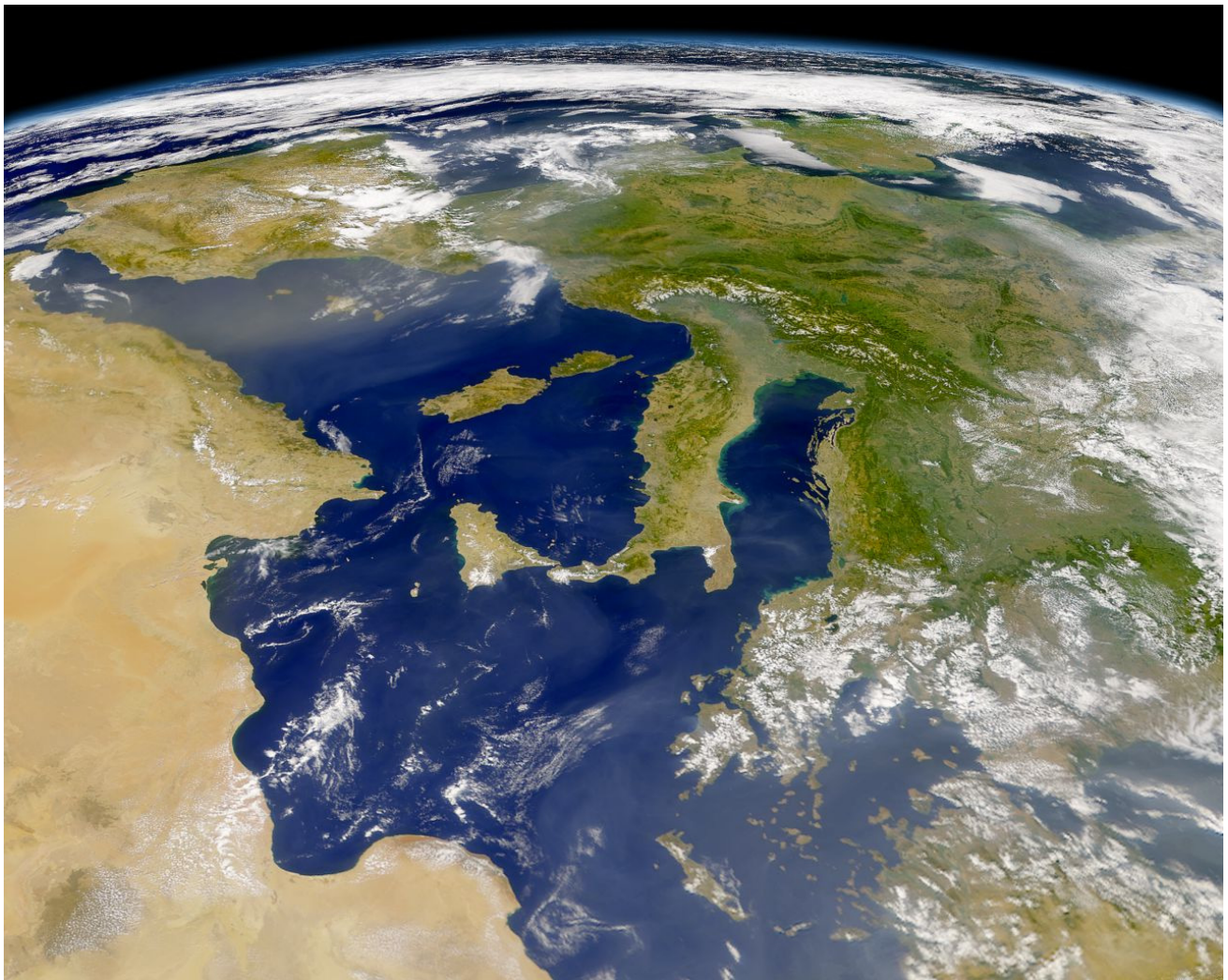


Fig. 186 - NASA-Shuttle view of the central western Mediterranean.

ve to the mantle with rates of about 49 mm/y, as computed adopting the hotspots reference frame. All Mediterranean orogens show typical thrust belt geometries with imbricate fan and antiformal stack associations of thrusts. The main difference between orogens and within the single belts is the variation in depth of the basal decollement. Deeper it is, higher is the structural and morphologic elevation of the related orogen.

Extensional basins have superimposed these orogenic belts, i.e., in the western side the Valencia, Provençal, Alboran, Algerian, Tyrrhenian Basins, and in the eastern side the Aegean Basin, and to the north the Pannonian Basin.

The Mediterranean can be divided into the western, central, and the eastern basins. The western Mediterranean is younger (mainly < 30 Ma) relative to the central and eastern Mediterranean areas, which are mainly relics

of the Mesozoic-Cenozoic(?) Tethys.

Positive gravity anomalies occur in deep basins (e.g., Provençal, Tyrrhenian and Ionian seas) where the mantle was uplifted by rifting processes. Negative gravity anomalies rather occur along the subduction zones.

A characteristic feature of the western Mediterranean is the large variation in lithospheric and crustal thickness. The lithosphere has been thinned to less than 60 km in the basins (50-60 km in the Valencia trough, 40 km in the eastern Alboran sea, and 20-25 km in the Tyrrhenian) while it is 65-80 km thick below the continental swells (Corsica-Sardinia and Balearic Promontory). The crust mimics these differences with a thickness of 8-15 km in the basins (Valencia trough, Alboran sea, Ligurian sea and Tyrrhenian sea) and 20-30 km underneath the swells (Balearic Promontory and Corsica-Sardinia), as inferred by seismic and gravity data. These lateral variations in

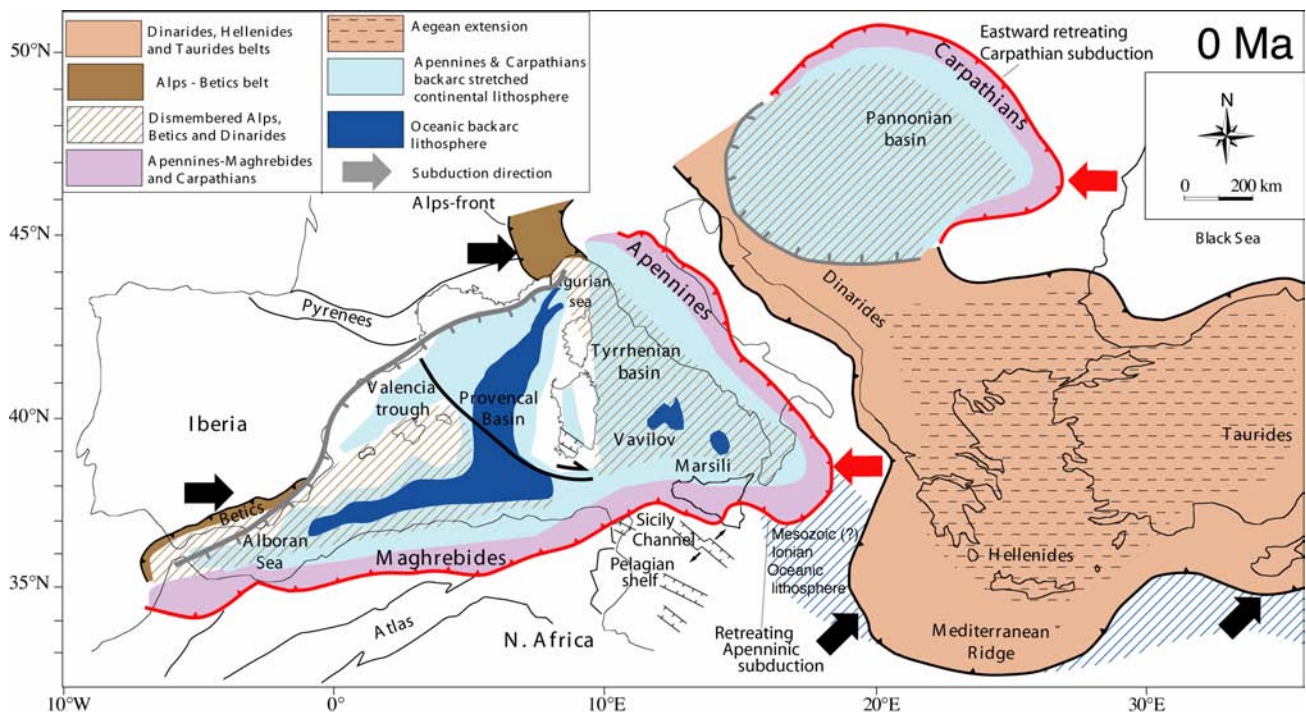


Fig. 187 - Present geodynamic framework. There are four subduction zones with variable active rates in the Mediterranean realm: the W-directed Apennines-Maghrebides; the W-directed Carpathians; the NE-directed Dinarides-Hellenides-Taurides; the SE-directed Alps. The Apennines-Maghrebides subduction-related backarc basin of the western Mediterranean stretched and scattered into the segmented basins most of the Alps-Betics orogen (after CARMINATI & DOGLIONI, 2004).

thickness and composition are related to the rifting process that affected the western Mediterranean, which is a coherent system of interrelated irregular troughs, mainly V-shaped, which began to develop in the Late Oligocene-Early Miocene in the westernmost parts (Alboran, Valencia, Provençal), becoming progressively younger eastward (Eastern Balearic, Algerian basins), up to the presently active E-W extension in the Tyrrhenian Sea. Heat flow data and thermal modelling show that the maximum heat flow values are encountered in the basins: 120 mW/m² in the eastern Alboran, 90-100 mW/m² in the Valencia trough, and more than 200 mW/m² in the Tyrrhenian Sea. All these sub-basins appear to be genetically linked to the backarc opening related to the coeval "E"-ward rollback of the W-directed Apennines-Maghrebides subduction zone. Extreme stret-

ching generated oceanic crust in the Provençal (20-15 Ma), Algerian (17-10), Vavilov and Marsili basins (7-0 Ma). During the 25-10 Ma time frame, the Corsica-Sardinia block rotated 60° counter clockwise.

In the southern Apennines, the choking of the subduction zone with the thicker continental lithosphere of the Apulia Platform slowed the E-ward migration of the subduction hinge, whereas in the central and northern Apennines and in Calabria the subduction is still active due to the presence in the foreland of thin continental lithosphere in the Adriatic Sea, and of Mesozoic(?) oceanic lithosphere in the Ionian Sea, allowing rollback of the subduction hinge.

The western Mediterranean basins tend to close both morphologically and structurally toward the southwest (Alboran Sea) and northeast (Ligurian Sea). The eastward migration

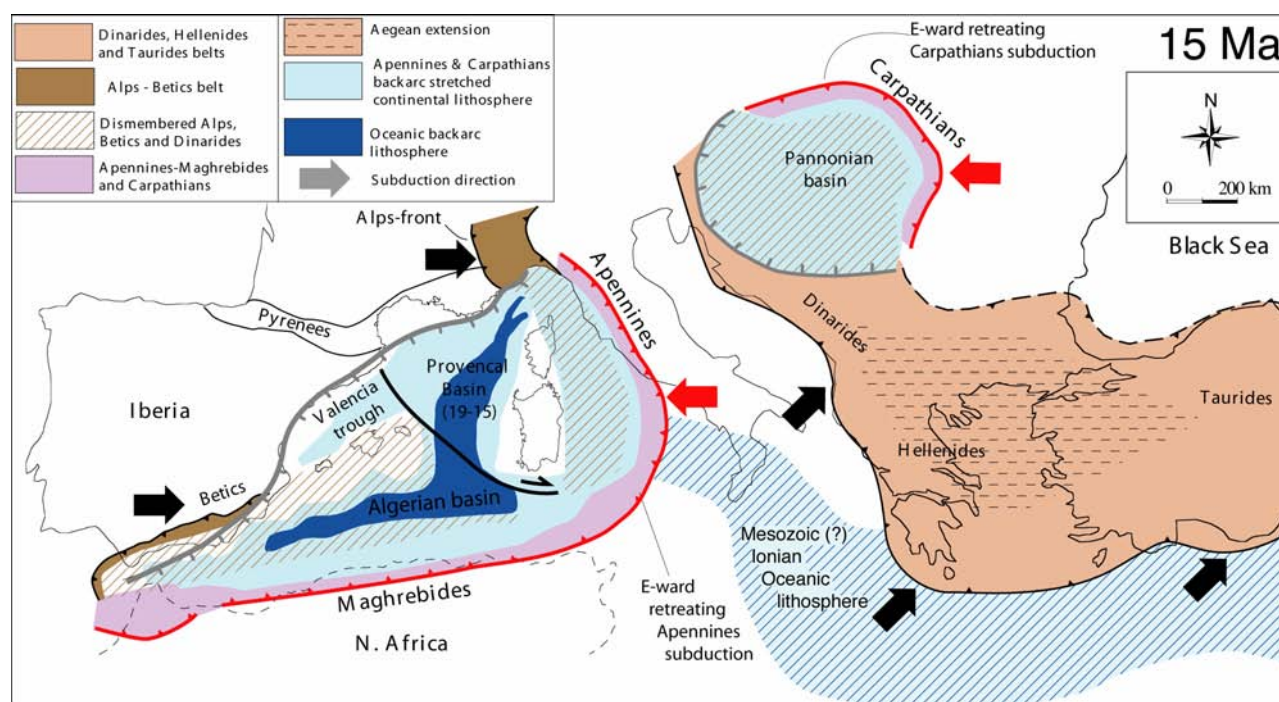


Fig. 188 - Paleogeodynamics at about 15 Ma. Note the "E"-ward vergence of both Apennines-Maghrebides trench and the backarc extensional wave. The Liguro-Provençal basin, the Valencia Trough and the North Algerian basin were almost completely opened at 10 Ma. The Dinarides subduction slowed down, due to the presence of the thick Adriatic continental lithosphere to the west, whereas to the south, the Hellenic subduction was very lively due to the presence in the footwall plate of the Ionian oceanic lithosphere. The Carpathians migrated E-ward, generating the Pannonian backarc basin, with kinematics similar to the Apennines (after CARMINATI & DOGLIONI, 2004).

of the arc associated with the W-directed subduction generated right-lateral transpression along the entire E-W-trending northern African belt (Maghrebides) and its Sicilian continuation, whereas left-lateral transtension has been described along the same trend in the backarc setting just to the north of the African margin. An opposite tectonic setting can be described in the northern margin of the arc. Subduction retreat generated calcalkaline and shoshonitic magmatic episodes particularly located in the western margins of the lithospheric boudins, later followed by alkaline-tholeiitic magmas in the backarc to the west. Extension partly originated in areas previously occupied by the Alps-Betics orogen, which formed since Cretaceous due to an "E"-directed subduction of Europe and Iberia underneath the Adriatic plate and an hypothetical Mesomediterranean plate. Once restored

Sardinia to its position prior to rotation, during the early Cenozoic the Alps were probably joined with the Betics in a double vergent single belt. The Western Alps, which are the forebelt of the Alps, were connected to Alpine Corsica; the Alps continued SW-ward into the Balearic promontory and Betics. The retrobelt of the Alps, i.e., the Southern Alps, were also continuing from northern Italy toward the SW. In a double vergent orogen, the forebelt is the frontal part, synthetic to the subduction, and verging toward the subducting plate; the retrobelt is the internal part, antithetic to the subduction, and verging toward the interior of the overriding plate. The W-directed Apennines-Maghrebides subduction started along the Alps-Betics retrobelt, where oceanic and thinned continental lithosphere was occurring in the foreland to the east. In fact the subduction underneath the

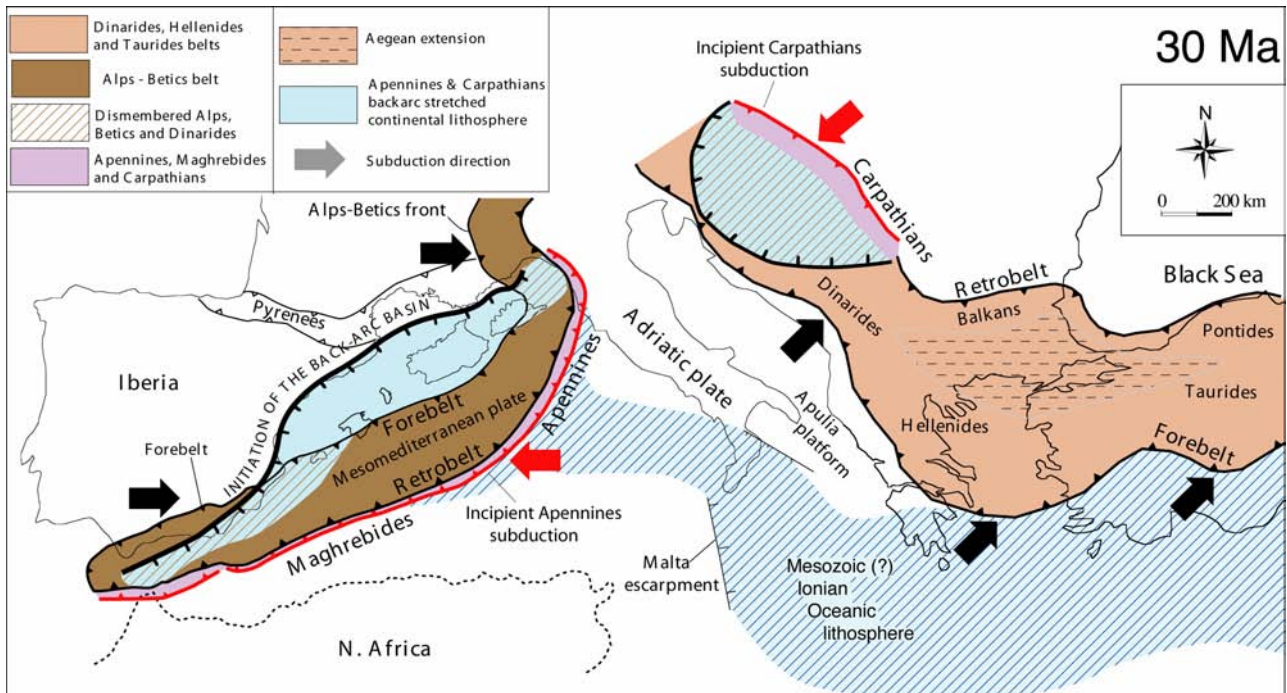


Fig. 189 - Paleogeodynamics at about 30 Ma. The location of the subduction zones is controlled by the Mesozoic paleogeography. The Alps-Betics formed along the SE-ward dipping subduction of Europe and Iberia underneath the Adriatic and Mesomediterranean plates. The Apennines developed along the Alps-Betics retrobelt, where oceanic or thinned pre-existing continental lithosphere was present to the east. Similarly, the Carpathians started to develop along the Dinarides retrobelt (i.e., the Balkans). The fronts of the Alps-Betics orogen are cross-cut by the Apennines-related subduction backarc extension (after CARMINATI & DOGLIONI, 2004).

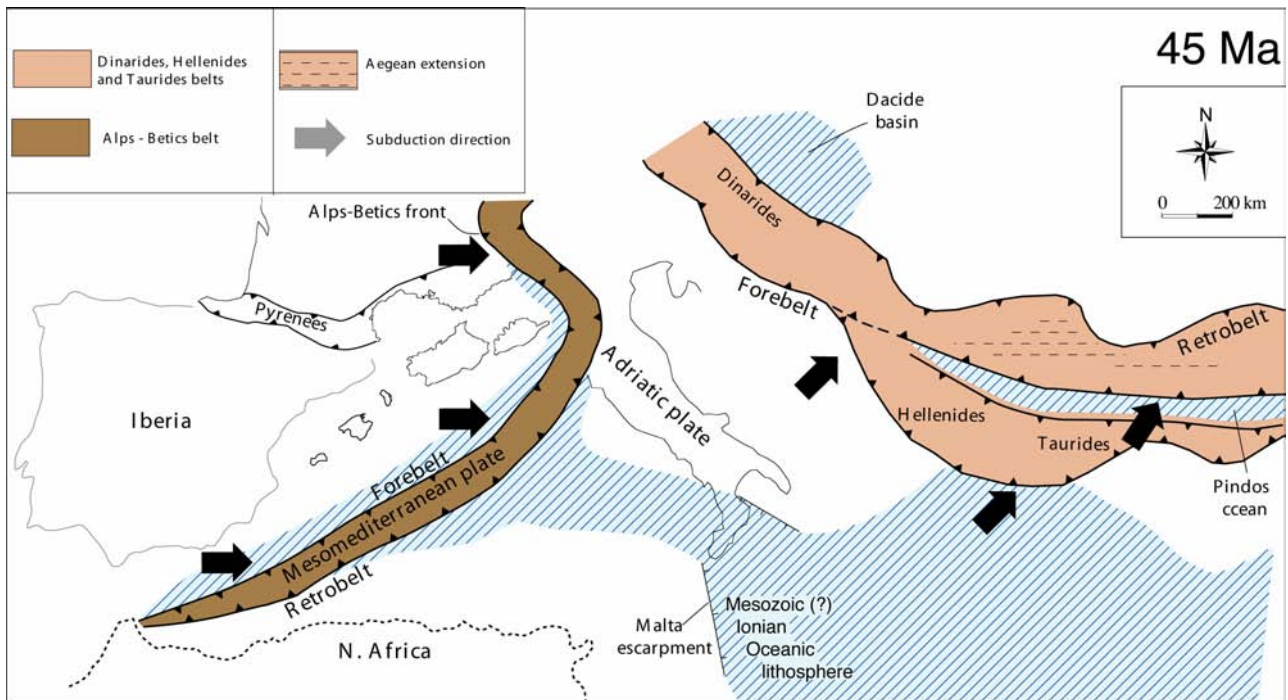


Fig. 190 - Paleogeodynamics at about 45 Ma. The Alps were a continuous belt into the Betics down to the Gibraltar consuming an ocean located relatively to the west (after CARMINATI & DOGLIONI, 2004).

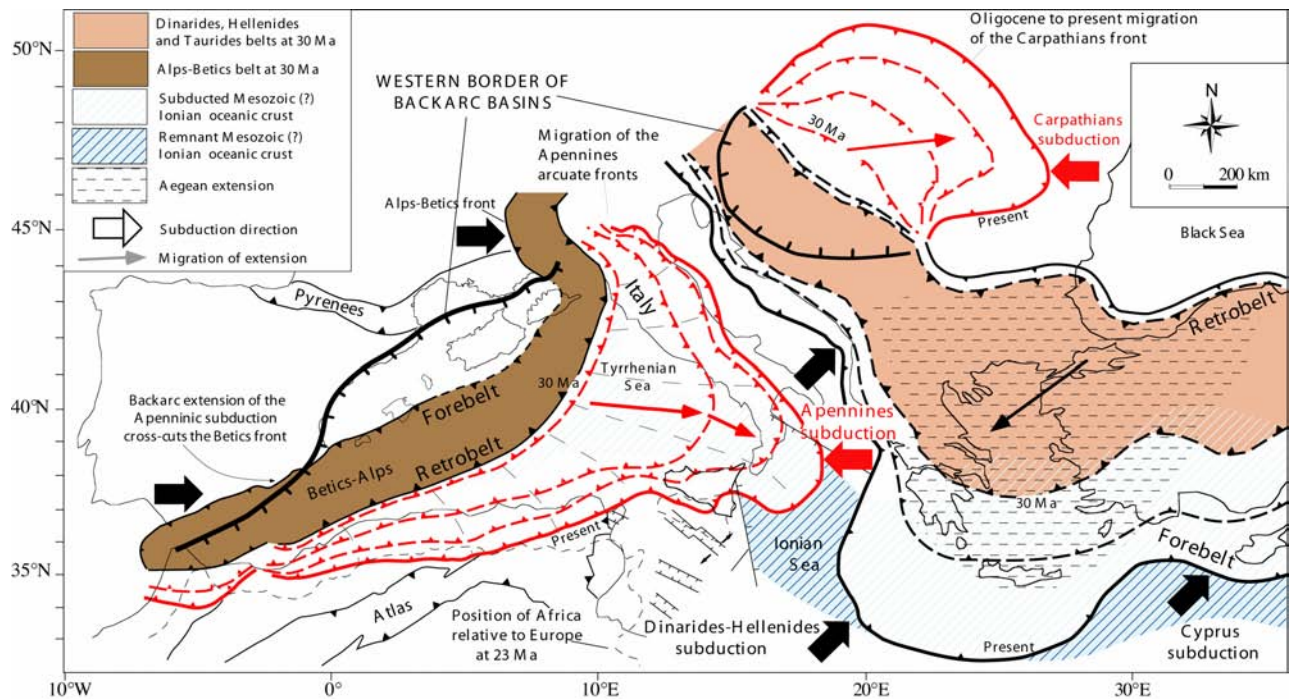


Fig. 191 - Main tectonic features of the Mediterranean realm, which has been shaped during the last 45 Ma by a number of subduction zones and related belts: the double vergent Alps-Betics; the single "E"-vergent Apennines-Maghrebides and the related western Mediterranean backarc basin; the double vergent Dinarides-Hellenides-Taurides and related Aegean extension; the single "E"-vergent Carpathians and the related Pannonian backarc basin; the double vergent Pyrenees (after CARMINATI & DOGLIONI, 2004).

Apennines-Maghrebides consumed inherited Tethyan domains. The subduction and the related arc migrated "E"-ward at speed of 25-30 mm/yr.

The western Late Oligocene-Early Miocene basins of the Mediterranean nucleated both within the Betics orogen (e.g., Alboran sea) and in its foreland (Valencia and Provençal troughs). At that time the N40°-70° direction of grabens was oblique to the coexisting N60°-80°-trending Betics orogen, indicating its structural independence from the Betics orogeny. Thus, as the extension cross-cuts the orogen and developed also well outside the thrust belt front, the westernmost basins of the Mediterranean developed independently from the Alps-Betics orogen, being rather related to the innermost early phases of the backarc extension in the hangingwall of the Apennines-Maghrebides subduction. In contrast with the "E"-ward migrating extensional basins and following the "E"-ward retreat of the Apennines subduction, the Betics-Balearic thrust front was migrating "W"-ward, producing interference or inversion structures.

The part of the Alps-Betics orogen was located in the area of the Apennines-Maghrebides backarc basin, it has been disarticulated and spread-out into the western Mediterranean (e.g., the metamorphic slices of Kabylie in N-Algeria, and Calabria in S-Italy). Alpine type basement rocks have been dragged in the Tyrrhenian Sea.

Similarly, boudinage of the pre-existing Alps and Dinarides orogens occurred in the Pannonian basin, which is the Oligocene to Present backarc basin related to the coeval E-ward retreating, W-directed Carpathians subduction zone. In the Pannonian basin, the extension isolated boudins of continental lithosphere previously thickened by the earlier Dinarides orogen, like the Apuseni Mountains that separate the Pannonian basin s.s. from the Transylvanian basin to the east. The western Mediterranean backarc setting is comparable with Atlantic and western Pacific backarc

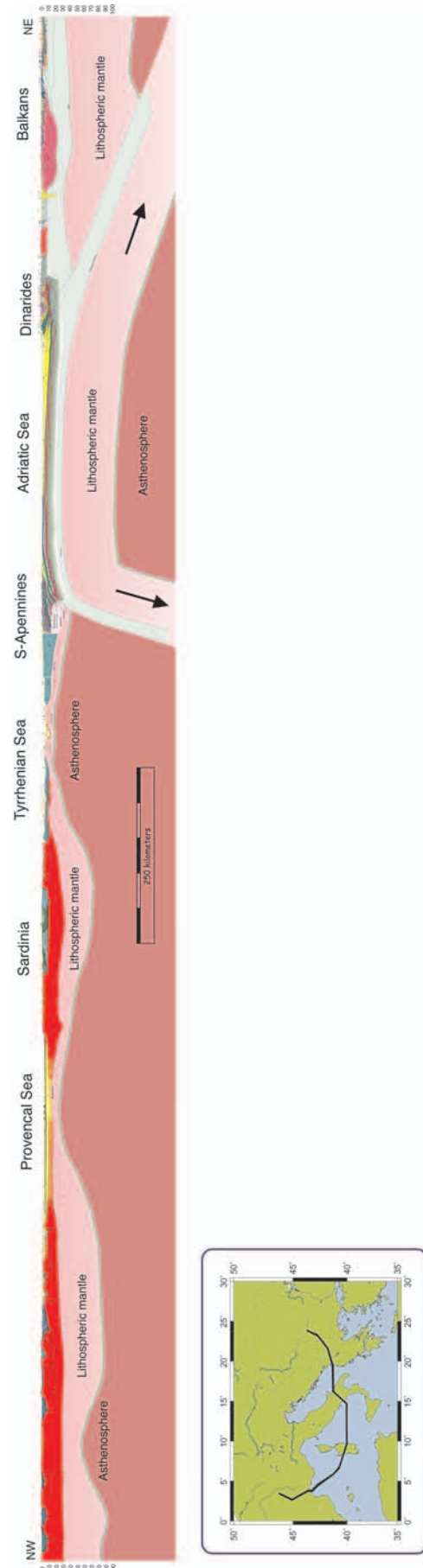


Fig. 192 - Transmed transect III. Modified after CARMINATI *et alii* (2004a).

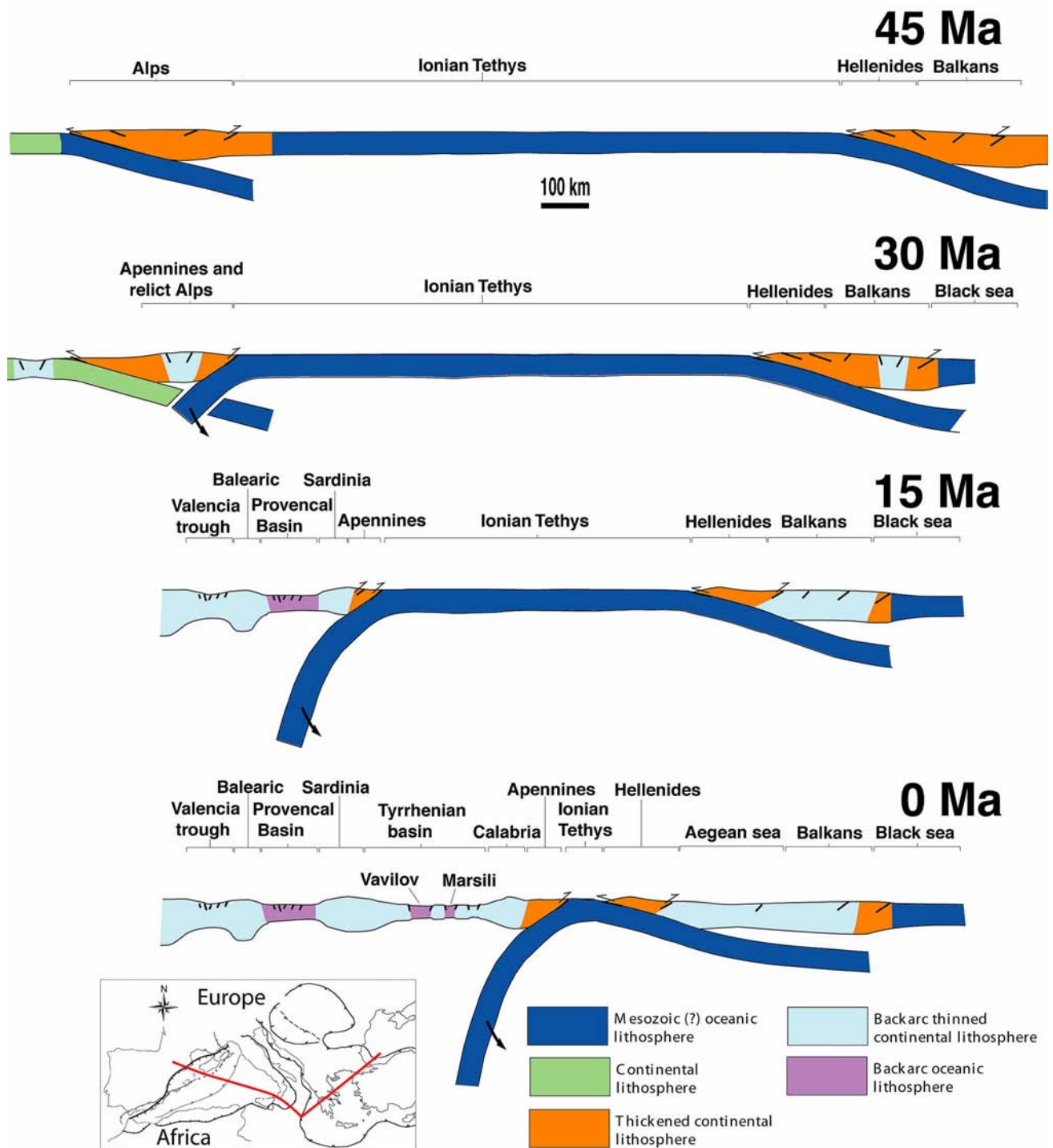


Fig. 193 - During the last 45 Ma, the evolution of the Mediterranean along the trace shown in the map is the result of three main subduction zones: i.e., the early E-directed Alpine subduction; the Apennines subduction switch along the Alps retrobelt; the Dinarides-Hellenides subduction. The last two slabs retreated at the expenses of the inherited Tethyan Mesozoic oceanic or thinned continental lithosphere. In their respective hangingwalls, a few rifts formed as backarc basins, progressively younger toward the subduction hinges. The slab is steeper underneath the Apennines, possibly due to the W-ward drift of the lithosphere relative to the mantle (after CARMINATI & DOGLIONI, 2004).

basins that show similar large-scale lithospheric boudinage, where parts of earlier orogens have been scattered in the backarc area, like the Central America Cordillera relicts that are dispersed in the Caribbean domain.

The Apennines accretionary prism formed in sequence at the front of the pre-existing Alpine retrobelt, and therefore the central western Apennines contain also the inherited Alpine orogen of Cretaceous to Miocene age. There has probably been a temporary coexistence of the opposite subductions during the Late Oligocene - Early Miocene. Structural and geophysical data support the presence of an

eastward migrating asthenospheric wedge at the subduction hinge of the retreating Adriatic plate. The flip of the subduction, from the Alpine E-directed to the Apennines W-directed subduction could have been recorded by the drastic increase of the subsidence rates in the Apennines foredeep during the Late Oligocene - Early Miocene. In fact, west-directed subduction zones such as the Apennines show foredeep subsidence rates up to 10 times faster (> 1 mm/yr) than to the Alpine foredeeps. The flip of the subduction could also be highlighted by the larger involvement of the crust during the earlier Alpine stages with

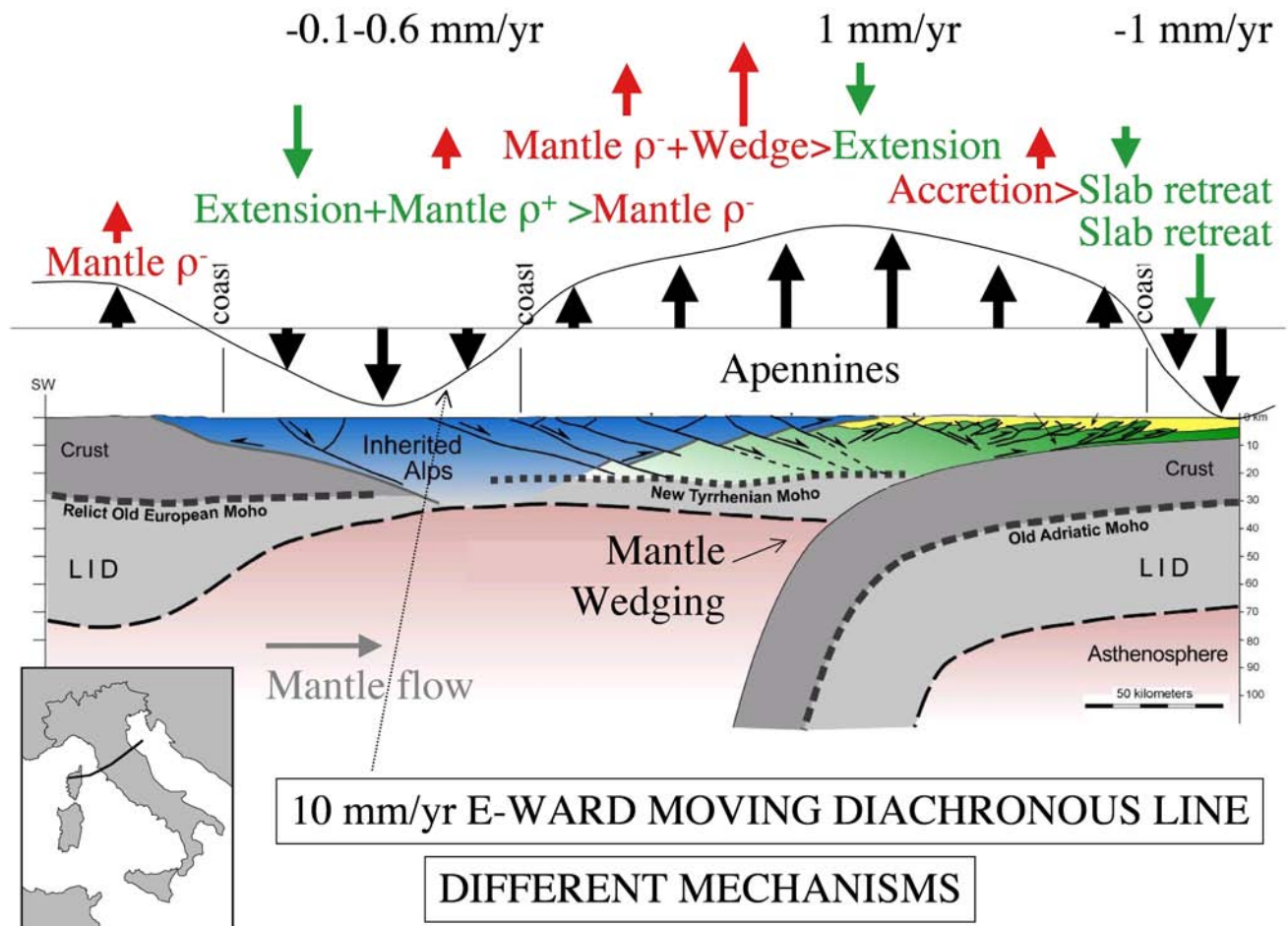


Fig. 194 - Cross-section of the Northern Apennines. The Alps are interpreted as a boudinaged relict stretched in the Tyrrhenian Sea and western Northern Apennines. The retrobelt of the Alps is considered the prolongation of the Southern Alps. The numbers are interpreted vertical and horizontal velocity rates. It shows how in the same tectonic system different geodynamic mechanisms may concur. Green and red arrows indicate subsidence and uplift mechanisms respectively. Modified after CARMINATI *et alii* (2004b).

respect to the Apennines décollements that mainly deformed the sedimentary cover and the phyllitic basement. It has been demonstrated that the load of the Apennines and Carpathians orogens is not sufficient to generate the 4-8 km deep Pliocene-Pleistocene fore-deep basins, and a mantle origin has been proposed as mechanism (slab pull and/or E-ward mantle flow).

Paradoxically the extension determining most of the western Mediterranean developed in a context of relative convergence between Africa and Europe. However it appears that the maximum amount of North-South Africa/Europe relative motion at the Tunisia longitude was about 135 km in the last 23 Ma, more than five times slower with respect to the eastward migration of the Apennines arc which moved eastward more than 700 km during the last 23 Ma. Therefore the eastward migration of the Apennines-Maghrebides arc is not a consequence of the relative N-S relative convergence between Africa and Europe, but it is rather a consequence of the Apennines-Maghrebides subduction rollback, which was

generated either by slab pull and/or the "E"-ward mantle flow relative to the lithosphere detected in the hotspot reference frame.

The development of the western Mediterranean occurred mainly after the terminal convergence in the Pyrenees at about 20 Ma, which formed due to the collision between Europe and the Late Cretaceous-Early Tertiary counter-clockwise rotating Iberia, contemporaneously to the opening of the Biscay Basin.

In northern Africa, south of the Maghrebides (and related Algerian Tell and Moroccan Riff), the Atlas mountains represent an intraplate inversion structure, where extensional (NNE-trending) and left-lateral (about E-W-trending) transtensional Mesozoic intercontinental rifts were later buckled and squeezed by Cenozoic compression and right-lateral transpression, in the foreland of the Apennines-Maghrebides subduction zone. This is also indicated by the thicker Mesozoic sequences in the Atlas ranges with respect to the adjacent not deformed mesetas.

10. Stratigraphy of the Dolomites

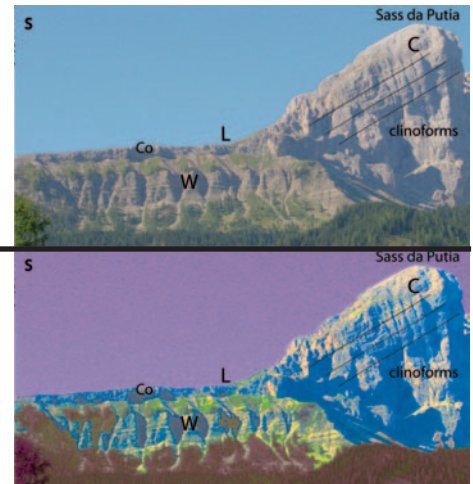


Fig. 195 - Phyllites recording Hercynian deformation in the NW-ward dipping basement of the Dolomites. 3 km south of Agordo. Chris Golding for scale.

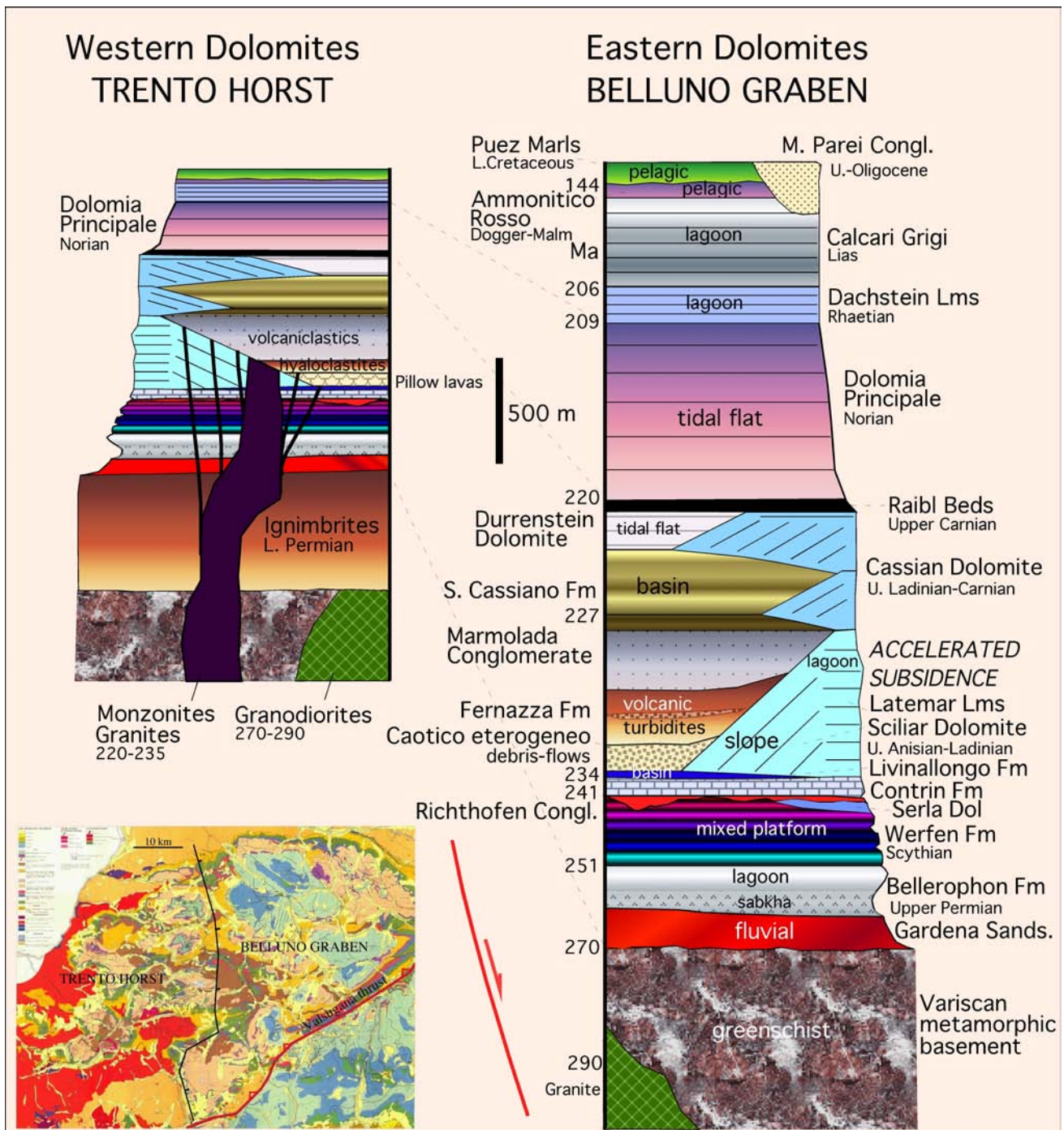


Fig. 196 - General stratigraphy of the Dolomites. The eastern side (Belluno Graben) underwent larger subsidence throughout the entire late Permian-Mesozoic. The differential subsidence was accommodated by a number of synsedimentary, roughly N-S-trending normal faults. The western side (Trento horst) has a thickness reduced to about a half with respect to the Belluno graben. Note that during the late Anisian-early Ladinian, the region had an accelerated subsidence (about 0.6 mm/yr) that allowed the fast aggradation and growth of the Sciliar Dolomite (Marmolada Lms). Most of the Mid-Triassic calcalkaline magmatism (e.g., intrusions of Predazzo and Monzoni) and the lower Permian porphyry (Piastrone porfirico Atesino) concentrated in the Trento horst.



Fig. 197 - Detail of the Permian-Triassic boundary (the largest extinction) in the Dolomites. From the bottom to the top: marls, gypsum and bituminous limestones of the upper Permian Bellerophon Fm (B); the first cliff is constituted by Triassic marly limestones of the Mazzin Member (M) of the Werfen Fm (Scythian); a yellow-orange level marks the occurrence of the evaporitic dolomites of the Andraz Horizon of the Werfen Fm (A); the topmost cliff (Siusi Member of the Werfen Fm, S) is made by marly and oolitic limestones with frequent intercalations (toward the top) of reddish siltstones. The picture was taken at the western end of the Pale di San Martino massif, near Passo Rolle.

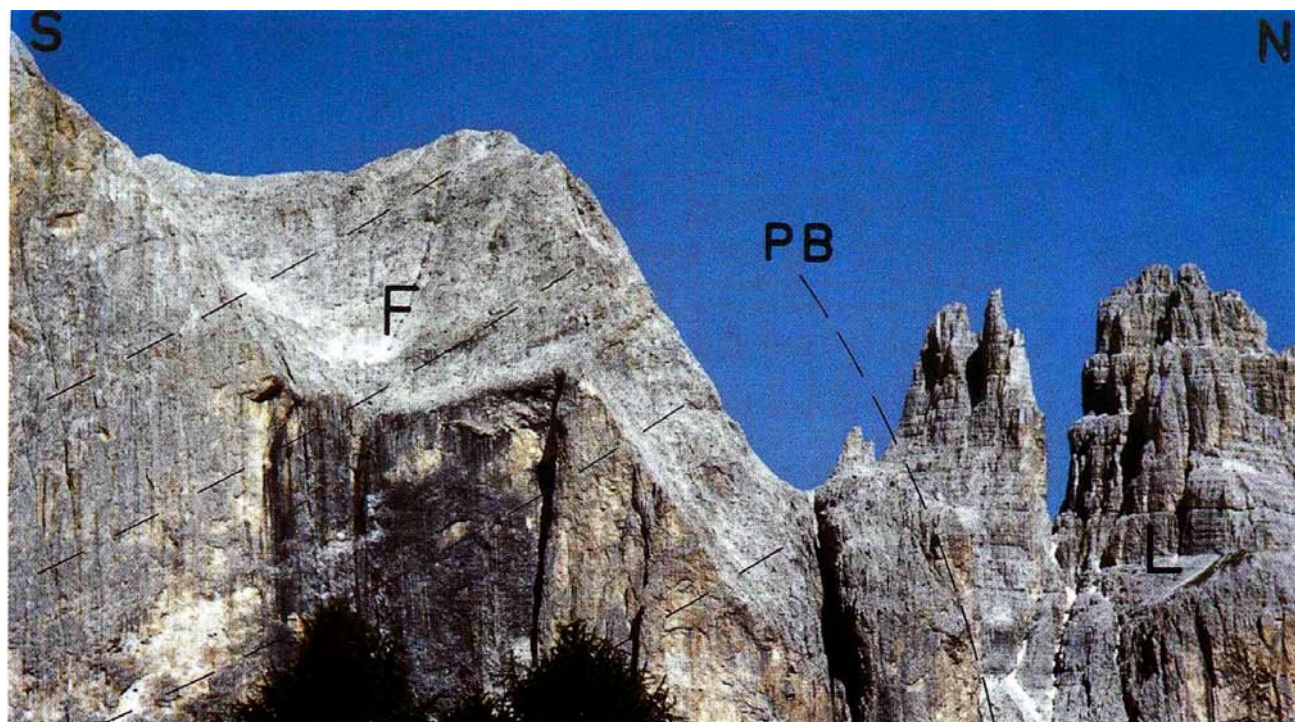


Fig. 198 - Transition (platform break plane, PB) between internal lagoon sediments (back reef, L) and clinostratified escarpment sediments (fore-reef, F) of the Ladinian Marmolada Limestone (or Sciliar Dolomite). The plane is steeply dipping, thus indicating strong aggradation. Photo taken in the Catinaccio Massif.

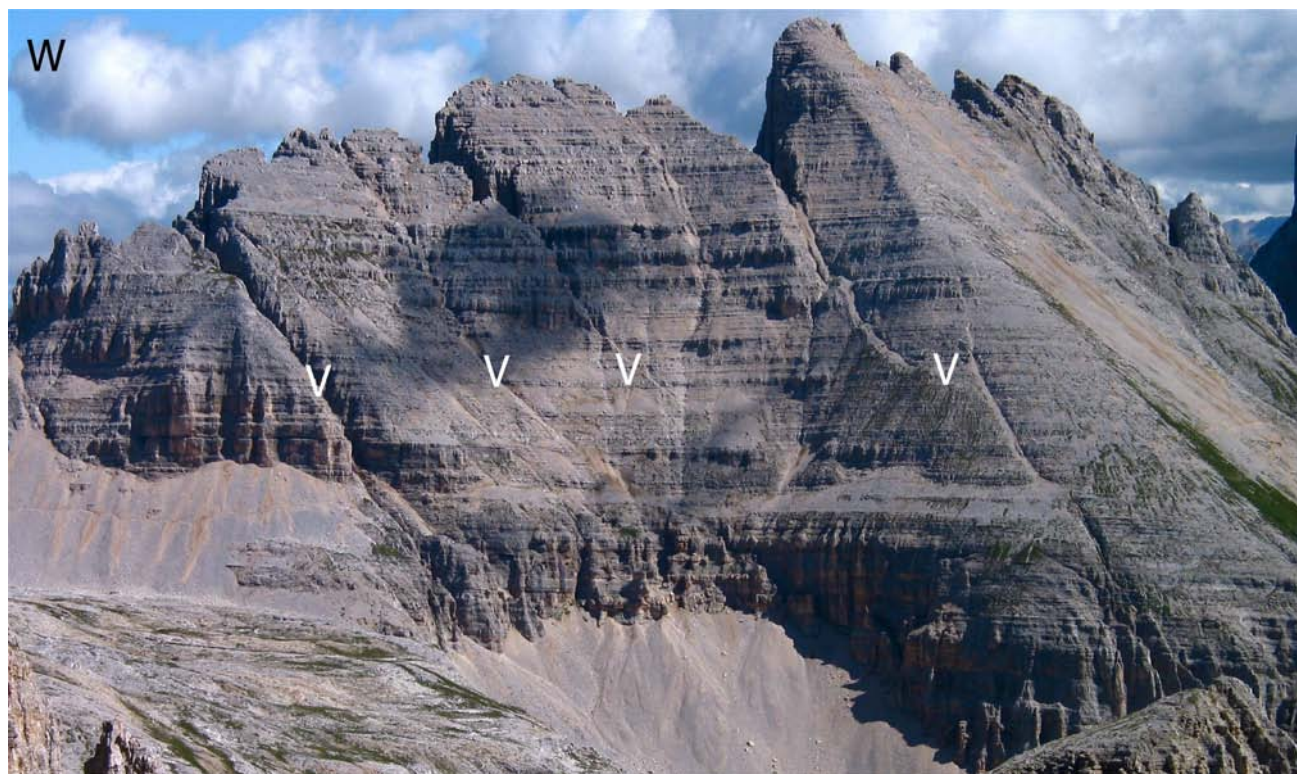


Fig. 199 - Latemar Massif, western Dolomites. The carbonate platform is showing its backreef or lagoon. V, late Ladinian volcanic dikes. There are different datings and genetic interpretations on the evolution of this platform (GAETANI *et alii*, 1981; GOLDHAMMER *et alii*, 1990; KENT *et alii*, 2004). Whatever the interpretation, the subsidence rate can be higher than 0.6 mm/yr, a rate typical of backarc basins associated to W-directed subduction zones.

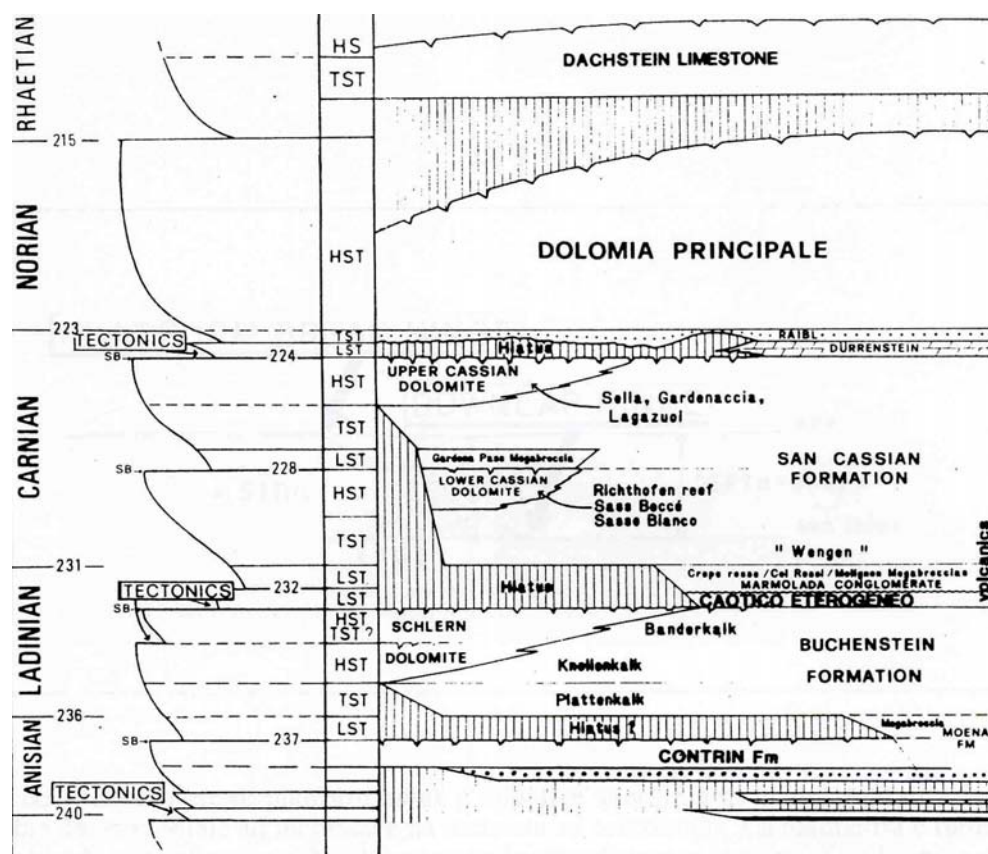


Fig. 200 - Chronostratigraphic chart of the Middle-Upper Triassic of the Dolomites, compared to the coastal onlap curve (after DOGLIONI *et alii*, 1989a).

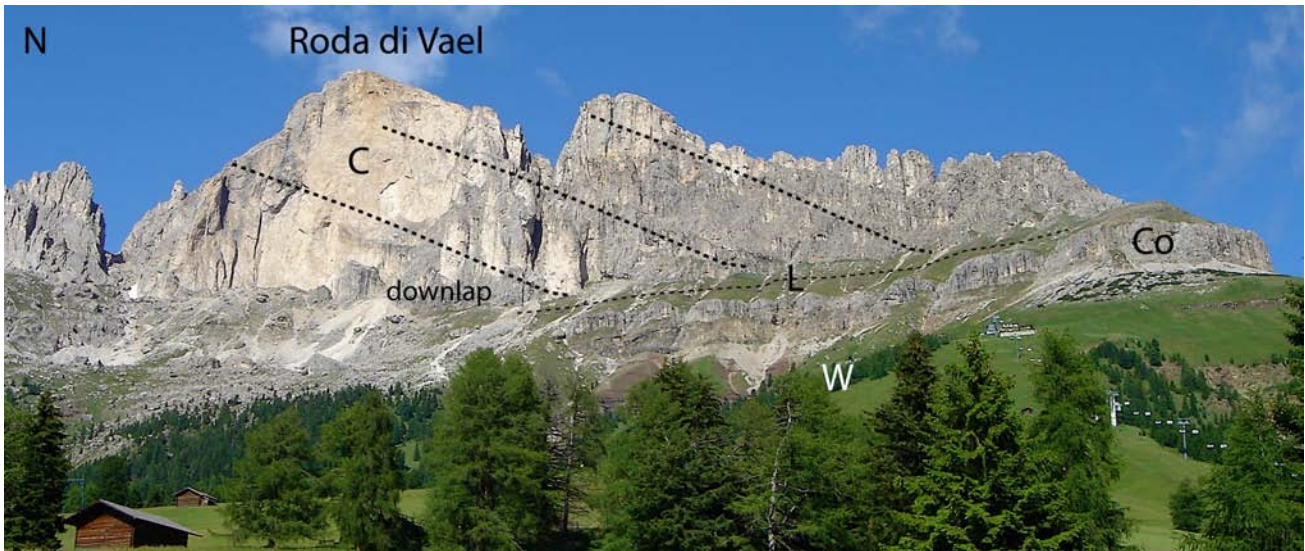


Fig. 201 - View of the southern outcropping termination of the Catinaccio prograding carbonate platform. C, Marmolada Limestone; L, Livinallongo Fm; Co, Contrin Fm; W, Werfen Fm. See next figure.

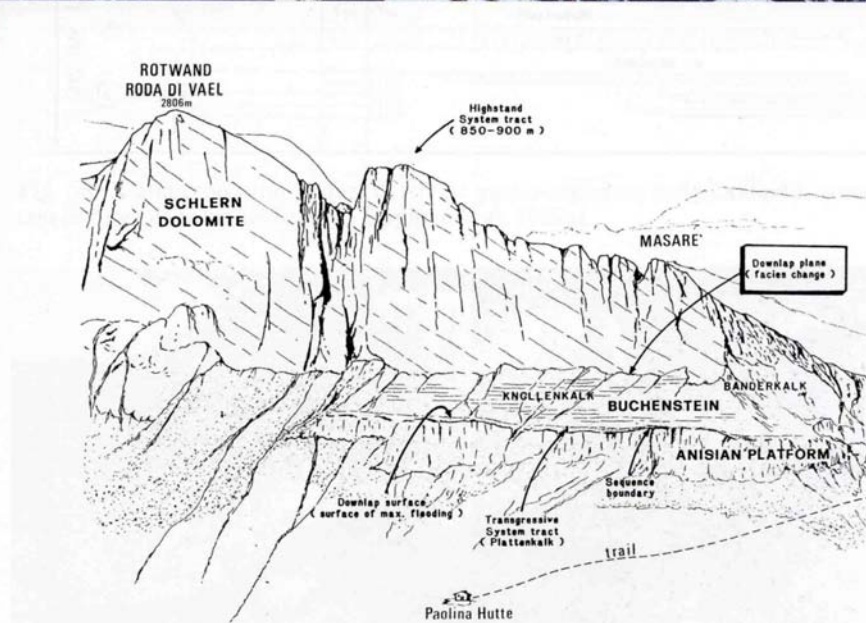


Fig. 202 - The Ladinian carbonate platform of the Catinaccio Massif, with its clinostratified megabreccias (D) prograding towards the south (to the right). Notice that the ledge of the Livinallongo Fm (L), made up of basinal sediments eropic to the platform, reduces and disappears moving to the left, at the core of the platform. Here, internal lagoon deposits directly overlie Anisian platform sediments (C). A syn-sedimentary fault probably accommodated a faster subsidence to the north, at the left margin of the picture above. W, Werfen Fm. The drawing below is the interpretation in terms of sequence stratigraphy of a detail of the southern margin of the picture (after BOSELLINI & DOGLIONI, 1988).

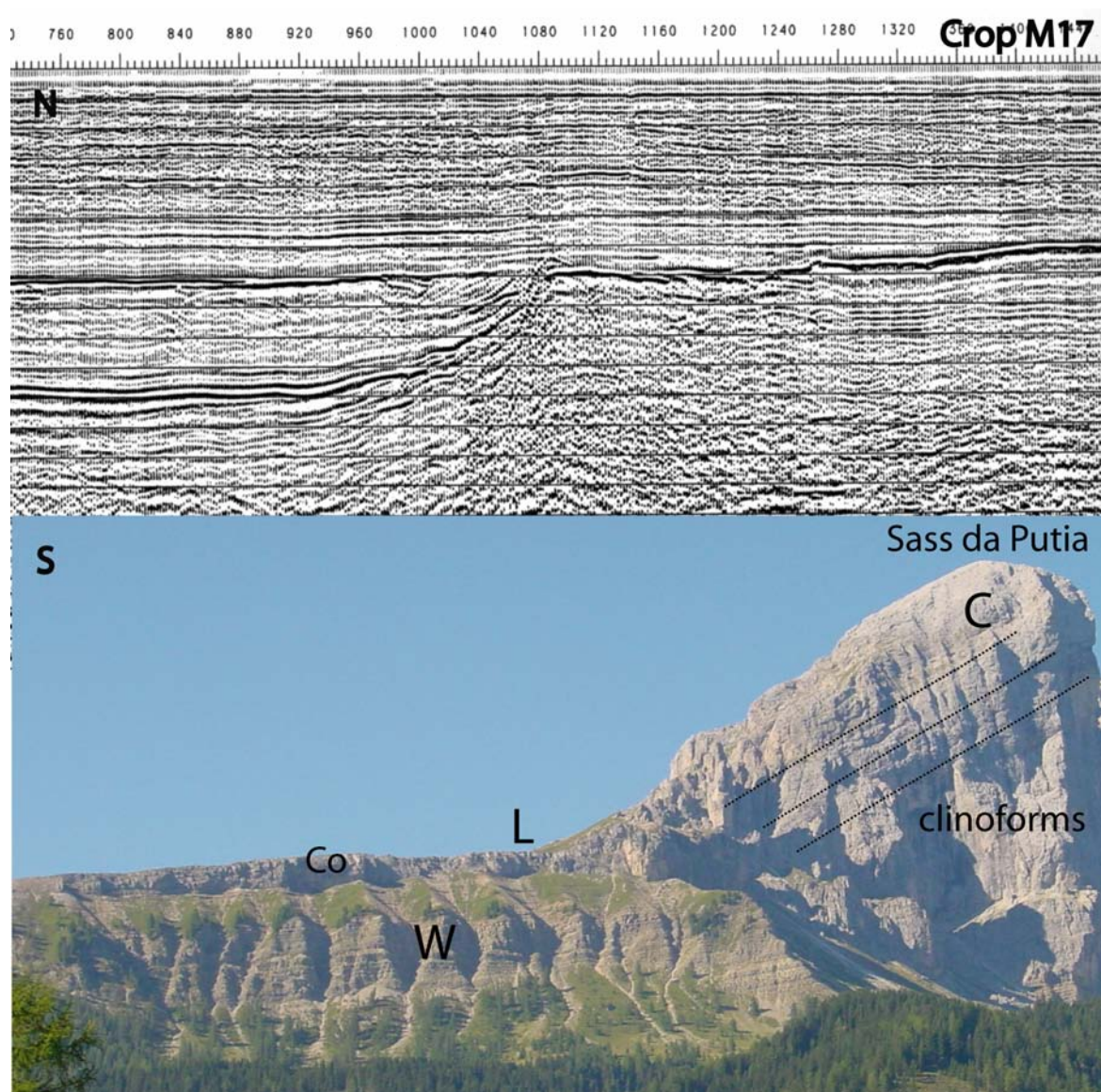


Fig. 203 - Above: seismic reflection profile in the Adriatic Sea (Crop Atlas, SCROCCA *et alii*, 2003) crossing the Mesozoic slope of a carbonate platform. Below: outcropping example of prograding margin of a Ladinian carbonate platform (C, Marmolada Limestone), over the basinal equivalent (L, Livinallongo Fm); W, Werfen Fm, Scythian; Co, Contrin Fm, Upper Anisian. Sass da Putia, northern Dolomites.

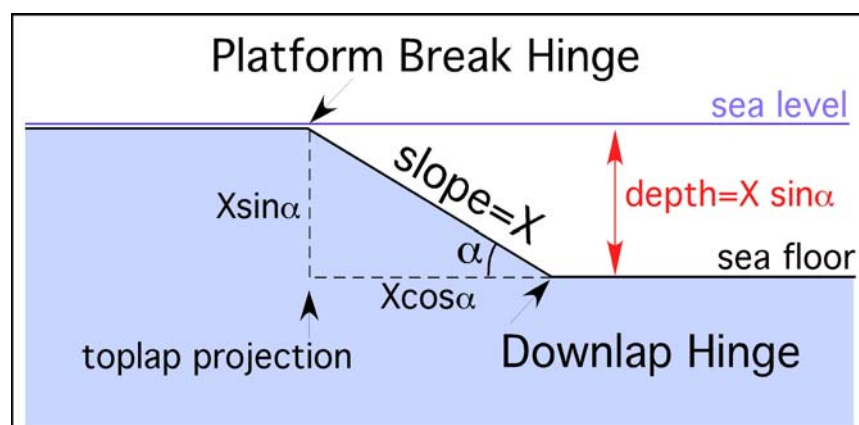


Fig. 204 - Platform break and downlap hinges are the points where stratification changes from horizontal to inclined and from inclined to horizontal. The sea depth is a function of the length of the slope (X) connecting the platform with the basin, and of the angle of the lower slope with the horizontal (α). Thus, $X \sin \alpha$ is almost equal to the depth of the basin, and $X \cos \alpha$ is the distance between the platform break projection and the downlap hinge (after DOGLIONI & BOSELLINI, 1989).

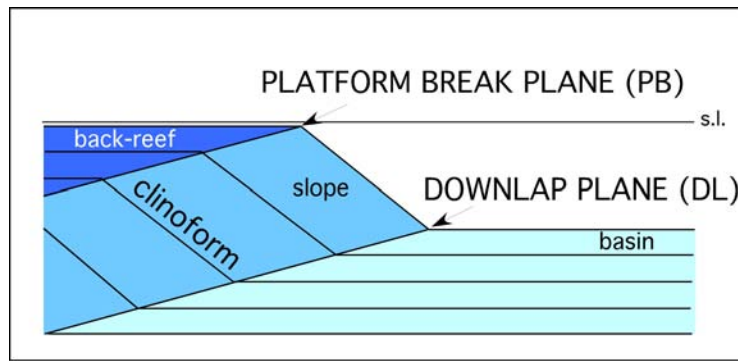


Fig. 205 - The platform break and downlap planes are the ideal planes intersecting respectively all the platform break and the downlap hinges in a progradational system (after DOGLIONI & BOSELLINI, 1989).

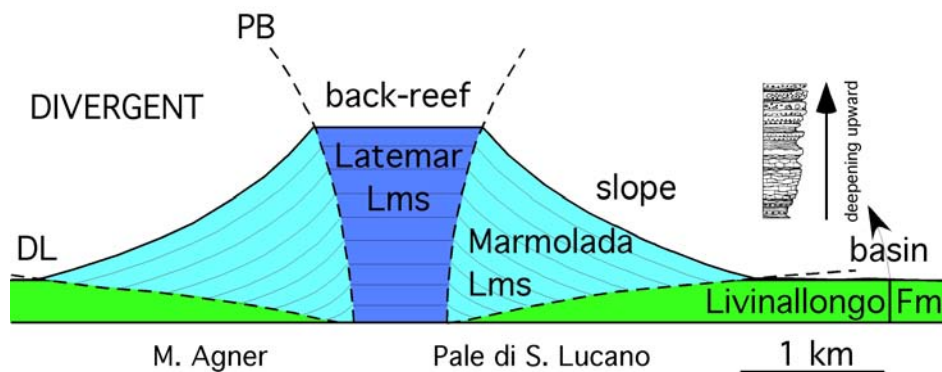


Fig. 206 - Reconstruction of the Ladinian Pale di San Lucano platform; NNW is to the right. Example of divergent platform break (PB) and downlap (DP) planes. Note that the basinal Livinallongo Formation shows a deepening upward sequence (1, black, laminated siliceous mudstone, starved basin; 2, nodular limestone; 3, graded calcarenites organized in small thickening-coarsening upward sequences). The Sciliar Dolomite (or Marmolada Limestone) is represented by megabreccias of the slope, whereas the Latemar Limestone consists of peritidal back-reef sediments (after DOGLIONI & BOSELLINI, 1989). The steep platform break is controlled by fast subsidence rate. It cannot be generated only by sea-level rise since the platform sequence is thicker than 1 km.

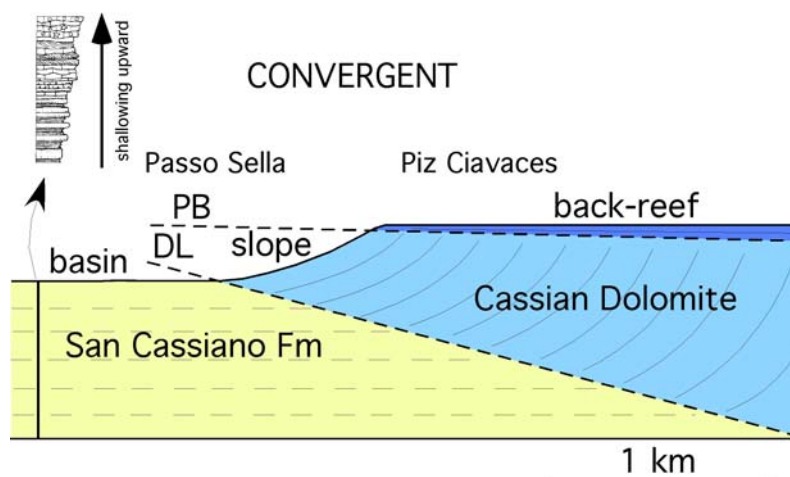


Fig. 207 - Reconstruction of the western margin of the Sella Carnian carbonate platform (Upper Cassian Dolomite). It is an example of convergence between the platform break plane (PB) and the downlap plane (DL). The coeval basin (San Cassiano Formation) consequently shows a shallowing upward sequence (1, graded calcarenites and breccias alternating with shale and mudstone; 2, nodular and wavy bedded limestones with traction-current structures; 3, wave bedded calcarenites). The flat and gentle dip of the platform break has to be related to absent or low subsidence rate.

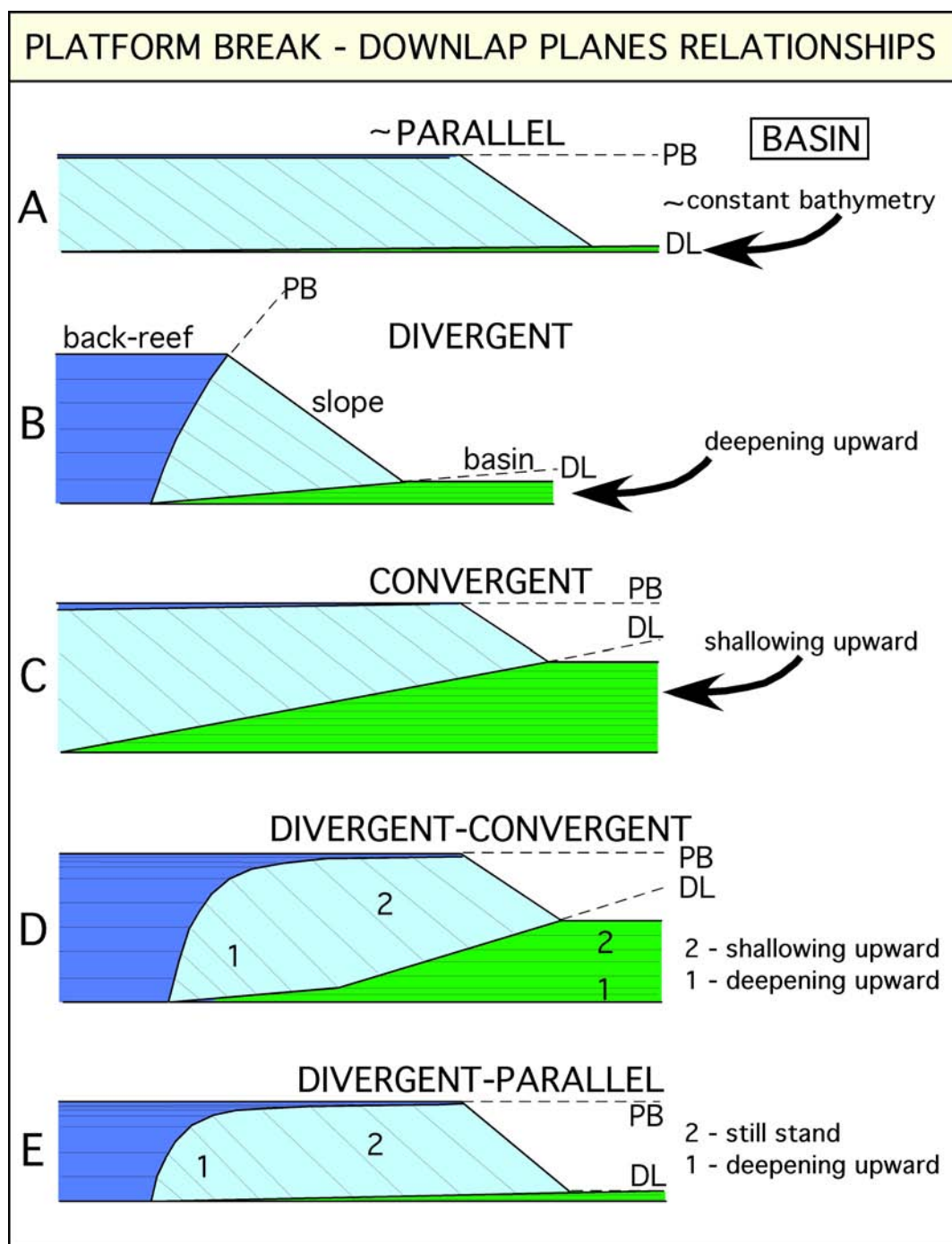


Fig. 208 - Different relationships between platform break and downlap planes in progradational systems produce different evolutions of the basin. A, parallel - constant bathymetry; B, divergent - deepening upward; C, convergent - shallowing upward; D, divergent-convergent - deepening and subsequent shallowing upward; E, divergent-parallel - deepening and subsequent still stand. PB, platform break plane; DL, downlap plane. The different kinds of geometries are principally controlled by subsidence rates, by sea-level eustatic oscillations, by carbonate productivity and by terrigenous input into the basin. Since subsidence and terrigenous input were variable from region to region in the Dolomites, during the same eustatic cycle carbonate platforms developed with different relationships between platform break and downlap planes (either convergent or divergent). For example, the Ladinian carbonate platforms of the Pale di San Lucano (B-type) and of the Catinaccio (E-type) developed contemporaneously in zones characterised by different subsidence (smaller, at a certain period, in the Catinaccio).

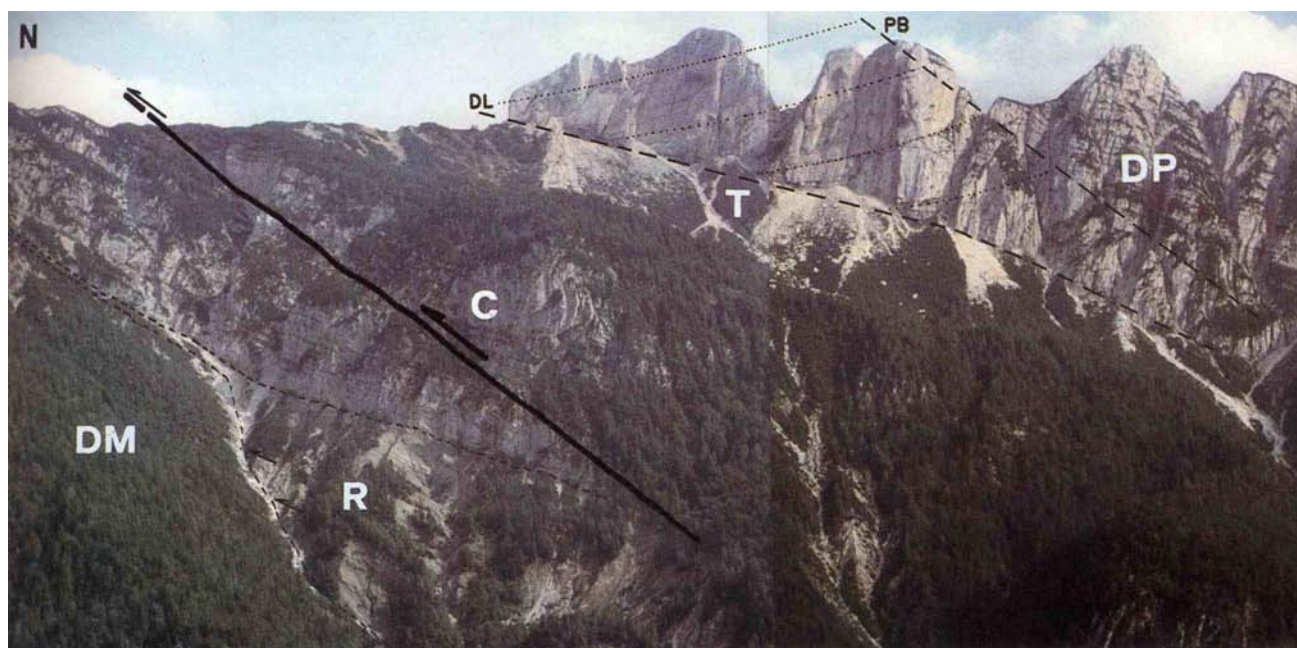


Fig. 209 - Natural section west of Raibl, in the Tarvisio area, between Portella and Mt. Guarda, to the right (eastern Southern Alps). DM, Ladinian Dolomia Metallifera, equivalent to the Sciliar Dolomite; R, Rio del Lago Fm, lower Carnian, consisting of marls and marly limestones onlapping the slope of the underlying platform (Dolomia Metallifera); C, Conzen Dolomite, middle Carnian; T, Tor Fm, upper Carnian, basinal equivalent of the upper Carnian-Norian Dolomia Principale (DP), consisting of classical peritidal dolomite to the right and of clinostratified megabreccias and calcarenites prograding towards the north in the central part of the picture. DL, Downlap plane; PB, Platform break plane.

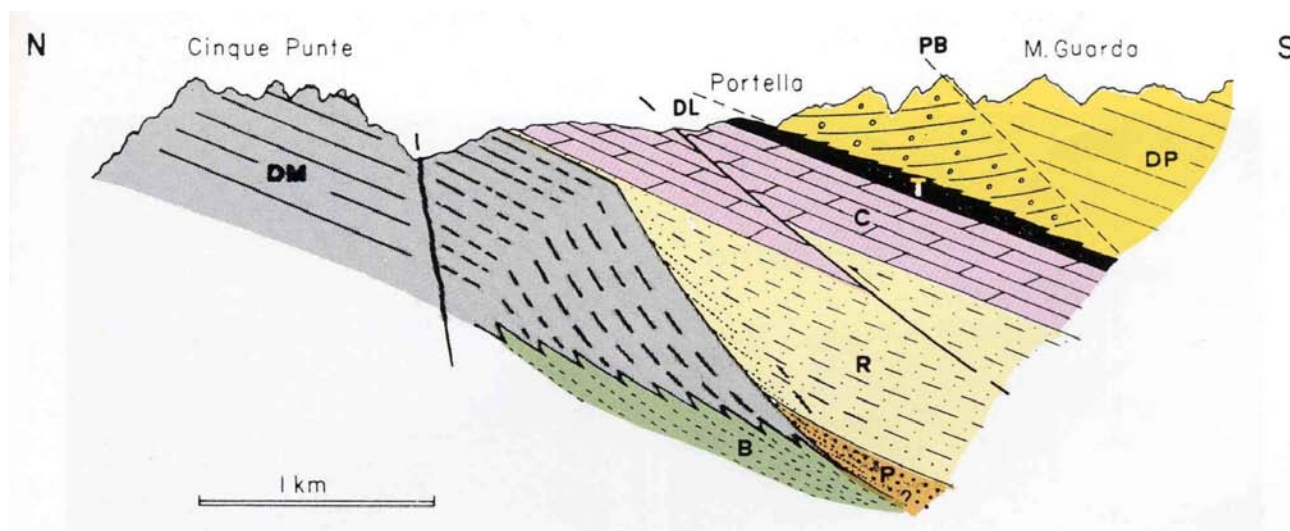


Fig. 210 - Section to the west of Raibl, Tarvisio area, between Cinque Punte and Mt. Guarda. DM, Dolomia Metallifera, Ladinian carbonate platform; B, Buchenstein (Livinallongo) Fm, Ladinian, basinal equivalent of the Dolomia Metallifera. P, Predil Limestone, lower Carnian; R, Rio del Lago Fm, lower Carnian, consisting of marls and marly limestones onlapping the slope of the underlying platform (Dolomia Metallifera); C, Conzen Dolomite, middle Carnian; T, Tor Fm, upper Carnian, basinal equivalent of the upper Carnian-Norian Dolomia Principale (DP), consisting of classical peritidal dolomite to the right and of clinostratified megabreccias and calcarenites prograding towards the north onto the Tor Fm; DL, Downlap plane; PB, Platform break plane. The picture of the previous figure represents the central-right part of the section.



Fig. 211 - Clinostratifications of the prograding megabreccias of the Ladinian Sciliar Dolomite, observable along the northern flank of the Cime di Focobon. Some latite-basaltic dykes (V) referred to the upper Ladinian volcanic event cut the platform sediments.

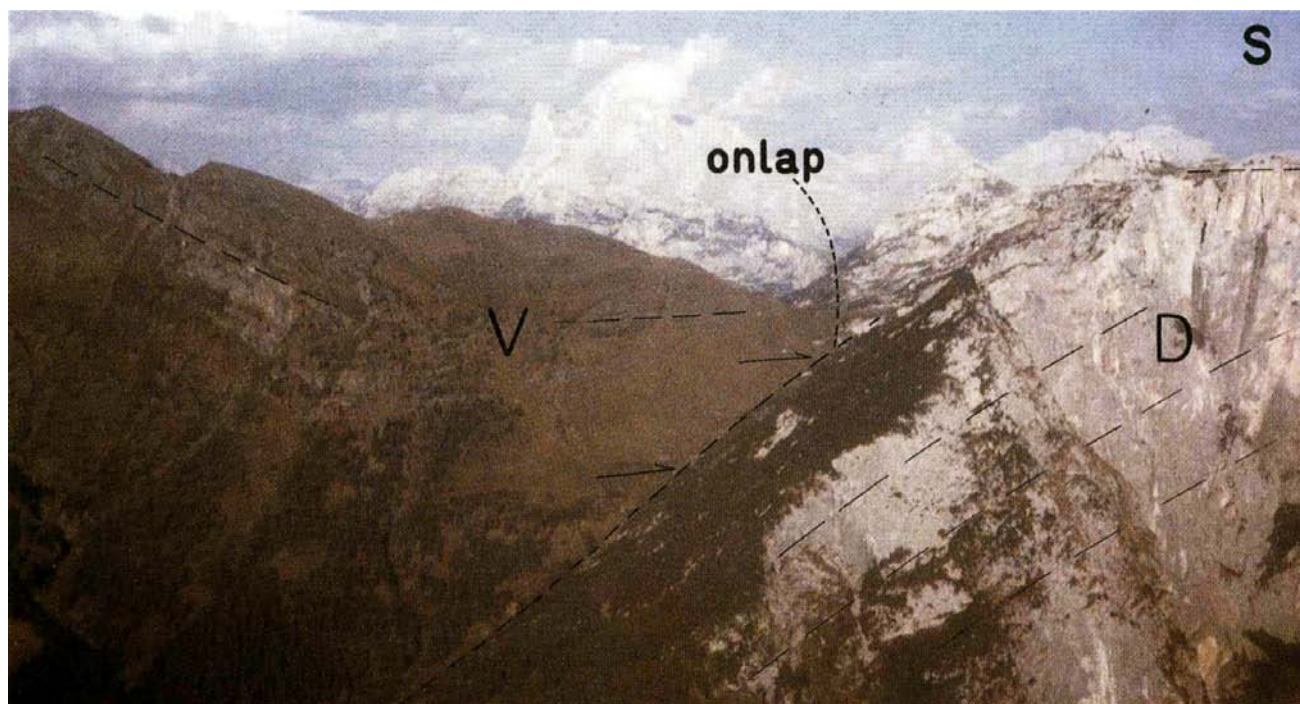


Fig. 212 - The famous onlap of the volcanic and volcanoclastic deposits (V) of Ladinian age onto the northern slope of the lower-middle Ladinian carbonate platform (D) of the Pale di San Lucano prograding towards the north, at the head of the Gares Valley.



Fig. 213 - Pillow lava of the Ladinian shoshonitic volcanic event in the Dolomites. Locality Colcuc, Andr  Droxler for scale.



Fig. 214 - Ladinian latit-basalt pillows covered (left) or lying on (right) and squeezing volcaniclastic turbidites. Locality Colcuc.



Fig. 215 - Caotico Eterogeneo, Ladinian mass flow deposit containing pebbles from the Upper Permian to the Ladinian. Volcanic rocks, basinal and platform fragments are included. Some elements are sheared or folded, and contained in the undeformed conglomerate, indicating Middle Triassic tectonics. Locality Lasta, Valle di Livinallongo.

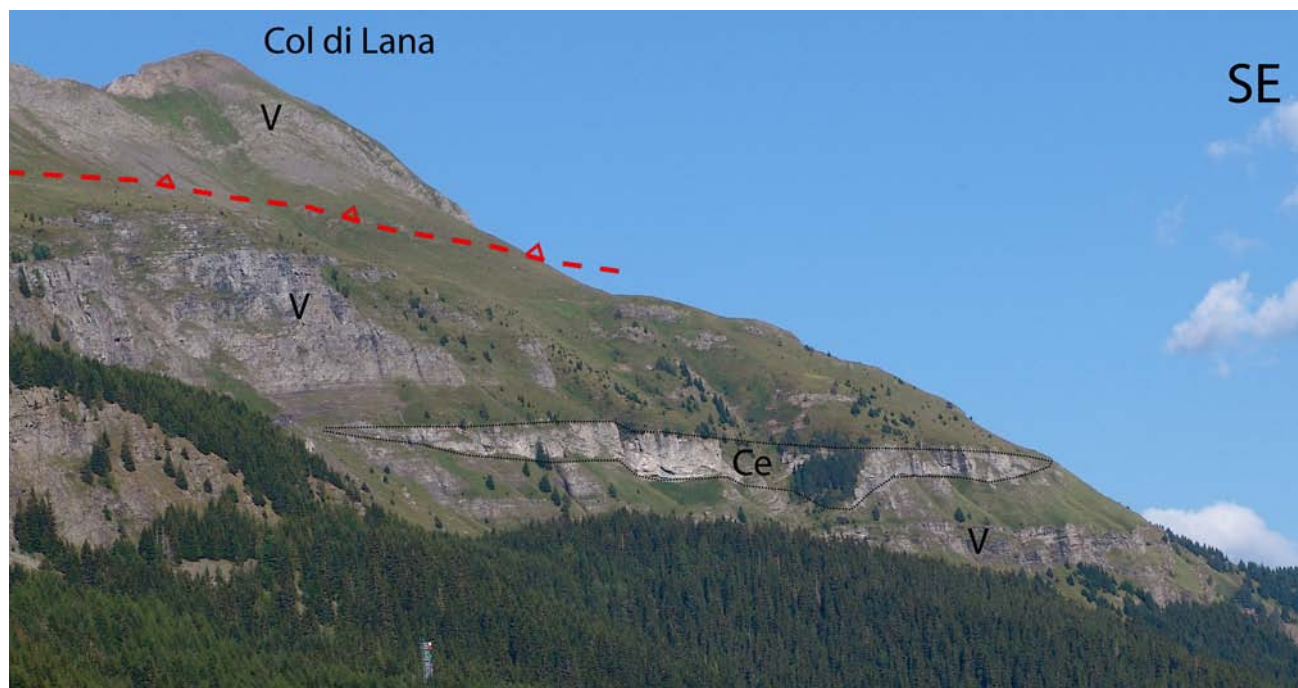


Fig. 216 - The Caotico Eterogeneo (Ce) occurs in channelized bodies interbedded in the turbiditic volcanoclastic sandstones of Ladinian age (V). This is an example in the Livinallongo Valley, in the southern slope of the Col di Lana, where the top is folded and thrusting toward the observer.



Fig. 217 - Carbonatic olistholith (Marmolada Limestone) included in the Upper Ladinian volcanic Marmolada Conglomerate. Road from Arabba to Passo Pordoi. Matteo Minervini, Elena Capoferri, David Hearty, Grant Ellis and others for scale.



Fig. 218 - Prograding Cassian Dolomite (D) of the Gardenaccia Massif over the San Cassiano Fm (S), toward the Val Badia. R, Raibl Fm; DP, Dolomia Principale.



Fig. 219 - Early Carnian San Cassiano Fm at Passo Sella. Carbonatic and volcanoclastic turbidites interfingered with emipelagic shales and marls. This basinal formation is eteropic to the Cassian Dolomite in the background. Silvia Campobasso, Cecile Huet, Eleonora Vitagliano, Daniele Fragola and others for scale.



Fig. 220 - Undolomitized olistolith of the Cassian Dolomite carbonate platform included in a coarse grained (volcaniclastic rich) turbiditic facies of the San Cassiano Fm, Passo Sella. Casey Moore for scale.

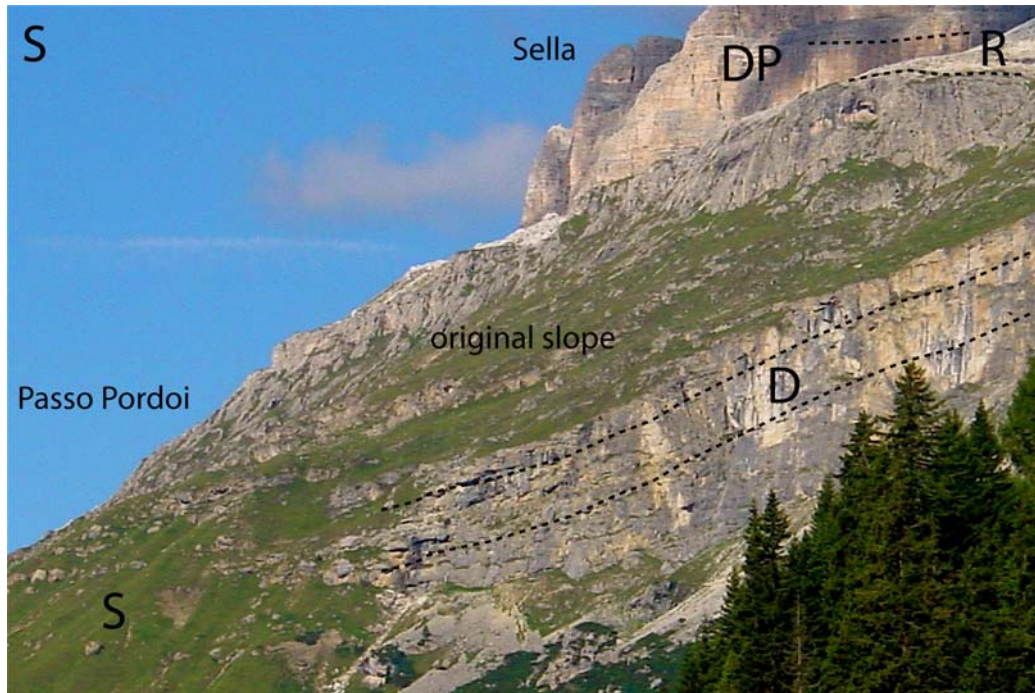


Fig. 221 - Interfingering between the clinoformed megabreccias of the Cassian Dolomite (D), representing the slope, and the basin of the San Cassiano Fm (S) in the green. R, Raibl Fm; DP, Dolomia Principale.



Fig. 222 - Stratigraphy of the western margin of the Sella Massif, central Dolomites. DP, Norian tidal flat Dolomia Principale; R, Upper Carnian Raibl Fm; Du, Carnian shallow water lagoon facies Dürrenstein Dolomite; D2, prograding megabreccias of the Carnian Upper Cassian Dolomite. S2, basinal sediments of the Carnian Upper San Cassiano Fm. In the background to the north toward Passo Gardena, D1, megabreccias of the Carnian Lower Cassian Dolomite, S1, the basinal sediments of the Lower San Cassiano Fm. In the Gardenaccia massif, the Dolomia Principale overrides the Cretaceous Puez Marls (K). Picture by Ulrich Prinz taken from a paraglide.



Fig. 223 - Carnian-Norian transition in the Mt. Faloria, southeast of Cortina. DP, Norian tidal flat Dolomia Principale; R, Upper Carnian Raibl Fm, here reddish, tidal flat and including some evaporites; Du, Carnian shallow water lagoon facies Dürrenstein Dolomite; D, megabreccias of the Carnian Cassian Dolomite.

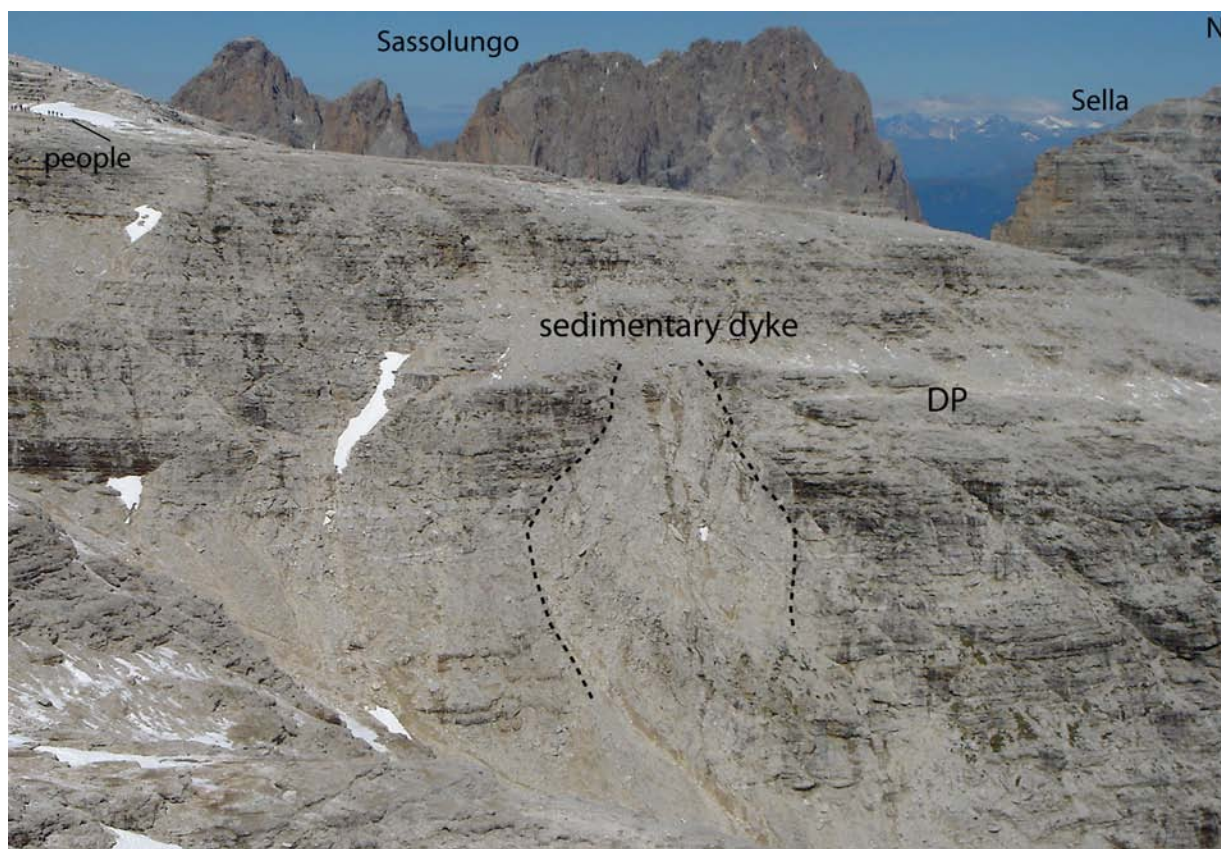


Fig. 224 - Intraformational sedimentary dyke in the Dolomia Principale (DP) near Sass Pordoi in the Sella Massif.

11. Tectonics of the Dolomites and the Venetian Alps

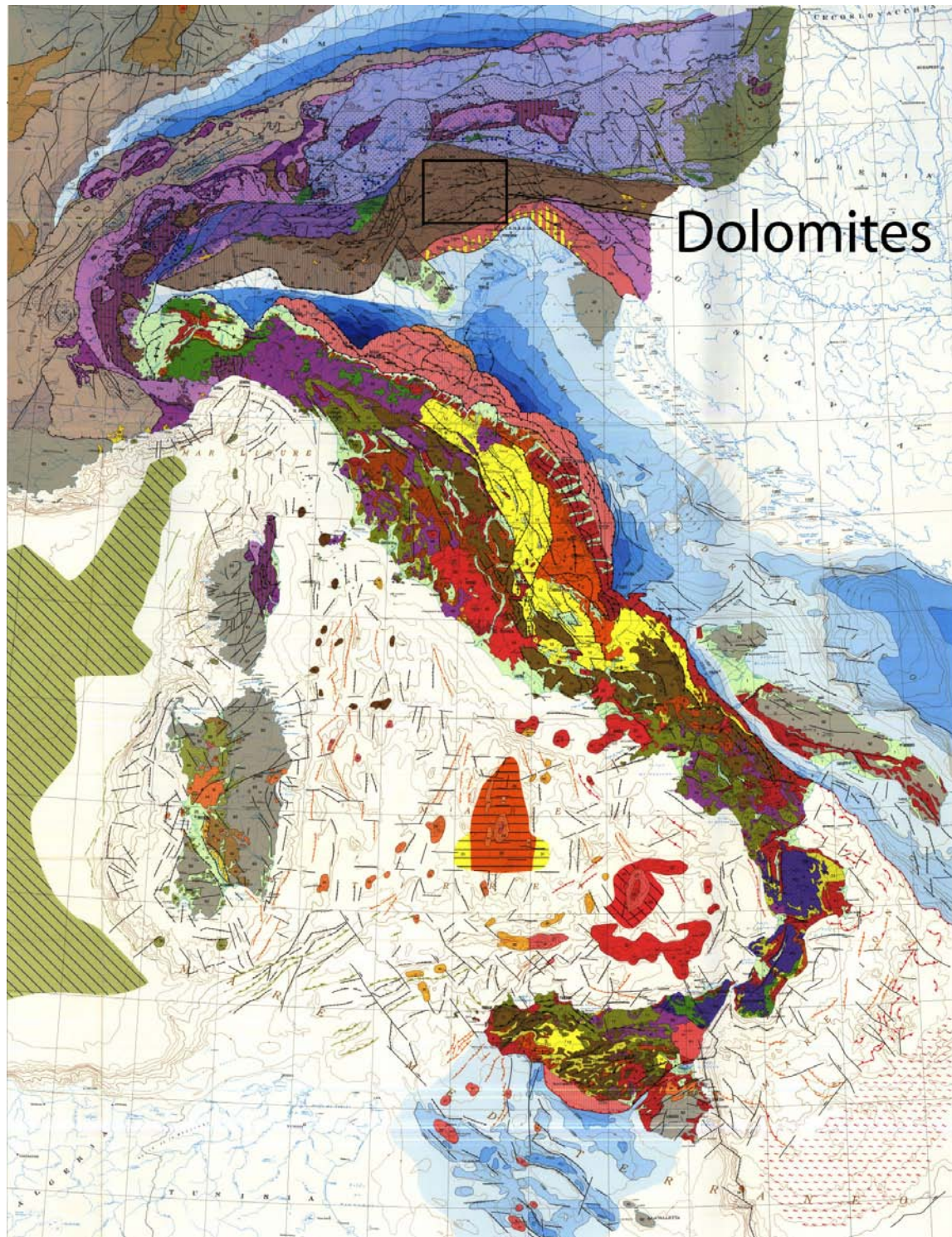


Fig. 225 - Structural Model of Italy (after BIGI *et alii*, 1989).

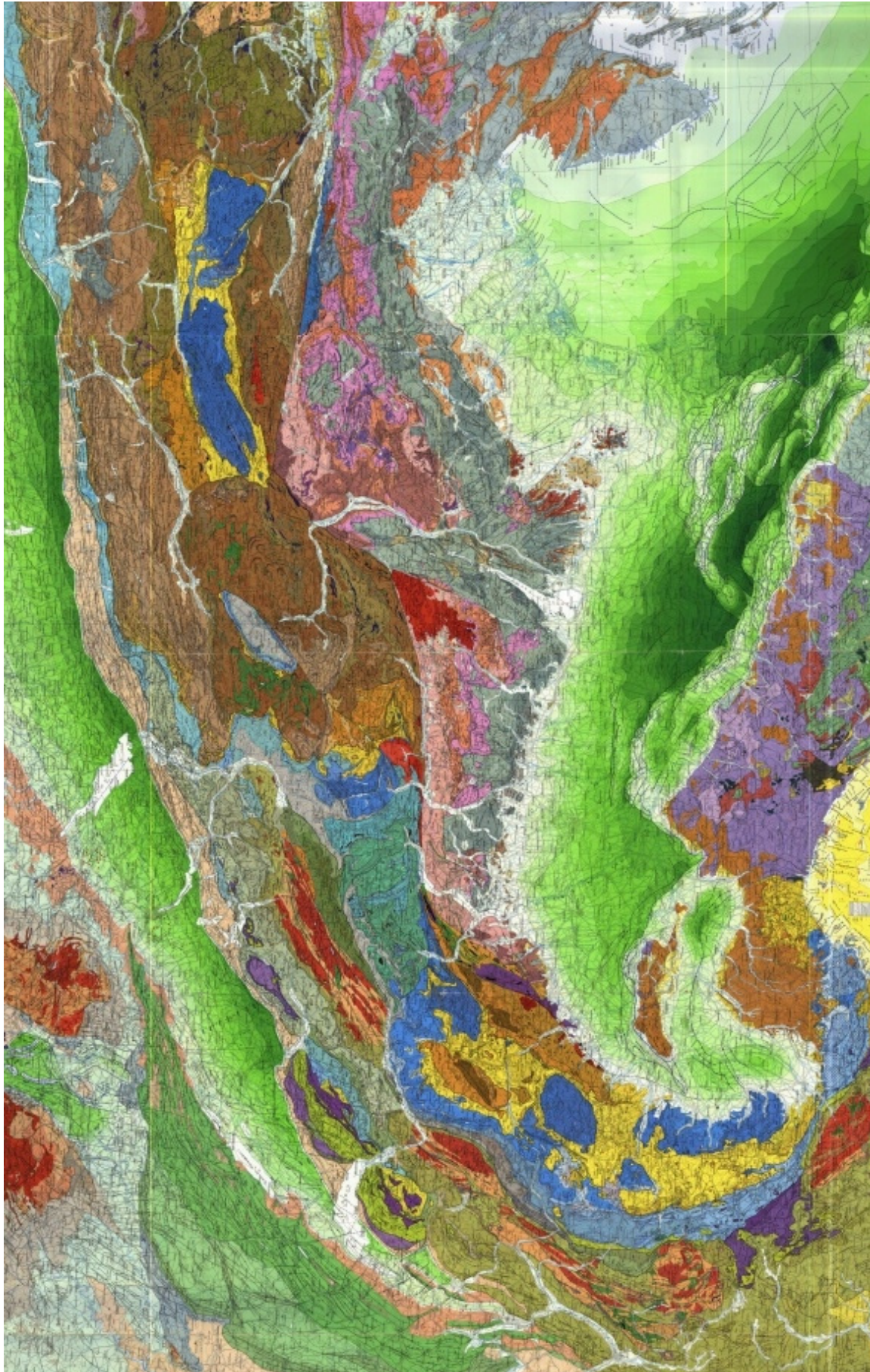


Fig. 226 - Structural model of the Alps and the Northern Apennines (Bigi *et alii*, 1989).

This chapter will describe the main structural grain of the Dolomites and the Venetian Alps, a part of the eastern Southern Alps, south of the Insubric Lineament (figs. 225 - 227; see also the map at the end of the book). It is a SSE-vergent fold and thrust belt (figs. 228 - 231) of mainly Paleogene-Neogene age (DAL PIAZ 1912; LEONARDI 1965; CASTELLARIN 1979; LAUBSCHER 1985, MASSARI *et alii* 1986; DOGLIONI 1987; ROEDER 1989) probably produced by the dextral transpression in the central-eastern Alps (LAUBSCHER 1983). The chain deformed a pre-existing Mesozoic passive continental margin (BOSELLINI 1965; 1973; BERNOULLI *et alii* 1979; Winterer & BOSELLINI 1981).

The Venetian Alps have been shortened main-

ly during Neogene times (VENZO 1939; MASSARI *et alii* 1986; DOGLIONI 1987) and not deformed by the Dinaric chain of which constituted the unfolded foreland during Paleogene times (DOGLIONI & BOSELLINI, 1987).

The Dolomites to the north, in post-Variscan times, underwent a number of tectonic events, which may be summarized as follows: Permian and Triassic rifting phases broke the area into N-S trending basins with different degrees of subsidence. A Middle Triassic transpressive-transpressive event then deformed the region along a N70°-90° trend, generating flower structures within the basement. Volcano-tectonic domal uplift and subsequent caldera formation occurred at the same time as the

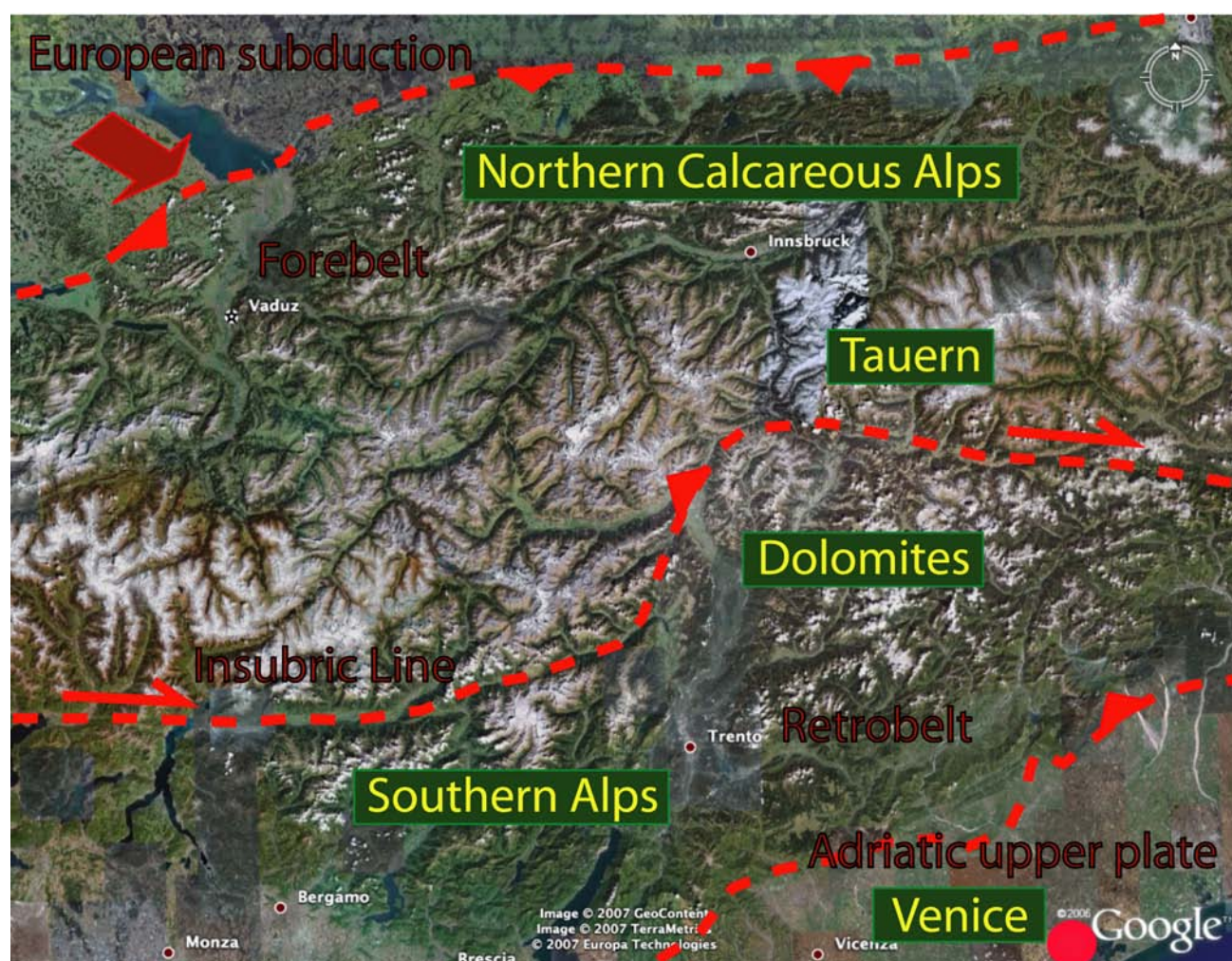


Fig. 227 - GoogleEarth map of the central-eastern Alps which formed by the subduction of the European plate beneath the Adriatic plate. The Dolomites are an element of the Southern Alps which constitutes the retrobelt of the Alpine orogen.

Late Ladinian magmatism. Early Jurassic rifting also controlled the subsidence which was larger in the eastern side of the Dolomites. This long period of generalized subsidence was followed by a pre-Neogene (Late Cretaceous-Paleogene?) ENE-WSW compression that generated a WSW-verging belt. This shortening amounts to at least 10 km. During the Neogene, the Dolomites as far north as the Insubric Lineament, were the innermost part of a S-verging thrust belt. The basement of the Dolomites was thrust southwards along the

Valsugana Line onto the sedimentary cover of the Venetian Prealps for at least 10 km. This caused a regional uplift of 3-5 km. The Valsugana Line and its backthrusts on the northern side of the central Dolomites generated a 60 km wide pop-up in the form of a synclorium within which the sedimentary cover adapted itself mainly by flexural slip often forming triangle zones. The shortening linked to this folding is about 5 km with Neogene thrusts faulting and folding the shallower WSW-verging pre-existing thrust planes. On

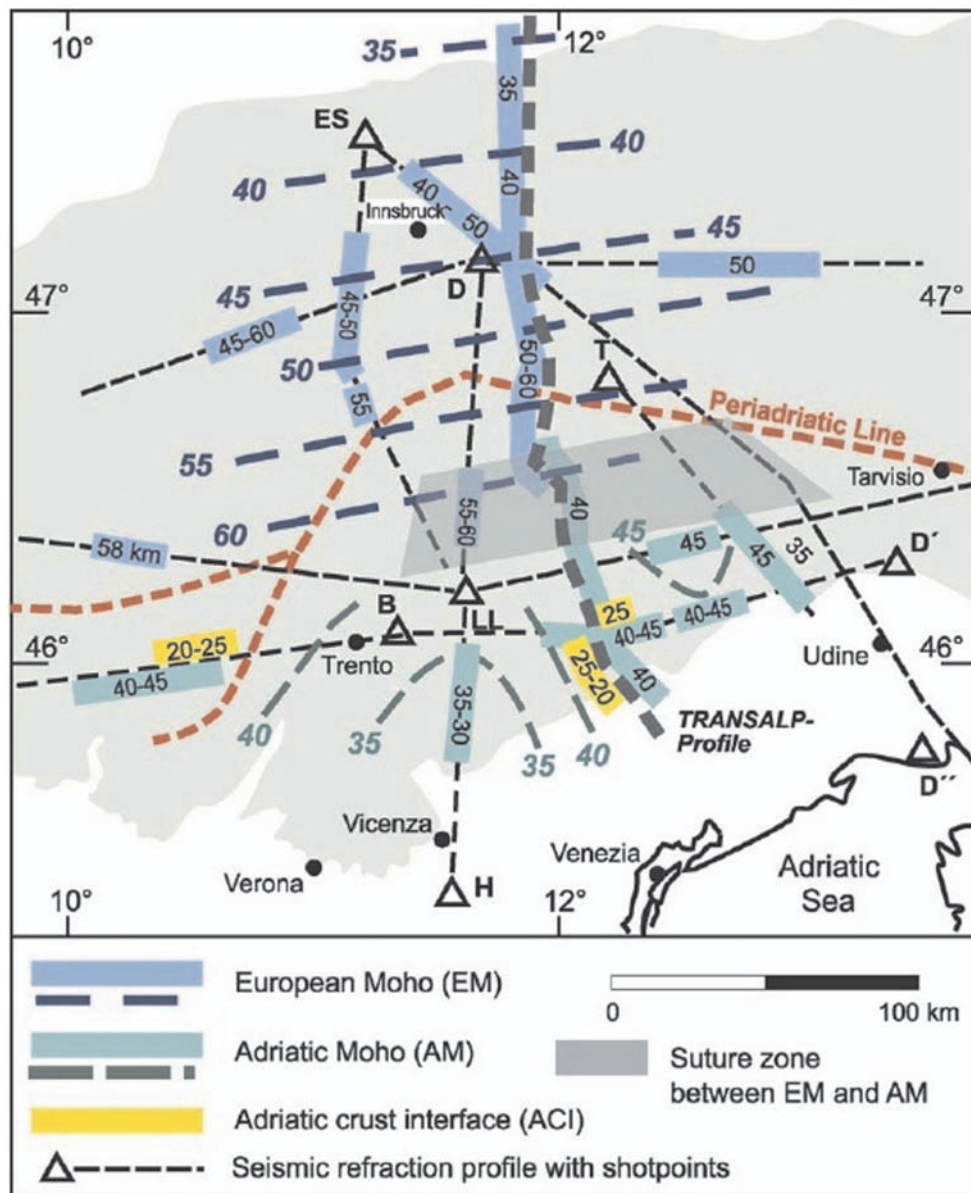


Fig. 228 - Moho depth in the central eastern Alps (after KUMMEROW *et alii*, 2004).

the north-eastern side of the Dolomites, Neogene deformation is apparently more strictly controlled by the transpressive effects of the Insubric Lineament (Pusteria Line) and shortening of the sedimentary cover may be greater than in the central Dolomites. Minor deformation linked to the Giudicarie belt is present in the western Dolomites. The eastern Dolomites are a recess of the earlier Alpine deformation where the ESE-verging Giudicarie system represents the left-lateral transpressive oblique ramp, and the WSW-verging Paleogene thrusts of the central eastern Dolomites are the right-lateral transpressive oblique ramp. The recess is located on the Permo-Mesozoic Trento Horst.

The present structure of the Dolomites is thus the result of a number of tectonic events of different significance and different strike. Only a 3-dimensional restoration can unravel the true structure of the area.

In the Dolomites, local compressive features of Middle Triassic age have been demonstrated by thrusts and folds cross-cut by volcanic dykes and plutonic bodies of Ladinian age and coeval sediments sealing these structures. The en-échelon distribution of grabens, folds and other structures suggest a left-lateral move-

ment along the basement involving N70°-90°-trend, particularly along the Stava and Trodena Lines, continuing along the northern limb of the Cima Bocche Anticline.

Tectonic features of magmatic origin are also present in the Dolomites. The radial pattern of faults and of the Ladinian volcanic dykes in the central-western part of the Dolomites suggests the presence of a domal uplift, genetically related to emplacement of the coeval magmatism. Subsequent calderas and volcano-tectonic basins complicate these structures in the Predazzo and Monzoni areas, which are located along the aforementioned alignment.

N-S or NNW-trending thrust and fold axes, accompanied by a corollary of consistent mesostructures, support the presence of a ENE-WSW-directed compression. These tectonic features are widespread throughout all the central-eastern Dolomites and involve up to Lower Cretaceous rocks. In the area of Monte Parei, north of Cortina, a lower Miocene conglomerate unconformably overlies these features. The thrusts are mostly thin-skinned with detachment horizons in the evaporitic Upper Permian Bellerophon Formation, plus a number of other shallower weak layers.

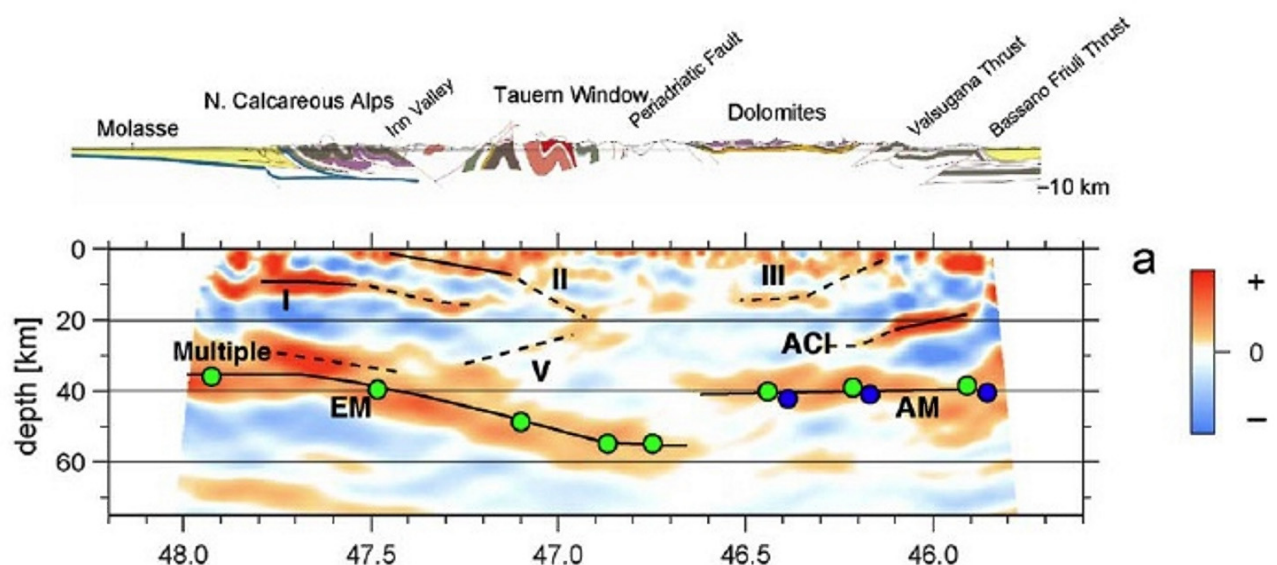


Fig. 229 - Evidence for the subduction of the European plate beneath the Adriatic plate from the TRANSALP profile in the central eastern Alps. EM, European Moho; AM, Adriatic Moho (after KUMMEROW *et alii.*, 2004).

In a N-S section, the central Dolomites form a wide synclinorium (figs. 232, 233), genetically related to the Valsugana thrust in the south, and its N-verging backthrusts to the north (Funes and Passo delle Erbe Lines). Therefore, the Dolomites are within a pop-up-related syncline generated by the two conjugate thrusts. The Valsugana thrust to the south over

Miocene sediments. The strike of Neogene thrusts and folds ranges from N90° to N50°. Conjugate strike-slip faults trend N30°-60°W (dextral transpression) and N0°-30° (sinistral displacement). Several valley in the central and northern Dolomites now lie along dextral strike-slip faults (e.g., Valparola, Valle di S. Vigilio). These strike-slip faults often show

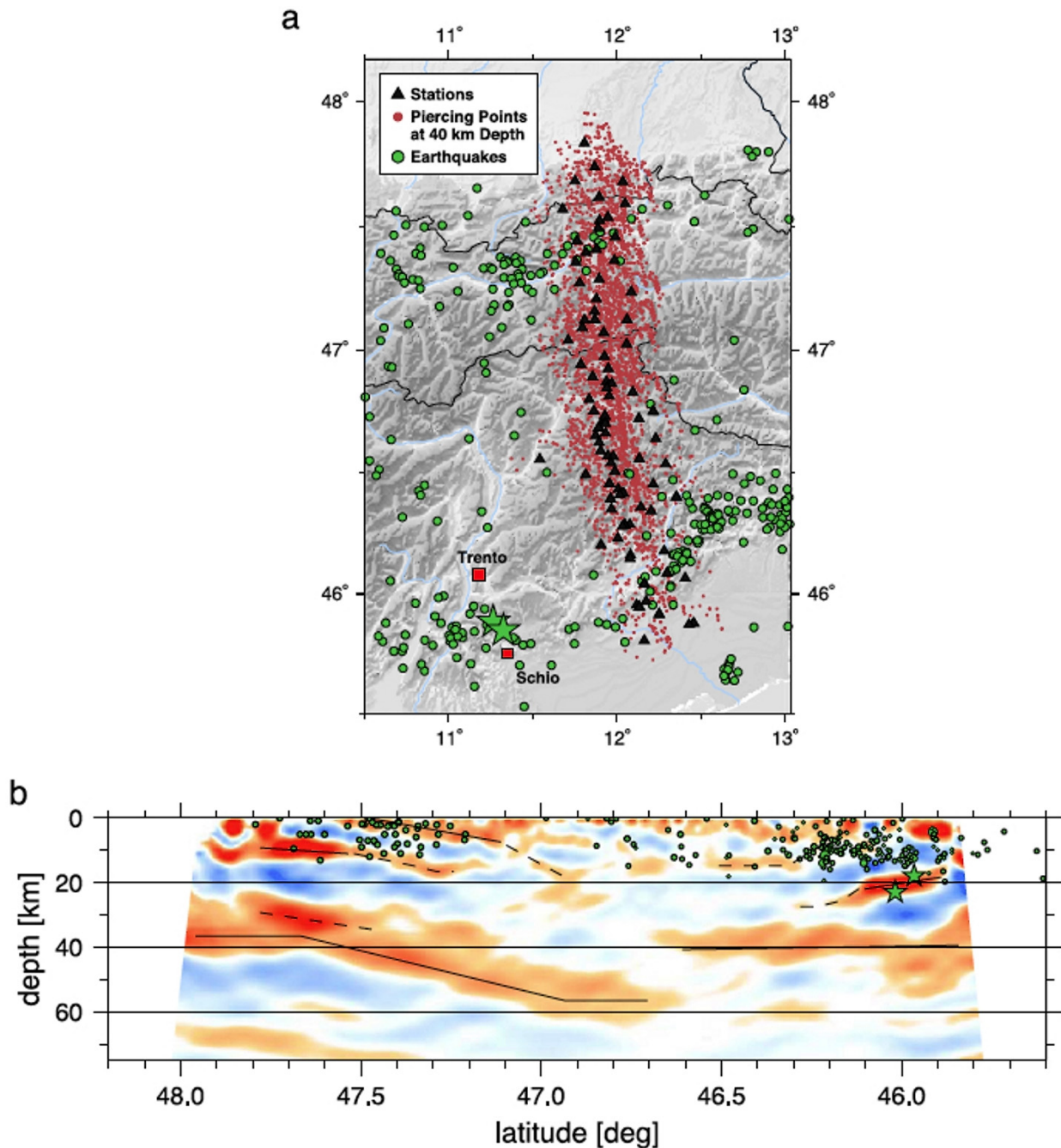


Fig. 230 - Seismicity distribution in the central-eastern Alps along the TRANSALP (after Kummerow et al., 2004). Note how seismicity is concentrated in areas of lower topography as suggested by CARMINATI *et alii* (2004).

both positive and negative flower structures. Neogene deformation generated most of the present elevation of the Dolomites, which form a slab of upper crust carried southwards by the Valsugana thrust.

The central Dolomites form the innermost part of the Southern Alps, the conjugate retro-belt of the Alpine subduction, where Europe subducted S-ward beneath the Adriatic plate. To the south of the Dolomites, the sedimentary cover of the Venetian Prealps is considerably shortened. In the central Dolomites, the sedimentary cover has rather been generally preserved, and the basement has been displaced southward by the Valsugana thrust for at least 8-10 km. The basement syncline, associated with the Valsugana thrust and the back-thrusts to the north, produced folding of the overlying sedimentary cover. The flower structures inherited from the Triassic times have complicated the core of the synclinorium. The sedimentary cover adapted itself to Neogene folding of the basement by generating semi-cylindrically shape folds by flexural slip or flexural shear. Thus the Neogene compression of the Dolomites apparently did not generate strong shortening within the sedimentary cover apart from the adaptation to

basement folding. Using an area balance, 10% (ca 5 km) Neogene shortening of the sedimentary cover in the central Dolomites, along a N-S cross-section, is about the same as that calculated by restoring the folding of the basement without taking into account inherited pre-Neogene structures (figs. 235 - 238).

Since the Dolomites stratigraphy contains a number of Triassic carbonate platforms and intervening basins, these inherited features represent mechanical discontinuities that influenced ramps and undulations of the thrust trajectories. The staircase trajectory of the thrusts is connected with marked differences in the rheological behavior of the different stratigraphic horizons.

The different tectonic phases of the Dolomites (figs. 239 - 268) formed mainly at low temperature (diagenesis) and are essentially brittle tectonics. However, Ladinian magmatism, Mesozoic burial and the Alpine event produced anchimetamorphic temperatures. Slow ductile behavior has been recognized for the Werfen Formation, and a temperature of about 200°, suggestive of anchimetamorphism conditions (Garzanti, 1985), has been proposed for Carnian sandstones in the western part of the Southern Alps.

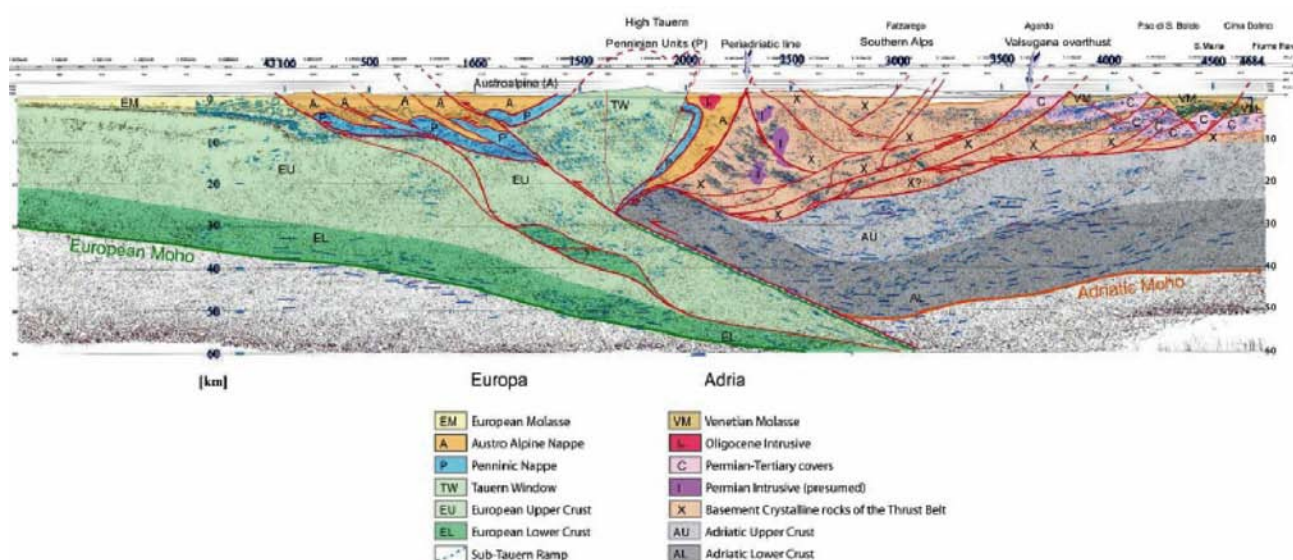


Fig. 231 - Interpretation of the TRANSALP profile after CASTELLARIN *et alii* (2006).

There are still doubts about the origin of the middle Triassic deformation and volcanism in the Dolomites. The models of an aborted rifting and the alternative interpretation of an ensialic subduction zone have been debated for long time.

Bob Goldhammer analyzed with incredible accuracy all the cycles of the Latemar carbonate platform, proposing an outstanding theory regarding their relationship with astronomical tuning (GOLDHAMMER *et alii*, 1990). Their interpretation has been debated in a number of articles where the interior of the platform was dated in detail, indicating a too fast cyclicity for being astronomically correlated (KENT *et alii*, 2004).

The origin of the Middle Triassic tectonics and related subsidence in the Dolomites, coeval to the growth of the Ladinian carbonate plat-

forms, has been interpreted in a number of ways, either as an aborted rift (e.g., BECHSTADT *et alii*, 1977), or as an ensialic subduction zone (CASTELLARIN *et alii*, 1979).

Whatever the origin of the Ladinian cycles is, in the Latemar massif they recorded a fast subsidence rate that can be estimated up to 600 m/Myr. This rate can be even higher in the eastern Dolomites, which subsided almost twice faster with respect to the western side from the Late Permian throughout the entire Mesozoic (e.g., BOSELLINI & DOGLIONI, 1986). Passive continental margin rates are generally much slower (even <50 m/Myr). The only extensional geodynamic setting where a subsidence rate similar to those recorded in the Latemar has been inferred is the backarc basin related to W-directed subduction zones (DOGLIONI, 1995).

W-directed subduction zones appear to nucleate along the retrobelt of pre-existing orogens related to E- to NE-directed subduction zones (DOGLIONI *et alii*, 1999). Examples are the Barbados subduction zone that developed along the retrobelt of the Central America cordillera, related to an E-directed subduction, and the Apennines, which started along the retrobelt of the south-westward prolongation of the Alps. East of the Dolomites there was the buried termination of the Hercynian retrobelt (e.g., Carnia, Friuli). Similarly to the quo-

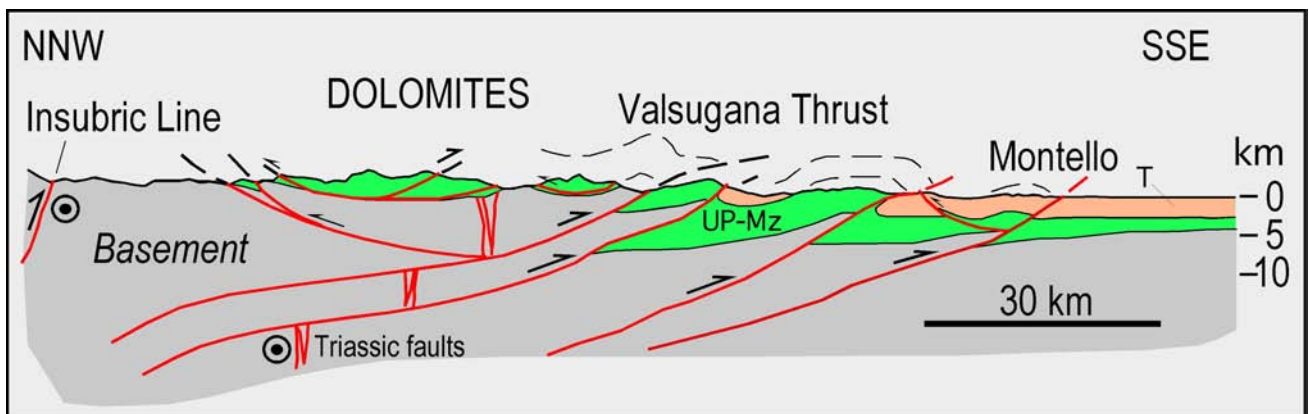
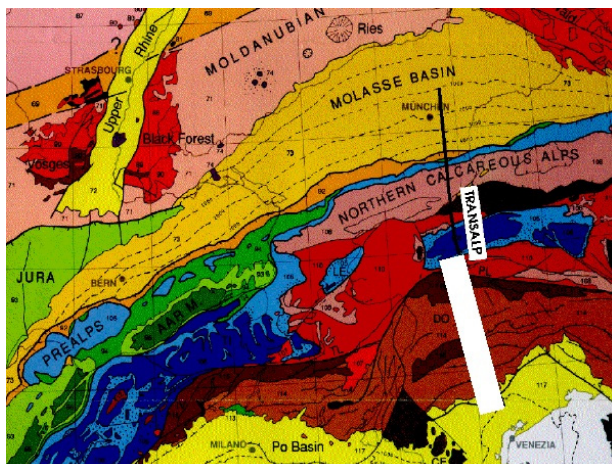


Fig. 232 - Cross-section of the Southern Alps along the southern segment of the Transalp (white thick line in upper map), modified after DOGLIONI, 1987. Map after Transalp Working Group. UP-Mz, Upper Permian-Mesozoic; T, Tertiary.

ted examples, if an oceanic or thinned continental lithosphere was occurring in the foreland of the Hercynian retrobelt during Late Permian or Early Triassic, a W-directed subduction zone could have taken place, retreating toward Slovenia, Hungary, being the relict of this hypothetical system now below the Pannonian basin. Therefore the Middle Triassic subsidence in the Dolomites is more compatible with a backarc setting of a W-directed subduction, and with the shoshonitic signature of the magmatic event that has been interpreted as subduction-related (PISA *et alii*, 1979).

Past plate motions in the Atlantic-Mediterranean-European realm have been reconstructed by a number of Authors (e.g., ZIEGLER, 1992; DERCOURT *et alii*, 2000). Since Paleozoic times, in the Atlantic area, E-W extension dominated, continuing with the Jurassic to Present oceanic spreading. To the east, the Cimmerian subductions system was NNE-directed. These reconstructions indicate an undulation in plate motions from E-W to

NNE in the past, which persisted during the Cenozoic and is still active today. This basic and simple observation would support the presence of a tectonic mainstream of plate motions (DOGLIONI, 1993; CRESPI *et alii*, 2007) active both in the geologic past and today. The tectonic mainstream has a sort of tectonic "equator" that is at about 25° with respect to the geographic equator, pointing for a rotational component of plate tectonics, tied to the tidal effects (SCOPPOLA *et alii*, 2006). If this is true, plate motions are constrained by Earth's rotation now and in the past.

The Venetian part of the Southern Alps (N-Italy) is a Neogene south-vergent thrust belt located to the south of the Dolomites. The minimum shortening of the chain is 30 km. Most of the thrusts trend N60°-80°E and show an inherited N10°W-N10°E normal faults pattern of the Mesozoic continental margin. These earlier features strongly conditioned the evolution of the following oblique thrust belt. Structural undulations along strike of folds and thrusts occur in correspondence



Fig. 233 - View of the southwestern Dolomites from the Sella Massif. The whole view is the southern limb of the Dolomites synclinoorium, being the Lagorai monocline related to the ramp of the Valsugana thrust.

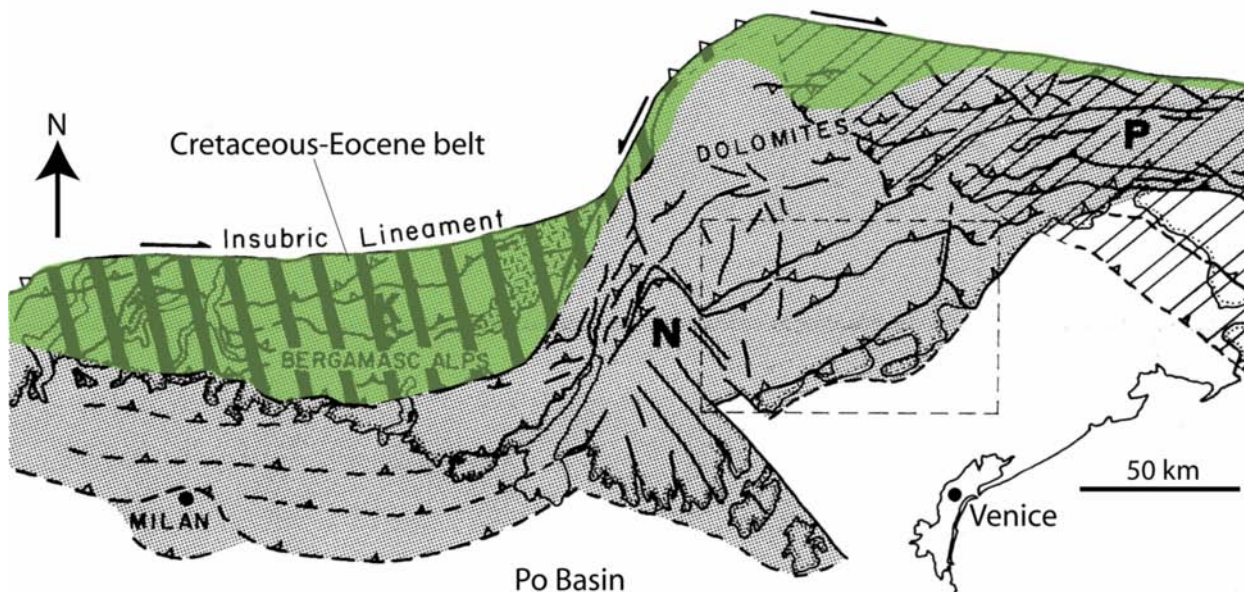


Fig. 234 - The Southern Alps underwent compressions at different times and in different areas. K: area of Late Cretaceous-Paleogene compression (green); P: Paleogene-Early Neogene compression (Dinarides); N: Paleogene-Neogene compression (Southern Alps). The rectangle indicates the area of the next figure which has been deformed only by the SSE-vergent Neogene Southalpine thrust belt and was located in the foreland of the Paleogene WSW-vergent Dinaric thrust belt. Note in the eastern side the overlap between Southern Alps and Dinarides.

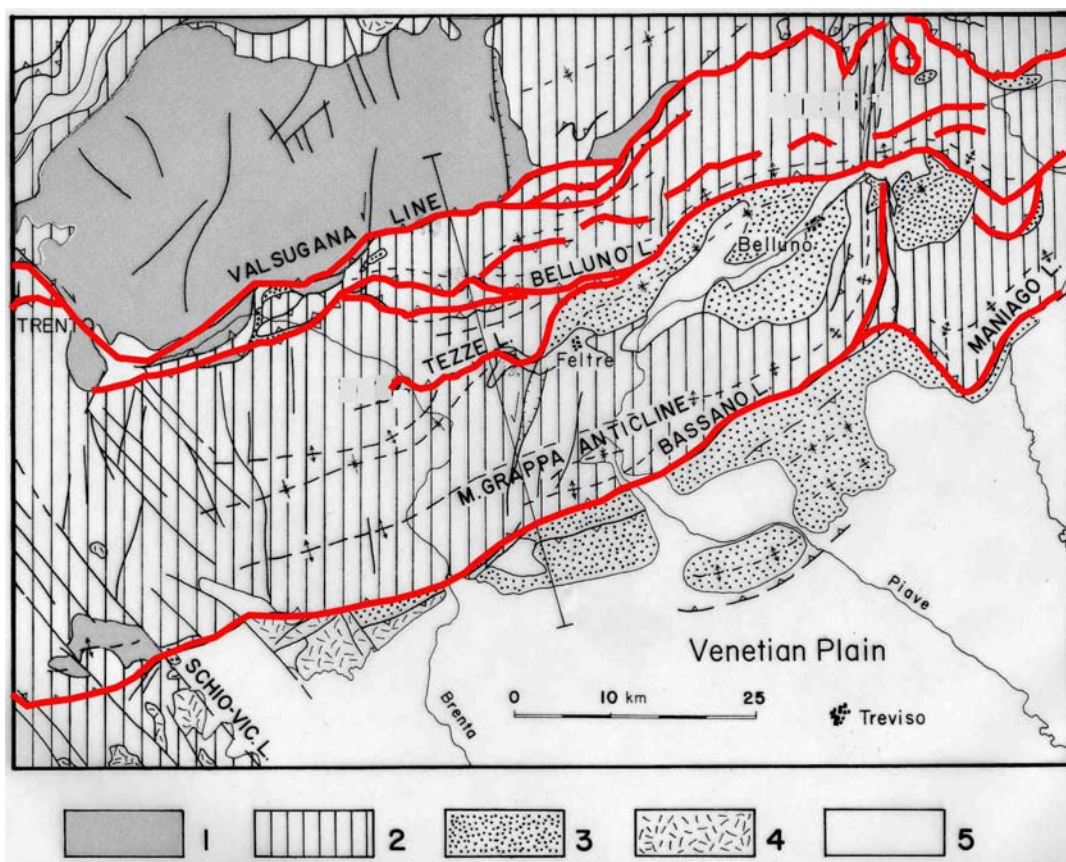


Fig. 235 - Simplified tectonic map of the Venetian Alps and location of the next section. 1) Hercynian crystalline basement and Permian ignimbrites; 2) Late Permian and Mesozoic sedimentary cover; 3) Tertiary sediments, Flysch and Molasse; 4) Triassic and Tertiary volcanics; 5) Quaternary. Red lines, thrusts.

to Mesozoic faults, thickness and facies variations. The thrusts are arranged in an imbricate fan geometry. A frontal triangle zone laterally ends at transfer faults. Earlier stages of the thrust belt were characterized by frontal triangle zones, which have later been involved and cut by the progression of the internal thrusts. The Southern Alps were part of a Mesozoic continental margin, according to stratigraphic analysis, i.e. facies and thicknesses changes (BERNOULLI *et alii* 1979; WINTERER & BOSELLINI 1981). The area can be divided into three main structural sectors during Mesozoic. These are, from west to east: the Trento Platform, the Belluno Basin and the Friuli Platform. True Mesozoic normal faults (i.e. Liassic) have been documented at the western border of the Trento Platform (CASTELLARIN 1972; DOGLIONI & BOSELLINI 1987) and proposed also at the eastern margin (WINTERER & BOSELLINI 1981; BOSELLINI *et alii* 1981; BOSELLINI & DOGLIONI 1986; MASETTI & BIANCHIN 1987, DOGLIONI & NERI 1988).

The Mesozoic normal faults trend mainly N10°W-N10°E. We can argue that the Trento Platform, the Belluno Basin and the Friuli

Platform were bounded by crustal normal faults, mainly N-S trending, acting at different times and with different displacements during Jurassic time and during at least the Early Cretaceous. The main Mesozoic tectonic features bordering the Belluno Basin are from west to east: the eastern margin of the Asiago Plateau, the Seren (Graben) Valley, the Cison Valley alignment (clearly seen on satellite images), the Passo Rolle Line, the S. Gregorio alignment, and to the east the Col delle Tosatte - Fadalto alignment. The Mesozoic alignments probably used inherited Variscan discontinuities as well. Platform and basinal Mesozoic facies do not coincide everywhere with the old horst and graben structure, i.e. the drowned Trento Platform, which acts as a horst with reduced basinal sequences after the Middle Jurassic until the Late Cretaceous. The geometry of the thrust belt is that of an imbricate fan with a main envelop angle produced by the thrust slices close to 7° (critical taper of wedge). The main thrusts are from the internal parts to the foreland, the Valsugana Line, the Belluno Line, the Moline Line, the Tezze Line, and the Bassano Line. The thrust

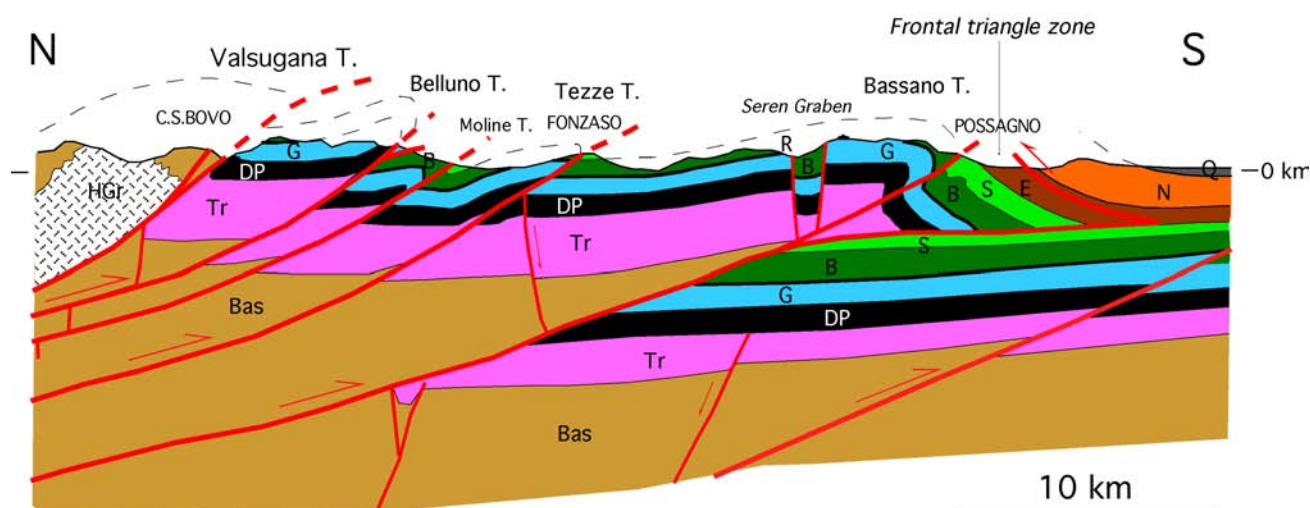


Fig. 236 - Balanced cross-section across the Venetian Alps. See Fig. 235 for location. Horizontal scale = vertical scale. Legend: Bas, crystalline basement; HGr, Late Hercynian granite; Tr, Late Permian-Lower and Middle Triassic formations; DP, Late Triassic (Dolomia Principale); G, Liassic platform facies (Calcari Grigi) gradually passing southward to Liassic-Dogger basinal facies in the Venetian Plain (Soverzene Formation, Igne Formation, Vajont Limestone); R, Dogger-Malm basinal facies (Lower and Upper Rosso Ammonitico, Fonzaso Formation; thin black layer) B, Early Cretaceous (Biancone); S, Late Cretaceous (Scaglia Rossa); E, Paleogene (Possagno Marls, etc.); N, Late Oligocene-Neogene Molasse; Q, Quaternary.

belt is not cylindrical in shape and the strain continuously changes along strike. In a map view of the area, the thrusts show an anastomosing pattern along strike, maintaining constant shortening which can conservatively be calculated as 30 km.

The structural evolution of the thrust belt shows a general rejuvenation from the internal thrust to the external ones. However the internal thrust sheets seem to have been reactivated also in recent times (SLEJKO *et alii* 1987). The crystalline basement outcrops in the hangingwall to the Valsugana thrust, and is composed of Variscan metamorphosed greenschist facies rocks intruded by Late Carboniferous granitic bodies. Basement depth in the Venetian Plain is inferred by magnetic data (CASSANO *et alii* 1986) and by the assumption of the general hinterland dipping monocline typical of thrust belts. This is consistent with the southward rising of the basement discovered in the Assunta Well at 4747 m where Late Triassic dolomites onlap a Late Ordovician granite (PIERI & GROPPi 1981). The basement is clear-

ly involved in the Valsugana Line, but balanced cross-sections would indicate a wider involvement by southern thrusts as well. We cannot exclude significant thickness variations of the sedimentary cover and minor dips of the thrusts which would considerably increase the amount of shortening along the thrust belt (ROEDER 1989). The main decollement of the thrust belt appears to be located in the basement (15-20 km in depth) beneath the Dolomites as suggested by the construction of balanced cross-sections (DOGLIONI 1987) and by focal mechanisms of earthquakes indicating low angle thrust planes (i.e. the Siusi event, SLEJKO *et alii* 1987). Triangle zones are present along the Valsugana thrust where the basement is sometimes wedged within the sedimentary cover, or it produces a triangle in the Valsugana Valley where the Valsugana thrust faces a north-vergent basement involving backthrust, to the north of the Asiago Plateau. Major undulations along the Valsugana thrust occur again in correspondence of inherited features, i.e. the sinistral N0°-10°E striking transpressive undulation of Borgo Valsugana which occurs in correspondence of an inherited structural high as supported by the reduced thickness of the sedimentary cover. The thrust is generally in ramp and abandoning earlier staircase trajectories in the sedimentary cover probably due to the poor possibility to fold by flexural slip.

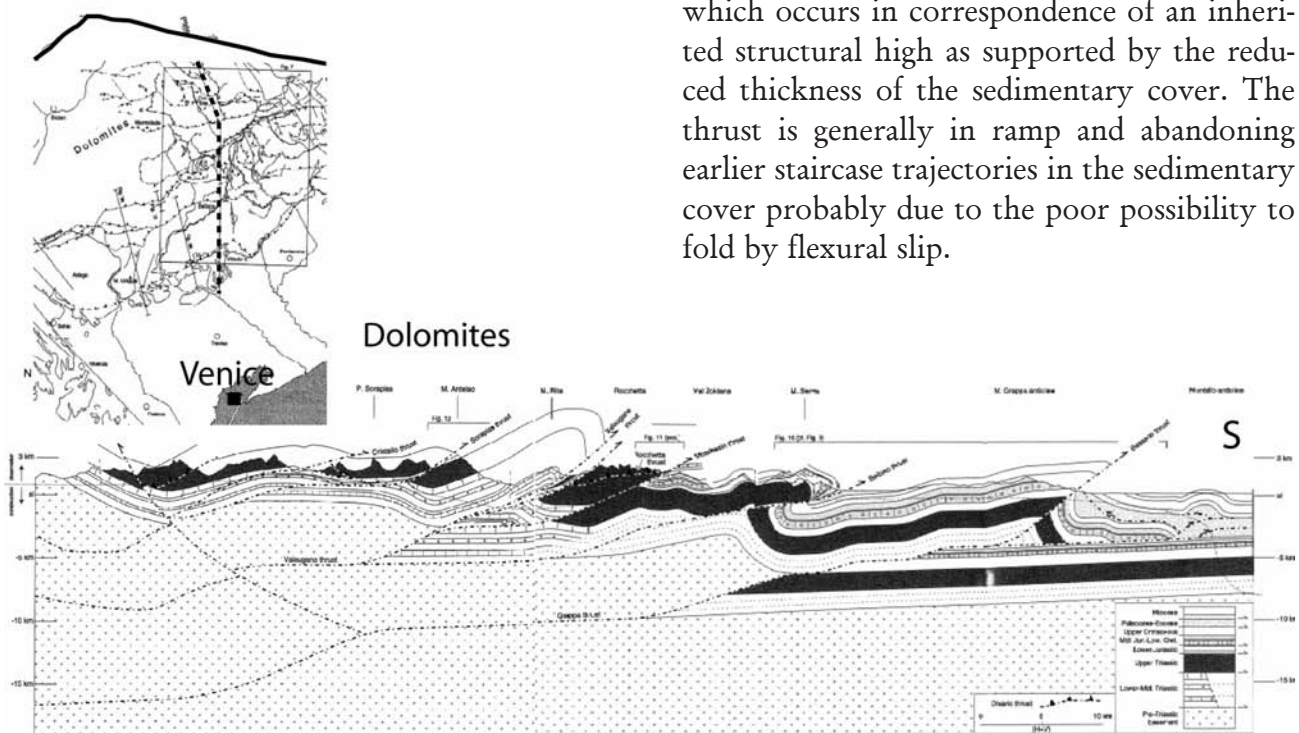


Fig. 237 - Cross-section of the Dolomites and eastern Venetian Prealps (after SCHÖNBORN, 1999).

Within the sedimentary cover the thrusts are characterized by cut-off angles ranging between 5° and 45° . Preferential decollement layers are the Tertiary Possagno Marls, the Late Cretaceous Scaglia Rossa, and other buried levels within the Late Permian and Triassic sequences. The thrust planes assume steeper angles when a footwall syncline is present. Footwall synclines are well developed in Cretaceous pelagic thin bedded rocks (Biancone and Scaglia Rossa) whose folding is accommodated by intense flexural slip. Chevron folds are particularly common in these two formations and their amplitude and wavelength decrease away from the thrust planes.

The frontal part of the thrust belt is characterized by a triangle zone (fig. 238) which generates a general southward dipping mono-

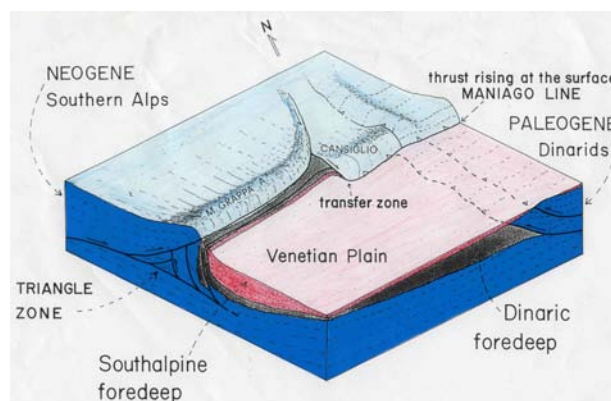


Fig. 238 - Schematic picture of the Venetian Alps front. The foothills are characterized by a triangle zone. The deep thrust plane (Bassano Line) reaches the surface (Maniago Line) through a transfer zone (Caneva Line). The Venetian Plain represents the foredeep of two opposite thrust belts. The geometry of the foreland basin changes from the triangle zone to the normal thrust to the east. In the first case the clastic sediments are pushed southwards, tilted and eroded. In the second case they are simply thrust.

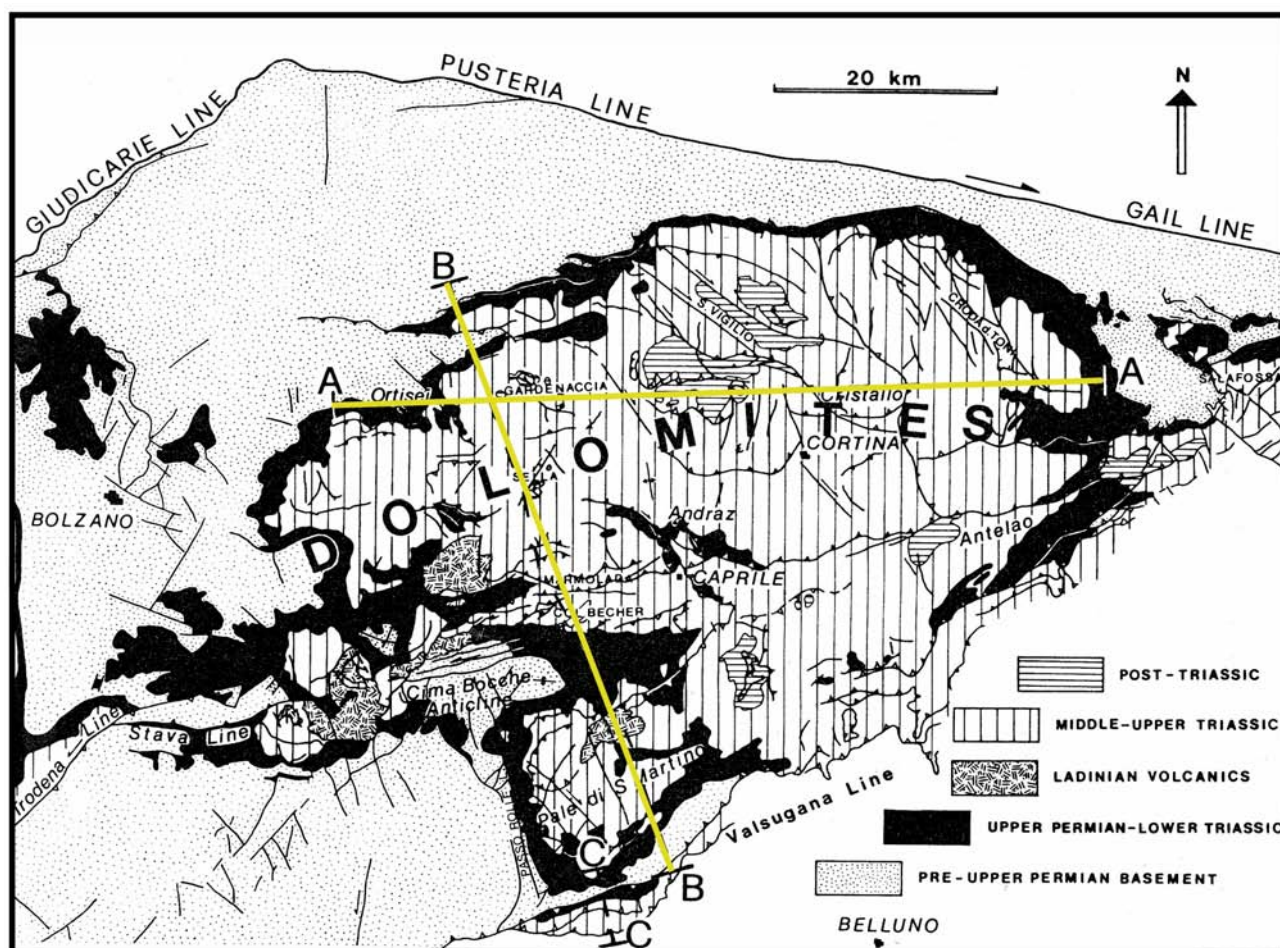


Fig. 239 - Simplified tectonic map of the Dolomites.

cline characteristic of the Venetian foothills between Bassano and Vittorio Veneto. The frontal triangle zone is the most peculiar structure of the foreland and its presence is indicated by: 1) the general absence of an important thrust at the base of the mountains (Monte Grappa - Visentin Anticline); 2) the necessity of a thrust at the base of the anticline to resolve the volume problem of the structural high; 3) the south-dipping monocline in the frontal part of the chain which is typical for the triangle zones (i.e. BALLY *et alii* 1966; JONES 1982; BOYER & ELLIOTT 1982); 4) the presence of north-vergent backthrusts (i.e. in the Possagno and Follina areas, BRAGA 1970; ZANFERRARI *et alii* 1982).

It is interesting to note that a similar triangle zone has been reported for the northern part of the Alps in the Bavarian foreland (MÜLLER *et alii* 1988). The triangle zone between Bassano (Schio?) and Vittorio Veneto seems to be connected with a ramp-flat geometry of the deep seated blind thrust which generated a thrust-

propagation fold (the Monte Grappa - Visentin Anticline). This was active at least during Late Miocene times because Tortonian and Messinian sediments onlap with a gradually smaller inclination the southern limb of the anticline (MASSARI *et alii* 1986). Sequence boundaries in the southern fold limb are marked by angular unconformities with decreasing angles toward the foredeep suggesting the coeval activity of the frontal fold (Monte Grappa - Visentin Anticline). It is clear that the unconformities are angular only along dip where the frontal fold is perpendicular to the assumed regional maximum Neogene stress (sigma 1: N20°-30°W) and the fold axis presents a "cylindric" trend. Where there are structural undulations in the fold axis (i. e. the sinistral transpressive zones of Valdobbiadene-Cornuda and the greater Fadalto alignment) the unconformities are marked by angular relationships along both dip and strike. In summary, structures control the nature of the unconformities. A growth fold, with constant

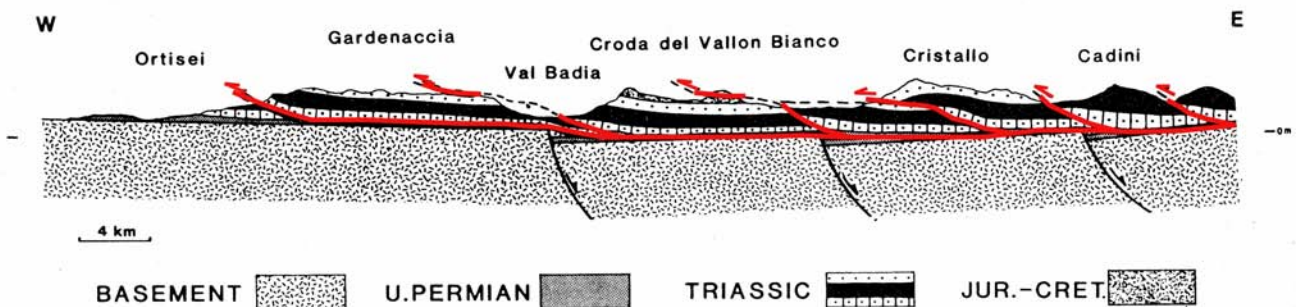


Fig. 240 - E-W cross-section of the Dolomites, showing WSW-vergence of thrusting. Location in figure 239.

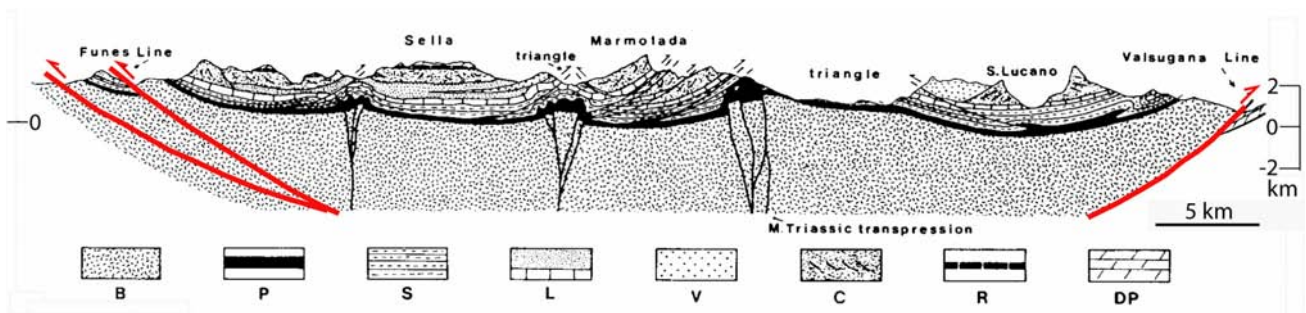


Fig. 241 - NNW-SSE cross-section of the Dolomites, showing the wide basement syncline generated by the pop-up. Location in fig- 239.

horizontal axis, generated by pure compression produces angular unconformities only along dip, while a growth fold generated by transpression produces angular unconformities both along dip and strike.

To the north, the Belluno Line may have been a blind thrust generating a triangle zone during earlier stages of the deformation, later rising at the surface in the northern limb of the Belluno Syncline. This is supported by the steep attitude of the northern limb of the Belluno Syncline which is difficult to explain geometrically as a simple footwall syncline. We also note that triangle zones mainly occur in the Mesozoic Belluno Basin, rather than in the neighboring platforms. In fact the Belluno Syncline is developed in the deepest structural zone with thick basinal lithofacies. This earlier structural situation had an important influence in the morphology and source areas of the hydrographic pattern during the Late Miocene.

In the Venetian segment of the Alps the thrusts became active during Late Oligocene to Quaternary times. Tortonian sandstones

are thrust by the Valsugana Line (VENZO 1939) and Pliocene shales are folded along the frontal triangle zone. Moreover Messinian-Pliocene onlap geometries in the southern border of the chain support a mainly Neogene age of the deformation. The extension of the unconformities within the molasse is a function of the thrust belt structure and reflects areas of stronger uplift. A problem is represented by the style and timing of the orogenic evolution: has the chain southward regularly risen in a continuum creep since Late Oligocene time and do the unconformities record moments of sea level fall (low stand)? Or was the chain generated step by step so that the unconformities simply mark moments of tectonic crisis? In general, plates move with a regular velocity suggesting that in areas of deformation the tectonic evolution should follow an almost constant activity. If the tectonic evolution generated with a constant regularity and tectonic crisis had a wavelength too short or too long with respect to the eustatic sea level changes, then an interesting problem appears in dating the thrust belt: the timing of



Fig. 242 - Croda del Vallon Bianco, northwest of Cortina. The thrust is WSW-verging and mainly Jurassic Calcarei Grigi outcrop both in the hangingwall and in the footwall. The geometry of the hangingwall cut-off allows to reconstruct the undulated geometry of the fault plane.

the tectonic crisis has been considered as the time missing at regional unconformities and the age of coarse-grained sediment supply (i.e. the Messinian Conglomerate) onlapping the discontinuity. But if the unconformities recorded only moments of general lowstand (in this case global or confined to the salinity crisis in the Mediterranean area) then we could argue that the chain developed more gradually and that the sea level oscillations orchestrated the arrangement of the syntectonic sedimentary sequences. The different interpretations of the unconformities and conglomeratic supply in the molassic sequences allow different tectonic reconstructions. With the sea level change interpretation (VAIL *et alii* 1977) the chain rises constantly during Late Oligocene-Neogene times, but if we assume the unconformities and conglomeratic supply to be tectonic-rela-

ted, then episodic tectonic activity existed, which is in contrast to the regular activity of the frontal growth fold and the general plate motion.

In the Belluno syncline an angular unconformity marks the Early Eocene Flysch - Late Oligocene Molasse contact. Moreover the Flysch seems to onlap the northern limb of the Belluno syncline and to the west the Seren Valley alignment. Consequently we cannot exclude that the area underwent compressive tectonics already during Paleogene times.

The basement and the sedimentary cover of the region were broken by N-S trending normal faults and N60°-90°E transfer faults (the paleo-Valsugana Line ?) during the Late Permian-Mesozoic rifting phases. These features have been cut, reused or deformed during the alpine inversion. Local structural undula-

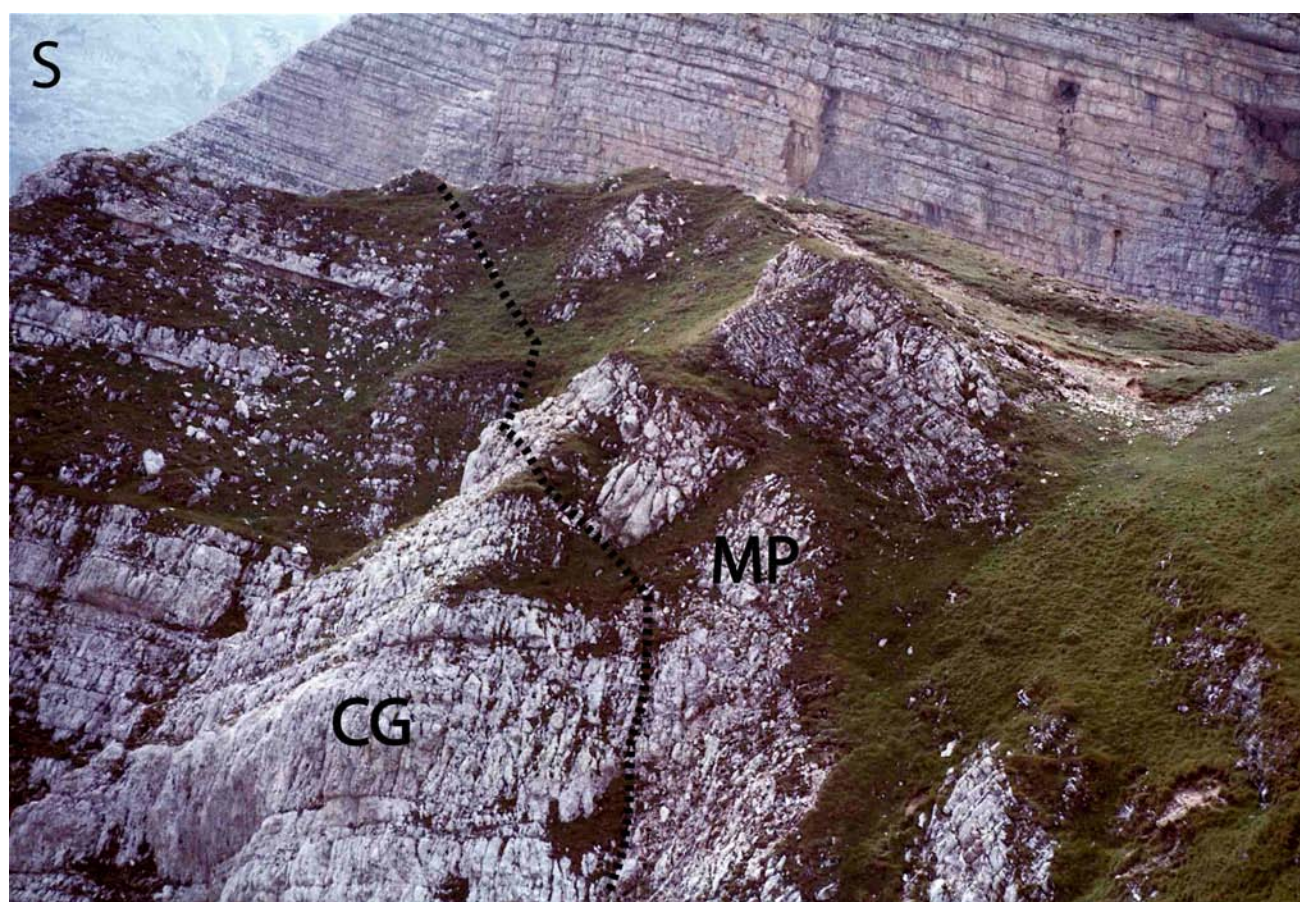


Fig. 243 - Upper Oligocene-Lower Miocene conglomerate (MP) at Mt. Parei - Col Bechei, to the northwest of Cortina, sealing an angular unconformity with the underlying Liassic Calcarei Grigi (CG) deformed by WSW-verging thrust and folds. This outcrop dates active pre-Late Oligocene WSW-verging shortening in the Dolomites.

tions in the general N60°-80°E trend of the chain (fold axis, direction of thrust planes, etc.) everywhere occur in correspondance to inherited features in the basement and in the Mesozoic sedimentary cover which is arranged in approximately N-S trending basins and

swells. The present tectonic configuration is due to the inherited Mesozoic background. The structural evolution of the area followed boundary features as transfer zones at horst margins (i.e. at the Trento Platform and Friuli Platform margins) which have influenced the

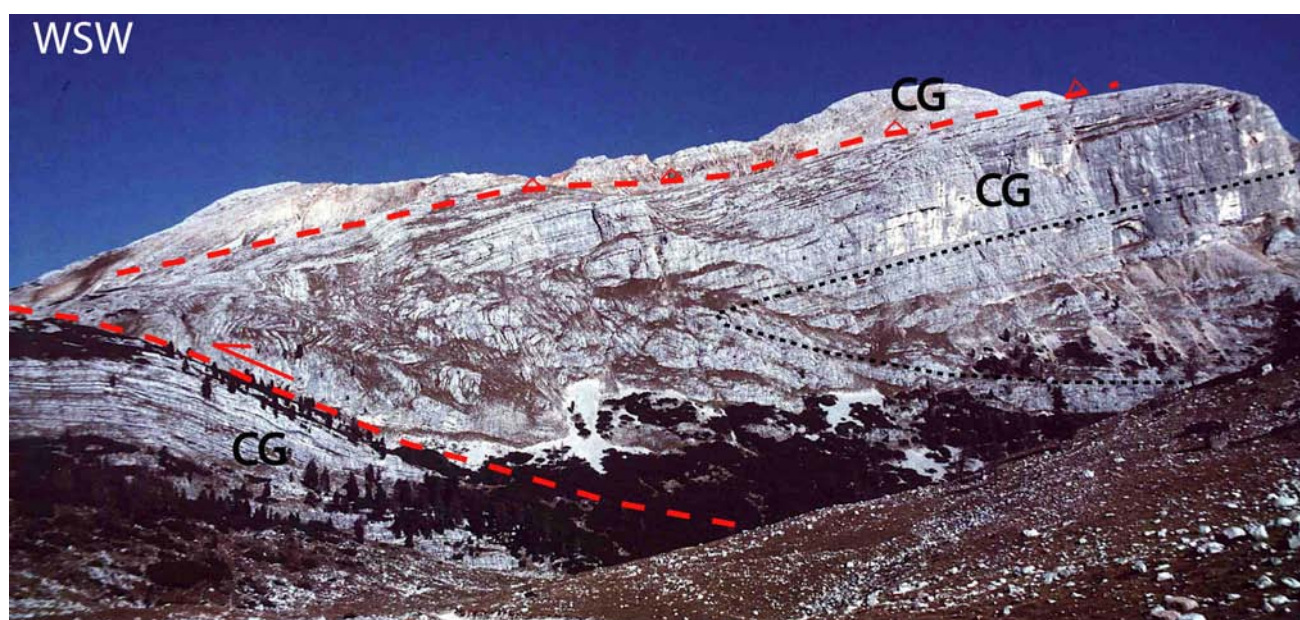


Fig. 244 - Col Bechei western side. The overturned fold in the hangingwall of a WSW-verging thrust, has been later cross-cut by a S-verging thrust. See following figure. CG, Liassic Calcarei Grigi.

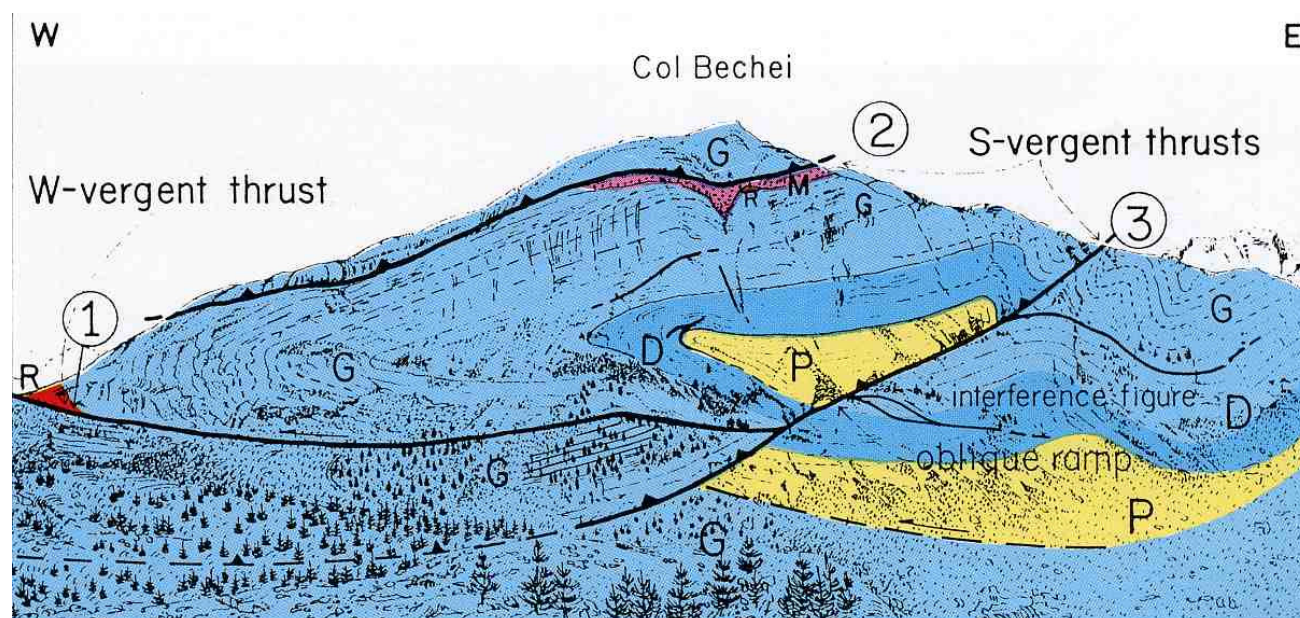


Fig. 245 - The Col Bechei structure, northwestward of Cortina. The WSW-verging thrust (1) is sealed by the Upper Oligocene Mt. Parei conglomerate. The thrust and the related fault-propagation recumbent fold are cross-cut by the later S-verging alpine thrusts (2, and 3). Numbers refer to the kinematic sequence. The two almost orthogonal compressive phases generated an interference structure. P, Dolomia Principale (Norian); D, Dachstein Limestone (Rhaetian); G, Calcarei Grigi (Liassic); R, Ammonitico Rosso (Dogger-Malm); M, Mt. Parei Conglomerate (Oligocene-Miocene). After DOGLIONI & SIORPAES (1990).

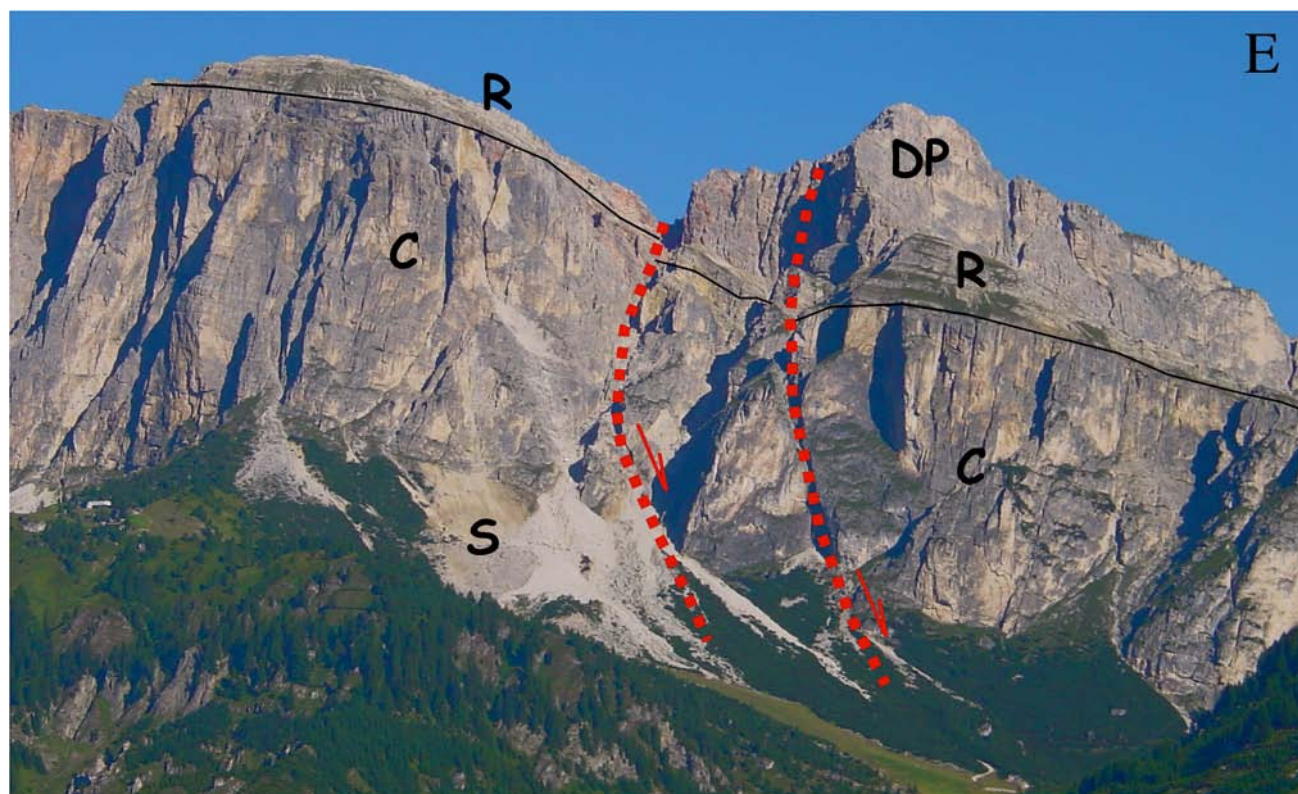


Fig. 246 - Southern view of the Puez-Gardenaccia Massif, showing N-S trending listric normal faults, above Colfosco, in Val Badia. The faults dip to the east and cut the succession up to the Dolomia Principale. They are somewhere accompanied by reddish oxidations and by sedimentary dykes. The grass ledge corresponds to peritidal deposits of the Dürrenstein or Raibl Fm. Legend, DP, Norian Dolomia Principale; R, Upper Carnian Raibl Fm; C, Lower Carnian Cassian Dolomite; S, San Cassiano Fm. Compare with the section of fig. 251 where the above shown tensional structures are represented below Gardenaccia.

geomorphologic evolution of the area. The Asiago pop-up (BARBIERI 1987) constitutes the western part of the study area, and is a wide plateau formed on the inherited Trento Platform (horst). The deformation at the western end of the Valsugana Line is transferred in the Trento area through the dextral transpressive Calisio Line to the sinistral transpressive Giudicarie Belt to the west. This undulation once again runs around a minor inherited Late Paleozoic and Mesozoic horst, within the wider Trento Platform. On the basis of thickness and facies changes the amplitude of the Trento Platform was probably wider in the east during Jurassic times (Seren Valley) and probably retreated (as horst, with basinal facies) by about 10 km during Cretaceous times (eastern margin of the Asiago Plateau, Valsugana Valley). The Tezze Line develops at this final eastern margin of

the Trento horst and undulates in oblique and lateral ramp (sinistral transpression) at the intersection with the inherited Seren Valley alignment. The Alpine deformation within the Belluno Basin is more diffuse, characterized by a larger number of thrust planes and reduced wavelength folds with respect to the lateral platform areas. The Belluno Line mainly develops to the east of the Trento Platform. It branches the Valsugana thrust and shows an eastward increase in displacement and amplitude of the fault-propagation folding and fault-bend folding in the hangingwall. Commonly, the inherited tensional Mesozoic areas have been reactivated in transpressive zones and are transfer zones between two different styles of deformation. For instance the N-vergent back-thrust in the hangingwall of the Belluno Line ends at the western margin of the Vette Feltrine at the intersection with the inherited

tensional zone of the Cismon Valley. The Caneva Line and the Fadalto Line are dextral and sinistral transpressive zones respectively at the eastern margin of the Belluno Basin. The Caneva Line represents the eastern transfer fault of the frontal triangle zone. The Fadalto transpression was emplaced at the western termination of the Friuli Platform. The study area was located in the foredeep of the Dinaric thrust belt during Paleogene times and suffered subsidence due to the load of the WSW-vergent Dinaric thrust sheets. A regional ENE-dipping monocline developed at that time and was inherited and involved in the younger SSE-vergent Neogene Southalpine deformation. The variations along strike of the deformation are reflected also in the Neogene and Quaternary foreland basin. The good outcrops and the clear interference between inherited features and Alpine tectonics make the Venetian Alps a classic example of

thrust belt. Earlier Mesozoic features strongly influenced the evolution of the chain. Any kind of structural undulation along strike of the thrust belt is associated with pre-existing synsedimentary faults, thickness and/or facies variations in the sedimentary cover. The thrusts are arranged in an imbricate fan geometry and show a frontal triangle zone which was probably present at earlier stages of the thrust belt in more internal zones. The variations along strike of the deformation are reflected also in the Neogene and Quaternary molasse. The frontal triangle zone appears to be a growth fold rising from Late Oligocene to Quaternary times because clastic sedimentation on the southern limb of the anticline shows onlap geometries and reduced thicknesses. According to this progressive evolution of the thrust belt, the unconformities within the molasse could record low-stands of eustatic cycles. The effects of four independent Neogene to

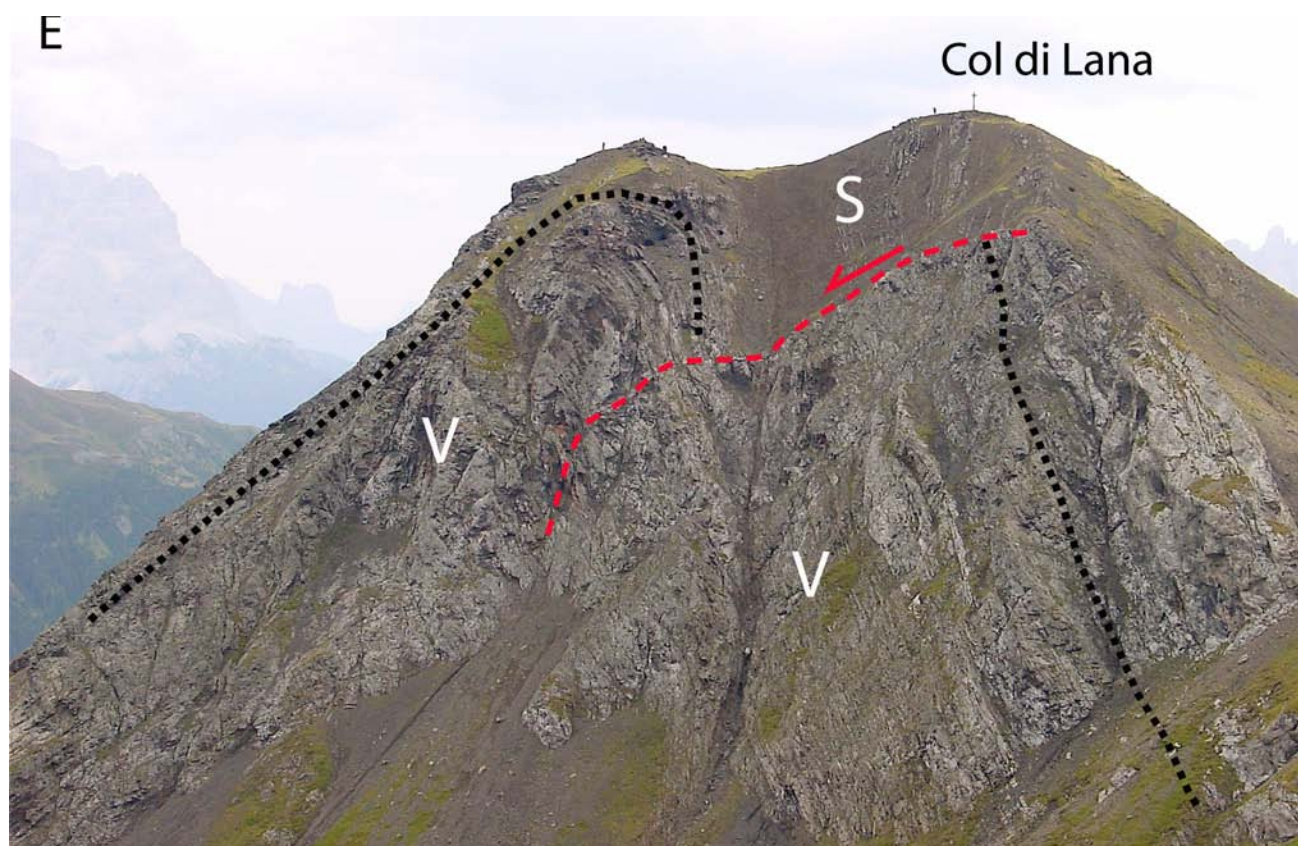


Fig. 247 - Example of a W-verging anticline inheriting a normal fault of Mesozoic(?) age at the top of the Col di Lana, central Dolomites. V, Upper Ladinian volcaniclastic sandstone; S, Lower Carnian San Cassiano Fm.

present subduction zones coexist in northeast Italy:

- 1) The dominant one is the Alpine subduction, where Europe subducted the Adriatic plate, and the Southern Alps are its related retrobelt.
- 2) The Alpine belt overlapped/interfered with the frontal thrust belt of the Dinarides, where the Adriatic plate rather subducted the Eurasia plate.
- 3) Moving eastward, normal faults of the Pannonian backarc basin of the Carpathians subduction crosscut the Northern Dinarides

and part of the Eastern Alps.

- 4) The hinge retreat of the Apennines subduction determines subsidence of the entire NE-Italy.

All these indicate that separate geodynamic settings can co-work in a given area, and their related stress fields may interact or overlap simultaneously.

- 1) The Transalp section (TRANSALP, 2002) confirmed the main double vergent structure of the Alps. It shows no N-S extension in the Alps, excluding significant orogenic collapse as

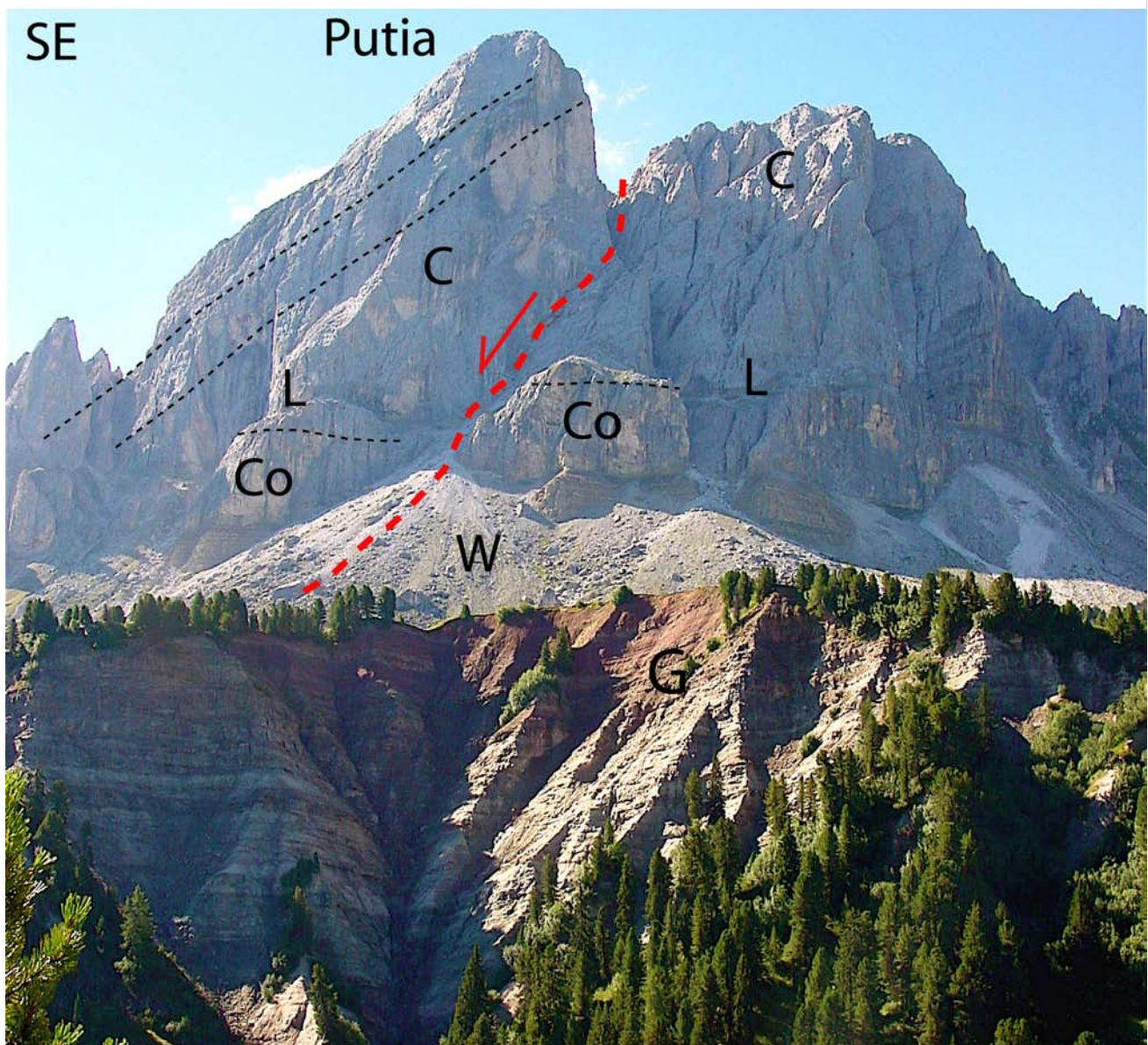


Fig. 248 - Northeastern slope of the Sass de Putia, northern Dolomites. A N-S trending normal fault lowers the eastern side of the massif. C, Marmolada Limestone; L, Livinallongo Fm; Co, Contrin Fm; W, Werfen Fm; G, Gardena Sandstone.

frequently proposed for orogens. The Southern Alps are notoriously bounded to the north by the right-lateral transpressive Insubric Lineament, but they are also considered the part of the orogen where the vergence of the thrusts is toward the subduction hangingwall, i.e., the Adriatic plate. Therefore, according to this second interpretation, the Southern Alps would extend in part also to the north of the Insubric Lineament, since several thrusts and folds present southward vergence. Pre-collision stage subduction zones exhibit well-developed retrobelts, such as the SubAndean belt, or the Rocky Mountains in the Southern and Northern America Cordilleras respectively. These analogues would suggest that the retrobelt in the Alps could have started since the early stages of the subduction.

2) The Dinarides and the Alps merged to generate a single belt in the Eastern Alps, but they remained two separated geodynamic processes, due to two independent subduction zones.

It is important to distinguish their meaning and kinematic overlap of the related thrust sheets. WSW-verging thrusts enter the Dolomites section of the Transalp profile.

3) The Carpathians subduction probably followed the same geodynamic scenario of the Apennines, which started to develop along the retrobelt of the Alps where in the foreland to the east there was oceanic or thinned continental lithosphere, like the W-directed subduction zones of the Barbados and the Sandwich arcs in the Atlantic ocean (DOGLIONI *et alii*, 1999). According to this interpretation, the Carpathians developed along the retrobelt of the northern Dinarides, such as the Balkans in the south, where oceanic or thinned continental lithosphere of the Dacide basin was located to the east of the retrobelt. The consumption of this basin accompanied the E-ward retreat of the subduction to the present position in Vrancea. This implies that in the Pannonian basin there are elements of both Alps and Dinarides stretched and scattered.

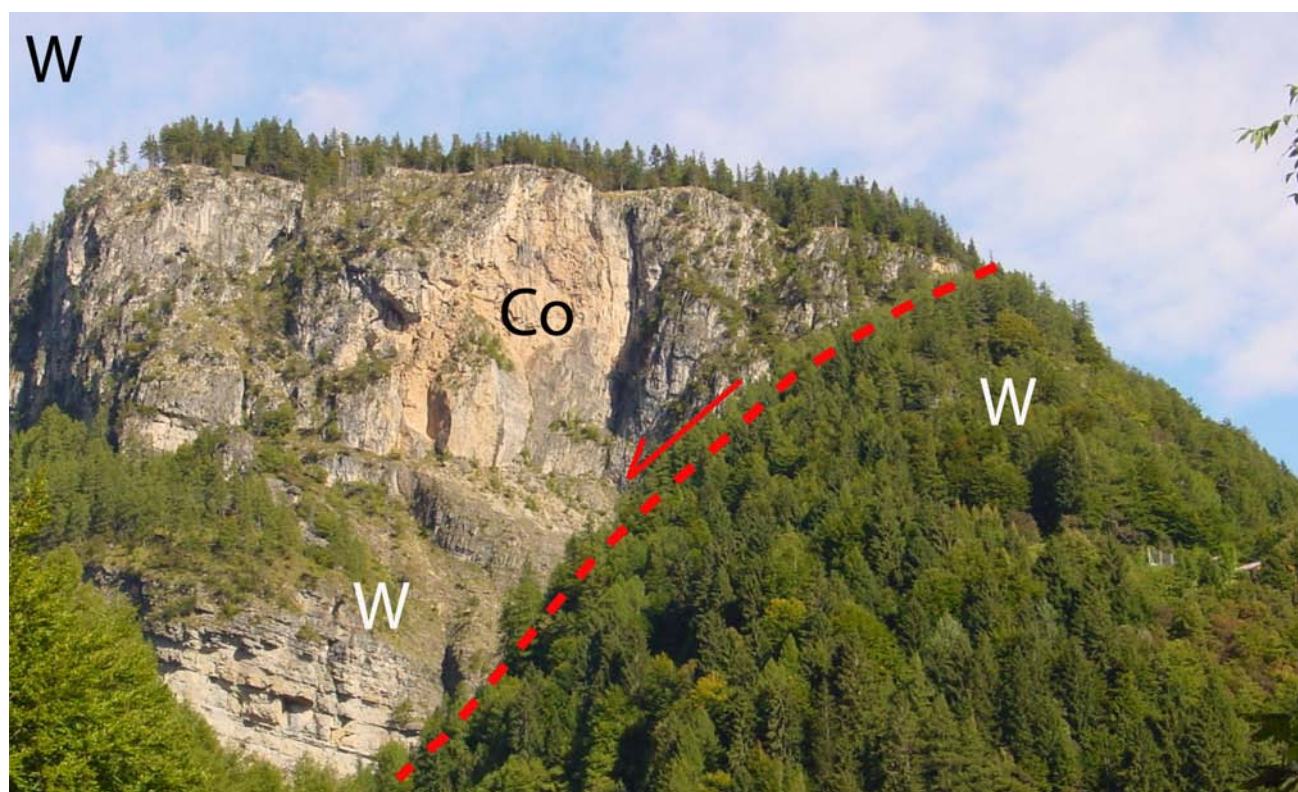


Fig. 249 - N-S trending normal fault likely of Mesozoic age outcropping near Cencenighe. Co, Contrin Fm; W, Werfen Fm.

4) Since the Paleogene, the Venetian and Friuli plains underwent subsidence due to the load of the Alpine and Dinarides thrust sheets, forming two related and anastomosed foredeeps. However, the thinning of the Pliocene-Quaternary sediments (MERLINI *et alii*, 2002), and the decrease of the regional monocline dip moving away from the Apennines front (MARIOTTI & DOGLIONI, 2000), they indicate an active subsidence all around this belt. The Apennines foreland subsidence affected most

of the Alps and external Dinarides. The long-term subsidence of Venice and other coastal cities appears determined by the retreat of the subduction hinge of the Adriatic plate dipping underneath the Apennines. The flexure of the subduction hinge affects areas more than 250 km far to the northeast of the Apennines front, providing data on the viscoelastic behavior of the Adriatic plate continental lithosphere. Slab rollback of such a continental lithosphere can only be ascribed to the

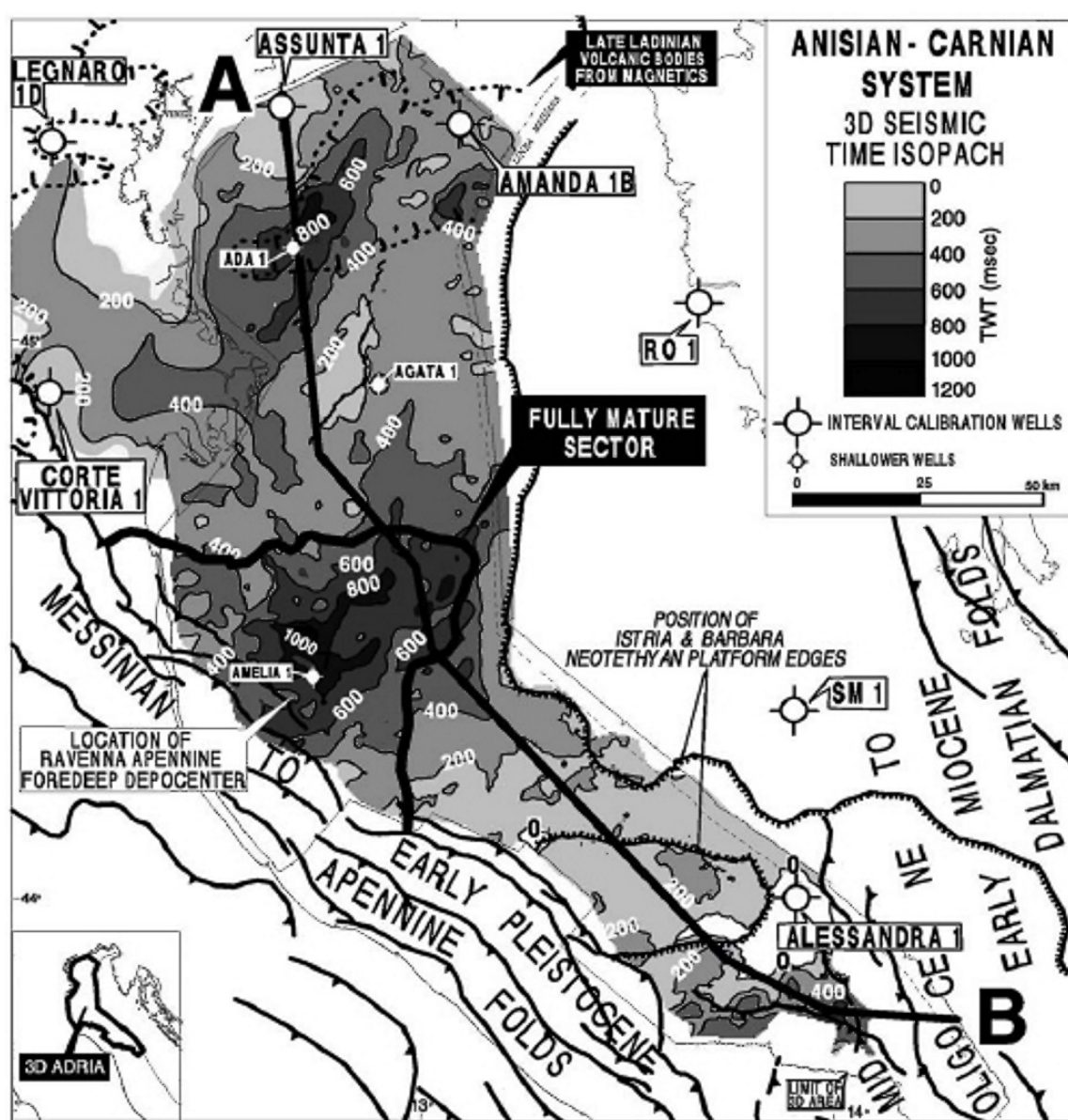


Fig. 250 - Evidences of Middle Triassic rifting in the Adriatic Sea, comparable to what outcropping in the Southern Alps. Front page, compressed random 3D seismic profile crossing the North Adriatic Mid Triassic depocenters and ridges. Above, two-way time isopach of Northadriatic Anisian-Carnian section. The mapped interval extends from the Midtriassic Unconformity to the base of Dolomia Principale, thus including the Late Carnian evaporite seal. After FRANCIOSI & VIGNOLO (2002), EAGE.

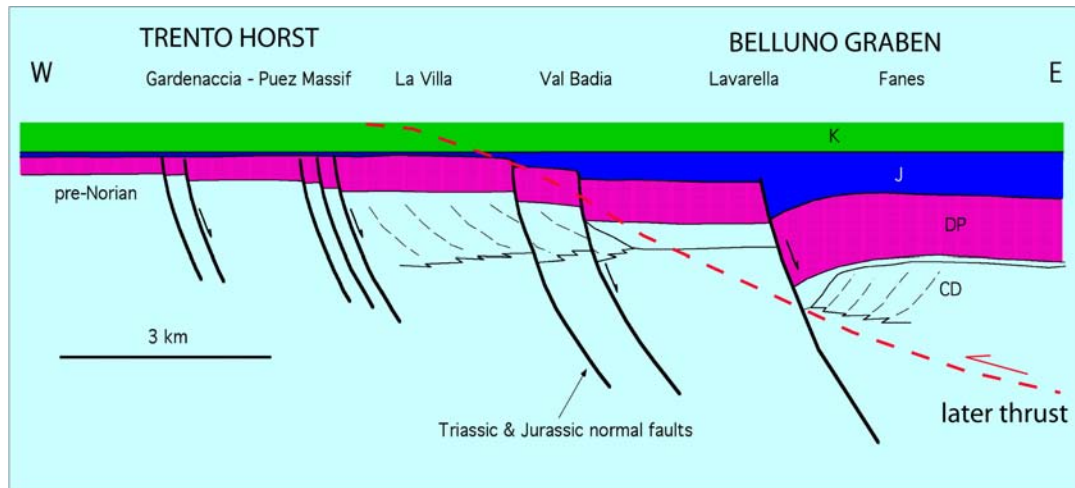


Fig. 251 - Paleotectonic section of the central-northern Dolomites between the Trento Horst to the west, and the Belluno graben to the east. All Mesozoic formations thicken moving eastward, suggesting active normal faulting at the hinge between the structural high and the low throughout the Triassic and Jurassic. Note how the extension and the differential subsidence is distributed in a number of normal faults, each one with relatively small offset. K, Cretaceous; J, Jurassic; DP, Norian Dolomia Principale; CD, Carnian Cassian Dolomite. Notice their regular spacing and the occurrence of the Calcarei Grigi only to the east (to the west the Jurassic J is represented by the Ammonitico Rosso). The extensional fault system seems to have been active also during the Triassic, as suggested by the westward thinning of the Dolomia Principale (P) and of the underlying sedimentary section. Also the Raibl Fm changes its facies and thins toward the west. K, Puez Marls Fm, Cretaceous. The WSW-vergent thrusts developed as ramps along inherited extensional zones, or a platform margin.

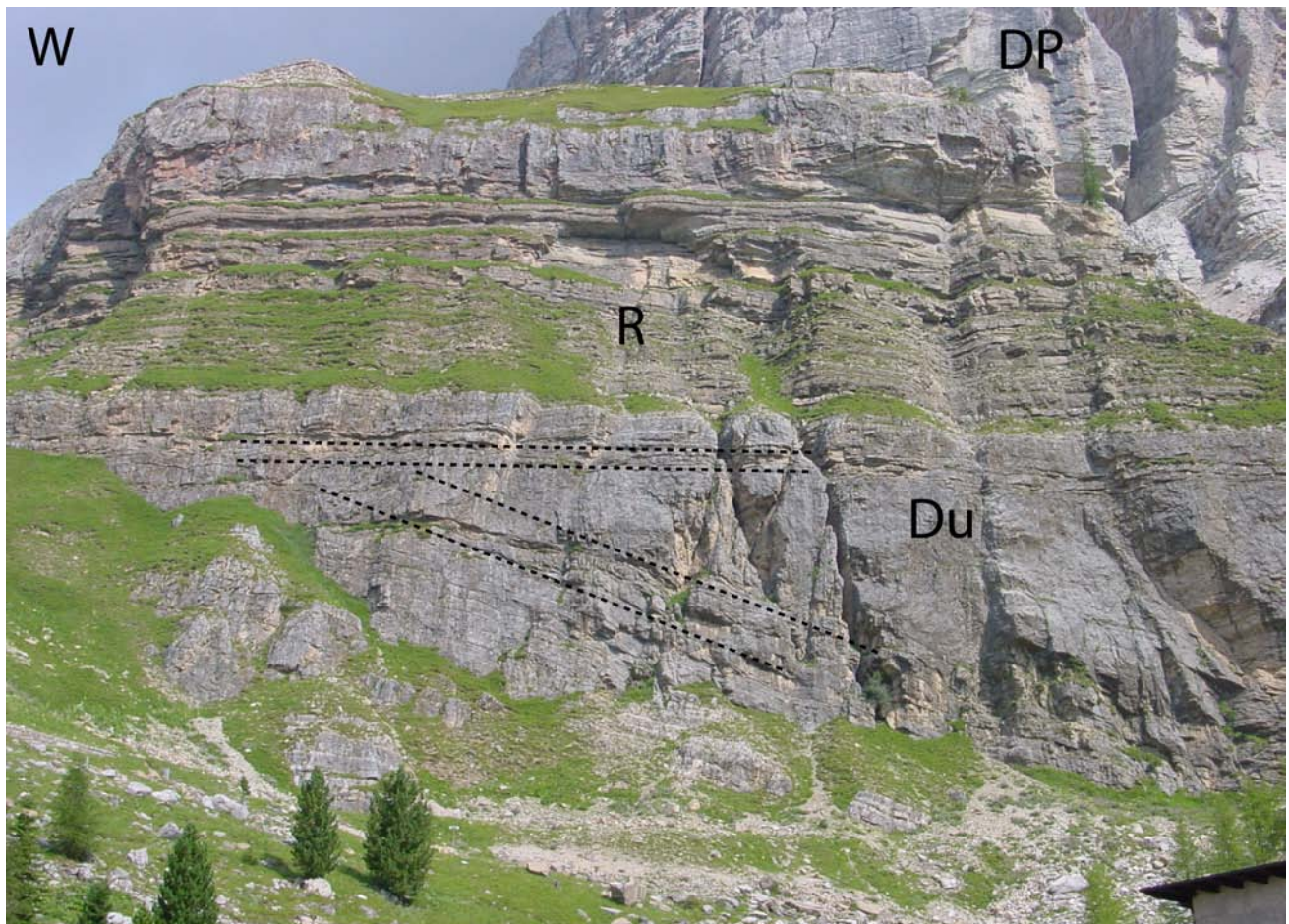


Fig. 252 - Angular unconformity between the Dürrenstein Dolomite (Du) and the overlying Raibl Fm (R) at the Rifugio Di Bona, beneath the Tofana Massif. DP, Dolomia Principale.

"eastward" relative mantle flow and not to slab pull.

Northeast Italy is usually interpreted as the area of N-S compression due to the African-Adriatic indenter. However, this comes from a misleading kinematic approach, where local stress field is assumed to be an indicator of plate motion. Stress field deviates along oblique plate margins, and the WNW-ward motion of the Adriatic plate relative to Europe can generate right-lateral transpression and consequent NW-SE to N-S compression along the central-eastern Alps. Moreover, the Adriatic plate and Europe, in an "absolute" reference frame (HEFLIN *et alii*, 2002), are both moving NE-ward, instead of N-S. European and Adriatic plates have different N-S component, but they move between 45°E and 52°E absolute directions.

The relatively high topography of the Alps is consistent with crustal scale thrusts (DOGLIONI, 1987; 1992; PFIFFNER *et alii*, 1997; Schönborn, 1999; Transalp Working Group, 2002), similarly to those observed in the Wind

River thrust in Wyoming (ALLMENDINGER *et alii*, 1983). In spite of the elevated topography and more than 50 km thick continental crust (KISSLING, 1993), the Alps, both in the frontal belt to the north and in the conjugate retrobelt to the south, present low dip of the foreland regional monocline (3°-5°), typical of "E"-directed subduction zones, in contrast with the Apennines, due to a "W"-directed subduction zone, where associated to low topography the monocline is at places even steeper than 20° (MARIOTTI & DOGLIONI, 2000). As a general rule, salients of the thrust belt in the Alps and adjacent orogens occur along inherited Mesozoic basins. Therefore the several transfer zones are related to pre-existing structural and stratigraphic lateral variations of the passive margin architecture (e.g., platform to basin transition, N-S trending horsts and grabens). Moving along strike from the Transalp section, thrust belt transfers occur mainly through lateral variations of the ramp distance.

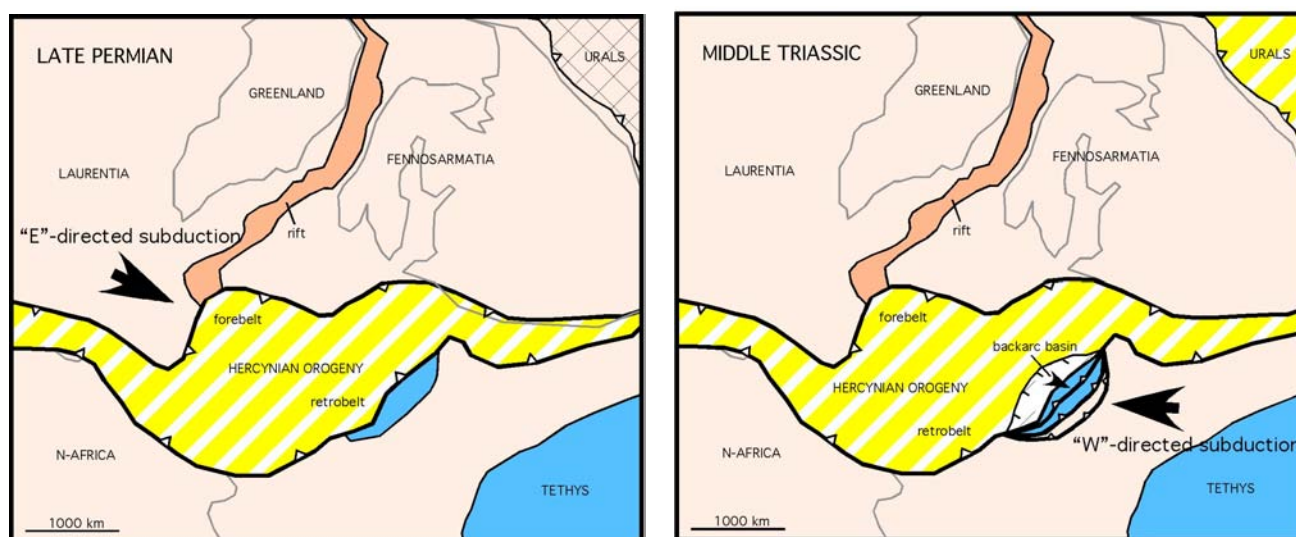


Fig. 253 - As in modern examples, where W-directed subduction zones developed along the retrobelt of an opposite subduction zone, the Middle Triassic of the Dolomites could have recorded the backarc rifting of such a setting. The Hercynian orogen was probably a collage of different subductions zones, but in general shows the characters of E-directed subductions zones, as the double vergence. If a small oceanic embayment was located east of the Hercynian retrobelt during Late Permian or Early Triassic, then a W-directed subduction zone could have developed, generating fast subsidence rate in the backarc basin (e.g., >600 m/Ma, Middle Triassic Southern Alps), and the shoshonitic magmatism.

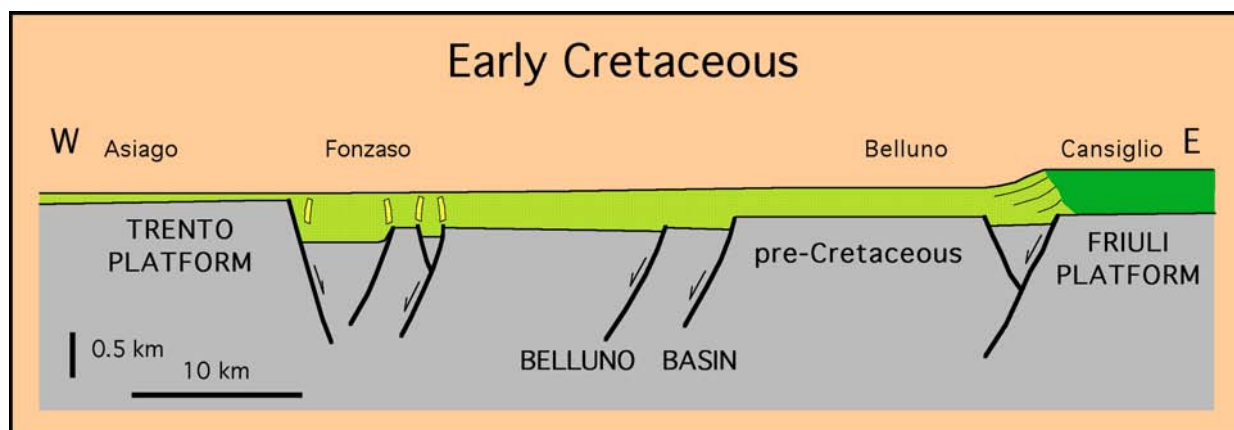


Fig. 254 - Interpreted W-E Early Cretaceous cross section from the Asiago plateau to the Cansiglio plateau, showing the coeval tensional tectonics, which produced differential subsidence in the area. Note the basinward prograding carbonate platform in the eastern side (M. Cavallo Limestone) and the different thicknesses in the basinal sedimentation (Biancone). Neptunian dikes (vertical yellow segments) characterize the zones of tensional tectonics (i.e. the Arsìe Lake, Fonzaso). The Neogene deformation has been strongly influenced by the pre-existing structural and stratigraphic geometries. See location and compare the general tectonics of the area with the inherited Mesozoic structural background in fig. 149.

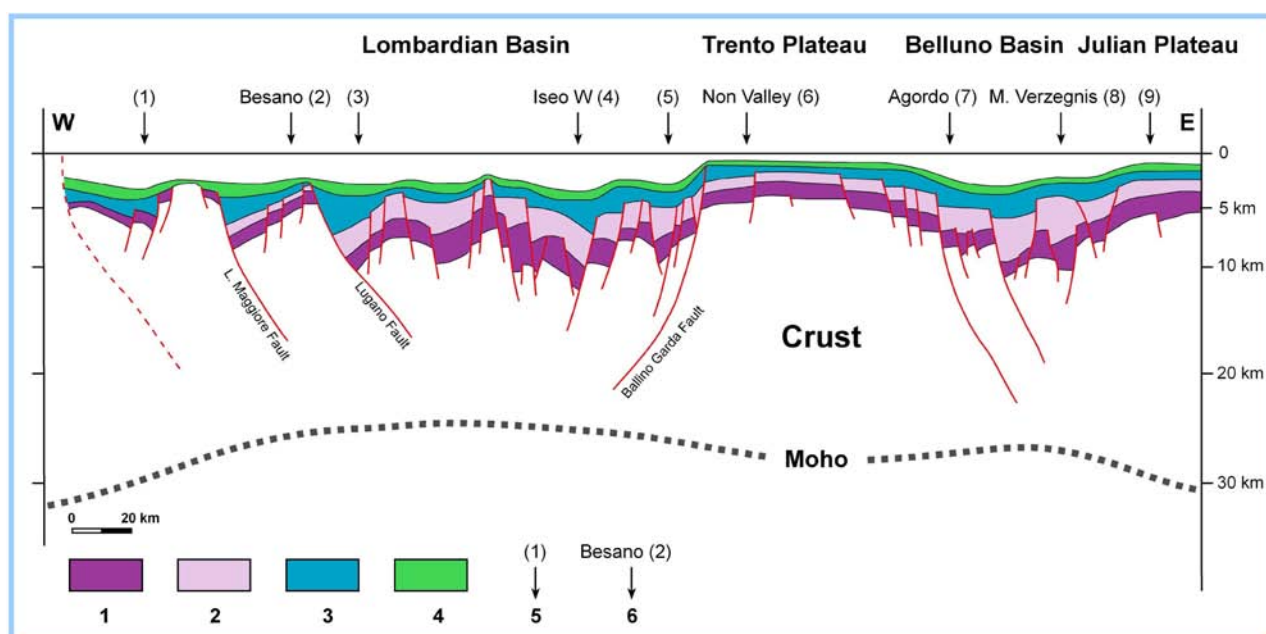


Fig. 255 - Extensional Mesozoic architecture of the Southern Alps at the end of Lower Cretaceous time. 1) Permian - Carnian p.p.; 2) Carnian p.p. - Rhaetian; 3) Hettangian - Bajocian; 4) Bathonian - Aptian p.p.; 5-6) Location where samples have been collected for organic matter maturity analyses and for thermal modelling (after FANTONI & SCOTTI, 2003). The Upper Cretaceous crustal structure is only speculative and does not reflect the present day crustal thicknesses, which have been increased by the Alpine compressional tectonics.

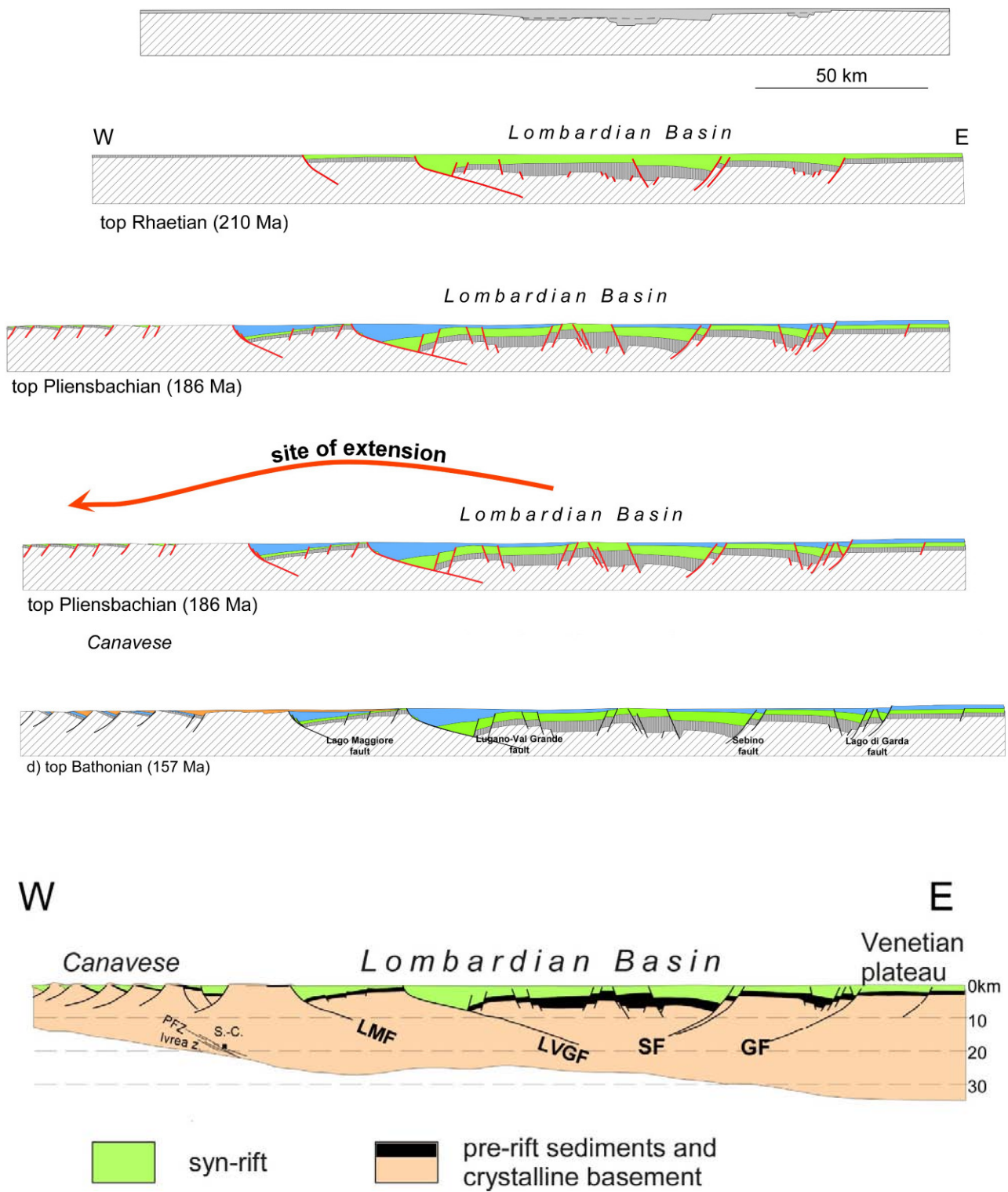


Fig. 256 - Reconstruction of the Late Triassic-Jurassic rifting in the central-western Southern Alps (after BERTOTTI *et alii*, 1993). The Venetian Plateau represents the Trento Horst.

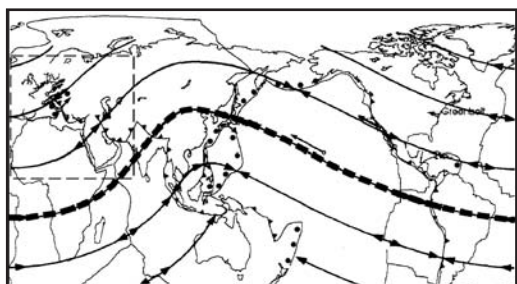
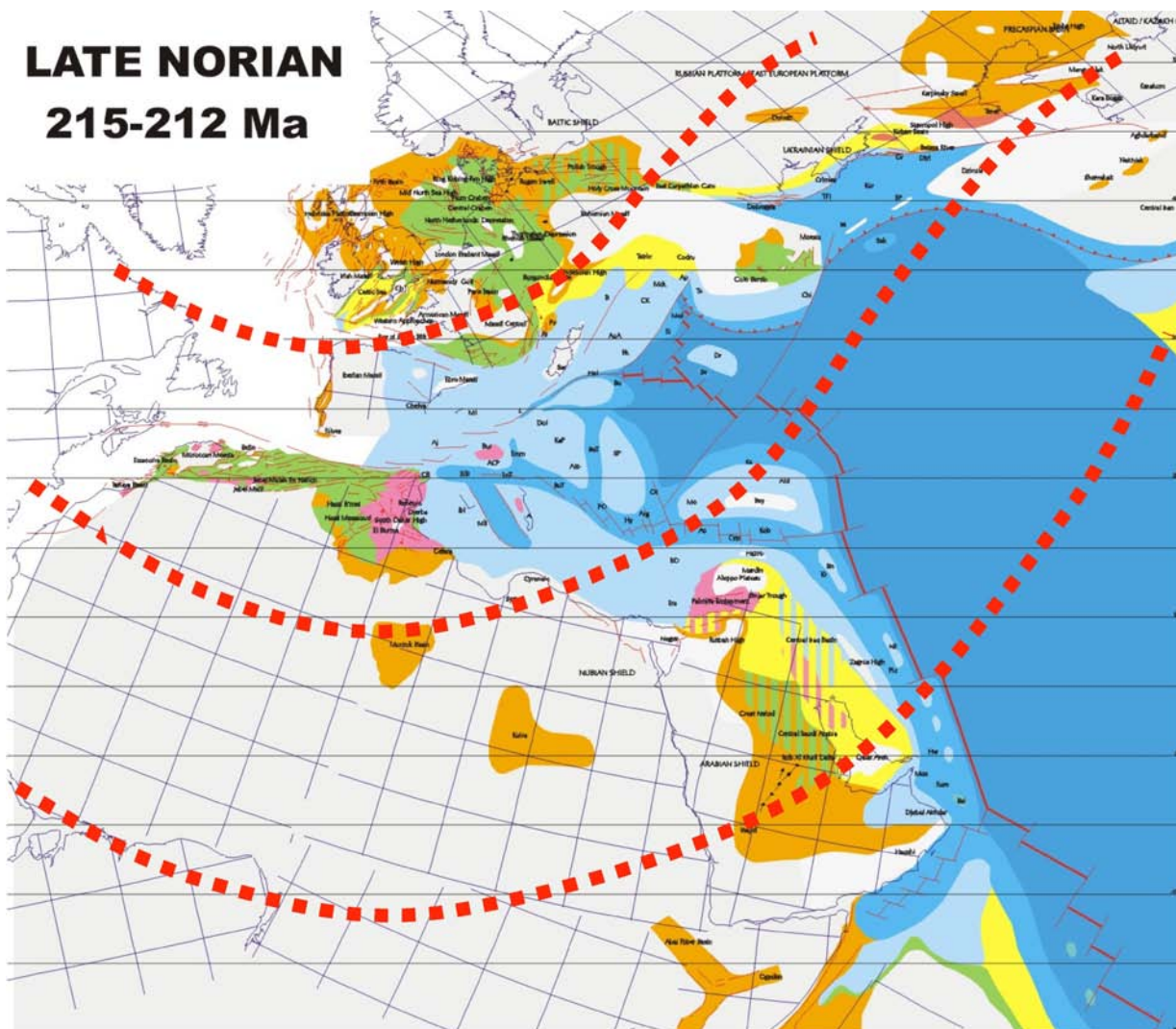


Fig. 257 - Panel to the left: Flow lines of plate motions during the last 45 Ma based on first order tectonic features. Upper panel: Paleogeography of the Late Triassic after GAETANI *et alii* (2003) on which the past plate motions have a similar undulation as today (inset of the panel to the left), indicating the persistence of the mainstream of plate motions even in the Mesozoic.

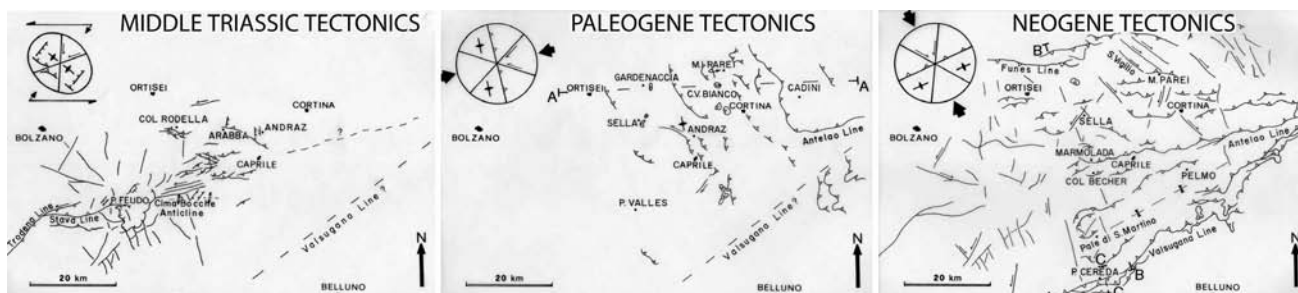


Fig. 258 - Main tectonic phases and related structures in the Dolomites after the Hercynian orogeny, apart the extensional Mesozoic tectonics (after DOGLIONI, 1987).

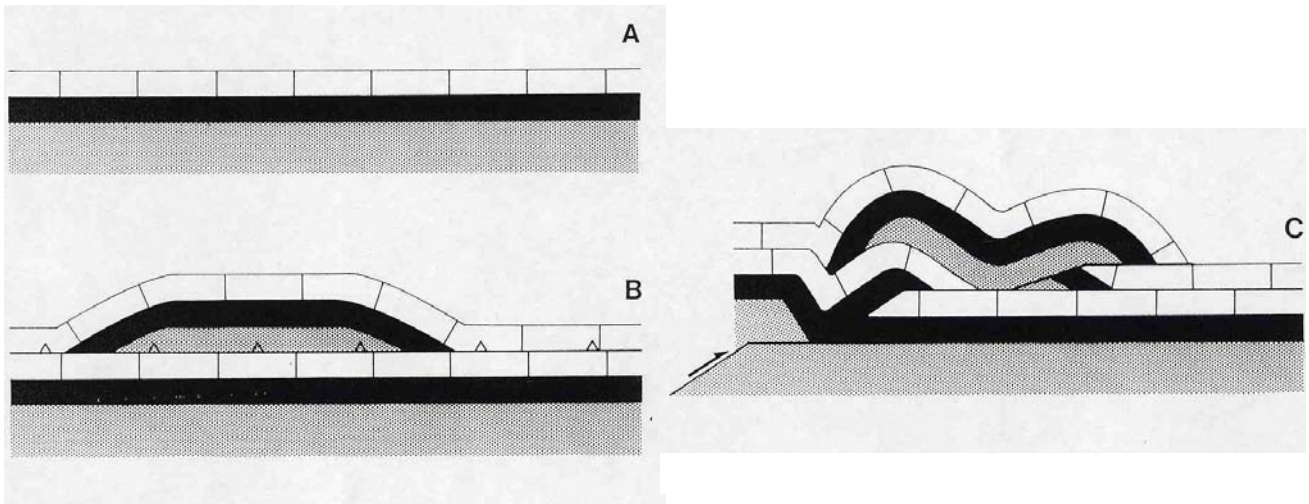


Fig. 259 - Overlap of two thrusts perpendicular to each other. A) pre-deformation stage; B) a thrust moves toward the reader with two lateral ramp cut-offs, strike view; C) later a thrust propagates with staircase trajectory, dip view. Assuming north to the left, this example could be applied to the interference pattern in the central-eastern Dolomites between older (Eocene?) WSW-verging thrusts and folds, later deformed by the deeper Miocene to Present SSE-verging thrusts and folds.

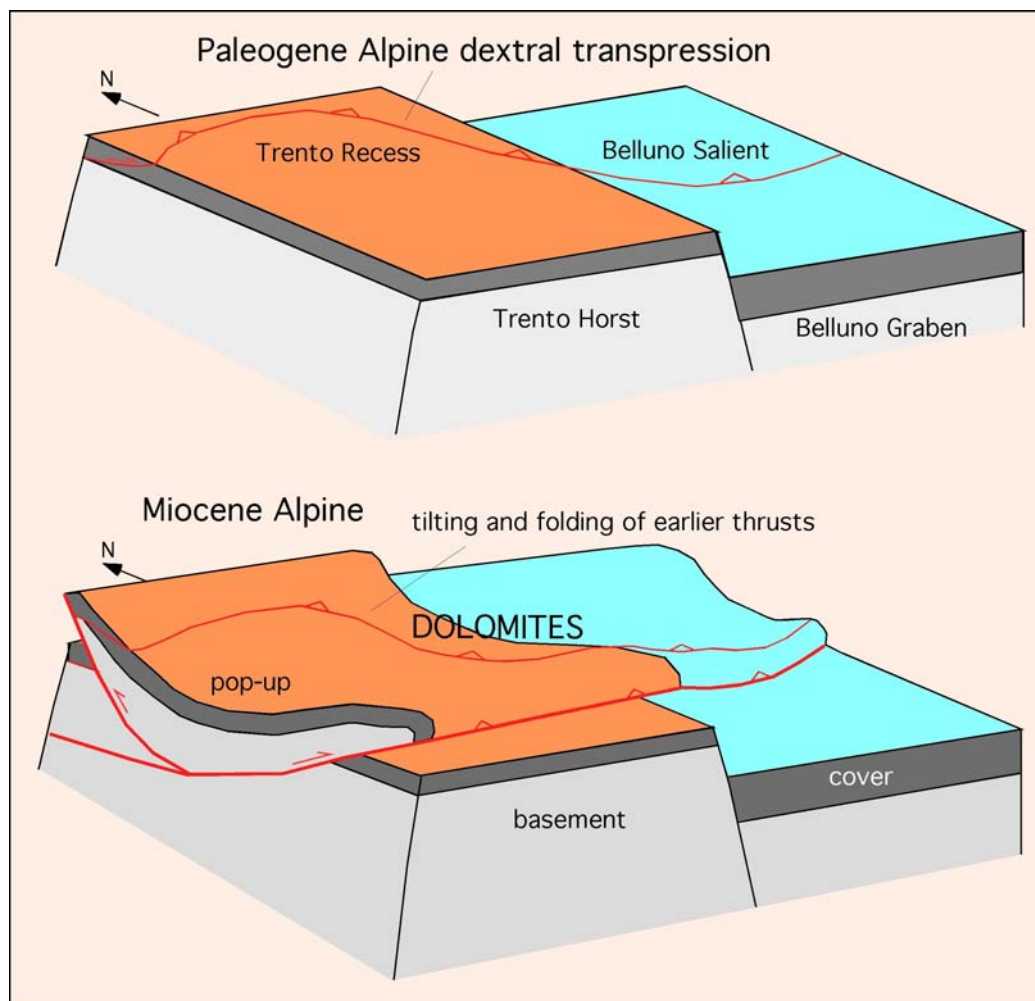


Fig. 260 - The earlier alpine deformation inherited the Trento horst determining a recess on the structural high, and a salient in the graben to the east. The transfer zone consists of right-lateral transpression with thin-skinned WSW-verging thrusts. The later deeper thick-skinned deformation, involving the basement, generated the Dolomites pop-up, folding and tilting the earlier shallower thrusts.

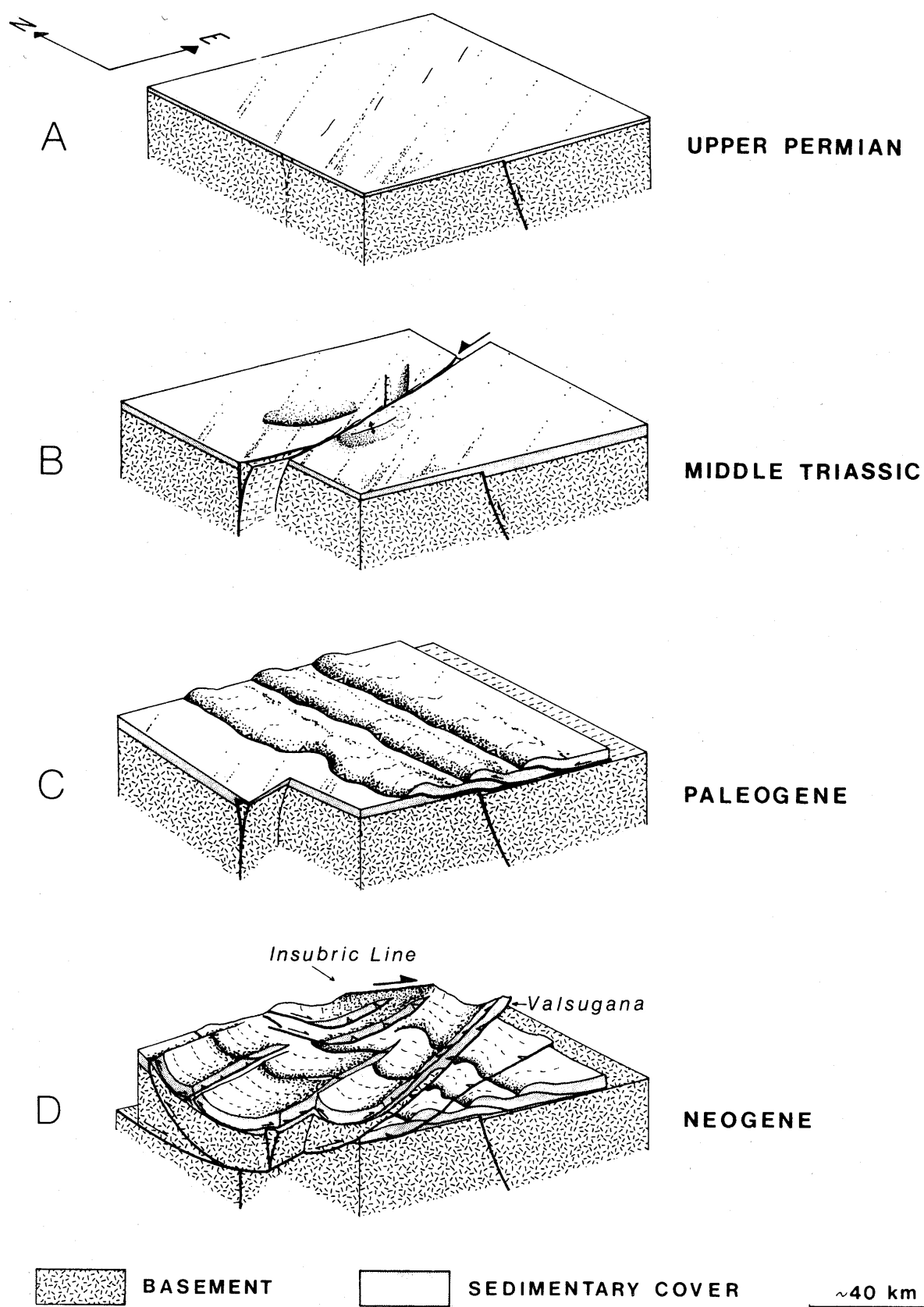


Fig. 261 - Main tectonic phases in the upper crust of the Dolomites. A, Permian-Triassic rifting; B, strike-slip tectonics (prevalent trans-tension with localized transpression) along a N70° trend; C, W-SW vergent thrusting of Paleogene age; D, Neogene SE-vergent thrusting, pop-up formation of the Dolomites synclinorium.

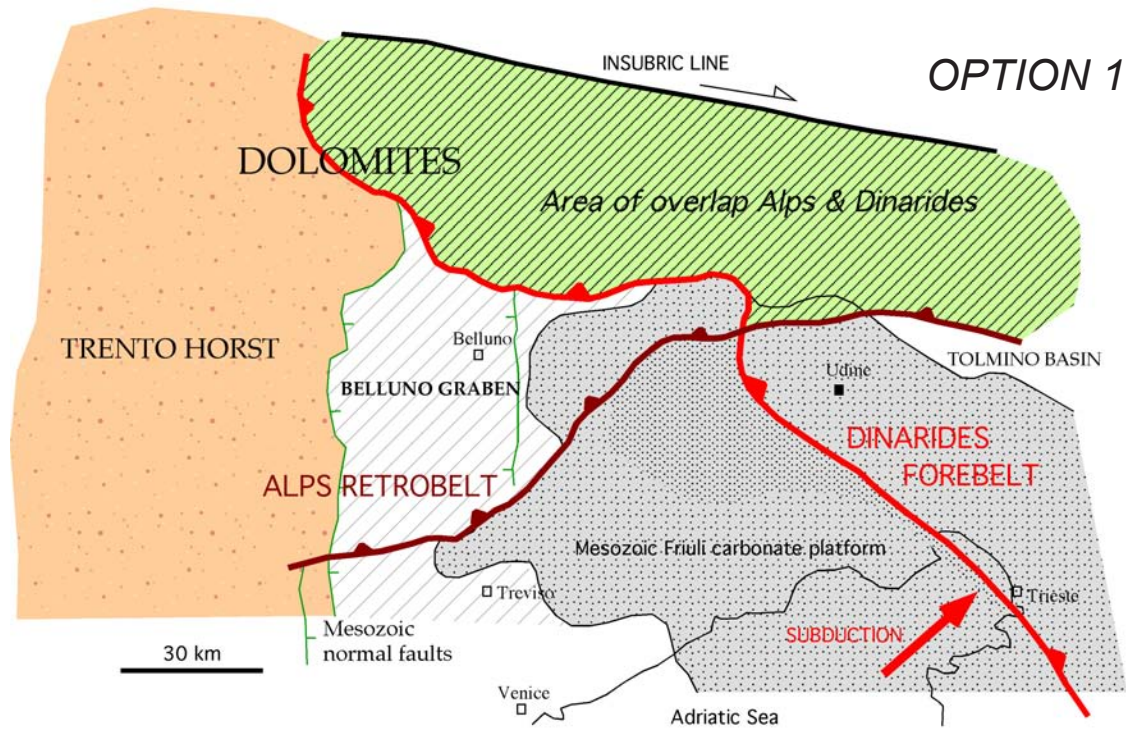


Fig. 262 - The WSW verging thrust structures of pre-Late Oligocene age in the Dolomites can be interpreted as the prolongation of the Dinarides front into the Southern Alps, in which there is a vast area of overlap and interference structures.

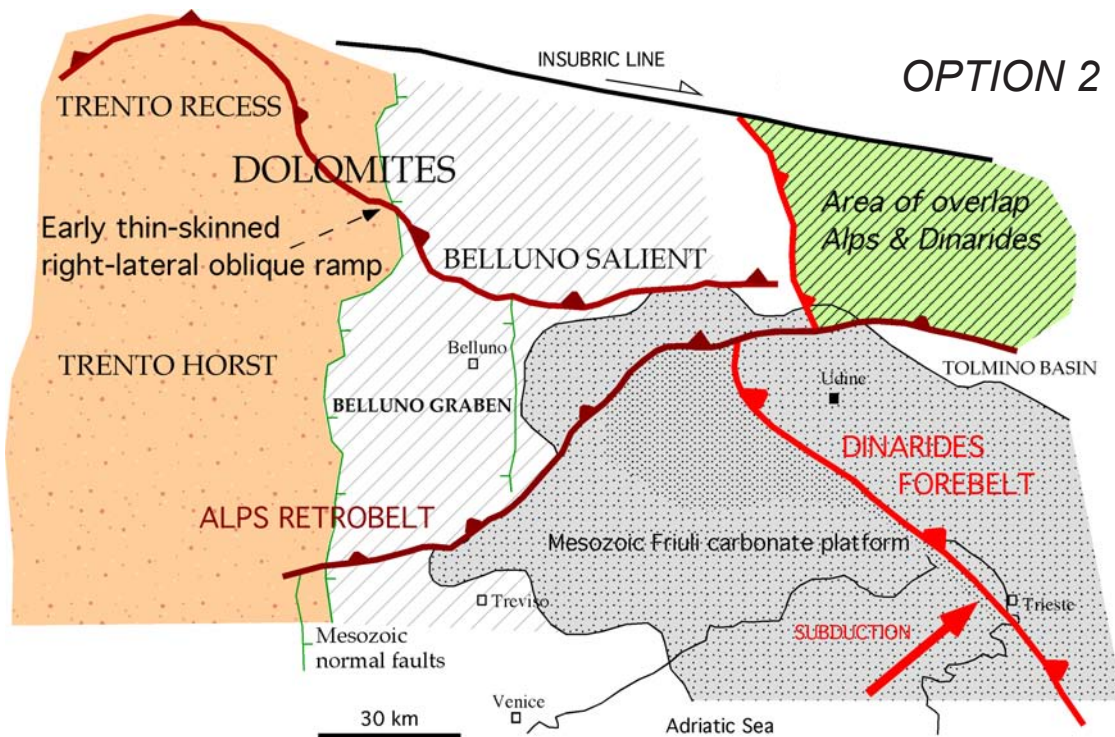


Fig. 263 - Alternatively to the previous figure, the WSW verging thrusts in the Dolomites are here interpreted as the oblique right-lateral transpressive ramp of the advancing Eocene alpine thrusting between the Trento recess and the Belluno salient. In this view the area of Alps-Dinarides overlap is more restricted to the east.

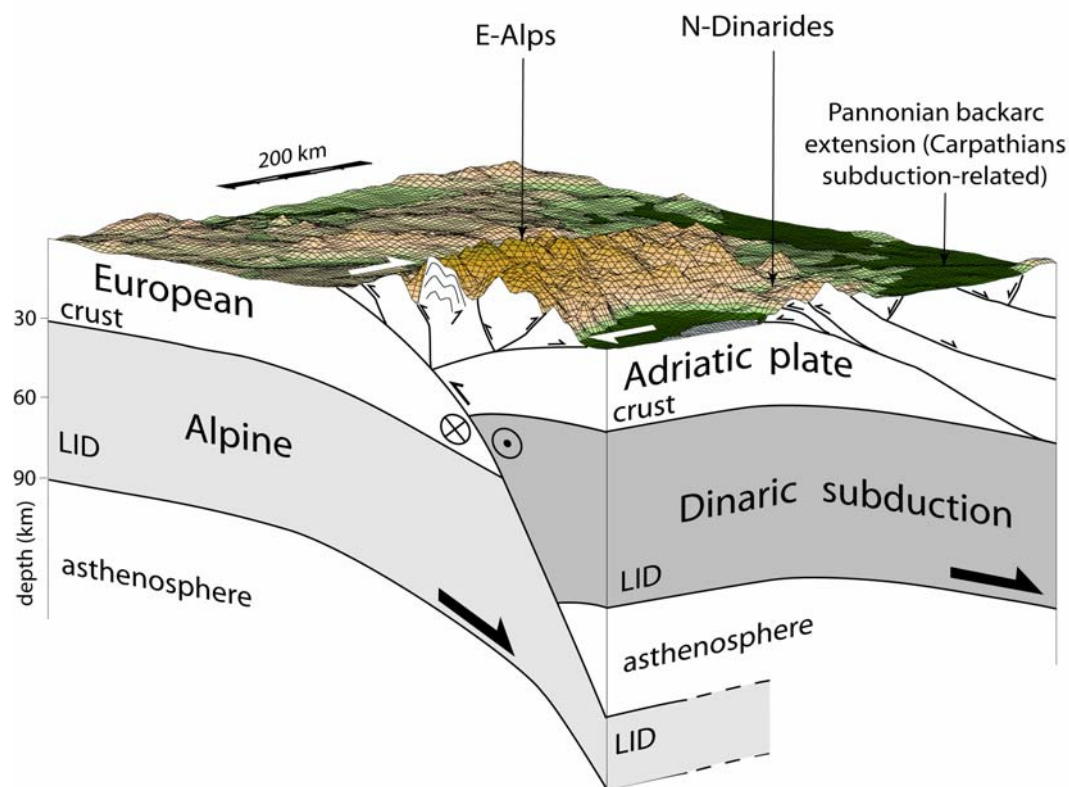


Fig. 264 - 3D view and interference between the Alpine and Dinaric subductions in northeastern Italy. The extension of the Pannonian, Carpathians subduction-related back-arc basin, crosscuts the Eastern Alps and the northern Dinarides. This indicates that, in the same area, independent geodynamic settings may concur and plate boundaries are passive features.

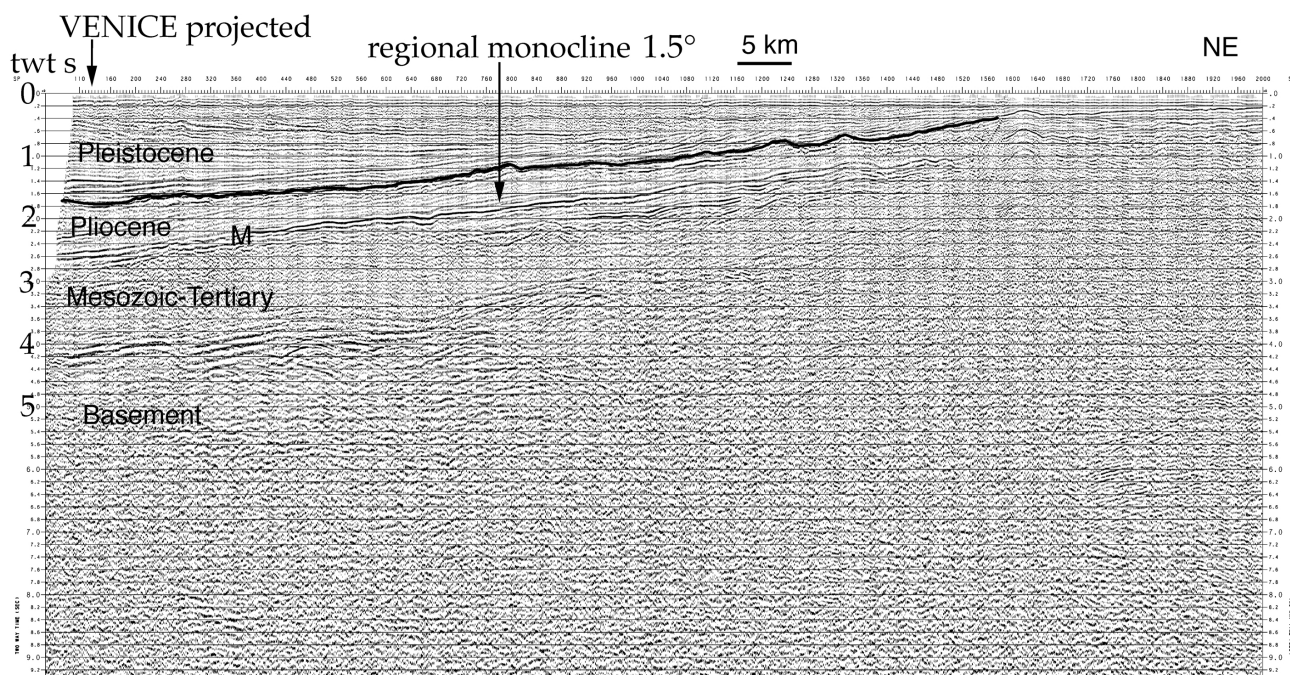


Fig. 265 - Seismic reflection profile (CROP M-18) of the northern Adriatic Sea, parallel to the coast, offshore Venice. Note the thinning of the Pleistocene sediments moving north-eastward, indicating coeval differential subsidence in the underlying rocks. The Pleistocene-Pliocene boundary is marked. M, Messinian unconformity. Vertical scale in seconds, two way time.

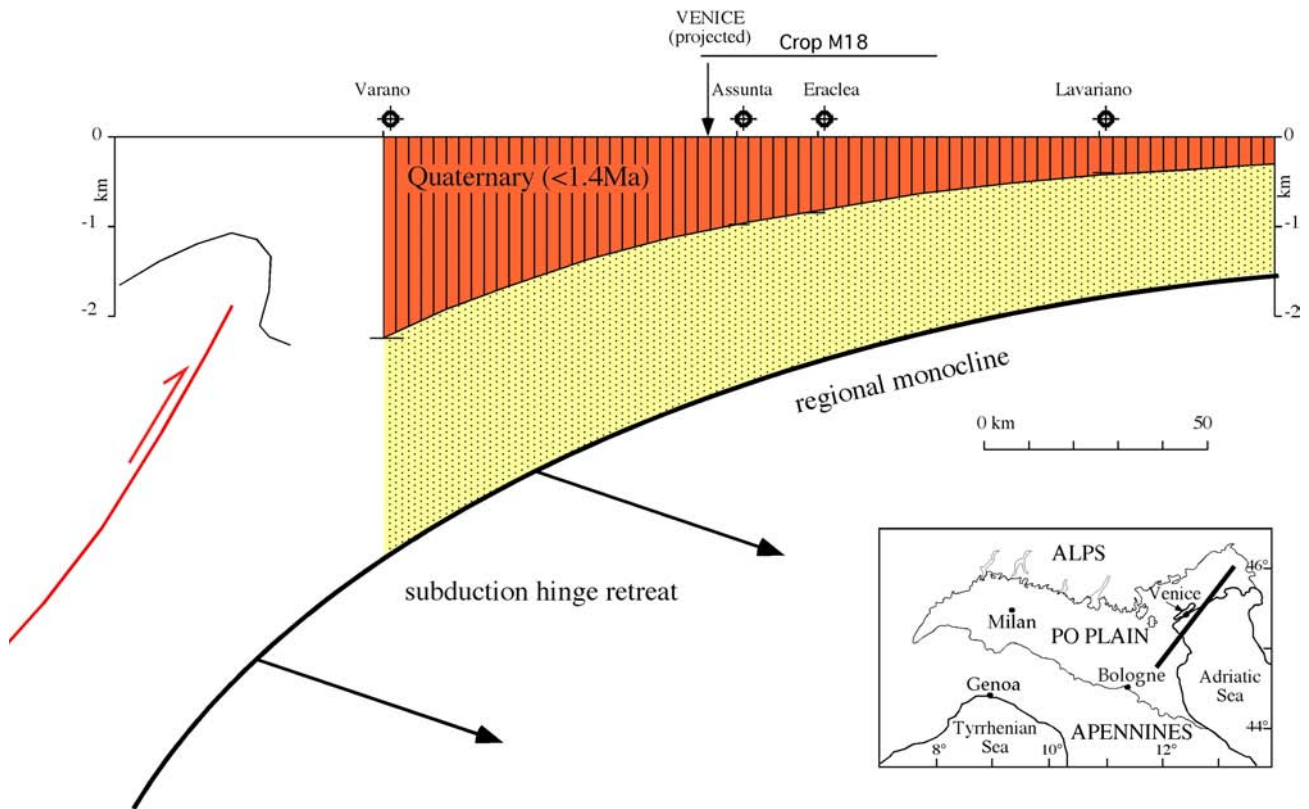


Fig. 266 - Seismic and borehole data constrain the geometry and southwestward thickening of the Pleistocene sediments in the Po Basin, northern Adriatic Sea and Friuli plain.

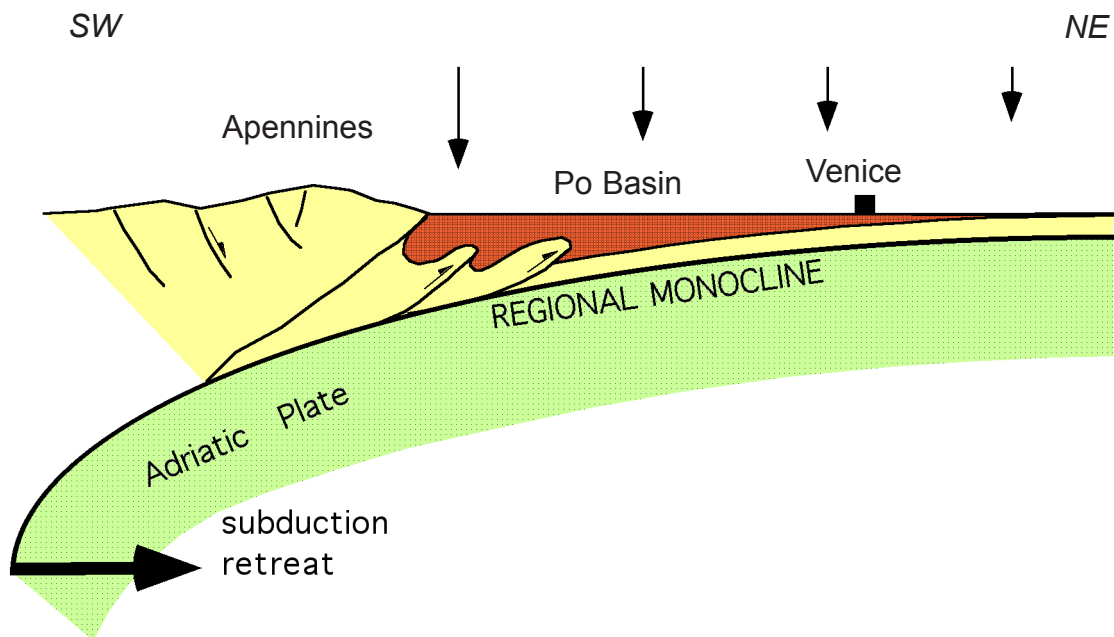


Fig. 267 - Schematic profile across the Apennines, Po Basin and Venetian area, showing the curvature of the Adriatic plate in the fore-land of the Apennines, associated to the slab retreat. The 1mm/yr subsidence rate of Venice is the distal effect of the Apennines subduction hinge retreat (after CARMINATI *et alii*, 2003).

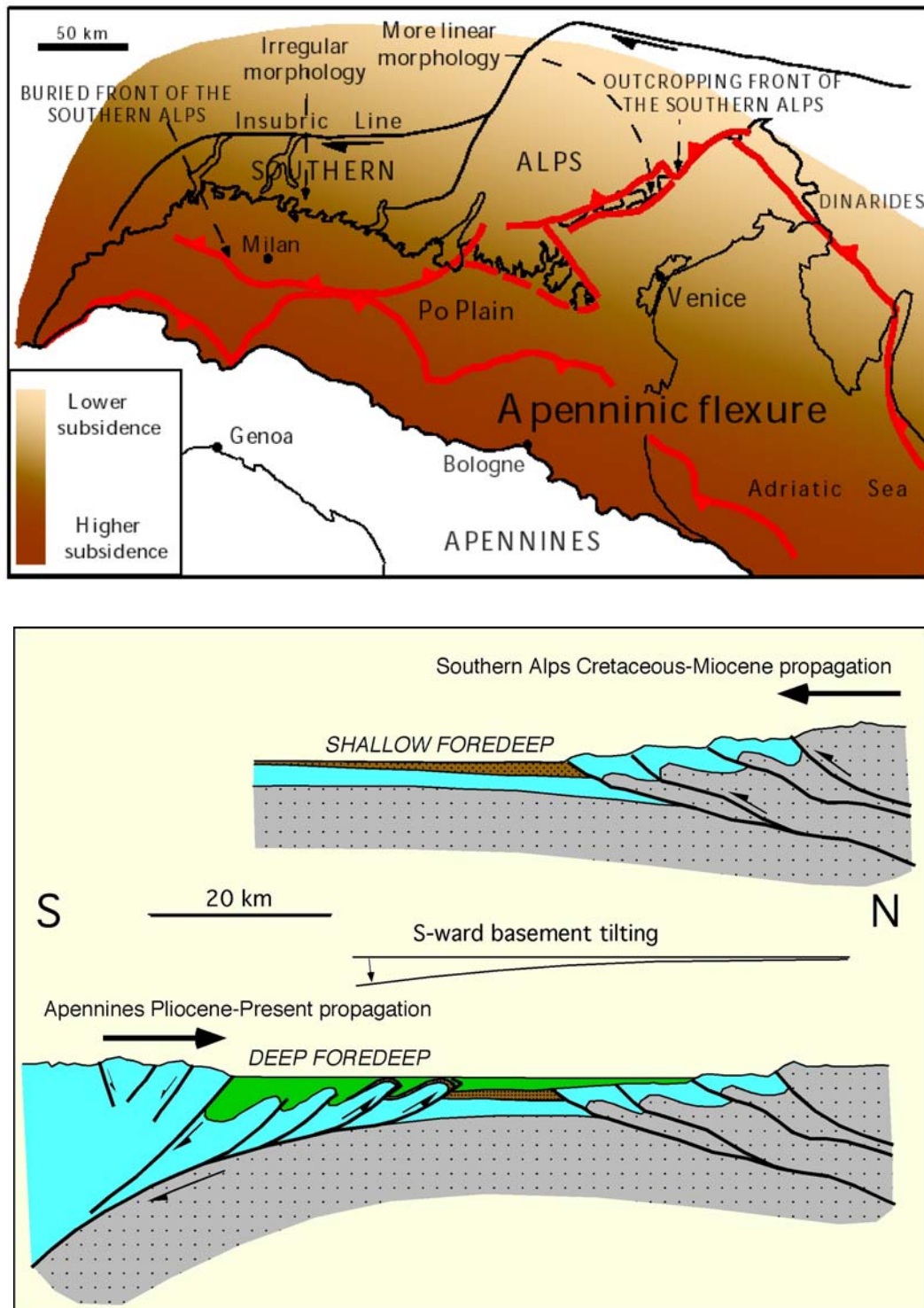


Fig. 268 - The subsidence related to the flexure induced by the Apennines subduction decreases from south to north. It affects all of the Po Plain basin and part of the Alps and of the Dinarides, where it contrasts the general uplift trend related to the orogenesis. Also the Dolomites are slightly affected by the Apennines subduction subsidence. The tectonic front of the Southern Alps corresponds to the alpine foothills in the eastern side, whereas it is buried in the western Po Basin due to the closer effect of the Apennines slab retreat. The lower panel represents an idealized cross-section between the northern Apennines and the western Southern Alps. The last ones are the south-vergent retrobelt of the right-lateral transpressive arm of the Alps, and formed between the Late Cretaceous and the Late Miocene, plus recent reactivations. Their shallow foredeep and the thrust planes have been southward tilted by the Late Miocene - Quaternary northward propagation of the basement monocline generated by the Apenninic subduction (after DOGLIONI, 1993; CARMINATI *et alii*, 2003).

Dolomites field-trip

The field trip is organized into five days with different main topics, such as the structure of the Southern Alps fold and thrust belt, the Triassic tectonics, the geometry of carbonate platforms and their control in the thrust tectonics, the relationship between the Tethyan rift and the Alpine tectonics. The program has to be considered flexible since weather condition can determine variations on the stop progression.

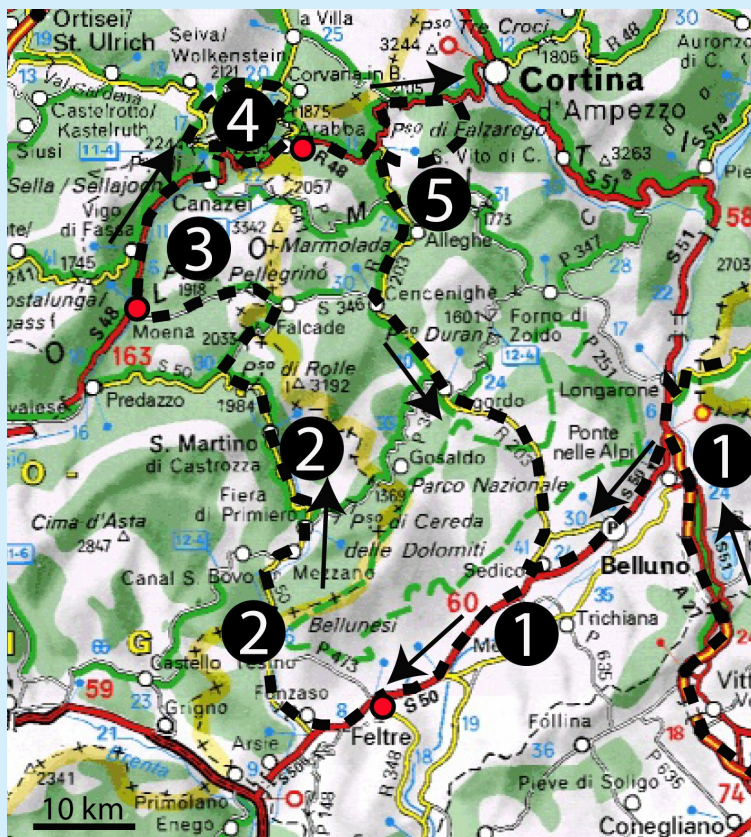
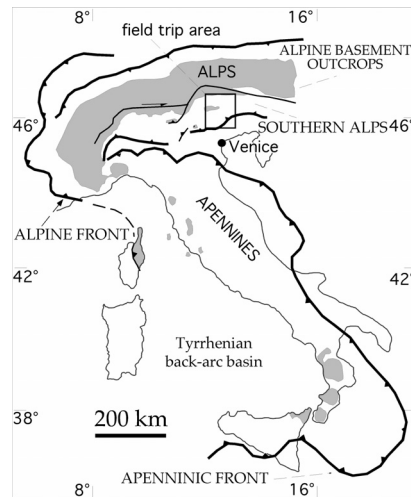


Fig. 269 - Location area of the field trip. Numbers indicate the days of the excursion.



Fig. 270 - View of the Southern Alps thrust belt from the Venetian foothills (left) to the Dolomites (right). Note the gradual increase in structural elevation and topography from the Venetian foothills moving northward.

1st Day



Fig. 1.0 - Itinerary: Longarone, Prealpi Bellunesi, Feltre. Google Earth view. Dashed red lines are the main thrusts of the area.

Subject: Mesozoic extensional structures and their alpine inversion

Mesozoic extensional structures have been often interpreted and described in literature on the basis of sudden variations of thickness and, eventually, of facies of the sedimentary cover. Seismic reflection studies confirmed such geometries and allowed the observation of typical morphologies of extensional structures. In the zone of Longarone, some tensional Mesozoic structures can be studied in outcrops that,

quite peculiarly, allow a 3D view of such structures. They are west-dipping faults that developed at the western margin of the Friuli Platform. Being located in the Southern Alps fold-and-thrust belt, often such structures were re-sheared, particularly those oriented N-S and dipping to the west.

This attitude made them particularly suitable to alpine inversion as sinistral transpressional faults (the regional sense of transport of thrust bodies is towards SSE), much more than east dipping faults.

Fig. 1.1 - Cross-section through the eastern Venetian Alps. The Belluno Thrust emplaced at the margin between the Belluno Basin sequence (in the hangingwall) and the Friuli Platform sequence (in the footwall). Legend: C, undifferentiated crystalline basement; T, Late Permian and Early-Middle Triassic formations; P, Late Triassic Dolomia Principale; J, undifferentiated Jurassic: platform facies (Calcari Grigi) in the southern part of the section, gradually passing northward to basinal facies (Soverzene Formation, Igne Formation, Vajont Limestone, Fonzaso Formation, Ammonitico Rosso); K, Cretaceous, platform facies (Calcare del Monte Cavallo, brick pattern) gradually passing northward to slope deposits and basinal facies (Calcare di Soccher, Biancone); S, Scaglia Rossa, Late Cretaceous - Paleocene; F, Eocene Flysch; M, Late Oligocene - Early-Middle Miocene Molasse; ME, Messinian conglomerates.

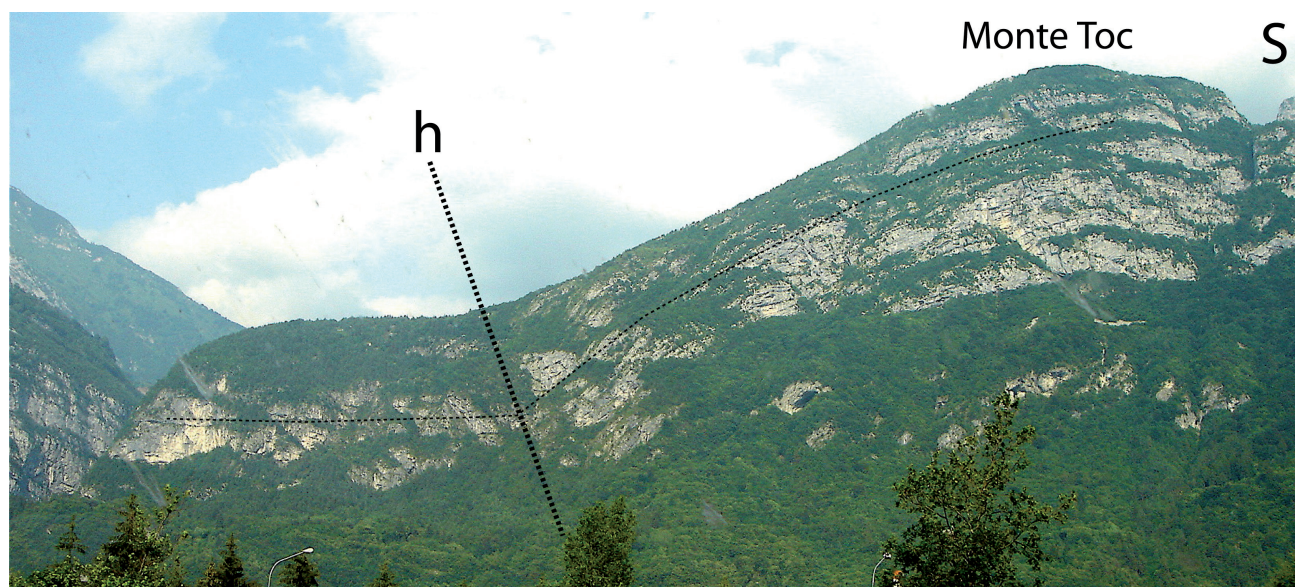
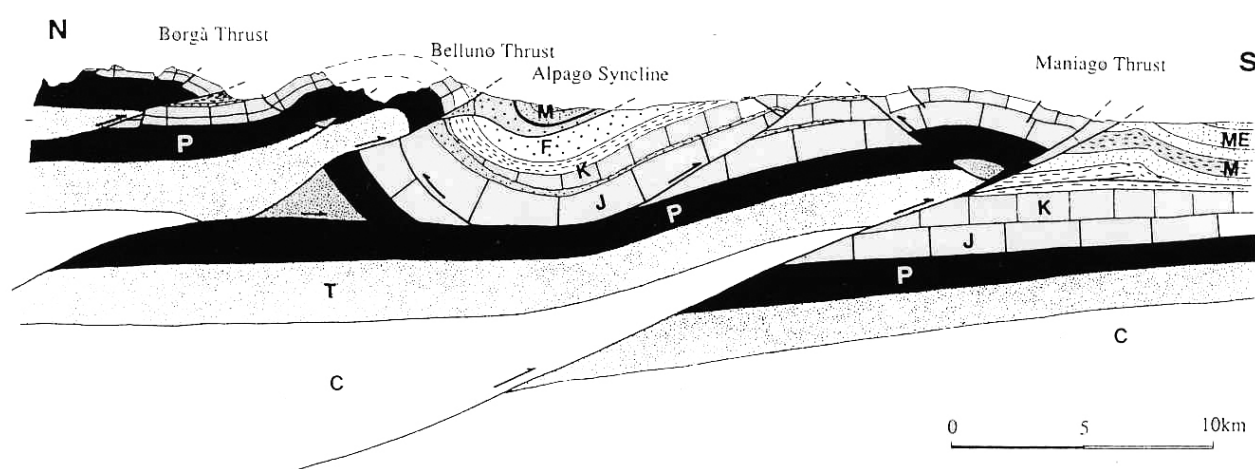
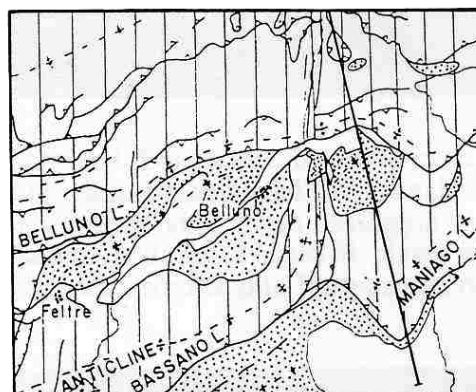


Fig. 1.2 - Eastern flank of the Piave Valley, near Longarone. The fold hinge (h) observable in the Calcare del Vajont (Dogger) belongs to the northern flank of the anticline developed in the hangingwall of the Belluno Thrust. It should correspond at depth to a transition from horizontal detachment to ramp of the thrust fault. The flank dipping to the north was the movement plane of the Vajont landslide, detached along the underlying Fonzaso Fm.

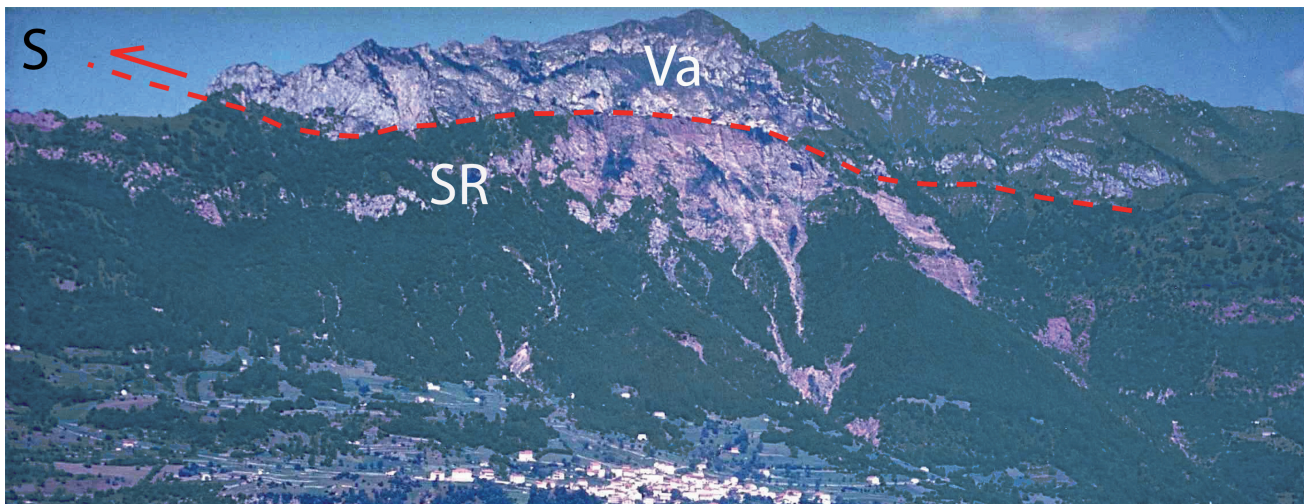


Fig. 1.3 - Western flank of the Piave Valley, above Longarone. Whitish Jurassic limestones (mostly Calcare del Vajont, Va) were thrust over the Scaglia Rossa (SR) along a sharp decollement plane. The thrust is a splay of the Valsugana Line. To the left, the thrust fault cuts downsection the Scaglia Rossa sediments, or it is folded by the deeper thrusts.

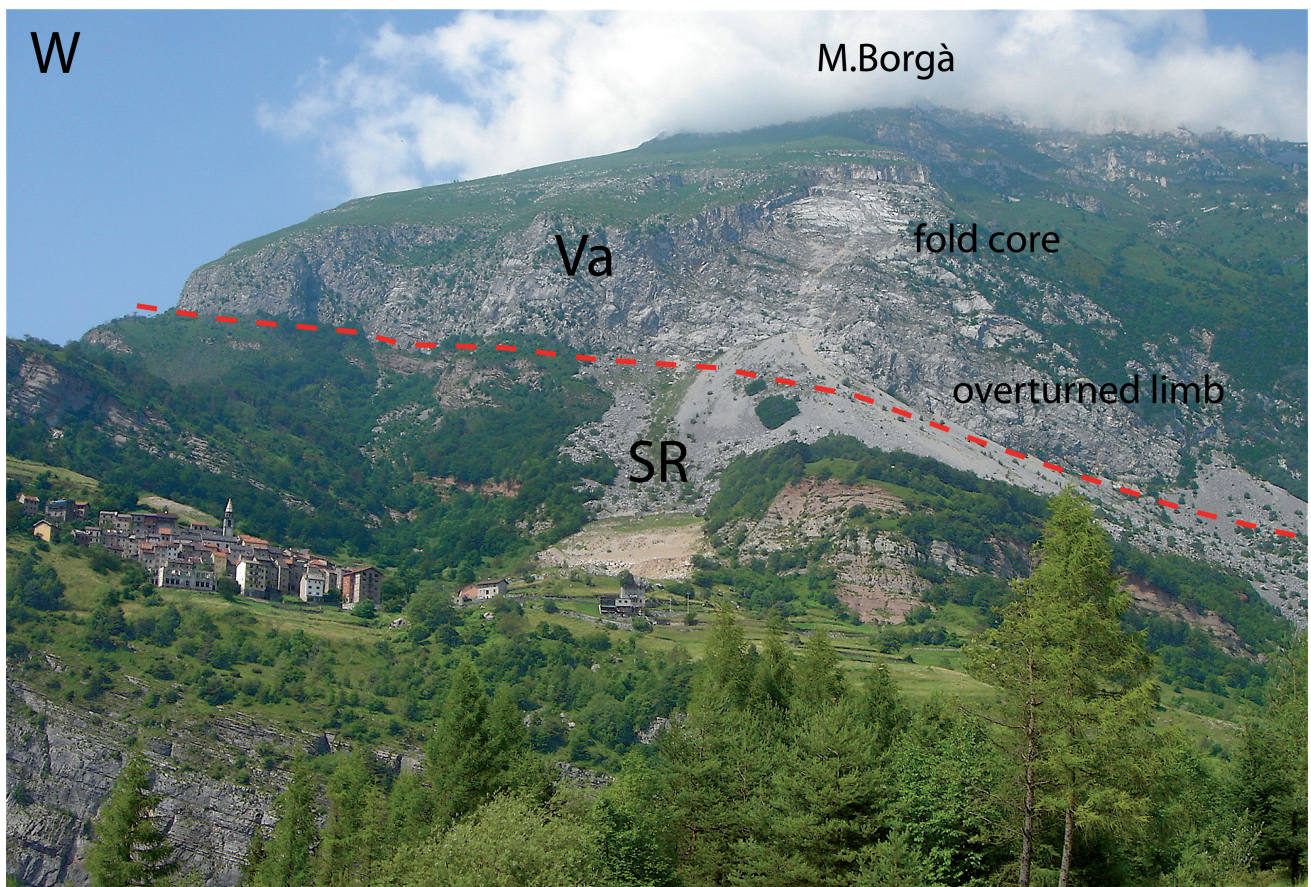


Fig. 1.4 - The eastward prolongation of a Valsugana Thrust splay outcropping in the southern cliff of the Mt. Borgà. The thrust is verging toward the observer and shows a lateral ramp geometry dipping to the east. In the hangingwall the overturned forelimb indicates fault-propagation fold kinematics. Va, Dogger Vajont Limestone; SR, Upper Cretaceous-Lower Tertiary Scaglia Rossa.

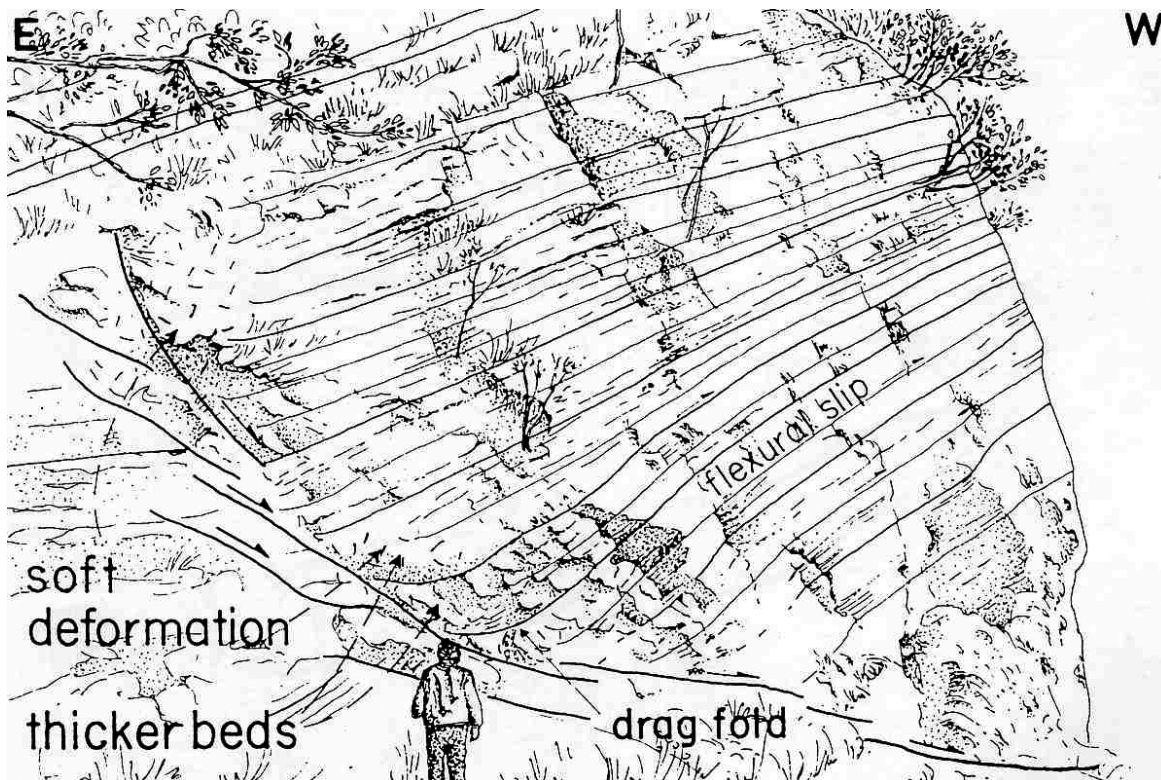


Fig. 1.5 - Natural cross-section of a small but significant synsedimentary Liassic fault in the Igne Fm, observable in the Vajont canyon, along the old ENEL road. In this outcrop it is possible to observe a rare example of listric fault in three dimensions. Notice the en echelon distribution of synthetic faults along the main shear zone, the deformation of unconsolidated sediments and the thickening of strata in the vicinity of the fault. At the top, the structure is sutured by undeformed strata.

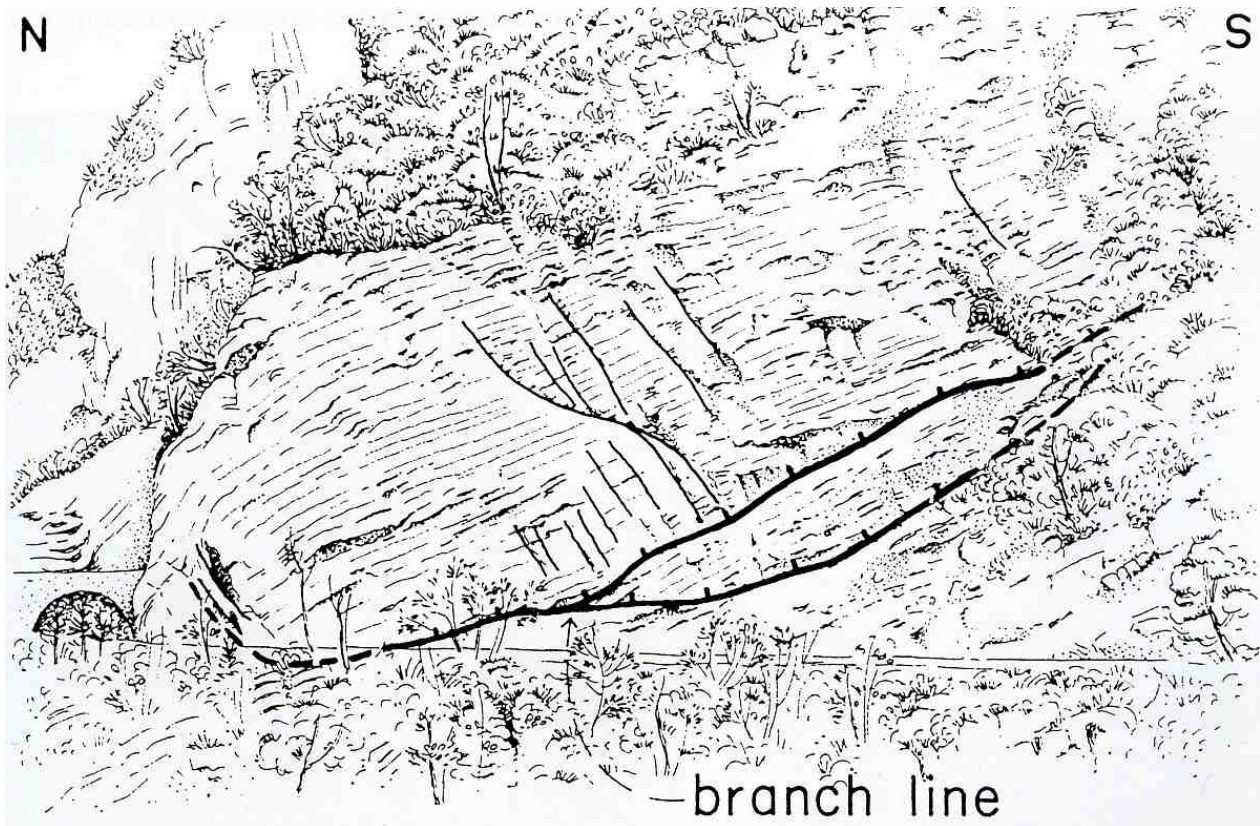


Fig. 1.6 - Frontal view of the Liassic growth fault in the basinal deposits of the Igne formation, in the Vajont canyon. Notice the ramification of the fault plane and the lateral and oblique ramp geometry of the fault. Extensional slickenfibers confirm that the hangingwall moved downward with respect to the footwall. Small conjugate fractures are confined to the hangingwall of the fault plane.

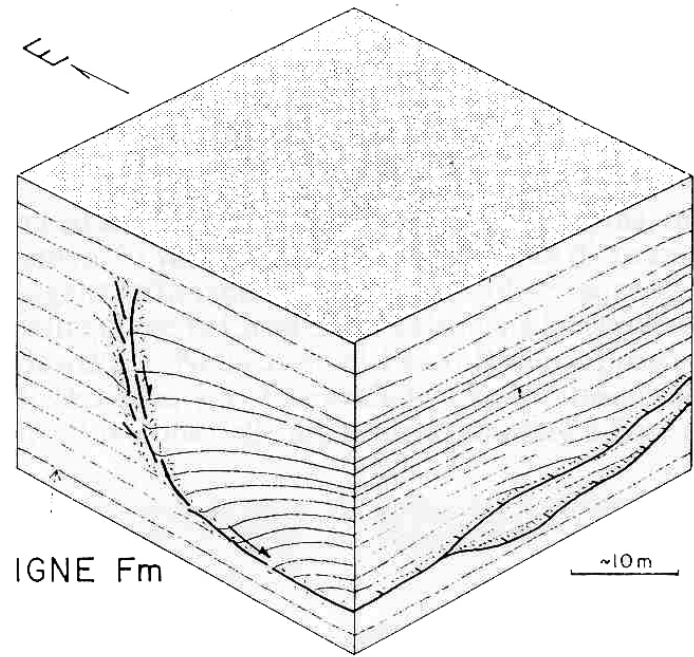


Fig. 1.7 - Schematic three-dimensional view of the extensional fault of the previous figures. A major regional extensional structure can be envisaged in the Col delle Tosatte Line, probably an extensional Mesozoic fault dipping to the west, reactivated as a sinistral transpressive fault during the Neogene Southalpine compressional deformation.



Fig. 1.8 - The landslide from Mt. Toc that generated the Vajont tragedy of the 9th October 1963, in which the water of the underlying artificial lake was squeezed out and devastated the city of Longarone with 1910 casualties. The decoupling surface is the basinal Middle Jurassic Fonzaso Fm, and the dip of the beds is due to the deeper S-verging ramp of the Belluno Thrust.

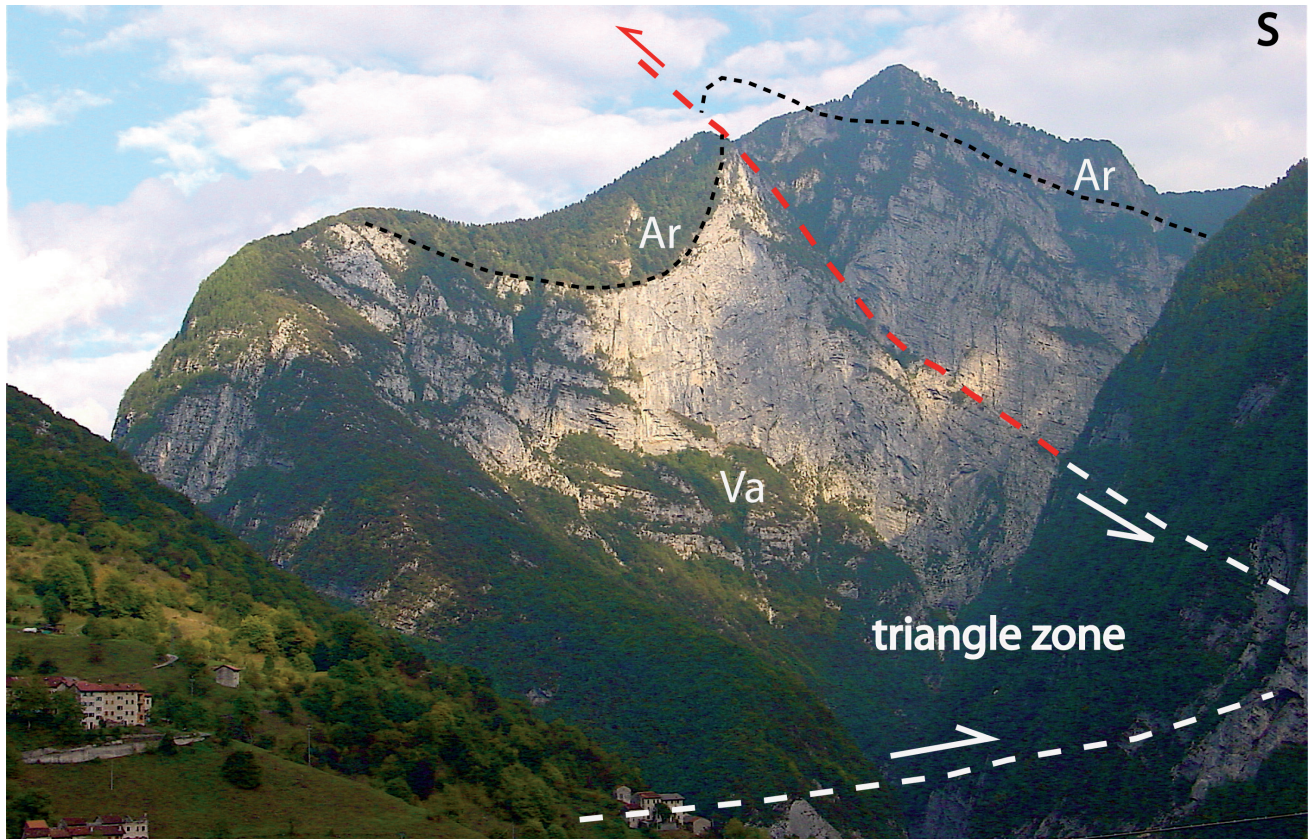


Fig. 1.9 - The thrust outcropping at the top of Mt. Borgà, has a lateral ramp cutting downsection eastward where it continues, east of the Vajont area, near Erto. Here it outcrops at lower elevation and generates a triangle zone as in this photo. The white part of the thrust is behind or below the ridge in the foreground. Ar, Ammonitico Rosso; Va, Vajont Lm.

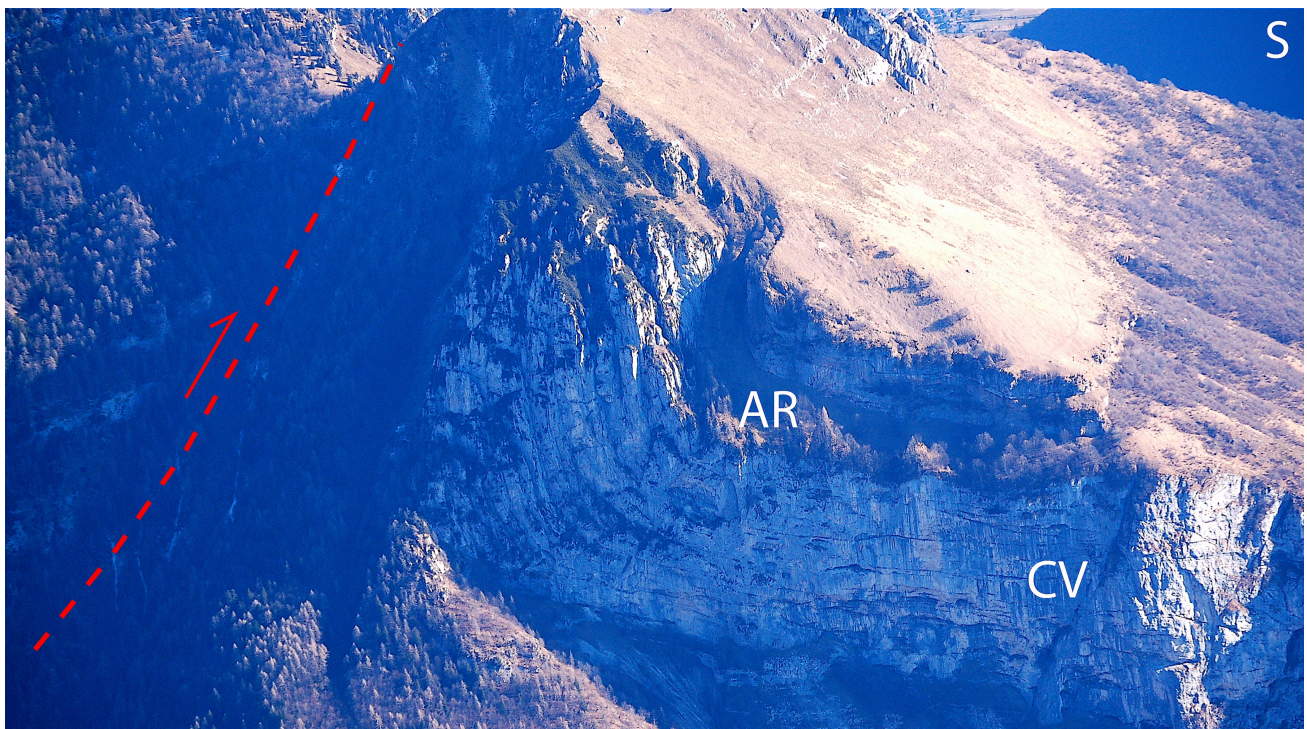


Fig. 1.10 - Footwall syncline beneath a branch of the Valsugana thrust in Val Zemola. CV, Middle Jurassic Vajont Limestone; AR, Upper Jurassic Ammonitico Rosso.



Fig. 1.11 - A branch of the Valsugana thrust system affects the Norian Dolomia Principale (DP) at the toe of the Duranno Mt., at the top of the Val Zemola. Note the different cutoff angles of the hangingwall and the footwall.

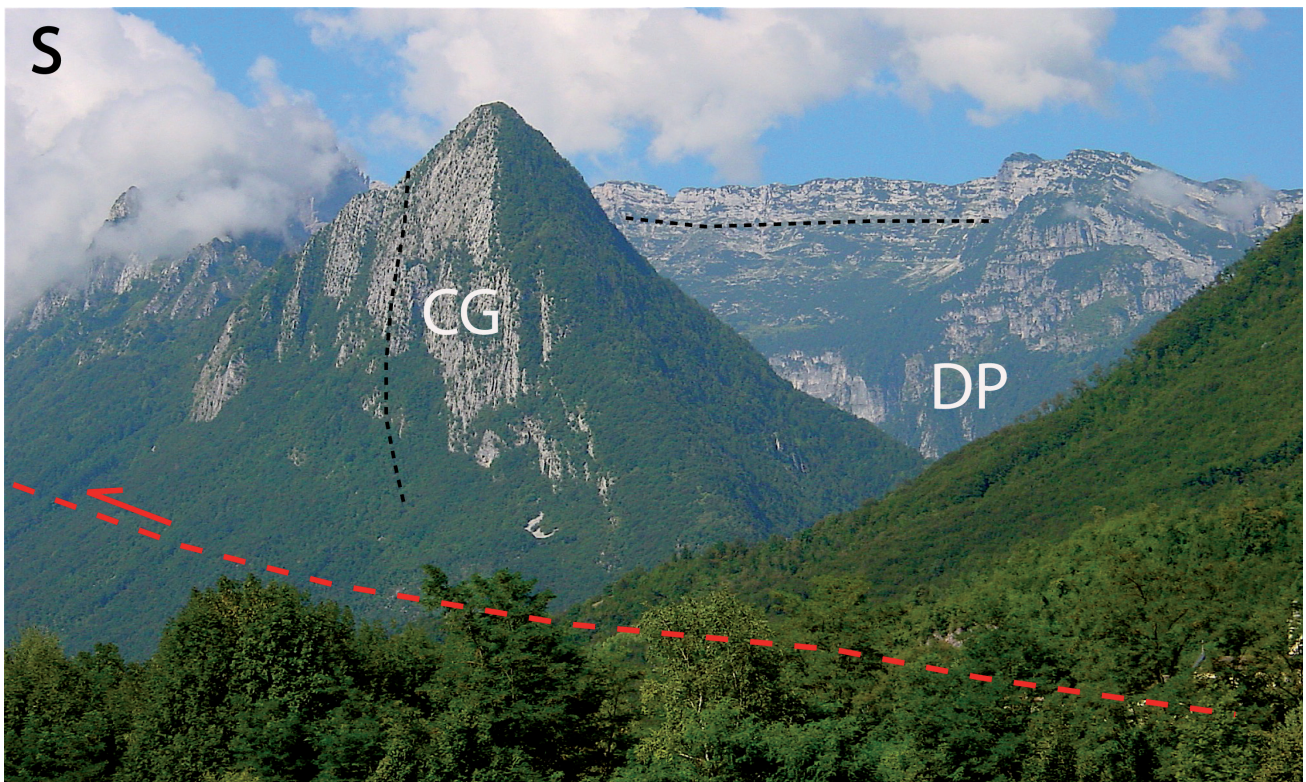


Fig. 1.12 - Fault-propagation fold in the hangingwall of the Belluno Thrust, west of Mas. CG, Liassic Calcarei Grigi; DP, Norian Dolomia Principale. Not visible in the footwall the Tertiary Molasse and Flysch.

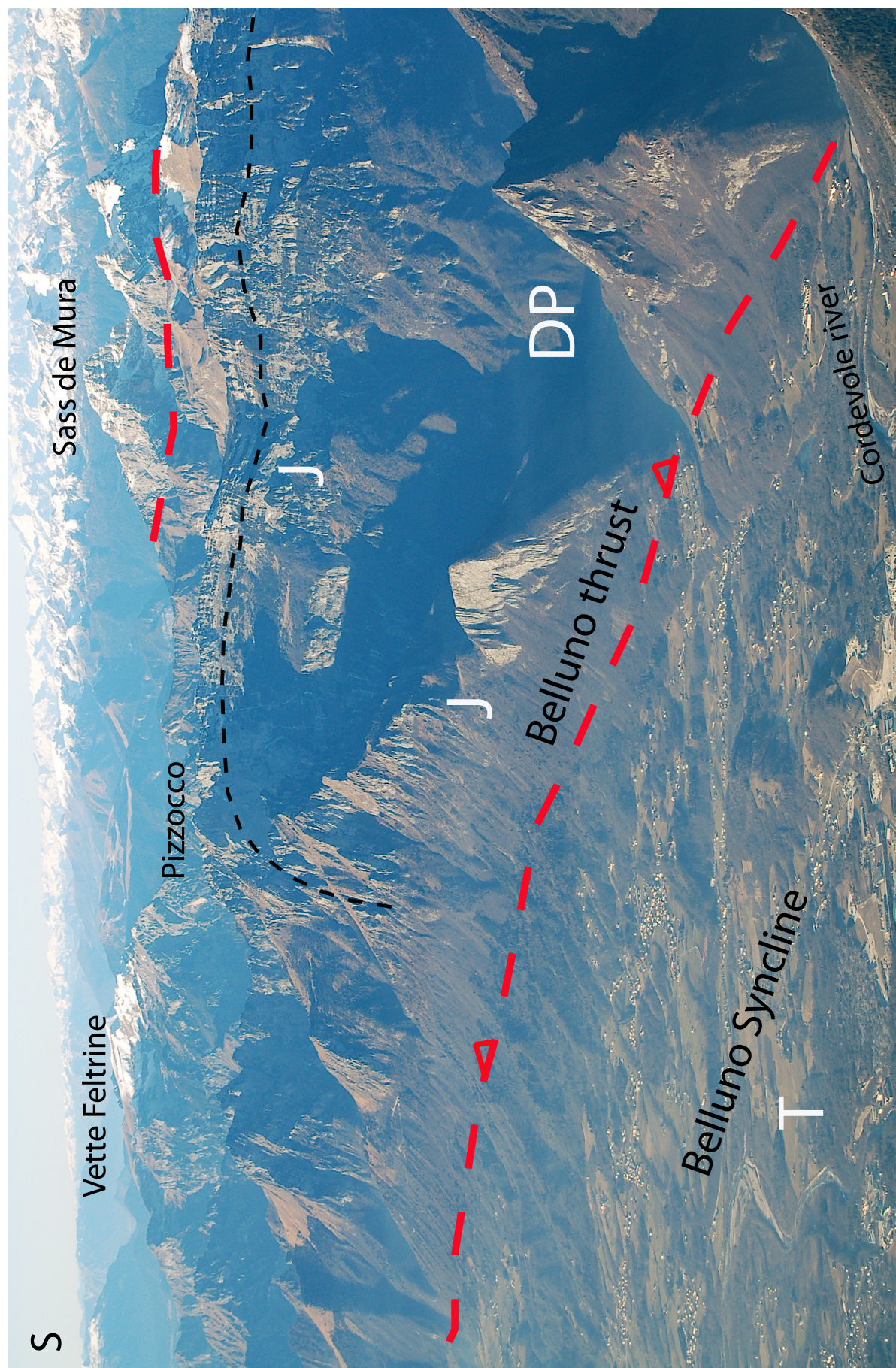


Fig. 1.13 - The anticline in the hangingwall of the Belluno thrust carries the Mesozoic sequence over the Tertiary Paleocene-Eocene flysch and the Oligo-Miocene molasses in the footwall. J, Jurassic; DP, Dolomia Principale; T, Tertiary.



Fig. 1.14 - The Eocene Flysch (F) covered unconformably by the Upper Oligocene Molasse (M) in the Belluno Syncline, in the footwall of the Belluno Thrust.

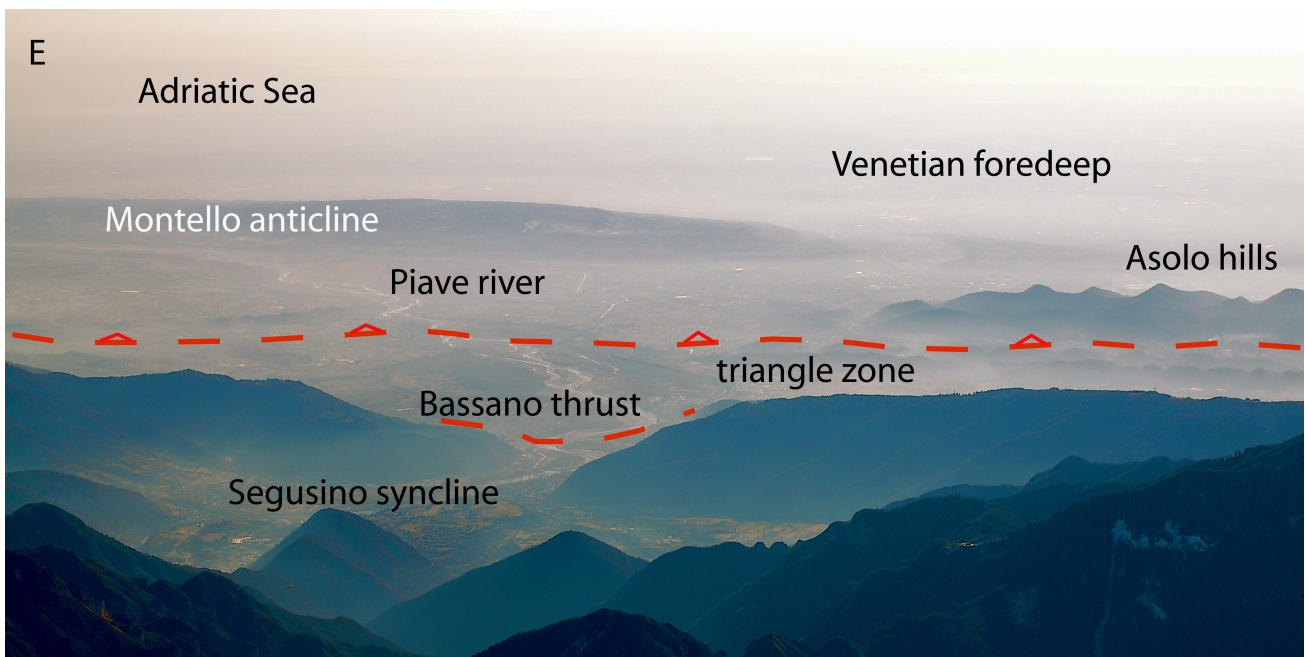


Fig. 1.15 - Southern view of the Southern Alps front with the active Montello anticline affecting Upper Miocene conglomerates and Pliocene shales.

2nd Day

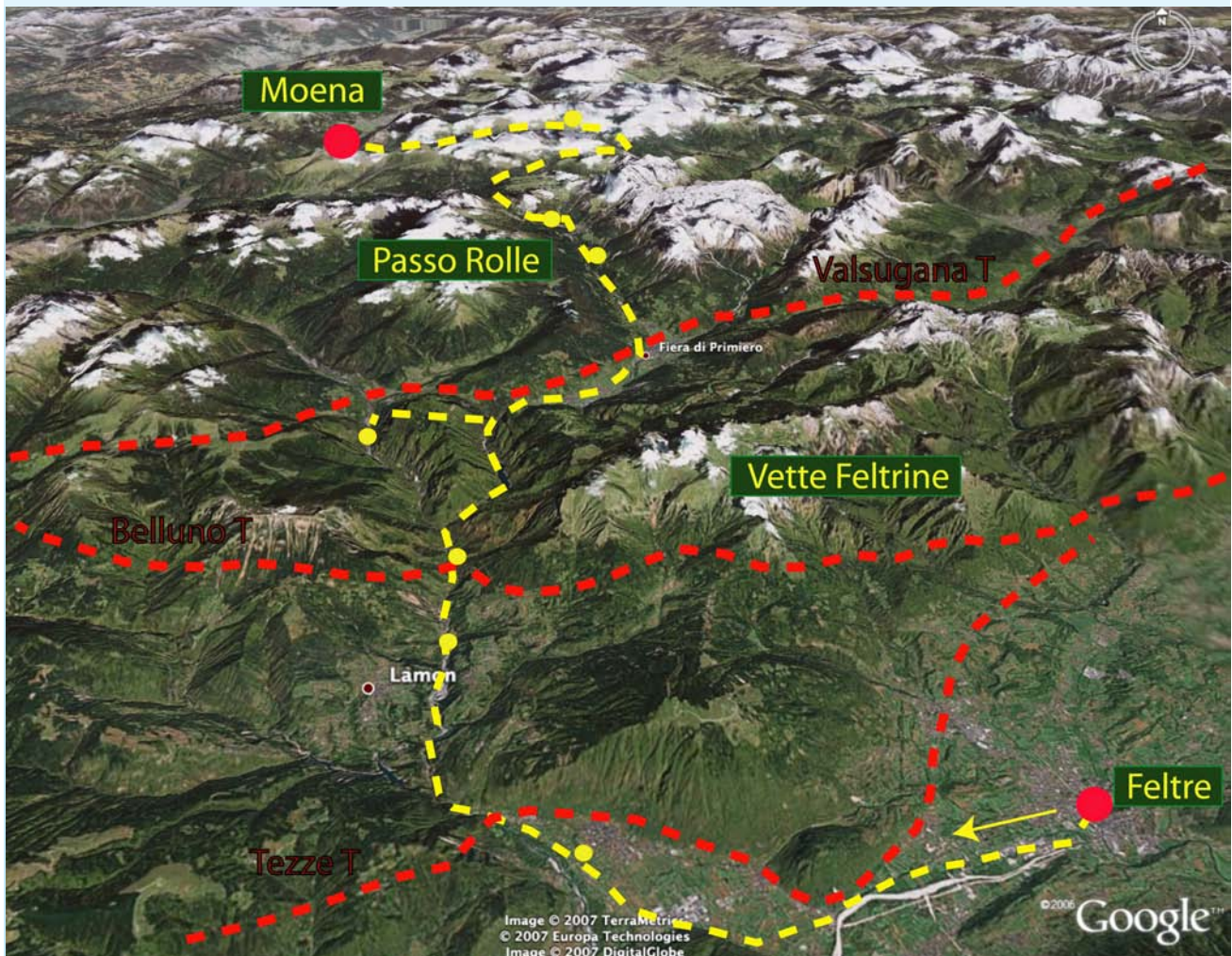


Fig. 2.0 - Itinerary: Feltre, Val Cismon, Passo Rolle, Passo Valles, Moena. Dashed red lines are the main thrusts.

Subject: Main structures of the fold-and-thrust belt, interference with the Mesozoic structures and stratigraphy

The daily excursion is a traverse through a typical cross-section of the eastern Southern Alps, characterized, in these areas, mainly by Neogene to present compressional deformation. We will observe the Tezze, Belluno and Valsugana thrusts, cropping out along the val-

ley of the Cismon river. It will be shown that the Valsugana Line inherited and cut the system of Mesozoic horsts and grabens. In the Passo Rolle area, the control of Mesozoic (both structural and stratigraphic) anisotropies on the alpine compressional tectonics can be studied in detail. Again in the Passo Rolle area we will observe one of the most evident flower structures that can be observed in the field.

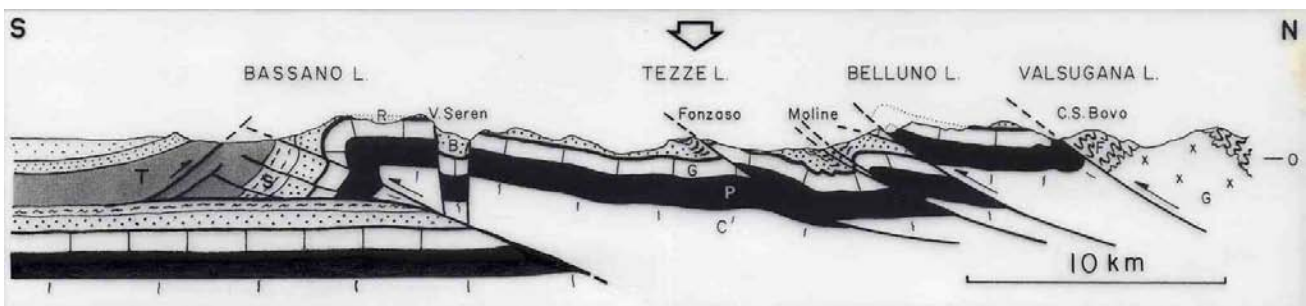
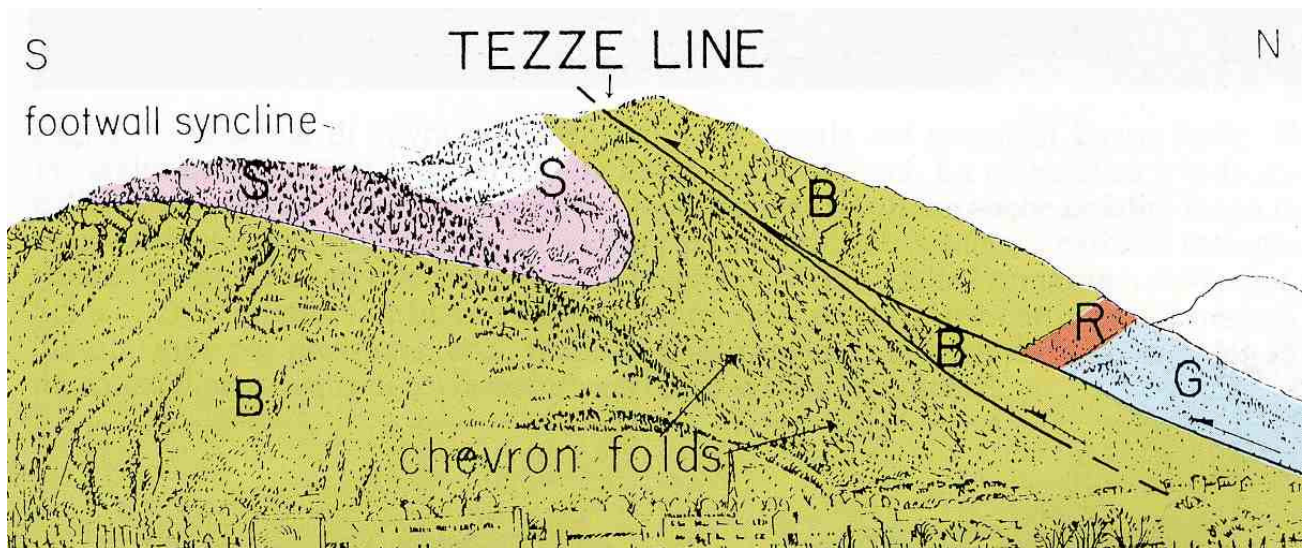


Fig. 2.1 - The Tezze thrust, near Fonzaso, west of Feltre. The syncline in the footwall suggests a fault-propagation-fold origin of the structure. Notice the chevron folds near the thrust fault. G, Calcari Grigi, Liassic; R, Ammonitico Rosso inferiore, Fonzaso Fm, Ammonitico Rosso superiore, Dogger and Malm; B, Biancone, Lower Cretaceous; S, Scaglia Rossa, Upper Cretaceous.

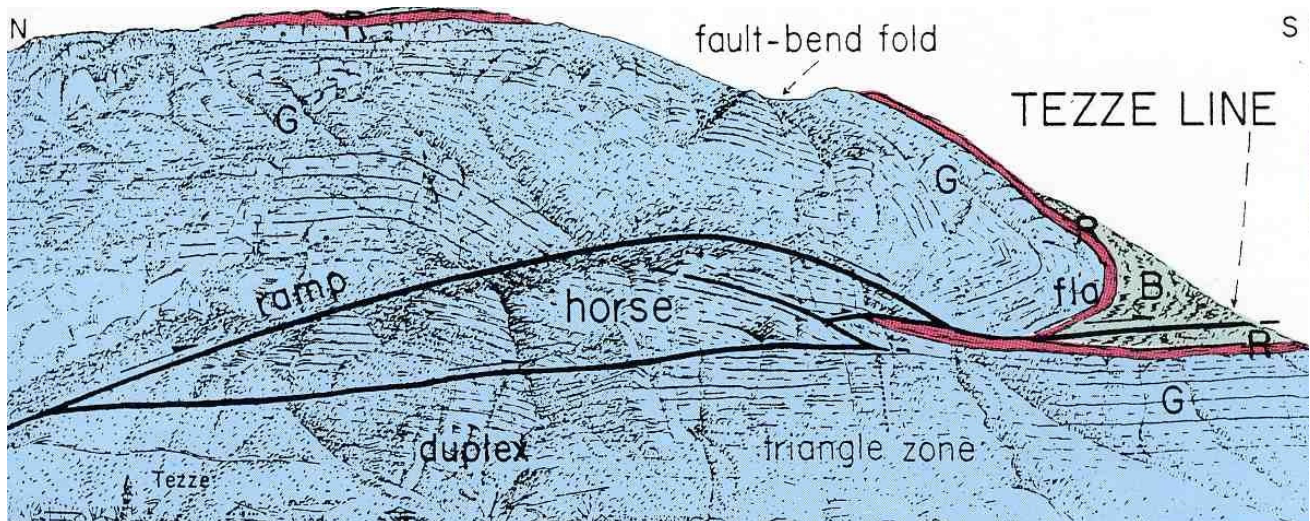


Fig. 2.2 - The Tezze thrust cropping out above the village of Tezze, in Valsugana. The frontal overturned limb of the fold suggests an origin by fault-propagation. This mechanism, however, was coupled to fault-bend folding, due to the ramp geometry of the fault in the Calcarei Grigi (G) and the flat geometry at the bottom of the Biancone (B). Ammonitico Rosso inferiore, Fonzaso Fm, Ammonitico Rosso superiore (R).

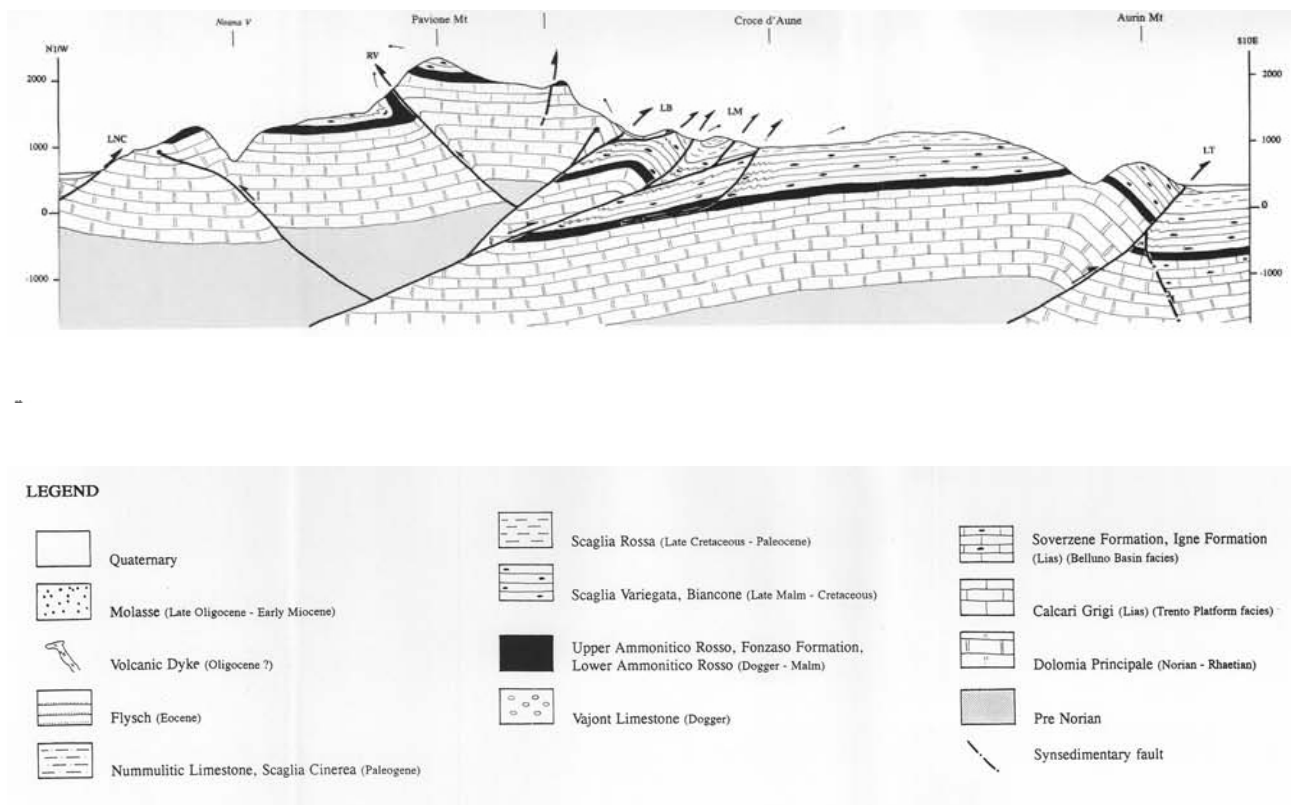


Fig. 2.3 - Cross-section of the Vette Feltrine, after D'ALBERTO *et alii* (1995).

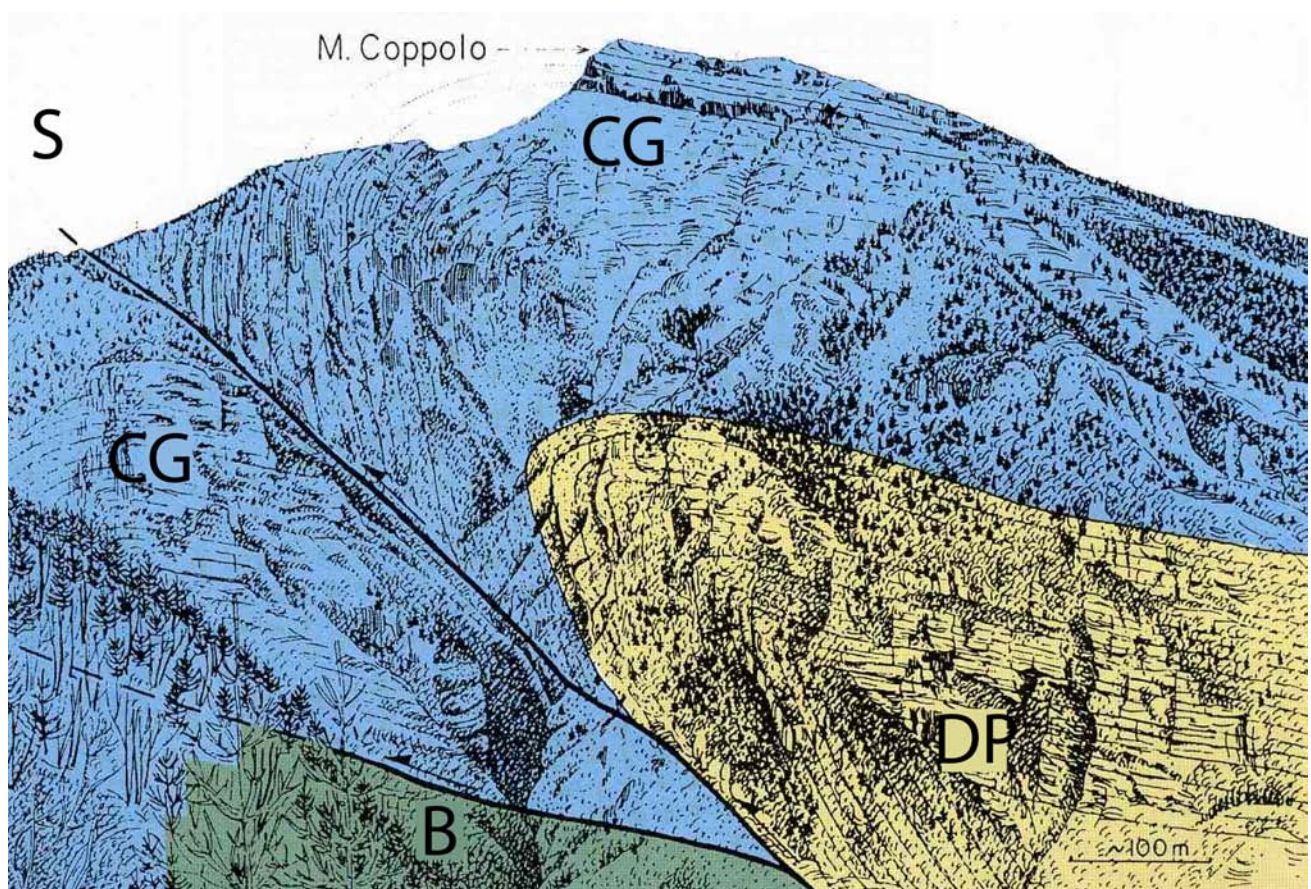


Fig. 2.4 - The Belluno thrust as it crops out along the western flank of the Cison valley. The vertical and somewhere overturned external flank of the hangingwall anticline indicates folding by fault-propagation. DP, Dolomia Principale (Norian); CG, Calcari Grigi (Lias); B, Biancone (Lower Cretaceous).

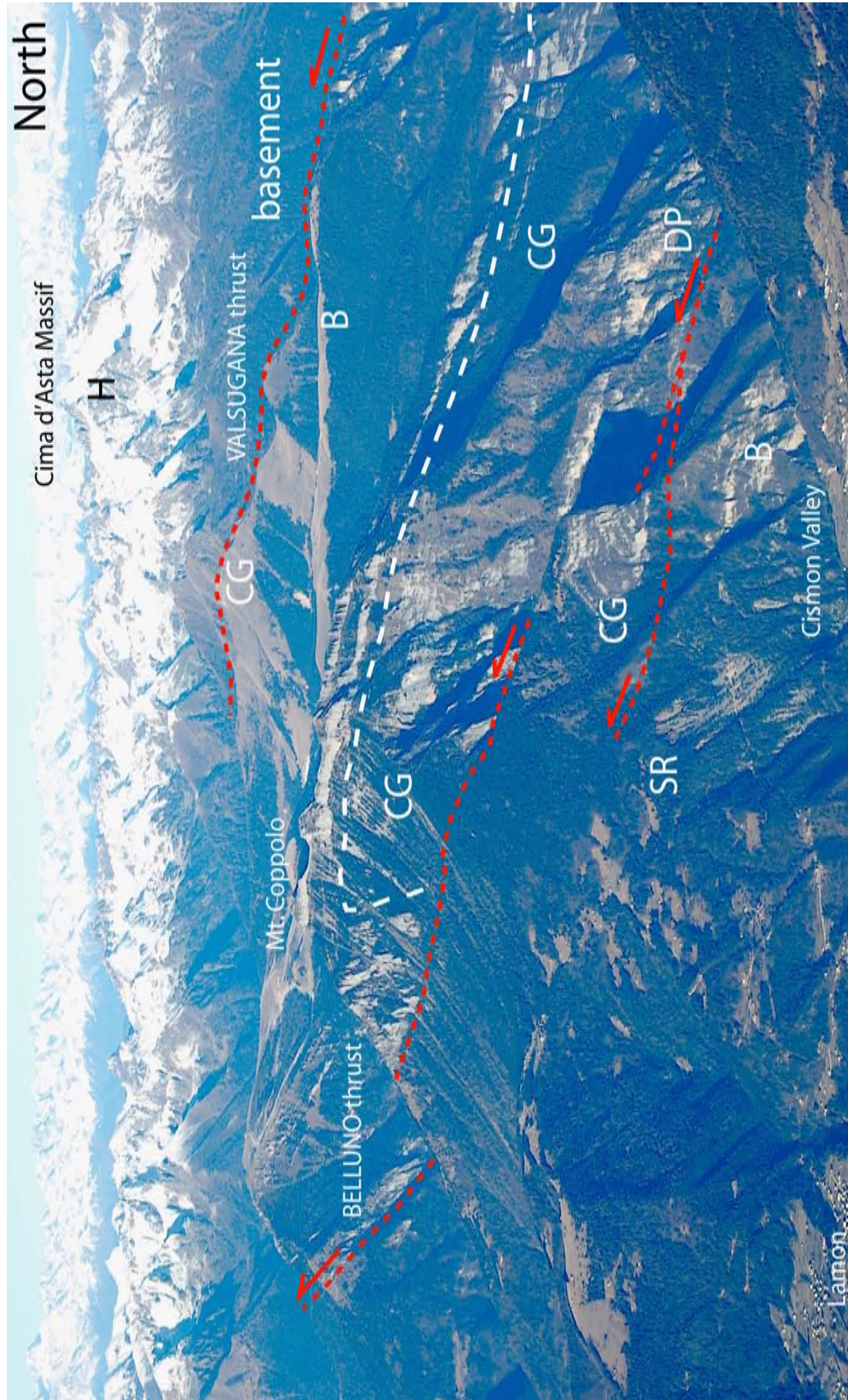


Fig. 2.5 - Same Belluno thrust as in Fig. 2.4. Note the short forelimb and the longer backlimb of the fault-propagation fold well exposed in the Coppolo mountain. To the north the Valsugana thrust where the crystalline basement outcrops in the hangingwall. H, Hercynian (Upper Carboniferous) intrusives and greenschist facies basement; DP, Dolomia Principale (Norian); CG, Calcarei Grigi (Lias); B, Biancone (Lower Cretaceous); SR, Scaglia Rossa (Upper Cretaceous).

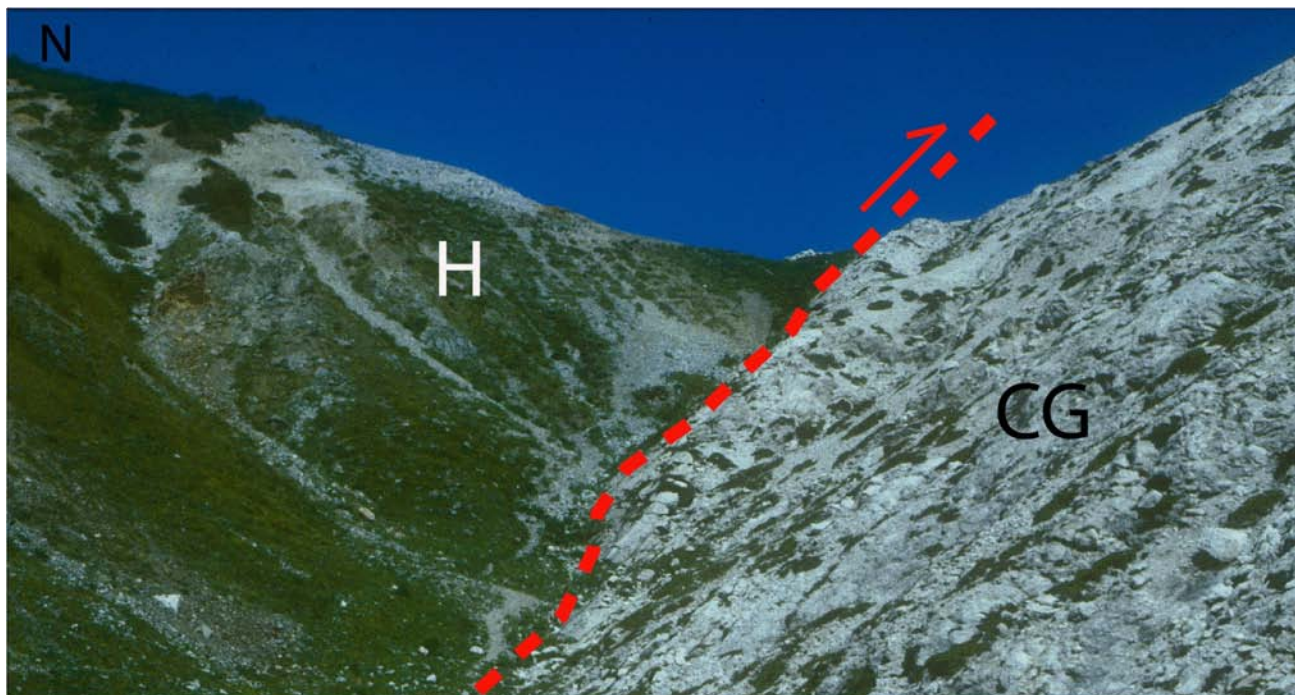


Fig. 2.6 - Valsugana thrust, north of Passo del Brocon. In the hangingwall the crystalline basement (H), here cropping out as an apophysis of the late-Hercynian Cima d'Asta granite. The basement is thrust towards the south over the Liassic Calcarei Grigi (CG).

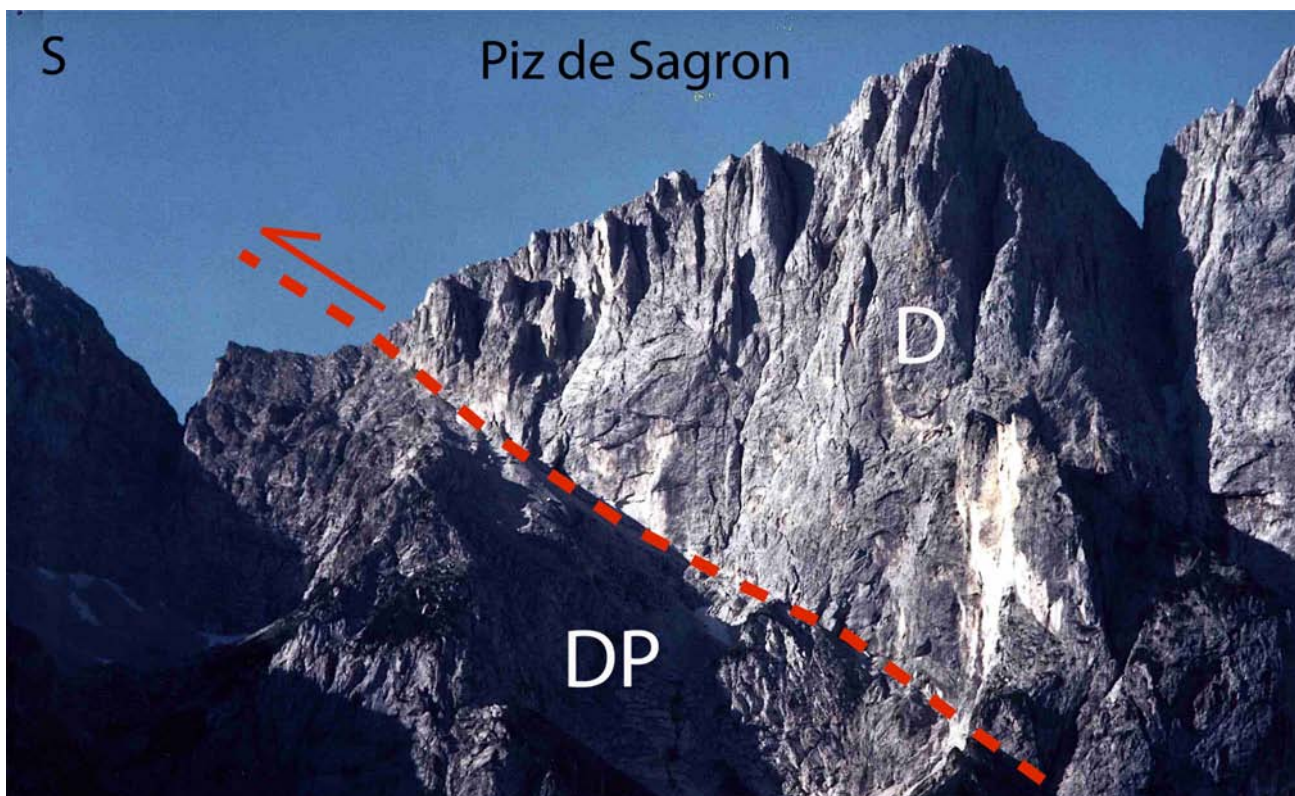


Fig. 2.7 - Same thrust as before, but more to the east: the Valsugana thrust outcrops with the Cassian Dolomite (Carnian, D) overlying the Dolomia Principale (Norian, DP).

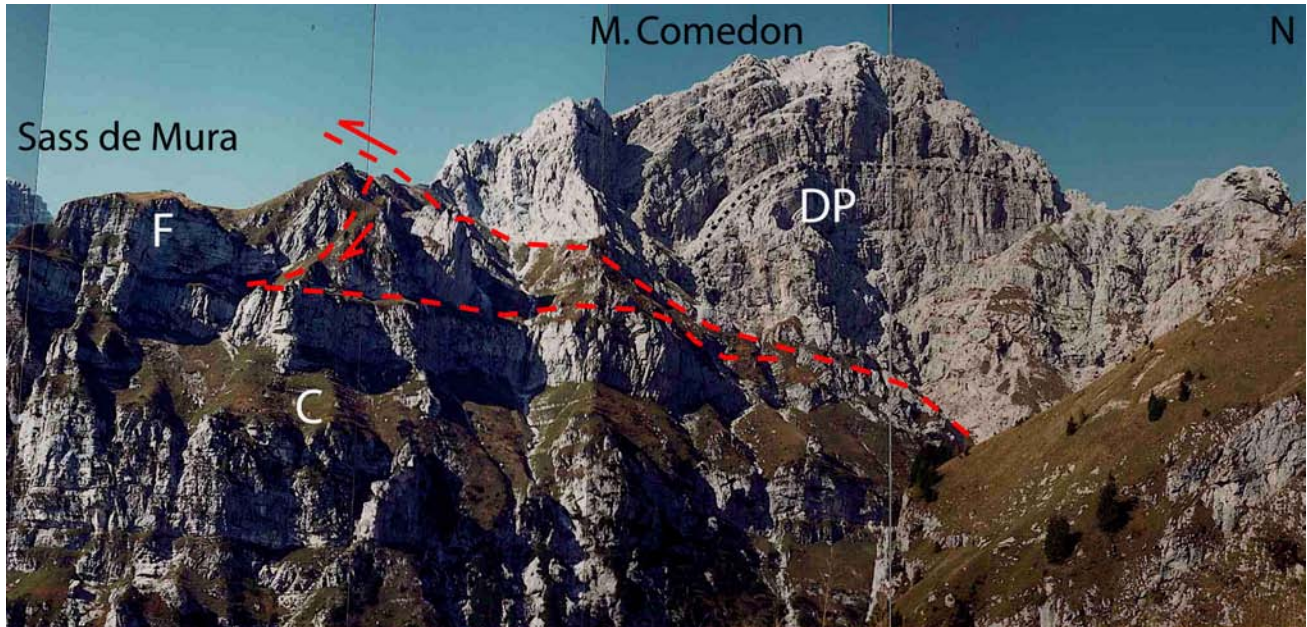


Fig. 2.8 - The Valsugana thrust in the southern cliff of the Mt. Comedon, Sass de Mura massif, Vette Feltrine. Note the triangle zone in the footwall. DP, Dolomia Principale (Norian); C, Calcarei Grigi (Lias); F, Fonzaso Fm (Dogger); Photo by Lucio D'Alberto.

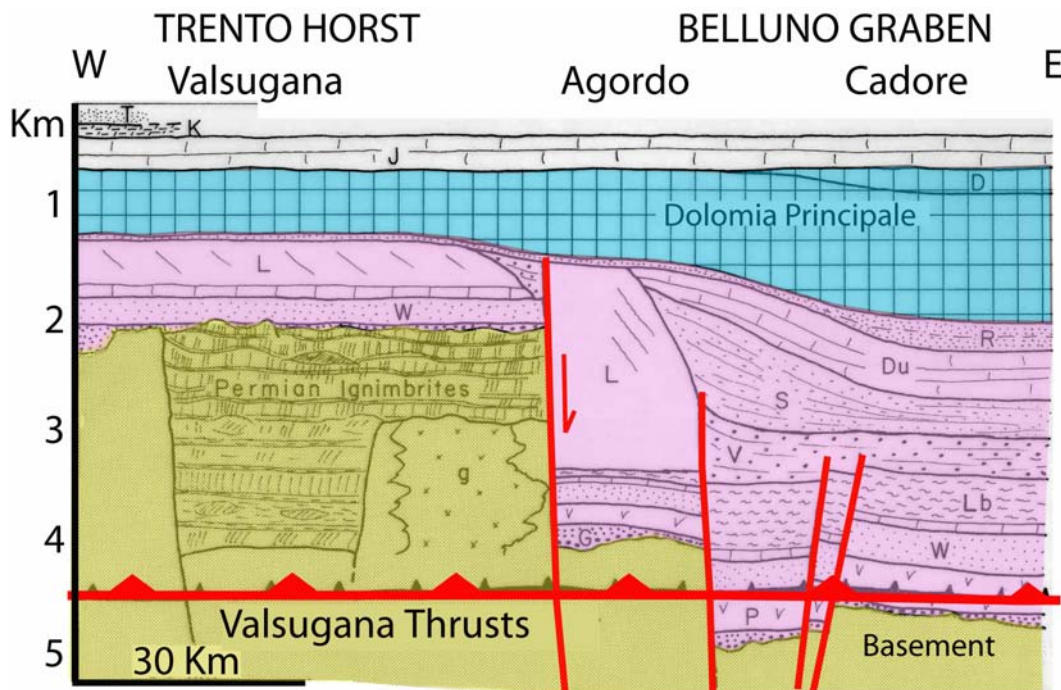


Fig. 2.9 - The Valsugana thrust cuts through inherited Mesozoic structures: the Trento (or Atesina) Platform and the Carnico-Bellunese Basin. This is evidenced by the thickness of the sedimentary cover that shows values around 2 km on the Trento horst and 4-5 km in the Carnico-Bellunese graben to the east (after BOSELLINI & DOGLIONI, 1986). The strike of the normal paleo-faults is always ca. N-S. Unlabelled yellow, crystalline basement; g, late-Hercynian granitoid; G, Gardena Sandstone (Upper Permian); P, Bellerophon Fm (Upper Permian); W, Werfen Fm (Scythian); Bricks, Anisian; L, Ladinian and Carnian carbonate platforms; Lb, Livinallongo Fm (Ladinian); V, volcanoclastic deposits (Late Ladinian); S, San Cassiano Fm (Carnian); Du, Dürrenstein Dolomite (Late Carnian); R, Raibl Fm (Late Carnian); DP, Dolomia Principale (Norian); J, Calcarei Grigi (Liassic); D, Dachstein Limestone (Rhaetian); K, Cretaceous; T, Tertiary. One of the main Mesozoic extensional faults accommodating differential subsidence between the platform and basin realms is the Passo Rolle Line, later reactivated as a transfer (mainly strike-slip) fault between the Lagorai monocline and the Pale di San Martino syncline.

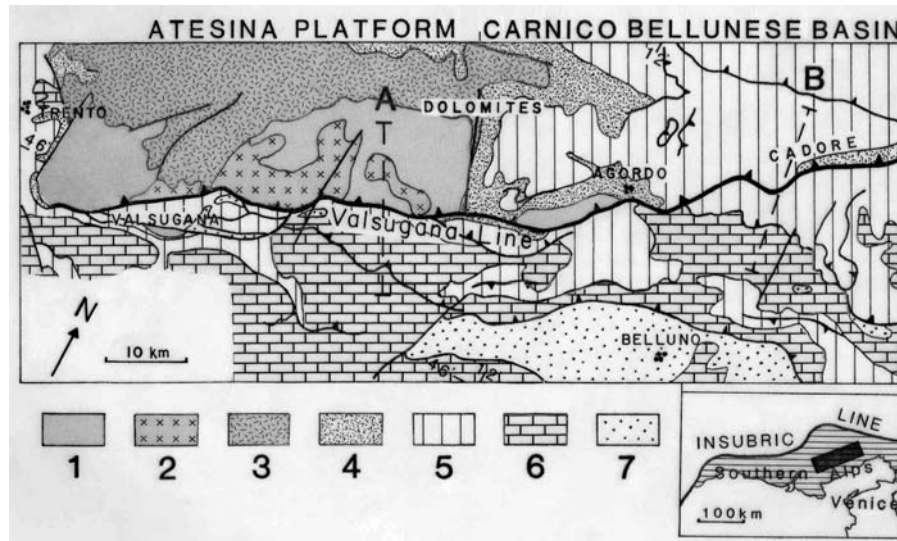


Fig. 2.10 - The Mesozoic structuration can be recognized also in geological maps that show a structural high of the basement in the hanging-wall of the Valsugana thrust between Trento and the Cison Valley, developed along the Passo Rolle Line. To the east of this lineament, the Valsugana Line cuts mainly through sedimentary cover, since this area was structurally depressed before the onset of compression. A and B are the traces of the cross sections of the next figure. 1, crystalline basement; 2, late-Hercynian granitoids; 3, Permian ignimbrites; 4, Upper Permian and Lower Triassic; 5, Upper-Middle Triassic; 6, Jurassic-Cretaceous; 7, Tertiary.

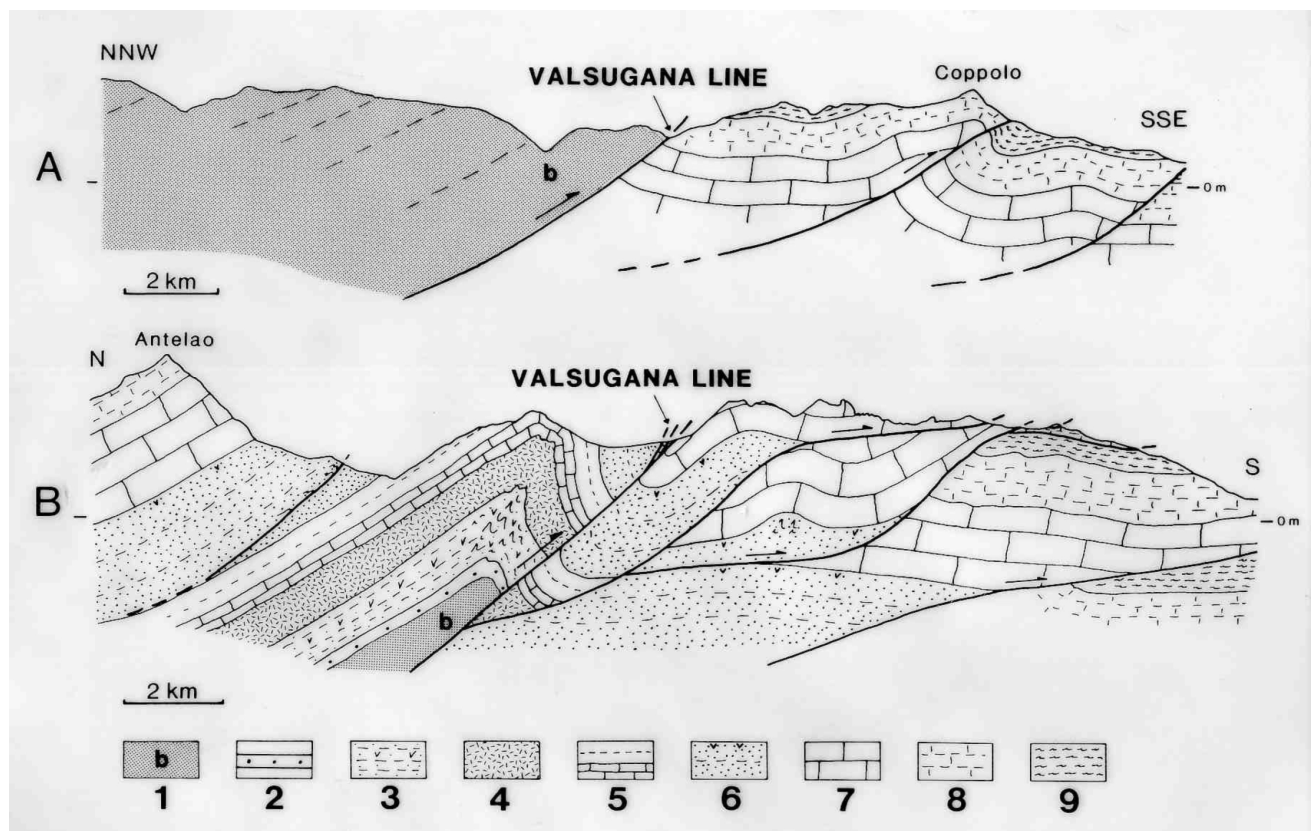


Fig. 2.11 - Geological cross-sections through the Valsugana Line: notice that along section A the basement (b) is more elevated in the hanging wall with respect to section B, although no significant differences of shortening occur between the two sections. This feature is explained by the fact that along section A the Valsugana Line cuts the horst of the Trento platform (or Atesina Platform) whereas in section B it cuts the Bellunese graben. 1, Undifferentiated crystalline basin; 2, Gardena Sandstone; 3, Bellerophon Fm; 4, Werfen Fm; 5, Anysian and Ladinian formations; 6, Carnian formations; 7, Dolomia Principale (Norian); 8, Jurassic limestones; 9, Cretaceous limestones and marls. The traces of the sections are shown in fig. 2.10.

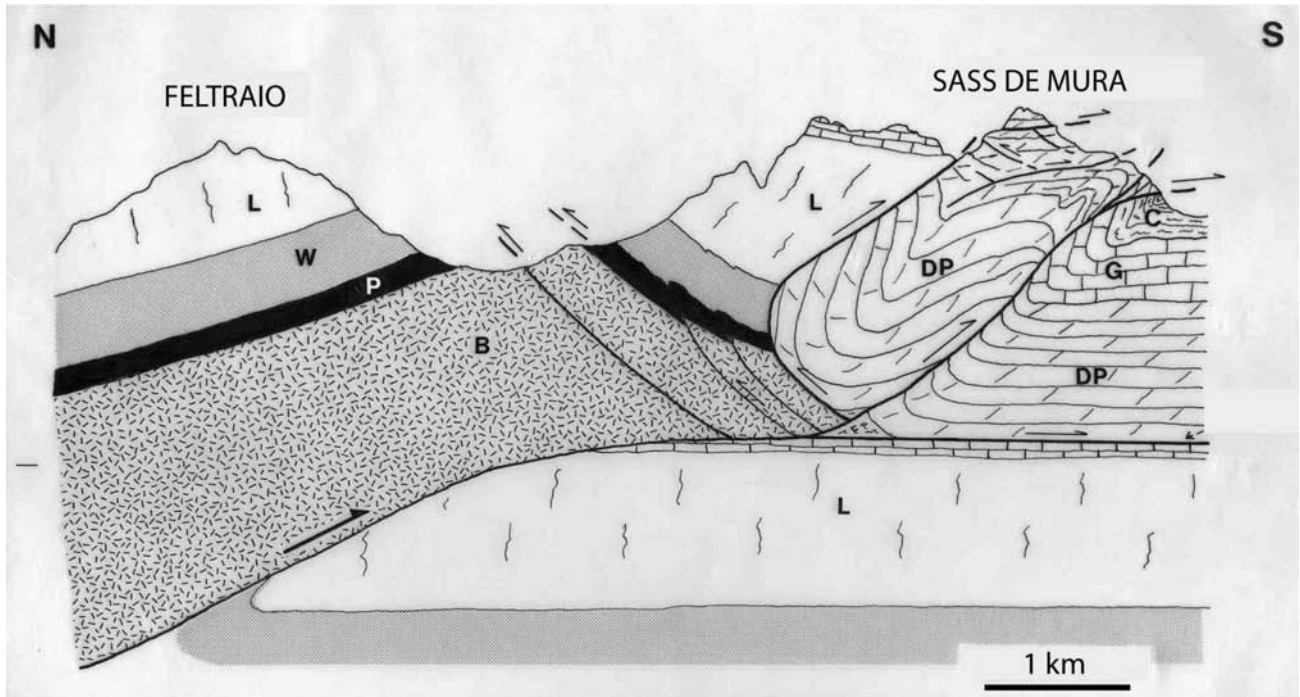


Fig. 2.12 - Cross-section across the Valsugana thrust, at the southern margin of the Dolomites, in the zone of Passo Cereda. The basement of the Dolomites (B) thrusts over and wedges within the sedimentary cover of the Venetian Prealps, developing a triangle structure. The basement shows a fault-bend-fold. The southern flank of the fold shows the Dolomia Principale (DP) wedging between the basement and Ladinian carbonates (L), generating thus another triangle structure, with the substitution of the cover at its bottom (direct contact between basement and Dolomia Principale). P, Upper Permian; W, Scythian and Anisian; G, Jurassic limestones; C, Cretaceous limestones and marls.

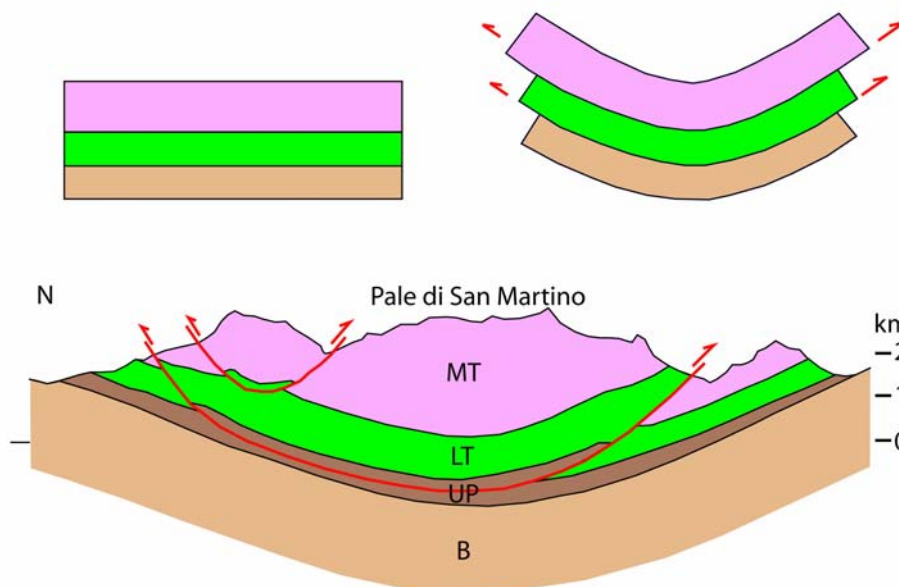


Fig. 2.13 - The Pale di San Martino are located at the core of a regional undifferentiated basement (B) syncline. The sedimentary cover accommodated the folding by flexural slip and shear, thus developing south-verging thrusts in the southern limb and north-vergent thrusts in the northern limb of the syncline. UP, Gardena Sandstone and evaporitic Bellerophon Fm (Upper Permian) which acted as a main decollement level between cover and basement (see next figure). LT, Lower Triassic; MT, Middle-Upper Triassic.

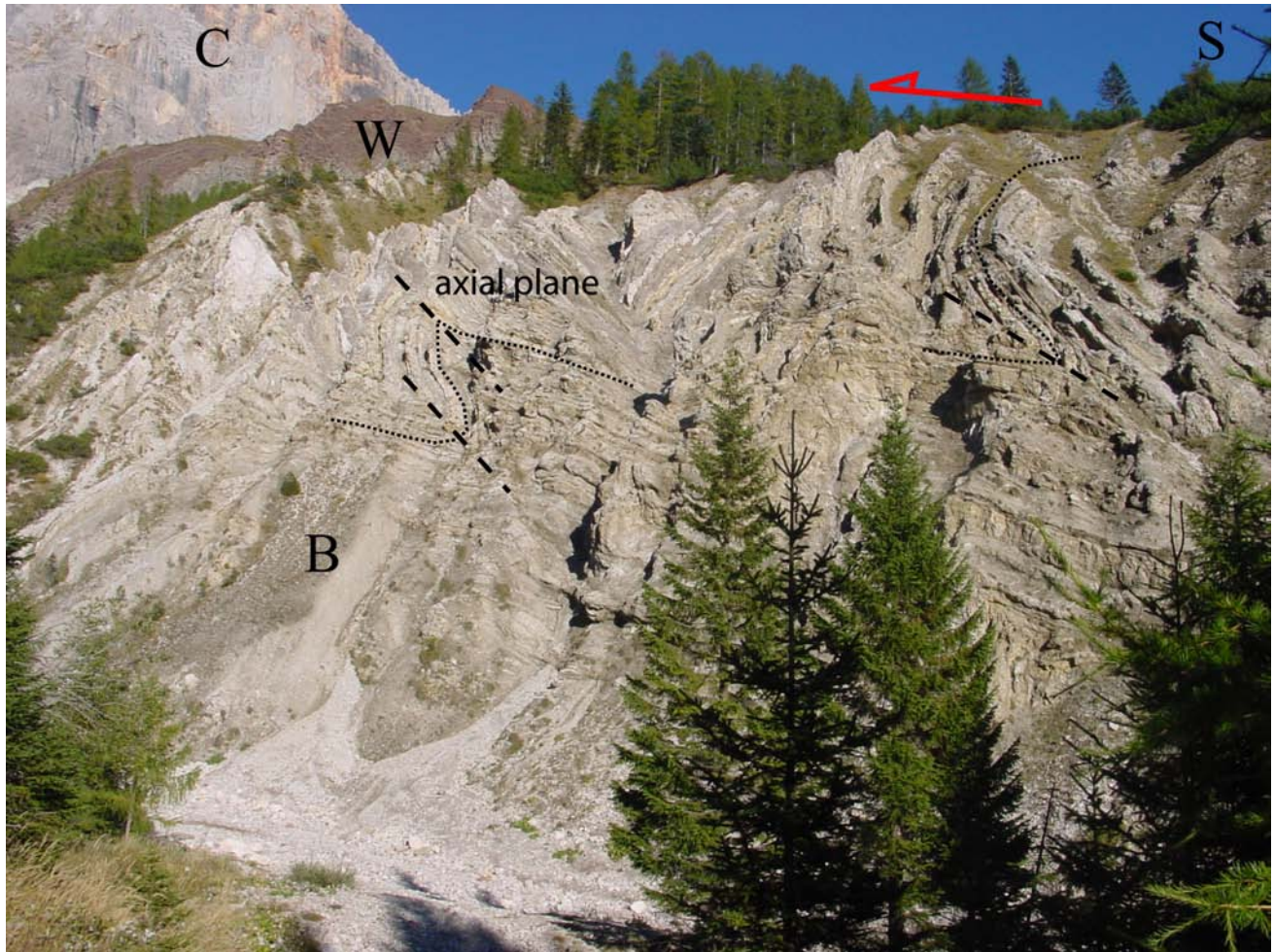


Fig. 2.14 - North-vergent en-echelon folds in the evaporitic Upper Permian Bellerophon Fm (B). The occurrence of gypsum and shales lowers the frictional resistance, thus enabling sliding. The outcrop is at the base of the Pale di San Martino massif, along the road to Passo Rolle from San Martino di Castrozza. Folds are confined within this formation made of shale, gypsum, marly limestone, and indicate a N-vergent decollement. Note the overlying unfolded Werfen Fm (W) and Marmolada Limestone (C). It testifies the flexural sliding (towards the north in this case, since the outcrop is positioned in the northern flank) of the sedimentary cover within the basement syncline.



Fig. 2.15 - Detail of the previous outcrop, Road from San Martino di Castrozza to Passo Rolle. The folds are within the Bellerophon Fm. Note the gypsum thickening in the hinge of the fold above to the left of the geologist.

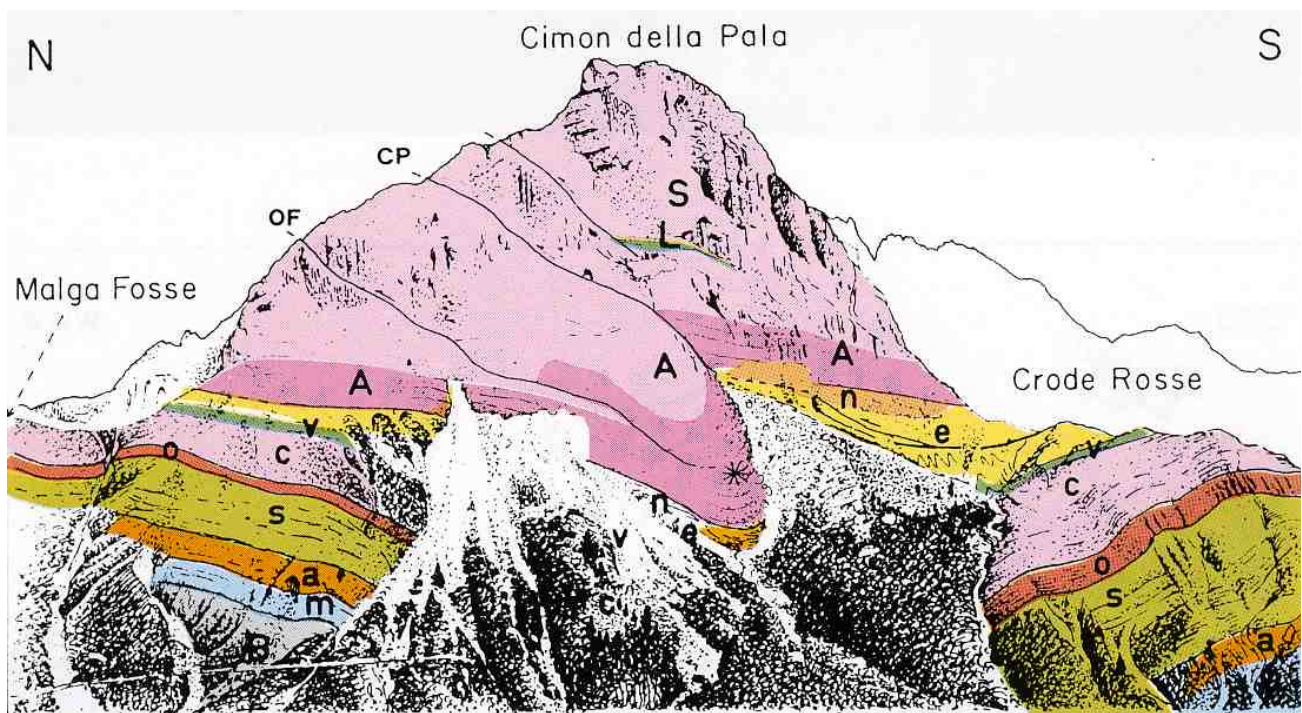


Fig. 2.16 - NW flank of Cimon della Pala massif, near Passo Rolle, at the northern margin of the Pale di San Martino regional basement syncline. Thrust faults verge northward due to the flexural sliding of the sedimentary cover accompanying the basement folding. Notice the thinning towards the left of the Werfen Fm, i.e., toward the Trento Horst: the Gastropod Oolite (o) can be taken as a reference. This layer is much thicker to the right (40 m) than to the left (20 m). Also the other members of the Werfen Fm, in particular the Siusi (s), Campil (c), Cencenighe (e) and San Lucano (n) members, show lateral variations of thickness. In the right portion of the figure, the lower section of the Cencenighe Member is characterized by evaporites (gypsum) and shales; these lithologies enabled the localization of the detachment plane of the Cimon della Pala thrust fault (CP). Where the evaporites terminate, the thrust fault is characterized by a ramp. A thrust sheet comprising the external syncline (out-of-syncline thrust, OF) characterizes the foot-wall syncline of the Cimon della Pala thrust (DOGLIONI & NERI, 1988). S, Sciliar Dolomite (Ladinian); L, Livinallong Fm (Ladinian); A, Anisian formations (lower Serla Dolomite, Voltago Conglomerate, upper Serla Dolomite, Morbiac Limestone, Contrin Fm). Werfen Fm (Scythian): n, San Lucano Member; e, Cencenighe Member; v, Val Badia Member; c, Campill Member; o, Gastropod Oolite; s, Siusi Member; a, Andraz horizon; m, Mazzin Member; B, Bellerophon Fm.

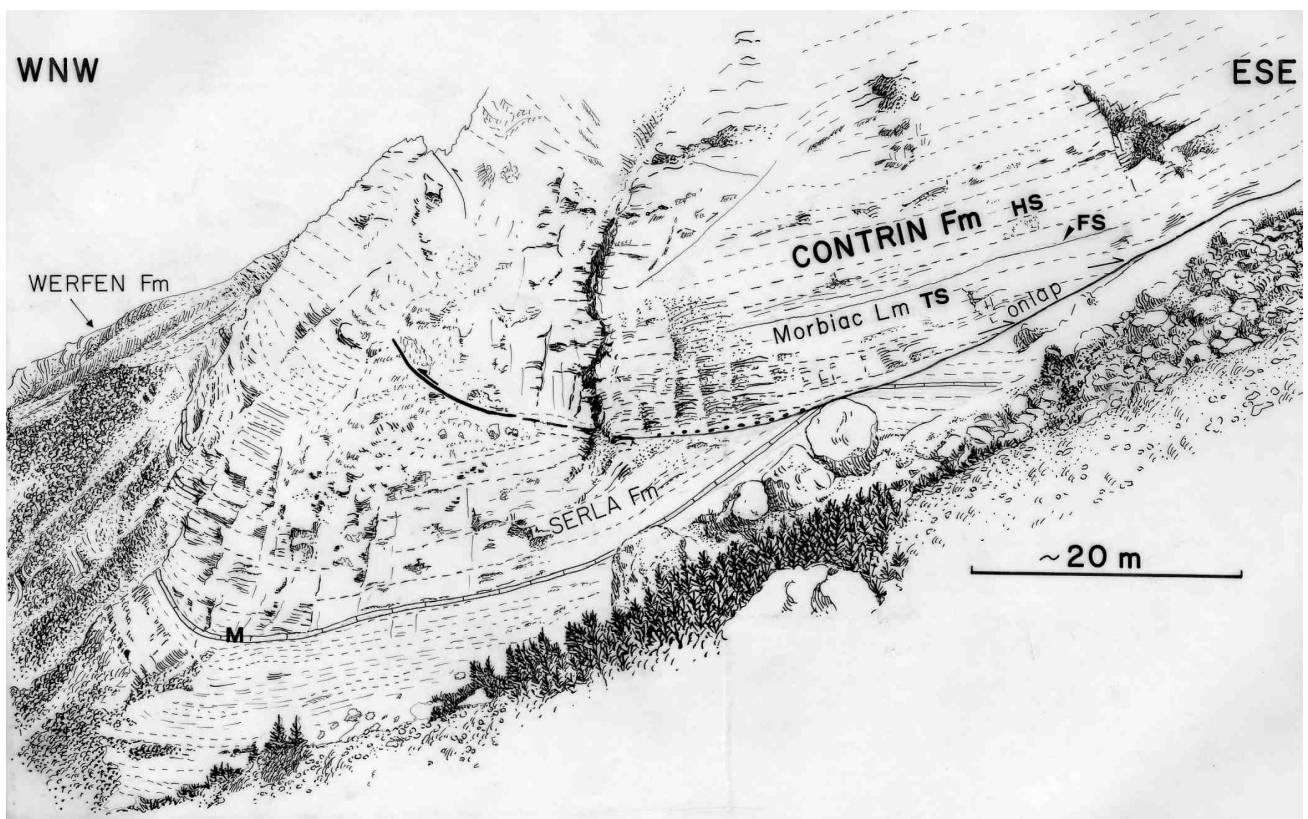
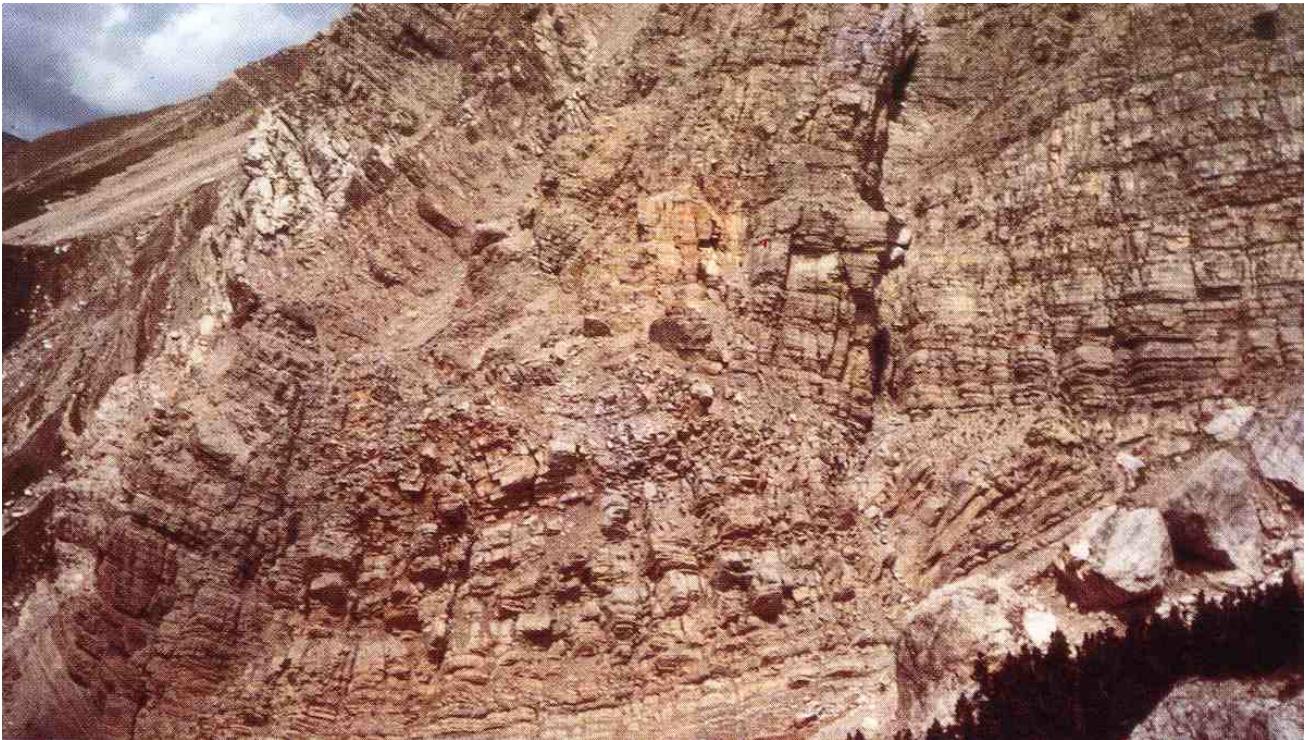


Fig. 2.17 - Geological drawing of the NW slope toe of the Cimon della Pala Mt. A N30-40°E trending anticline involving Pelsonian rocks is eroded and covered unconformably by conglomerates pockets and marly limestones of the Morbiac Limestone, which onlaps the unconformity. In terms of sequence stratigraphy we interpret the Morbiac Limestone as a transgressive system tract (TS) and the Contrin Formation as the highstand system tract (HS) of the Illyrian cycle. The boundary between the two units is the maximum flooding surface (FS). To the left the unconformity has been used as detachment plane by an out-of-syncline thrust located in the foot-wall of the Cimon della Pala thrust. M, marker bed.

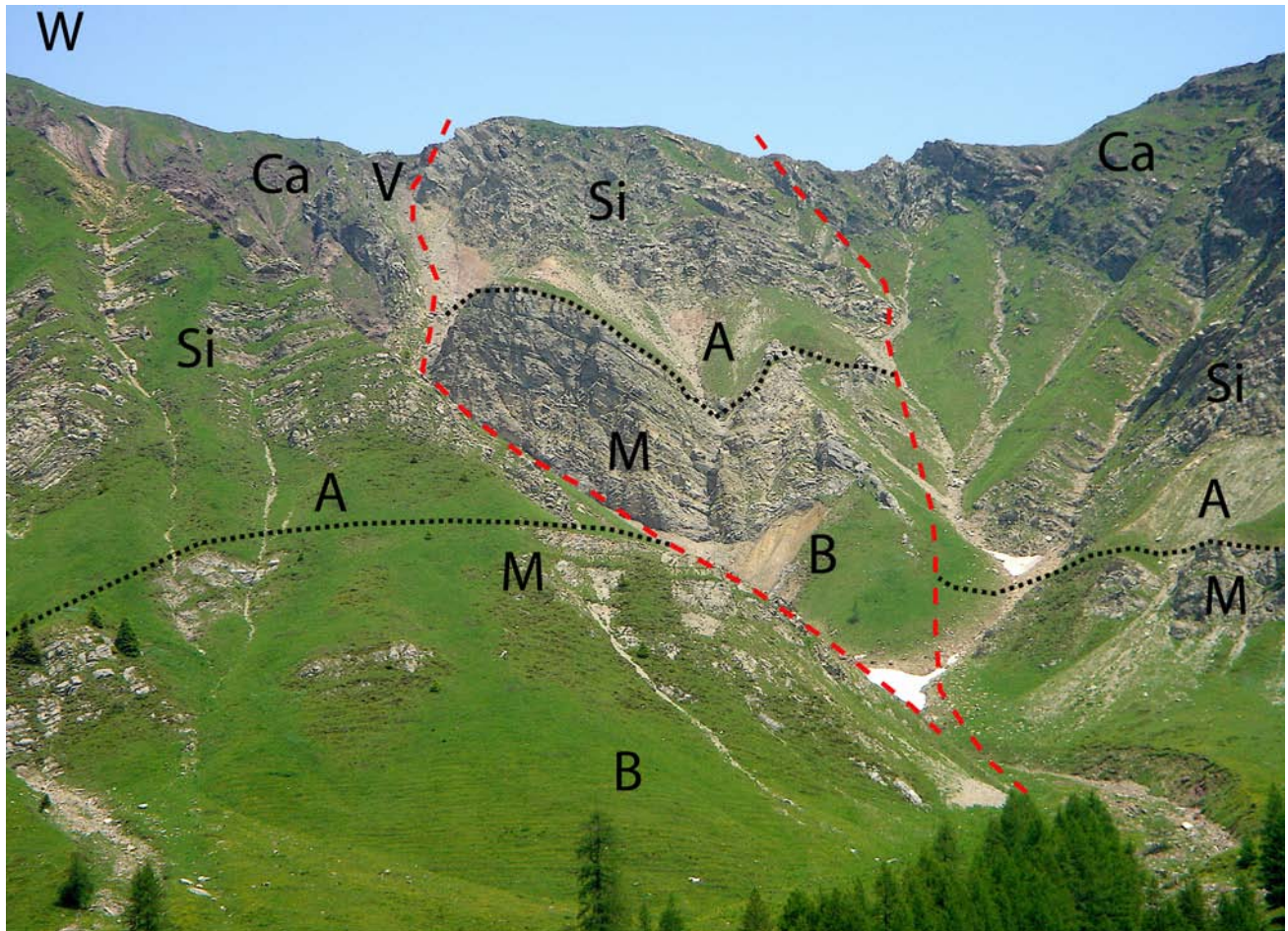


Fig. 2.18 - Positive flower structure cropping out near Passo Rolle (locality Malga Fosse). Notice the uplifted wedge between two high angle faults which branch at the bottom of the picture. The structure is oriented N5°-10°E and shows a sinistral shear. Note that moving up along the faults the undulated geometry determines either normal or reverse offset. A, Andraz horizon that, as reference level, marks the vertical throws. The outcrop shows various levels of the Werfen Fm (Scythian). At the bottom of the flower structure, the faults converge in the Bellerophon Fm (B) evaporites (Upper Permian). A dark Ladinian volcanic dyke (v) is subparallel to the western fault. Legend: M, Mazzin Member; A, Andraz horizon; Si, Siusi Member; Ca, Campil Member; V, volcanic dyke.

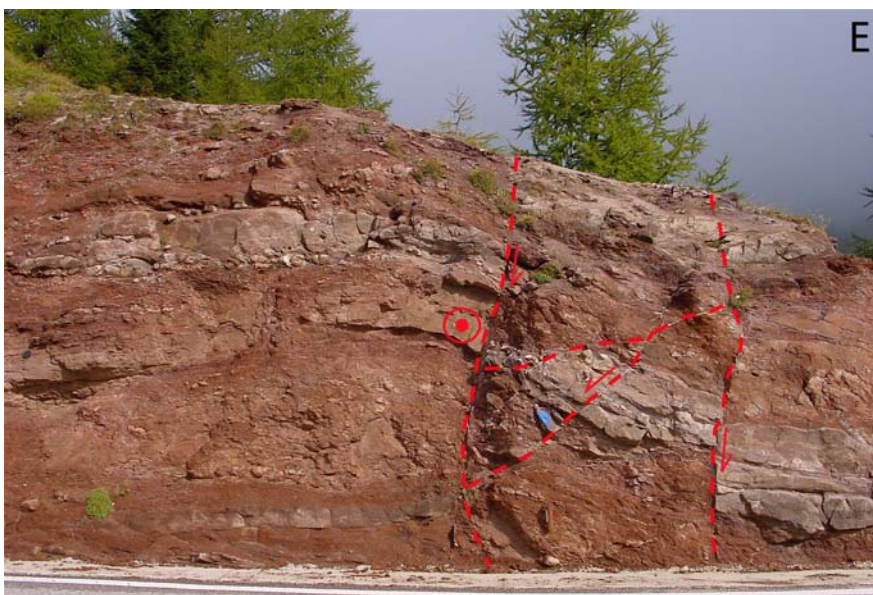


Fig. 2.19 - Upper Permian Gardena Sandstone near Malga Fosse, Passo Rolle. They represent fluvial facies reworking the underlying ignimbrites. The faults show extensional movement later reactivated into left-lateral transpression. This kinematic evolution is consistent with 1) the regional setting of Mesozoic extension between the Trento Horst to the west and the Belluno Graben to the east, and 2) the Alpine reactivation of this hinge separating the regional NNW-dipping monocline of the Lagorai massif in the hangingwall of the Valsugana Thrust with respect to the S-dipping northern limb of the Pale di San Martino syncline.

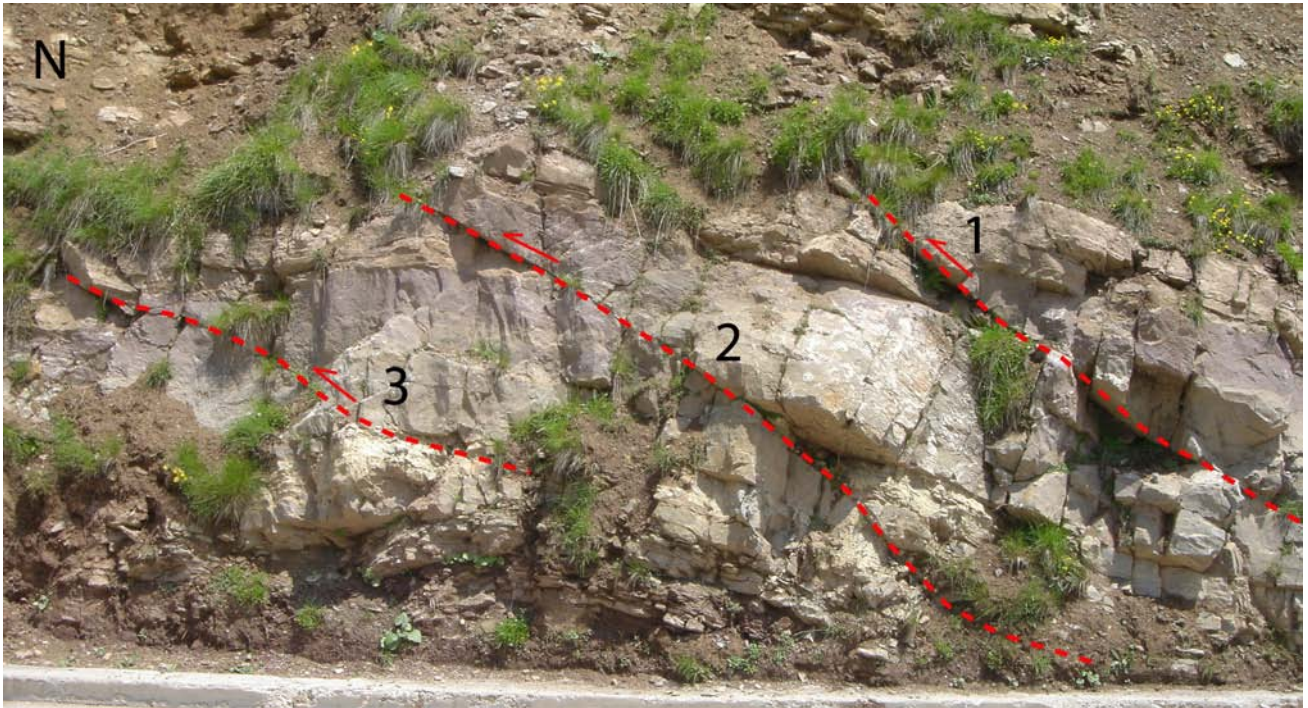


Fig. 2.20 - System of mesoscale thrust faults near Passo Rolle. The imbricated fan propagated from right to left. The kinematics are indicated by the dip of the fault planes: the fault to the right (1) is more inclined and reflects the transport along the ramp of the thrust in the middle (2). The distance among fault planes is constant since the lithologies (oolitic limestones, marly limestones and siltstones of the Siusi Member of the Werfen Fm, Scythian, Lower Triassic) cross-cut by the faults do not change laterally. Micro- and meso-structures, slickenlines, small conjugate backthrusts, pressure solution and other features make of this small outcrop a miniature of a fold-and-thrust belt such as the Southern Alps.



Fig. 2.21 - A Ladinian latit-basaltic dyke at Passo Rolle cross-cutting the Upper Permian Gardena Sandstone. The alpine deformation concentrated in the dyke where mesoscale N0-10° trending left-lateral strike slip faults can be observed.

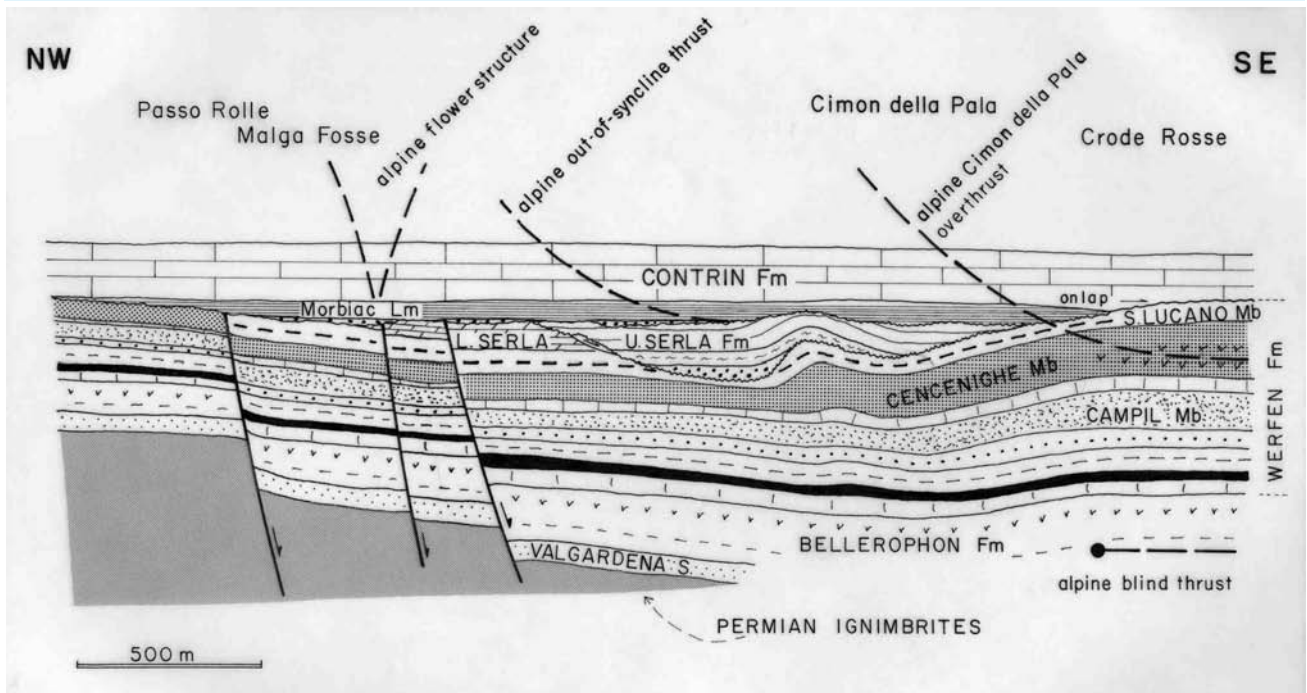


Fig. 2.22 - Geological reconstruction of the Passo Rolle area in the Anisian. Notice that the area is located in the tensional hinge zone between the Trento Horst and the Belluno Graben. This is evidenced by the occurrence of the extensional fault system of the Passo Rolle Line, by the thinning of the Scythian and Anisian formations and, at places, by the lack of some levels of the series towards the north-west (DOGLIONI & NERI, 1988). The Anisian unconformities are sutured by late Anisian formations. The alpine compressional deformation inherited this complex architecture: for example, the thrust fault of the Cimon della Pala becomes horizontal in the evaporitic level of the Cencenighe Member. The flower structure of Malga Fosse (Fig. 2.18) is probably related to sinistral transfer motions along the Passo Rolle Line and re-sheared a Mesozoic tensional structure. Moreover, the Upper Permian Bellerophon Fm is characterized by a blind thrust that generated an accommodation fold in the overlying cover, now visible between Crude Rosse and Malga Fosse.



Fig. 2.23 - The about N-S trending Cismon Valley, with the Passo Rolle at its head, is the seat of normal faults separating the Trento Horst and the Belluno Graben to the east. Since the Permo-Triassic thickness of the sedimentary cover in the Trento Horst is about half (2 km) of the cover to the east, this supports a long lasting history of this hinge, acting as one of the major hinge zones during the Tethyan rift. During the Alpine shortening, the hinge was reactivated as a left-lateral strike-slip transfer zone. In the hangingwall of the Valsugana thrust, to the west the basement dips steadily northward about 30°, parallel to the deep thrust plane. To the east, the basement and the cover are folded within the Pale di San Martino syncline.

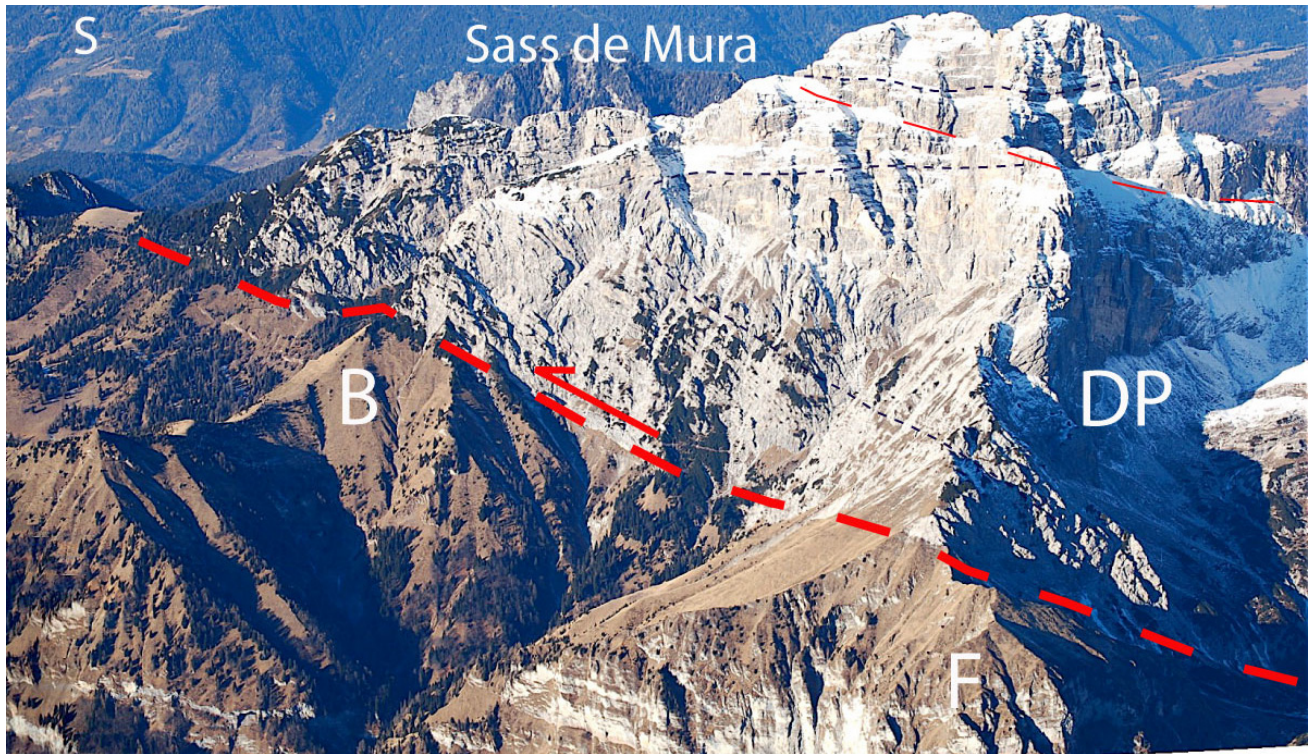


Fig. 2.24 - South of the Pale di San Martino, the S-verging Valsugana thrust carries the fault-propagation fold of Norian Dolomia Principale (DP) over the Lower Cretaceous Scaglia Variegata, Biancone (B) and the Middle-Upper Jurassic Fonzaso Fm (F). Note the long overturned forelimb.

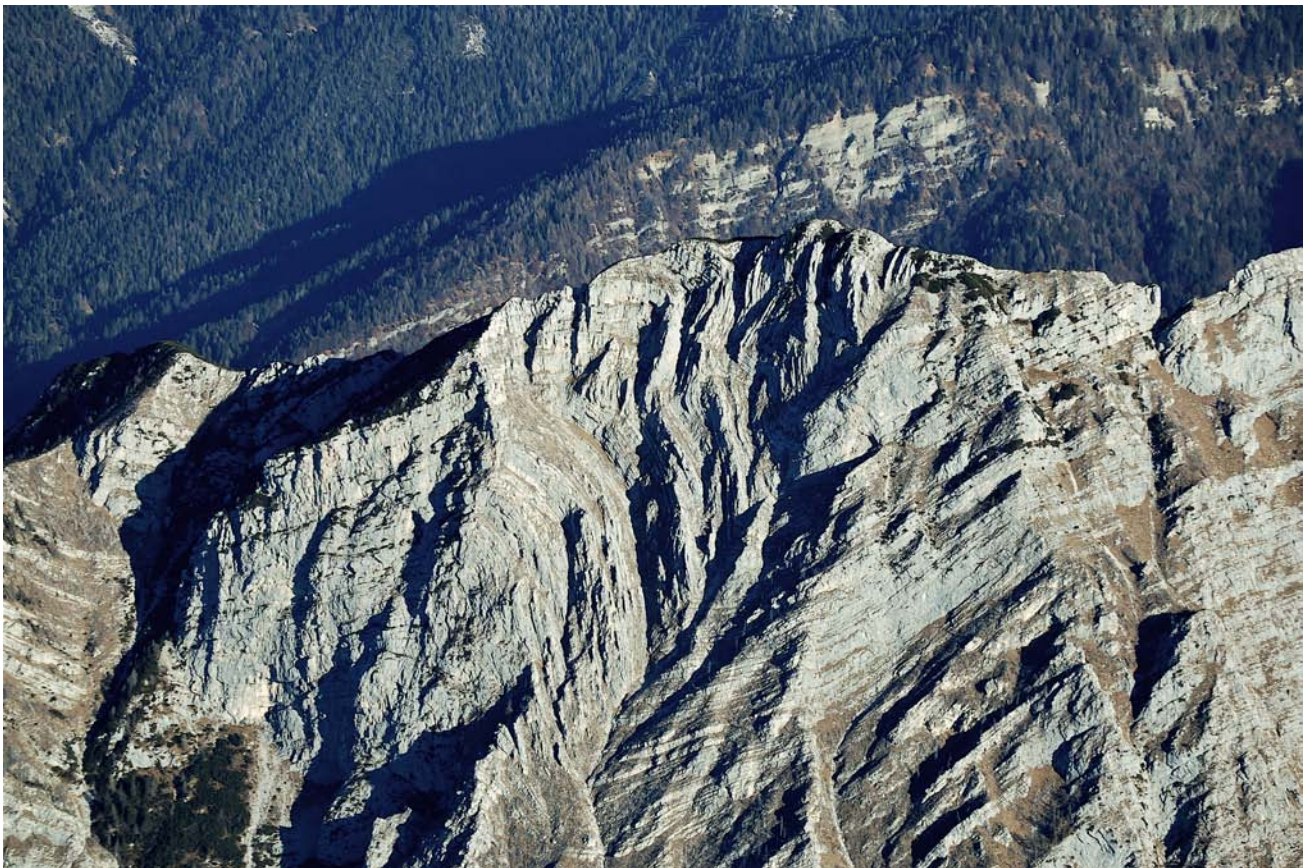


Fig. 2.25 - Valsugana thrust footwall syncline affecting Liassic Calcarei Grigi, south of Agordo in the Mt. Cielo.

3rd Day

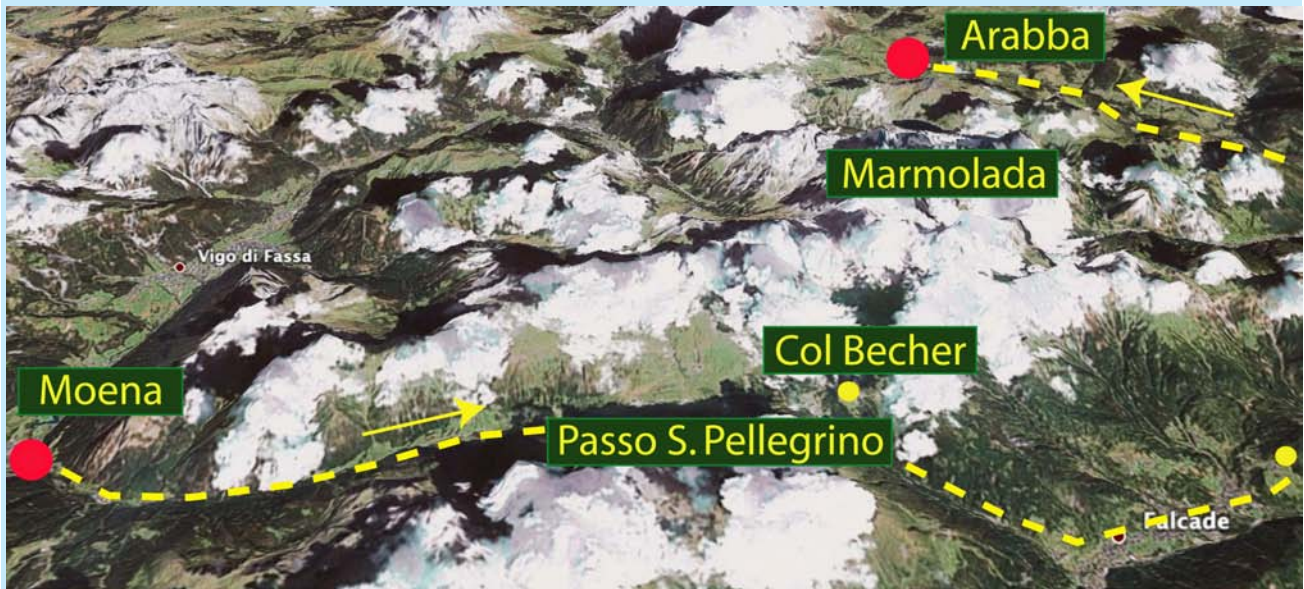


Fig. 3.0 - Itinerary: Moena, Passo S. Pellegrino, Avoscan, Arabba

Subject: Transpressional Triassic tectonics and related diapiric structures

The Dolomites are crossed by an important structural alignment involving the basement oriented N70°-90°E consisting, from west to east by: the Stava Line, the Trodena Line, the Cima di Bocche anticline and the fault system that truncates the anticline to the north and continues, with the same orientation, towards the eastern Dolomites. This alignment is cut by the Ladinian intrusive bodies of Predazzo-Monzoni and deforms all the succession up to the Lower-Middle Ladinian, thus suggesting a Middle Triassic age. Volcanic dykes cutting folds and upper Ladinian volcanoclastic conglomerates unconformably deposited on folds and thrusts confirm the Triassic age of an important deformation phase in the

Dolomites. The alignment is characterized by high angle to subvertical faults with both normal and reverse kinematics. Additional structures related to this tectonic phase are en-echelon thrust faults (Costabella, Marmolada, Col Rodella and Livinallongo valley) and diapiric structures triggered by transpressional tectonics within the basin with, at the core, the evaporitic facies of the Permian Bellerophon Fm piercing the sedimentary cover right above the structural alignment cutting the basement. The most significant structures are located in the Col Becher, Val San Nicolò, Passo Selle and Avoscan areas. The flower structures along the Stava Line-northern flank of the Cima Bocche anticline alignment and various other en-echelon structures indicate a transpressive sinistral motion. Along the alignment, narrow and elongated depressions limi-

ted by high angle reverse faults (e.g., Passo San Pellegrino) can be observed, together with long and narrow uplifted blocks (Monte Rocca). Both these structures are referred to strike-slip zones. In the Triassic rocks of the Dolomites, extensional syn-sedimentary faults oriented N-S coexisting with above described strike slip tectonics can be also observed. These extensional tectonics are consistent with the occurrence of 1-2 km thick carbonate platforms of Middle-Upper Triassic age that required a comparable subsidence for their deposition. This amount of subsidence cannot be accommodated in a compressional or transpressional environment. The transpressional structures, moreover, are localized to very limited areas and are confined to the north and to the south by sinistral transpressional shear zones oriented N70°-90°E.

This favors an interpretation of such compressional areas as local push-ups. The geological significance of these tectonics has been long disputed through the years. A first interpretation suggests the development of an aborted

rift to explain the considerable Middle Triassic subsidence and its cessation in the Upper Triassic (BECHSTADT *et alii*, 1977).

A second hypothesis explains the Middle Triassic compressional structures and the calcalkaline shoshonitic magmatism with the existence of a Middle Triassic subduction zone (CASTELLARIN *et alii*, 1979). A further scenario suggests a continuous rifting from Permian to Lower Cretaceous, with a strong continental extensional crisis in the Middle Triassic. The cause of this rifting (either backarc extension or linear Atlantic-type rifting) is unclear. According to some researchers, the calcalkaline chemistry of the Triassic magmatism could reflect an Hercynian inheritance in the mantle. It remains open the possibility of a west-dipping subduction (localized in the area of Hungary?) generating calcalkaline magmatism, backarc extension and local transpressional zones. A present-day example is the Tyrrhenian Basin, where, at the eastward margin, local transpressional structures have been described.

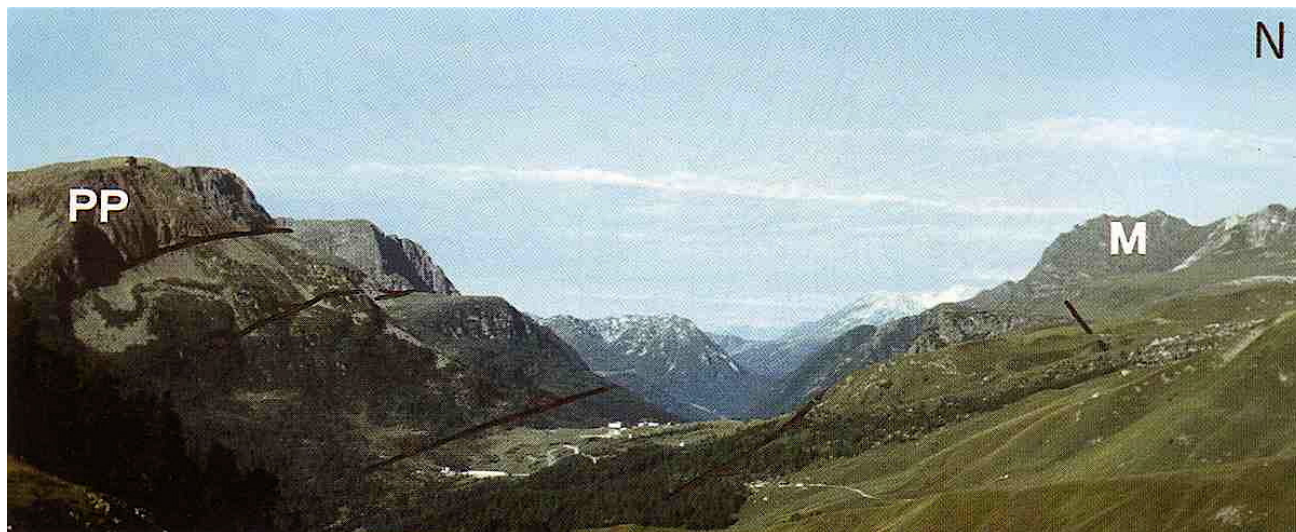


Fig. 3.1 - View towards the west of the northern flank of the Cima Bocche (the mountain in the left part of the picture) anticline, characterized by the outcrop at its hinge of Permian porphyroids (PP). The fold is truncated along its northern flank by N70°E reverse subvertical faults belonging to the Stava Line-Cima Bocche anticline structural system. In the foreground, Passo San Pellegrino (where Permian porphyrites and minor Gardena Sandstone rocks crop out) is located in the structural depression. In the background, along the alignment, Passo Feudo (Fig. 3.2) can be observed. The Upper Ladinian Monzoni intrusives (M) were emplaced along the sinistral transpressional alignment. These can be recognized by the dark color, and crop out to the right of Passo San Pellegrino, confirming the Middle Triassic age of structures in this area.



Fig. 3.2 - Passo Feudo, along the Stava Line, west of Predazzo. A latitic-basaltic dyke (V) of upper Ladinian age cuts chevron faults developed in the dark limestones of the Upper Anisian Moena Fm (Mo), dating to the Middle Triassic the age of deformation.

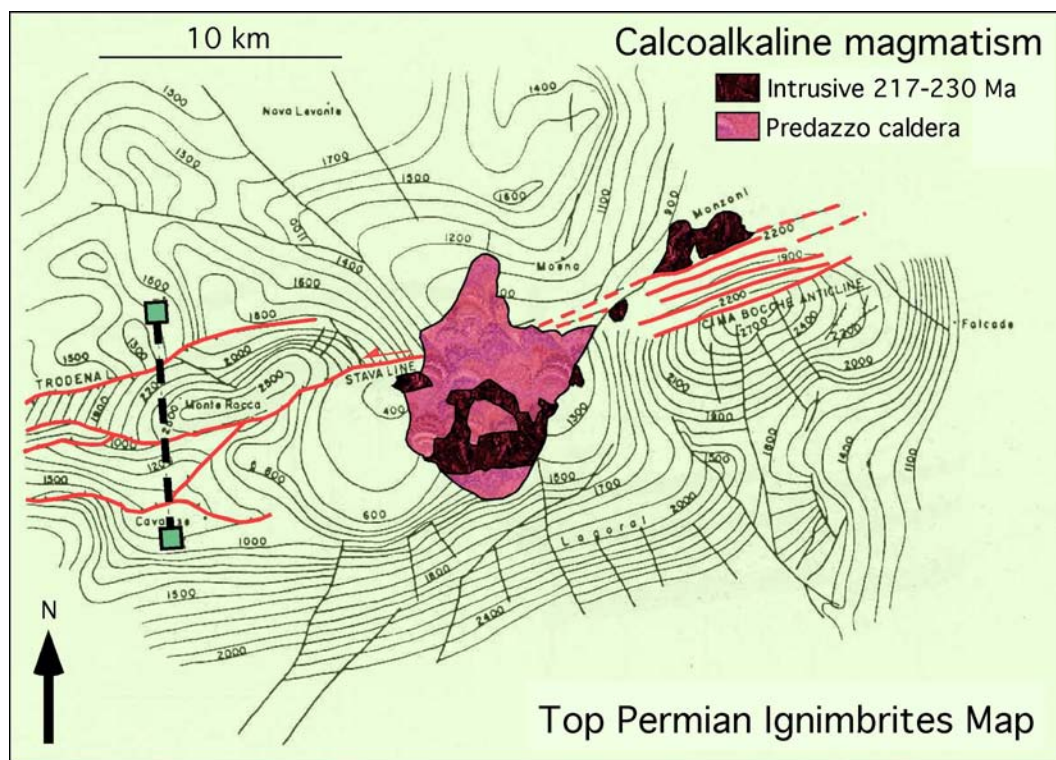


Fig. 3.3 - Morphological map of the basement (top of the Permian porphyrites) in the central-western Dolomites. The contour lines (every 100 m) are referred to the mean sea level. Notice that the northern flank of the Cima Bocche anticline is truncated by a fault system that seems to continue, to the west, in the Trodena and Stava Lines (Monte Rocca structure, Fig. 3.4). The motion along the alignment is sinistral transpressive. The Upper Ladinian-Lower Carnian(?) plutonic bodies and the Predazzo caldera cut, and therefore date this N70°E alignment (Stava Line-northern flank of the Cima Bocche anticline) that deformed sedimentary rocks up to the upper Ladinian. Notice that volcanism also developed along the alignment. In the left part of the figure, the opposite vergence of the Stava and Trodena Lines can be observed. Such opposite vergence has been interpreted as the result of a flower structure. The thick dashed line is the trace of Fig. 3.4).

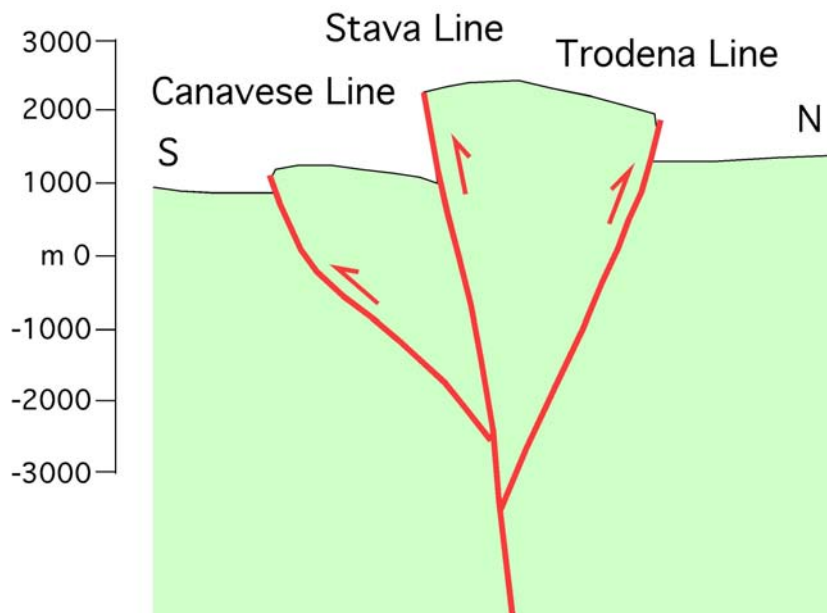


Fig. 3.4 - Approximately N-S sketch profile across the undifferentiated basement (including the Permian porphyrites) about 12 km west of Predazzo: the Monte Rocca structure is a positive flower structure, triggered by sinistral transpression along the Triassic N70E° Dolomitic alignment.

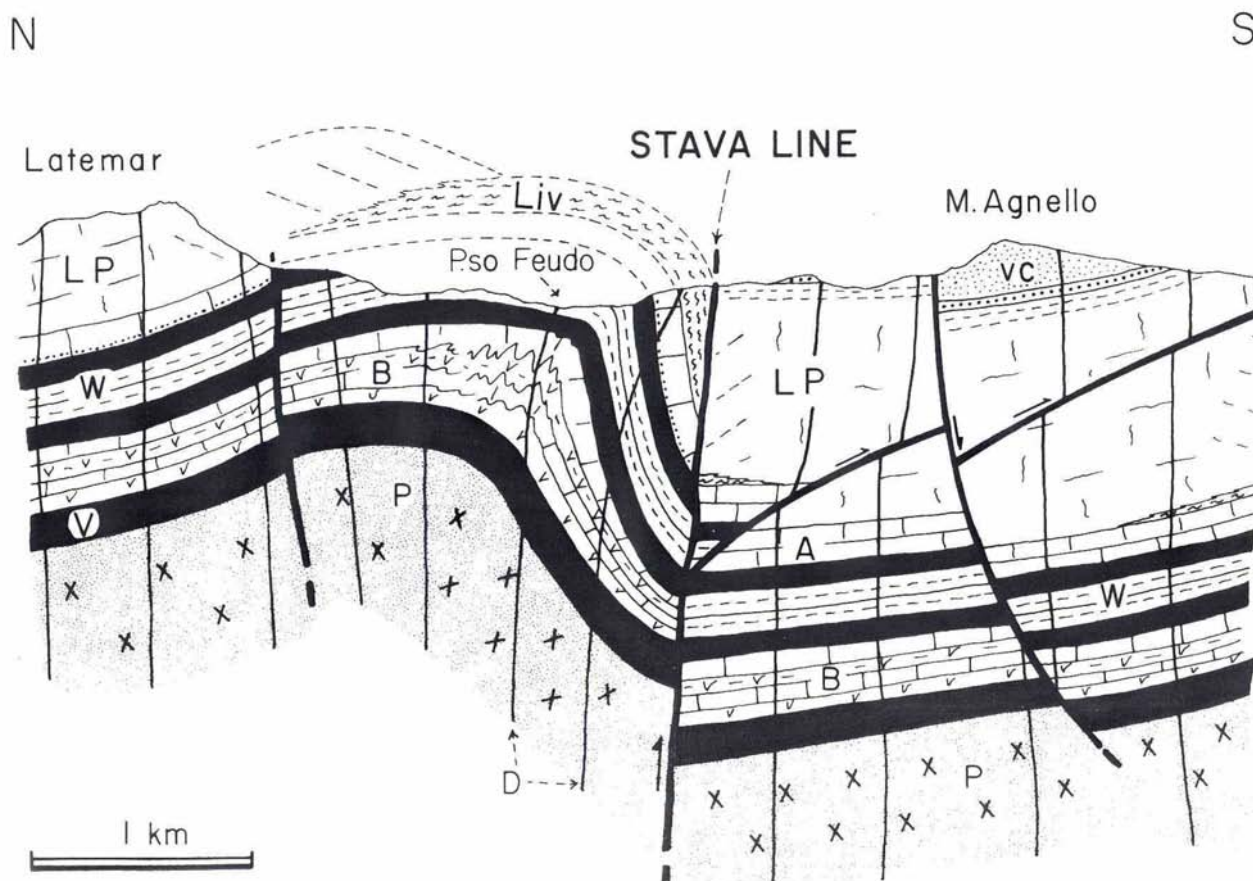


Fig. 3.5 - Cross section through the Stava Line, near Passo Feudo, west of Predazzo. The section is evidently not-retrodeformable in two dimensions. This suggests strike-slip kinematics for the Stava Line. Notice the subvertical geometry of the Livinallongo Fm (Liv) tectonically in contact with the Monte Agnello subhorizontal carbonate platform sediments (LP). LP, Sciliar Dolomite and Latemar Limestone (Ladinian); Liv, Livinallongo Fm (coeval Ladinian basinal facies); D, Ladinian volcanic dykes; VC, Upper Ladinian lavas and volcanoclastic deposits; A, Upper Anisian: Moena Fm north of the Stava Line, Contrin Fm and Serla Dolomite south of the line; W, Scythian Werfen Fm; B, Upper Permian Bellerophon Fm; V, Upper Permian Gardena Sandstone; P, Permian Ignimbrites. Numerous volcanic dykes are not represented.

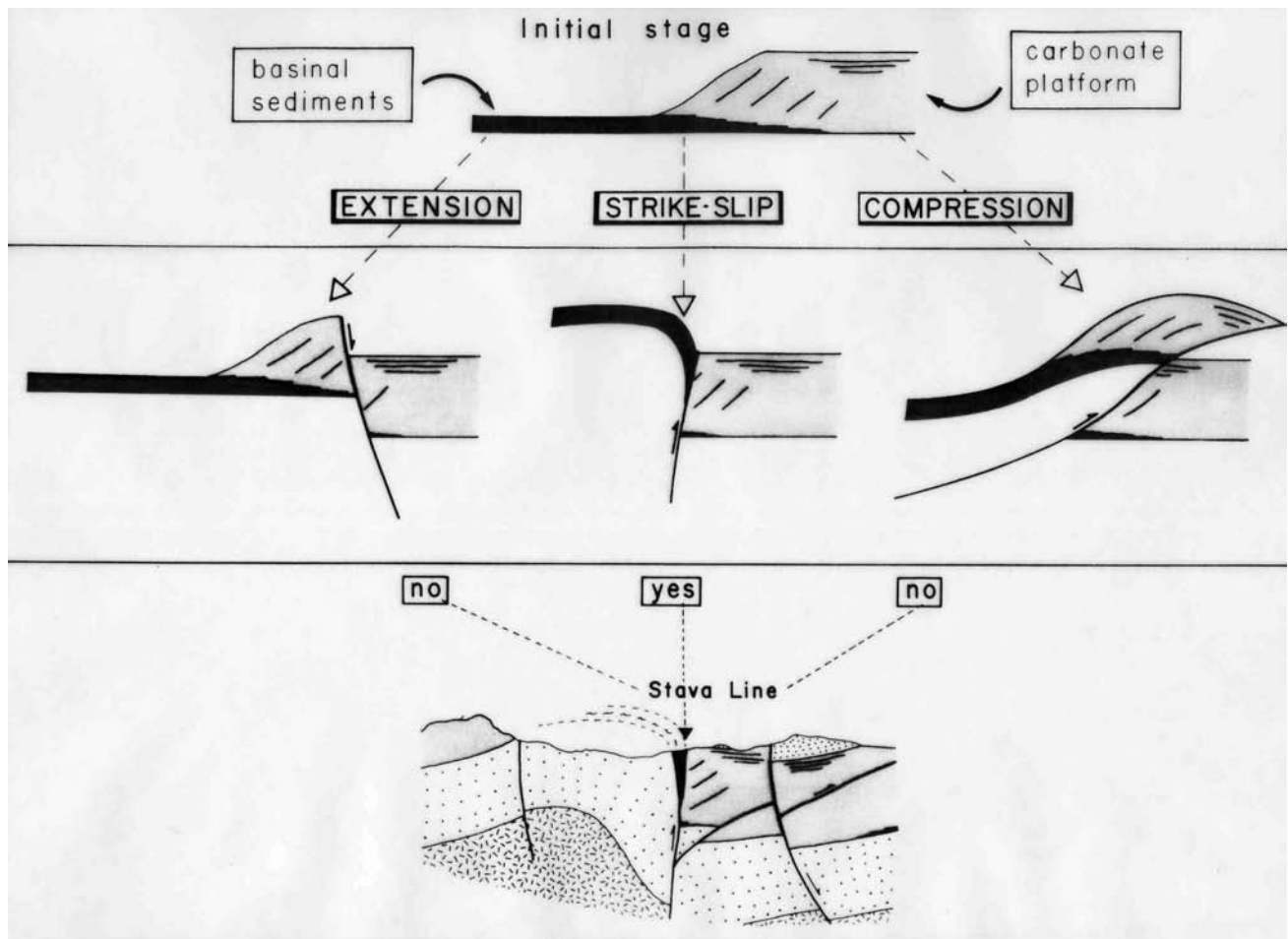


Fig. 3.6 - Scheme illustrating that both extensional and compressional deformation affecting a platform-basin system can be retro-deformed, contrary to strike-slip motions, as seen for the Stava Line, near Passo Feudo (Fig. 3.5). Notice that in the strike-slip panel the toe wedge of the carbonate platform is missing.

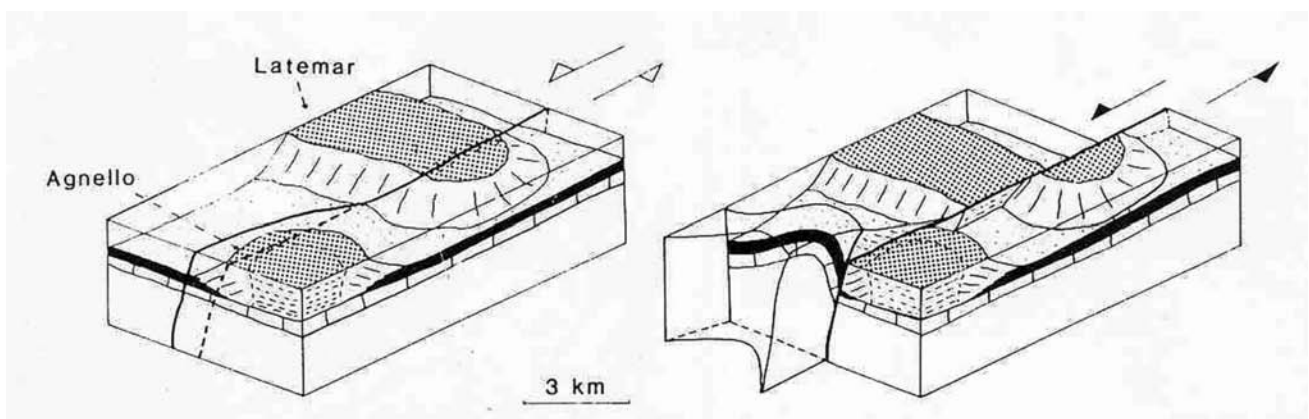


Fig. 3.7 - Reconstruction of the Monte Agnello and Latemar carbonate platforms before the strike-slip motion occurred along the Stava Line and of the volcanic event that cut the Stava tectonic alignment. North is to the left.

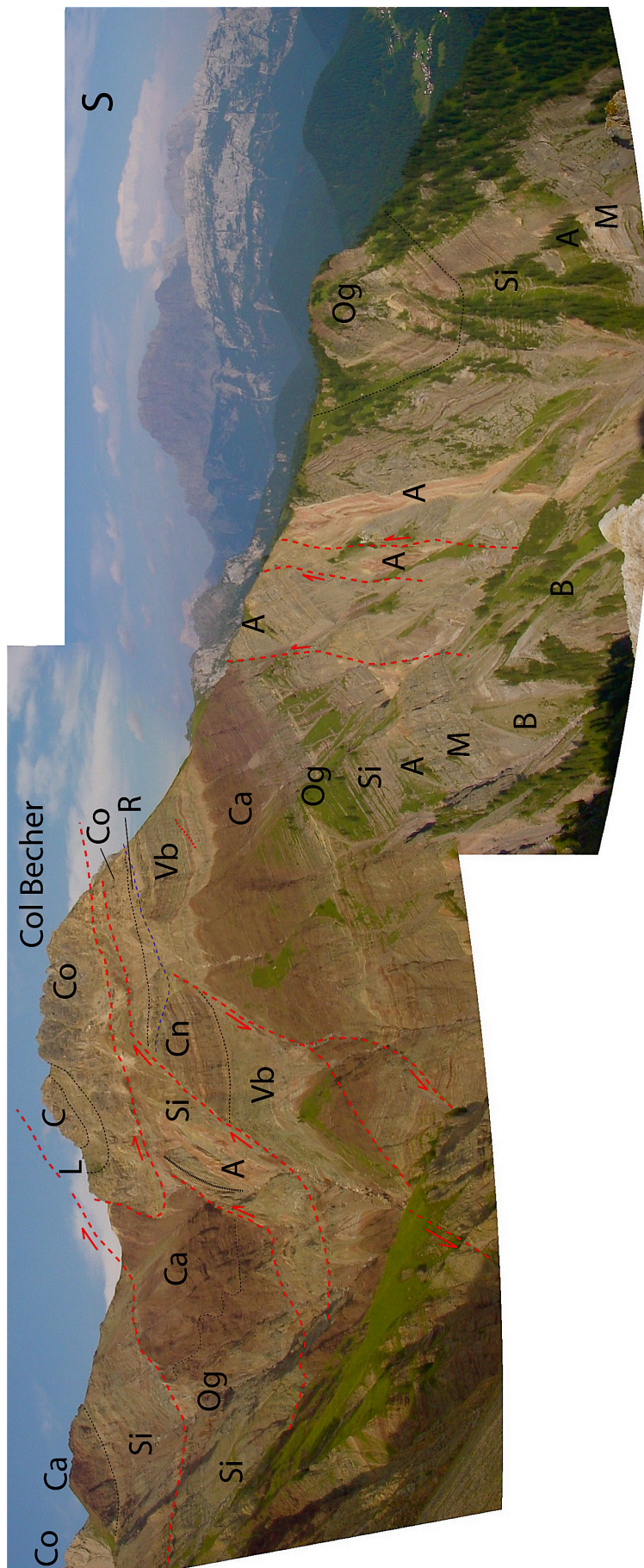


Fig. 3.8 - The Col Becher is one of the most impressive and original outcrops of the Dolomites from a structural geology point of view, near the San Pellegrino Pass. The picture was taken from the west. A diapiric structure triggered by the Bellerophon Fm evaporites (not cropping out) intrudes the Werfen Fm. Legend, Ladinian: C, Marmolada Limestone; L, Livinallongo Fm; Upper Anisian: Co, Contrin Fm; R, Richthofen Conglomerate; Scythian: Werfen Fm: Cn, Cencenighe Mb; Vb, Val Badia Mb; Ca, Campil Member; Og, Gastropod Oolite; Si, Siusi Mb; A, Andraz horizon; M Mazzin Mb, Late Permian; B, Bellerophon Fm. The piercing structure (where A is uplifted on the left side of the picture) is truncated by a thrust sheet of younger (Anisian-Ladinian) formations. The thrust fault was later folded (left of Col Becher). An extensional or transensional Anisian fault, older than the above described deformation, was sutured by the Upper Anisian Richthofen Conglomerate (R). The following deformation phases can be thus recognized: 1) extensional or transensional Anisian fault; 2) Diapir development, possibly triggered by deep seated basement involving N70°E left-lateral transensional/transpressional faults; 3) truncation of the upper part of the diapiric structure by the Col Becher thrust fault; 4) folding of the thrust fault. The Upper Ladinian age of the diapiric structure is suggested by analogy with similar structures (e.g., Passo Serle, in the San Nicolò Valley) that present folds and faults cut by Ladinian magmatism and, at places, eroded and overlain unconformably by submarine landslides of the Caotico ete-rogeneo and by Upper Ladinian volcanoclastic deposits. Moreover, the structure is localized along the Stava-Cima Bocche Line that is, as already mentioned, cut by Middle Triassic vol-
canism. Compare with the map and sections of Fig. 3.12 and 3.13.

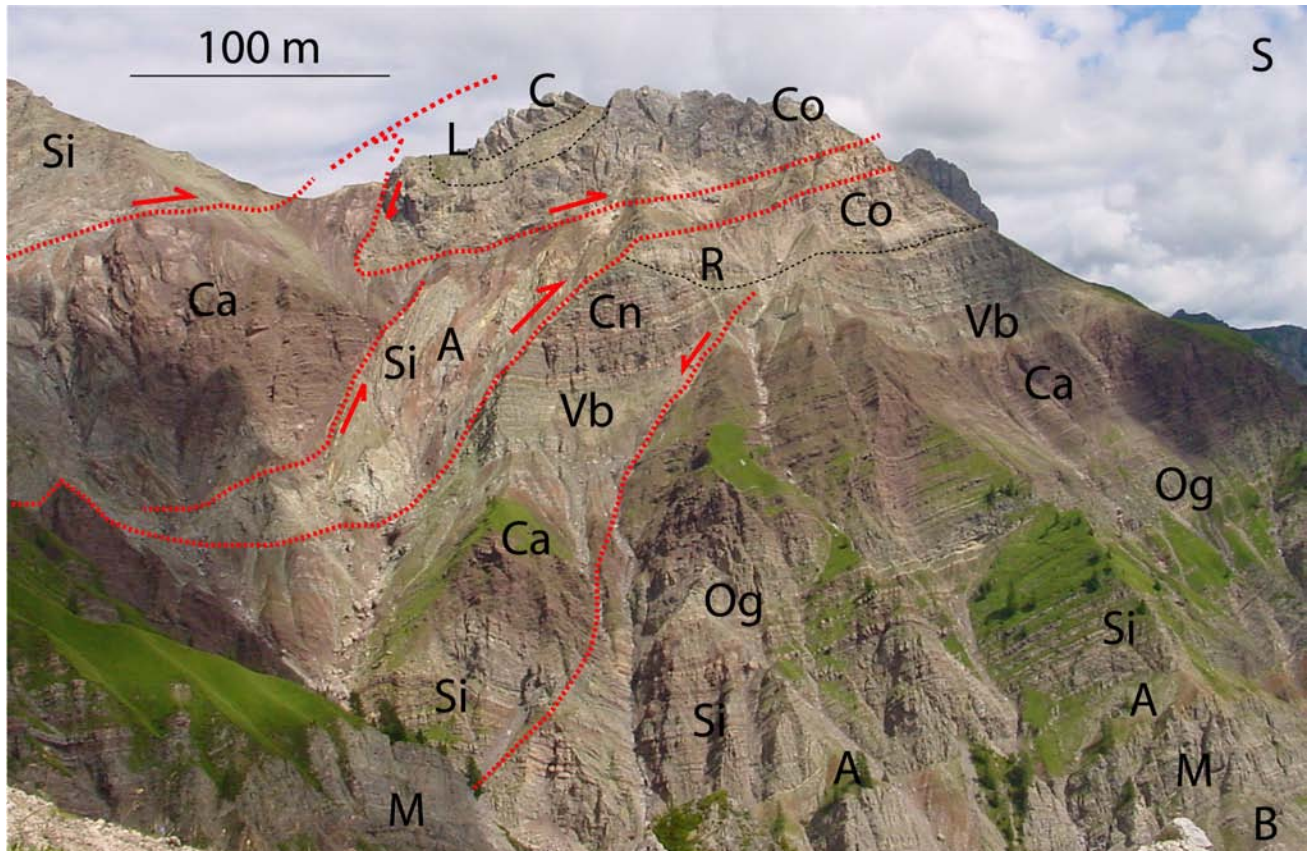


Fig. 3.9 - Detail beneath the Col Becher. The piercing "diapiric" structure has been decapitated by the upper thrust, which has later been folded. In the center is also visible the Anisian transtensional fault sealed by the Richthofen Conglomerate. Legend, Ladinian: C, Marmolada Limestone; L, Livinallongo Fm; Upper Anisian: Co, Contrin Fm; R, Richthofen Conglomerate; Scythian: Werfen Fm: Cn, Cencenighe Mb; Vb, Val Badia Mb; Ca, Campil Mb; Og, Gastropod Oolite; Si, Siusi Mb; A, Andraz horizon; M, Mazzin Mb. Late Permian: B, Bellerophon Fm).

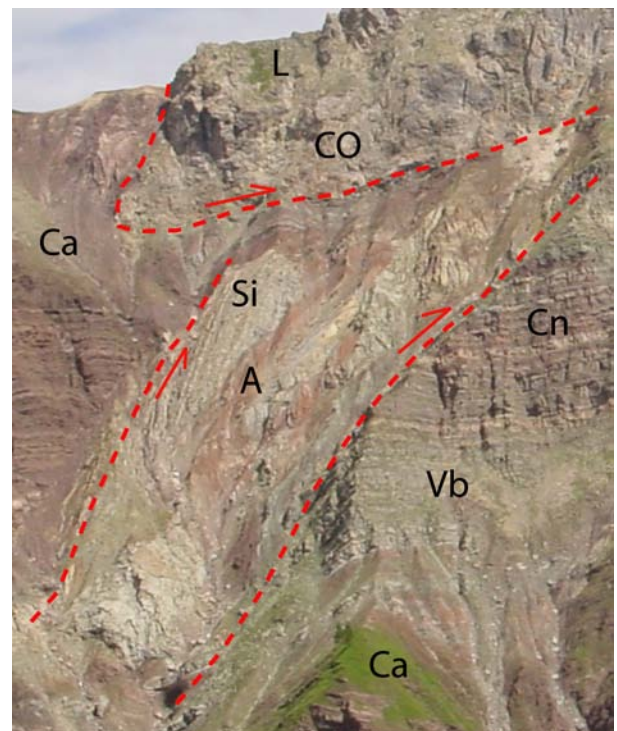


Fig. 3.10 - Detail of the previous panoramic view, with the "diapiric" intrusion of disrupted Werfen Fm, bounded by two faults cross-cut by the upper thrust of the Col Becher. In the core of the intrusion can be inferred the evaporitic Bellerophon Fm. Legend: L, Livinallongo Fm; Co, Contrin Fm; Cn, Cencenighe Mb; Vb, Val Badia Mb; Ca, Campil Mb; Si, Siusi Mb; A, Andraz horizon.

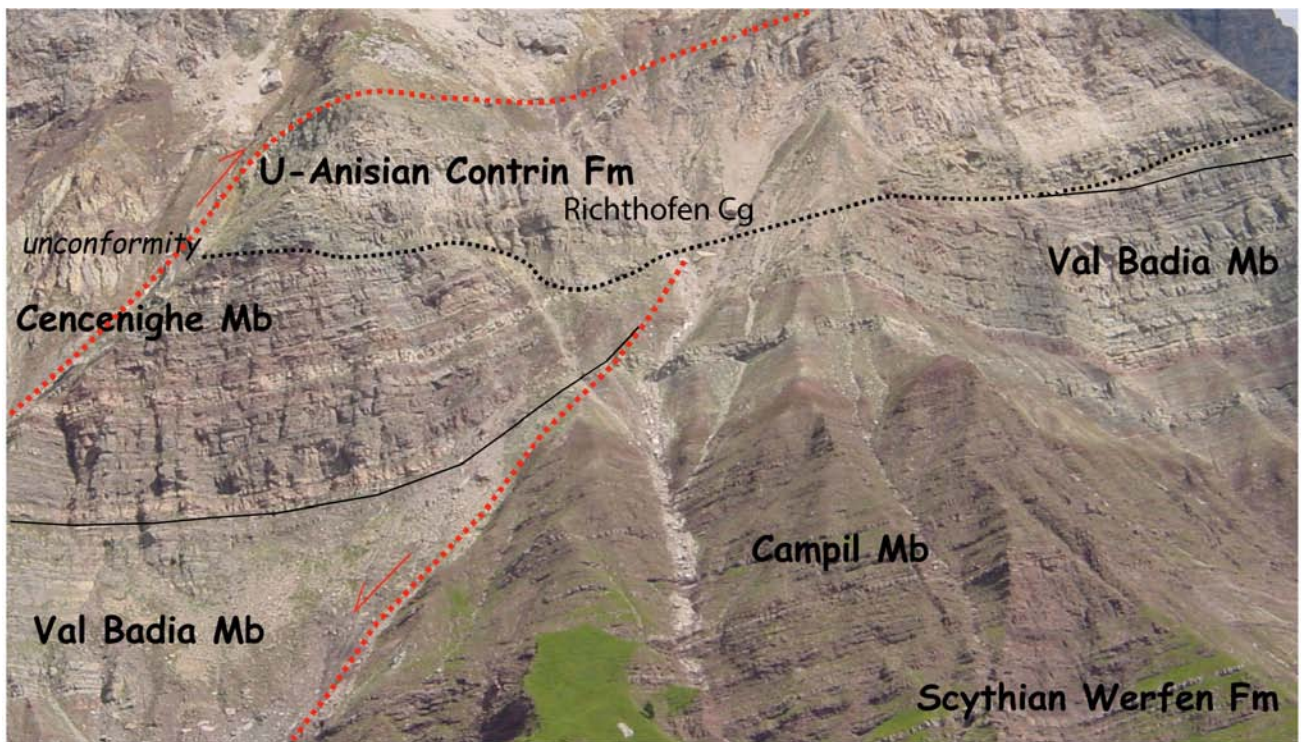


Fig. 3.11 - Detail of the Col Becher structure: the Anisian fault lowered the Cencenighe Mb of the Werfen Fm, now in contact with the Campil Mb (dark red) in the footwall. The Richtofen Conglomerate and the Upper Anisian Contrin Fm unconformably overlie the erosional surface that leveled the extensional structure. Notice, in the Cencenighe Mb of the hanging wall a drag fold associated to the normal or transtensional fault. Above, the Col Becher thrust fault with reddish siltstones of the Werfen Fm overriding the Anisian dolomites. C, Campil Mb; V, Val Badia Mb; E, Cencenighe Mb; R, Richthofen Conglomerate; CO, Contrin Fm. See also the map and the sections in the following figures.

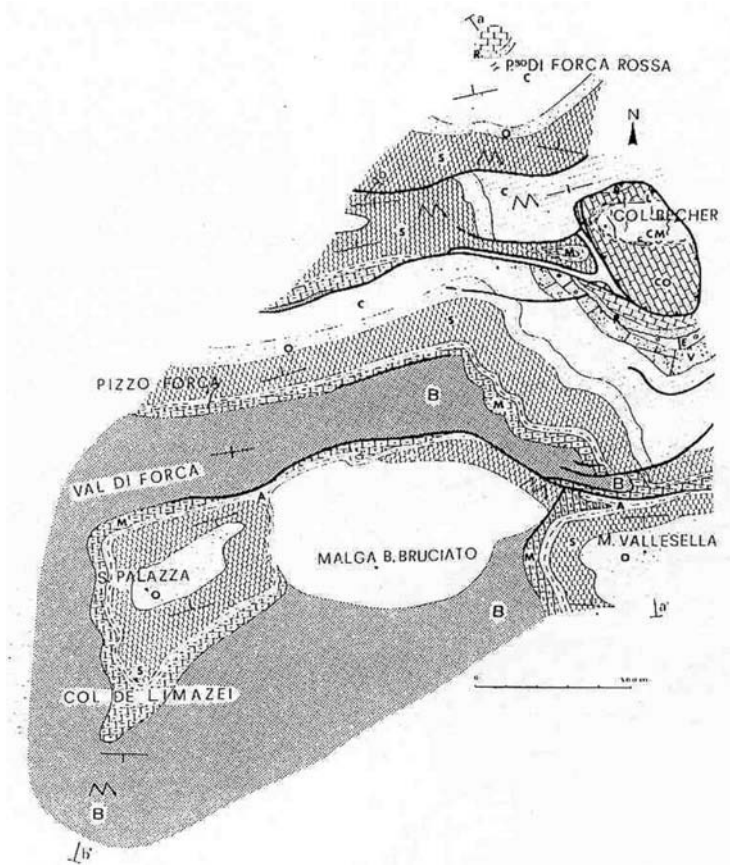


Fig. 3.12 - Geological map of the Col Becher structure. The top of Col Becher is a small klippe. Other diapiric structures occur north of the Vallesella syncline, in structural continuity with the Val di Forca diapiric anticline, and at Col de Limazei, to the southwest. B, Bellerophon Fm; M, Mazzin Mb; A, Andraz horizon; S, Siusi Member; O, Gastropod Oolite; C, Campil Mb; V, Val Badia Mb; E, Cencenighe Mb; R, Richthofen Conglomerate; Co, Contrin Fm; L, Livinallongo Fm; CM, Marmolada Limestone.

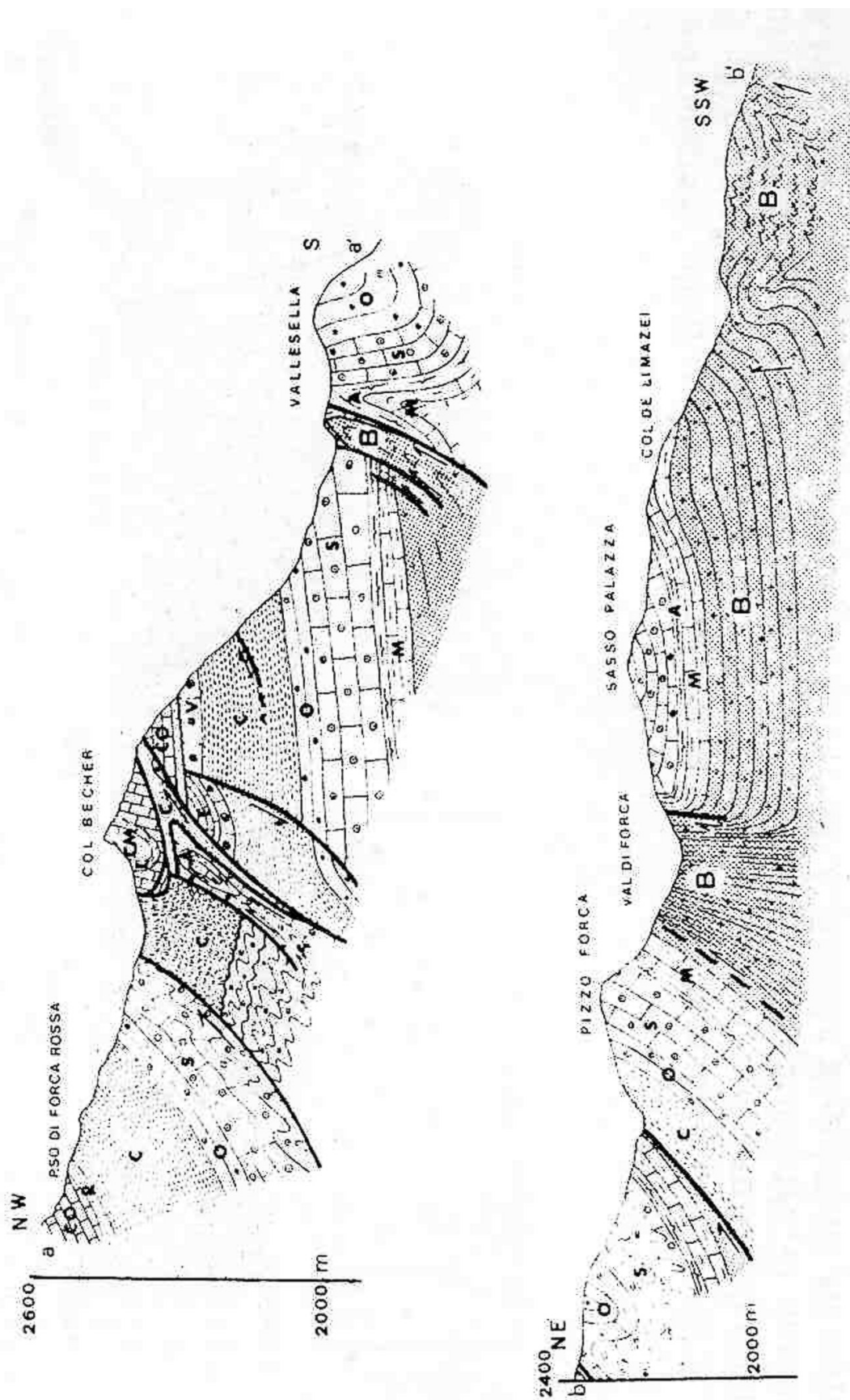


Fig. 3.13 - Geological cross-sections of the Col Becher area. B, Bellerophon Fm; M, Mazzin Mb; A, Andraz horizon; S, Siusi Mb; O, Gastropod Oolite; C, Campil Mb; E, Cencenighe Mb; R, Richthofen Conglomerate; Co, Contrin Fm; L, Livinallongo Fm; CM, Marmolada Limestone.

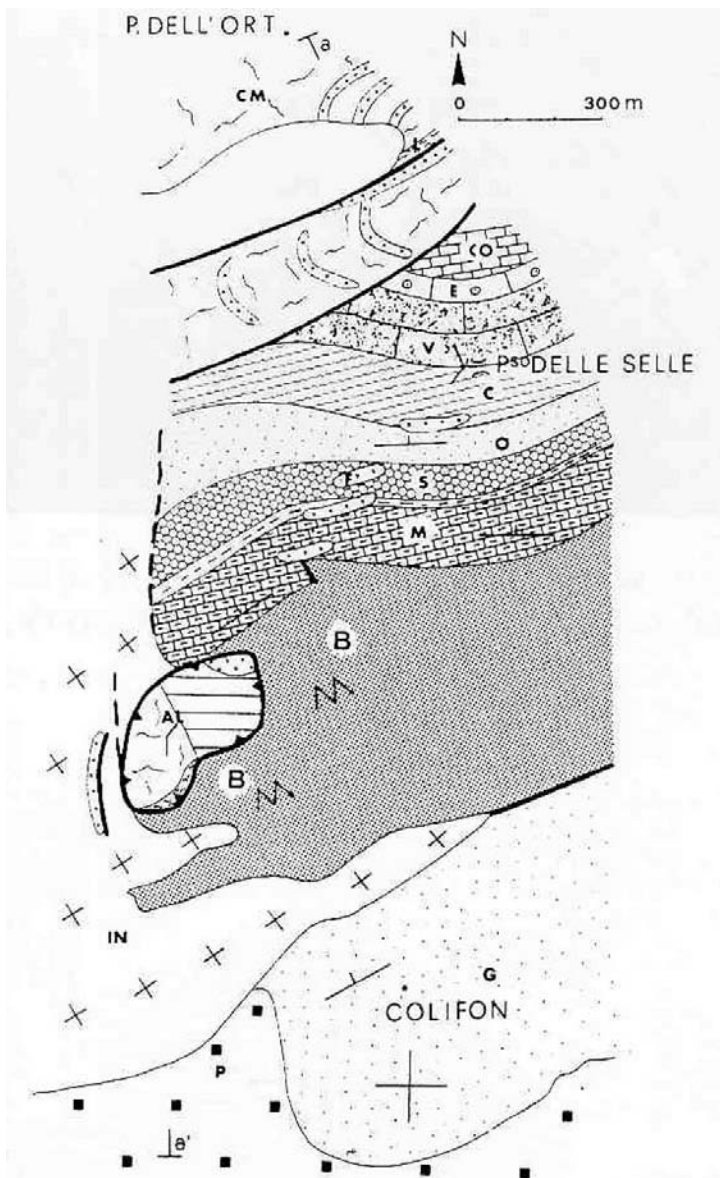
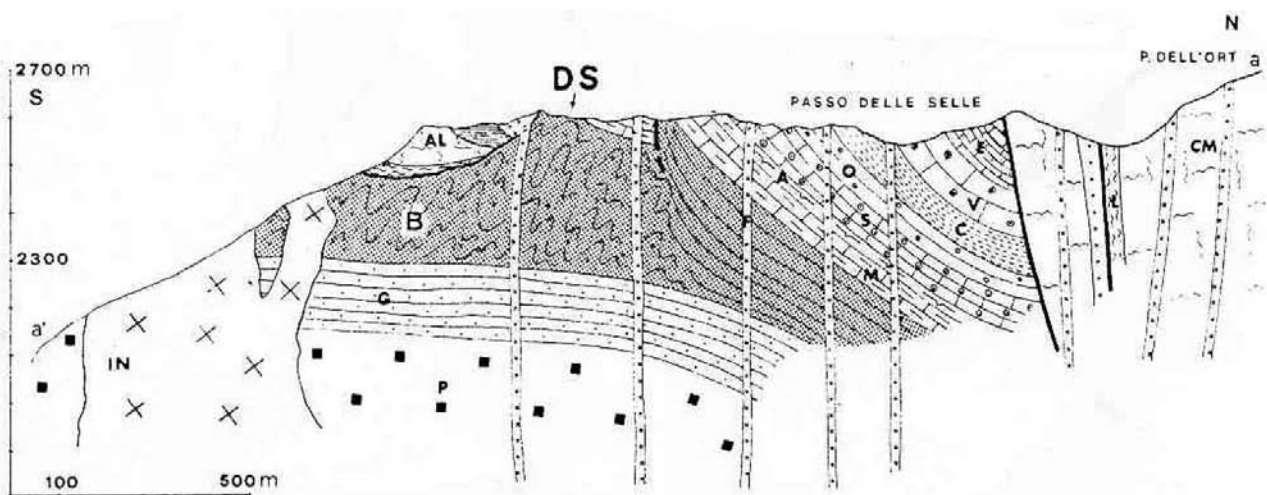


Fig. 3.14 - Geological map and section of the diapiric anti-cline of Passo Selle, metamorphosed by the contact with the monzonitic intrusion, northwest of Passo San Pellegrino. P, Permian porphyrites; G, Gardena Sandstone; B, Bellerophon Fm; M, Mazzin Mb; A, Andraz horizon; S, Siusi Mb; O, Gastropod Oolite; C, Campil Mb; V, Val Badia Mb; E, Cencenighe Mb; R, Richthofen Conglomerate; CO, Contrin Fm; L, Livinallongo Fm; CM, Marmolada Limestone; AL, allochthonous carbonatic block of Latemar or Marmolada Limestone, thrust and metamorphosed; F, latit-basaltic dykes; IN, monzonitic intrusion; DS, diapiric structure.



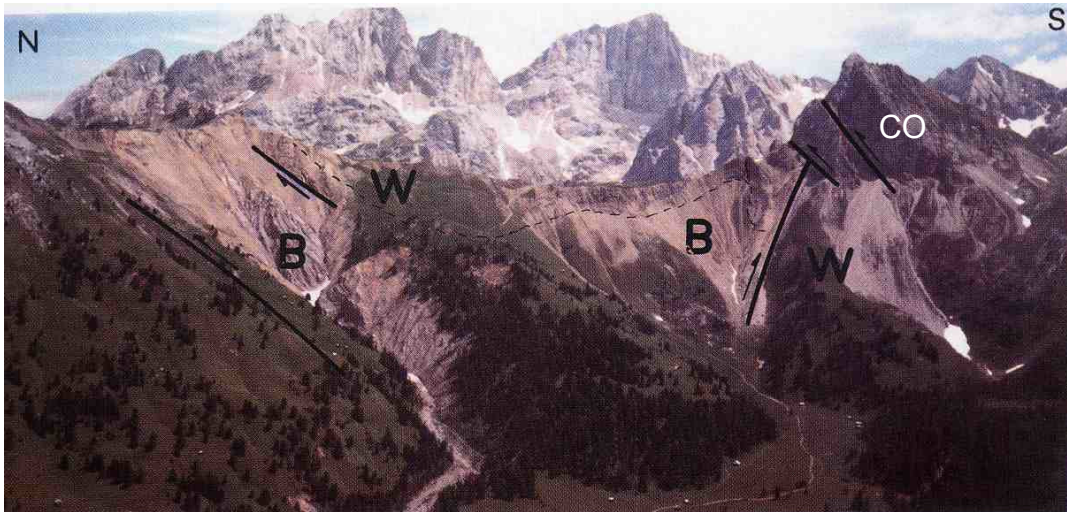


Fig. 3.15 - Diapiric anticline of Val San Nicolò, a lateral valley of Val di Fassa. View from the west. B, Bellerophon Fm; W, Werfen Fm; CO, Anisian carbonates. See the map and section of Fig. 3.16.

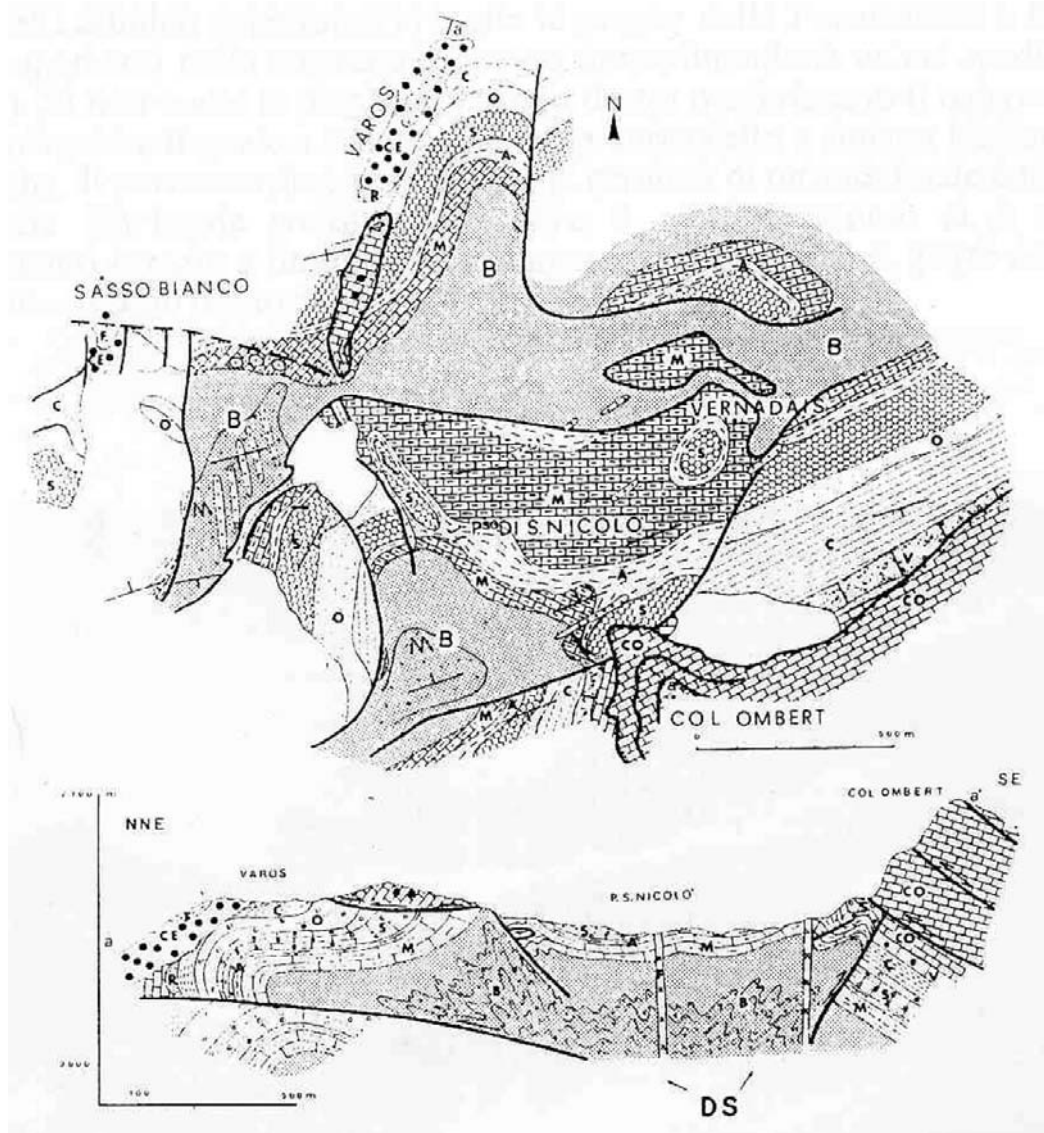


Fig. 3.16 - Geological map and cross section of the double vergent diapiric anticline of Val San Nicolò. B, Bellerophon Fm; M, Mazzin Mb; A, Andraz horizon; S, Siusi Mb; O, Gastropod Oolite; C, Campil Mb; V, Val Badia Mb; E, Cencenighe Mb; R, Richthofen Conglomerate; CO, Moena Fm, Contrin Fm; F, latitic-basaltic dykes, diatremes and subvolcanic bodies; CE, Caotico ete-rogeo; DS, diapiric structure.

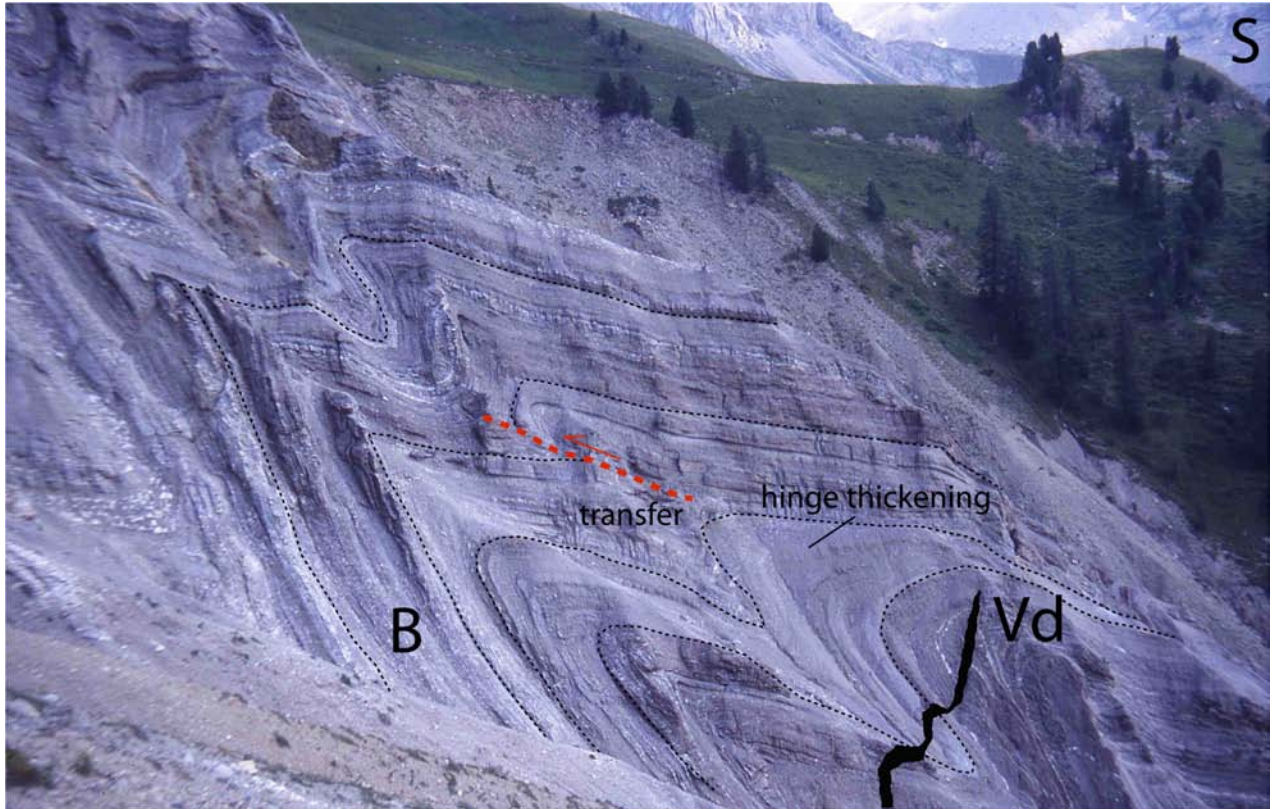


Fig. 3.17 - Northern head of Val San Nicolò. To the right an Upper Ladinian latitic-andesitic dyke (Vd) cuts the folds of the diapiric structure in the Upper Permian Bellerophon Fm (B), constraining their Middle Triassic age (Rossi, 1977). Notice that the folds (right bottom) transfer the shortening to a thrust fault that terminates, leaving the pace to other folds (top left). The thrust fault generates at the hinge of an anticline and terminates at the hinge of an overlying syncline. The two tip lines of the small thrust transfer the shortening into the folds. Where the shortening is accommodated by the thrust fault (due to relatively more competent lithologies; central part of the photo), folds are much less frequent. In the more shaly layers the folds show hinge thickening.



Fig. 3.18 - Synsedimentary syncline filled by nodular limestones of the Livinallongo Fm (L), south of the top of Col Ombert mountain, south of the diapiric structure of Valle di San Nicolò. This structure testifies the Ladinian transpressional tectonics of the central Dolomites. The Contrin Fm (C) is folded with synclinal geometry due to a pop-up structure produced by conjugate thrust faults.



Fig. 3.19 - Detail of the previous structure: the southern limb of the synsedimentary syncline, with onlap geometries within the Livinallongo Fm, characterized by massive calcarenites passing laterally into reddish nodular limestones. The picture was taken north of the Massiccio della Costabella, between Passo Pasche and Col Ombert. Alberto Boz for scale.

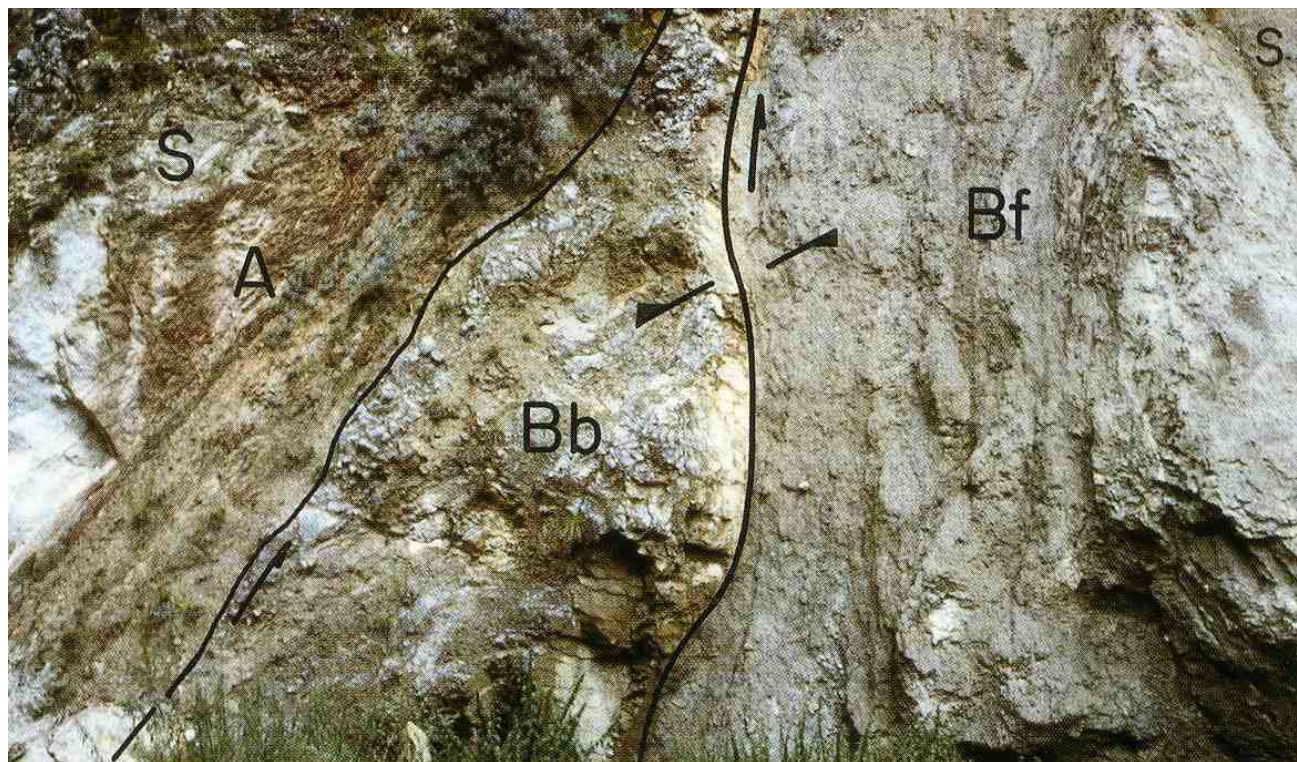


Fig. 3.20 - Detail of the northern flank of the Avoscan (locality Roi, see also the following picture) diapiric anticline. The Bellerophon Fm (Bf) in the “fiammazza” (evaporitic) facies is in tectonic contact with a slice of the same formation with a “badiotta” (lagoon) facies (Bb). The main movement plane is characterized by both vertical and horizontal slickenlines. (A) Andraz horizon and (S) Siusi Member of the Scythian Werfen Fm.

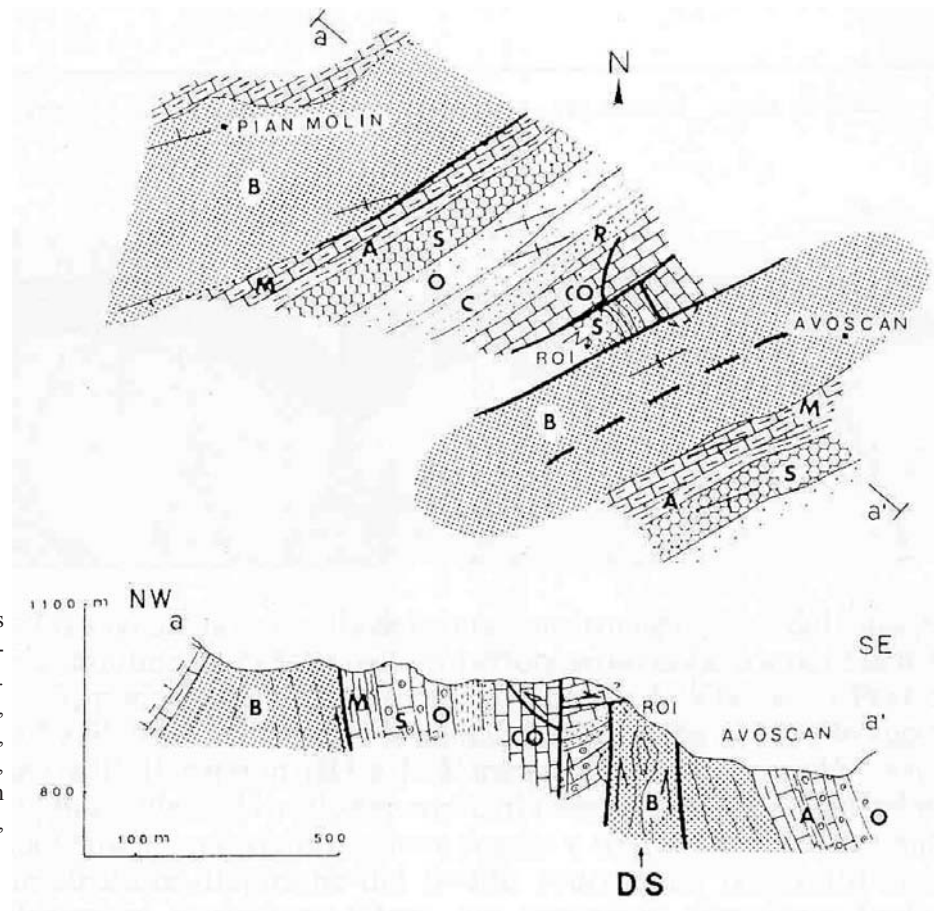


Fig. 3.21 - Geological map and cross section of the Avoscan diapiric anticline, between Cencenighe and Alleghe. B, Bellerophon Fm; Werfen Fm: M, Mazzin Mb; A, Andraz horizon; S, Siusi Mb; O, Gastropod Oolite; C, Campil Mb; R, Richthofen Conglomerate; CO, Contrin Fm; DS, diapiric structure.

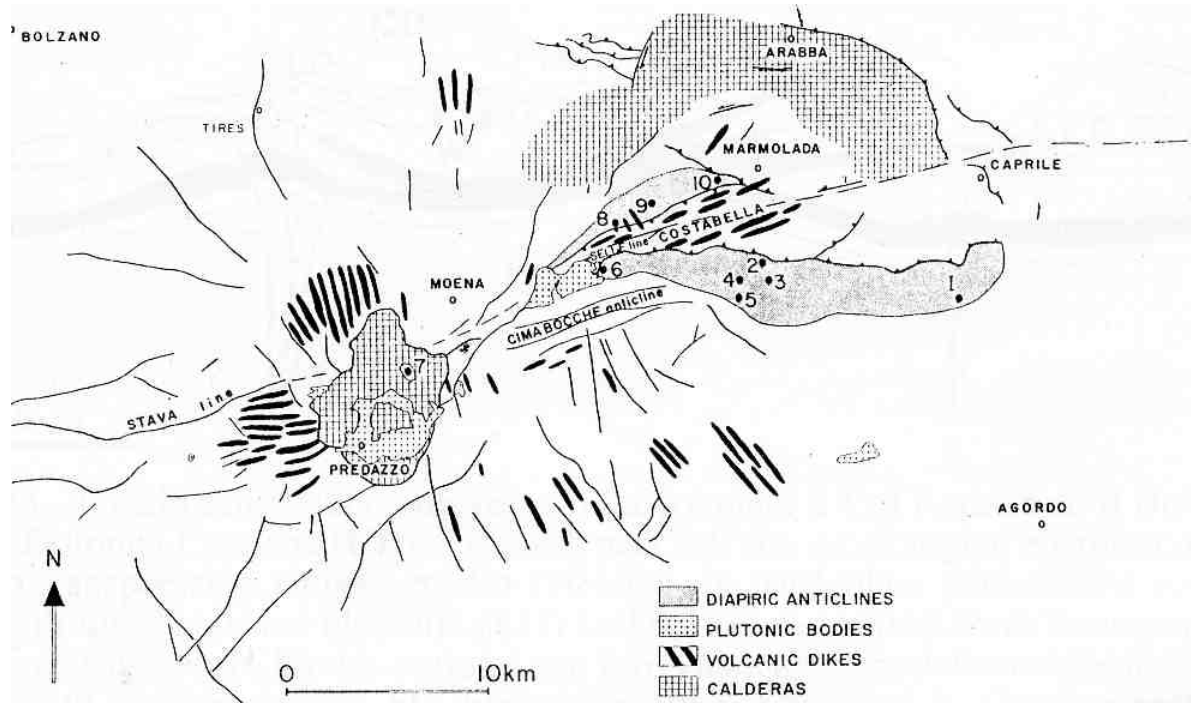


Fig. 3.22 - Structural scheme of the Ladinian tectonics of the Dolomites. The following tectonic phases can be distinguished: 1) development of the (numbered) diapiric anticlines along the N70°E-trending transpressional Stava-Cima Bocche alignment; 2) truncation of the diapiric structures by the thrust faults of Costabella, characterized by opposite vergence, a feature typical of flower structures, and by the en-echelon thrusts of Marmolada and Col Rodella; 3) development of extensional faults with radial pattern around the Predazzo and Monzoni magmatic centers; such faults possibly accommodated with a dome shape the magma upraise and the emplacement of the radial dykes.

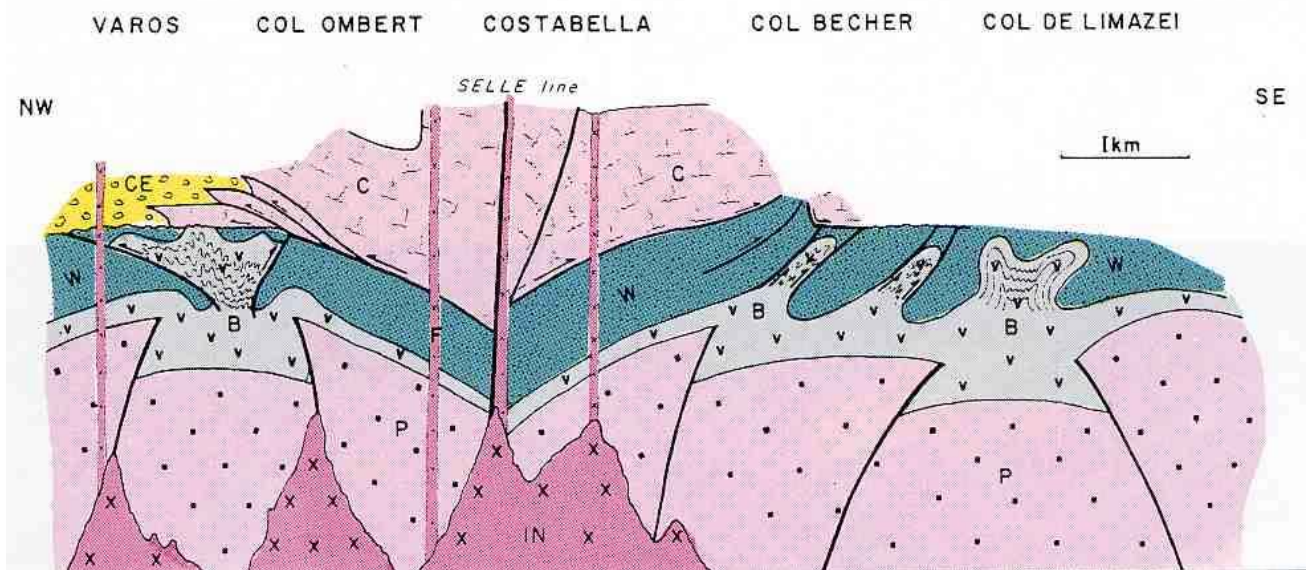


Fig. 3.23 - Relationship between the transpressional deformation of the basement P (top of the Permian Ignimbrites) and the diapiric structures in the sedimentary cover to the north of the Cima Bocche anticline. Notice the following three different structural levels: (1) at their bottom the ignimbrites suffered brittle deformation that triggered the diapiric anticlines in the above layer (2), where the Bellerophon Fm (B) and the Werfen Fm (W) show a more ductile deformation; in the uppermost level (3) the Anisian and Ladinian carbonates (C) display again brittle deformation and are thrust over the diapiric anticlines of the middle layer, truncating them at their top. In the structural highs of the diapiric anticlines, a Ladinian (Varos) erosional surface, unconformably overlain by a volcaniclastic conglomerate (CE, Caotico eterogeneo) is at places observed. The monzonitic intrusion (IN) fossilized the deformation.

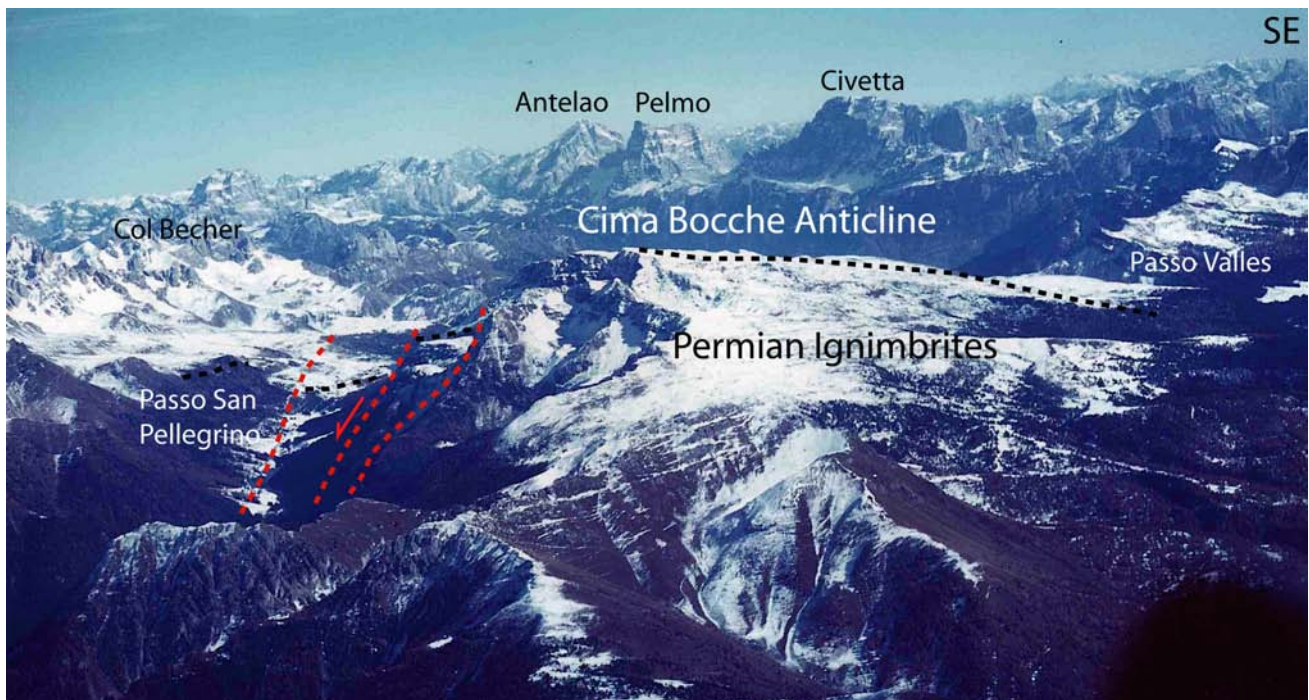


Fig. 3.24 - The Cima Bocche Anticline involves the basement and the overlying Permian Ignimbrites. Its northern limb is truncated by few subvertical N70-90° trending, possibly left-lateral strike-slip faults along the Passo San Pellegrino.

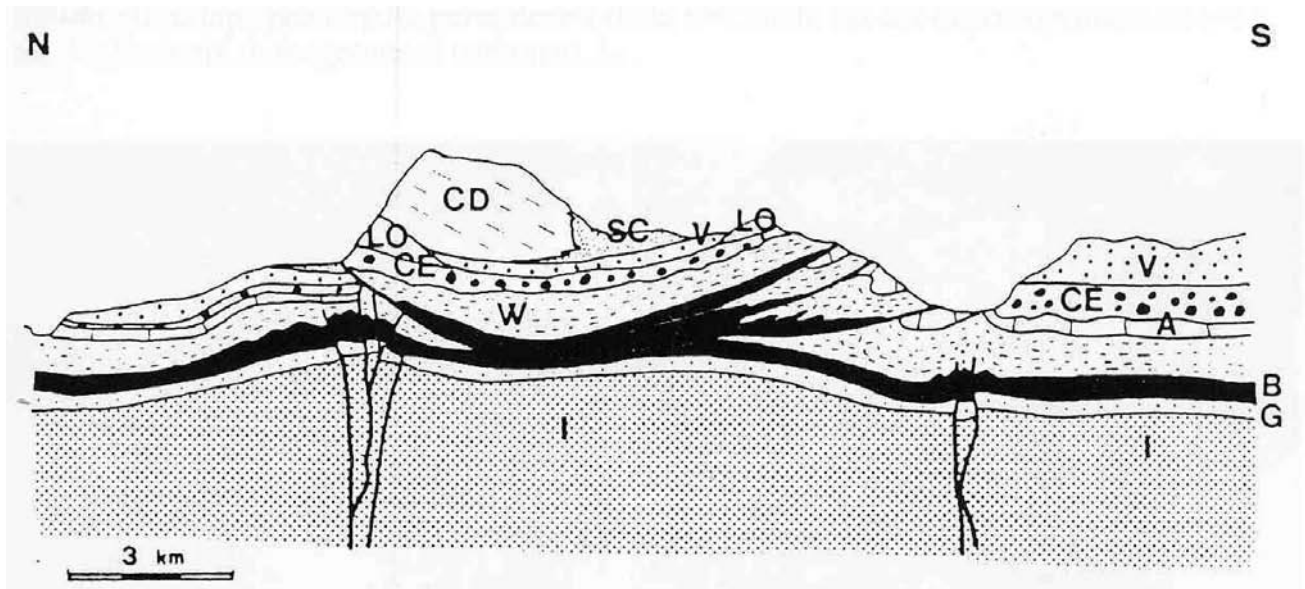


Fig. 3.25 - Schematic profile through the Sassolungo, Col Rodella and Buffaure massifs. The Cassian Dolomite (CD) developed on the morphological and structural high generated by a sinistral transpressional push-up of Middle Triassic age. In particular, the push-up nucleated beneath a giant olistolite (LO) included in the marine landslide deposits of the Caotico eterogeneo (CE). The section is not retrodeformable due to the strong out-of-section component of deformation. SC: San Cassiano Fm; V, Marmolada Conglomerate, volcaniclastic deposits and lavas; A, Livinallongo and Contrin Fms.; W, Werfen Fm; B, Bellerophon Fm; G, Gardena Sandstone; I, Ignimbrites, Permian rhyolites and crystalline basement. The main detachments are located in the Bellerophon Fm. Notice the two transpressional systems to the north and to the south, respectively the westward prosecutions of the Passo Gardena and Passo Fedaia alignments. South of Val di Fassa (right in the drawing), the Buffaure massif represented a sort of small foredeep basin for the push-up structure developed between the two transpressional belts. Here the volcaniclastic deposits are much thicker (800-1000 m) with respect to the 100-200 m thick volcaniclastic sediments in the push-up zone (Sassolungo and Col Rodella Massifs).



Fig. 3.26 - The Crepe Rosse synsedimentary syncline (located near Passo Fedaia) developed right to the south of the Triassic sinistral transpressional alignment of the Fedaia Lake, that is here buried. Notice the onlaps, especially on the right flank of the syncline, of both volcaniclastic deposits and the interfingering carbonatic megabreccias.

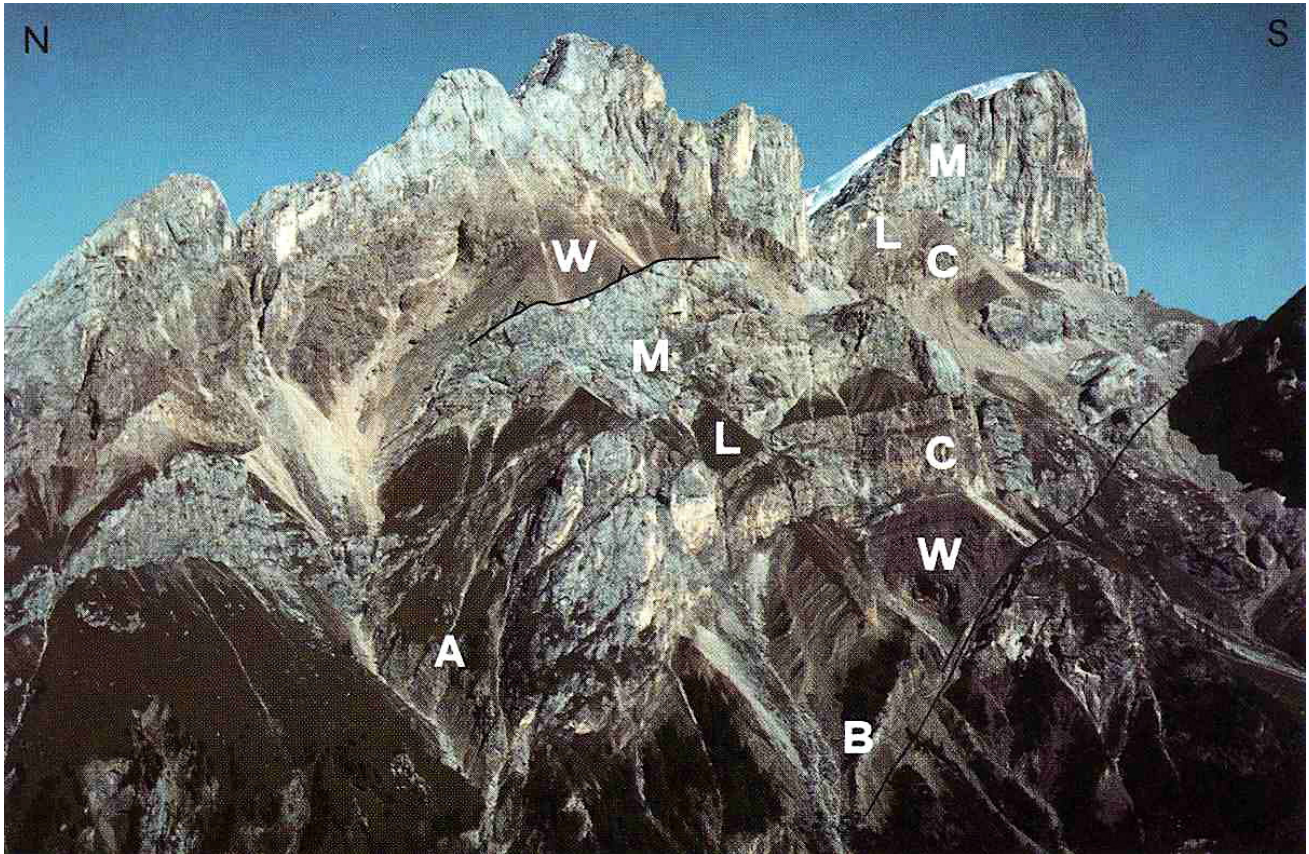


Fig. 3.27 - The southern cliff of the Marmolada massif is extremely complicated by SW-vergent thrusts. B, Bellerophon Fm; W, Werfen Fm; C, Contrin Fm; L, Livinallongo Fm; M, Marmolada Limestone; A, Caotico eterogeneo.



Fig. 3.28 - Northern slope of the Marmolada Ladinian carbonate platform (left), overlapped by Upper Ladinian volcanic and volcanoclastic rocks of the Padon ridge (right). North to the right, looking west. In the valley the Fedaia lake. Cristina Bagolan and Virginio Doglioni for scale.

Fig. 3.29 - Schematic geological map of the Southern Alps at the Ladinian. Notice the en-echelon distribution of basins and structural highs with respect to the border between the Northern Zone and the Southern Mobile Belt (sensu BRUSCA, 1981). The distribution suggests a sinistral shear. In the Northern Zone both carbonate platforms and basins developed (with higher sedimentary thicknesses in the basins), whereas in the Southern Mobile Belt the basement was cropping out (PIERI & GROPPi, 1981; BRUSCA *et alii*, 1981; DE ZANCHE & MIETTO, 1984; GARZANTI, 1985).

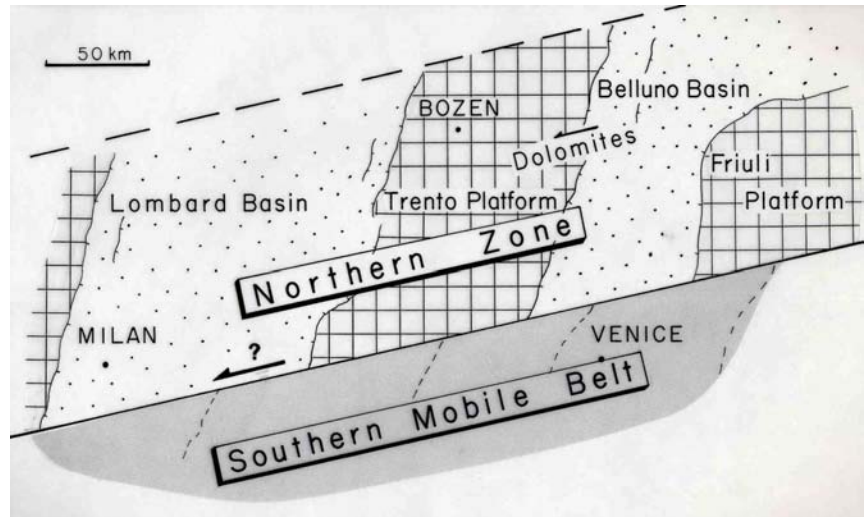


Fig. 3.30 - Upper-Middle Triassic geodynamic reconstruction (modified after BERNOULLI & LEMOINE, 1980, BRANDNER, 1984, MASSON & MILES, 1986). Notice the sinistral relative motion between Africa and Europe, coeval to the Atlantic rift. The magmatic centers (black dots) are localized within rift zones and transform zones characterized by mainly transtensional kinematics (e.g., Terranova-Azores-Gibraltar; Pyrenees). X-X' is the trace of the section of the following figure and the rectangle indicates the approximate position of the previous figure.

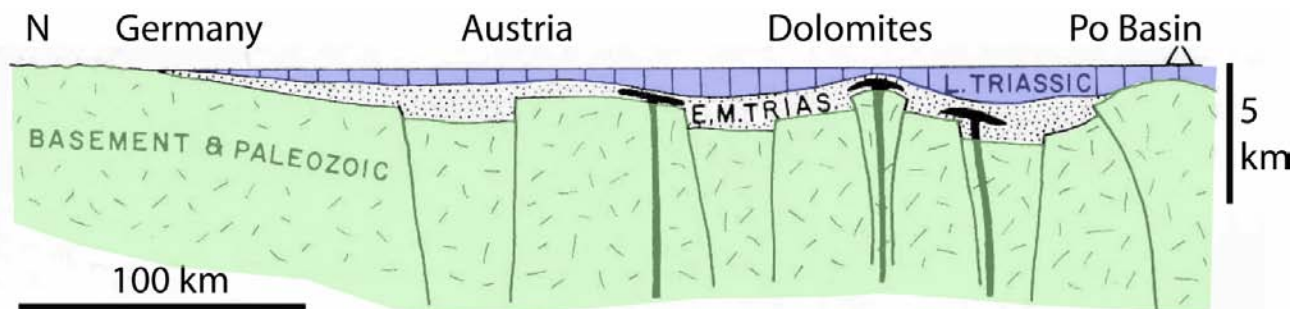
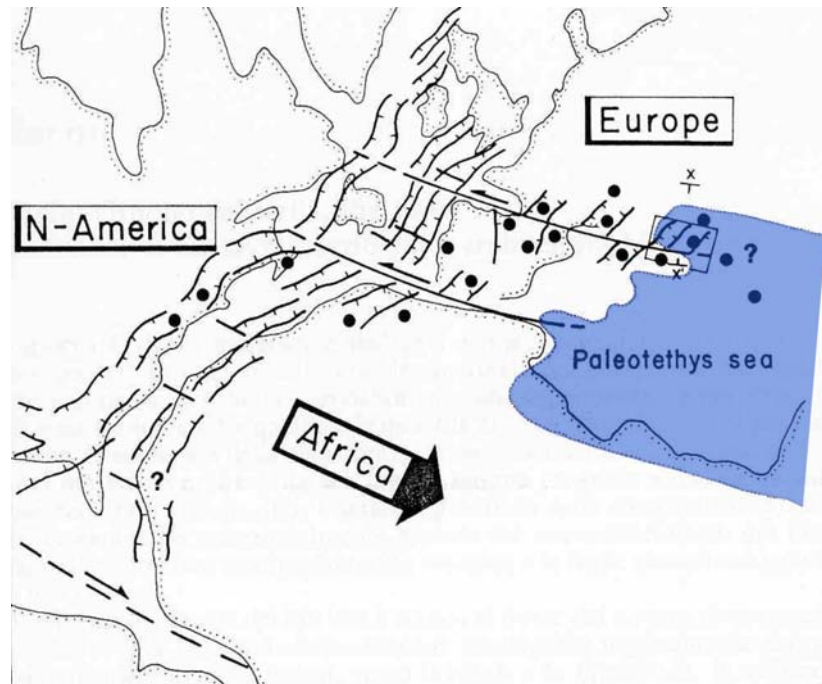


Fig. 3.31 - Idealized section through Europe and the Po Plain in the Upper Triassic. Notice the occurrence of a structural high under the Po Plain. Several positive (i.e., transpressional) flower structures (e.g., Dolomites) occur within an area prevalently characterized by subsidence (transtension).

4th Day

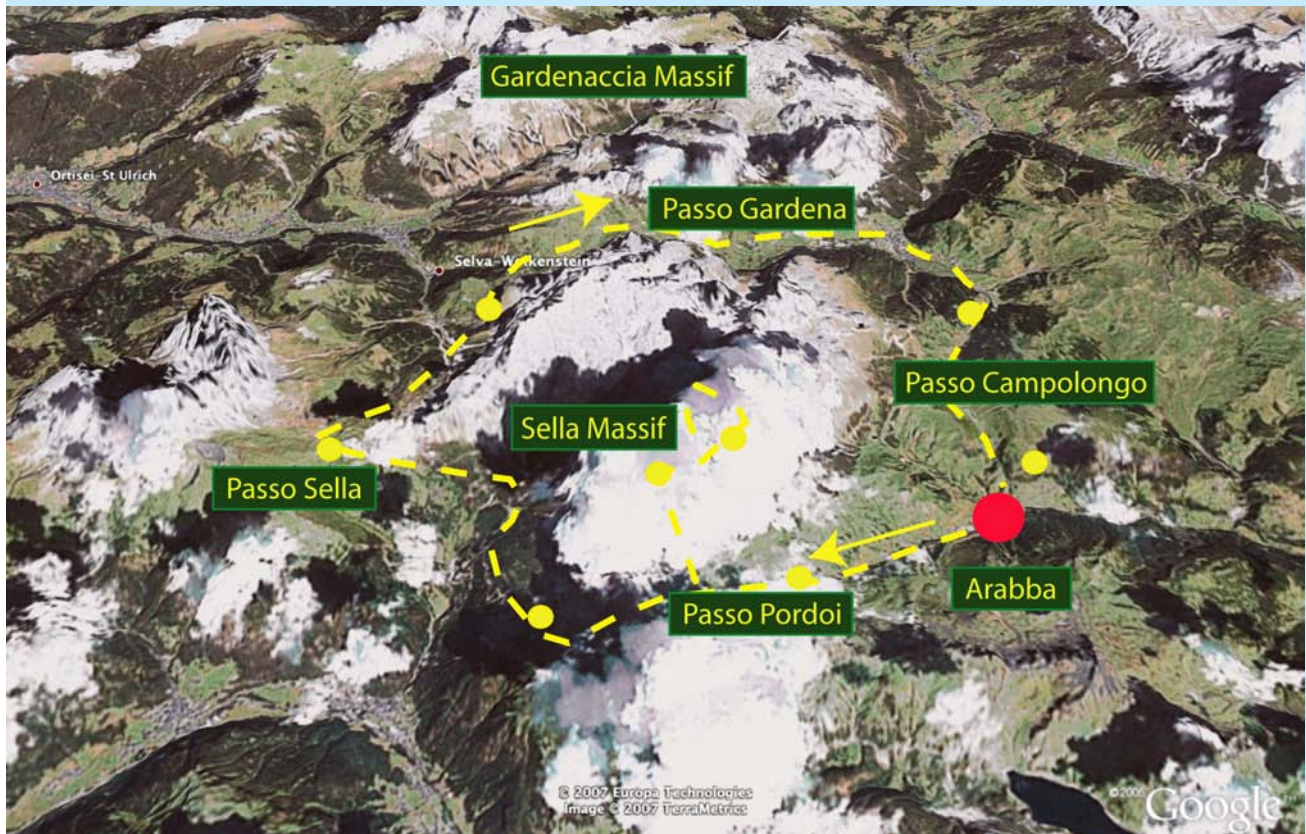


Fig. 4.0 - Itinerary: Sella massif, Piz Boè

Subject: Analysis of a thrust; Mesozoic architecture.

This day is entirely dedicated to the geology of the Sella Massif, at the heart of the Dolomites, in the core of the large basement syncline where the sedimentary cover crops out. The Sella Massif is probably one of the most fascinating mountains from the geological point of view. The quality and quantity of geological observations is extraordinary: the geometry of the Carnian carbonate platform that forms the basal portion of the massif that radially progrades from the internal lagoon to the adjacent

basin of the San Cassiano Fm; the effects of compaction on the basinal deposits; the geometries of the beautifully exposed thrust of the Piz Boè; the control of stratigraphic architecture on tectonics and synsedimentary faults. The peak thrust of the Piz Boè is located at the front of the W-SW vergent thrust system of the central-western Dolomites, that can be regionally related to the Dinaric belt, or to an alpine oblique ramp associated to the transfer between a recess and a salient. It is possible to analyze the thrust architecture in three dimensions, observing the lateral ramps connecting decollement planes and frontal ramps.

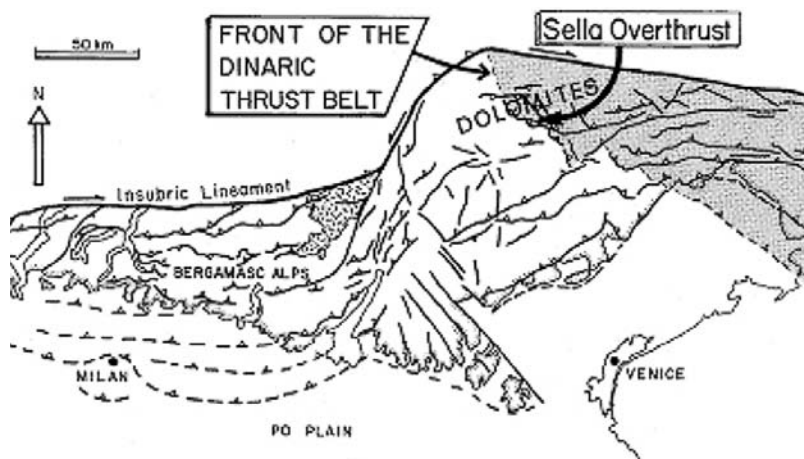


Fig. 4.1 - The Sella thrust might represent the front of the WSW-vergent Dinaric fold and thrust belt, of Paleogene-Lower Neogene age. The front of the Dinarides cuts obliquely the eastern Southern Alps and was dissected by later (Neogene) southalpine thrusts. Alternatively, the WSW-vergent thrusts in the Dolomites, as discussed earlier, could represent an earlier Alpine right-lateral undulation along the eastern margin of the Trento Horst, conjugate to the left-lateral transpression along the Giudicarie belt, emplaced along the western margin of the Trento Horst.

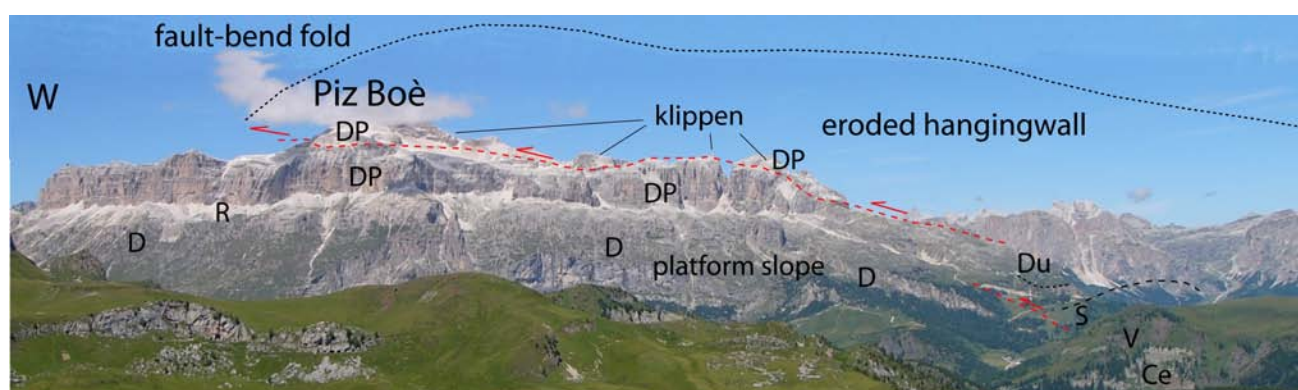


Fig. 4.2 - View of the Sella Massif from the south. The basal part consists of Cassian Dolomite (D) of Middle Carnian age. The overlying debris in the middle consists of rocks belonging to the Upper Carnian Raibl Fm (R). The upper cliff is made of Norian Dolomia Principale (DP). Du, Dürrenstein Dolomite, S, San Cassiano Fm; V, Volcanoclastic sandstones; Ce, Caotico Eterogeneo. The thrust followed the shape of the Carnian platform slope, it continued in ramp into the Dolomia Principale, and with a staircase trajectory arrived at the top of the Piz Boè with its classic summit klippe geometry. The top klippe overlies a condensed Jurassic-Cretaceous succession.



Fig. 4.3 - Val Lasties, looking to the west from the Sella Massif. Beyond the Sella Massif, the Sassolungo Massif can be recognized. Observing the right flank of the valley, the basal cliff is still constituted by upper Cassian Dolomite (CD), the gentle slope by Raibl Fm (R) and the upper cliff by Dolomia Principale (P). Note that the Raibl Fm thickens moving away from the platform: at the outermost peak of the Sella Massif (Piz Ciavaces), the Raibl Fm is some 80 m thick, whereas it dies out at the core of the Sella Massif. The Sella plateau, like other Dolomitic massifs is characterized by large fossil erosional terraces that according to Rossi (1957) could be related to an Oligocene erosional surface.

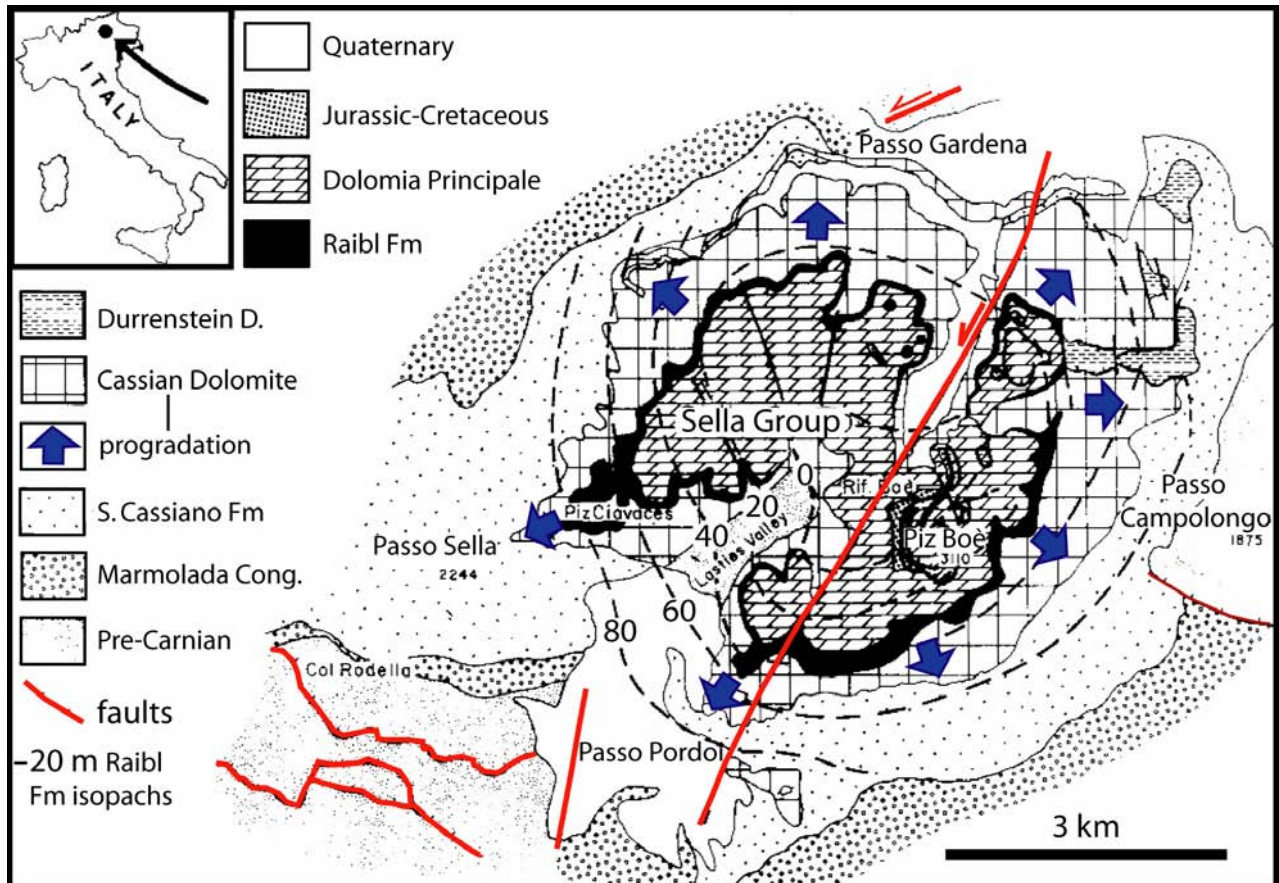


Fig. 4.4 - Geological map of the Sella Group. Notice the radial progradation of the Carnian carbonate platform (Cassian Dolomite). The Sella group is a perfectly preserved atoll (Leonardi, 1967). The isopachs of the Raibl Fm indicate a thickening of the formation away from the Carnian platform. This suggests a relationship between the geometry of the Raibl Fm deposits and the underlying platform-basin system. To the right, south of Campolongo Pass a SSW-vergent thrust fault sutured by basinal deposits of the San Cassiano Fm can be observed (DOGLIONI & GOLDHAMMER, 1988).

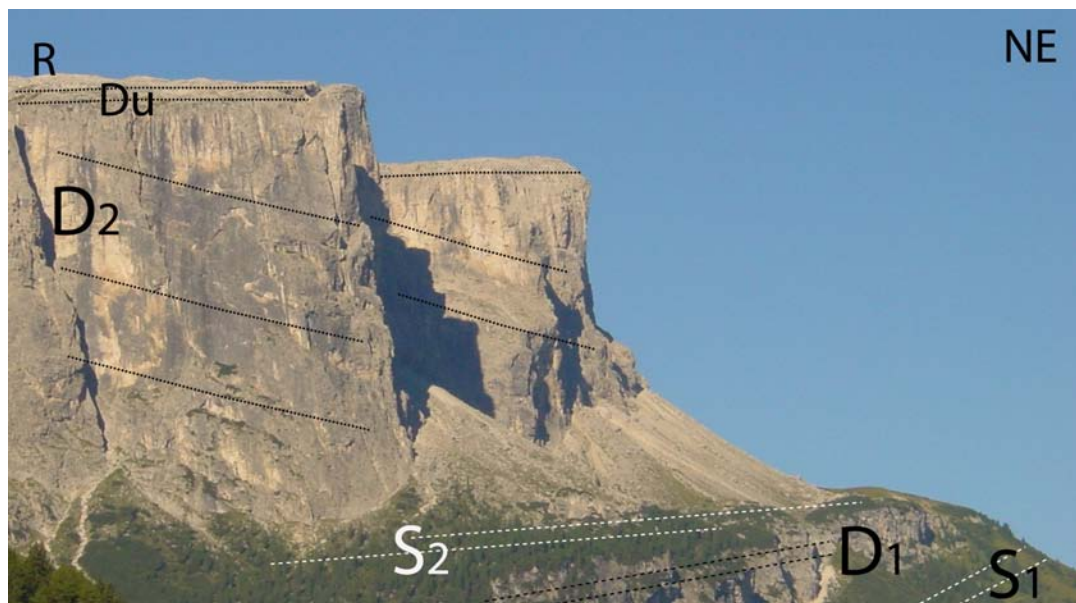


Fig. 4.5 - Northern slope of the Sella Massif, west of Corvara. The Cassian Dolomite (upper platform D2) progrades northward over the San Cassiano Fm (S2). A lower Cassian Dolomite (D1) and related basin (S1) are below. Du, Dürrenstein Dolomite, R, Raibl Fm.

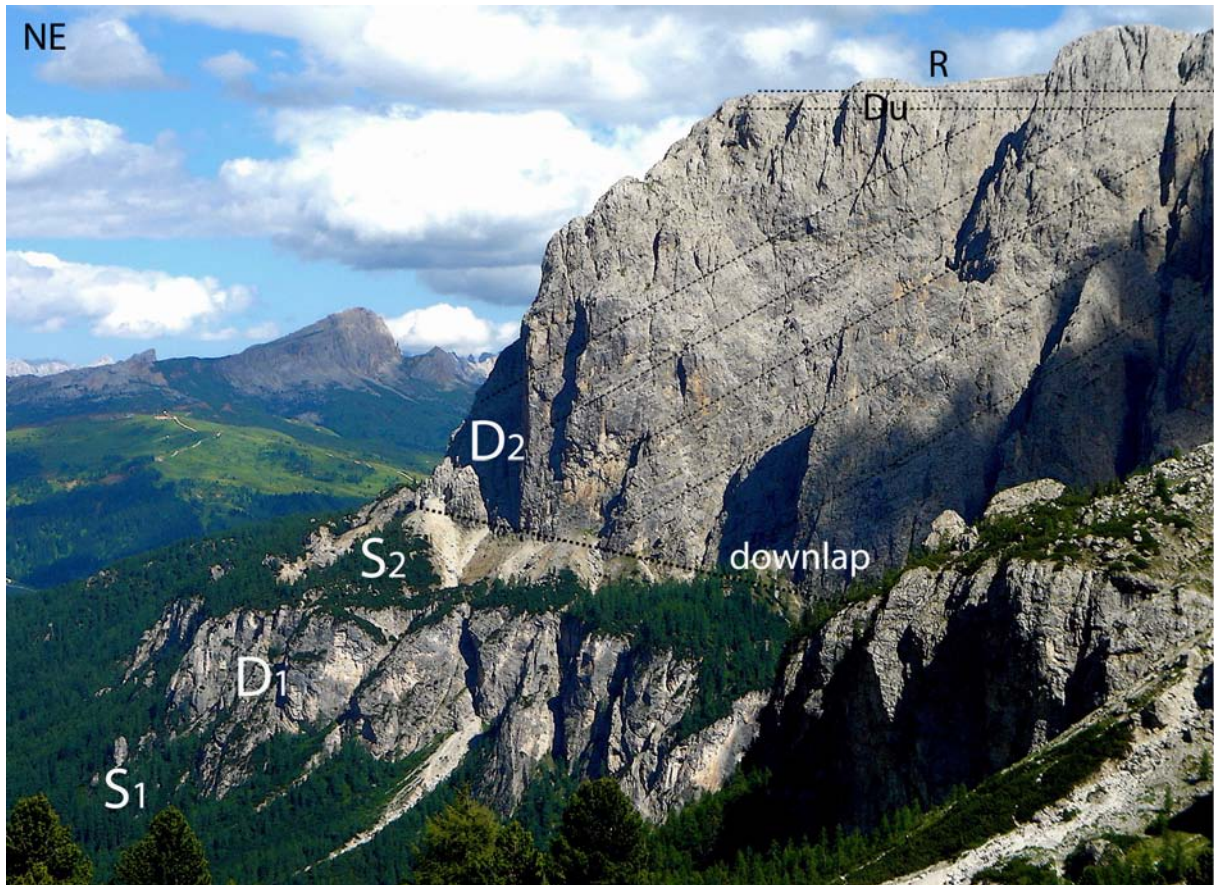


Fig. 4.6 - Northeastern slope of the Sella Massif. The Cassian Dolomite (upper platform D2) progrades northeastward over the San Cassiano Fm (S2). A lower Cassian Dolomite (D1) and related basin (S1) are below. Du, Dürrenstein Dolomite, R, Raibl Fm.

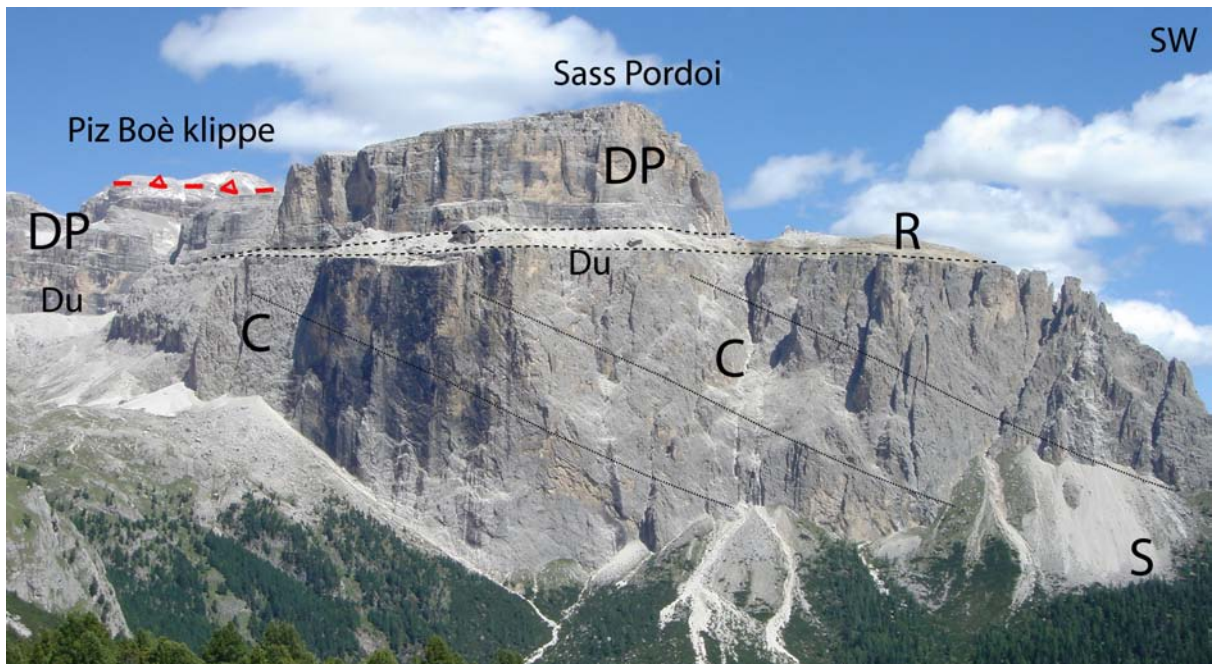


Fig. 4.7 - Southwestern margin of the Sella massif. The Carnian Cassian Dolomite (C) with its lagoon Dürrenstein Dolomite (Du) progrades over the basinal equivalent San Cassiano Fm (S). The Raibl Fm (R) above thins toward the interior of the atoll, for the larger subsidence of the platform margin over the basinal sediments. DP, Norian Dolomia Principale.

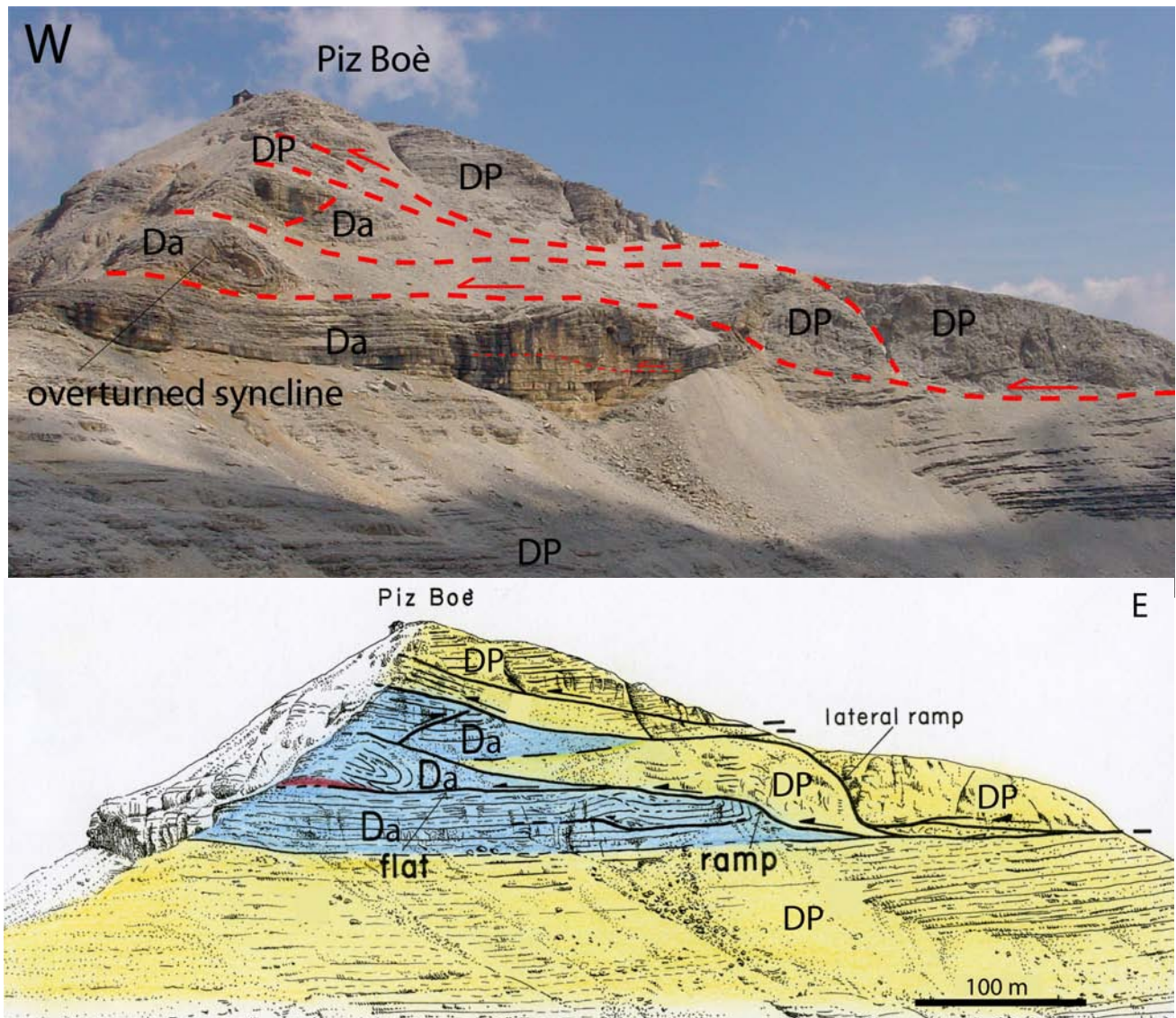
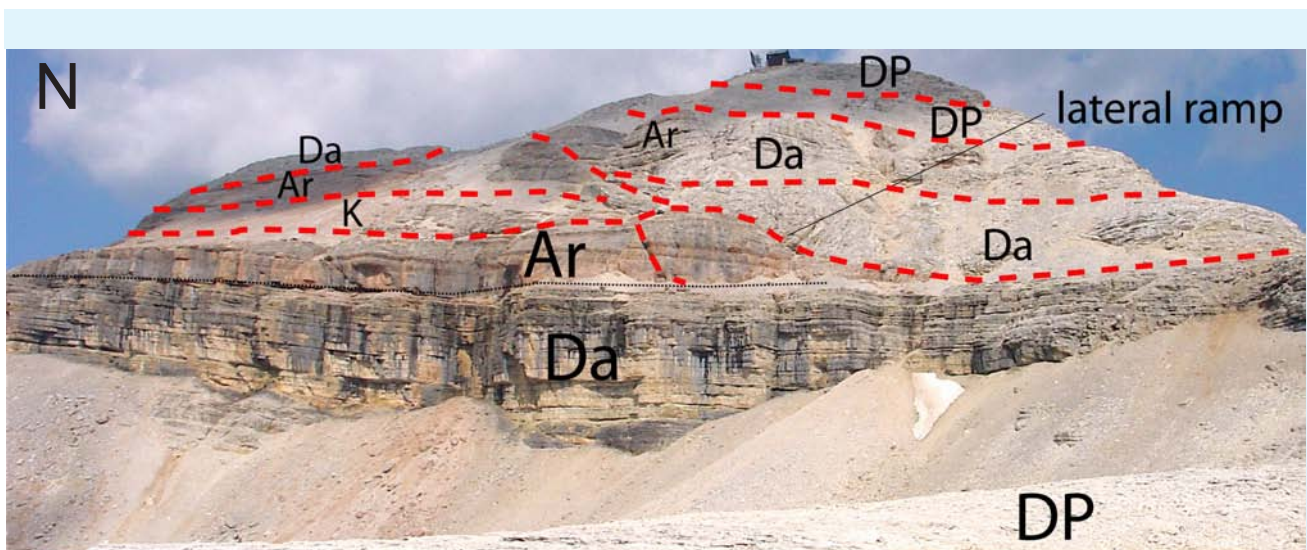


Fig. 4.10 - Southern view of the Piz Boè. The thrusts show staircase geometry with décollements at the top of the Dolomia Principale (P) and of the Dachstein Limestone (D), with connection ramps. Compare with Fig. 4.11 and Fig. 4.12 to appreciate how deformation varies along the strike of the thrust fault. Legend, DP, Dolomia Principale; Da, Dachstein Limestone (after DOGLIONI, 1990).



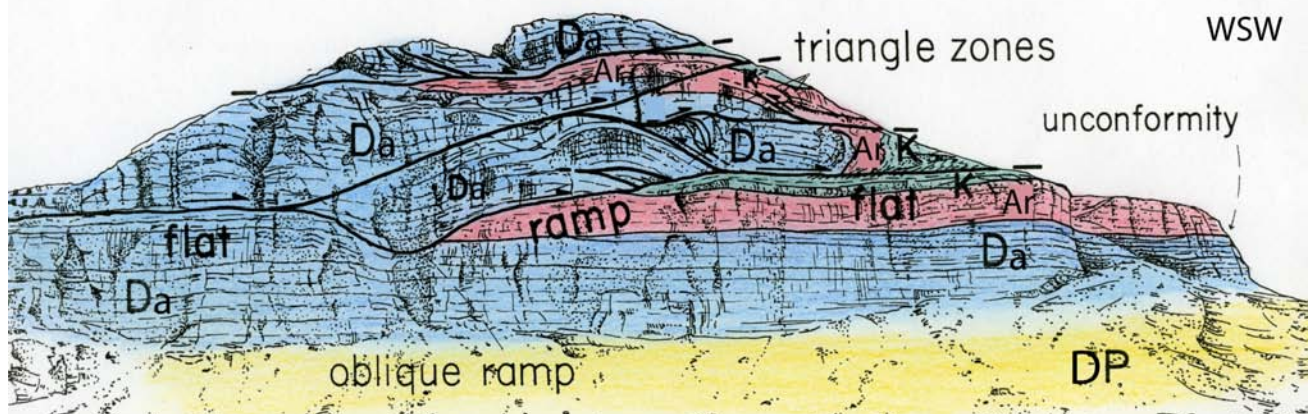
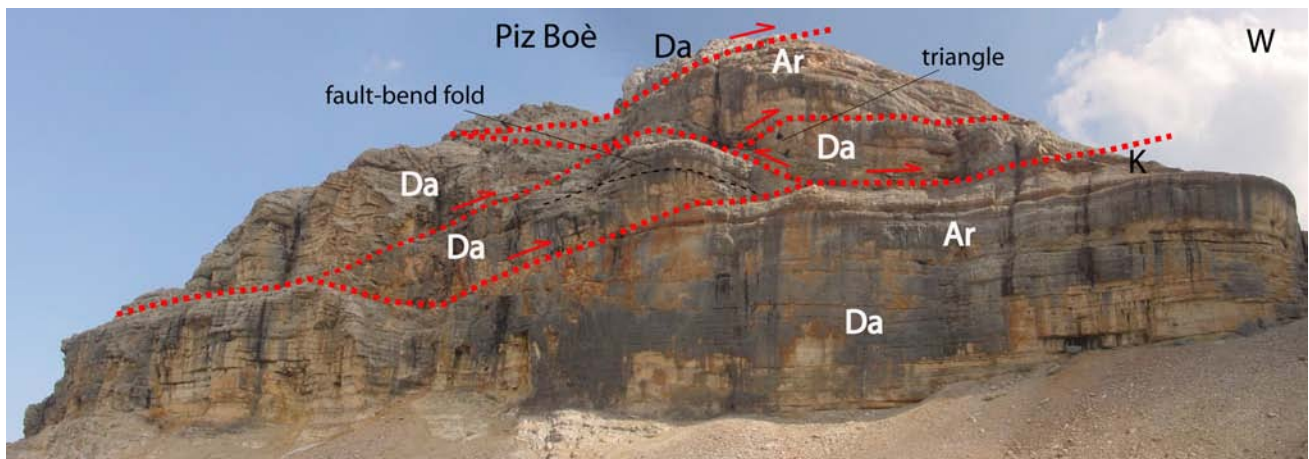


Fig. 4.11 - Northern view of the Piz Boè. Notice the various triangle structures and the ramp-flat geometry controlled by stratigraphy. The basal surface of the thrust system is stratigraphically higher with respect to the southern section of Piz Boè (Fig. 4.10). This is explained by the occurrence of an intermediate lateral ramp (Fig. 4.12). Legend, DP, Dolomia Principale, Norian; Da, Dachstein Limestone, Rhaetian; Ar, Ammonitico Rosso, M-U Jurassic; K, Puez Marls, Cretaceous (after DOGLIONI, 1990).

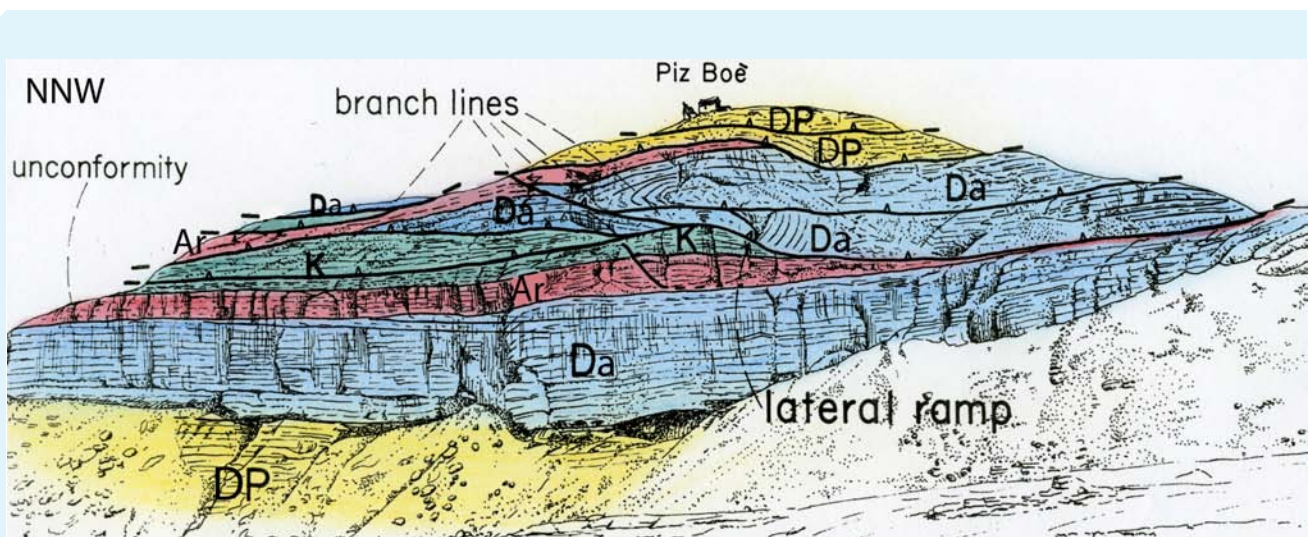


Fig. 4.12 - Western view of the Piz Boè (left front page), a natural section along the strike of the thrust system, that verges towards the observer. The structural link between the previous two sections can be observed. Notice the numerous branches and the main lateral ramp connecting the basal decollements of the northern and southern sections. There is, thus, a continuous structural variation along strike. It is interesting to notice, in the hangingwall of the lateral ramp, a fold whose axis is parallel to the transport direction. Legend, DP, Dolomia Principale; Da, Dachstein Limestone; Ar, Ammonitico Rosso; K, Puez Marls.

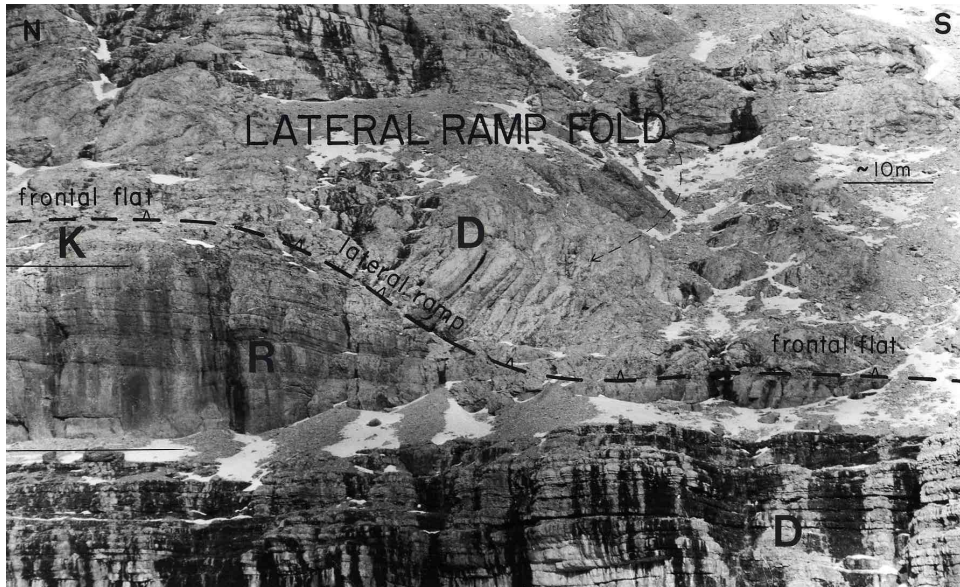


Fig. 4.13 - Detail of the lateral ramp of the previous figure, after DOGLIONI (1990).

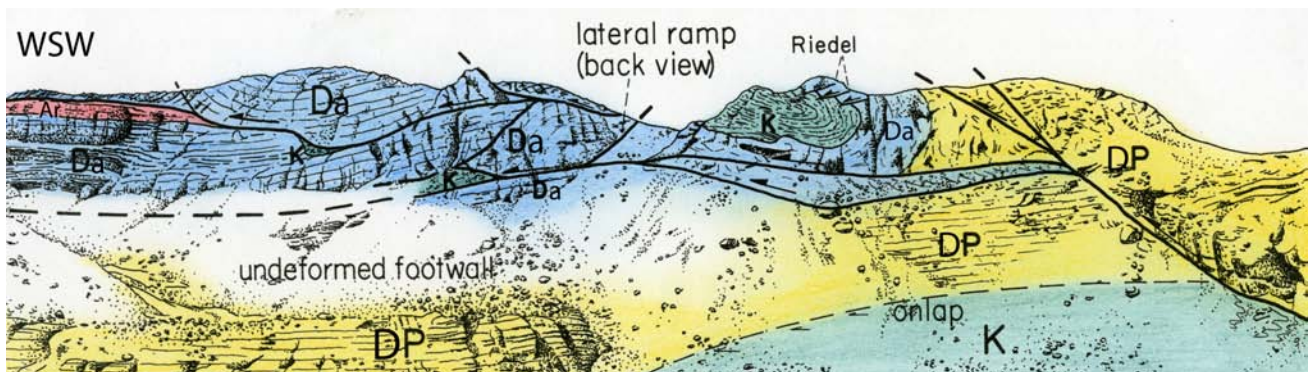


Fig. 4.14 - Eastern view of Piz Boè. Note the constant undulate trajectory of the thrust planes. At the bottom right, a deep scar in the Norian Dolomia Principale (P) is filled by the Early Cretaceous Puez Marls (K). R, Rosso Ammonitico (Middle-Late Jurassic); D, Dachstein Limestone (Rhaetian).

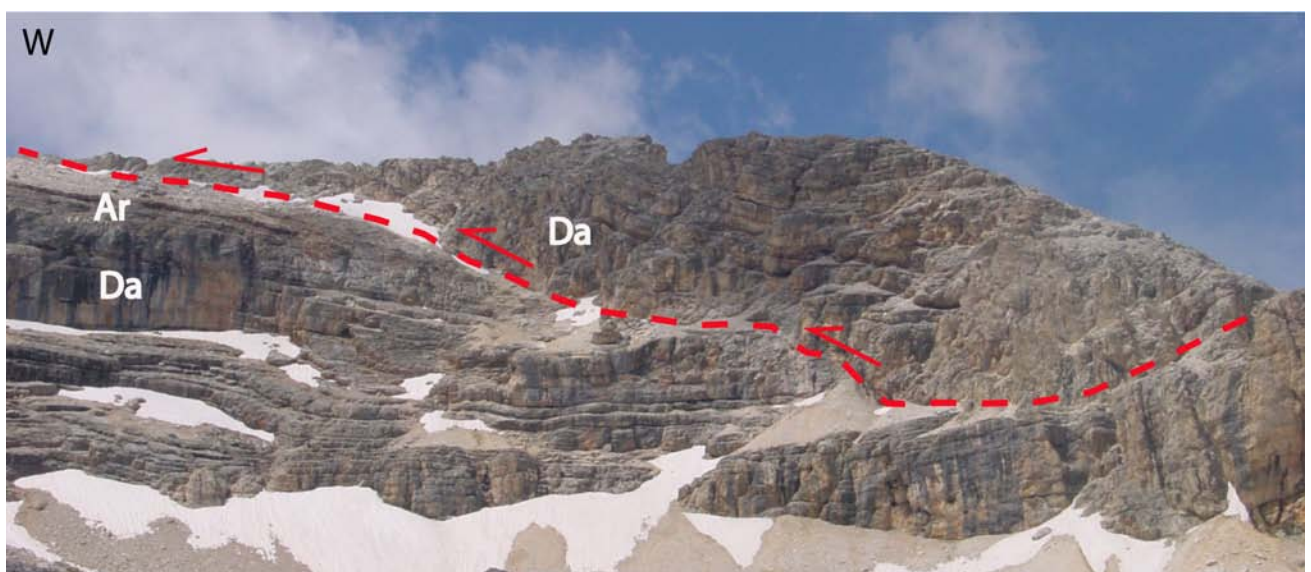


Fig. 4.15 - Detail of the left upper part of the previous drawing. The topmost thrust of the imbricate system of thrusts of the Sella Massif showing undulated geometry with ramps and flats. Da, Dachstein Limestone; Ar, Ammonitico Rosso.

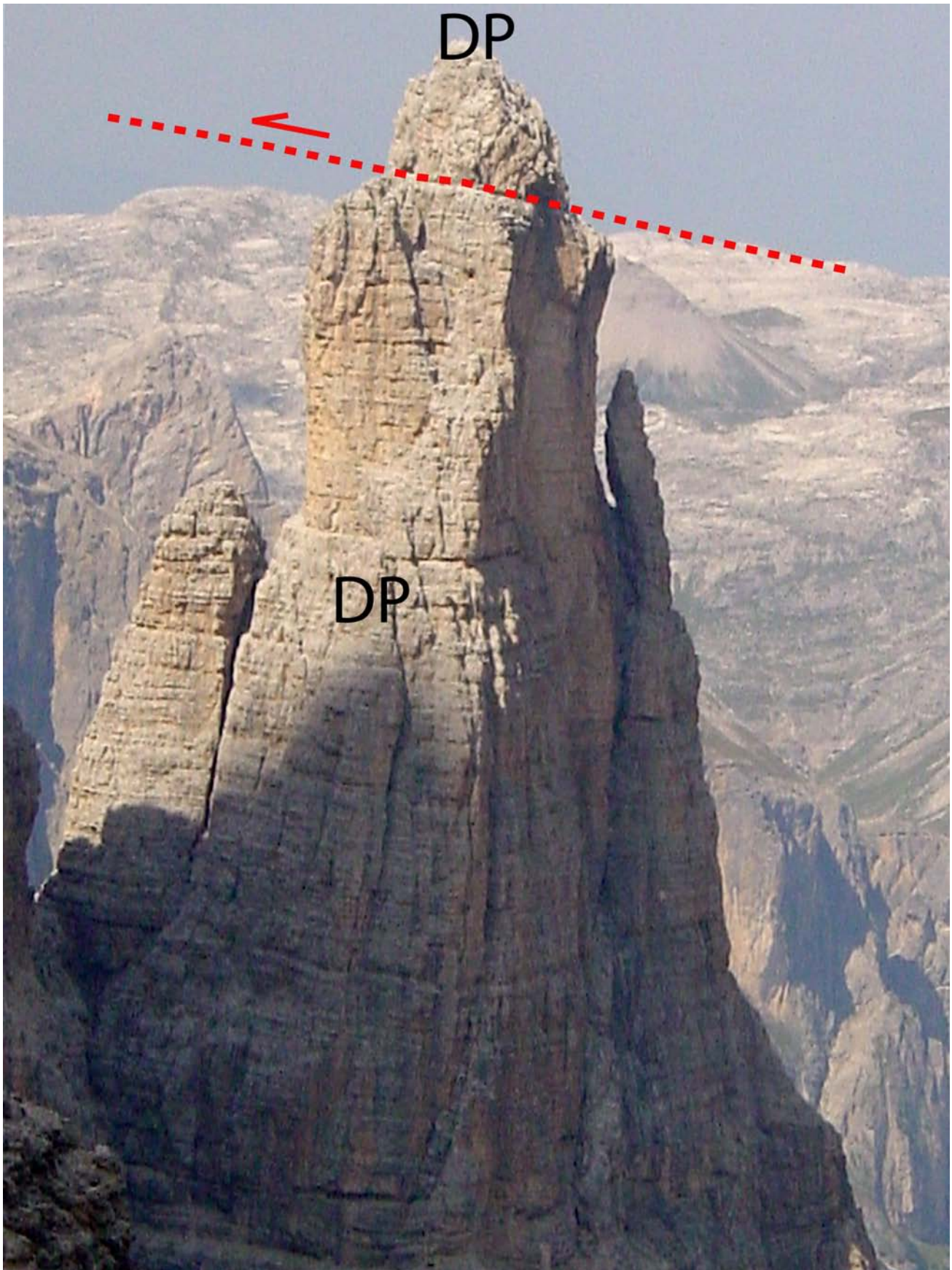


Fig. 4.16 - Classical klippe with Dolomia Principale (DP) both in the footwall and in the hangingwall of a tower located in the left flank of the Val de Mesdi, north of Piz Boè.

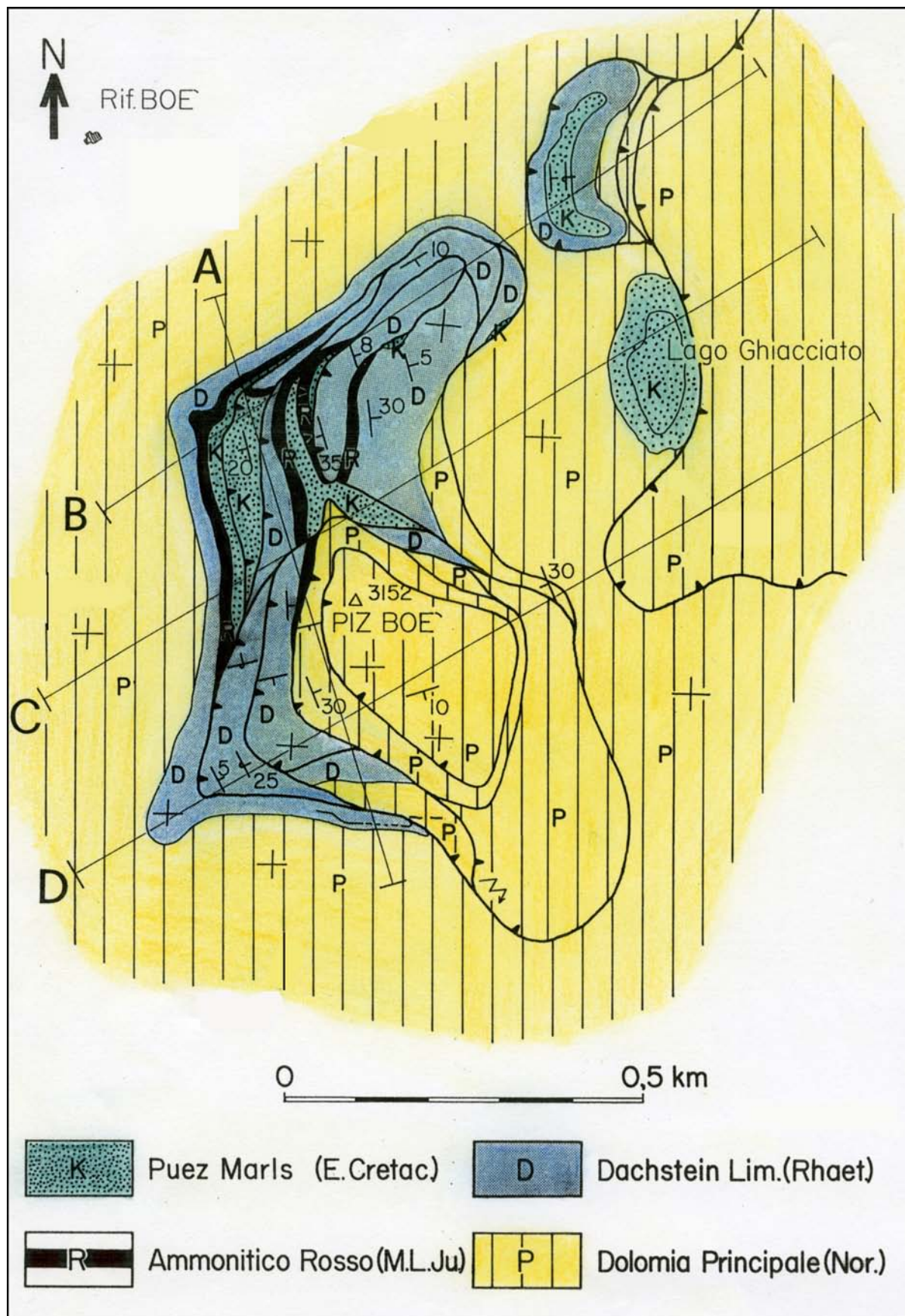


Fig. 4.17 - Geological map of Piz Boè, at the top of the Sella Massif (after DOGLIONI, 1990).

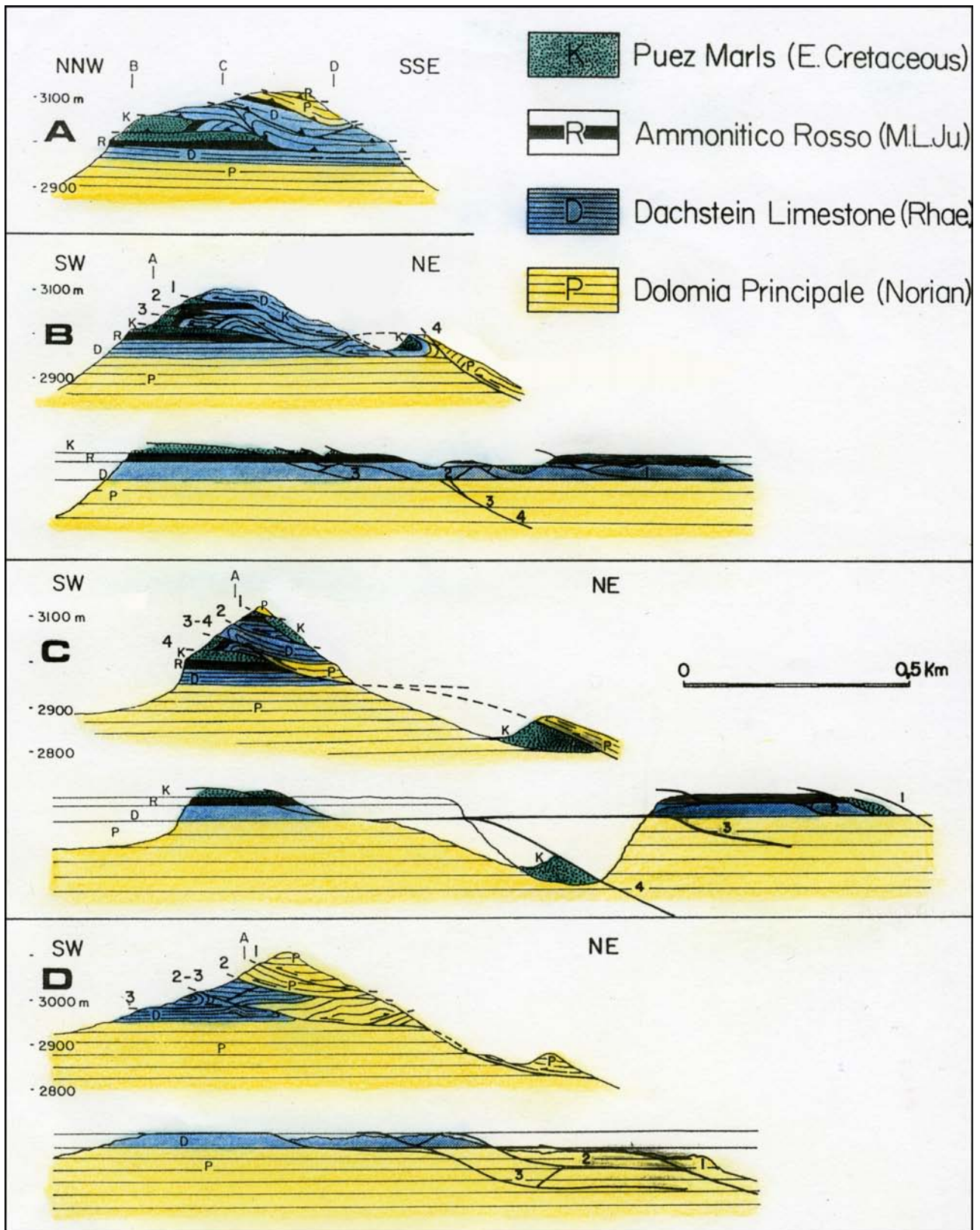


Fig. 4.18 - Geological cross sections across Piz Boè. A is a longitudinal section showing the lateral ramp and the thrust branches that allow the continuous variation of the geometries along strike. The structure is very irregular although the shortening (about 1 km) remains quite constant. The numbers indicate the reconstructed kinematics of the thrust faults. The occurrence of deep scars filled by Puez Marls explains the tectonic transport of Cretaceous sediments above older rocks (e.g., section C). The location of the cross sections is in the previous figure.

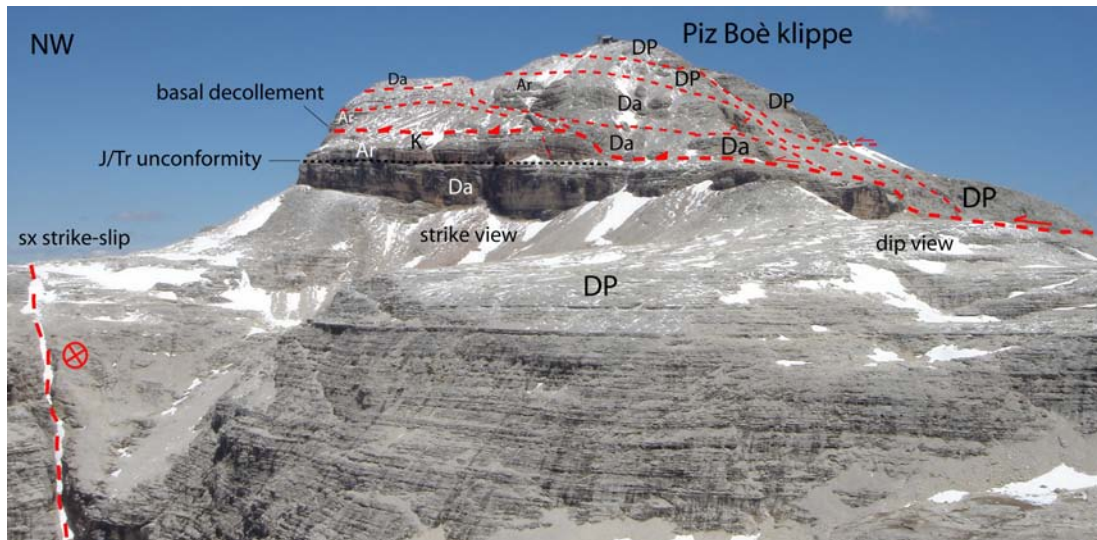


Fig. 4.19 - General view of the top of the Sella Massif, i.e., the Piz Boè with its klippe made of a stack of thrusts with small lateral continuity and a number of branch lines.

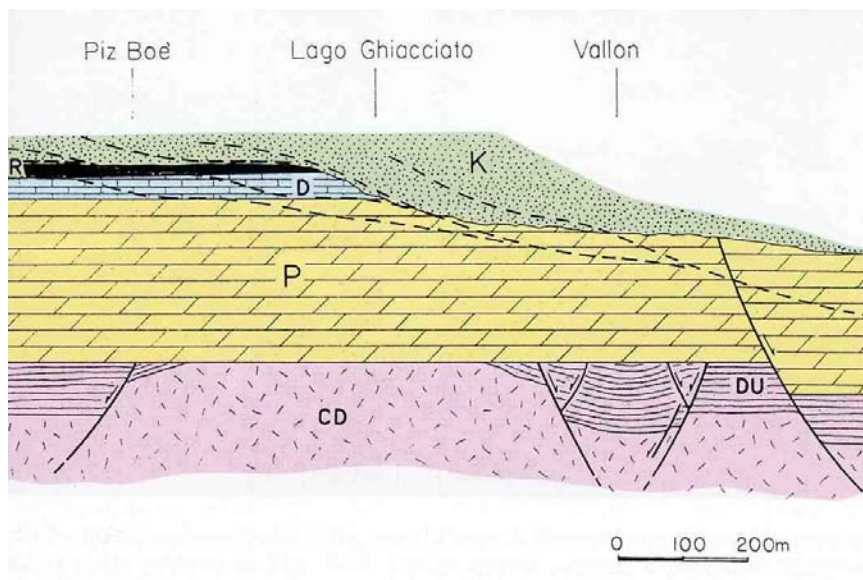


Fig. 4.20 - Stratigraphic relationships in the upper part of the Sella Massif and location of the thrust faults. Sequence boundaries are frequently detachment planes. The thrust faults cut pre-existing Mesozoic extensional faults. Notice also the Cretaceous erosional surface. CD, Cassian Dolomite (Middle Carnian); DU, Dürrenstein Dolomite (Upper Carnian); P, Dolomia Principale (Norian); D, Dachstein Limestone (Rhetian); R, Ammonitico Rosso (Middle-Upper Jurassic); K, Puez Marls (Lower Cretaceous).

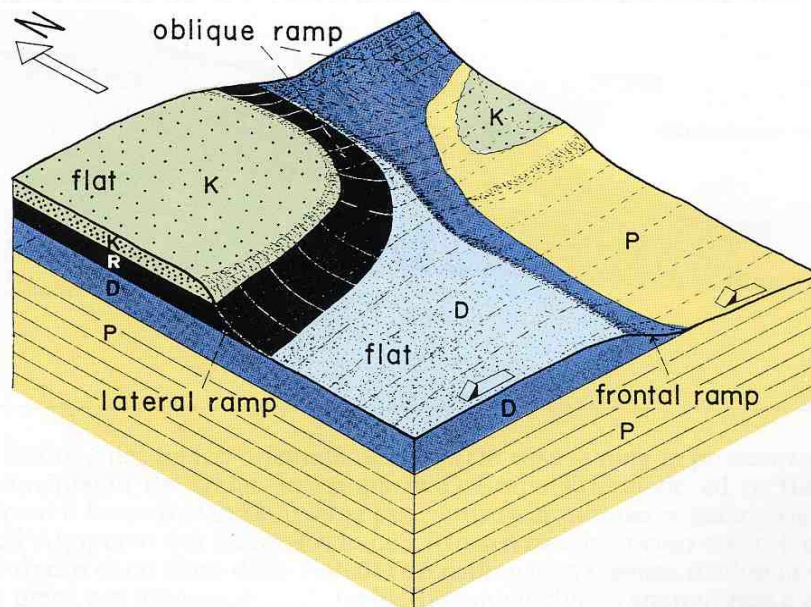


Fig. 4.21 - Geometry of the basal detachment surface of the Sella thrust. P, Dolomia Principale; D, Dachstein Limestone; R, Ammonitico Rosso; K, Puez Marls (after DOGLIONI, 1990).

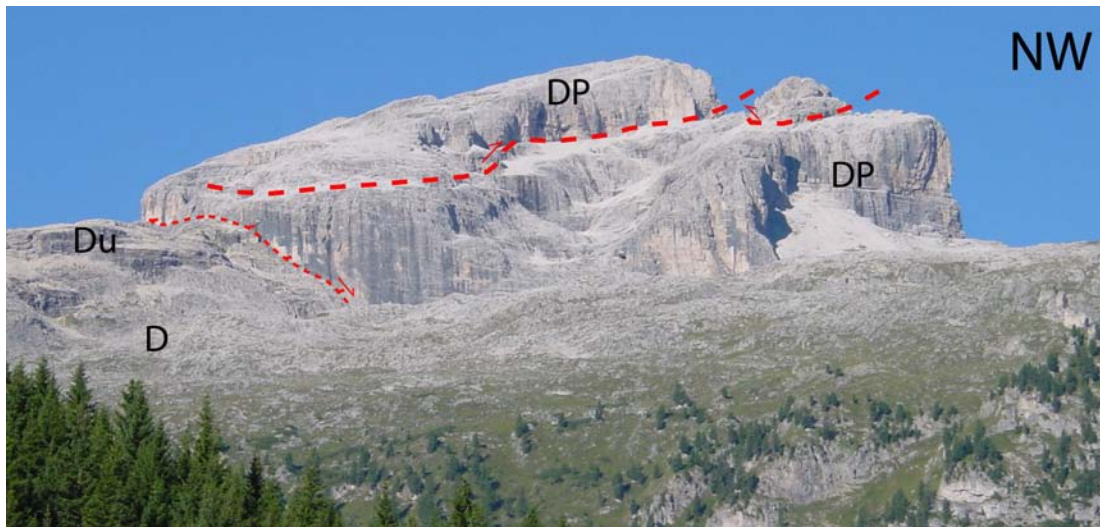


Fig. 4.22 - Eastern ramp of the Sella Thrust, where two klippen of Dolomia Principale (DP) crop out in the northeastern part of the massif. View from the road between Corvara and the Campolongo Pass. Du, Dürrenstein Dolomite; D, Cassian Dolomite.

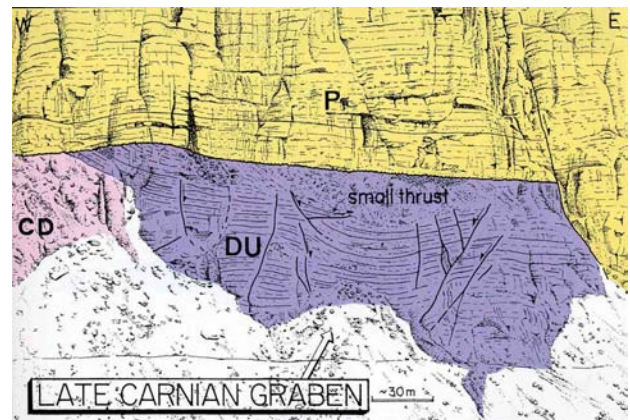
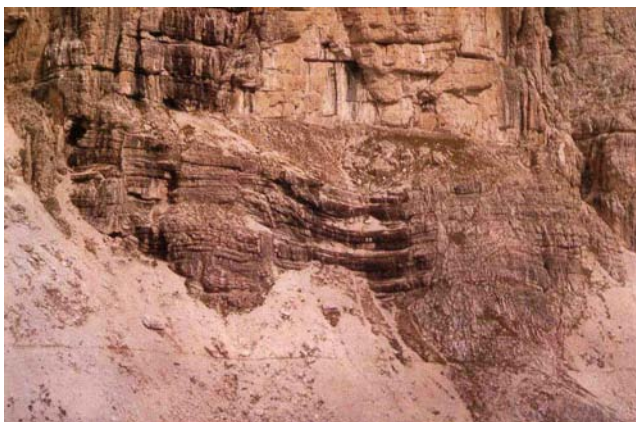
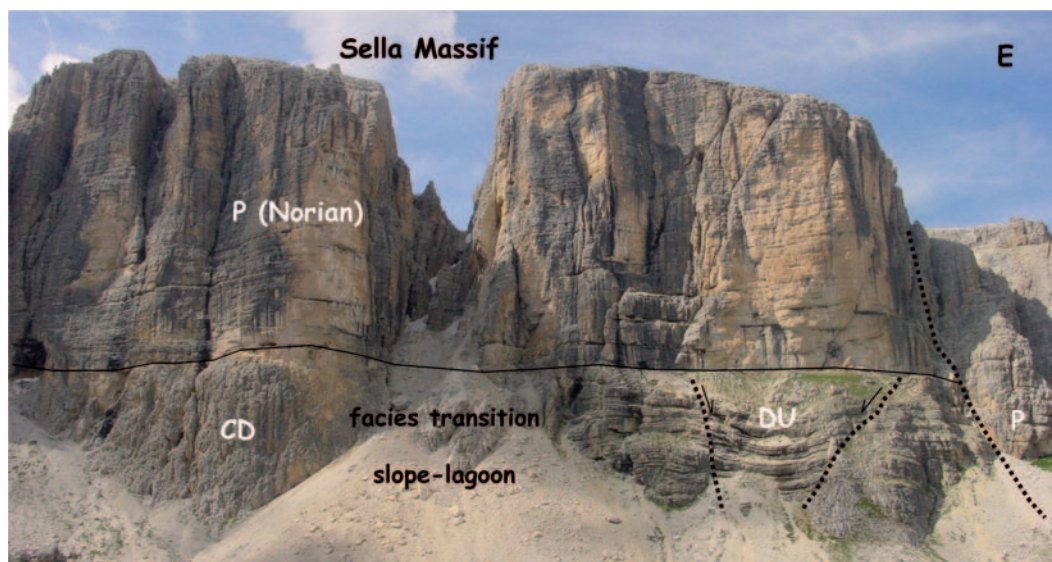


Fig. 4.23 - In the Vallon del Serla (Serla canyon), east of Piz Boè, an Upper Carnian N-S oriented graben, sealed by the Dolomia Principale, crops out undeformed in the footwall of the Sella thrust. P, Dolomia Principale (Norian) above the unconformity; DU, Dürrenstein Dolomite; CD, Cassian Dolomite.

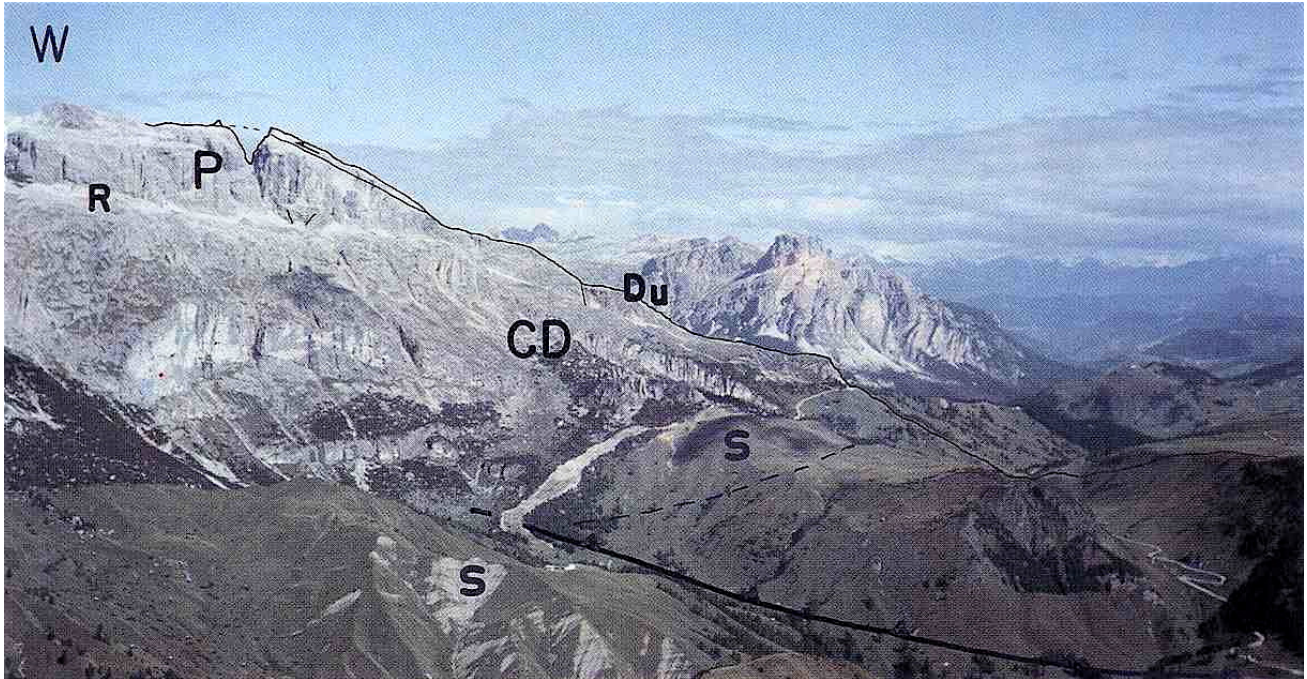


Fig. 4.24 - Eastern flank of the Sella Group and Campolongo Pass. The black profile shows the trace of the section of Fig. 4.25. Along this section the eastward continuation of the Sella thrust to lower stratigraphic levels can be observed. CD, Cassian Dolomite (Middle Carnian); S, San Cassiano Fm (Middle Carnian); Du, Dürrenstein Dolomite (Upper Carnian); R, Raibl Fm; P, Dolomia Principale (Norian). In the foreground, near Arabba, the Livinè Line (a thrust fault sealed by the San Cassiano Fm, 600-700 m thick to the left and only 150-200 m to the right) is indicated.

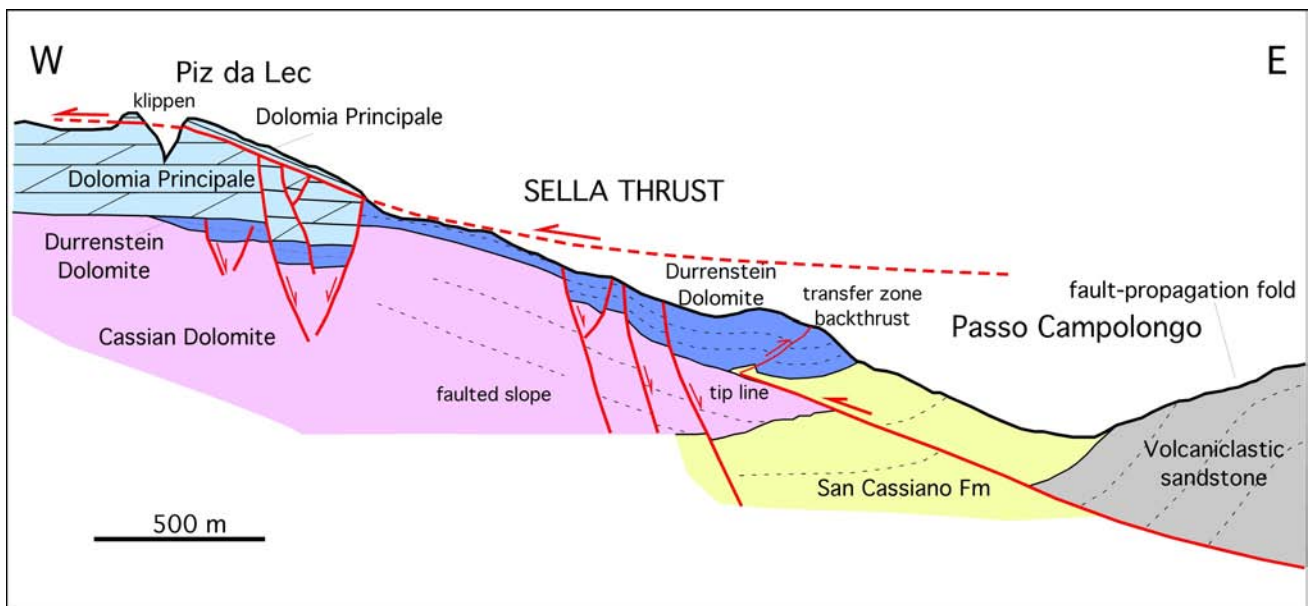


Fig. 4.25 - Geological section of the eastern flank of the Sella Massif. The eastward continuation of the Sella thrust (ramp in the Dolomia Principale and flat at its top) can be observed. Towards the bottom of the section, the thrust plane is partly eroded and crops out again more to the east in the meadows of the Altipiano del Chertz-Pralongià. A blind thrust, however, occurs above the slope of the Carnian carbonate platform (Cassian Dolomite) and is associated to a fault propagation fold. The inclined stratigraphic plane was thus a heterogeneity that controlled the distribution of the shortening. N-S trending synsedimentary extensional faults disrupted the continuity of the slope. They are upper Carnian (syn-Dürrenstein Dolomite) or younger (after DOGLIONI, 1992).

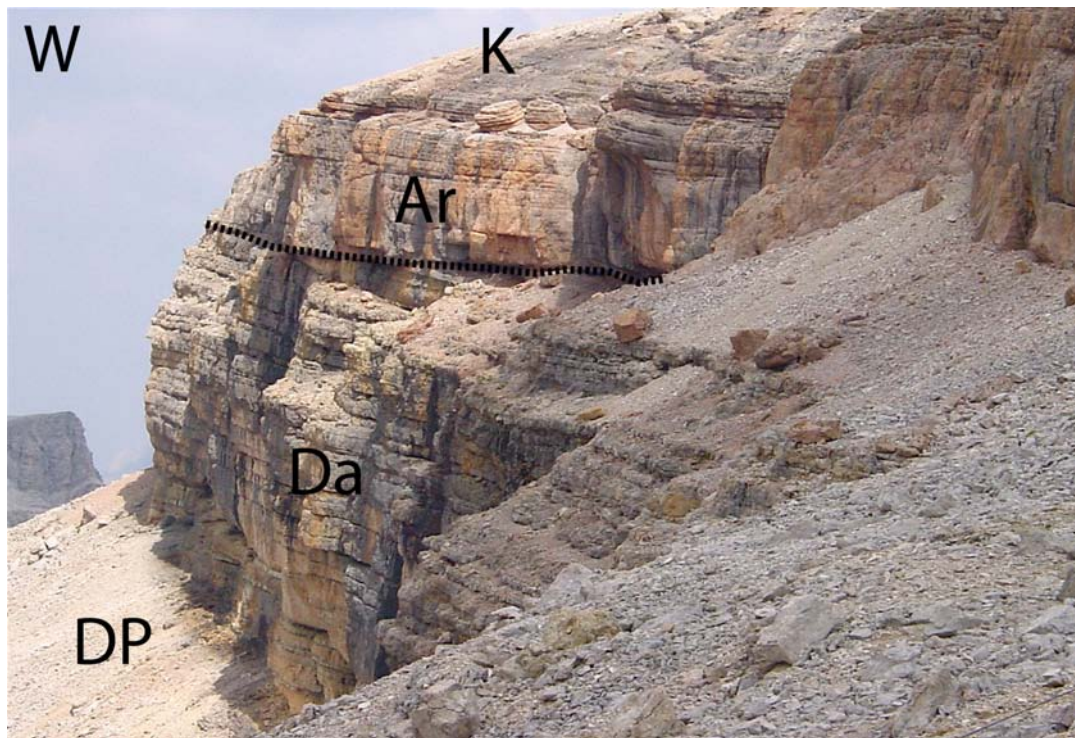


Fig. 4.26 - Angular unconformity between the Middle-Late Jurassic condensed sequence of the Ammonitico Rosso (Ar) and the underlying Rhaetian Dachstein Limestone (Da). DP, Dolomia Principale; K, Puez Marls. At the unconformity occurs a several cm thick hardground. Note the absence of the Liassic Calcarei Grigi in this part of the Trento Horst. Moving eastward, the early Jurassic appears with few hundred meters thickness, suggesting synsedimentary tectonics.

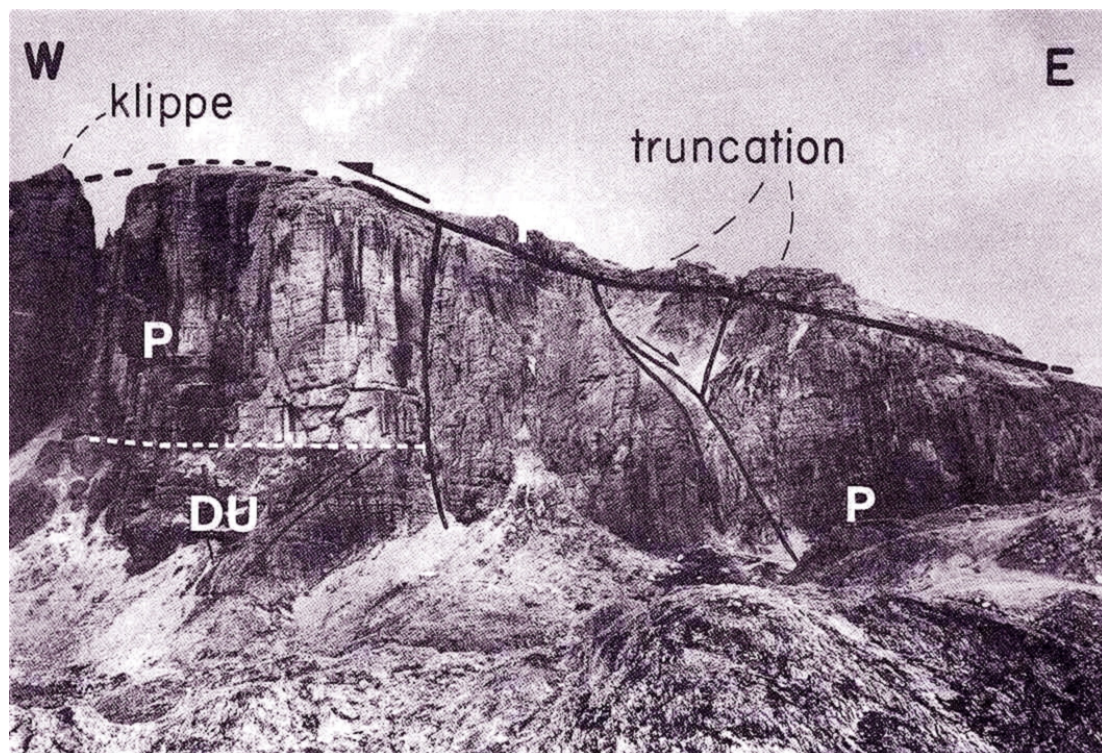


Fig. 4.27 - Detail of the western part of the section of Fig. 4.25. Vallon del Serla, east of Piz Boè. Note the W-vergent thrust with ramp and flat geometry. The dislocation plane cuts N-S trending extensional faults. P, Dolomia Principale; DU, Dürrenstein Dolomite. The hangingwall is made of Dolomia Principale.

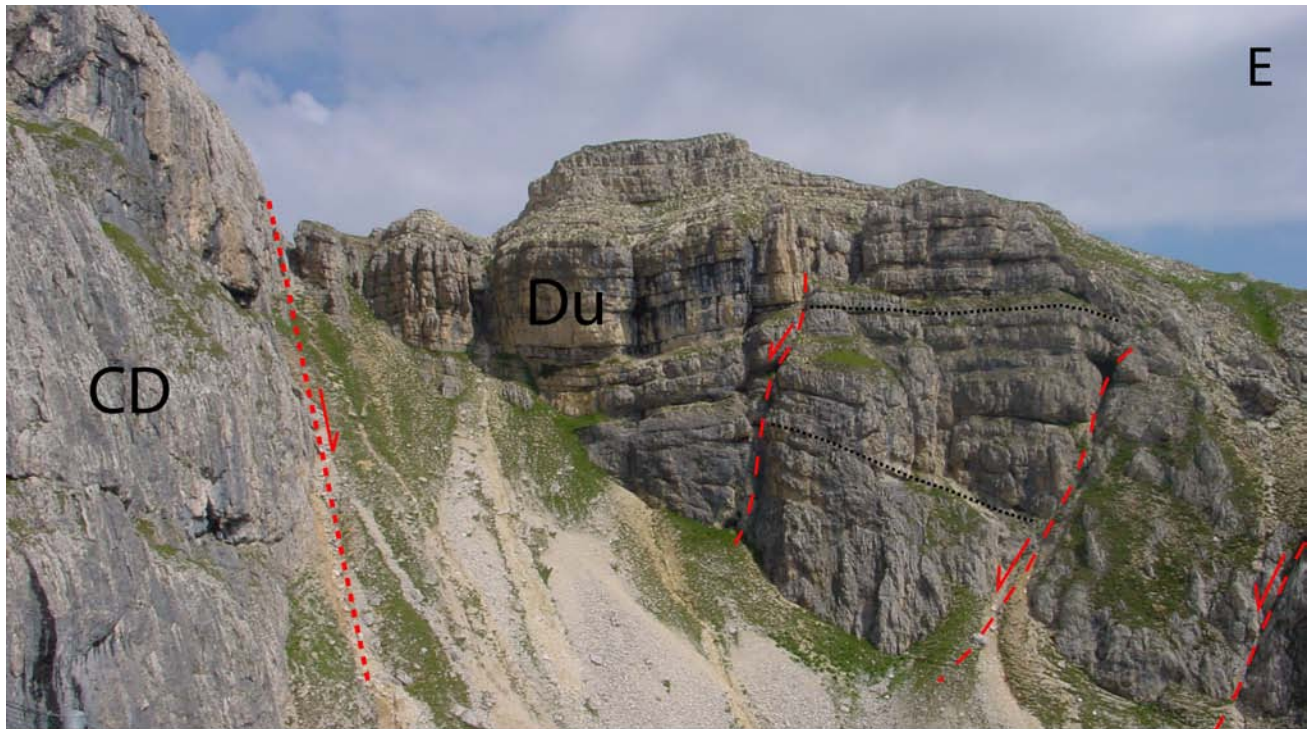


Fig. 4.28 - Detail of the central part of the section of Fig. 4.25. The syndimentary character of the N-S extensional faults is evidenced by the angular unconformities within the Dürrenstein Dolomite (Du). CD, Cassian Dolomite.

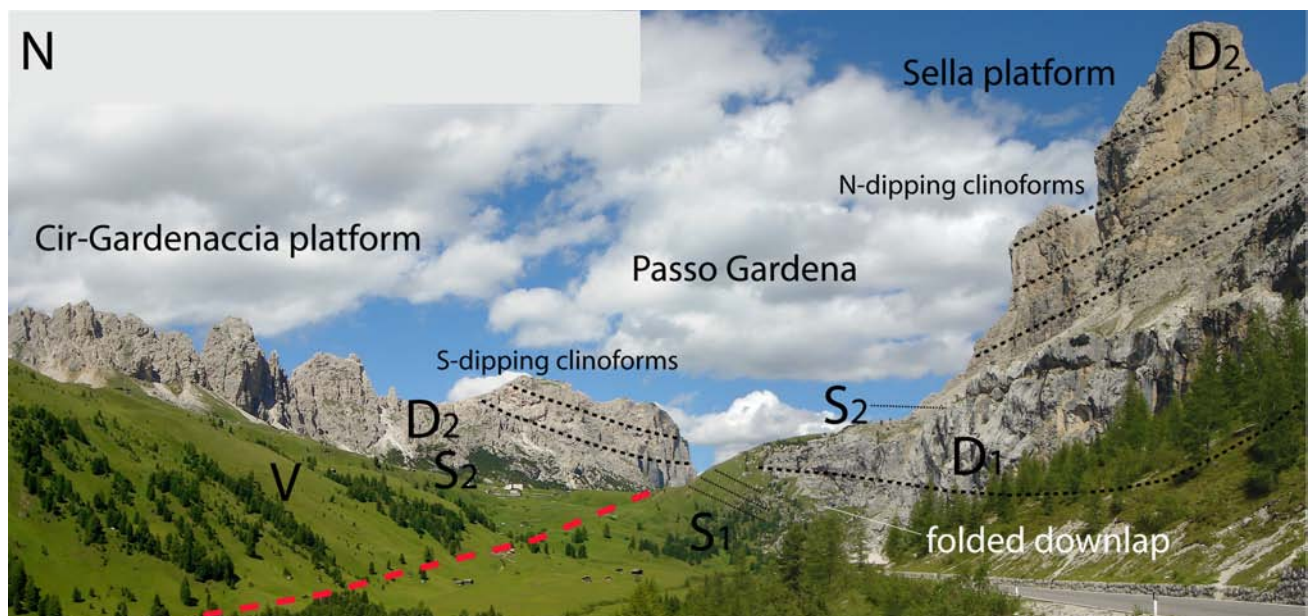


Fig. 4.29 - Two opposite prograding platforms border the Passo Gardena. A fault, possibly with a left-lateral component, runs across the pass. To the south the lower part of the Sella megabreccias are folded and thicker, suggesting a syndimentary Carnian origin of the deformation since the upper part is undeformed, as shown by the angle between the upper clinoforms and the lower ones. See the interpretation in the next figure. Carnian, D2, Upper Cassian Dolomite; S2 Upper San Cassiano Fm; D1, Lower Cassian Dolomite; S1, Lower San Cassiano Fm; Ladinian, V, volcanoclastic sandstone. Note in the northern side, that V is at the same structural elevation of D1 south of the fault, and the missing (or highly reduced?) D1 and S1.

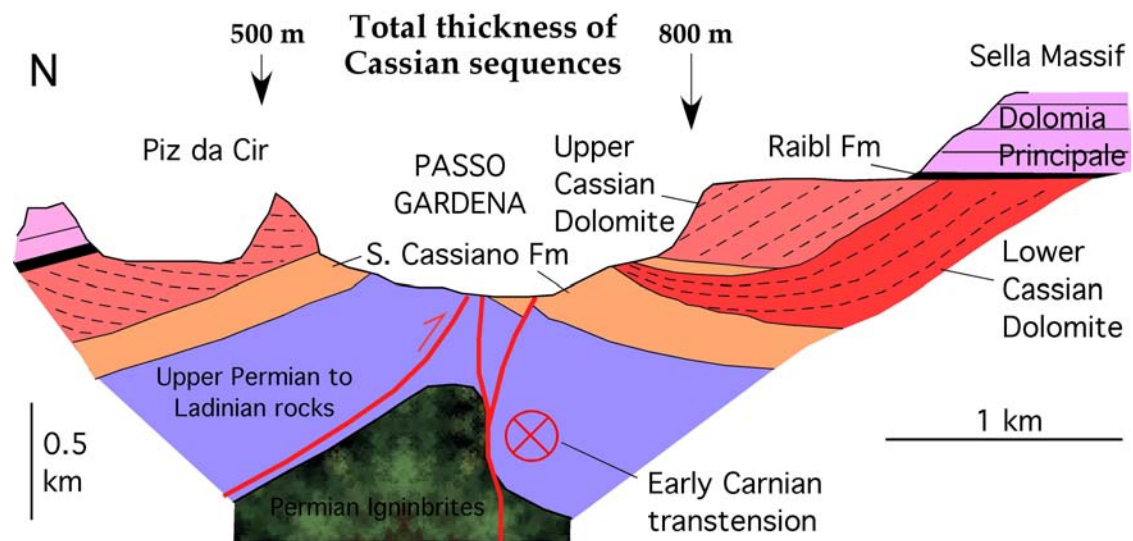


Fig. 4.30 - Geological section of the northern side of the Sella Group, through the Gardena Pass, where two Carnian carbonate platforms converge with their progradation. At the Gardena Pass, a sinistral transtensional fault system, Triassic in age and trending roughly E-W, crops out. The kinematics of the fault system is indicated by slickenlines, attitude of the fault plane and changes of sediment thicknesses left and right of the fault. For example, to the south (right) of the fault, the lower Cassian Dolomite occurs, whereas it is not present to the left. Moreover, the same dolomite is folded syndepositionally in its lower part, near the Passo Gardena Line. A S-vergent Alpine thrust complicates the structure (after CHANNELL & DOGLIONI, 1994).

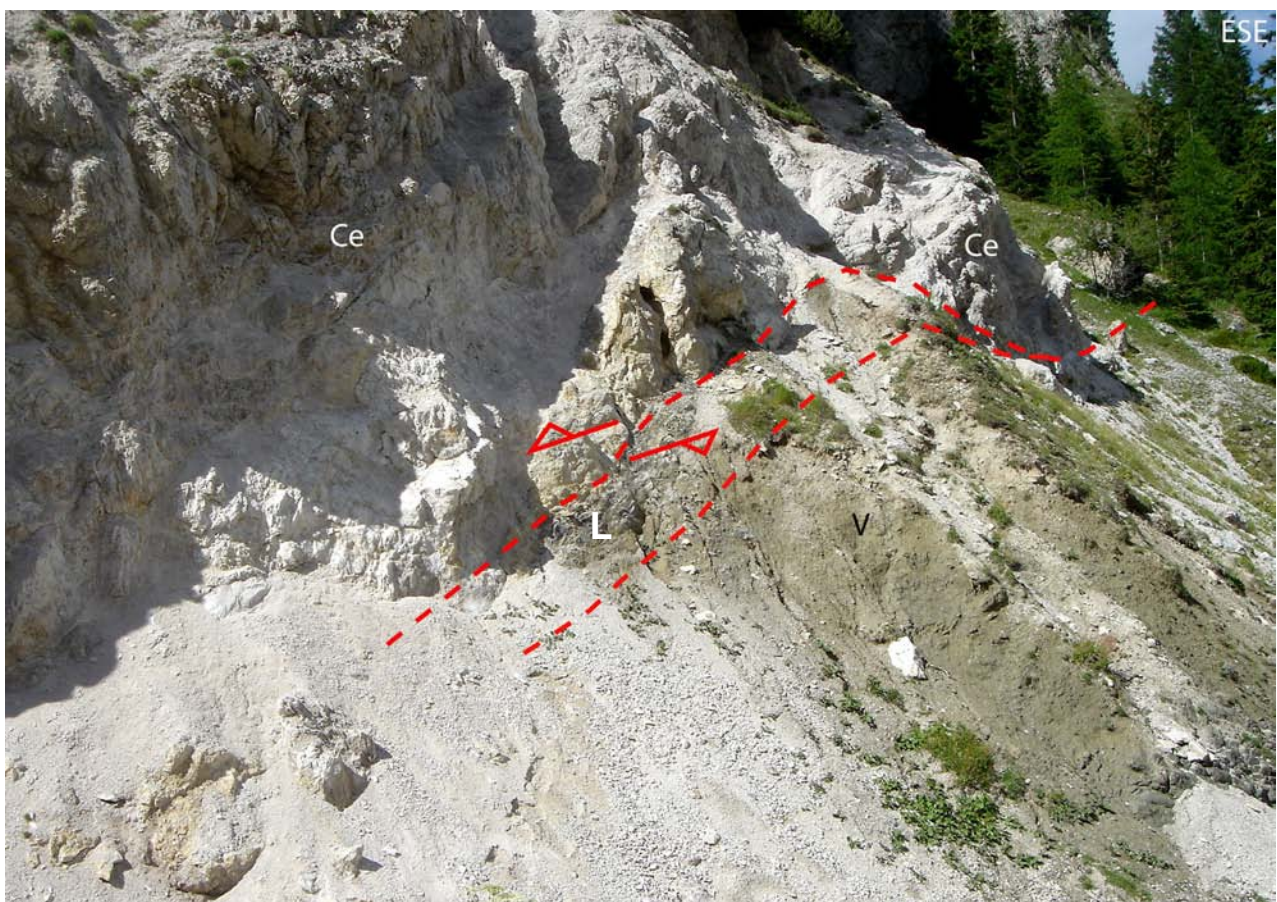


Fig. 4.31 - Outcrop of the Passo Gardena Line, along the road between Corvara and Passo Gardena. Ce, olitoslith of Contrin Fm included in the Ladinian Caotico Eterogeneo; L, Livinallongo Fm, dark marly limestones; V, volcanoclastic sandstones. On the sub-vertical N70°-90°E trending fault plane there is evidence for left-lateral transtensive/transpressive component.

5th Day

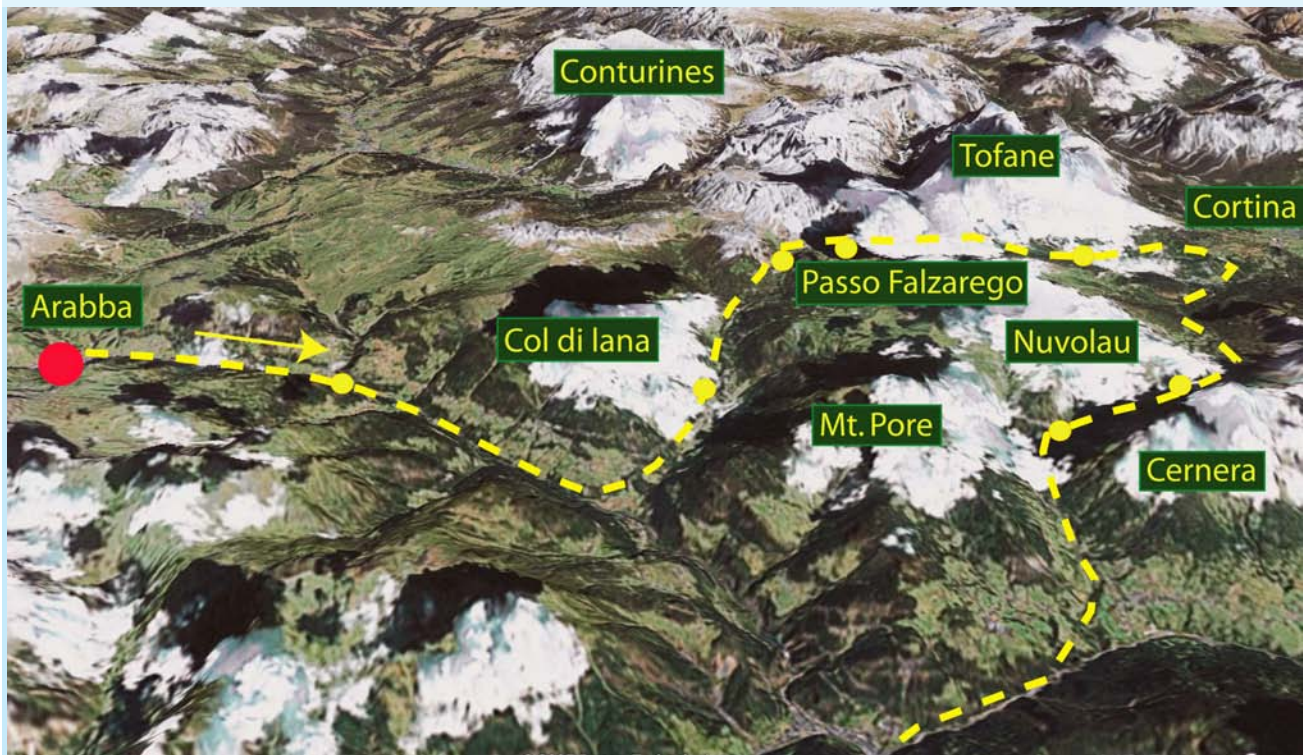


Fig. 5.0 - Itinerary: Passo di Campolongo, Passo Falzarego, Passo Giau, Agordo.

Subject: Tectonics-stratigraphy relationship, Mesozoic extension and inversion structures

In the Middle Triassic of the Dolomites, extensional tectonics and local compressional effects coexisted. This can be explained by the occurrence of a transtensional regime with local transpressional effects. Near Arabba, both aspects can be observed in the field: the Livinè Line (a Middle Triassic thrust fault en-echelon with the transcurrent faults) and the Varda Line (an Upper Ladinian extensional fault). The Dolomites are characterised by extensional synsedimentary structures excellently exposed and preserved from the Alpine shortening. The extensional faults are characterised by a quite stable N-S trend, as in the whole Tethyan, African and North Atlantic domain, suggesting a global significance for such a regularity. The age is variable from Upper Permian

to Scythian, to Ladinian, Carnian and Jurassic. The spacing between the main normal faults is quite regular. A major subsidence step reported in literature at least for the Liassic is located in Val Badia, between the Puez Massif to the west (without Calcarei Grigi Fm in the stratigraphic sequence) and the Fanes massif to the east (characterised by several hundred meters of Calcarei Grigi Fm). This extensional zone is the border between the Trento Platform and the Belluno Basin and was inverted and re-sheared as a ramp by later WSW-vergent thrust faults. The interference between paleostructures and tectonics can be excellently studied also at the Falzarego Pass. Here, in the hangingwall of the Falzarego thrust, a Carnian graben was cut passively since it is characterised by high angle extensional faults at approximately 90° with respect to the direction of compression. Moreover, the margin of the

Lagazuoi carbonate platform influenced the thin-skin geometry of the thrust that forms a lateral ramp where the carbonate platform terminates. During this day we will study various structures formed by the tectonic interference between the earlier WSW-verging thrusts and the younger SE-verging thrust.

Moreover, we will cross the belt towards the foreland, crossing the Valsugana thrust (cropping out just after Agordo), the Belluno thrust and the frontal triangle structure. In previous stages of the belt, the Belluno Line was likely the front of the belt and could have been itself a triangle zone, similar to that now observed at the northern margin of the Venetian plain.

In the Mesozoic, the regularity of extensional faults and transfer zones suggests the occurrence of a relative flow between lithosphere and sub-lithospheric mantle. Lateral heterogeneities and distribution and shape of lithospheric anisotropies control the subductions and, therefore, the geometry and evolution of mountain chains. Consequently, from the geometry of mountain belts it is possible to reconstruct the zones of thinned lithosphere (i.e., the Mesozoic basinal areas). These informations are of fundamental importance when reconstructing the paleogeography of the Mediterranean area.

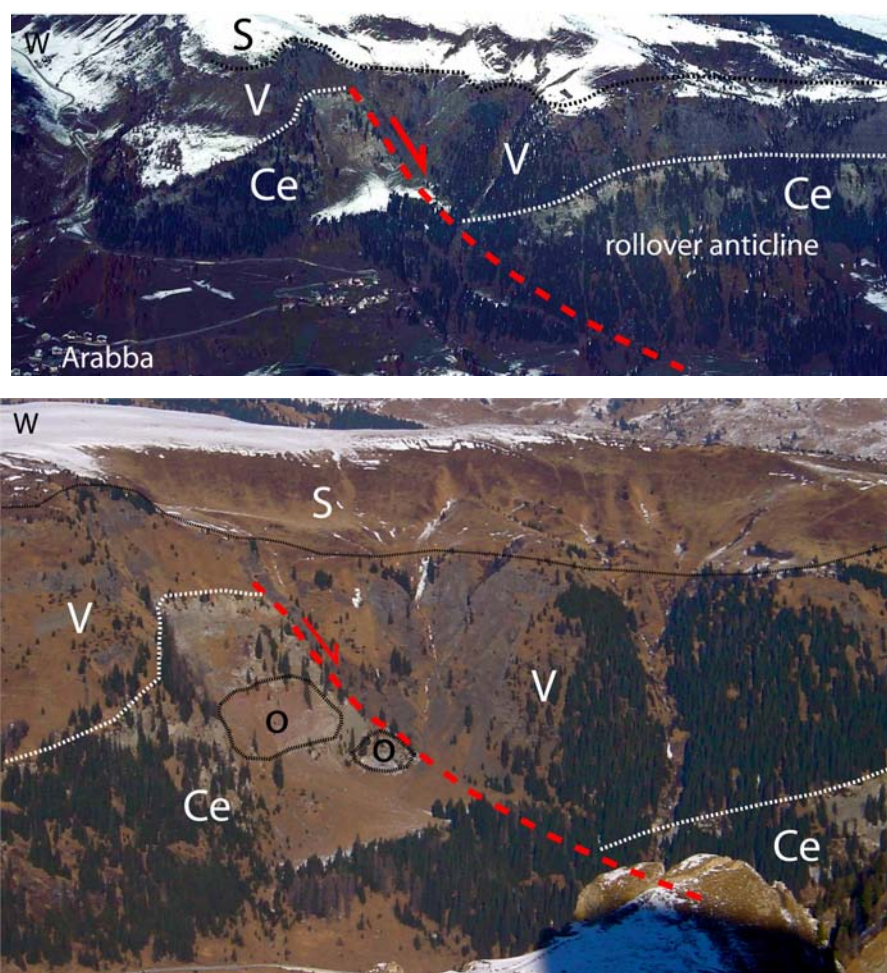


Fig. 5.1 - Distal (above) and closer (below) view of the Varda Line, a N-S synsedimentary extensional fault of upper Ladinian age, near the village of Varda, close to Arabba, Central Dolomites. The throw is evidenced by the greyish formation of the Caotico Eterogeneo (Ce), a conglomerate with poligenic clasts of volcaniclastic and of sedimentary (including large olistholiths (o) of the Werfen Fm and Marmolada Limestone) origin. A gentle rollover anticline occurs in the hangingwall, downthrown to the right, of the fault. The volcanoclastic sandstones (V) of the Upper Ladinian (Fernazza Hyaloclastites, Wengen group) seal the fault with 150 m of thickness to the right and 30-40 m in the footwall. S, Carnian San Cassiano Fm.

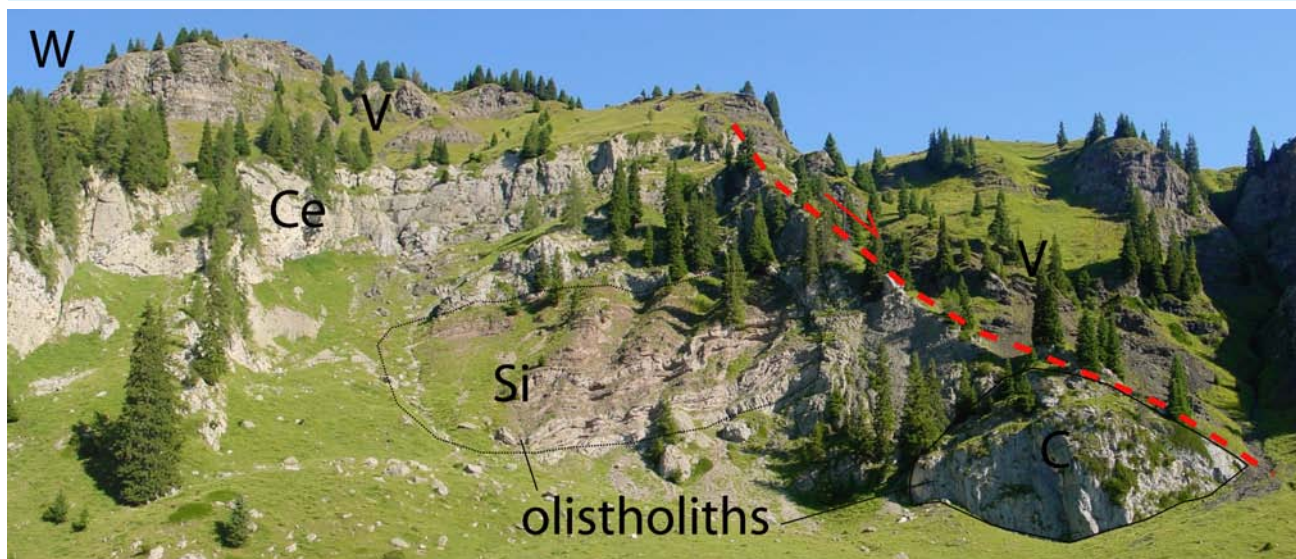


Fig. 5.2 - Detail of the previous figure, where several tens of meters wide olistholiths outcrop in the footwall of a synsedimentary normal fault. The biggest olistholith is made of Siusi Mb (Si) of the Werfen Fm, and Marmolada Limestone (C) included in the Caotico Eterogeneo (Ce). The volcanoclastic Wengen Fm (V) are thicker than 150 m in the hangingwall of the fault, and thinner than 50 m in the footwall indicating the Ladinian growth nature of the listric normal fault.

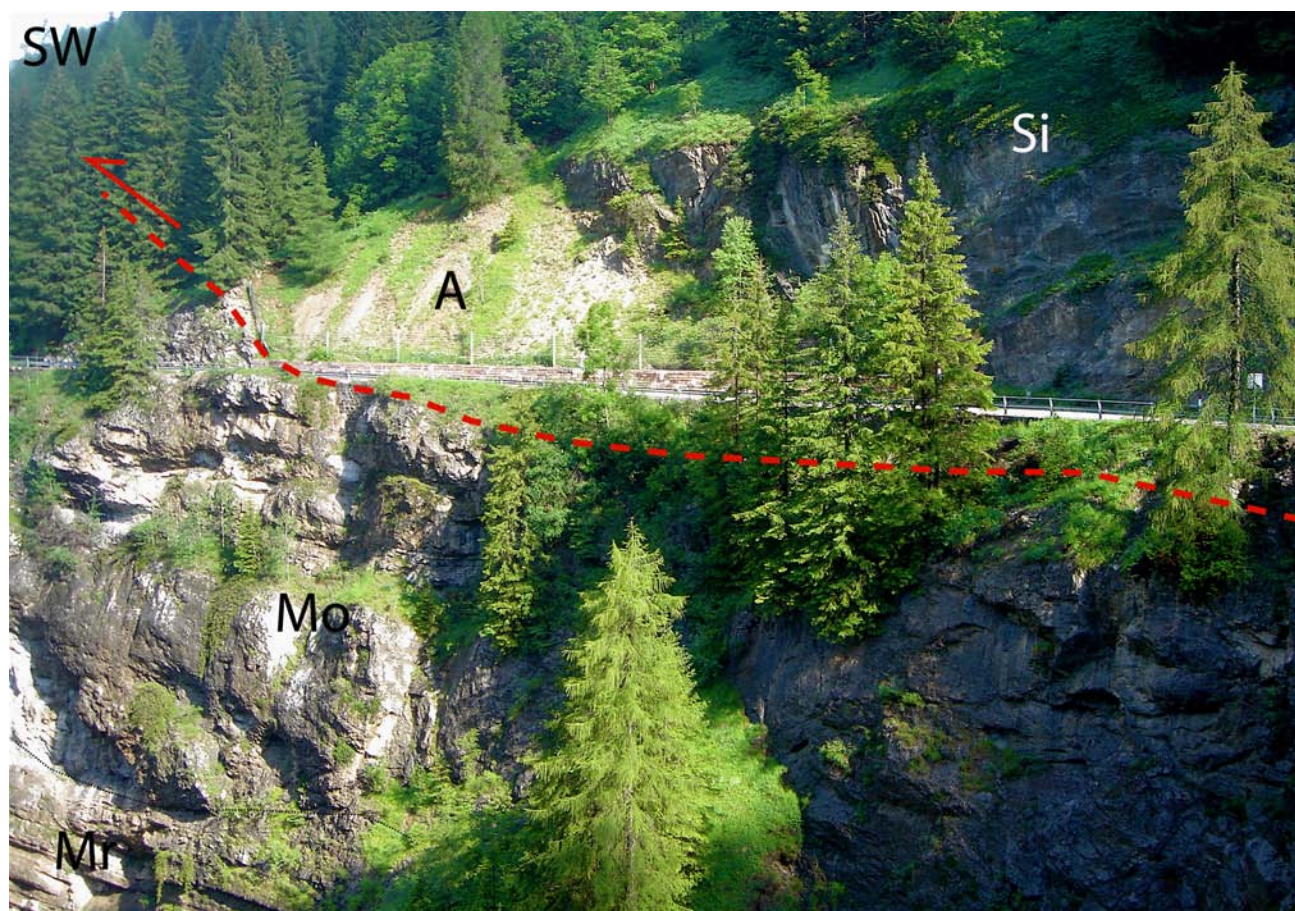


Fig. 5.3 - The Livinè Thrust in the Livinallongo Valley, 4 km east of Arabba. Legend, in the footwall, channelized breccias of the Late Anisian Moena Fm (Mo) over the Morbiac Lm (Mr); in the hangingwall, Scythian Werfen Fm, Siusi Mb (Si), and Andraz horizon (A).

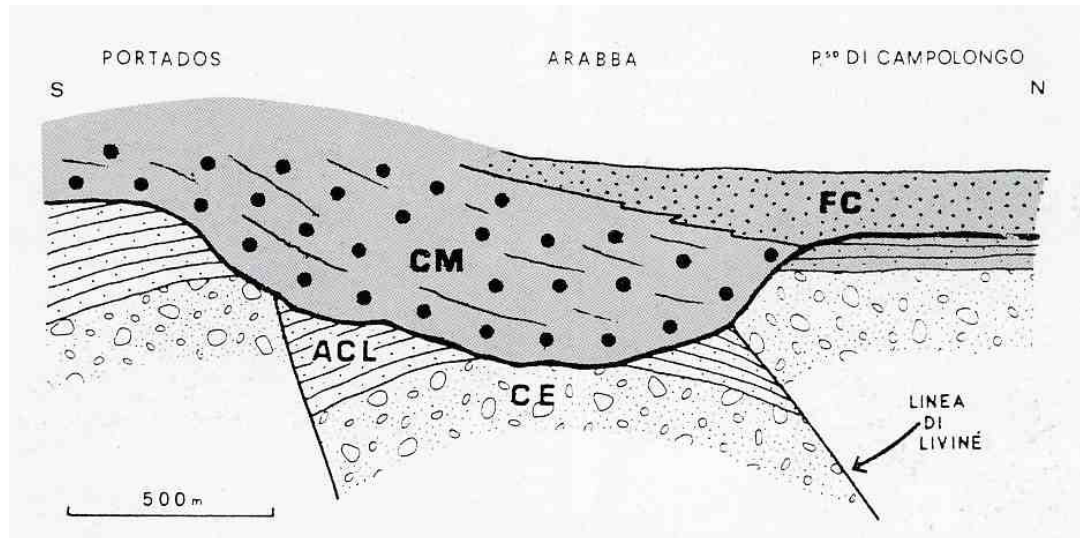


Fig. 5.4 - N-S geological section reconstructed at the Upper Ladinian-Lower Carnian for the Arabba area. The Marmolada Conglomerate (CM) seals an irregular morphology and middle Triassic faults (e.g., the transpressional Livinè Line). The conglomerates pass laterally to sandstones (FC) stratigraphically located at the bottom of the San Cassiano Fm. CE, Caotico Eterogeneo; ACL, Volcaniclastic sandstones, Fernazza Hyaloclastites. Notice that the N 70°-130° trending transpressional structures, as the Livinè Line, coexist with coeval extensional structures trending N-S.

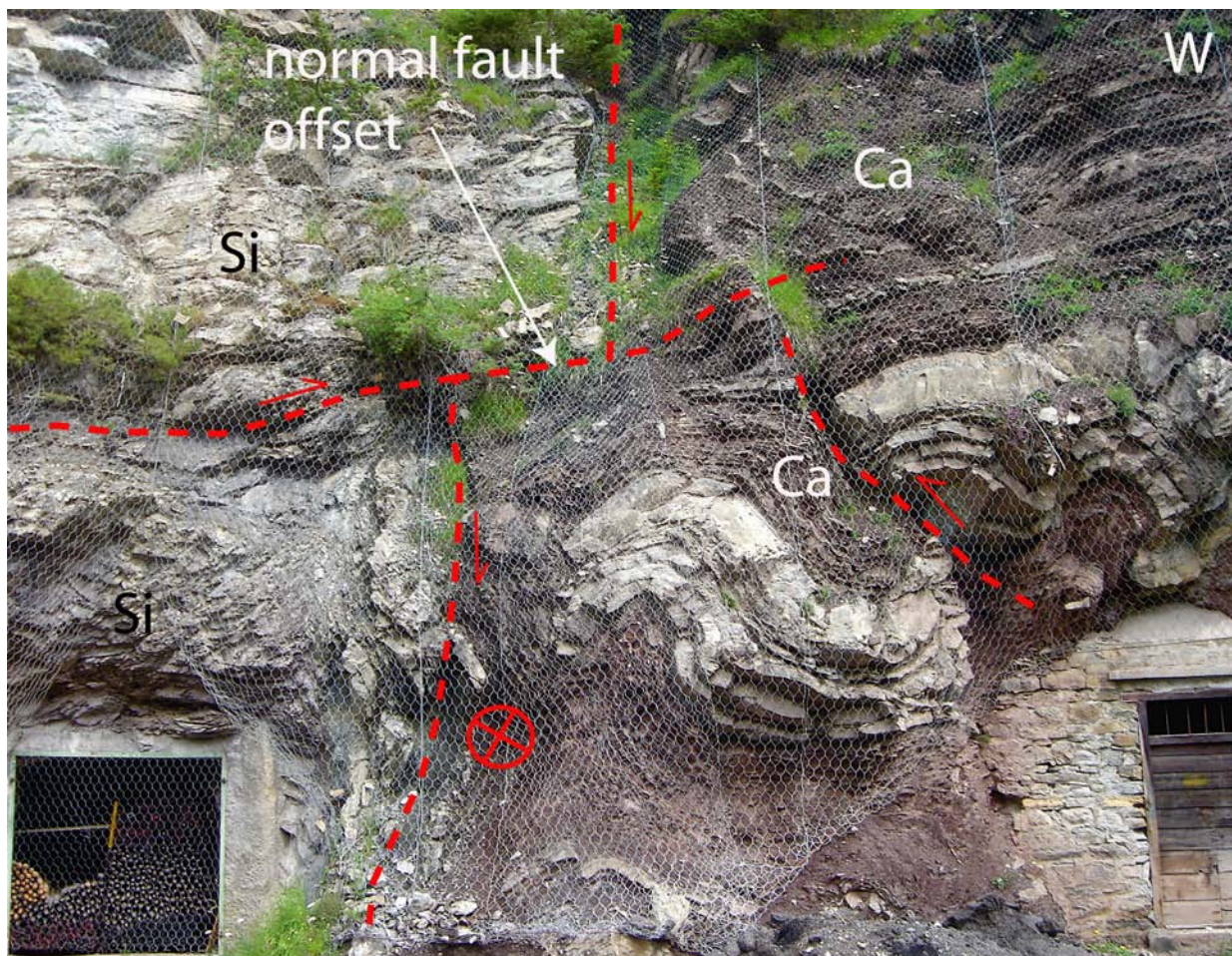


Fig. 5.5 - A N-S trending normal fault in the Werfen Fm (Scythian), sealed by Upper Anisian sequences (not visible in the picture) has been cross-cut and folded by a later E-verging thrust, and the whole visible rocks have been squeezed and buckled. It appears as a meso-scale example of inversion tectonics such as those observed in the North Sea. The N-S pre-existing normal fault has been re-sheared also by left-lateral strike-slip motion during alpine compression. Si, Siusi Mb; Ca, Campil Mb. 1 km west of Andraz.

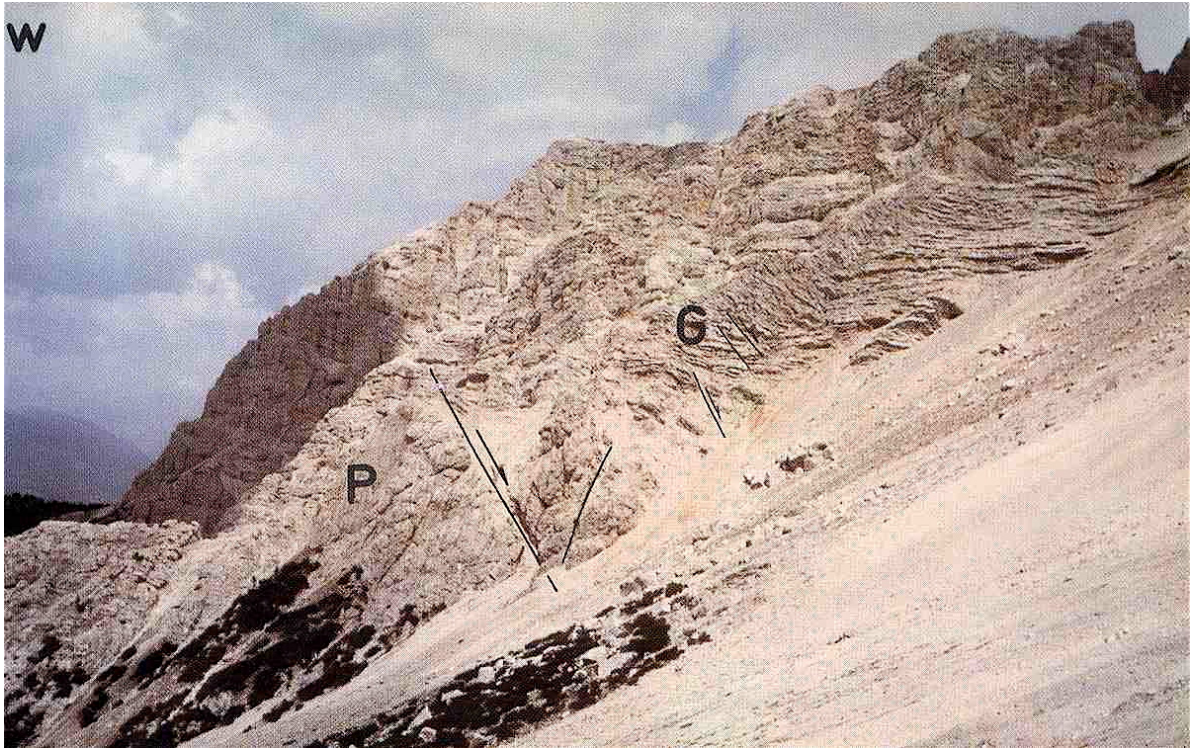


Fig. 5.6 - N10°W trending extensional fault cropping out on the western flank of the Lavarella mountain. Right of the fault, the fan shape of the Calcari Grigi (G) suggests a growth geometry. In the footwall of the fault it occurs the Dolomia Principale (P).

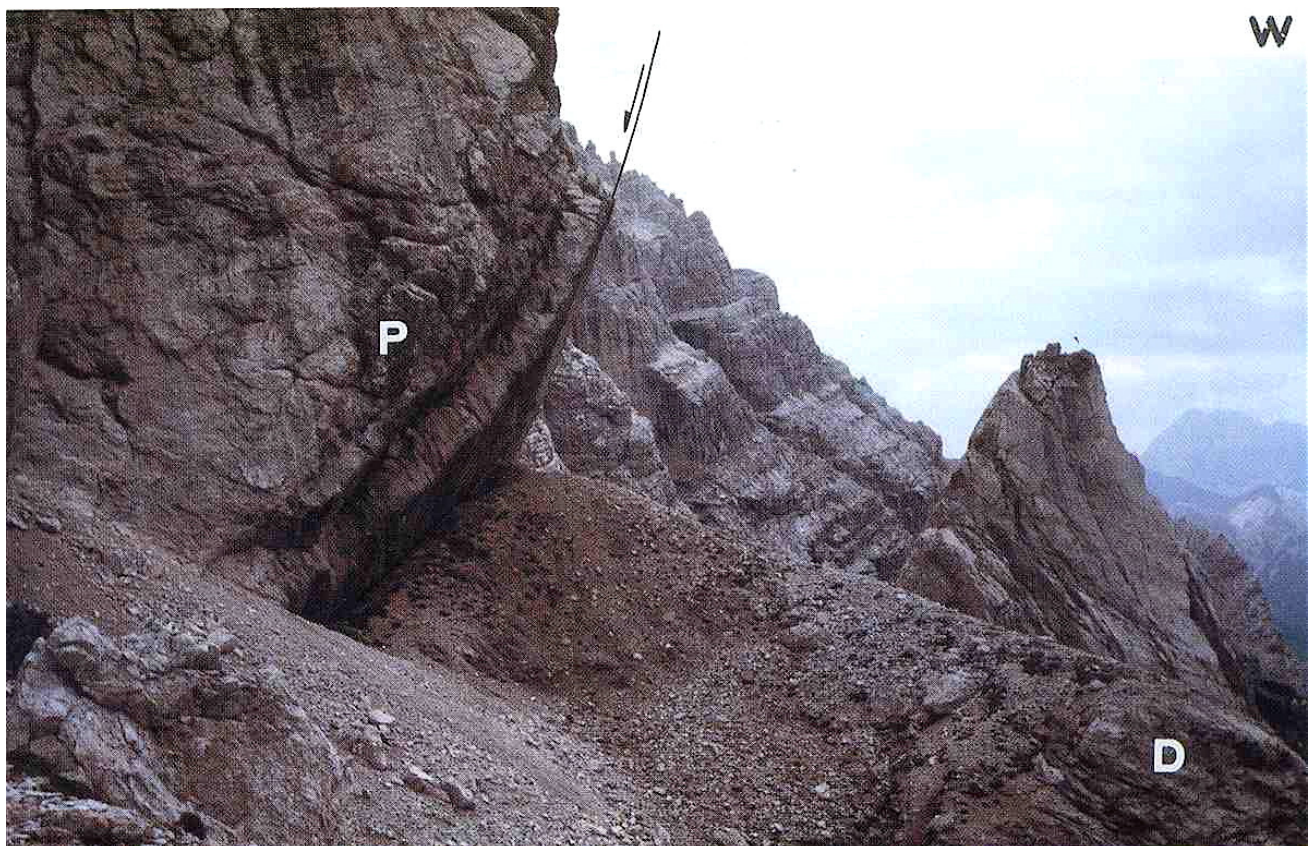


Fig. 5.7 - Detail of the extensional fault of Fig. 5.6, as cropping out to the south. The Dolomia Principale (P) is in the hangingwall and Carnian marls and Cassian Dolomite (D) in the footwall. The slickenlines on the fault surface are subvertical. The fault dips to the east (left) and is underlined by a thin reddish-blackish oxidised crust.

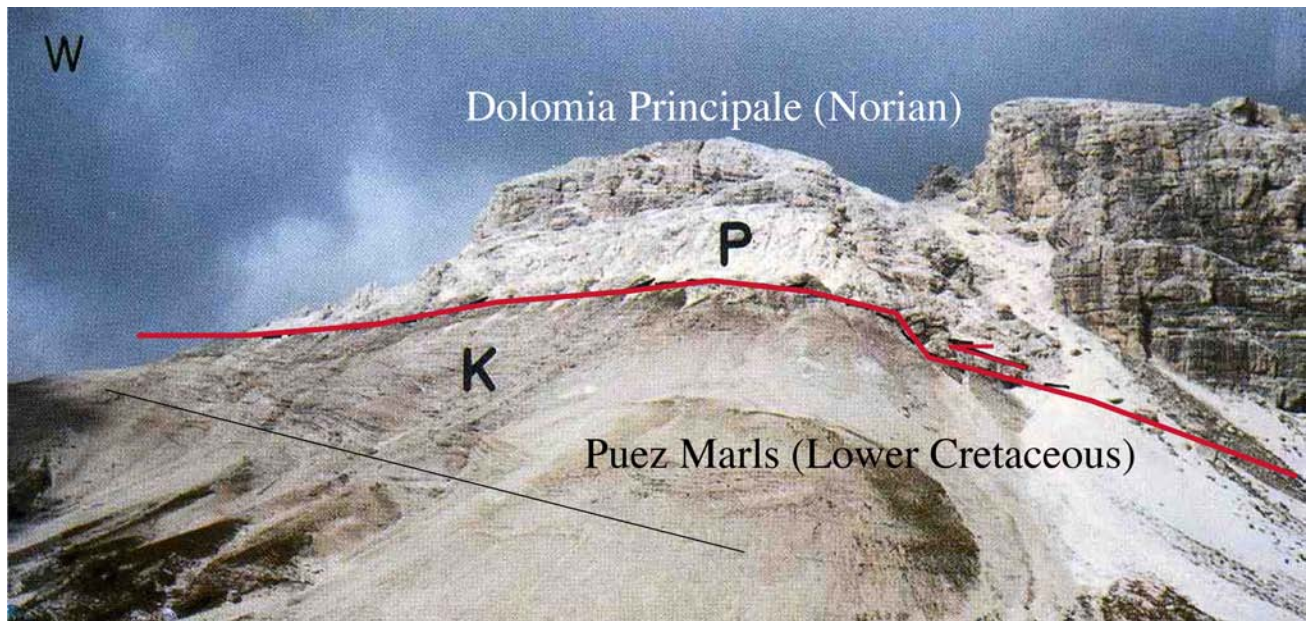


Fig. 5.8 - The Puezt thrust, described very well by ACCORDI already in 1955. In the hangingwall the Norian Dolomia Principale (P) and in the footwall the Cretaceous Puezt Marls (K), extremely laminated and affected by minor fault planes close to the main thrust fault. The thrust is W-SW vergent (to the left). It is noteworthy that the thrust plane is gently tilted, with a dip towards the south. The Southalpine N-vergent Funes thrust fault (not visible here), with a ramp geometry in the basement, tilted the Paleogene WSW-verging structures.

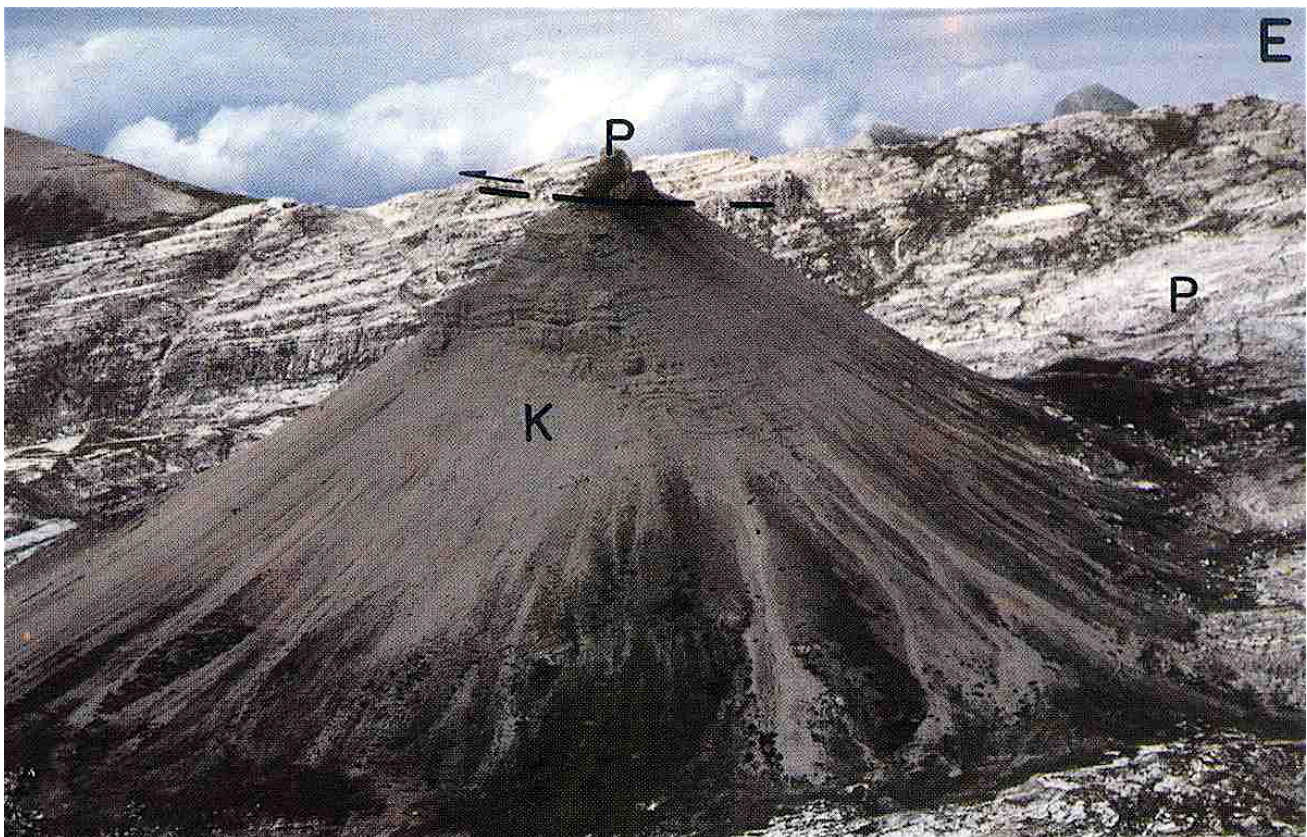


Fig. 5.9 - Altipiano del Puezt, with Cretaceous Puezt Marls (K) preserved by a very small klippe of Dolomia Principale (P) in the hangingwall of the thrust. Notice the absence of the Liassic Calcarei Grigi in the stratigraphy.

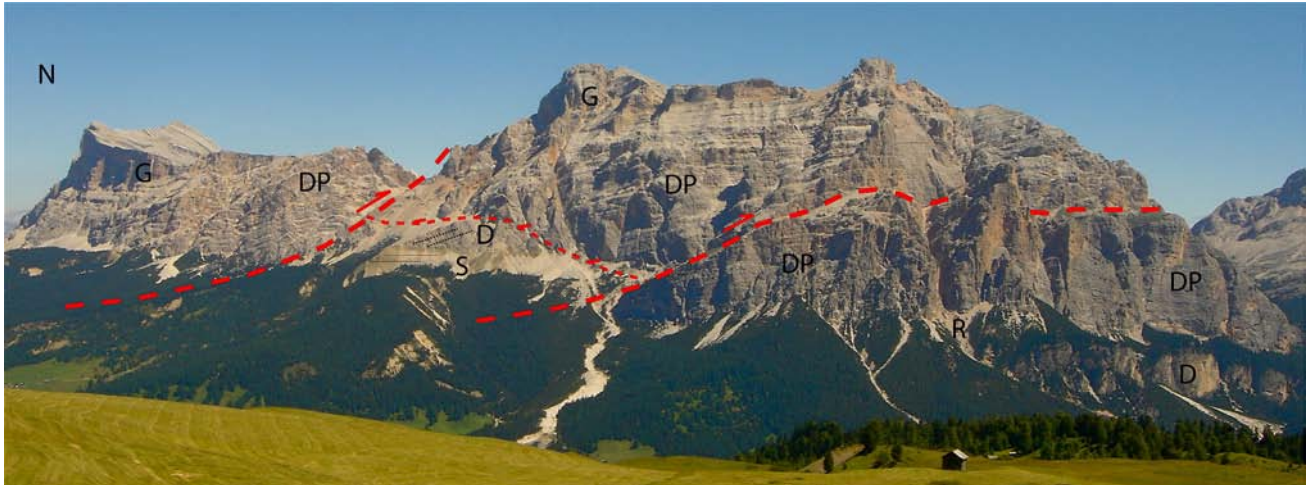


Fig. 5.10 - Conturines and Lavarella massifs. S, San Cassiano Fm; D, Cassian Dolomite; R, Raibl Fm; DP, Dolomia Principale; G, Calcarei Grigi. The two thrusts cross-cut a pre-existing N-S trending normal fault.

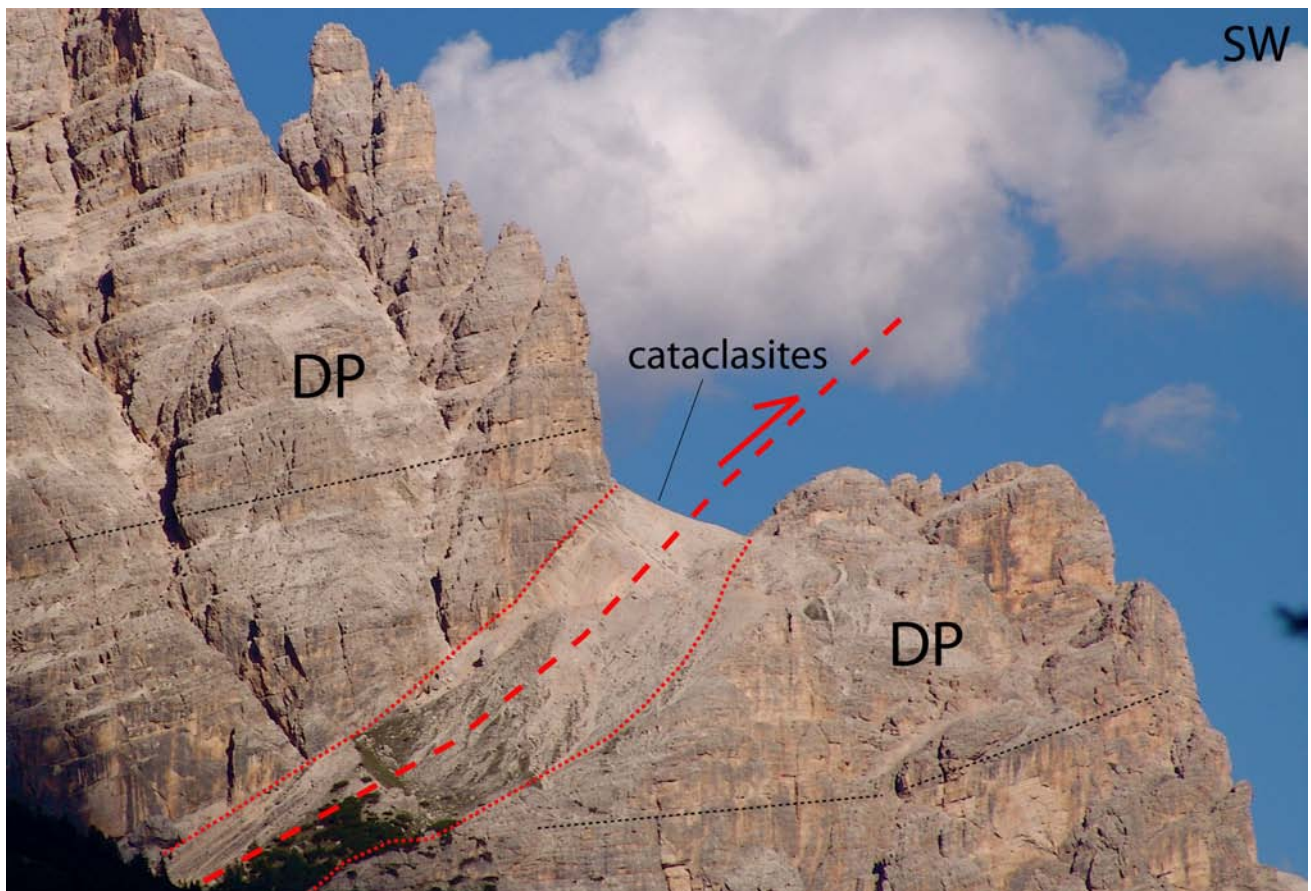


Fig. 5.11 - Detail of the Conturines Thrust viewed from Valparola. Note the footwall and hangingwall cutoff, and the 30-40 m thick cataclasites forming the gentle slope of the fault debris. The hangingwall cutoff indicates reduced shortening, limited to the thrust ramp. DP, Dolomia Principale.



Fig. 5.12 - Detail of the central part of the figure 5.10. A relict of the lower slope of a prograding Carnian Cassian Dolomite (D) over the basin of the San Cassiano Fm (S) is crosscut by a normal fault which has been in turn offset by the two thrusts. Conturines Massif.

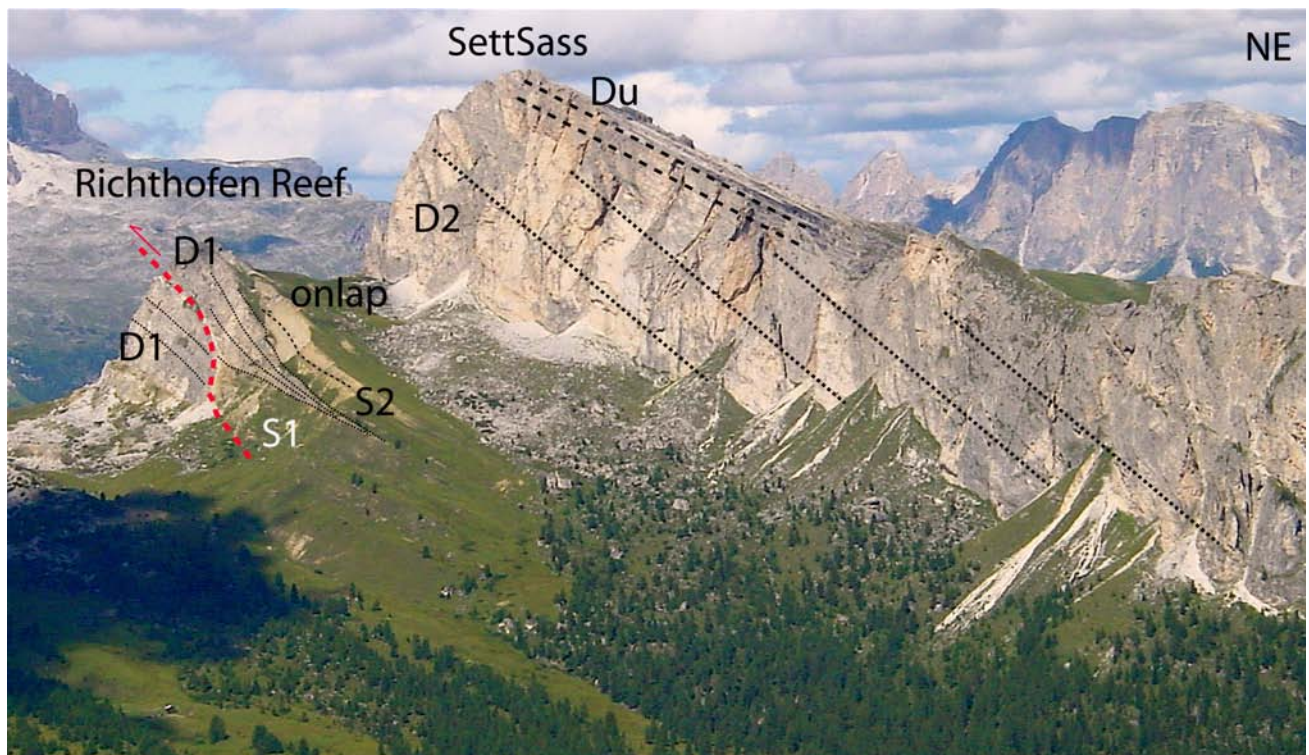


Fig. 5.13 - The Richthofen Reef to the left and the Settsass to the right, respectively formed by the Lower (D1) and Upper (D2) Cassian Dolomite, testifying two third order Carnian cycles. The two dolomites should represent the relative highstand phases, prograding onto the adjacent basin of the Lower (S1) and Upper (S2) San Cassiano Fm. At the sequence boundary, the San Cassiano Fm onlaps the mega-breccias of the Lower Cassian Dolomite. The thrusting thickened the Richthofen Reef. Du, Dürrenstein Dolomite.

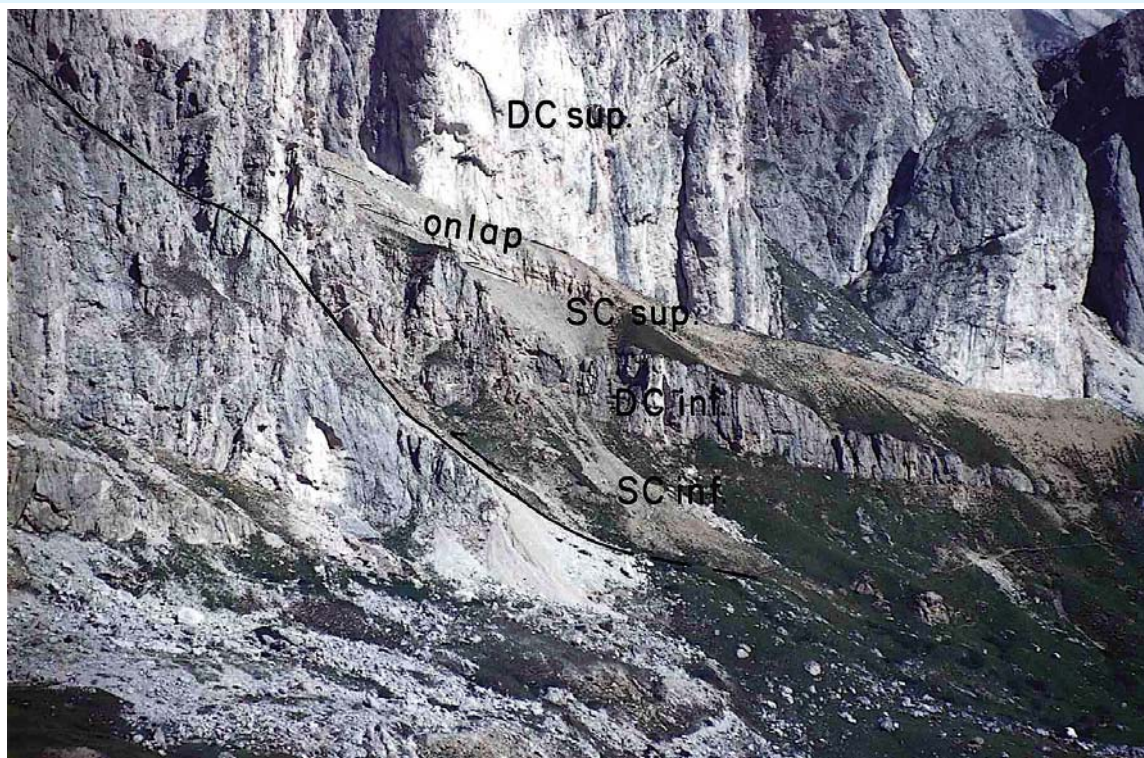


Fig. 5.14 - Detail of the Richthofen Reef. DC sup., Upper Cassian Dolomite; SC sup., Upper San Cassiano Fm; DC inf., Lower Cassian Dolomite; SC inf., Lower San Cassiano Fm.

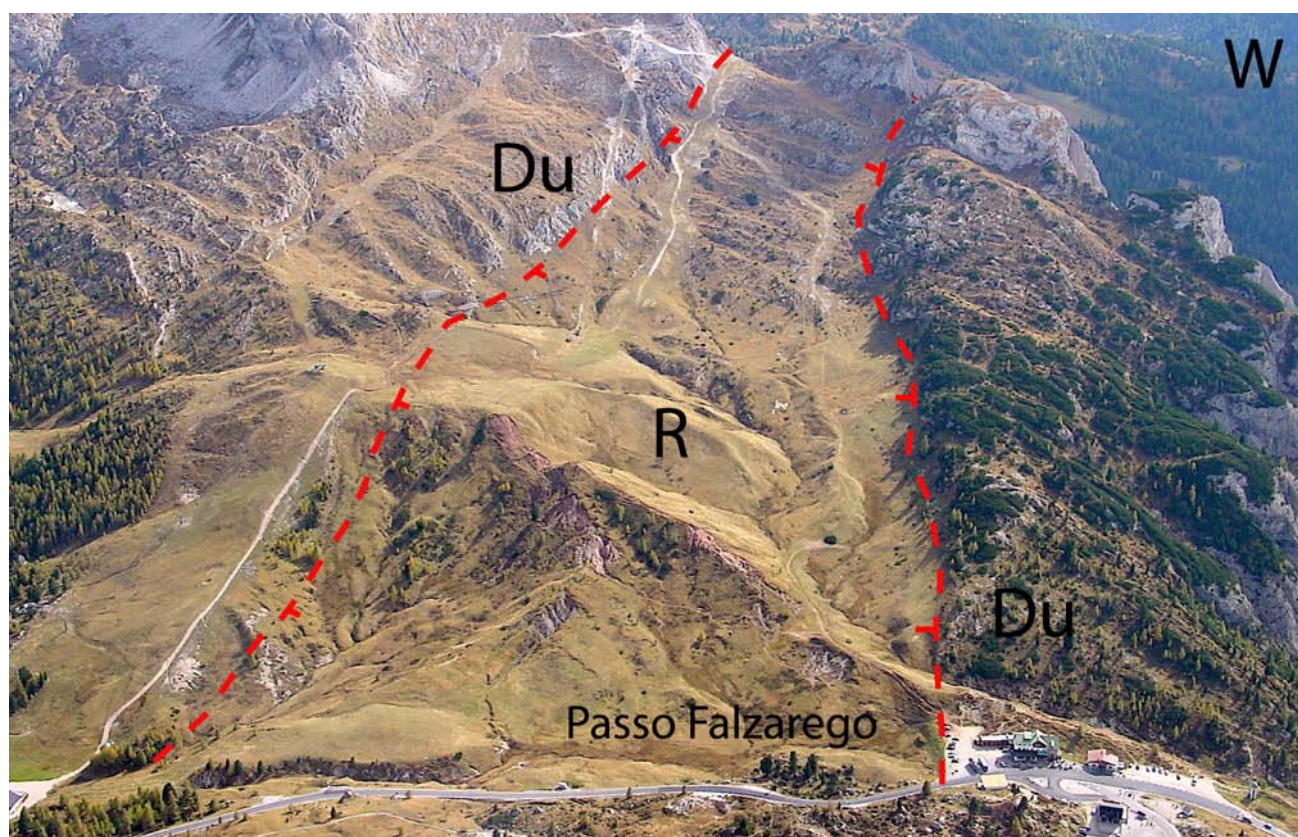


Fig. 5.15 - N-S-trending graben at Falzarego Pass. As typically occurs, normal faults are not straight planes, but are rather undulated. The axis of the graben is tilted to northeast because it is in the hangingwall of a SW-directed thrust. R, Raibl Fm; Du, Dürrenstein Dolomite. The Raibl Fm is thicker within the graben, indicating a Late Carnian age of the structure.

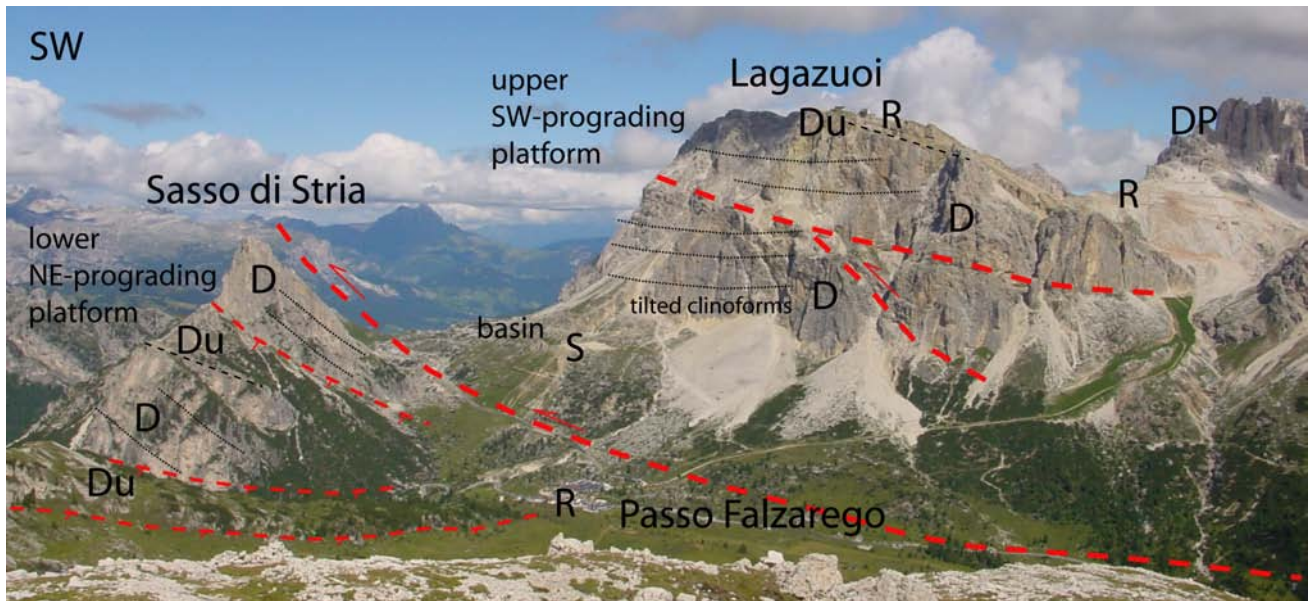


Fig. 5.16 - Two independent, opposite prograding Carnian carbonate platforms of Cassian Dolomite (D) were juxtaposed with the sandwiched intervening basin of the San Cassiano Fm (S). The lagoonal deposit of the Dürrenstein Dolomite (Du), overlain by the shallow water Raibl Fm (R) are visibly duplicated at the top of Lagazuoi Massif. DP, Norian Dolomia Principale. The thin-skinned tectonics of the Falzarego thrust was controlled by the shape of the Lagazuoi carbonate platform. The lateral ramp developed where the carbonate platform terminates and the frontal ramp followed the escarpment of the Sasso di Stria platform. Pre-existing Mesozoic (?) normal faults are well visible in the footwall.

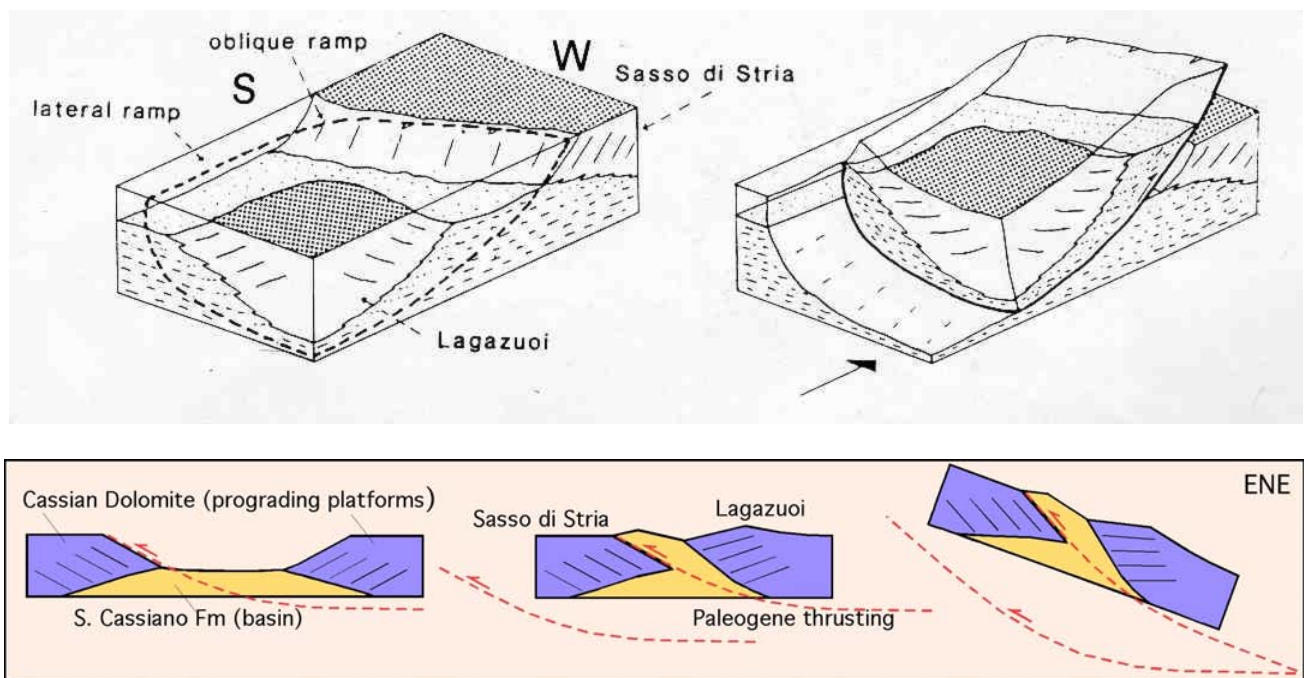


Fig. 5.17 - Sketches of the Falzarego thrust where the Lagazuoi Carbonate platform overrode the Sasso di Stria Platform. The geometry of the upper platform determined the undulation (frontal and lateral ramp) of the Falzarego Thrust. Upper panel viewed from NE, lower panel from S.

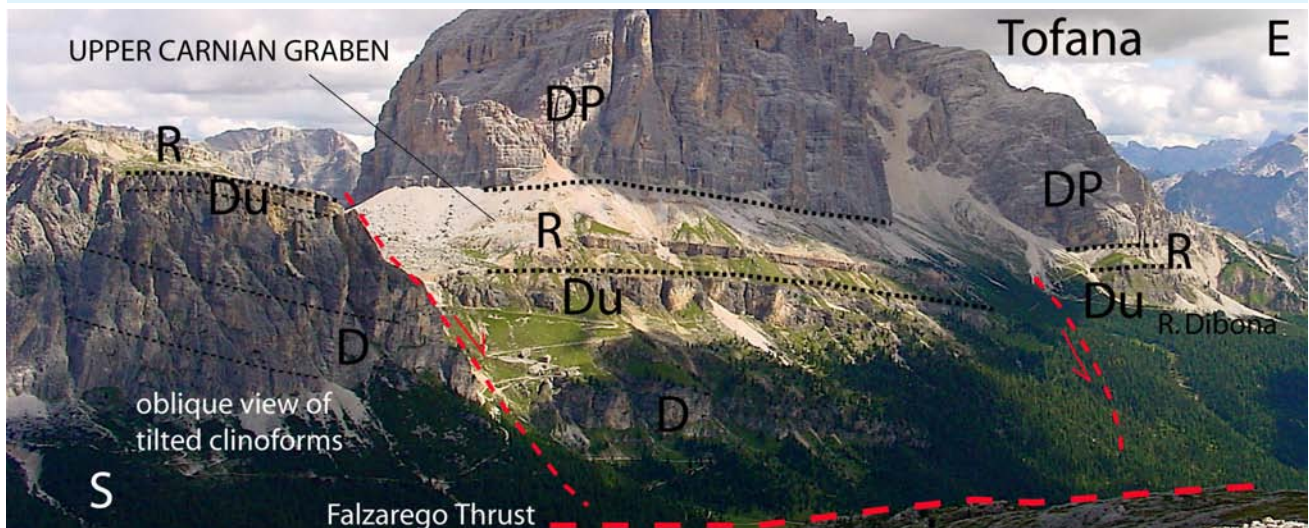


Fig. 5.18 - Southern cliff of the Lagazuoi and Tofane massifs, along the valley from the Passo Falzarego to Cortina. DP, Norian Dolomia Principale; R, Upper Carnian Raibl Fm; Du, Carnian Dürrenstein Dolomite; D, Lower Carnian Cassian Dolomite; S, San Cassiano Fm. See the thicker Raibl Fm in the center with respect to the same formation to the right in the footwall of the normal fault, indicating a syndepositional Late Carnian origin of the graben. See also the drawing in the following figure from a more perpendicular view.

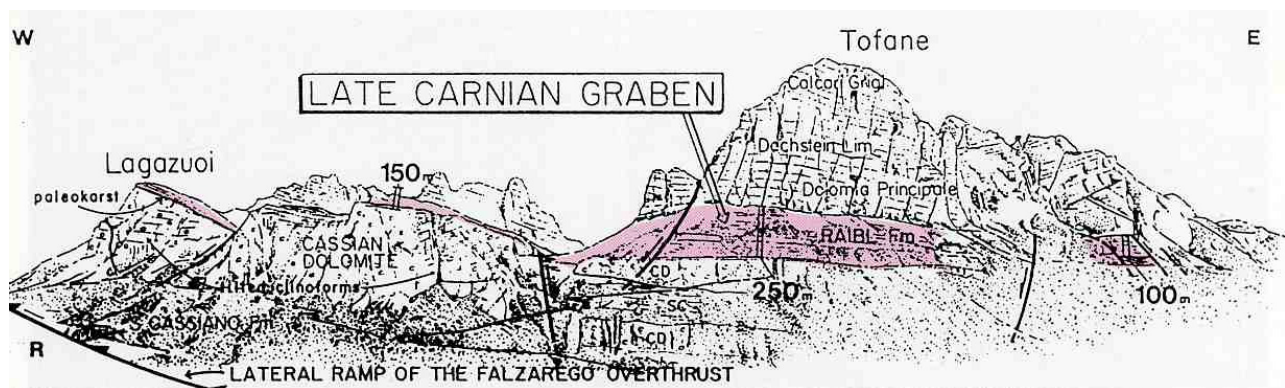


Fig. 5.19 - An Upper-Carnian graben, syn-Raibl Fm, is preserved in the hangingwall of the Falzarego thrust. Its occurrence is evidenced by the sudden changes of sedimentary thicknesses between the adjacent horsts and the graben (after DOGLIONI *et alii*, 1989b).

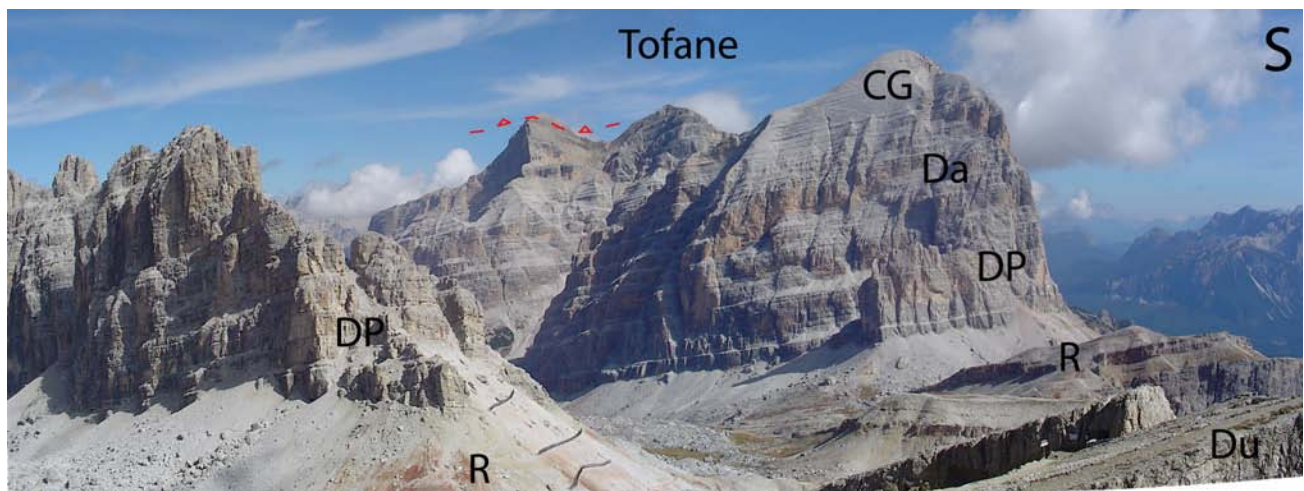


Fig. 5.20 - View from the Lagazuoi toward the Tofane. The earlier WSW-verging thrust of the Tofana III has been tilted by the northern general dip related to the deeper ramp of the Falzarego Thrust. CG, Calcarei Grigi; Da, Dachstein Lm; DP, Dolomia Principale; R, Raibl Fm; Du, Dürrenstein Dolomite.

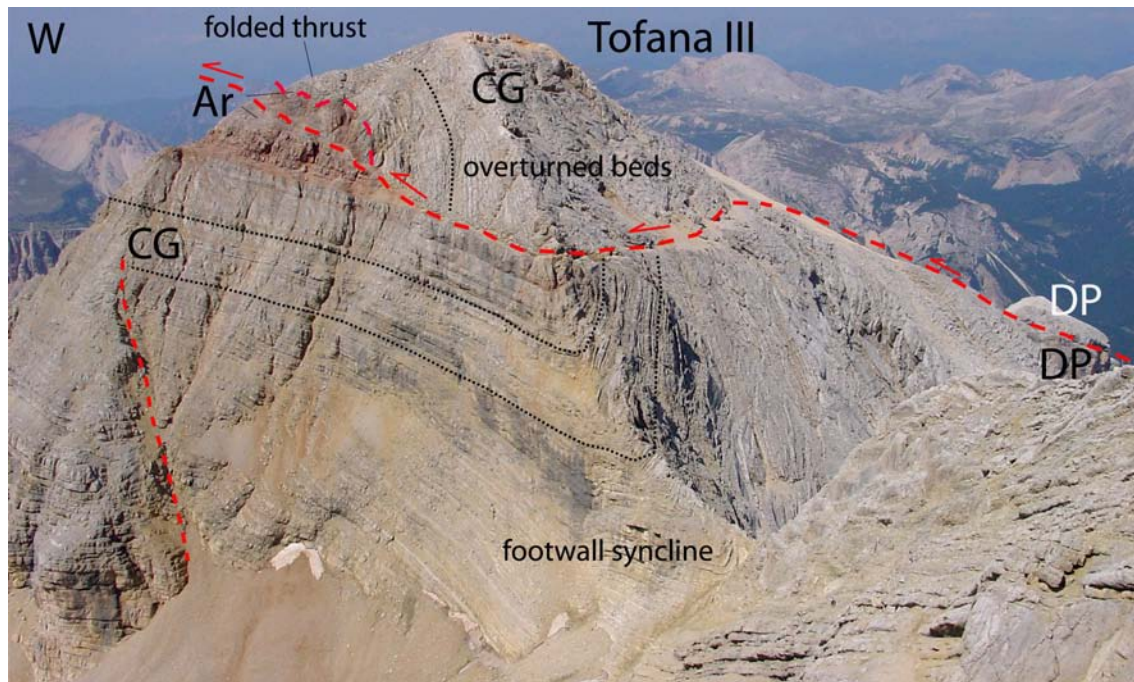


Fig. 5.21 - The W-vergent thrust of the Tofana III. Notice the transition from ramp to flat and the occurrence of an antiformal stack duplex, with the Calcarei Grigi (CG) in the hangingwall, and the Ammonitico Rosso (Ar) in the footwall and in the duplex horse. In the footwall of the main thrust, a vertical flank of a syncline occurs. This suggests that a fault-propagation fold was later truncated along the elongated limb and was later deformed by fault-bend folding. The flat developed along the horizontal flank of the syncline (to the left). To the right, the ramp is visible at the base of a klippe in the Dolomia Principale (DP).

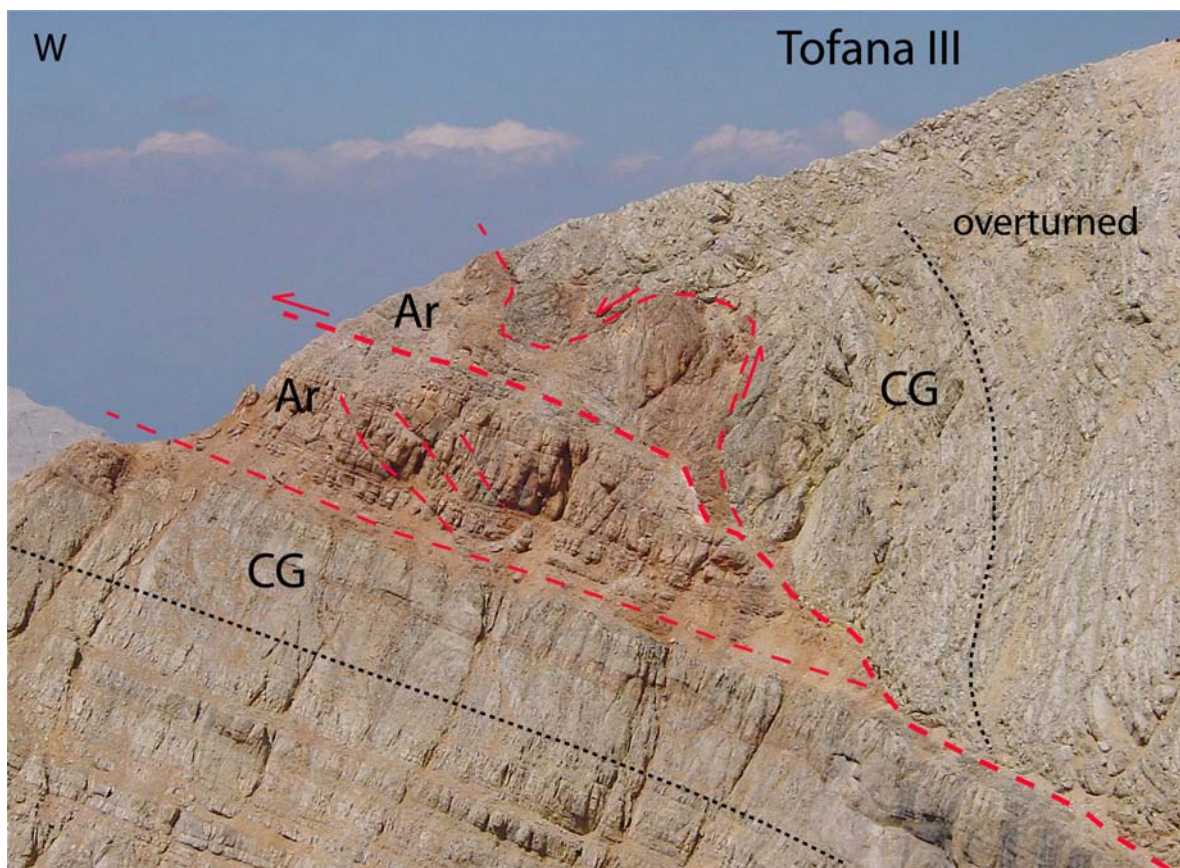


Fig. 5.22 - Detail of the Tofana III Thrust with an antiformal stack where the upper fault plane has been folded and passively transported. Ar, Ammonitico Rosso; CG, Calcarei Grigi.

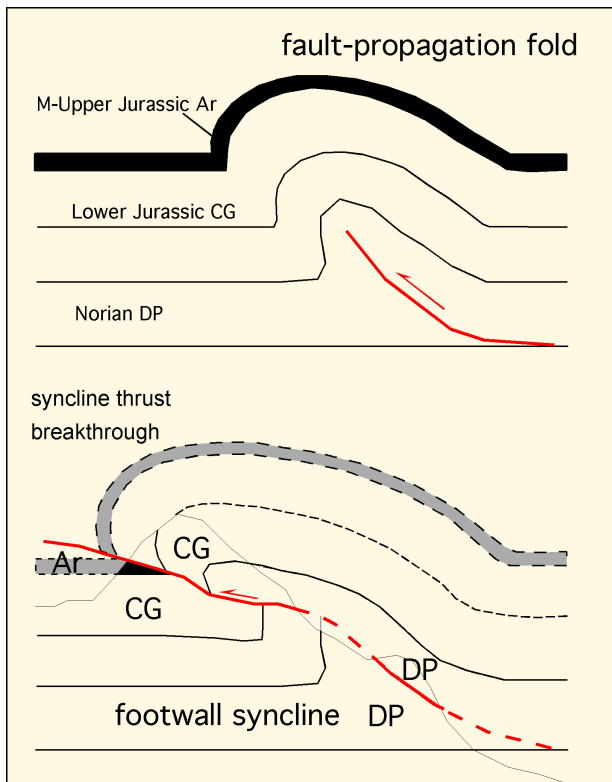


Fig. 5.23 - Kinematic sketch of the Tofana III evolution.



Fig. 5.24 - The famous section between the Lastoi de Formin and the Cernera Group, where the Upper Ladinian volcaniclastic deposits onlap on the platform escarpment, in the right side of the picture. The contact was later weakly reactivated by a W-vergent thrust fault (see next figure). The Carnian carbonate platform prograding margin of the Cassian Dolomite (D) in the left passes to the internal lagoonal facies of the Dürrenstein Dolomite (Du). S, San Cassiano Fm; V, volcaniclastic deposits; Ce, Caotico Eterogeneo; C, Marmolada Limestone.

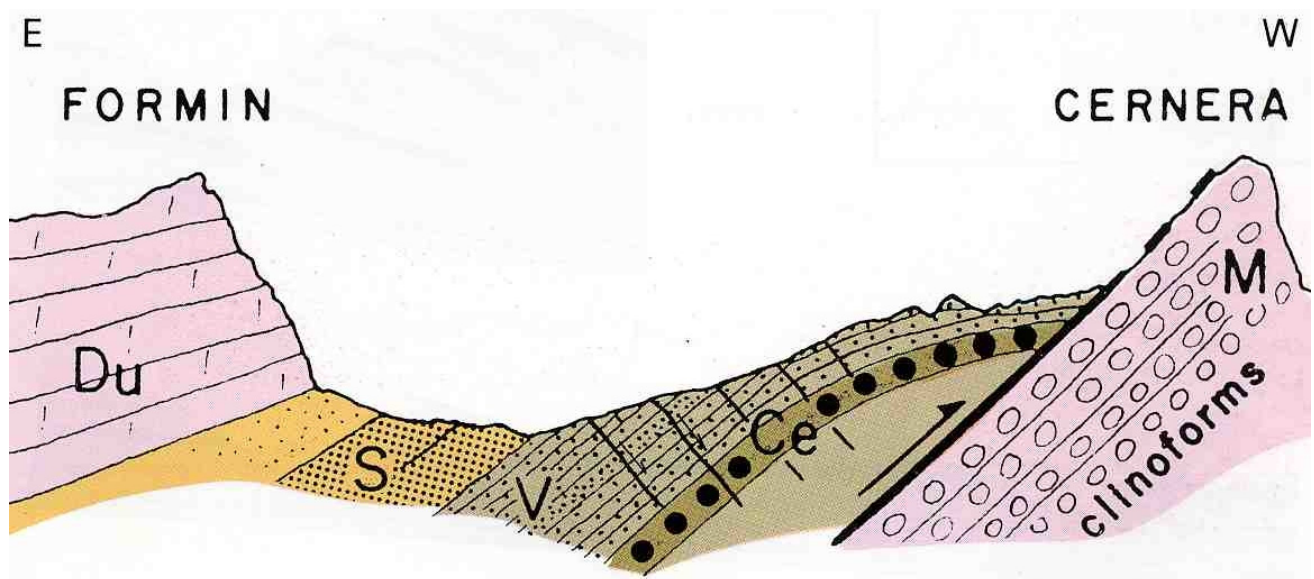
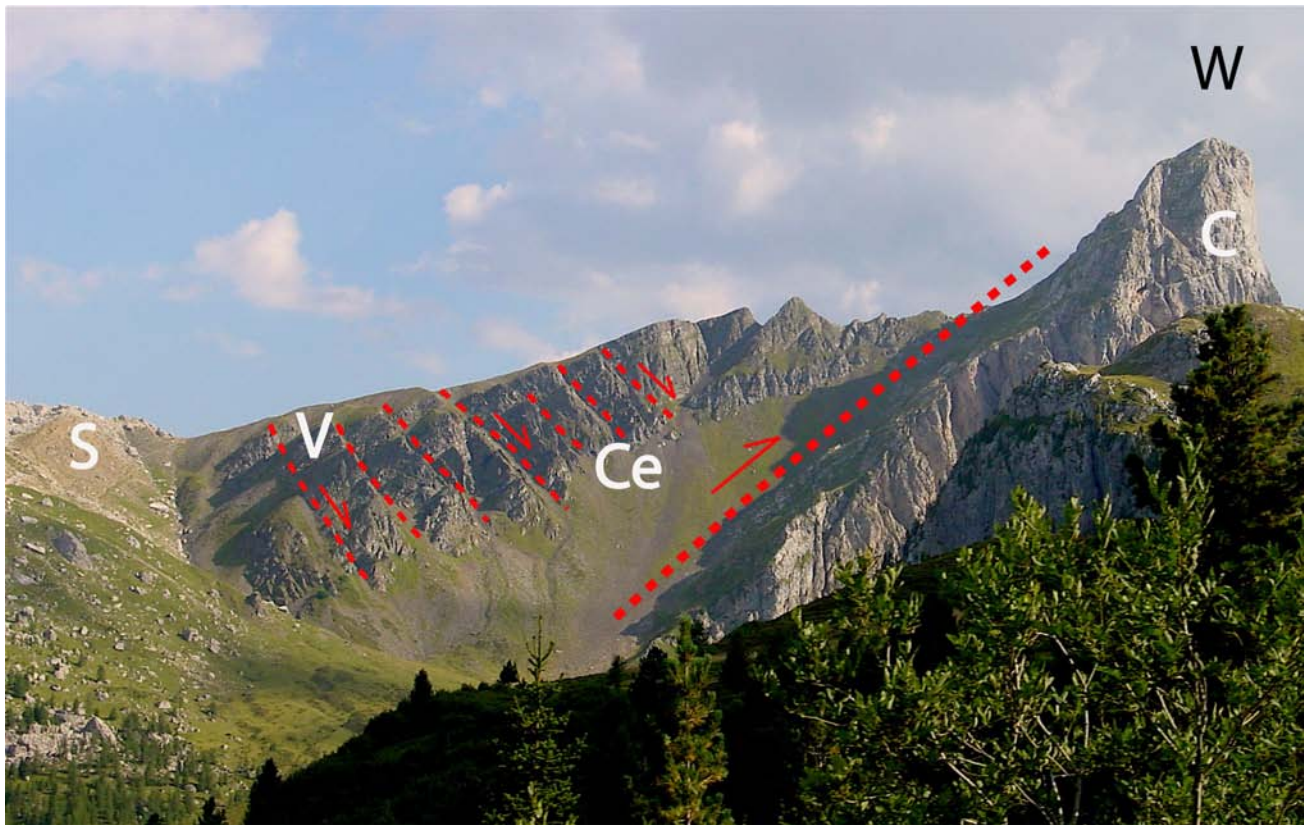


Fig. 5.25 - The Cernera Ladinian Carbonate platform slope of the Marmolada Limestone (C in upper panel and M in lower panel), originally onlapped by volcanoclastic rocks (V) and the Caotico Eterogeneo (Ce), has been partly inverted by a thrust. An open fold, and small-scale, regularly spaced normal faults affected the volcanic rocks in the hangingwall. S, Carnian San Cassiano Fm; Du, Dürrenstein Dolomite.



Fig. 5.26 - Detail of the central part of figure 5.24. The interior of the Lastoi de Formin lagoonal facies of the Carnian Dürrestein Dolomite is cross-cut by a set of normal faults with a domino array, possibly related to the Norian-Jurassic rifting.

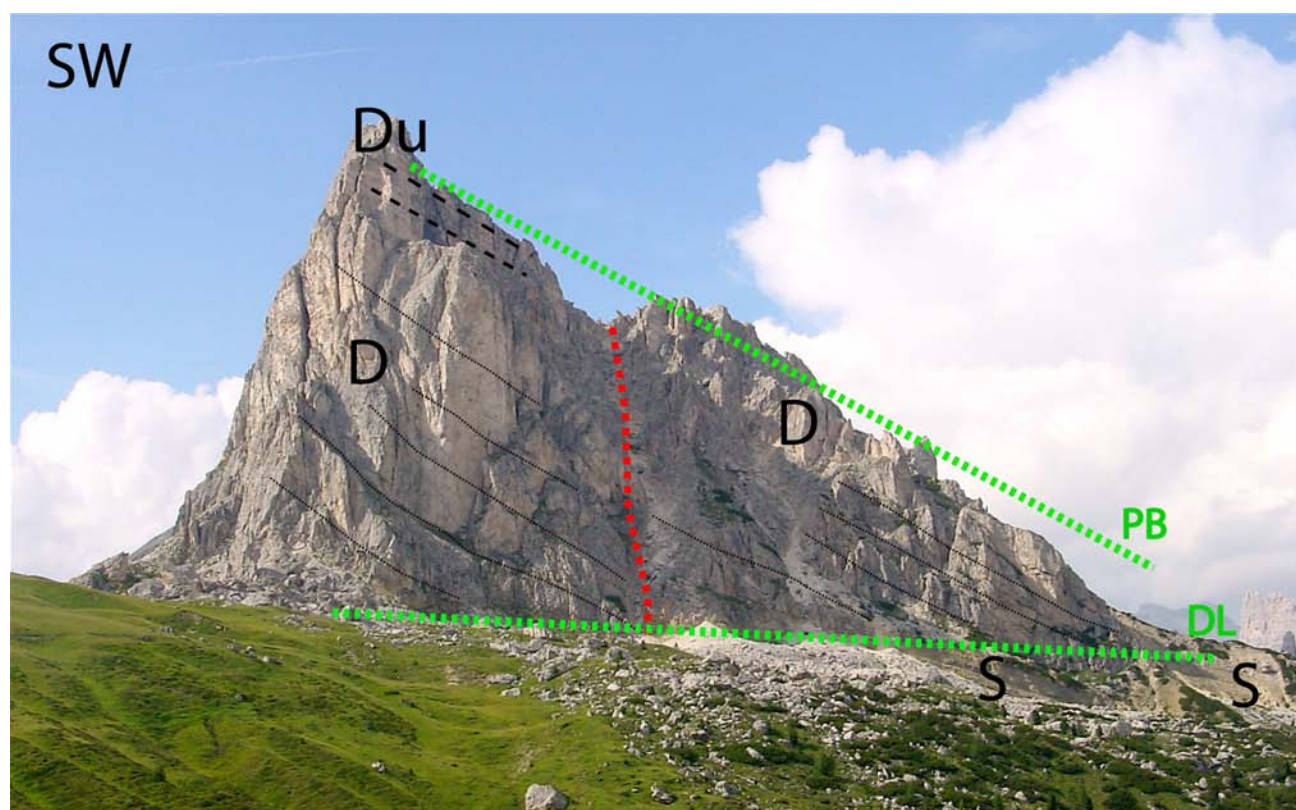


Fig. 5.27 - The Gusela del Nuvolao, near Passo Giau. Some 20°-25° of the present day clinoforms dip are due to an underlying ramp of a W-vergent thrust fault. Retrodeforming the Cassian Dolomite (D) prograding onto the San Cassiano Fm (S), a convergent geometry between the platform break (PB) and the downlap (DL) surfaces can be observed. This suggests a decrease of bathymetry in the basin facing the platform. Near the peak, the Dürrenstein Dolomite (Du) crops out. Minor faults complicate the structure.

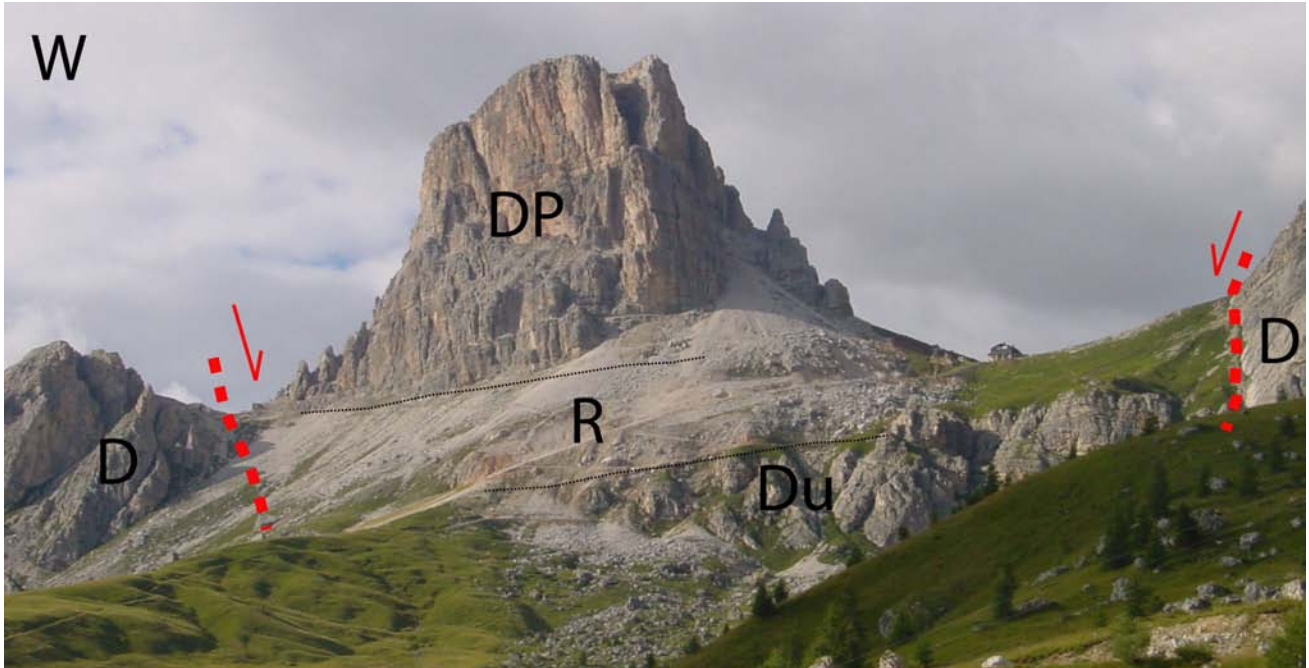


Fig. 5.28 - The Averau graben, again oriented roughly N-S, in the vicinity of the Giau Pass. D, Cassian Dolomite; Du, Dürrenstein Dolomite; R, Raibl Fm; DP, Dolomia Principale. Here extensional tectonics is post-Norian (Liassic?).

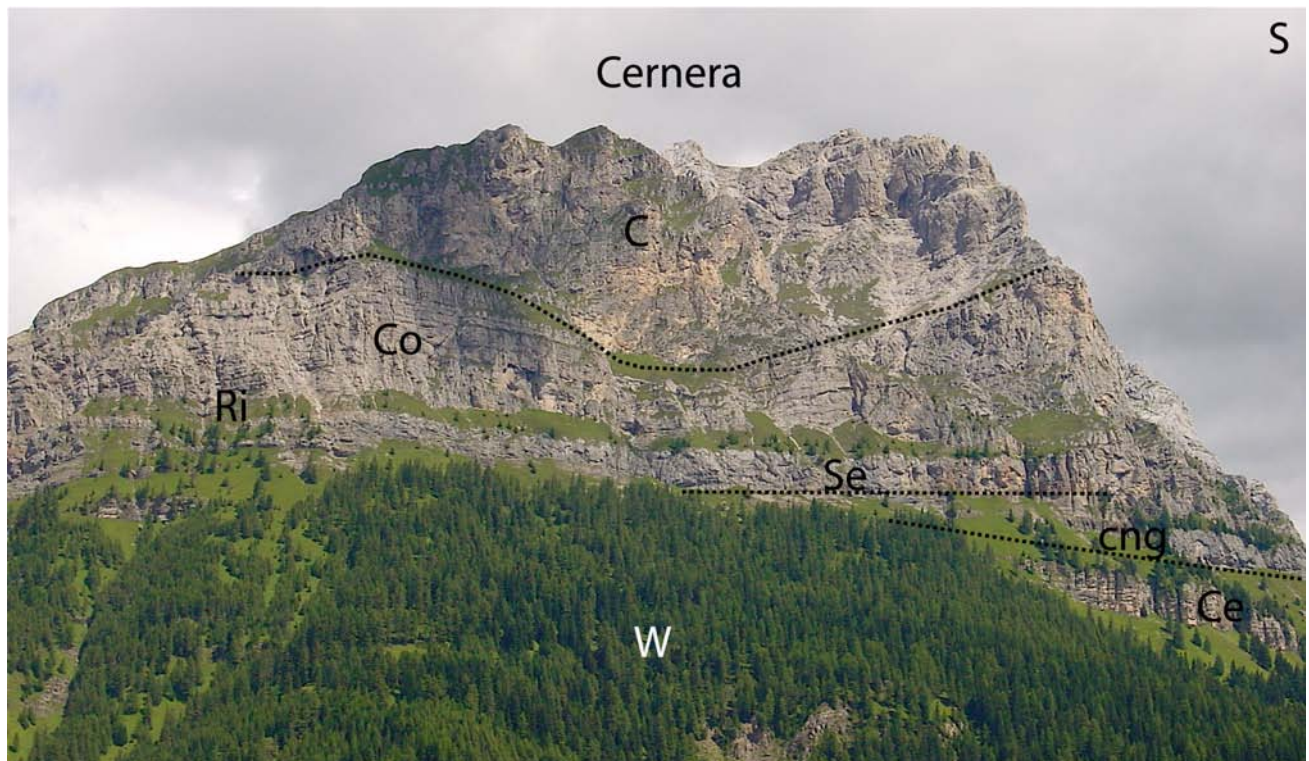


Fig. 5.29 - A channel in the Upper Anisian shallow platform facies of the Contrin Fm (Co) is filled by megabreccias of the Marmolada Limestone (C). Below, the fluvial Richthofen Conglomerate (Ri) overlies the Lower Anisian Serla Dolomite (Se) and a conglomerate (cng), which are sealing an unconformity with the underlying tilted Werfen Fm (W) and its upper Cencenighe Mb (Ce). View of the Mt. Cenera from the Fiorentina Valley.

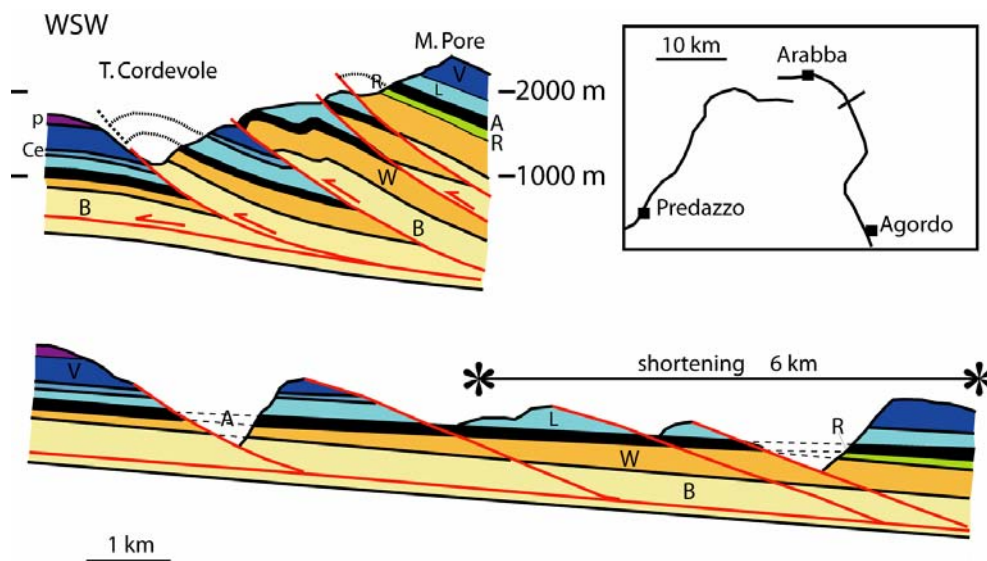


Fig. 5.30 - Balanced cross-section of a frontal segment of the earlier WSW-verging thrusting, between the Pore and Digonera mountains. The imbricated fan structure is detached along the Permian evaporites of the Bellerophon Fm (B). The shortening calculated from the retrodeformation is about 6 km. The various thrust units are characterized by different sediment thicknesses. For example, the Werfen Fm (W) thickens towards the east, since the intensity of the Anisian erosion diminishes eastward. Also the Richthofen Conglomerate (R) thickens towards the east. A, Anisian Carbonates (Contrin Fm), with facies variations along the section; L, Livinallongo Fm and Zoppè Sandstones; V, Volcaniclastic sandstones, with, at their base, intercalated levels of Caotico Eterogeneo; P, Pillow lavas.



Fig. 5.31 - The WSW-vergent thrust near Digonera, along the road to Laste. It is the most external thrust plane of the previous section. In the hangingwall of the main thrust fault: S, Siusi Mb; A, Andraz Horizon; M, Mazzin Mb (Werfen Fm, Scythian). In the foot-wall: V, Volcaniclastic sandstones (Ladinian). The contacts among the levels of the Werfen Fm were resheared to form an antiformal stack duplex. The Mazzin Mb and the Andraz Horizon are strongly foliated by S-C structures. Intense pressure solution, diminishing away from the main fault plane, can be observed in the outcrop. At regional scale, the fault plane can be connected to the Sella and Civetta thrusts klippen (see next figure).

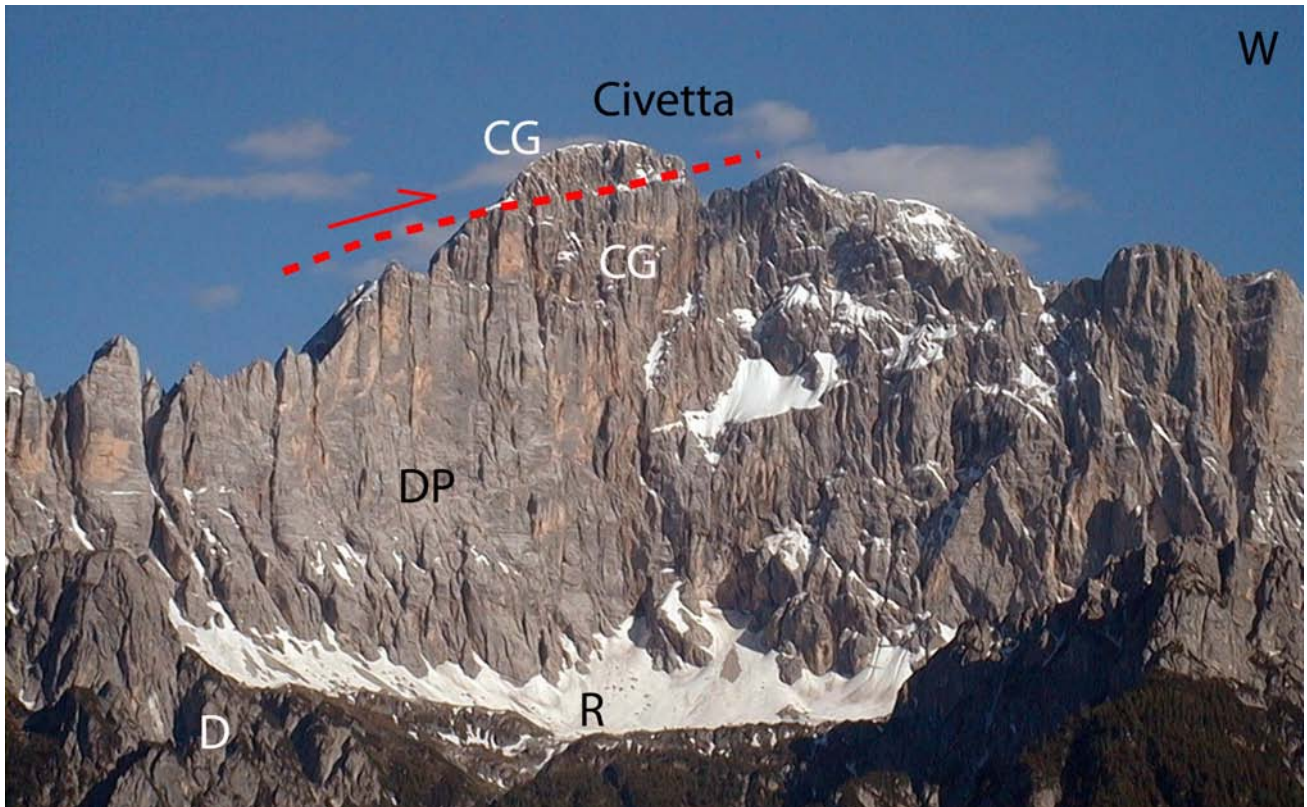


Fig. 5.32 - Northern cliff of the Civetta Massif. Note the klippe at the top. Moreover the thickness of the Dolomia Principale is about twice (>500 m) than at the Piz Boè (250 m), indicating Norian synsedimentary tectonics. CG, Calcarei Grigi; DP, Dolomia Principale; R, Raibl Fm; D, Cassian Dolomite.



Fig. 5.33 - The fault of the Digonera dam. It is a S-vergent Southalpine thrust fault (compare with Fig. 5.35) with the Werfen Fm in the hangingwall and Ladinian volcanoclastic sandstones in the footwall. Note the chevron folds in the thinly bedded rocks of the hangingwall. The thrust displaces W-vergent paleostructures.

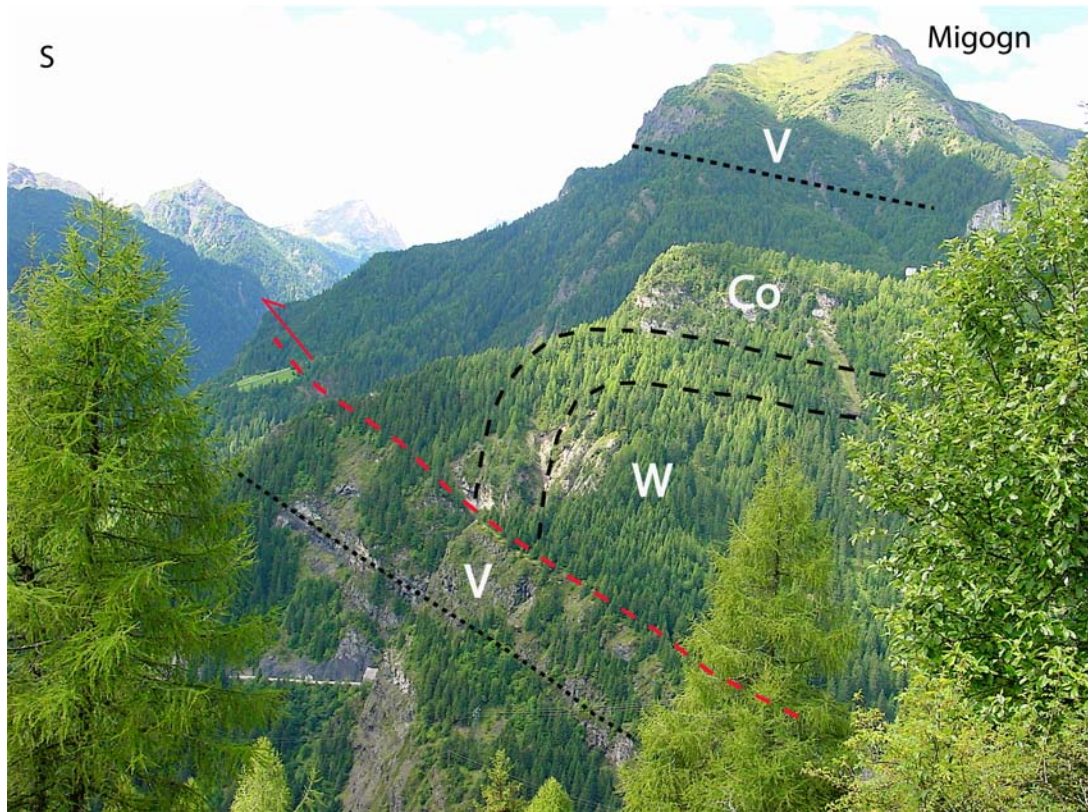


Fig. 5.34 - The Digionera thrust, the same of the dam of the previous figure, seen from the other side of the valley, from the road from Caprile to Selva di Cadore. The hangingwall fold with the vertical forelimb indicates a fault-propagation fold origin. V, Ladinian volcanoclastic sandstones; Co, Upper Anisian Contrin Fm; W, Scythian Werfen Fm.

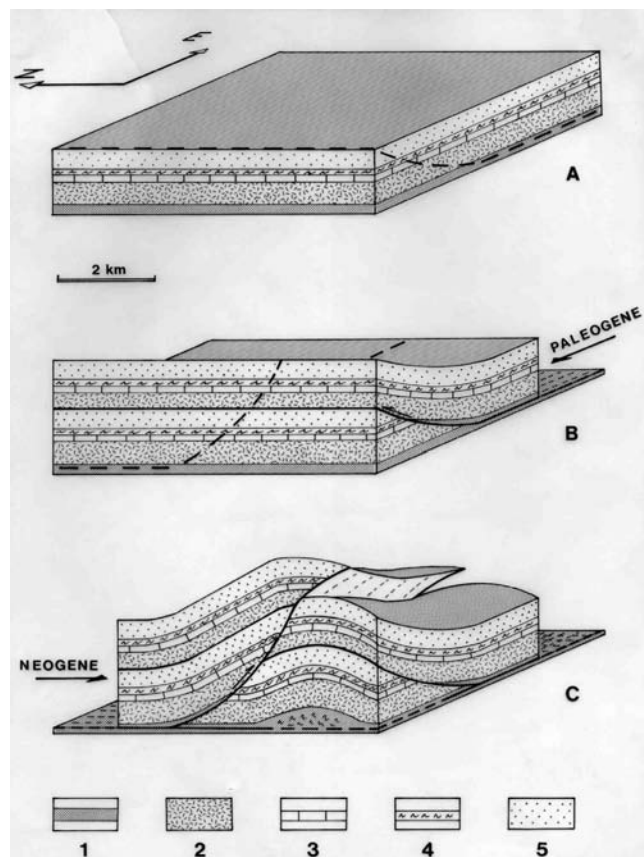


Fig. 5.35 - In the Caprile zone, the interference between the W-vergent Paleogene Dinaric structures and the S-vergent Neogene Southalpine faults, that cut and folded the earlier WSW-verging structures, can be observed. 1, Bellerophon Fm; 2, Werfen Fm; 3, Contrin Fm; 4, Livinallongo Fm; 5, volcaniclastic deposits.

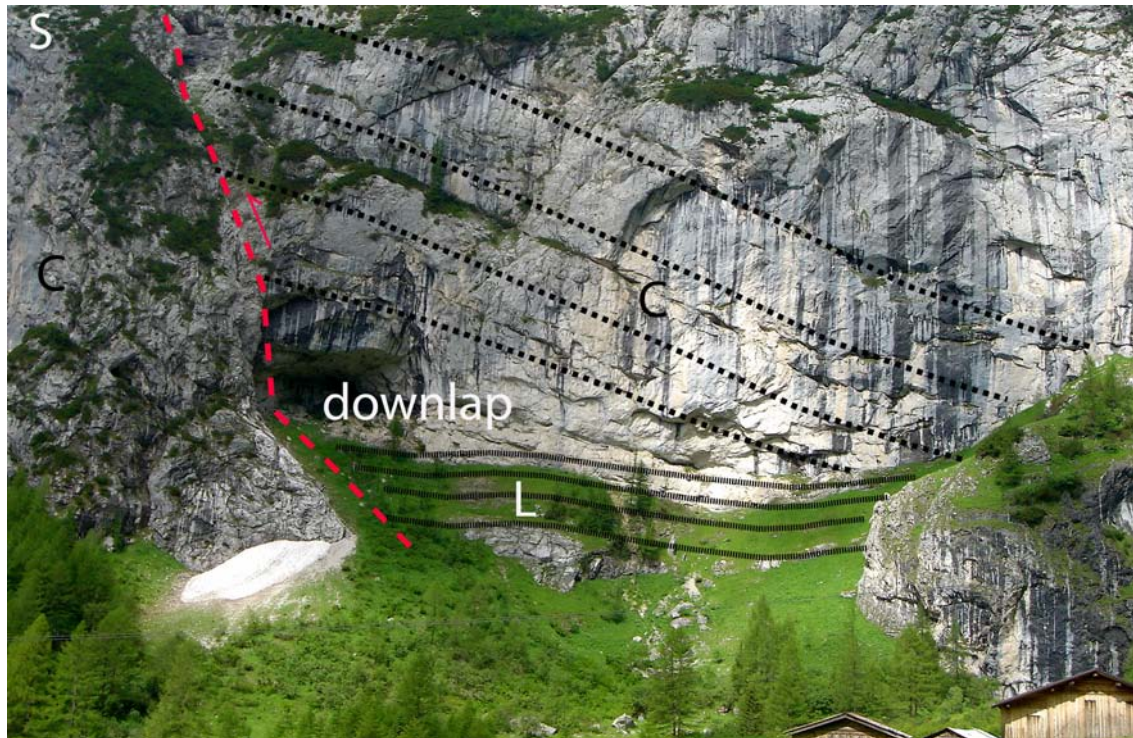


Fig. 5.36 - Downlap of the Ladinian megabreccias of the Marmolada Limestone (C) over the basinal equivalent of the Livinallongo Fm (L). Road from Malga Ciapela to Fedaia Pass.



Fig. 5.37 - Fault-propagation fold in the Dolomia Principale along the Cordevole Valley, south of Agordo. The axial plane is marked by a fracture. The thrust fault shows an undulated trajectory and spaced Riedel planes generate a weak foliation in the hangingwall. The structure is N-vergent and represents a backthrust of the Belluno Thrust.

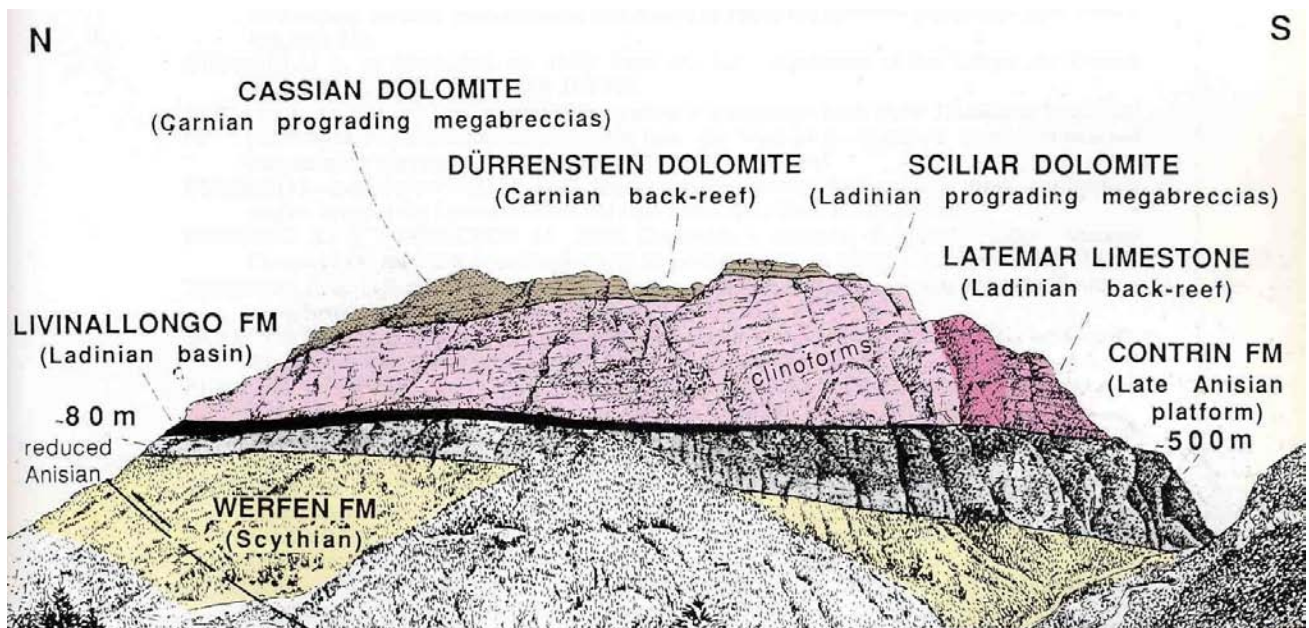
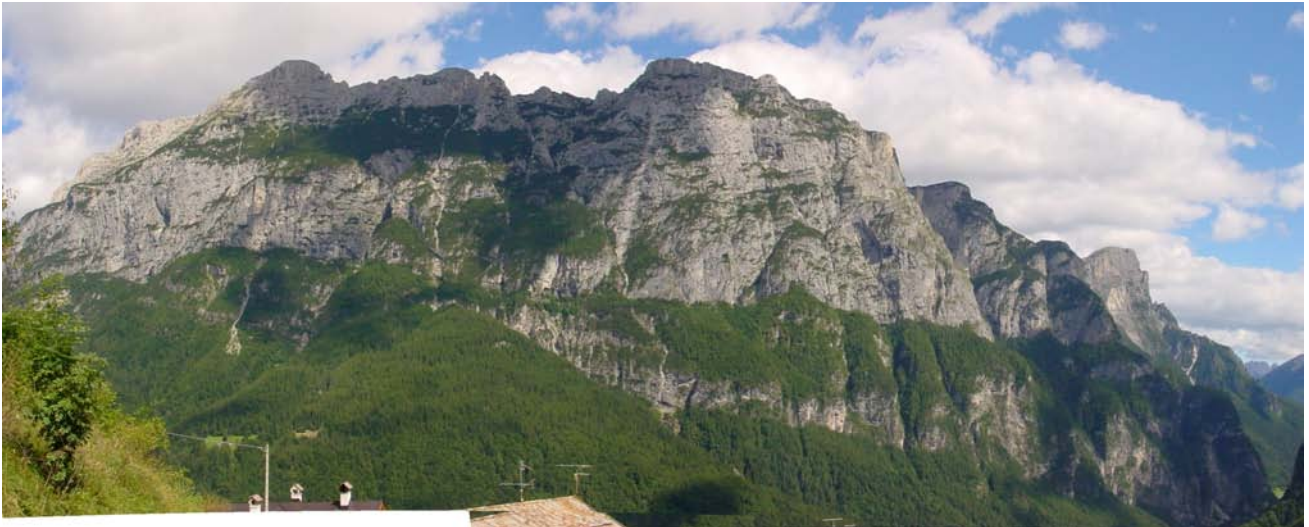


Fig. 5.38 - Natural section along the western flank of the Civetta Group, Monte Alto di Pelsa. View from the west, above Cencenighe. Notice the marked lateral variation of the thickness of the various formations, such as the thinning of the Livinallongo Fm towards the south, the southward thickening of the tilted and truncated underlying Anisian carbonates, and the Ladinian Platform prograding toward the north. It is a noteworthy example of field "seismic section".



Fig. 5.39 - Detachment fold in the Cencenighe Mb of the Werfen Fm. The symmetric buckle fold is decoupled in a siltstone-shaly layer where the thickness of beds changes. The overlying thinner strata allow easier flexural slip than the underlying thicker more competent beds. The outcrop is 5 m wide, along the road cut 2 km west of Cencenighe.

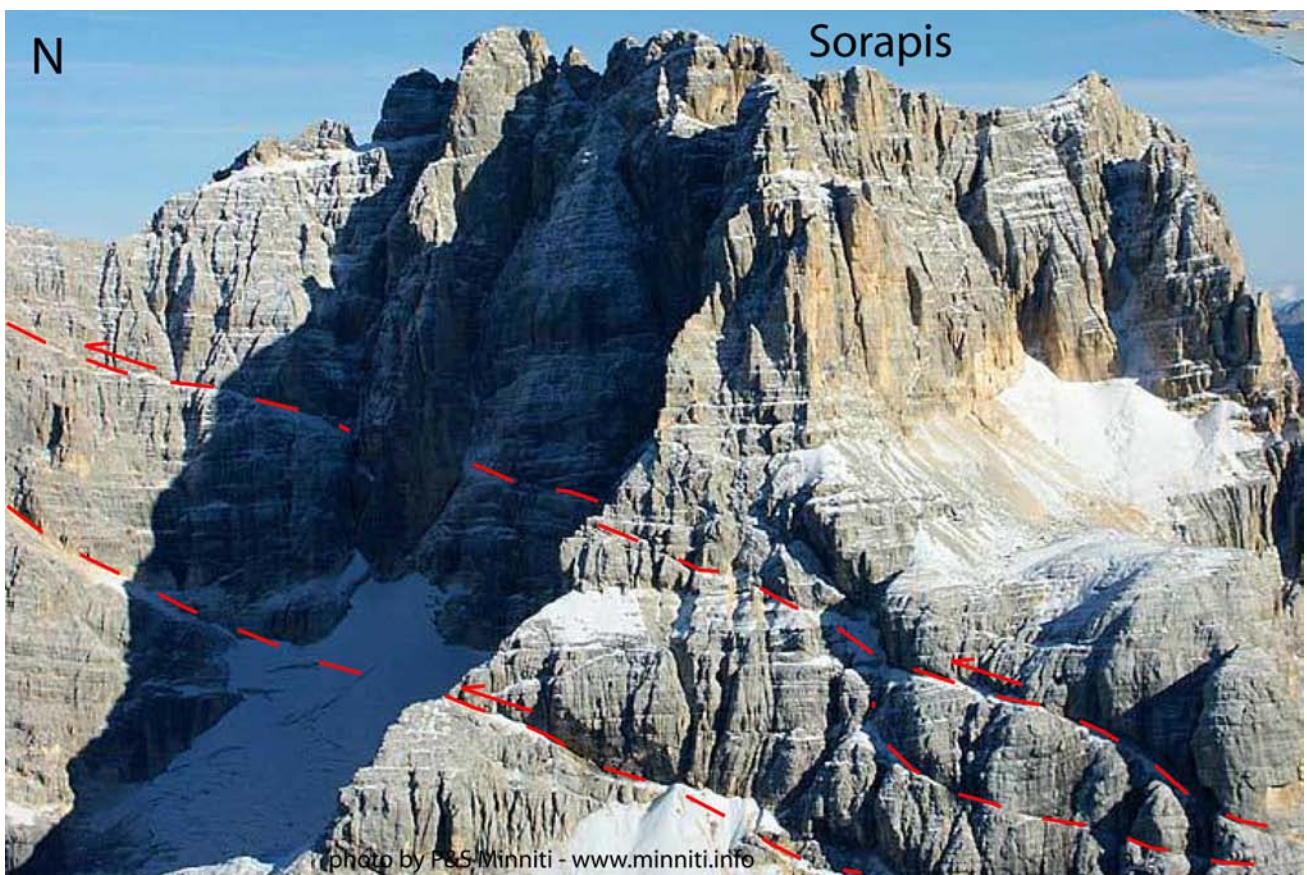


Fig. 5.40 - Ramp geometries in the Sorapis backthrust affecting the Dolomia Principale (photo by Minniti).

ACKNOWLEDGMENTS

Many thanks to Eni and the Italian Geological Survey for sponsoring the publication. We are particularly indebted to JONATHAN CRAIG, MAURIZIO ORLANDO, GIORGIO GIORGETTA, CIRO PAGANO, UMBERTO VERGINE for Eni E&P, LEONELLO SERVA, DOMENICO TACCHIA and SILVANA FALCETTI for the Italian Geological Survey. ROBERTO GATTI stimulated this volume and RODOLFO CAROSI kindly reviewed the manuscript.

REFERENCES

- ACCORDI B. (1955) - *Le dislocazioni delle cime (Gipfelfaltungen) delle Dolomiti*. Ann. Univ. Ferrara (9), Sci. geol. paleont. 2: 65-188.
- ALLMENDINGER R.W., BROWN L.D., OLIVER J.E. & KAUFMAN S. (1983) - COCORP deep seismic profiles across the Wind River mountains, Wyoming. In: A.W. BALLY (Ed.), *Seismic expression of structural styles*. Amer. Ass. Petrol. Geol., Studies in Geology, v. 15, 3.2.1.29-3.2.1.33 pp.
- ALLMENDINGER R.W. (1998) - *Inverse and Forward numerical modeling of trishear fault-propagation folds*. Tectonics, v. 17: 640-656.
- ANDERSON E.M. (1905) - *The dynamics of faulting*, Transactions of the Edinburgh Geological Society, 8: 387-402, 1905.
- ASSERETO R. et alii (1977) - *The Pb-Zn mineralization in the Triassic of the Dolomites*. Geological History and genetic interpretations. L'industria mineraria, nov.-dic., 367-402.
- BACHMANN G.H. & KOCH K. (1983) - *Alpine Front and Molasse Basin, Bavaria*. In: Seismic expression of structural styles; a picture and work atlas; Volume 3. A-W BALLY (editor), Am. Ass. Petrol. Geol. Studies in Geology, 15: 3.4.1-27-3.4.1-32.
- BADLEY M.E. (1985) - *Practical Seismic Interpretation*, New Jersey, Prentice Hall.
- BALLY A.W. (1984) - *Tectogenèse et sismique réflexion*. Bull. Soc. géol. France, 7: 279-285.
- BALLY A.W., GORDY P.L. & STEWART G.A. (1966) - *Structure, seismic data and orogenic evolution of Southern Canadian Rocky Mountains*. Bull. Canad. Petrol. Geol., 14: 337-381.
- BARBIERI G. (1987) - *Lineamenti tettonici degli Altipiani Trentini e Vicentini tra Folgaria e Asiago (Prealpi Venete)*. Mem. Scienze Geol., 39: 257-264, Padova.
- BECHSTADT T. & BRANDNER R. (1970) - *Das Anis zwischen St.Vigil und dem Holensteintal (Pragser und Olanzer Dolomiten, Südtirol)*. Beiträge zur Mikrofazies und Stratigraphie von Tirol und Voralberg. (Festb.Geol. Inst., 300-J. Feier Univ. Innsbruck), 9-103.
- BECHSTADT T., BRANDNER R., MOSTLER H. & SCHMIDT K. (1977) - *Aborted rifting in the Triassic of the Eastern and Southern Alps*. N. Jb. Geol. Palaont. Abh., 156, 2: 157-178.
- BERGE T.B. & VEAL S.L. (2005) - *Structure of the Alpine foreland*. Tectonics, 24, TC5011, doi: 10.1029/2003TC001588.
- BERNOULLI D. (1964) - *Zur Geologie des Monte Generoso (Lombardische Alpen)*. Beitr. Geol. Karte Schweiz, Neue Folge, Bern, 134.
- BERNOULLI D., BICHSEL M., BOLLI H., HAERING H., HOCHULI P. & KLEBOTH P. (1981) - *The Missaglia Megabed, a catastrophic deposit in the upper Cretaceous Bergamo Flysch (Northern Italy)*. Eclogae Geol. Helv., 74/2, 421-442.
- BERNOULLI D., CARON C., HOMEWOOD P., KALIN O. & VON STUIJVENBERG J. (1979) - *Evolution of continental margins in the Alps*. Schweiz. Mineral. Petrogr. Mitt., 59: 165-170.
- BERNOULLI D., HEITZMANN P. & ZINGG A. (1990) - *Central and southern Alps in southern Switzerland: tectonic evolution and first results of reflection seismics*. Mém. Soc. géol. France 156: 289-302.
- BERNOULLI D. & LEMOINE M. (1980) - *Birth and Early Evolution of the Tethys: the Overall Situation*. Mem. B.R.G.M., 115: 168-179.
- BERNOULLI D. & WINKLER W. (1990) - *Heavy mineral assemblages from Upper Cretaceous South- and Austroalpine flysch sequences (Northern Italy and Southern Switzerland): source terranes and paleotectonic implications*. Eclogae Geol. Helv., 83/2: 287-310.
- BERSEZIO R. & FORNACIARI M. (1987) - *Cretaceous sequences in the Lombardy Basin: stratigraphic outline between the Lakes of Lecco and Iseo*. Mem. Soc. Geol. It., 40: 187-197.
- BERSEZIO R. & FORNACIARI M. (1988) - *Geometria e caratteri stratigrafici della Sequenza Cenomaniana nel Bacino Lombardo (Alpi Meridionali)*. Riv. It. Paleont. Strat., 94/3: 425-454.
- BERSEZIO R. & FORNACIARI M. (1988) - *Tectonic framework of the Lombardy foothills (Southern Alps) between Brianza and Lake Iseo*. Rend. Soc. Geol. It., 11: 75-78.
- BERTOTTI G. (1990) - *The deep structure of the Monte Generoso basin: an extensional basin in the south-Alpine Mesozoic passive continental margin*. Mém. Soc. géol. France 156: 303-308.
- BERTOTTI G., PICOTTI V., BERNOULLI D. & CASTELLARIN A. (1993) - *From rifting to drifting: tectonic evolution of the South-Alpine upper crust from the Triassic to the Early Cretaceous*. Sedimentary Geology, 86: 53-76.
- BIGI G., CASTELLARIN A., CATALANO R., COLI M., COSENTINO D., DAL PIAZ G.V., LENTINI F., PAROTTO M., PATACCA E., PRATURLON A., SALVINI F., SARTORI R., SCANDONE P. & VAI G.B. (1989) - *Synthetic structural-kinematic map of Italy, scale 1:2.000.000*. CNR, Progetto Finalizzato Geodinamica, Roma.
- BLENDINGER W. (1983) - *Anisian sedimentation and tectonics of the M.Pore-M.Cernera area (Dolomites)*. Riv. It. Paleont.Strat., 89: 175-208.
- BLENDINGER W. (1985) - *Middle Triassic strike-slip tectonics and igneous activity of the Dolomites (Southern Alps)*.

- Tectonophysics, **113**: 105-121.
- BLENDINGER W. (1986) - *Isolated stationary carbonate platforms: the Middle Triassic (Ladinian) of the Marmolada area, Dolomites, Italy*. Sedimentology, **31**: 1-24.
- BOSELLINI A. (1965) - *Lineamenti strutturali delle Alpi Meridionali durante il Permo-Trias*. Mem. Museo St. Nat. Ven. Trid., **15**, 3: 1-72.
- BOSELLINI A. (1968) - Paleogeologia pre-anisica delle Dolomiti centro-settentrionali. Atti Acc. Naz. Lincei, Rend. Cl. Sc. Fis. Mat. Nat., **89**: 1-32.
- BOSELLINI A. (1973) - *Modello geodinamico e paleotettonico delle Alpi Meridionali durante il Giurassico-Cretacico*. Sue possibili applicazioni agli Appennini. In: B. ACCORDI (ed) *Moderne vedute sulla geologia dell'Appennino*, Accad. Naz. Lincei, **183**: 163-205, Roma.
- BOSELLINI A. (1982) - *Geologia dei passi dolomitici circostanti il Gruppo di Sella*. In: Guida alla Geologia del Sudalpino centro-orientale. Eds. A. CASTELLARIN & G.B. VAI, Guide Geol. Reg. Soc. Geol. It., 267-272.
- BOSELLINI A. (1984) - *Progradation geometries of carbonate platforms: examples from the Triassic of the Dolomites, northern Italy*. In: *Reefs in Time and Space* Ed. by L.F. LAPORTE, Spec. Publ. Soc. econ. Paleont. Miner., **18**: 209-233.
- BOSELLINI A. (1991) - *Geology of the Dolomites, An introduction*. Dolomieu Conference on Carbonate Platforms and Dolomitization, 1-43.
- BOSELLINI A. (1996) - *Geologia delle Dolomiti*. 1-192 pp., Athesia, Bolzano.
- BOSELLINI A. & DOGLIONI C. (1986) - *Inherited structures in the hangingwall of the Valsugana Overthrust (Southern Alps, Northern Italy)*. Journ. Struct. Geol., **8**, 5: 581-583.
- BOSELLINI A. & DOGLIONI C. (1988) - *Progradation Geometries of Triassic Carbonate Platforms of the Dolomites, and their Large-Scale Physical Stratigraphy*. Am. Assoc. Petrol. Geol. Nice Conference, Guide Book field trip **6**: 1-42.
- BOSELLINI A. & FERRI R. (1980) - *La Formazione di Livinallongo (Buchenstein) nella Valle di S. Lucano (Ladinico inferiore, Dolomiti Bellunesi)*. Ann. Univ. Ferrara, **IX**, **6**: 63-89.
- BOSELLINI A., GIANOLLA P. & STEFANI M. (2003) - *Geology of the Dolomites*. Episodes, **26**, 3: 181-185.
- BOSELLINI A. & HARDIE L.H. (1973) - *Depositional theme of a marginal marine evaporite*. Sedimentology, **20**: 5-27.
- BOSELLINI A. & MASETTI D. (1972) - *Ambiente e dinamica deposizionale del calcare del Vajont (Giurassico medio, Prealpi Bellunesi e Friulane)*. Annali Univ. Ferrara, **5**, 4: 87-100.
- BOSELLINI A., MASETTI D. & SARTI M. (1981) - *A Jurassic "Tongue of the ocean" infilled with oolitic sands: the Belluno trough, Venetian Alps, Italy*. Mar. Geol., **44**: 59-95.
- BOSELLINI A. & NERI C. (1991) - *The Sella Platform (Upper Triassic, Dolomites, Italy)*. Dolomieu Conference on Carbonate Platforms and Dolomitization. Guidebook Excursion B, 1-30.
- BOSELLINI A. & ROSSI D. (1974) - *Triassic carbonate buildups of the Dolomites, Northern Italy*. In: *Reef in Time and Space*, L.F. LAPORTE (Ed), Spec. publ. Soc. econ. Paleont. Miner., **18**: 209-233.
- BOSELLINI A. & STEFANI M. (1991) - *The Rosengarten: A platform-to-basin carbonate section (Middle Triassic, Dolomites, Italy)*. Dolomieu Conference on Carbonate Platforms and Dolomitization. Guidebook Excursion C, 1-24.
- BOSTROM R.C. (1971) - *Westward displacement of the lithosphere*. Nature, **234**: 536-538.
- BOYER G.R. (1914) - *Étude géologique des environs de Longarone (Alpes Venetiennes)*. Bull. Soc. Géol. France, **4**, **13** (1913), **8**: 451-485.
- BOYER S.E. & ELLIOTT D. (1982) - *Thrust systems*. Amer. Ass. Petrol. Geol., **66**: 1196-1230, Tulsa.
- BOZZO G.P. & SEMENZA E. (1973) - *Nuovi elementi tettonici del vallone di Fadalto e loro inquadramento nella struttura del veneto nordorientale*. Boll. Mus. Civ. St. Nat. Venezia, suppl. **12**: 11-25, Venezia.
- BRACE W. F. & KOHLSTEDT D. L. (1980) - *Limits on lithospheric stress imposed by laboratory experiments*, J. Geophys. Res., **85**: 6248-6252.
- BRACK P. (1981) - *Structures in the south western border of the Adamello intrusion (Alpi Bresciane, Italy)*. Schweiz. Mineral. Petr. Mitt., **61**: 37-50.
- BRACK P. (1983) - *Multiple intrusions-examples from the Adamello batholith (Italy) and their significance on the mechanisms of intrusion*. Mem. Soc. Geol. It., **26**: 145-157.
- BRACK P. (1984) - *Geologie der Intrusiva und Rahmengesteine des SW-Adamello*. Diss. nr. 7612, ETH, Zürich.
- BRACK P., MUNDIL R., OBERLI F., MEIER M., & RIEBER H. (1996) - *Biostratigraphic and radiometric age data question the Milankovitch characteristics of the Latemar (Southern Alps, Italy)*. Geology, **v. 24**: 371-375 pp.
- BRACK P. & RIEBER H. (1993) - *Towards a better definition of the Anisian/Ladinian boundary: New stratigraphic data and correlations of boundary sections from the Southern Alps*. Eclogae geol. Helvetiae, **v. 86/2** 415-527 pp.
- BRAGA G.P. (1970) - *L'assetto tettonico dei dintorni di Possagno (Trevigiano occidentale)*. Acc. Naz. Lincei, **48**: 451-455.
- BRAGA G.P., GATTO G.O., GATTO A., GRENNANIN A., MASSARI F., MEDIZZA F., NARDIN M., PERNA G., ROSSI D., SACERDOTI M., SEMENZA E., SOMMAVILLA E., ZIRPOLI G. & ZULIAN T. (1971) - *Note illustrative della Carta Geologica Italiana alla scala 1:100.000, Foglio 22, Feltre*. Serv. Geol. It., 1-149, Roma.
- BRANDNER R. (1984) - *Meeresspiegelschwankungen und Tektonik in der Trias des NW-Tethys*. Jahrb. Geol. Bundesanst., **126**, 4: 435-475.
- BRANDNER R., FLÜGEL E., KOCH R. & YOSE L.A. (1991) - *The Northern Margin of the Schlern/Scliar. Rosengarten/Catinaccio Platform*. Dolomieu Conference on Carbonate Platforms and Dolomitization. Guidebook Excursion A, 1-61.
- BRANDNER R. & MOSTLER H. (1982) - *Der geologische Aufbau des Schlerngebietes und seiner weiteren Umgebung. Exkursions-führer, jahrestagung der Österreichischen Geologischen Gesellschaft*, 1-43.

- BROGLIO LORIGA C., MASETTI D. & NERI C. (1982) - *La Formazione di Werfen (Scitico) delle Dolomiti occidentali: sedimentologia e biostratigrafia*. Riv. It. Paleont. Strat., **88**, 4: 501-598.
- BRUSCA C., GAETANI M., JADOUL F. & VIEL G. (1981) - *Paleogeografia Ladino-Carnica e Metallogenesi del Sudalpino*. Mem. Soc. Geol. It., **22**: 65-82.
- BUSATTA C. (1991) - *Geologia del fianco nordoccidentale del Monte Civetta (Dolomiti centrali)*. Tesi di laurea, 1-125, Ferrara.
- BUXTORF A. (1916) - *Prognosen und Befunde beim Hauensteinbasis und Grenchenbergstunnel und die Bedeutung der letzteren für die Geologie des Jura Gebirges*. Verhandlungen der Natforschenden Gesellschaft in Basel, **27**: 184-254, Basel.
- BYERLEE J.D. (1978) - *Friction of rocks*. Pure Appl. Geophys., **116**: 615-626.
- CADELL H.M. (1889) - *Experimental researches in mountain building*. Transactions of the Royal Society of Edinburgh, **1**: 337-357.
- CALCAGNILE G. & PANZA G.F. (1980) - *The main characteristics of the lithosphere-asthenosphere system in Italy and surrounding regions*. Pure Applied Geophysics, **119**: 865-879 pp.
- CARMINATI E. & DOGLIONI C. (2004) - *Europe. Mediterranean tectonics*. In Encyclopedia of Geology. Elsevier, 135-146.
- CARMINATI E., DOGLIONI C., ARGNANI A., CARRARA G., DABOVSKI C., DUMURDZANOV N., GAETANI M., GEORGIEV G., MAUFFRET A., NAZAI S., SARTORI R., SCIONTI V., SCROCCA D., SÉRANNE M., TORELLI L. & ZAGORCHEV I. (2004) - *TRANSMED Transect III*, in: W. CAVAZZA, F. ROURE, W. SPAKMAN, G.M. STAMPFLI & P.A. ZIEGLER, (Eds.), The TRANSMED Atlas. The Mediterranean Region from Crust to Mantle, Springer-Verlag, Berlin, 141pp.
- CARMINATI E., DOGLIONI C. & BARBA S. (2004) - *Reverse migration of seismicity on thrusts and normal faults*. Earth Sci. Rev., **65**: 195-222.
- CARMINATI E., DOGLIONI C. & SCROCCA D. (2003) - *Apennines subduction-related subsidence of Venice*. Geophys. Res. Lett. **30**, 13, 1717, doi: 10.1029/2003GL017001.
- CARMINATI E., DOGLIONI C. & SCROCCA D. (2004) - *Alps Vs Apennines*. Special Volume of the Italian Geological Society for the IGC 32 Florence-2004, 141-151.
- CARMINATI E., DOGLIONI C. & SCROCCA D. (2005) - *Magnitude and causes of long-term subsidence of the Po Plain and Venetian region*. Flooding and Environmental Challenges for Venice and its Lagoon: State of Knowledge, eds. C. A. FLETCHER & T. SPENCER WITH J. DA MOSTO & P. CAMPOSTRINI. Cambridge University Press.
- CARMINATI E., NEGREDO A.M., VALERA J.L. & DOGLIONI C. (2005) - *Subduction-related intermediate-depth and deep seismicity in Italy: insights from thermal and rheological modelling*. Phys. Earth Planet. Int., **149**: 65-79.
- CARMINATI E. & SANTANTONIO M. (2005) - *Control of differential compaction on the geometry of sediments onlapping paleoescarpments: insights from field geology (Central Apennines, Italy) and numerical modeling*. Geology, **33**: 353-356.
- CARMINATI E. & SILETTO G.B. (1997) - *The effects of brittle plastic transitions in basement involved foreland belts: The central Southern Alps (N. Italy) case*. Tectonophysics, **280**: 107-123.
- CARMINATI E. & SILETTO G.B. (2005) - *The Central Southern Alps (N. Italy) paleoseismic zone: A comparison between field observations and predictions of fault mechanics*. Tectonophysics, **401**: 179-197, 2005.
- CARMINATI E., WORTEL M. J. R., SPAKMAN W. & SABADINI R. (1998) - *The role of slab detachment processes in the opening of the western-central Mediterranean basins: some geological and geophysical evidence*. Earth Planet. Sci. Lett., **160**: 651-665 pp.
- CARTER N.L. & TSENN M.C. (1987) - *Flow properties of continental lithosphere*. Tectonophysics, **136**: 27-63.
- CASATI P., JADOUL F., NICORA A., MARINELLI M., FANTINI SESTINI N. & FOIS E. (1982) - *Geologia della Valle dell'Ansiei e dei Gruppi M. Popera*. Tre Cime di Lavaredo (Dolomiti Orientali). Riv. It. Paleont. Strat., **87**, 3: 371-510.
- CASATI P. & TOMAI M. (1969) - *Il Giurassico ed il Cretacico del versante settentrionale del Vallone Bellunese e del Gruppo del Monte Brandol*. Riv. Ital. Paleont. Strat., **75**, 2: 205-340, Milano.
- CASON C., GRANDESSO P., MASSARI F. & STEFANI C. (1981) - *Depositi deltizi nella molassa cattiano-burdigaliana della bellunese (Alpi Meridionali)*. Mem. Sc. Geol., **34**: 325-354, Padova.
- CASSANO E., ANELLI L., FICHERA R. & CAPPELLI V. (1986) - *Pianura Padana, Interpretazione integrata di dati geofisici e geologici*. Agip, 73° Congresso Soc. Geol. Ital., Roma, 1-27.
- CASTELLARIN A. (1972) - *Evoluzione paleotettonica sinsedimentaria del limite tra "piattaforma veneta" e "bacino lombardo", a nord di Riva del Garda*. Giorn. Geol., **37** (1970), s. 2, 1, 11-212, Bologna.
- CASTELLARIN A. (1979) - *Il problema dei raccorciamenti crostali nel sudalpino*. Rend. Soc. Geol. It., **1** (1978), 21-23, Roma.
- CASTELLARIN A. (1981) - *Carta tettonica delle Alpi Meridionali alla scala 1:200.000*. CNR, pubbl. **441**: 1-220, Tecnoprint, Bologna.
- CASTELLARIN A. (1982) - *Lineamenti ancestrali sudalpini*. In: CASTELLARIN & VAI (Eds.): Guida alla Geologia del Sudalpino centro-orientale. Guide Geol. Reg., Soc. Geol. It., 41-55.
- CASTELLARIN A., LUCCHINI F., ROSSI P.L., SIMBOLI G., BOSELLINI A. & SOMMAVILLA E. (1979) - *Middle-Triassic magmatism in Southern Alps II: A geodynamic model*. Riv. It. Paleont. Strat., **85**: 3-4, 1111-1124.
- CASTELLARIN A., LUCCHINI F., ROSSI P.L., SELLI L. & SIMBOLI G. (1988) - *The Middle Triassic magmatic-tectonic*

- arc development in the Southern Alps*. Tectonophysics, **146**: 79-89.
- CASTELLARIN A., LUCCHINI F., ROSSI P.L., SARTORI R., SIMBOLI G. & SOMMAVILLA E. (1982) - *Note geologiche sulle intrusioni di Predazzo e dei Monzoni*. In: CASTELLARIN & VAI (Eds): Guida alla Geologia del Sudalpino centro-orientale. Guide Geol. Reg., Soc. Geol. It., 211-220.
- CASTELLARIN A., LUCCHINI F., ROSSI P.L., SIMBOLI G., BOSELLINI A. & SOMMAVILLA E. (1979) - *Middle-Triassic magmatism in Southern Alps II: A geodynamic model*. Riv. It. Paleont. Strat., **85**: 3-4, 1111-1124.
- CASTELLARIN A., NICOLICH R., FANTONI R., CANTELLI L., SELLA M. & SELLI L. (2006) - *Structure of the lithosphere beneath the Eastern Alps (southern sector of the TRANSALP transect)*. Tectonophysics **414**: 259-282.
- CASTELLARIN A., ROSSI P.L., SIMBOLI G., SOMMAVILLA E. & DE LUCA A. (1977) - *Dati geologici e petrografici sul Gruppo del Buffaure*. Miner. Petrogr. Acta, **21**: 165-187.
- CASTELLARIN A., SELLI L., PICOTTI V., & CANTELLI L. (1998) - *La tettonica delle Dolomiti nel quadro delle Alpi Meridionali orientali*. Memorie della Società Geologica Italiana, v. **53**, 133-143 pp.
- CASTELLARIN A. & VAI G.B. (1981) - *Importance of Hercynian tectonics within the framework of the Southern Alps*. J. Struct. Geol., **3**, 4: 477-486.
- CASTELLARIN A. & VAI G.B. (1982) - *Introduzione alla geologia strutturale del sudalpino*. In CASTELLARIN & VAI (Eds), Guida alla geologia del Sudalpino centro-orientale. Guide Geol. Reg., Soc. Geol. It., 1-22.
- CASTIGLIONI B. (1931) - *Il Gruppo della Civetta (Alpi Dolomitiche)*. Mem. Ist. Geol. Mineral. Univ. Padova, **9**: 1-83.
- CASTIGLIONI B. (1939) - *Il Gruppo delle Pale di S.Martino e le valli limitrofe (Alpi Dolomitiche)*. Mem. Ist. Geol. R. Univ. Padova, **13**: 1-104.
- CASTIGLIONI B., BOYER G., DAL PIAZ G., LEONARDI P., VENZO S., VIALI V. & ZENARI S. (1941) - *Foglio 23, Belluno, della Carta Geologica delle Tre Venezie*, alla scala 1:100.000. Uff. Idrogr. Mag. Acque, Venezia.
- CATALANO R., D'ARGENIO B. & DOGLIONI C. (1989) - *Triassic and Liassic transensional tectonics and later inversion in Italy*. 28th International Geological Congress, Washington, v. **1**, 251.
- CATALANO R., DOGLIONI C. & MERLINI S. (2001) - *On the Mesozoic Ionian basin*. Geophysical Journal International, **144**: 49-64 pp.
- CATI A., SARTORIO D. & VENTURINI S. (1987) - *Carbonate platforms in the subsurface of the northern Adriatic area*. Mem. Soc. Geol. It., **40**: 295-308.
- CELLA F., FEDI M., FLORIO G. & RAPOLLA A. (1998) - *Gravity modeling of the litho-asthenosphere system in the Central Mediterranean*. Tectonophysics, **287**: 117-138 pp.
- CHANNELL J.E.T. & DOGLIONI C. (1994) - *Early Triassic paleomagnetic data from the Dolomites (Italy)*. Tectonics, **13**, 1: 157-166.
- CHAMBERLIN R.T. (1910) - *The Appalachian folds of central Pennsylvania*. J. Geol., **18**: 228-251.
- CHANNELL J.T.E., DOGLIONI C. & STONER J. (1991) - *New paleomagnetic data from the Southern Alps*. In: IUGG, General Assembly XX, Vienna. Tethyan Paleomagnetism and tectonics.
- CHANNELL J.E.T. & DOGLIONI C. (1994) - *Early Triassic paleomagnetic data from the Dolomites (Italy)*. Tectonics, **13**, 1: 157-166.
- CHANNELL J.T.E., DOGLIONI C. & STONER J. (1992) - *Jurassic and Cretaceous paleomagnetic data from the Southern Alps (Italy)*. Tectonics, **11**, 4: 811-822.
- CHRISTOVA C. & NIKOLOVA S. B. (1993) - *The Aegean region: deep structures and seismological properties*. Geophysical Journal International, **115**: 635-653 pp.
- CITA M.B. & ROSSI D. (1959) - *Prima segnalazione di Aptiano-Albiano nelle Dolomiti*. Rend. Acc. Naz. Lincei, **8**, 6, 8.
- COLACICCHI R. (1960) - *Le dislocazioni delle cime (Gipfelfaltungen) nelle Dolomiti*. Gruppo del Civetta. Mem. Ist. Geol. Mineral. Univ. Padova **22**: 1-49.
- CORTI G., CARMINATI E., MAZZARINI F. & OZIEL GARCIA M. (2005) - *Active strike-slip faulting in El Salvador (Central America)*, Geology, **33**: 989-992.
- CORTI G., CUFFARO M., DOGLIONI C., INNOCENTI F. & MANETTI P. (2006) - *Coexisting geodynamic processes in the Sicily Channel*. In: Y. DILEK & S. PAVLIDES (Eds), Postcollisional tectonics and magmatism in the Mediterranean region and Asia, Geol. Soc. Am. Sp. Paper, **409**: 83-96.
- COSTA V. & DOGLIONI C. (1989) - *Tettonica del Foglio 1:50.000. 063 Belluno*. Note Illustrative della Carta Geologica d'Italia, Serv. Geol. It., Roma, in press.
- COTTON J.T. & KOYI H.A. (2000) - *Modeling of thrust fronts above ductile and frictional detachments: Application to structures in the Salt Range and Potwar Plateau, Pakistan*, GSA Bulletin, **112**: 351-363.
- COUSIN M. (1981) - *Les rapports Alpes-Dinarides. Les confins de l'Italie et de la Yougoslavie*. Soc. Géol. du Nord, **5**, I,1-521, II,1-521.
- CRANE R.C. (1987) - *Geologic interpretation of thrust belts. Alaskan north slope geology*, **2**: book 50, 621-630 pp., Santa Fe.
- CRESPI M., CUFFARO M., DOGLIONI C., GIANNONE F. & RIGUZZI F. (2007) - *Space geodesy validation of the global lithospheric flow*. Geophysical Journal International, **168**: 491-506, doi: 10.1111/j.1365-246X.2006.03226.x.
- CROS P. (1966) - *Age oligocène supérieur d'un poudingue (du Monte Parei) dans le Dolomites centrales italiennes*. C.R. somm. Soc. géol. France **7**: 250-252.
- CROS P. (1974) - *Evolution sédimentologique et paléostrutturale de quelques plate-formes carbonatées biogènes (Trias des Dolomites Italiennes)*. Sciences Terre, **19**: 299-379.
- CROS P. (1978) - *Interprétation des relations entre sédiments continentaux intrakarstiques et molasses littorales Oligo Miocènes des Dolomites centrales Italiennes*. Atti Congr. "Processi Paleocarsici e Neocarsici", Napoli.

- CROWELL J.C. (1974) - *Origin of late Cenozoic basins in southern California*, Special Publication - Society of Economic Paleontologists and Mineralogists, **22**: 190-204.
- CRUCIANI C., CARMINATI E. & DOGLIONI C. (2005) - *Slab dip vs. lithosphere age: no direct function*. *Earth Planet. Sci. Lett.*, **238**: 298-310.
- CUFFARO M., CAPUTO M. & DOGLIONI C. (2004) - *On the sub-rotation of a plate*. *Journal of Virtual Explorer*, ISSN 1441-8142, **14**, **2**: 1-15.
- DAHLSTROM C.D.A. (1969) - *Balanced cross sections*. *Can. J. Earth Sci.*, **6**: 743-757, 1969.
- DAHLSTROM C.D.A. (1970) - *Structural geology in the eastern margin of the Canadian Rocky Mountains*. *Bull. Can. Petrol. Geol.*, **18**: 332-406.
- D'ALBERTO L., BOZ A. & DOGLIONI C. (1995) - *Structure of the Vette Feltrine (Eastern Southern Alps)*. *Memorie di Scienze Geologiche*, Padova, **47**: 189-199.
- DAL PIAZ G. (1907) - *Le Alpi Feltrine*. *Mem. R. Ist. Veneto Sc. Lett. Arti*, 1-176, Venezia.
- DAL PIAZ G. (1912) - *Studi geotettonici sulle Alpi Orientali (Regione tra il Brenta ed il Lago di Santa Croce)*. *Mem. Ist. Geol. R. Univ. Padova*, **1**: 1-196.
- DAL PIAZ G.V. (1976) - *Alcune riflessioni sulla evoluzione geodinamica alpina delle Alpi*. *Rend. Soc. It. Miner. Petr.*, **XXXII**, 380-385.
- DAL PIAZ G.V., BISTACCHI A. & MASSIRONI M. (2003) - *Geological outline of the Alps*. *Episodes*, **26**, **3**, 175-180.
- DAL PIAZ G.V. & LOMBARDO B. (1986) - *Early Alpine eclogite metamorphism in the Penninic Monte Rosa*. *Gran Paradiso basement nappes of the northwestern Alps*, *Geol. Soc. Amer. Mem.*, **164**: 249-265.
- D'AMICO C. (1962) - *La zona cristallina Agordo-Cereda*. *Mem. Ist. Geol. Min. Univ. Padova*, **23**: 3-77.
- D'AMICO C. (1986) - *Volcanic sequence in Trentino. Alto Adige*. In: AA. VV., *Permian and Permian-Triassic boundary in the South-Alpine segment of the Western Tethys*. IGCP Project 203. Field Conference preceedings, 1-158.
- DAVIES S.J., DAWERS N.H., MCLEOD A.E. & UNDERHILL J.R. (2000) - *The structural and sedimentological evolution of early synrift successions: the Middle Jurassic Tarbert Formation, North Sea*, *Basin Research*, **12**: 343-365.
- DAVIS D., SUPPE J. & DAHLEN F.A. (1983) - *Mechanics of fold-and-thrust belts and accretionary wedges*, *J. Geophys. Res.*, **88**: 1153-1172.
- DAVIS G.H. & REYNOLDS S.J. (1996) - *Structural Geology of Rocks and Regions*. New York, John Wiley & Sons, Inc.
- DE CONCINI C., DE FLORENTIS N., GATTO G.O. & ILLICETO V. (1980) - *Movimenti attuali nelle Alpi orientali rilevati mediante livellazioni ripetute*. *Mem. Sc. Geol. Padova*, **34**: 53-66.
- DE PAOR D.G. (1988) - *Balanced section in thrust belts; Part 1, Construction*. *Am. Assoc. Petrol. Geol. Bull.*, **72**: 73-90.
- DERCOURT J., GAETANI M., VRIELYNCK B., BARRIER E., BIJU-DUVAL B., BRUNET M.F., CADET J.P., CRASQUIN S. & SANDULESCU M. (2000) - *Peri-Tethys palaeogeographical atlas*. 24 maps and explanatory notes: I-XX. CCGM/CGMW, Paris, 269 pp.
- DE SITTER L.U. & DE SITTER KOOMANS C.M. (1949) - *The geology of the Bergamasc Alps, Lombardia, Italy*. *Leidse Geol. Mededl.*, **14 B**, 1-257, Leiden.
- DE VOOGD B., TRUFFERT C., CHAMOT-ROOKE N., HUCHON P., LALLEMANT S. & LE PICHON X. (1992) - *Two-ship deep seismic soundings in the basins of the Eastern Mediterranean Sea (Pisiphae cruise)*. *Geophysical Journal International*, **109**: 536-552 pp.
- DE ZANCHE V. & FARABEGOLI E. (1981) - *Scythian tectonics in the Southern Alps: Recoaro Phase*. *Geol. Palaeont. Mitt. Innsbruck*, **10**, **10**: 289-304.
- DE ZANCHE V. & MIETTO P. (1984) - *Testimonianze di attività tettonica tardotriassica nelle Prealpi Vicentine*. *Riv. It. Paleont. Strat.*, **89**, **3**: 335-342.
- DI NAPOLI ALLIATA E. & PROTO DECIMA F. (1968) - *Segnalazione di una lacuna stratigrafica tra il "Flysch superiore" e la "Glanconia cattiana" del Vallone Bellunese*. *Boll. Soc. Geol. It.*, **87**: 233-234, Roma.
- DOGLIONI C. (1982) - *Tettonica Triassica nella Valle di Livinallongo (Dolomiti centrali)*. *Ann. Univ. Ferrara, sez. IX, Scienze Geol. Paleont.*, v. VIII, n.1, 1-21.
- DOGLIONI C. (1983) - *Duomo medio-triassico nelle Dolomiti*. *Rend. S.G.I.*, **6**: 13-16.
- DOGLIONI C. (1984) - *Triassic diapiric structures in the central Dolomites (Northern Italy)*. *Eclogae Geol. Helv.*, **77/2**: 261-285.
- DOGLIONI C. (1984) - *Tettonica triassica transpressiva nelle Dolomiti*. *Giornale di Geologia*, **46**, **2**: 47-60, Bologna.
- DOGLIONI C. (1985) - *Geometrie lungo l'asse di una kink-band centimetrica*. *Boll. S.G.I.*, **104**, **1**: 81-86.
- DOGLIONI C. (1985) - *The overthrusts in the Dolomites: ramp-flat systems*. *Eclogae Geol. Helv.*, **78/2**: 335-350.
- DOGLIONI C. (1987) - *Tectonics of the Dolomites (Southern Alps, Northern Italy)*. *Journ. Struct. Geol.*, **9**, **2**: 181-193.
- DOGLIONI C. (1988) - *Examples of strike-slip tectonics on platform-basin margins*. *Tectonophysics*, **156**: 293-302.
- DOGLIONI C. (1990) - *Anatomy of an overthrust*. *Annales Tectonicae*. v. IV/1: 68-82.
- DOGLIONI C. (1990) - *Thrust tectonics examples from the Venetian Alps*. *Studi Geologici Camerti*, vol. spec. 117-129.
- DOGLIONI C. (1990) - *The global tectonic pattern*. *Journal of Geodynamics*, **12**, **1**: 21-38.
- DOGLIONI C. (1991) - *The Venetian Alps thrust belt*. In: K. McCLAY (Ed): *Thrust Tectonics*, Chapman and Hill, London.
- DOGLIONI C. (1991) - *Una interpretazione della tettonica globale*. *Le Scienze*, **270**: 32-42, febbraio.
- DOGLIONI C. (1991) - *A proposal for the kinematic modelling of W-dipping subductions. possible applications to the Tyrrhenian-Apennines system*. *Terra Nova*, **3**, **4**: 423-434.
- DOGLIONI C. (1992) - *Relationships between Mesozoic extensio-*

- nal tectonics, stratigraphy and Alpine inversion in the Southern Alps.* *Eclogae Geologicae Helveticae*, **85**, 1: 105-126.
- DOGLIONI C. (1992) - *The Venetian Alps thrust belt.* In: K.R. MCCLAY (Ed): *Thrust Tectonics*, Chapman and Hall, 319-324, London.
- DOGLIONI C. (1992) - *Escursione nel Sudalpino Orientale (Dolomiti e Prealpi Venete).* Agip Adde, 1-118.
- DOGLIONI C. (1992) - Main differences between thrust belts. *Terra Nova*, **4**, 2: 152-164.
- DOGLIONI C. (1993) - *Geological evidence for a global tectonic polarity.* *Journal of the Geological Society, London*, **150**: 991-1002.
- DOGLIONI C. (1993) - *Some remarks on the origin of foredeeps.* *Tectonophysics*, v. **228**: 1-2, 1-20 pp.
- DOGLIONI C. (1994) - *Foredeeps versus subduction zones.* *Geology*, **22**, 3: 271-274.
- DOGLIONI C. (1995) - *Geological remarks on the relationships between extension and convergent geodynamic settings.* *Tectonophysics*, **252**: 1-4, 253-267.
- DOGLIONI C., AGOSTINI S., CRESPI M., INNOCENTI F., MANETTI P., RIGUZZI F. & SAVASCIN Y. (2002) - *On the extension in western Anatolia and the Aegean sea.* *Journal Virtual Explorer*, **7**: 117-131.
- DOGLIONI C. & BOSELLINI A. (1987) - *Eoalpine and Mesoalpine tectonics in the Southern Alps.* *Geol. Rundschau*, **76/3**: 735-754.
- DOGLIONI C. & BOSELLINI A. (1989) - *Platform break. downlap planes relationship in prograding carbonate platforms: a tool for the reconstruction of basin evolution.* *Boll. Soc. Geol. It.*, **108**, 1: 175-182.
- DOGLIONI C., BOSELLINI A. & VAIL P.R. (1989a) - *Stratal patterns: classification and examples from the Dolomites.* *Basin Research*, **2**: 83-95.
- DOGLIONI C. & CARMINATI E. (2002) - *The effects of four subductions in NE Italy.* *Transalp Conference, Mem. Scienze Geol.*, **54**: 1-4.
- DOGLIONI C., CARMINATI E. & BONATTI E. (2003) - *Rift asymmetry and continental uplift.* *Tectonics*, **22**, 3: 1024, doi:10.1029/2002TC001459.
- DOGLIONI C., CARMINATI E. & CUFFARO M. (2006) - *Simple kinematics of subduction zones.* *Int. Geol. Rev.*, **48**, 6: 479-493.
- DOGLIONI C., CARMINATI E., CUFFARO M. & SCROCCA D. (2007) - *Subduction kinematics and dynamic constraints.* *Earth Science Reviews*, **83**: 125-175.
- DOGLIONI C., D'AGOSTINO N. & MARIOTTI G. (1998) - *Normal faulting versus regional subsidence and sedimentation rate.* *Mar. Petrol. Geol.*, **15**: 737-750.
- DOGLIONI C. & FLORES G. (1997) - *Italy.* In: MOORES & FAIRBRIDGE (Eds), *Encyclopedia of European and Asian Regional Geology.* CHAPMAN & HALL, 414-435.
- DOGLIONI C. & GOLDHAMMER R.K. (1988) - *Compaction-induced Subsidence in a margin of a carbonate platform.* *Basin Research*, **1/4**: 237-246.
- DOGLIONI C., GUEGUEN E., SABAT F. & FERNANDEZ M. (1997) - *The western Mediterranean extensional basins and the Alpine orogen.* *Terra Nova*, **9**, 3: 109-112.
- DOGLIONI C., GUEGUEN E., HARABAGLIA P. & MONGELLI F. (1999) - *On the origin of W-directed subduction zones and applications to the western Mediterranean.* *Geol. Soc. Sp. Publ.*, v. **156**: 541-561 pp.
- DOGLIONI C., HARABAGLIA P., MERLINI S., MONGELLI F., PECCERILLO A. & PIROMALLO C. (1999) - *Orogens and slabs vs their direction of subduction.* *Earth Science Reviews*, **45**: 167-208.
- DOGLIONI C., MASETTI D. & NERI C. (1989b) - *Late Carnian extensional tectonics in the Dolomites.* *Rendiconti Società Geologica Italiana*, **14**: 43-48.
- DOGLIONI C., MERLINI S. & CANTARELLA G. (1999) - *Foredeep geometries at the front of the Apennines in the Ionian sea (central Mediterranean).* *Earth and Planetary Science Letters*, **168**, 3-4: 243-254.
- DOGLIONI C., MONGELLI F. & PIALI G.P. (1998) - *Boudinage of the Alpine belt in the Apenninic back-arc.* *Mem. Soc. Geol. It.*, **52**: 457-468.
- DOGLIONI C., MORETTI I. & ROURE F. (1990) - *Basal lithospheric detachment, eastward mantle flow and Mediterranean Geodynamics: a discussion.* *Journal of Geodynamics*, **13**, 1: 47-65.
- DOGLIONI C. & NERI C. (1988) - *Anisian tectonics in the Passo Rolle Area.* *Rend. S.G.I.*, **11**: 197-204.
- DOGLIONI C. & PROSSER G. (1997) - *Fold uplift versus regional subsidence and sedimentation rate.* *Marine and Pet. Geology*, **14**, 2: 179-190.
- DOGLIONI C. & SABADINI R. (2003) - *Mantle dynamics and plate kinematics.* In *Encyclopedia of Life Support Systems (EOLSS)*, UNESCO, Eolss Publishers, Oxford, <http://www.eolss.net>.
- DOGLIONI C. & SORPAES C. (1990) - *Polyphase deformation in the Col Bechei area (Dolomites-Northern Italy).* *Eclogae Geol. Helv.*, **83/3**: 701-710.
- DURAND B., JOLIVET J., HORVÁTH F. & SÉRANNE M. (1999) - *The Mediterranean Basins: Tertiary extension within the Alpine orogen.* *Geological Society of London, Special Publication*, **156**: 1-584 pp.
- EGENHOFF E., PETERHANSEL A., BECHSTADT T., ZUHLKE R. & GROTSCH J. (1999) - *Facies architecture of an isolated carbonate platform: tracing the cycles of the Latemar (Middle Triassic, northern Italy).* *Sedimentology*, **46**: 893-912.
- ENGELDER T. (1999) - *Transitional-tensile fracture propagation: a status report.* *J. Struct. Geol.*, **21**: 1049-1055.
- ERSLEV E.A. (1991) - *Trishear fault-propagation folding.* *Geology*, **19**: 617-620.
- FABIANI R. (1915) - *Il Paleogene nel Veneto.* *Mem. Ist. Geol. R. Univ. Padova*, **3**: 1-336, Padova.
- FANTONI R. & SCOTTI P. (2003) - *Thermal record of the Mesozoic extensional tectonics in the Southern Alps.* *Atti Ticinesi Sc. Terra*, **SS9**, 96-101.
- FARABEGOLI et alii (1976) - *Risultati preliminari sull'Anisico della Conca di Agordo e dell'Alta Val di Zoldo (Dolomiti Sudorientali).* *Boll. Soc. Geol. It.*, **95**: 659-703.
- FERASIN F. (1958) - *Il "Complesso di scogliera" cretaceo del*

- Veneto centro-orientale. Mem. Ist. Geol. Miner. Univ. Padova, 21: 1-54, Padova.
- FOIS E. (1982) - *The Sass da Putia carbonate buildup (western Dolomites): biofacies succession and margin development during the Ladinian*. Riv. It. Paleont. Strat., 87, 4: 565-598.
- FOIS E. & GAETANI M. (1981) - *The northern margin of the Civetta buildup. Evolution during the Ladinian and the Carnian*. Riv. It. Paleont. Strat., 86, 3: 469-542.
- FORCELLA F. (1988) - *Assetto strutturale delle Orobie orientali tra la Val Seriana e la Val Camonica*. Rend. Soc. Geol. It., 11: 269-278.
- FORCELLA F., FERRARI L., TIBALDI A. & ZANCHI A. (1990) - *Tettonica a thrusts nelle Orobie Orientali*. Field trip B4 of the 75° Congress of the "Società Geologica Italiana".
- FORT X., BRUN J.P. & CHAUVEL F. (2004) - *Salt tectonics on the Angolan margin, synsedimentary deformation processes*. Am. Assoc. Petrol. Geol. Bull., 88: 1523-1544.
- FRANCIOSI R. & VIGNOLO A. (2002) - *Northern Adriatic foreland - A promising setting for the Southalpine Mid-Triassic petroleum system*. EAGE, 64th Conference & Exhibition, Florence, Italy, 27-30 May, H-25.
- FRIZON DE LAMOTTE D., SAINT BEZAR B., BRACENE R. & MERCIER E. (2000) - *The two main steps of the Atlas building and geodynamics of the western Mediterranean*. Tectonics, 19, 4: 740-761 pp.
- FUGANTI A. (1964) - *Le "pulsazioni tettoniche" turoniane nel Trentino occidentale (Alpi orientali)*. St. Trent. Sci. Nat., 41: 138-158.
- FURLANI M. (1909) - *Zur Tektonik der Sellagruppe in Gröden*. Mitt. geol. Ges. Wien 2: 445-461.
- GAETANI M. (1979) - *Field-Guide Book, Riccardo Assereto and Giulio Pisa Symposium on Triassic stratigraphy in Southern Alps, Bergamo, Italy*. Univ. Milano, 1-73.
- GAETANI M., DERCOURT J. & VRIELYNCK B. (2003) - *The Peri-Tethys Programme: achievements and results*. Episodes, 26, 2: 79-93.
- GAETANI M., FOIS E., JADOUL F. & NICORA A. (1981) - *Nature and evolution of Middle-Triassic carbonate buildups in the Dolomites (Italy)*. Mar. Geol. 44: 25-57.
- GAETANI M. & JADOUL F. (1979) - *The structure of the Bergamasc Alps*. Rend. Acc. Naz. Lincei, 65: 411-416.
- GARZANTI E. (1985) - *Petrography and diagenesis of Upper Triassic volcanic arenites (S. Giovanni Bianco, Gorno & Val Sabbia Formations, Bergamasc Alps)*. Boll. Soc. Geol. It., 104, 1: 3-20.
- GARZANTI E., DOGLIONI C., VEZZOLI G. & ANDÒ S. (2007) - *Orogenic Belts & Orogenic Sediment Provenances*. J. Geol., 115: 315-334.
- GAWTHORPE R.L. & LEEDER M. R. (2000) - *Tectono-sedimentary evolution of active extensional basins*, Basin Research, 12: 195-218.
- GEISER P.A. (1988) - *Mechanisms of thrust propagation: some examples and implications for the analysis of overthrust terranes*. J. struct. Geol. 10/8: 829-845.
- GELATI R., CASCONI A. & PAGGI L. (1982) - *Le unità stratigrafiche aptiano-maastrichtiane delle Prealpi Bergamasche*. Riv. It. Paleont. Strat., 74, 1: 63-70.
- GELATI R., NAPOLITANO A. & VALDISTURLO A. (1988) - *La "Gonfolite Lombarda": stratigrafia e significato nell'evoluzione del margine sudalpino*. Riv. It. Paleont. Strat., 94/2: 285-332.
- GIANOLLA P., DE ZANCHE V. & MIETTO P. (1998) - *Triassic Sequence Stratigraphy in the Southern Alps*. Definition of sequences and basin evolution. in: P.C. DE GRACIANSKY, J. HARDENBOL, T. JACQUIN, P.R. VAIL & D. ULMER-SCHOLLE (Eds.): Mesozoic-Cenozoic Sequence Stratigraphy of European Basins: SEPM Special Publication n°60, 723-751 pp.
- GIANOLLA P., RAGAZZI E. & ROGGI G. (1998) - *Upper Triassic amber from the Dolomites (Northern Italy)*. A paleoclimatic indicator?: Rivista Italiana di Paleontologia e Stratigrafia, v. 104: 381-390 pp.
- GIBBS A.D. (1984) - *Structural evolution of extensional basin margins*, J. geol. Soc. Lond., 141: 609-620.
- GIBBS A.D. (1990) - *Linked fault families in basin formation*, Journal of Structural Geology, 12: 795-803.
- GNACCOLINI M. (1967) - *Il Flysch dell'Alpago*. Riv. It. Paleont., 73, 3: 889-906, Milano.
- GNACCOLINI M. (1968) - *Caratteristiche sedimentologiche del Flysch del Vallone Bellunese*. Riv. Ital. Paleont., 74, 1: 63-70, Milano.
- GNACCOLINI M. & JADOUL F. (1990) - *Carbonate platform, lagoon and delta "high frequency" cycles from the Carnian of Lombardy (Southern Alps, Italy)*. Sedimentary Geology, 67: 143-159.
- GOETZE C. & EVANS B. (1979) - *Stress and temperature in the bending lithosphere as constrained by experimental rock mechanics*. Geophys. J. R. Astron. Soc., 59: 463-478.
- GOLDHAMMER R.K. (1987) - *Platform Carbonate Cycles, Middle Triassic of Northern Italy: The Interplay of local tectonics and Global Eustasy*. Ph.D. Thesis, Johns Hopkins University, Baltimore, 1-468.
- GOLDHAMMER R.K., DUNN P.A. & HARDIE L.A. (1987) - *High frequency glacio-eustatic sealevel oscillations with Milankovitch characteristics recorded in Middle Triassic platform carbonates in Northern Italy*. Am. J. Sci., 287: 853-892.
- GOLDHAMMER R.K., DUNN P.A. & HARDIE L.A. (1990) - *Depositional cycles, composite sea-level changes, cycle stacking patterns, and the hierarchy of stratigraphic forcing*. Geol. Soc. Amer. Bull., 102: 535-562.
- GOLDHAMMER R.K. & HARRIS M.T. (1989) - *Eustatic controls on the stratigraphy and geometry of the latemar buildup (Middle Triassic), the Dolomites of northern Italy*. In: CREVELLO et alii (eds), Controls on carbonate platform and basin development. SEPM Spec. Publ., 44: 323-338.
- GRANDESSO P. (1976) - *Biostratigrafia delle formazioni terziarie del Vallone Bellunese*. Boll. Soc. Geol. It., 94 (1975), 1323-1348, Roma.
- GRELAUD S., BUIL D., HARDY S. & FRIZON DE LAMOTTE D. (2000) - *Trishear kinematic model of fault-propagation folding and sequential development of minor structures: the Oupia Anticline (NE Pyrenees, France) case study*. Bull.

- Soc. Geol. Fr., v. 171; no. 4; 441-449 pp.; DOI: 10.2113/171.4.441.
- GRIPP A.E. & GORDON R.G. (2002) - *Young tracks of hot-spots and current plate Velocities*. Geophys. J. Int., **150**: 321-361.
- GUEGUEN E., DOGLIONI C. & FERNANDEZ M. (1998) - *On the post 25 Ma geodynamic evolution of the western Mediterranean*. Tectonophysics, **298**: 259-269.
- GUERRERA F., MARTIN-ALGARRA A. & PERRONE V. (1993) - *Late Oligocene-Miocene syn-/late orogenic successions in western and central Mediterranean chain from the betic cordillera to the southern Apennines*. Terra Nova **5**: 525-544 pp.
- HANDIN J. (1969) - *On the Coulomb-Mohr failure criterion*. J. Geophys. Res., **74**: 5343-5348.
- HARDING T.P. (1983) - *Divergent wrench fault and negative flower structure, Andaman Sea*. in A.W. BALLY ed., Seismic expression of structural styles: American Association of Petroleum Geologists Studies in Geology Series no. 15, v. 3, 4.2-1-8 pp.
- HARDING T.P., GREGORY R.F. & STEPHENS L.H. (1983) - *Convergent wrench fault and positive flower structure, Ardmore Basin, Oklahoma*, in A.W. BALLY ed., Seismic expression of structural styles: American Association of Petroleum Geologists Studies in Geology Series no. 15, v. 3, 4.2-13-17 pp.
- HARDIE L.A., BOSELLINI A. & GOLDHAMMER R.K. (1986) - *Repeated subaerial exposure of subtidal carbonate platforms, Triassic, Northern Italy: evidence for high frequency sea-level oscillations on a 10(4) year scale*. Paleogeography, **1**: 447-457.
- HARDIE L.A., NEWTON WILSON E. & GOLDHAMMER R.K. (1991) - *Cyclostratigraphy and dolomitization of the Middle Triassic Latemar buildup, the Dolomites, northern Italy*. Dolomieu Conference on Carbonate Platforms and Dolomitization. Guidebook Excursion F, 1-56.
- HUDEC M.R. & JACKSON M.P.A. (2004) - *Regional restoration across the Kwanza Basin, Angola: Salt tectonics triggered by repeated uplift of a metastable passive margin*. Am. Assoc. Petrol. Geol. Bull., **88**: 971-990.
- HEFLIN M. *et alii* (2002) - <http://sideshow.jpl.nasa.gov/mbh/series.html>
- HUIQI L., MCCLAY K.R. & POWELL D. (1992) - *Physical models of thrust wedges*. In: K.R. MCCLAY (Ed): Thrust Tectonics, Chapman and Hall, 71-81, London.
- HUGUEN C., MASCLE J., CHAUMILLON E., WOODSIDE J.M., BENKHELIL J., KOPF A. & VOLKONSKAIA A. (2001) - *Deformational styles of the eastern Mediterranean Ridge and surroundings from combined swath mapping and seismic reflection profiling*. Tectonophysics, **343**: 21-47 pp.
- JACKSON M.P.A. & TALBOT C.J. (1991) - *A Glossary of Salt Tectonics*, Bureau of Economic Geology, University of Texas at Austin.
- JACKSON M.P.A. & VENDEVILLE B.C. (1994) - *Regional extension as a geologic trigger for diapirism*, GSA Bulletin, **106**: 57-73.
- JADOUL F. (1986) - *Stratigrafia e Paleogeografia del Norico nelle Prealpi Bergamasche occidentali*. Riv. It. Paleont. Strat., **91**, 4: 479-512.
- JADOUL F. (1990) - *Il Norico superiore delle Prealpi Bergamasche occidentali*. Field trip A2 of the 75° Congress of the "Società Geologica Italiana".
- JAEGER J.C. & COOK N.G.W. (1979) - *Fundamentals of rock mechanics*, 3rd Edition, London, Mathuen, 593 pp.
- JONES P.B. (1982) - *Oil and gas beneath east-dipping underthrust faults in the Alberta foothills*. In R.B. POWERS (Ed.): Geologic Studies of the Cordilleran Thrust Belt. Rocky Mountain Ass. Geol., 61-74, Denver.
- JORDAN T.H. (1974) - *Some Comments on Tidal Drag as a Mechanism for Driving Plate Motions*. J. Geophys. Res., **79**, 14: 2141-2142.
- KALIN O. & TRÜMPY R. (1977) - *Sedimentation und Paleotektonik in den westlichen Sudalpen: Zur Triassisch-Jurassischen Gescichte des Monte Nudo-Beckens*. Eclogae Geol. Helv., **70**: 295-350.
- KASTENS K., MASCLE J., AUROUX C., *et alii* (1988) - *ODP Leg 107 in the Tyrrhenian Sea: Insights into passive margin and back-arc basin evolution*. Geological Society of America Bulletin, **100**: 1140-1156 pp.
- KEARY P. & VINE F. (1992) - *Global Tectonics*, Blackwell Science, 333 pp.
- KENT D.V., MUTTONI G. & BRACK P. (2004) - *Magnetostratigraphic confirmation of a much faster tempo for sea-level change for the Middle Triassic Latemar platform carbonates*, Earth Planet. Sci. Lett., **228**: 369-377.
- KENTER J.A.M. (1990) - *Carbonate platform flanks: slope angle and sediment fabric*. Sedimentology, **37**: 777-794.
- KHALIL S. (1998) - *Tectonic Evolution of the Eastern Margin of the Gulf of Suez, Egypt*. PhD Thesis, Royal Holloway, University of London, 349 pp.
- KHALIL S.M. & MCCLAY K.R. (2001) - *Tectonic evolution of the northwestern Red Sea-Gulf of Suez system*, Special Publication-Geological Society Of London, **187**: 453-473.
- KISSLING E. (1993) - *Deep structure of the Alps; what do we really know?* Phys. Earth Planet. Int., v. **79**, 1-2, 87-112 pp.
- KOBER L. (1908) - *Das Dachsteinkalkegebirge zwischen Garder, Rienz und Boite*. Mitt. Geol. Ges. **1**, Wien.
- KOYI H.A., HESSAMI K. & TEIXELL A. (2000) - *Epicenter distribution and magnitude of earthquakes in fold-thrust belts: insights from sandbox models*, Geophys. Res. Lett., **27**: 273-276.
- KUMMEROW J., KIND R., ONCKEN O., GIESE P., RYBERG T., WYLEGALLA K., SCHERBAUM F. & TRANSALP Working Group (2004) - *A natural and controlled source seismic profile through the Eastern Alps*: TRANSALP. Earth and Planetary Science Letters **225**: 115-129.
- LAUBSCHER H.P. (1971) - *Das Alpen-Dinariden-Problem und die Palinspastik der südlichen Tethys*. Geol. Rundschau, **60**, 3: 813-833.
- LAUBSCHER H.P. (1983) - *The Late Alpine (Periadriatic intrusions and the Insubric Line*. Mem. Soc. Geol. It., **26**: 21-30, Roma.
- LAUBSCHER H.P. (1985) - *Large scale, thin skinned thrusting in the Southern Alps: kinematic models*. Geol. Soc. Amer.

- Bull., **96**: 710-718, Tulsa.
- LAWTON T.F., BOYER S.E. & SCHMITT J.G. (1994) - *Influence of inherited taper on structural variability and conglomerate distribution, Cordilleran fold and thrust belt, western United States*. *Geology*, **22**: 339-342.
- LENCI F. & DOGLIONI C. (2007) - *On some geometric prism asymmetries*. In: *Thrust belts and Foreland Basins: From Fold Kinematics to Hydrocarbon Systems*, O. LACOMBE, J. LAVÉ, F. ROURE & J. VERGES (Eds.), *Frontiers in Earth Sciences*, Springer, 41,60.
- LEONARDI P. (1955) - *Breve sintesi geologica delle Dolomiti occidentali*. *Boll. Soc. Geol. It.*, **74**: 1-79.
- LEONARDI P. (1962) - *Il Gruppo dello Sciliar e le scogliere coralligene dolomitiche*. *Ann. Univ. Ferrara*, IX, III, 6-82.
- LEONARDI P. (1965) - *Tectonics and Tectonogenesis of the Dolomites*. *Eclogae Geol. Helv.*, **58**, 1: 49-62, Basel.
- LEONARDI P. et alii (1967) - *Le Dolomiti. Geologia dei Monti tra Isarco e Piave*. Ed. Manfrini, Rovereto, vols.1-2, 1-981.
- LÜSCHEN E., LAMMERER B., GEBRANDE H., MILLAHN K., NICOLICH R. & TRANSALP Working Group, (2004) - *Orogenic structure of the Eastern Alps, Europe, from TRANSALP deep seismic reflection profiling*. *Tectonophysics* **388**: 85-102
- MARIOTTI G. & DOGLIONI C. (2000) - *The dip of the foreland monocline in the Alps and Apennines*. *Earth and Planet. Sci. Lett.*, v. **181**, 191-202 pp.
- MARTINIS B. (1966) - *Prove di Ampì sovrascorimenti nelle Prealpi friulane e venete*. *Mem. Ist. Geol. Miner. Univ. Padova*, **25**.
- MASETTI D. & BIANCHIN G. (1987) - *Geologia del Gruppo della Schiara*. *Mem. Sc. Geol.*, **39**: 187-212, Padova.
- MASETTI D. & NERI C. (1980) - *L'Anisico della Val di Fassa (Dolomiti occidentali): sedimentologia e paleogeografia*. *Ann. Univ. Ferrara*, **7/1**, 1-19.
- MASETTI D., NERI C. & BOSELLINI A. (1991) - *Deep-water asymmetric cycles and progradation of carbonate platforms governed by high-frequency eustatic oscillations (Triassic of the Dolomites, Italy)*. *Geology*, **19**, 4: 336-339.
- MASSARI F., GRANDesso P., STEFANI C. & JOBSTRAIBIZER P.G. (1986) - *A small polyhistory foreland basin evolving in a context of oblique convergence: the Venetian basin (Chattian to Recent, Southern Alps, Italy)*. *Spec. Publs. Int. Ass. Sediment.*, **8**: 141-168, Oxford.
- MASSARI F., MELLERE D. & DOGLIONI C. (1990) - *Cyclicity in nonmarine foreland basin sedimentary infill: the Messinian Conglomerate-bearing succession of the Eastern Southern Alps (Italy)*. *Lisboa Meeting Preceedings*.
- MASSARI F. & NERI C. (1997) - *The infill of a supradetachment (?) basin: the continental to shallow-marine Upper Permian succession of Dolomites and Carnia (Italy)*. *Sedimentary Geology*, v. **110**, 181-221 pp.
- MASSON D.G. & MILES P.R. (1986) - *Development and Hydrocarbon Potential of Mesozoic Sedimentary Basins Around Margins of North Atlantic*. *Amer. Ass. Petrol. Geol. Bull.*, **70**, 6: 721-729.
- MCCLAY K.R. (1989) - *Analogue models of inversion tectonics*, in M. A. COOPER & G. D. WILLIAMS, eds., *Inversion tectonics*: Geological Society of London, Sp. Publ. **44**: 41-59.
- MCCLAY K.R. (1992) - *Glossary of thrust tectonics terms*. In K.R. MCCLAY (Ed.) "Thrust tectonics", Chapman & Hall, London, United Kingdom, 419-433.
- MCCLAY K. R., DOOLEY T. WHITEHOUSE P. & MILLS M. (2002) - *4-D evolution of rift systems: Insights from scaled physical models*. *Am. Assoc. Petrol. Geol. Bull.*, **86**: 935-959.
- MCNEILL L.C., PIPER K.A., GOLDFINGER C., KULM L.D. & YEATS R.S. (1997) - *Listric normal faulting on the Cascadia continental margin*, *J. Struct. Geol.*, **102**, 12, 123-12, 138.
- MCQUARRIE N. (2004) - *Crustal scale geometry of the Zagros fold-thrust belt, Iran*. *J. Struct. Geol.*, **26**, 519-535.
- MERLA G. (1931) - *Osservazioni morfologiche e tettoniche sugli altipiani ampezzani (Fosses-Sennes-Fanes)*. *Atti Soc. Toscana Sc. Nat.*, Mem. **42**, Pisa.
- MERLINI S., DOGLIONI C., FANTONI R. & PONTON M. (2002) - *Analisi strutturale lungo un profilo geologico tra la linea Fella-Sava e l'avampaese adriatico (Friuli Venezia Giulia-Italia)*. *Mem. Soc. Geol. It.*, **57**: 293-300.
- MILANI E.J. & DAVISON I. (1988) - *Basement control and transfer tectonics in the Reconcavo-Tucano-Jatoba rift, Brazil*. *Tectonophysics*, **154**: 41-70.
- MITRA S. (1986) - *Duplex structures and imbricate thrust systems*. *Amer. Ass. Petrol. Geol.*, **70/9**: 1087-1112.
- MITRA S. (1988) - *Three-dimensional geometry of the Pine Mountain thrust system, Southern Appalachians*. *Amer. Geol. Soc. Bull.*, **100**: 72-95.
- MITRA S. (2002) - *Fold-accommodation faults*. *Am. Assoc. Petrol. Geol. Bull.*, **86**: 671-693.
- MITRA S. & NAMSON J. (1989) - *Equal-area balancing*. *Amer. J. Sci.*, **289**: 563-599.
- MOHR M., KUKLA P.A., URAI J.L. & BRESSER G. (2005) - *Multiphase salt tectonic evolution in NW Germany: seismic interpretation and retro-deformation*. *Int. J. Earth Sci. (Geol Rundsch)*, **94**: 917-940.
- MOHR M., KUKLA P.A., URAI J.L. & BRESSER G. (2006) - *Mapping, modeling and evolution of salt structure geometries: implications for improved sub-salt exploration*. *Am. Ass. Petrol. Geol. Annual Convention*.
- MOJSISOVICS VON E. (1879) - *Die Dolomit-Riffe von Südtirol und Venetien*. *Beiträge zur Bildungsgeschichte der Alpen*. **1**, 1-552, Hölder, Wien.
- MORELLATO C., REDINI F. & DOGLIONI C. (2003) - *On the number and spacing of faults*. *Terra Nova*, **15**, 315-321, doi: 10.1046/j.1365-3121.2003.00501.x
- MORLEY C.K. (2002) - *Evolution of large normal faults: Evidence from seismic reflection data*. *Am. Assoc. Petrol. Geol. Bulletin*, **86**: 961-978.
- MÜLLER M., NIEBERDING F. & WANNINGER A. (1988) - *Tectonic style and pressure distribution at the northern margin of the Alps between Lake Constance and River Inn*. *Geol. Rund.*, **77**, 3, 787-796, Stuttgart.
- MUELLER S. & PANZA G.F. (1986) - *Evidence of a deep-rea-*

- ching lithospheric root under the Alpine Arc. In: *The Origin of Arcs*: F.C. WEZEL (Ed.), Elsevier, v. 21, 93-113 pp.
- MUTTI E. (1985) - *Turbidite systems and their relations to depositional sequences*. In: G.G. ZUFFA (Ed), *Provenance of arenites*: NATO-ASI Series, Reidel Publishing Co., 65-93.
- MUTTI E. & NORMARK W.R. (1987) - *Comparing examples of modern and ancient turbidite systems: Problems and concepts*. In: J.K. LEGGET & G.G. ZUFFA (Eds), *Deep Water Clastic Deposits: Models and Case Histories*. Graham & Trotman, 1-38.
- MUTTI E., SEGURET M. & SGAVETTI M. (1988) - *Sedimentation and Deformation in the Tertiary Sequences of the Southern Pyrenees*. Am. Assoc. Petrol. Geol. Mediterranean Basins Conference, Nice, Field Trip guide book 7: 1-157.
- NEWTON WILSON E., HARDIE L.A. & PHILLIPS O.M. (1990) - *Dolomitization front geometry, fluid flow patterns, and the origin of massive dolomite: the Triassic Latemar buildup, northern Italy*. Amer. Journ. Science, 290: 741-796.
- OGILVIE GORDON M.M. (1910) - *Die Überschiebung am Giepfel des Sellamassiv in Südtirol*. Verhandl. Geol. Reichsanstalt, Wien.
- OGILVIE GORDON M.M. (1929) - *Geologie des Gebietes von Pieve (Buchenstein), St. Cassian, und Cortina d'Ampezzo*. Jahrb. Geol. Bundesanst., Bd., 79, Heft 3-4, Wien.
- OGILVIE GORDON M.M. (1934) - *Geologie von Cortina d'Ampezzo und Cadore*. Jahrb. Geol. Bundesanst., Bd. 84, Heft. 1-4, Wien.
- PANZA G.F. & MUELLER S. (1978) - *The plate boundary between Eurasia and Africa in the Alpine area*. Mem. Ist. Geol. Mineral. Univ. Padova, 33: 43-50.
- PANZA G.F., PONTEVIVO A., CHIMERA G., RAYKOVA R. & AOUDIA A. (2003) - *The Lithosphere-Asthenosphere: Italy and surroundings*. Episodes, 26, 3: 169-174.
- PANZA G., RAYKOVA R.B., CARMINATI E. & DOGLIONI C. (2007) - *Upper mantle flow in the western Mediterranean*. Earth Planet. Sci. Lett., 257: 200-214.
- PEACOCK D.C.P. (2002) - *Propagation, interaction and linkage in normal fault systems*. Earth Sci. Rev., 58: 121-142.
- PEACOCK D.C.P. & SANDERSON D.J. (1994) - *Geometry and development of relay ramps in normal fault systems*, Am. Assoc. Petrol. Geol. Bulletin, 78: 147-165.
- PIFFNER O.A., LEHNER P., HEITZMANN P., MUELLER S. & STECK A. (1997) - *Results of NRP20-Deep structure of the Alps*. Birkhäuser Verlag, Basel.
- PIA J. (1937) - *Stratigraphie und Tektonik der Pragser Dolomiten in Südtirol*. 1-248, Wien.
- PIERI M. (1983) - *Three seismic profiles through the Po Plain*. In: *Seismic expression of structural styles* (Ed A.W. BALLY), Am. Ass. Petrol. Geol. Studies in Geology 15 (1983) 3.4.1/8-26
- PIERI M. & GROPPi G. (1981) - *Subsurface geological structure of the Po plain, Italy*. Prog. Final. Geod., Pubbl. 414, 1-13 pp., Roma.
- PISA G., CASTELLARIN A., LUCCHINI F., ROSSI P.L., SIMBOLI G., BOSELLINI A. & SOMMAVILLA E. (1979) - *Middle Triassic magmatism in Southern Alps. I: a review of general data in the Dolomites*. Riv. It. Paleont. Strat., 85, 3-4: 1093-1110.
- PISA G., FARABEGOLI E. & OTT E. (1978) - *Stratigrafia e paleogeografia dei terreni anisici della Conca di Agordo e dell'Alta Val di Zoldo (Dolomiti sudorientali)*. Mem. Soc. Geol. It., 18: 63-92.
- PLATT N., PHILIP P. & STEWARD W. (1993) - *Going for the play: Structural interpretation in offshore Congo*. Oilfield Review.
- POSENATO R. (1988) - *The Permian-Triassic boundary in the Western Dolomites, Italy*. Review and proposal. Ann. Univ. Ferrara, 1, 3: 31-45.
- PREMOLI SILVA I. & LUTERBACHER H. (1966) - *The Cretaceous-Tertiary boundary in the Southern Alps (Italy)*. Riv. It. Paleont., 72: 1183-1266.
- PRETO N., HINNOV L.A., HARDIE L. & DE ZANCHE V. (2001) - *Middle Triassic orbital signature recorded in the shallow-marine Latemar carbonate buildup (Dolomites, Italy)*. Geology, v. 29, n. 12, 1123-1126 pp.
- RAMSAY J.G. & HUBER M. (1987) - *Modern structural geology, Folds and fractures*. Vol. II, Academic Press, London, 309-700 pp.
- RANALLI G. & MURPHY D.C. (1987) - *Rheological stratification of the lithosphere*. Tectonophysics, 132: 281-295.
- RÉHAULT J.P., MASCLE J. & BOILLOT G. (1984) - *Evolution géodynamique de la Méditerranée depuis l'Oligocène*. Memorie Società Geologica Italiana, 27, 85-96 pp.
- REITHOFER O. (1928) - *Geologie der Sellagruppe (Südtiroler Dolomiten)*. Jb. geol. Bundesanst. (Wien) 78/3-4, 529-579.
- RICARD Y., DOGLIONI C. & SABADINI R. (1991) - *Differential rotation between lithosphere and mantle: a consequence of lateral mantle viscosity variations*. Journ. Geophysical Research, 96: 8407-8415.
- RIVA M., BESIO M., MASETTI D., ROCCATI F., SAPIGNI M. & SEMENZA E. (1990) - *Geologia delle valli Vajont e Gallina (Dolomiti orientali)*. Ann. Univ. Ferrara 2, 4, 53-76.
- ROEDER D. (1985) - *Geodynamics of Southern Alps. Seminar paper given at University of Milan*, Anschutz Corporation Exploration Research Division, 1-22, Denver.
- ROEDER D. (1989) - *South-Alpine thrusting and trans-Alpine convergence*. In: M.P. COWARD, D. DIETRICH & R.G. PARK (Eds), *Alpine Tectonics*, Geol. Soc. Spec. Publ., 45: 211-227.
- ROSSI D. (1957) - *Gli aspetti morfologici delle cime dolomitiche*. Boll. Soc. Geol. Ital., 76: 46-66.
- ROSSI D. (1962) - *Geologia della parte meridionale del Gruppo della Marmolada*. Mem. Mus. Storia Nat. Venetia Tridentina, 14, 1b, 1-189.
- ROSSI D. (1977) - *Un esempio di tettonica preladinica forse diapirica nelle Dolomiti occidentali (Val di S. Nicolò)*. Ann. Univ. Ferrara, 5, 12, 213-221.
- ROSSI P.L. SIMBOLI G. & SOMMAVILLA E. (1974) - *La serie vulcanica medio-triassica della Catena del Padon (Gruppo della Marmolada, parte settentrionale)*. Miner. Petrogr. Acta, 20:

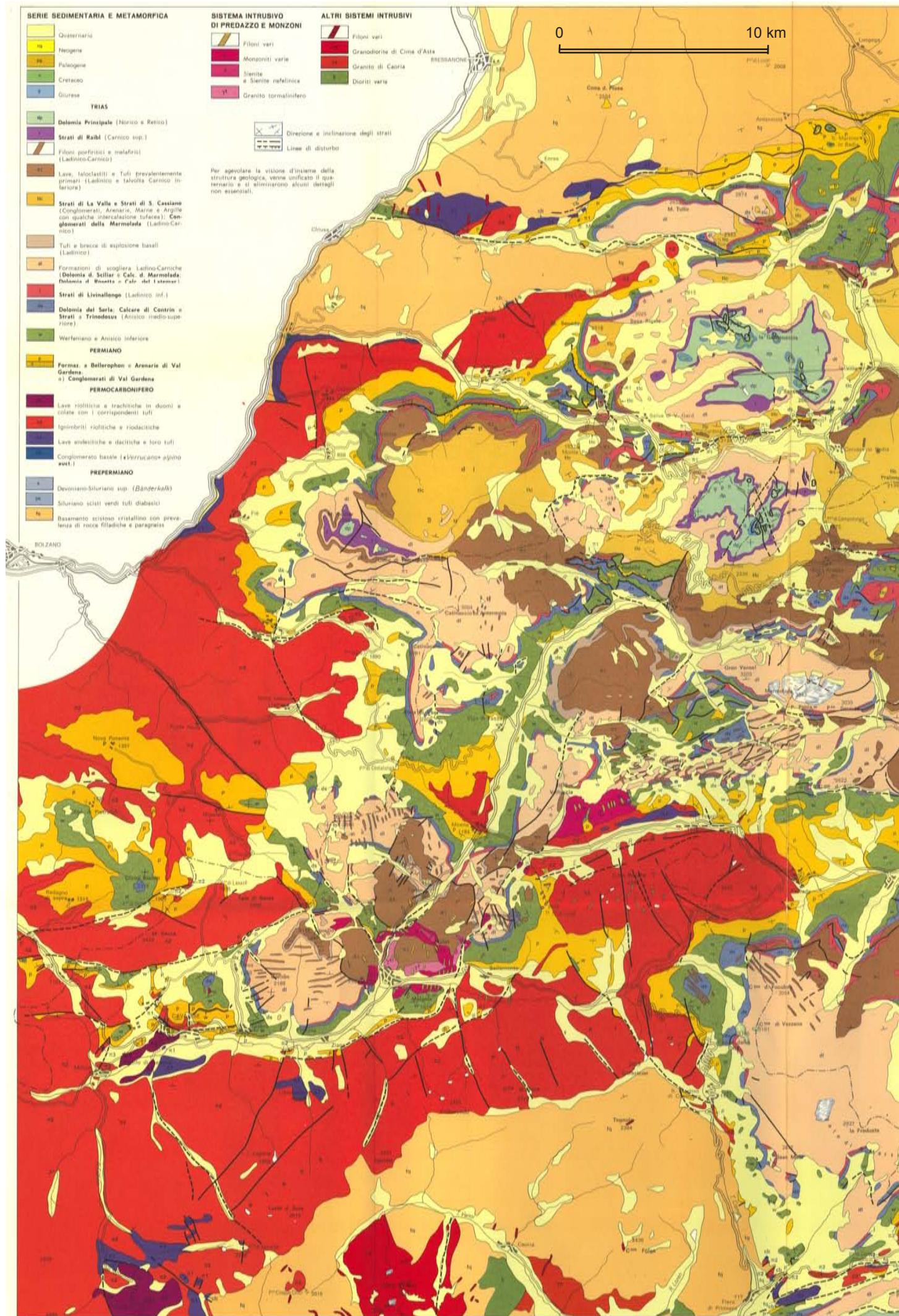
- 1-48.
- ROSSI P.M. & JADOUL F. (1982) - *Evoluzione paleogeografico-strutturale e vulcanismo triassico nella Lombardia centro-occidentale*. In CASTELLARIN & VAI (Eds), Guida alla geologia del Sudalpino centro-orientale. Guide Geol. Reg., Soc. Geol. It., 143-156.
- ROSSI M.E. & ROGLEDI S. (1988) - *Relative sea-level changes, local tectonic settings and basin margin sedimentation in the interference zone between two orogenic belts: seismic stratigraphic examples from Padan foreland basin, northern Italy*. In: NEMEC & STEEL (Eds), Fan Deltas: Sedimentology and Tectonic Settings, Blackie & Son, 368-384.
- RUDOLF K.W., SCHLAGER W. & BIDDLE K.T. (1989) - *Seismic models of a carbonate foreslope-to-basin transition, Picco di Vallandro, Dolomite Alps, northern Italy*. Geology, 17, 5: 389-484.
- RUSSO F., NERI C., MASTANDREA A. & LAGHI G. (1991) - *Depositional and diagenetic history of the Alpe di Specie (Seeland alpe) fauna (Carnian, Northeastern Dolomites)*. Facies, 25: 187-210.
- RUSSO F., MASTRANDREA A., STEFANI M. & NERI C. (2000) - *Carbonate facies dominated by syndepositional cements: a key component of Middle Triassic platforms. The Marmolada case history (Dolomites, Italy)*. Facies, v. 42, 211-226 pp.
- RUSSO F., NERI C. & MASTRANDREA A. (1998) - *Le comunità costruttrici delle piattaforme triassiche delle Dolomiti: Memorie della Società Geologica Italiana*, v. 53, 479-488 pp.
- SABADINI R., DOGLIONI C. & YUEN D.A. (1990) - *Eustatic sea-level fluctuations induced by polar wander*. Nature, 345: 708-710.
- SACERDOTI M. & SOMMAVILLA E. (1962) - *Pillowlave, ialoclastiti e altre formazioni vulcanoclastiche nella Regione Dolomitica occidentale*. Studi Trent. Sci. Nat., 39: 423-473.
- SARTI M. & ARDIZZONI F. (1984) - *Tettonica triassica nel Gruppo di Cima Pape. Pale di Sanson (Dolomiti Bellunesi)*. Mem. Sci. Geol., 36: 353-370.
- SCHLAGER W., BIDDLE K.T. & STAFLEU J. (1991) - *Picco di Vallandro (Dürrenstein) a platform-basin transition in outcrop and seismic model*. Dolomieu Conference on Carbonate Platforms and Dolomitization. Guidebook Excursion D, 1-22.
- SCHMID S.M., AEBLI H.R., HELLER F. & ZINGG A. (1989) - *The role of the Periadriatic Line in the tectonic evolution of the Alps*. In: COWARD et alii (eds), Alpine tectonics. Spec. Publ. geol. Soc. London 45: 153-171.
- SCHOLZ C.H. (1990) - *Mechanics of earthquakes and faulting*. Cambridge University Press, Cambridge, England, 439 pp.
- SCHÖNBORN G. (1999) - *Balancing cross sections with kinematic constraints: The Dolomites (northern Italy)*. Tectonics, 18, 3, 527-545 pp.
- SCHWINNER R. (1915) - *Zur Tektonik der Ampezzaner Dolomiten*. Mitt. Geol. Ges. 8, Wien.
- SCOPPOLA B., BOCCALETTI D., BEVIS M., CARMINATI E. & DOGLIONI C. (2006) - *The westward drift of the lithosphere: a rotational drag?* Bull. Geol. Soc. Am., 118, 1/2: 199-209 pp.; doi: 10.1130/B25734.1.
- SCROCCA D., DOGLIONI C. & INNOCENTI F. (2003) - *Constraints for an interpretation of the Italian geodynamics: a review*. In: D. SCROCCA, C. DOGLIONI, F. INNOCENTI, P. MANETTI, A. MAZZOTTI, L. BERTELLI, L. BURBI, S. D'OFFIZI (Eds.): "CROP Atlas: seismic reflection profiles of the Italian crust". Mem. Descr. Carta Geol. It., 62: 15-46.
- SCROCCA D., DOGLIONI C., INNOCENTI F., MANETTI P., MAZZOTTI A., BERTELLI L. BURBI L. & D'OFFIZI S. (Editors), 2003. "CROP Atlas: seismic reflection profiles of the Italian crust". Mem. Descr. Carta Geol. It., 62, 194 pp.
- SCROCCA D., CARMINATI E., DOGLIONI C. & MARCANTONI D. (2007) - *Slab retreat and active shortening along the central-northern Apennines*. In: Thrust belts and Foreland Basins: From Fold Kinematics to Hydrocarbon Systems, O. LACOMBE, J. LAVÉ, F. ROURE & J. VERGES (Eds.), Frontiers in Earth Sciences, Springer, in press.
- SCUDELLER BACCCELLE L. & SEMENZA E. (1974) - *Flysch terrigeno con strutture contornitiche nel Cretacico delle Dolomiti Ampezzane*. Caratteristiche sedimentologiche e significato geodinamico. Ann. Univ. Ferrara, 5/9, 165-199.
- SELLI R. (1947) - *La Geologia dell'Alto Bacino dell'Isonzo (stratigrafia e tettonica)*. Giorn. Geol., 2, XIX, 1-153.
- SELLI R. (1963) - *Schema geologico delle Alpi Carniche e Giulie Occidentali*. Giorn. Geol., 2, 30, 1-121.
- SEMENTA E. (1959) - *Osservazioni sulla tettonica del fianco sinistro della Valle del Piave nel tratto tra Loggò e Pieve di cadore*. Rend. Acc. Naz. Lincei, 8, 27/6, 397-404.
- SEMENTA E. (1960) *Nuovi studi tettonici nella Valle del Vajont e zone limitrofe*. Rend. Acc. Naz. Lincei, Cl. Sc. fis. mat. e nat., S.VIII, 28, 2, Roma.
- SEMENTA E. (1974) - *La fase giudicariense nel quadro di una nuova ipotesi sull'orogenesi alpina nell'area italo-dinarica*. Mem. Soc. Geol. It., 13, 187-226, Roma.
- SEMENTA E., BIANCHIN G. & MAZZEO G. (1984) - *Geologia dei Monti a Sud di Costa Vedorcia (Cadore sudorientale)*. Ann. Univ. Ferrara, 8/11, 145-167.
- SHAW J.H., CONNORS C. & SUPPE J. (2005) - *Seismic interpretation of contractional fault-related folds*. Am. Assoc. Petrol. Geol. Seismic Atlas. Studies in Geology n. 53.
- SIBSON R.H. (1981) - *Controls on low-stress hydro-fracture dilatancy in thrust, wrench and normal fault terrains*. Nature, 289: 665-667.
- SIBSON R.H. (1990) - *Rupture nucleation on unfavorably oriented faults*. Bulletin of the Seismological Society of America, 80: 1580-1604.
- SIBSON R.H. (1998) - *Brittle failure mode plots for compressional and extensional tectonic regimes*. J. Struct. Geol., 20: 655-660.
- SIBSON R.H. (2001) - *Seismogenic framework for hydrothermal*

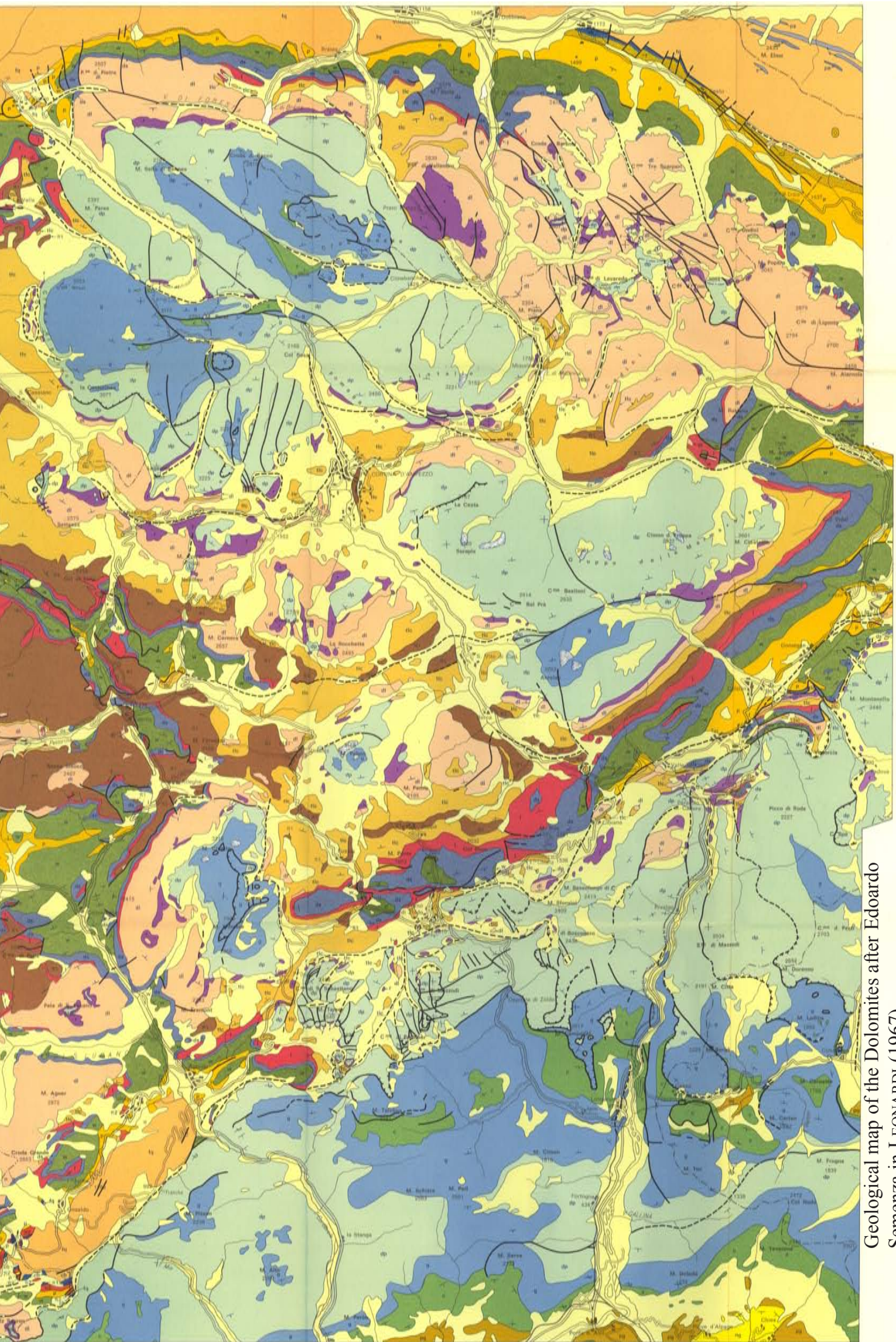
- transport and ore deposition. Soc. Economic Geol. Rev., 14: 25-50.
- SIGNORINI R. (1954) - Osservazioni sulla struttura e la morfologia delle Dolomiti Orientali. Boll. Soc. Geol. It., 70, 3, 545-564.
- SKUCE A.G. (1994) - A structural model of a graben boundary fault system, Sirte Basin, Libya: Compaction structures and transfer zones. Can. J. Expl. Geophys., 30: 84-92.
- SLEIKO D., CARULLI G.B., CARRARO F., CASTALDINI D., CAVALLIN A., DOGLIONI C., ILICETO V., NICOLICH R., REBEZ R., SEMENZA E. ZANFERRARI A. & ZANOLLA C. (1987) - Modello sismotettonico dell'Italia nord-orientale. CNR, GNDT, Rend. 1: 1-82, Trieste.
- STAMPFLI G., BOREL G., CAVAZZA W., MOSAR J. & ZIEGLER P. A. (2001) - The paleotectonic atlas of the Peri-Tethyan domain. European Geophysical Society, CD rom.
- STANLEY D.J. & WEZEL F.C. (Eds) (1985) - Geological Evolution of the Mediterranean Basin. Springer-Verlag, 1-589 pp.
- STEFANINI G. (1915) - Il Neogene del Veneto. Mem. Ist. Geol. R. Univ. Padova, 3:1-286, Padova.
- SUNWALL M.T., MCQUILLAN K.A. & NICK C.J. (1983) - Salt diapir; Gulf of Mexico. Am. Assoc. Petrol. Geol. Studies in Geology, 15, 2.3.2-32-2.3.2-37 pp.
- SUPPE J. (1983) - Geometry and Kinematics of fault-bend folding. Amer. J. Sci. 283: 684-721.
- SUPPE J. (1985) - Principles of Structural Geology. Prentice-Hall, 1-537.
- SUPPE J. & MEDWEDEFF D.A. (1990) - Geometry and kinematics of fault-propagation folding. Eclogae geol. Helv. 83/3, 409-454.
- TARAMELLI T. (1882) - Geologia delle Provincie Venete con Carte Geologiche e Profili. Atti Acc. Naz. Lincei, Mem. Cl. Sc. Fis., 3, 13, 1-536 Roma.
- TOWNEND J. & ZOBACK M.D. (2000) - How faulting keeps the crust strong. Geology, 28: 399-402.
- TRACCANELLA E. (1987) - Itinerari geologici nella zona della Marmolada e nell'Alta Val Cordevole. Agip, Sepi, 1-86.
- TAPPONNIER P. & MOLNAR P. (1977) - Active faulting and tectonics in China. J. Geophys. Res., 82: 2905-2930.
- TRANSALP Working Group 2002, First deep seismic reflection images of the Eastern Alps reveal giant crustal wedges and transcrustal ramps. Geophys. Res. Lett., 29, 10, 10.1029/2002GL014911.
- TRENER G.B. (1909) - Geologische Spezialkarte der Oest. Ung. Mon. 1:75.000, Blatt: Borgo und Fiera di Primiero. K.K. Geol. R.A., Wien.
- TREVISAN L. (1939) - Il Gruppo di Brenta. Mem. Ist. Geol. Univ. Padova, 13: 1-128.
- TREVISAN L. (1941) - Profili tettonici nella regione della bassa Sarca (Trentino). Studi Trentini Sc. Nat., Anno XXII, 1: 1-8, Trento.
- TREVISAN L. (1941) - Caratteri particolari della tettonica dell'Altopiano dei Sette Comuni (Vicenza). Studi Trent. Sc. Nat., 22, 2, 79-88, Trento.
- TRUMPY R. (1980) - An outline of the geology of Switzerland. Schweiz. Geol. Komm., Geology of Switzerland, a guide-book, A, 1-104.
- TRUMPY R. (1982) - Alpine Paleogeography: a Reappraisal. In: K.J. HSU (ed), Mountain building processes. Academic Press, 149-156.
- TRUSHEIM F. (1960) - Mechanism of salt migration in northern Germany. Am. Ass. Petrol. Geol. Bull., 44: 1519-1540.
- TWISS R.J. & MOORES E.M. (1992) - Structural geology, W.H. Freeman and Compan, New York, 531 pp.
- VAI G.B., BORIANI A., RIVALENTI G. & SASSI P.F. (1982) - Catena Ercinica e Paleozoico nelle Alpi Meridionali. In: AA.VV. Cento anni di Geologia Italiana. Soc. Geol. It., Tecoprint Bologna, 133-154.
- VAI G.B. & MARTINI P. (Eds) (2001) - Anatomy of an Orogen: the Apennines and Adjacent Mediterranean Basins. Kluwer Academic Publisher, Dordrecht, The Netherlands, 1-632 pp.
- VAIL P.R., MITCHUM R.M.JR. & THOMPSON S.III (1977) - Seismic stratigraphy and Global Changes of Sea Level, Part 4: Global Cycles of Relative Changes of Sea Level. In: Seismic Stratigraphy. applications to hydrocarbon exploration, Amer. Ass. Petrol. Geol. Mem., 26: 83-98, Tulsa.
- VAN BEMMELEN R.W. (1966) - The structural evolution of the Southern Alps. Geol. Mijnbouw, 45: 405-444.
- VARDABASSO S. (1930) - Carta geologica del territorio eruttivo di Predazzo e Monzoni nelle Dolomiti di Fiemme e di Fassa. R. Scuola d'Ingegneria, Padova.
- VARDABASSO S. (1931) - Profili geologici attraverso le Dolomiti occidentali. Min. Lav. Pubbl. Uff. Idrogr. R. Mag. Acque, Venezia.
- VENZO G.A. (1958) - La Linea di Trodena e la struttura geologica della struttura Occlini. Altipiano di Lavazè (Trentino Alto Adige). St. Trent. Sc. Nat., 35, 2-3, 99-106.
- VENZO S. (1939) - Nuovo lembo tortoniano strizzato tra le filladi ed il permiano a Strigno di Valsugana (Trentino meridionale orientale). Boll. Soc. Geol. It., 58, 1, 175-185, Roma.
- VENZO S. (1939) - Osservazioni geotettoniche e geomorfologiche sul rilevamento del foglio Belluno. Boll. Soc. Geol. It., 58, 2-3, 433-451, Roma.
- VENZO S. (1940) - Studio geotettonico del Trentino meridionale-orientale tra Borgo Valsugana e M. Coppolo. Mem. Ist. Geol. Univ. Padova, 14: 1-86, Padova.
- VENZO S. (1954) - Stratigrafia e tettonica del Flysch (Cretacico-Eocene) del Bergamasco e della Brianza orientale. Mem. Descr. Carta Geol. Italia, 31: 1-133.
- VENZO S. (1977) - I depositi Quaternari e del Neogene superiore nella bassa Valle del Piave da Quero al Montello e del Paleopiave nella Valle del Soligo (Treviso). Mem. Ist. Geol. Miner. Univ. Padova, 30: 1-63, Padova.
- VIEL G. (1979) - Litostratigrafia Ladinica: una revisione. Ricostruzione paleogeografica e paleostrutturale dell'area Dolomitico-Cadorina (Alpi Meridionali); I e II parte. Riv. It. Paleont. Strat., 85, 1, 85-125; 85, 2, 297-352.
- XIAO H. & SUPPE J. (1992) - Origin of rollover. Am. Assoc. Petrol. Geol. Bull., 76: 509-529.

- WENDT J. (1982) - *The Cassian patch reefs* (Lower Carnian, Southern Alps). *Facies*, **6**: 185-202.
- WEISSERT H.J. & BERNOULLI D. (1985) - *A transform margin in the Mesozoic Tethys: evidence from the Swiss Alps*. *Geol. Rund.*, **74**: 665-679.
- WILSON M. & BIANCHINI G. (1999) - *Tertiary-Quaternary magmatism within the Mediterranean and surrounding regions*. Geological Society Special Publication, **156**, 141-168 pp.
- WINTERER E.L. & BOSELLINI A. (1981) - *Subsidence and Sedimentation on a Jurassic Passive Continental Margin (Southern Alps, Italy)*. *Amer. Ass. Petrol. Geol. Bull.*, **65**: 394-421, Tulsa.
- WOODCOCK N.H. & FISCHER M. (1986) - *Strike-slip duplexes*, *J. Struct. Geol.*, **8**: 725-735.
- ZAMPIERI D. (1987) - *Le piattaforme carbonatiche triassiche delle Pale di San Martino (Dolomiti)*. *Mem. Sc. Geol., Padova*, **73-84**.
- ZANFERRARI A. (1973) - *Osservazioni geologiche sui terreni attraversati dalle gallerie dell'autostrada di Alemagna presso Vittorio Veneto*. Significato dei dati in rapporto alla tettonica del margine meridionale del Cansiglio. *Mem. Soc. Geol. It.*, **12**, 4, 529-548.
- ZANFERRARI A., BOLLETTINARI G., CAROBENE L., CARTON A., CARULLI G.B., CASTALDIN D., CAVALLIN A., PANIZZA M., PELLEGRINI G.B., PIANETTI F. & SAURO U. (1982) - *Evoluzione neotettonica dell'Italia nord-orientale*. *Mem. Sc. Geol.*, **35**: 355-376, Padova.
- ZENARI S. (1934) - *Sulla tettonica dei dintorni di Lozzo in Cadore*. *Atti Acc.Sc.Ven.Trent.Istr.*, **24**: 3-7.
- ZIEGLER P.A. (1988) - *Evolution of the Arctic-North Atlantic and Western Tethys*. *Amer. Ass. Pet. Geol. Memoir*, **43**: 1-206.
- ZIEGLER P.A. (1992) - *European Cenozoic rift system*. *Tectonophysics*, **208**: 91-111.

INDEX

1. Elements of rheology	pag.	9
2. Fault mechanics: some basic aspects	“	15
3. Thrusts, folds and orogens	“	23
4. Normal faults and rift zones	“	63
5. Strike-slip faults - Opposite migration of seismicity	“	81
6. Salt tectonics	“	91
7. Geodynamic framework of subduction zones	“	99
8. Tectonics and Sedimentation	“	109
9. Mediterranean Geodynamics	“	137
10. Stratigraphy of the Dolomites	“	147
11. Tectonics of the Dolomites	“	163
Dolomites field trip - 1 st day excursion	“	197
2 nd day excursion	“	209
3 rd day excursion	“	225
4 th day excursion	“	243
5 th day excursion	“	261
<i>References</i>	“	283





Geological map of the Dolomites after Edoardo Semenza in LEONARDI (1967).



Eugenio Carminati

eugenio.carminati@uniroma1.it

http://tetide.geo.uniroma1.it/sciterra/sezioni/carminati/carminati_intro.html



Carlo Doglioni

carlo.doglioni@uniroma1.it

<http://tetide.geo.uniroma1.it/DST/doglioni>

